UNIVERSIDADE FEDERAL DO ESPÍRITO SANTO
CENTRO DE CIÊNCIAS EXATAS
PROGRAMA DE PÓS-GRADUAÇÃO EM QUÍMICA

Synthesis and Biological Evaluation of Cytotoxic Paeonol Derivatives, Aryne-Functionalized Naphthoquinones with Trypanocidal Activity, and BODIPY-Based Fluorophores

Laura Patricia Rocha Figueroa

Tese de Doutorado em Química

Vitória
2025

Laura Patricia Rocha Figueroa

Synthesis and Biological Evaluation of Cytotoxic Paeonol Derivatives, Aryne-Functionalized Naphthoquinones with Trypanocidal Activity, and BODIPY-Based Fluorophores

Tese apresentada ao Programa de Pós-Graduação em Química do Centro de Ciências Exatas da Universidade Federal do Espírito Santo como requisito parcial para obtenção do Título de Doutor em Química

Área de Concentração: Química

Linha de Pesquisa: Síntese Orgânica e Medicinal.

Orientador: Prof. Dr. Warley de Souza Borges

Co-orientador(a): Prof. Dr. Eufrânio Nunes da Silva Junior

VITÓRIA
2025

Ficha catalográfica disponibilizada pelo Sistema Integrado de Bibliotecas - SIBI/UFES e elaborada pelo autor

---

Rocha Figueroa, Laura Patricia, 1996-
R672s Synthesis and Biological Evaluation of Cytotoxic Paeonol Derivatives, Aryne-Functionalized Naphthoquinones with Trypanocidal Activity, and BODIPY-Based Fluorophores / Laura Patricia Rocha Figueroa. - 2025.
259 f. : il.

Orientador: Warley de Souza Borges.
Coorientador: Eufrânio Nunes da Silva Junior.
Tese (Doutorado em Química) - Universidade Federal do Espírito Santo, Centro de Ciências Exatas.

1. Química orgânica. 2. Síntese orgânica. I. de Souza Borges, Warley. II. Nunes da Silva Junior, Eufrânio. III. Universidade Federal do Espírito Santo. Centro de Ciências Exatas. IV. Título.

CDU: 54

Synthesis and Biological Evaluation of Cytotoxic Paeonol Derivatives, Aryne-Functionalized Naphthoquinones with Trypanocidal Activity, and BODIPY-Based Fluorophores

Laura Patricia Rocha Figueroa

Tese submetida ao Programa de Pós-Graduação em Química do Centro de Ciências Exatas da Universidade Federal do Espírito Santo como requisito parcial para a obtenção do Grau de Doutor(a) em Química.

Aprovada em 11/12/2025 por:

Prof.(a) Dr.(a) Warley de Souza Borges
Orientador(a)
UFES

Prof.(a) Dr.(a) Eufranio da Silva Junior
Coorientador(a)
UFMG

Prof.(a) Dr.(a) Vanessa Nascimento
UFF

Prof.(a) Dr.(a) Juliana Christina Thomas
UFRGS

Prof.(a) Dr.(a) Amanda Silva de Miranda
UFMG

Prof.(a) Dr.(a) Luis Octavio Regasini
UNESP

Prof.(a) Dr.(a) Alvaro Cunha Neto
UFES

Universidade Federal do Espírito Santo
Vitória, dezembro de 2025

Datas e horários baseados em Brasília, Brasil
Sincronizado com o NTP.br e Observatório Nacional (ON) em 12/12/2025 às 10:29:51

AtaAprovação_Laura Patricia Rocha Figueroa

Data e Hora de Criação: 12/12/2025 às 10:29:39

Documentos que originaram esse envelope:
- AtaAprovação_Laura Patricia Rocha Figueroa.pdf (Arquivo PDF) - 2 página(s)
- FolhaRegistro_Laura Patricia Rocha Figueroa.pdf (Arquivo PDF) - 1 página(s)
- FolhaAssinaturas_Laura Patricia Rocha Figueroa.pdf (Arquivo PDF) - 1 página(s)

Hashs únicas referente à esse envelope de documentos

[SHA256]: 50abb5b07a9ab5fd534231469eff45ccbdbf6a451d52d465f4e64ea6ebc70298
[SHA512]: 903f6cf6de9cd83f01a32019b2284f0f0cb10b27b8e87ac9c8e3492f37b861fa747a1f0507604bd4cf5a34ed922fbc499a563852c7629ed7f0e367c2f8d2e34c

Lista de assinaturas solicitadas e associadas à esse envelope

ASSINADO - Warley De Souza Borges (warley.borges@ufes.br)
Data/Hora: 12/12/2025 - 10:32:26, IP: 179.102.131.66, Geolocalização: [-20.274883, -40.303760]
[SHA256]: 37f899f99e666994cfed5518d117fdf10b836facc77745be1ee53886a7e3bdbb
Assinatura Eletrônica Avançada (Conforme Lei nº 14.063/20, art. 4º, II)

ASSINAR
Eufranio Nunes da Silva Junior (eufranio@qui.ufmg.br)
[aguardando ação do usuário]

ASSINAR
Vanessa Nascimento (nascimentovanessa@id.uff.br)
[aguardando ação do usuário]

ASSINAR
Juliana Christina Thomas (juliana.thomas@ufrgs.br)
[aguardando ação do usuário]

ASSINAR
Amanda Silva de Miranda (a.s.miranda@hotmail.com)
[aguardando ação do usuário]

ASSINAR
Luis Octavio Regasini (luis.regasini@unesp.br)
[aguardando ação do usuário]

ASSINAR
Alvaro Cunha Neto (alvaro.cunha@ufes.br)
[aguardando ação do usuário]

Histórico de eventos registrados neste envelope

12/12/2025 10:32:26 - Assinatura realizada por warley.borges@ufes.br, IP 179.102.131.66
12/12/2025 10:32:20 - Envelope visualizado por warley.borges@ufes.br, IP 179.102.131.66
12/12/2025 10:29:53 - Envelope registrado na Blockchain por kieza.pereira@ufes.br, IP 200.137.65.103
12/12/2025 10:29:51 - Envelope encaminhado para assinaturas por kieza.pereira@ufes.br, IP 200.137.65.103
12/12/2025 10:29:41 - Envelope criado por kieza.pereira@ufes.br, IP 200.137.65.103

Datas e horários baseados em Brasília, Brasil
Sincronizado com o NTP.br e Observatório Nacional (ON) em 14/12/2025 às 13:00:38

AtaAprovação_Laura Patricia Rocha Figueroa_251212_165641

Data e Hora de Criação: 12/12/2025 às 17:04:18

Documentos que originaram esse envelope:
- AtaAprovação_Laura Patricia Rocha Figueroa_251212_165641.pdf (Arquivo PDF) - 5 página(s)

Hashs únicas referente à esse envelope de documentos

[SHA256]: 3344bef53e000e4eb0eef93a3230db8bc23b53933ad36173a33a732fe65afa8f
[SHA512]: 676e44b4b9514e1964f966bbe9babc50646c8d1e4d90852ddf5543716fd5f12dd5e458b23189d9dcb634c4b4bb9ef4f8e31ae8d5382eab9e790ef9c794dc9b73

Lista de assinaturas solicitadas e associadas à esse envelope

ASSINADO - Alvaro Cunha Neto (alvaro.cunha@ufes.br)
Data/Hora: 12/12/2025 - 17:07:21, IP: 200.137.65.100
[SHA256]: 675de77bfe39268aacd2ef10ad54dd5a179adf37a7eb73a54da7ec55b01105f9
Assinatura Eletrônica Avançada (Conforme Lei nº 14.063/20, art. 4º, II)

ASSINADO - a.s.miranda@hotmail.com
Data/Hora: 12/12/2025 - 17:57:08, IP: 191.185.79.182
[SHA256]: 52ea02d5ee12bf07274b8d486cf80fdd53b049fabe9f98041f3ff87ac5ee383a
Assinatura Eletrônica Avançada (Conforme Lei nº 14.063/20, art. 4º, II)

ASSINADO - eufranio@qui.ufmg.br
Data/Hora: 14/12/2025 - 13:00:38, IP: 177.86.37.140
[SHA256]: 43f0b00ab6f6889a8af2ab50b47f186cadc8f51da1387357e51d1ad11f817c76
Assinatura Eletrônica Avançada (Conforme Lei nº 14.063/20, art. 4º, II)

ASSINADO - juliana.thomas@ufrgs.br
Data/Hora: 12/12/2025 - 20:19:58, IP: 189.6.253.231, Geolocalização: [-30.045026, -51.122727]
[SHA256]: 15b621a2fec164bd11587f6bf4a17762c7ded6fca39e58f9009de8a16b7cd536
Assinatura Eletrônica Avançada (Conforme Lei nº 14.063/20, art. 4º, II)

ASSINADO - luis.regasini@unesp.br
Data/Hora: 13/12/2025 - 10:23:20, IP: 187.181.208.70
[SHA256]: da8258df77894ca7dad1175cbcc2fc5cb5396181601c90e495cb344141d710e1
Assinatura Eletrônica Avançada (Conforme Lei nº 14.063/20, art. 4º, II)

ASSINADO - nascimentovanessa@id.uff.br
Data/Hora: 13/12/2025 - 08:30:48, IP: 177.12.16.252
[SHA256]: dea6365508dede2c6c750162a06cb5933648595f63f675b2b0a8ad42dd6b8f7f
Assinatura Eletrônica Avançada (Conforme Lei nº 14.063/20, art. 4º, II)

ASSINADO - Warley De Souza Borges (warley.borges@ufes.br)
Data/Hora: 12/12/2025 - 17:10:10, IP: 179.102.141.163, Geolocalização: [-20.342170, -40.292968]
[SHA256]: dd327948a27391e0c82d25283c094e6124e2cfb6e0f1463fab6f50986c85eb0a
Assinatura Eletrônica Avançada (Conforme Lei nº 14.063/20, art. 4º, II)

Histórico de eventos registrados neste envelope

14/12/2025 13:00:38 - Envelope finalizado por eufranio@qui.ufmg.br, IP 177.86.37.140
14/12/2025 13:00:38 - Assinatura realizada por eufranio@qui.ufmg.br, IP 177.86.37.140
13/12/2025 10:23:20 - Assinatura realizada por luis.regasini@unesp.br, IP 187.181.208.70
13/12/2025 10:22:55 - Envelope visualizado por luis.regasini@unesp.br, IP 187.181.208.70
13/12/2025 08:30:48 - Assinatura realizada por nascimentovanessa@id.uff.br, IP 177.12.16.252
13/12/2025 08:30:41 - Envelope visualizado por nascimentovanessa@id.uff.br, IP 187.19.161.165
12/12/2025 20:19:58 - Assinatura realizada por juliana.thomas@ufrgs.br, IP 189.6.253.231
12/12/2025 20:19:46 - Envelope visualizado por juliana.thomas@ufrgs.br, IP 189.6.253.231
12/12/2025 17:57:08 - Assinatura realizada por a.s.miranda@hotmail.com, IP 191.185.79.182

Datas e horários baseados em Brasília, Brasil
Sincronizado com o NTP.br e Observatório Nacional (ON) em
14/12/2025 às 13:00:38

AtaAprovação_Laura Patricia Rocha Figueroa_251212_165641

Data e Hora de Criação: 12/12/2025 às 17:04:18

Documentos que originaram esse envelope:

- AtaAprovação_Laura Patricia Rocha Figueroa_251212_165641.pdf (Arquivo PDF) - 5 página(s)

Hashs únicas referente à esse envelope de documentos

[SHA256]: 3344bef53e000e4eb0eef93a3230db8bc23b53933ad36173a33a732fe65afa8f
[SHA512]: 676e44b4b9514e1964f966bbe9babc50646c8d1e4d90852ddf5543716fd5f12dd5e458b23189d9dcb634c4b4bb9ef4f8e31ae8d5382eab9e790ef9c794dc9b73

Histórico de eventos registrados neste envelope

12/12/2025 17:56:52 - Envelope visualizado por a.s.miranda@hotmail.com, IP 191.185.79.182
12/12/2025 17:10:10 - Assinatura realizada por warley.borges@ufes.br, IP 179.102.141.163
12/12/2025 17:10:09 - Envelope visualizado por warley.borges@ufes.br, IP 179.102.141.163
12/12/2025 17:07:21 - Assinatura realizada por alvaro.cunha@ufes.br, IP 200.137.65.100
12/12/2025 17:05:23 - Envelope registrado na Blockchain por marcos.a.ribeiro@ufes.br, IP 200.137.65.107
12/12/2025 17:05:22 - Envelope encaminhado para assinaturas por marcos.a.ribeiro@ufes.br, IP 200.137.65.107
12/12/2025 17:04:21 - Envelope criado por marcos.a.ribeiro@ufes.br, IP 200.137.65.107

I dedicate this thesis to my parents, Laura and Alberto, and to my brother, Pablo, for their unwavering support, their encouragement, and for inspiring me to always strive to be a better version of myself.

ACKNOWLEDGMENTS

To my father, Alberto Rocha, and my mother, Laura Figueroa, for being the greatest role models I could ever ask for, and for their constant love, encouragement, and unwavering belief in me throughout this journey. To my brother, Pablo Rocha, for inspiring me to grow and for the invaluable gift of our shared friendship and complicity. And to my family as a whole, thank you for surrounding me with affection and strength.

To my advisor, Professor Warley de Souza Borges, for all the guidance and support since my arrival in Brazil, for providing the tools that shaped me into a better professional, and for always believing in my potential.

To my co-advisor, Professor Eufranio da Silva Junior, for welcoming me into his remarkable research group and for enriching my academic path with meaningful opportunities.

To all my colleagues from the laboratory — Amanda Eiriz, Ana Alves, Ana Luísa, Breno Urcine, Dandara Borges, Eduardo Guimarães, Emilay Baessa, Esther Regina, Gabriel, Luisa, Ícaro Antônio, Jennifer Pardo, José Manuel, Joyce Cristina, Luana Machado, Renata Gomes, Renato Carvalho, William Cezar, and many others who were part of the lab — thank you for the companionship, collaboration, and support that made this path lighter, happier, and far more rewarding.

To Jennifer and Juliana, for starting this academic adventure by my side and for becoming lifelong friends.

To my circle of friends and support network — both Brunas, Bárbara, Jairo, Fernanda, Mariana, David, Eduardo, Esther, and Jesús — thank you for lifting me up during difficult moments and for becoming my family away from home throughout these years.

To Castelões, for your support and companionship during this final stretch. Without you, this process would not have reached such a beautiful ending.

I would also like to acknowledge the dear friends and colleagues I met during my stay in Germany — Heinrich, Jonas, Malini, Pedram, Daniil, Ishika, Julia, Noushine, Anselm, Arthur, Veronica, Anjuli, and Richard — who made that experience unforgettable. I am especially grateful to Jasper Mindner and Yuriy Kononevich for

their kindness, for giving me the opportunity to learn from the best, and for teaching me with patience and generosity. Our friendship will always stay with me.

To Dr. Daniel Werz, for warmly welcoming me into his laboratory in Freiburg and for his valuable contribution to my work.

To Professors Javier Ellena, Valdemar Lacerda Junior, Letícia V. Costa-Lotufo, Rubem F. S. Menna-Barreto, and John F. Bower, for the important roles they played in the development of these projects.

To the staff of the Chemistry Department, especially those in the Graduate Program, for their continuous assistance and support.

To the NMR Laboratory, the Petroleomics Laboratory, the Instrumentation Laboratory, and the entire LabPetro group for their essential analytical contributions.

To the committee members who kindly accepted the invitation to evaluate and contribute to this work.

Finally, I express my gratitude to the Coordenação de Aperfeiçoamento de Pessoal de Nível Superior – Brasil (CAPES), as well as to CNPq, CAPES, and FAPES, whose financial support made this research possible.

FIGURES LIST

SCHEMES LIST

TABLES LIST

ABBREVIATIONS

CCDC	Cambridge Crystallographic Data Centre
CD	Chagas disease
DCM	dichloromethane
DG	directing group
DMF	N,N-dimethylformamide
DMSO	dimethyl sulfoxide
EDGs	electron donating groups
ESI-MS	electrospray ionization mass spectrometry
equiv.	equivalent(s)
HMBC	heteronuclear multiple bond correlation
HRMS	high resolution mass spectrometry
IC_{50}	inhibitory concentration of 50% of the parasitary population
IUPAC	International Union of Pure and Applied Chemistry
IR	infrared spectroscopy
J	coupling constant
MeCN	acetonitrile
MeOH	methanol
MS	mass spectrometry
NMR	nuclear magnetic resonance
ROS	reactive oxygen species
R.T.	room temperature
TLC	thin layer chromatography
THF	tetrahydrofuran
UV	ultraviolet

ABSTRACT

This work presents three projects related to the organic synthesis of natural product derivatives and bioluminescent moieties with different applications. The first project focused on Paeonol-related compounds and their biological potential through the synthesis of Paeonol-derived ethers and benzofurans *via* bimolecular nucleophilic substitution reactions. A total of four ether derivatives and seven benzofuran derivatives were obtained. The cytotoxic activity of all synthesized compounds was evaluated, and three compounds were active against the HCT116 cell line, showing over 60% growth inhibition. Notably, compound 44e exhibited a strong IC_{50} value of 0.2 μM, supporting its potential as an anticancer agent. The second study explored the regioselective synthesis of functionalized 1,4-naphthoquinones *via* aryne chemistry, through the generation and trapping of naphthoquinonynes. Twelve amine derivatives and six pyridine *N*-oxide derivatives were obtained, providing access to A-ring–functionalized naphthoquinones, including nine new compounds. Their trypanocidal activity was evaluated, and fourteen naphthoquinones showed higher activity than benznidazole, the current drug used for Chagas disease. Two compounds were approximately ten times more potent. These results highlight the value of this approach for the discovery of new trypanocidal agents and demonstrate the efficiency and versatility of the methodology. The third chapter showed the design and synthesis of BODIPY-based fluorescent molecules. A series of krypto-BODIPY and *meso*-phenyl-BODIPY derivatives was synthesized, including eight new compounds such as mono- and di-halogenated scaffolds, acetylated analogues, Sonogashira coupling products, and a symmetric bis-BODIPY alkyne. The results demonstrate that both kryptopyrrole and *meso*-phenyl frameworks tolerate electrophilic substitution, C–H activation, and Pd-catalyzed cross-coupling reactions, enabling efficient diversification of BODIPY fluorophores. Overall, this work demonstrates the development of efficient synthetic strategies for biologically relevant and fluorescent molecular scaffolds, contributing new compounds and methodologies with potential applications in medicinal chemistry and chemical biology.

Key words: Paeonol Derivatives, Cytotoxic Activity, Aryne Chemistry, Trypanocidal 1,4-Naphthoquinones Derivatives, BODIPY Fluorophores.

RESUMO

Este trabalho apresenta três projetos relacionados à síntese orgânica de derivados de produtos naturais e de unidades bioluminescentes com diferentes aplicações. O primeiro projeto teve como foco compostos relacionados ao paeonol e seu potencial biológico, por meio da síntese de éteres e benzofuranos derivados do paeonol *via* reações de substituição nucleofílica bimolecular. Ao todo, foram obtidos quatro derivados éter e sete derivados benzofurânos. A atividade citotóxica de todos os compostos sintetizados foi avaliada, e três deles apresentaram atividade contra a linhagem celular HCT116, com inibição do crescimento superior a 60%. Destaca-se o composto 44e, que exibiu um valor de IC_{50} de 0,2 μM, sustentando seu potencial como agente anticancerígeno. O segundo estudo explorou a síntese regioseletiva de 1,4-naftoquinonas funcionalizadas por meio da química de arinos, através da geração e captura de naftoquinoninas. Foram obtidos doze derivados de aminas e seis derivados de *N*-óxido de piridina, permitindo o acesso a naftoquinonas funcionalizadas no anel A, incluindo nove novos compostos. A atividade tripanocida desses compostos foi avaliada, e quatorze naftoquinonas apresentaram atividade superior à do benznidazol, fármaco atualmente utilizado no tratamento da doença de Chagas. Dois compostos mostraram-se aproximadamente dez vezes mais potentes. Esses resultados destacam o valor dessa abordagem para a descoberta de novos agentes tripanocidas e demonstram a eficiência e versatilidade da metodologia. O terceiro capítulo apresentou o planejamento e a síntese de moléculas fluorescentes baseadas em BODIPY. Uma série de derivados krypto-BODIPY e *meso*-fenil-BODIPY foi sintetizada, incluindo oito novos compostos, como estruturas mono- e di-haletadas, análogos acetilados, produtos de acoplamento de Sonogashira e um alquino bis-BODIPY simétrico. Os resultados demonstram que tanto os sistemas de krypto-pirrol quanto os de *meso*-fenil toleram reações de substituição eletrofílica, ativação C–H e acoplamentos cruzados catalisados por paládio, permitindo a diversificação eficiente de fluoróforos BODIPY. De modo geral, este trabalho demonstra o desenvolvimento de estratégias sintéticas eficientes para a obtenção de estruturas moleculares biologicamente relevantes e fluorescentes, contribuindo com novos compostos e metodologias com potencial aplicação em química medicinal e biologia química.

Palavras-chave: Derivados de Paeonol, Atividade Citotóxica, Química de Arinos, Derivados Tripanocidas de 1,4-Naftoquinona, Fluoróforos BODIPY.

CONTENTS

CHAPTER 1

Paeonol-derived benzofurans and ethers with cytotoxic activity

1.1 INTRODUCTION

1.1.1 Paeonol:

Paeonol (**1**), also known as 2-hydroxy-4-methoxyacetophenone (HARADA & YAMASHITA, 1969), is the main active compound found in the root bark of peonies, including *Paeonia suffruticosa*, *Paeonia moutan*, *Paeonia lactiflora* Pall., among others (LIU, Yanze *et al*., 2015). These species belong to the Paeoniaceae family and are among the most widely used herbs in traditional Chinese medicine for over 1,000 years (ADKI & KULKARNI, 2021).

PAE is not only found in the Paeoniaceae family but also in other natural species, such as *Dioscorea japonica* and *Arisaema erubescens* (TSAI, Chia-Ying *et al*., 2016). This compound is a bioactive monoterpene glycoside (**Figure 1**) that exhibits a wide range of significant biological activities and possesses extensive pharmacological properties (TIAN, Mingfa *et al*., 2024).

Figure 1. Structure of 2-hydroxy-4-methoxyacetophenone (paeonol) isolated from *Paeonia suffruticosa*.

Paeonia suffruticosa

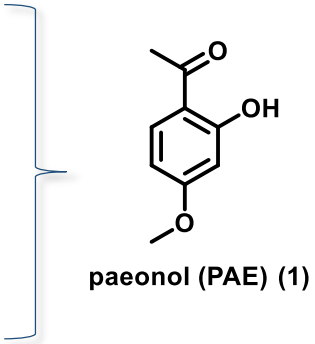

paeonol (PAE) (1)

Regarding its pharmacological profile, PAE has been approved by the CFDA (China Food and Drug Administration) for its anti-inflammatory properties in various pharmaceutical formulations, such as tablets, ointments, patches, and injections (HU, Yang Sheng *et al*., 2020). It is clinically used to manage inflammation, pain, fever, headaches, neuralgia, muscle pain, rheumatoid arthritis, and several dermatological conditions, and has also shown efficacy in allergic rhinitis and cold prevention. Nonetheless, other potential pharmacological effects of PAE have not yet achieved broad clinical application (ZHANG; LI & LIU, 2019).

PAE has been extensively studied for a range of pharmacological effects, including its analgesic properties (CHOU, Tz-Chong, 2003), anti-diabetic effects (LAU,

C.H. *et al*., 2007), anti-cancer activity (YIN, Juan *et al*., 2013), anti-atherogenic effects (ZHAO, Jin-Feng *et al*., 2013), anti-allergic activity (LEE, Bomi *et al*., 2008), and its use in the treatment and prevention of thromboembolic diseases. It is also known for its antioxidant properties (CHEN, NING & YANG, 2012).

Figure 2 below provides a summary of the various pharmacological effects of paeonol:

Figure 2. Summary of the pharmacological effects of paeonol.

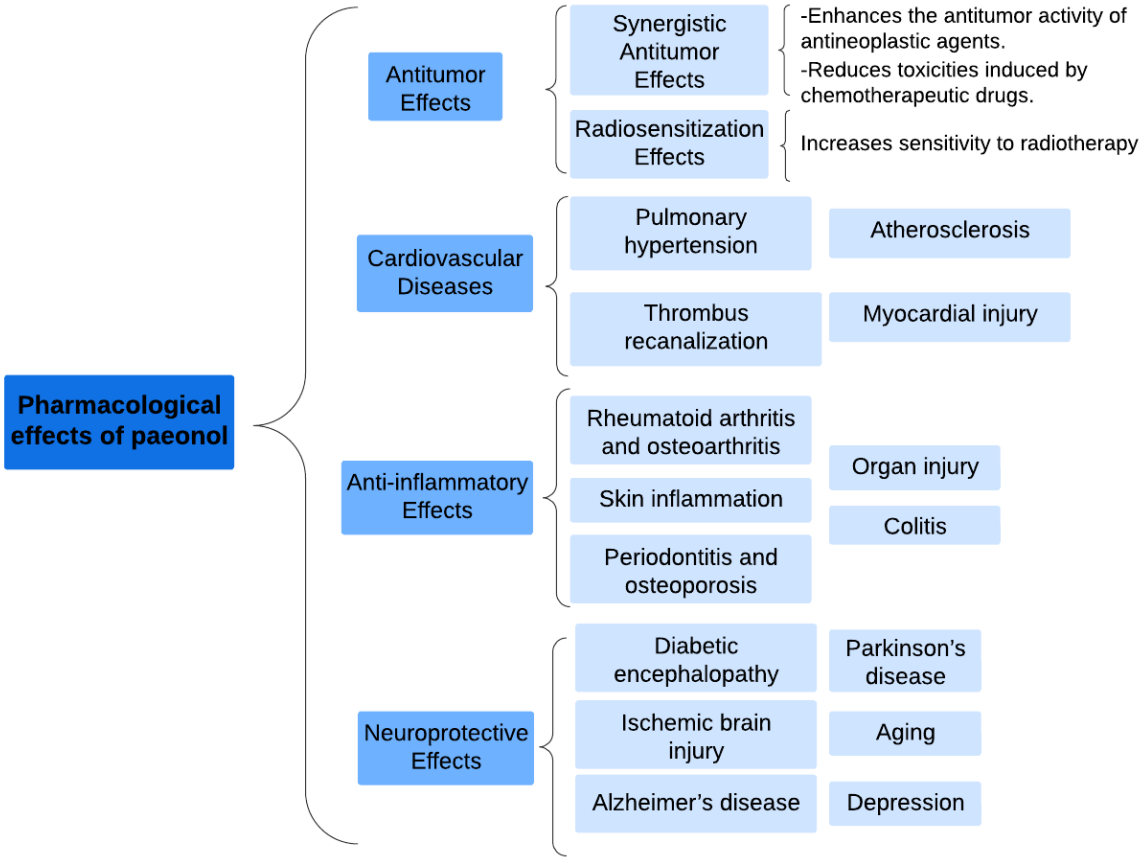

PAE can be obtained either from natural sources or through synthetic methods. It is obtained from natural sources using techniques such as ultrasonic extraction, solid-phase extraction, and Soxhlet extraction, reaching purity levels above 95% after purification (YAN, Binjun *et al*., 2018; Li, Qian *et al*., 2021). Among the synthetic approaches, the two most widely employed are its production from resorcinol (**2**) *via* acetylation (**3**) and methylation (**1**) with dimethyl sulfate (KUMAR, Sarvesh *et al*., 2012), and from *m*-methoxyphenol (**4**) through Friedel–Crafts acylation (**1**) (ROMAGNA, Rodrigo de Almeida *et al*., 2024) (**Scheme 1**).

Scheme 1. Representative Synthetic Routes to PAE.

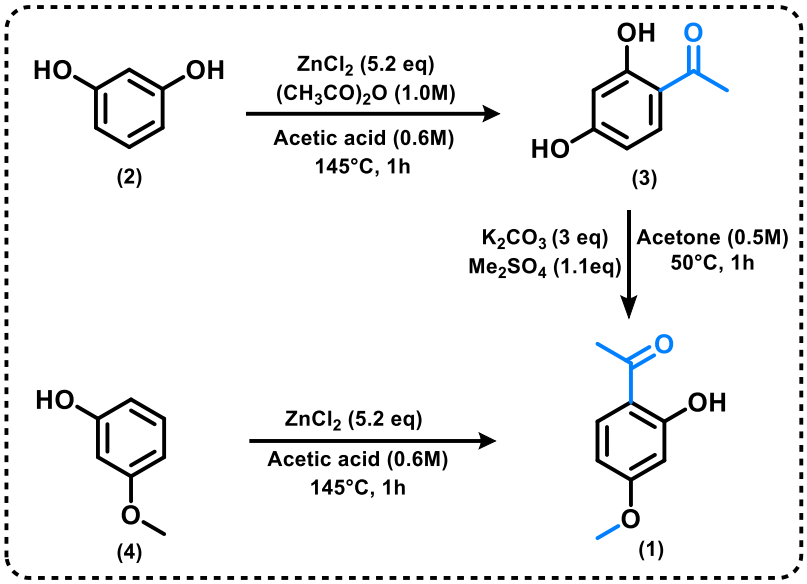

Since PAE has the potential to be developed as a commercial product due to its multi-faceted pharmacological properties, it is currently available on the market and is primarily manufactured by Sigma-Aldrich and TCI Chemicals, CAS number 552-41-0. It is sold as a crystalline powder at a price of approximately R$ 1,278.00 for 20 g (Sigma-Aldrich Brasil site, consulted on 05-11-2025). Therefore, based on all the above-mentioned considerations, PAE has been selected for the synthesis of new derivatives.

1.1.2 Synthesis of paeonol derivatives:

Despite its promising biological activities, the therapeutic application of PAE is limited by its low water solubility, poor stability, and restricted bioavailability, underscoring the need to develop more effective derivatives (CHEN, Z.X. *et al*., 2017; ZONG, Shi-yu *et al*., 2017). Its molecular scaffold has multiple modification sites, and broad-spectrum biological activities highlight its strong potential as a drug lead, providing a solid foundation for the discovery of new molecules (YIN, Wanying *et al*., 2024; CHE, Zhiping *et al*., 2022).

Most studies on PAE derivatives have focused on modifications of the ketone carbonyl side chain and the hydroxyl group at positions C-1 and C-2 respectively (**Figure 3**) (ZHOU, An *et al*., 2015; HU, Yang Sheng *et al*., 2020). In contrast, modifications at the 3- and 5-position of PAE and their associated biological activities

remain poorly explored (ZHANG, Famin *et al*., 2025). In this section, some of the most relevant derivatives structures are presented.

Figure 3. PAE positions and examples of most studies modifications.

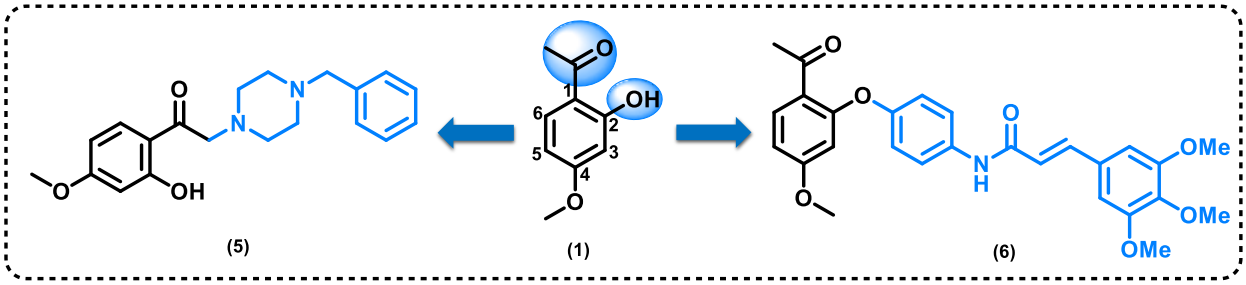

The research group led by Qin and collaborators (QUIN, Dong-Dong *et al*., 2010) reported the synthesis of water-soluble Schiff base complexes derived from PAE with Cu(II) and Ni(II) (**7**), which exhibited both DNA-binding activity and high antioxidant potential (QUIN, Dong-Dong *et al*., 2009). One year later, another type of Schiff base complex of PAE with Cu(II) (**8**-**11**) was synthesized, showing potential antioxidant activity, moderate DNA-binding capacity, and significant cytotoxicity against human Hep-2 (laryngeal) carcinoma cell lines (**Figure 4**).

Figure 4. Schiff base complex derivatives of PAE with Cu (II), Ni (II).

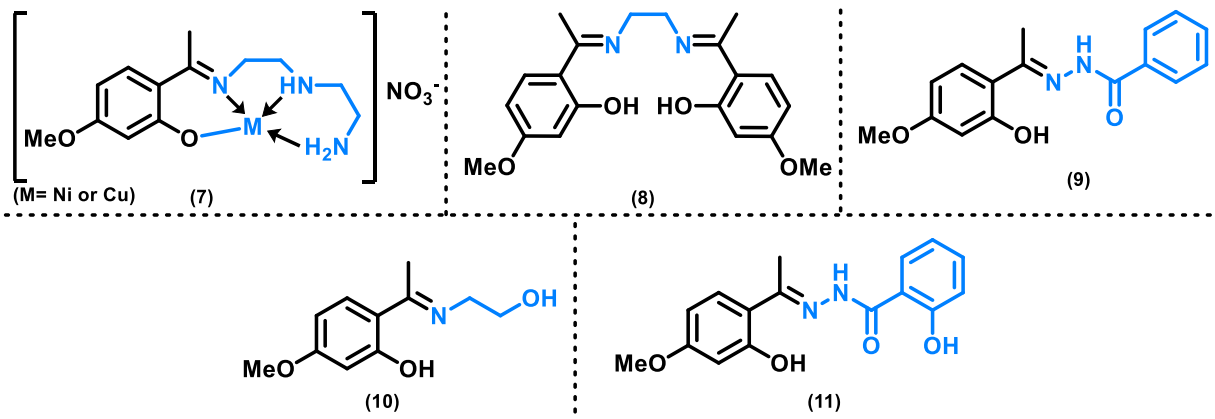

Moreover, Schiff bases derived from PAE containing a 1,2,3-triazole moiety, such as **12,** were synthesized using a one-pot, three-component method with propargylamine and various phenyl azides (JIANG, Yuqin *et al*., 2020). The optimized reaction conditions are summarized in **Scheme 2**. The resulting derivatives exhibited higher activity against human lung cancer A549 cell lines *in vitro*, as evaluated by the MTT assay, compared to PAE.

Scheme 2. Synthesis of Schiff bases derivatives from PAE with a 1,2,3-triazole moiety.

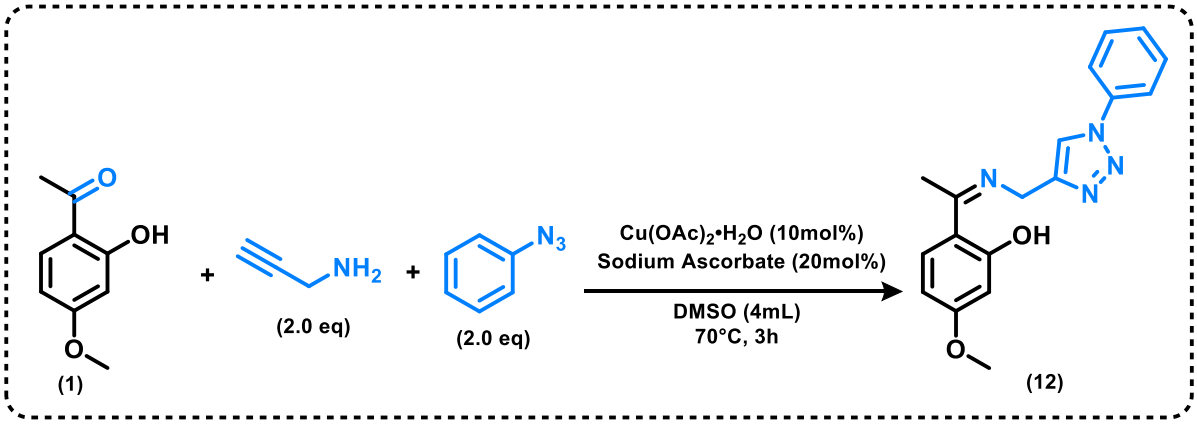

In another study, Fu and colleagues synthesized aminothiazole–paeonol derivatives (APDs) by incorporating 2-aminothiazole units into PAE (**Scheme 3, 14** and **15**), with the aim of treating acute lung injury (ALI) and acute respiratory distress syndrome (ARDS) (FU, Pin-Kuei *et al*., 2017). This approach was based on the recognition that the 2-aminothiazole scaffold is a well-established pharmacophore with applications in various therapeutic areas (WANG, Jilei *et al*., 2019).

Scheme 3. Synthesis of aminothiazole-paeonol derivatives (APDs) with pharmacological activity.

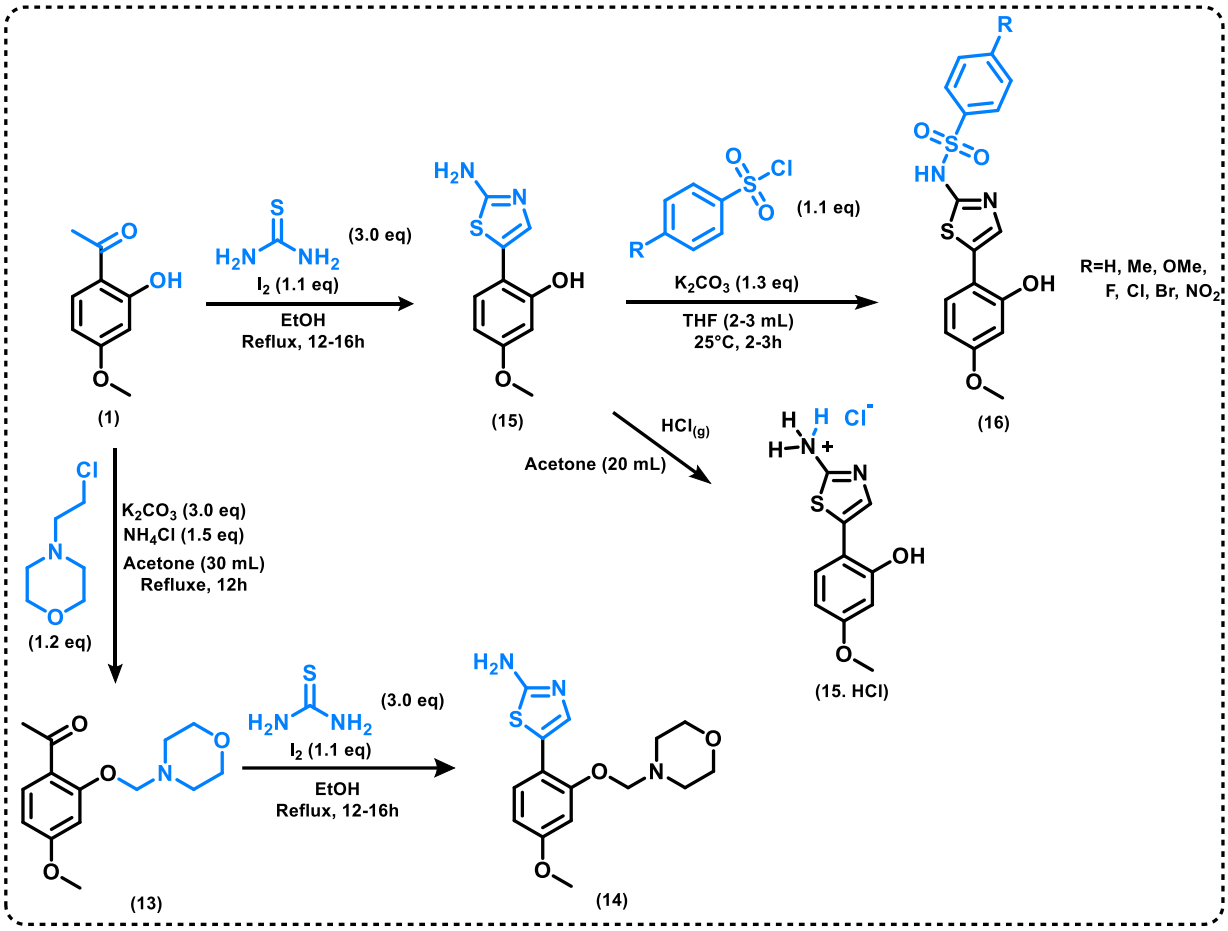

Additionally, PAE derivatives incorporating 1,4-benzoxazinone and 1,2,3-triazole moieties with potential anticancer activity were synthesized through a five-step route (**Scheme 4**). In this project, PAE was first nitrated at the C-3 position (**17**) and subsequently reduced to obtain the corresponding amine (**18**), which was then subjected to amidation and cyclization to yield the 1,4-benzoxazinone intermediate (**19**). Further *N*-alkylation afforded the precursor (**20**) for the final step, where a series

of derivatives (**21**) were generated by 1,3-dipolar Huisgen cycloaddition with different phenyl azides (YANG, Tingting *et al*., 2019).

Scheme 4. Synthesis of PAE derivatives linked to 1,4-benzoxazinone and 1,2,3-triazole molecules.

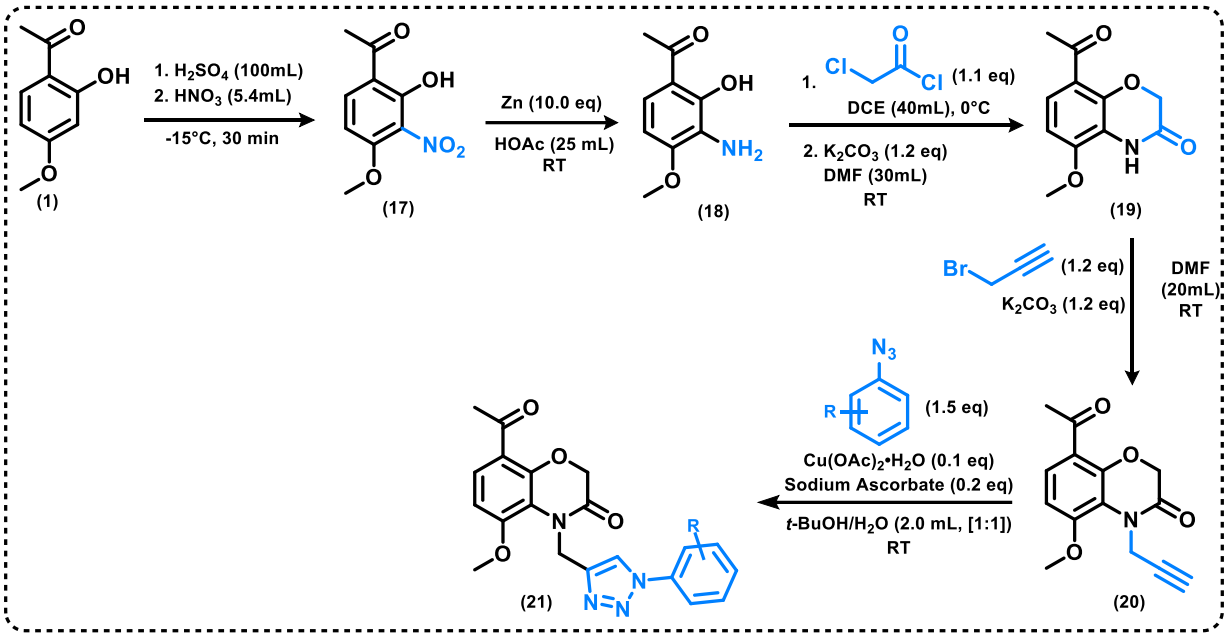

Another click reaction was carried out by Son and collaborators using a microwave reactor. In this procedure, tryptamine azide and propargylated PAE (**22**) were reacted in acetone in the presence of $Cu(PPh_3)_3Br$ at 65 °C for 30 minutes, yielding a hybrid tryptamine–triazole compound (**23**) with butyrylcholinesterase inhibitory activity (SON, Minky *et al*., 2019) (**Scheme 5**).

Scheme 5. Synthesis of paeonol-derived tryptamine-triazole hybrid.

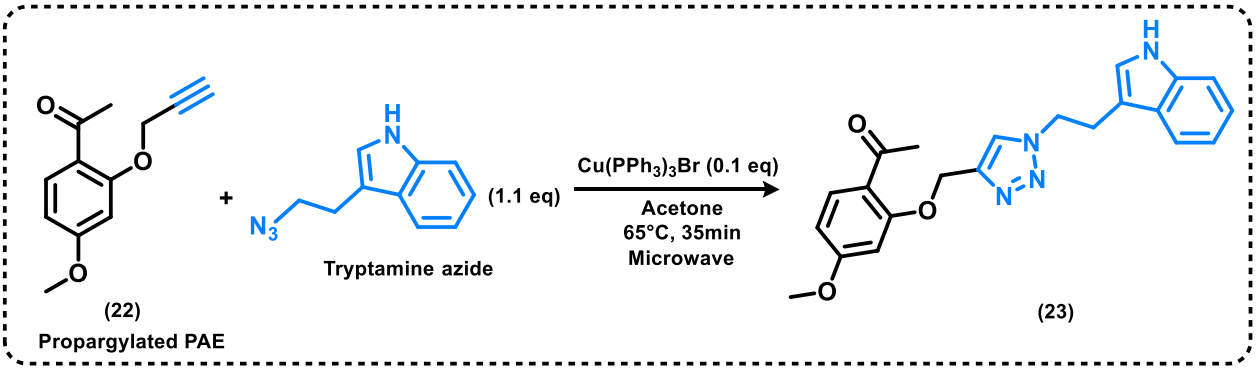

Additional 1,2,3-triazole derivatives of PAE (**24**) were synthesized, along with ether-type derivatives (**25**) obtained through nucleophilic substitution of the hydroxyl group at position C-2 (**Scheme 6**). The antibacterial activity of all compounds was thoroughly evaluated using a microdilution assay against standard Gram-positive (*S.*

aureus) and Gram-negative (*E. coli*) bacterial strains (FIGUEROA, Laura Patricia *et al*., 2023). This study represents the first effort by our group to investigate PAE derivatives with potential biological activity.

Scheme 6. Synthesis of 1,2,3-triazole and ether PAE derivatives at position 2.

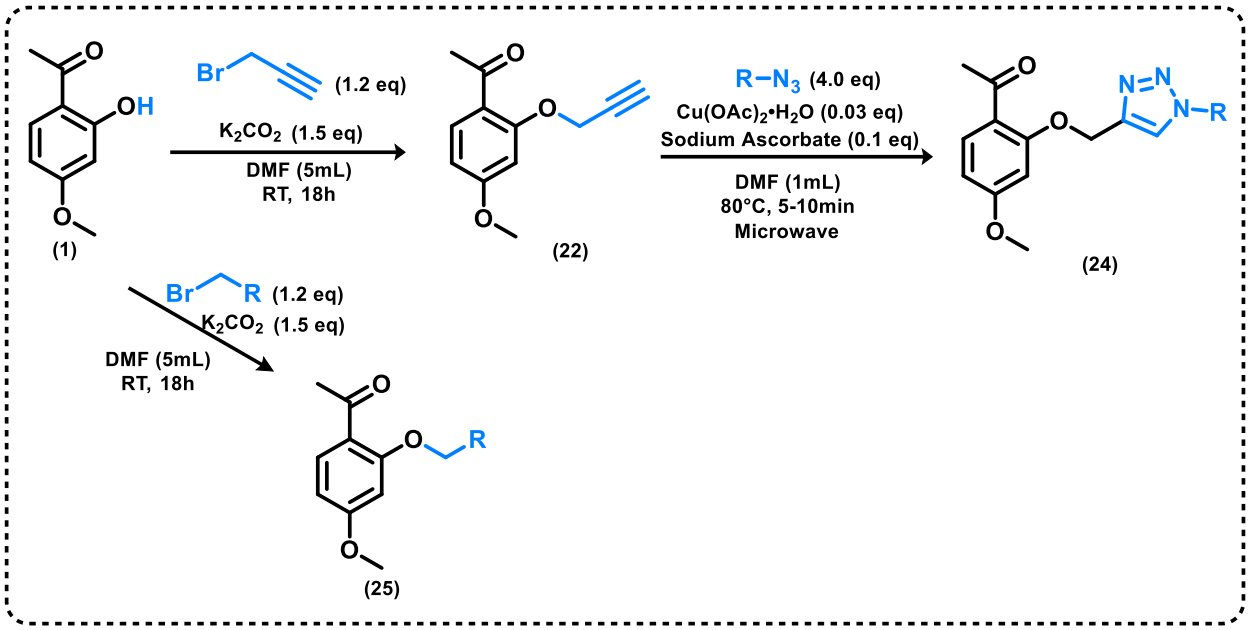

Similarly, further research has been conducted on PAE ether derivatives. In this study, a series of alkyl ether analogs of PAE (26) were synthesized and characterized to evaluate their anti-inflammatory activity (HUANG, Ligua *et al*., 2016). These analogs were obtained through etherification with alkyl halides in the presence of acetone and potassium carbonate. Additionally, brominated alkyl ether derivatives were prepared by direct bromination of PAE at position C-5 (**27**), followed by etherification (**28**) under similar conditions (**Scheme 7**) (ADKI & KULKARNI, 2020).

Scheme 7. Synthesis of PAE alkyl ether derivatives.

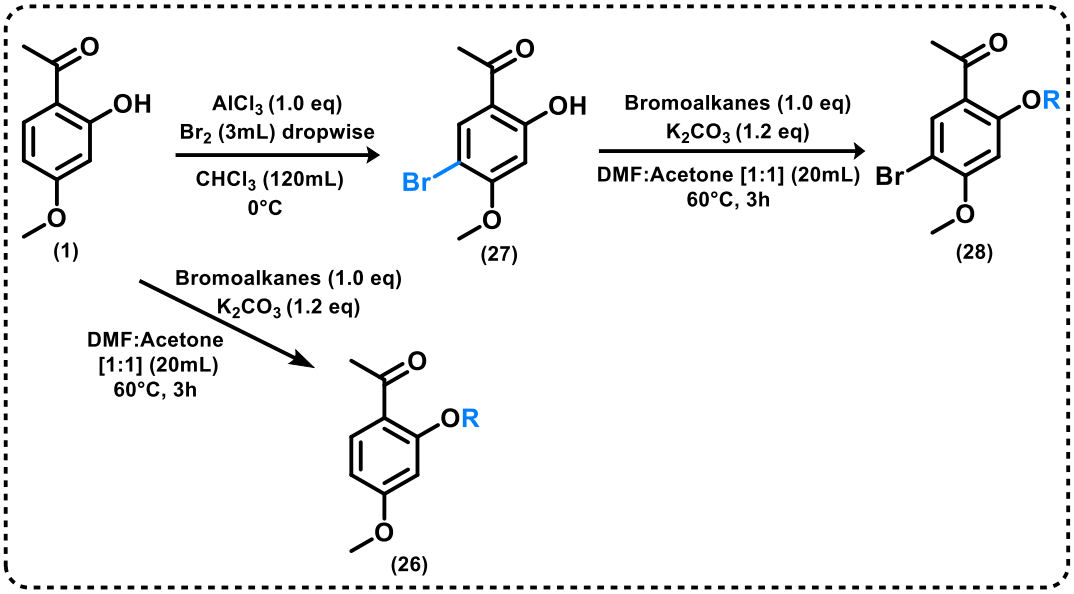

Conversely, studies by YU and collaborators on other oxygenated derivatives of PAE reported the synthesis of acetylferulic paeonol ester (APE, **29**) and ferulic paeonol ester (FPE, **30**). The synthetic pathway for these PAE ester derivatives is illustrated in **Scheme 8**. Furthermore, their antioxidant activity was thoroughly evaluated (YU, Lijuan *et al*. 2021).

Scheme 8. Synthetic route of PAE ester derivatives: APE and FPE.

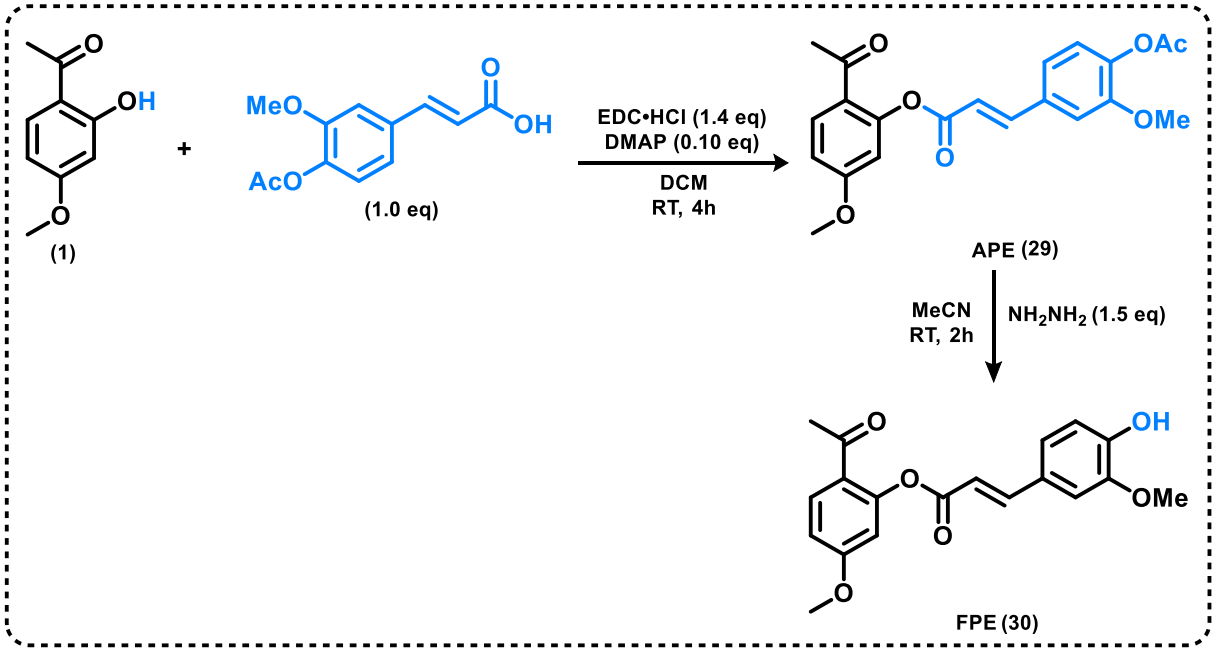

PAE derivatives have been shown to exhibit a wide range of biological activities. ADKI and KULKARNI, 2020, conducted a comprehensive review of these compounds, identifying heterocyclic compounds, triazole derivatives, nitrogen-containing derivatives, sulfonated derivatives, among others, and, to a lesser extent, oxygenated derivatives. This highlights the importance of developing PAE-derived oxygenated compounds as part of ongoing research into natural products with potential biological activities.

1.1.3 Oxygenated heterocyclic compounds: Benzofurans and ethers

The majority of medications and drugs sold on the market (60%) belong to the class of heterocyclic compounds or contain at least one heterocyclic core in their structure (McGRATH, BRICHACEK & NJARDARSON, 2010). Heterocyclic compounds play a vital role in human cellular metabolism, as they are often found in significant proportions in biomolecules such as enzymes, vitamins, and natural products (DWARAKANATH & GAONKAR, 2022; AL-MULLA, Abbas 2017).

Heterocyclic compounds represent a diverse class of molecules characterized by their cyclic structure and the presence of heteroatoms (i.e. O, N, S or Se) within their framework (GUPTA, KUMAR & GUPTA, 1985). The significance of heterocycles is well-established both biologically and medicinally, as they are widely found in vitamins, pharmaceuticals, biomolecules, natural products, and other biologically active compounds. These include antibiotics, antitumor agents, anti-inflammatory drugs, antimalarials, antidepressants, anti-HIV agents, antibacterials, antivirals, antidiabetics, antifungals, herbicides, fungicides, and insecticides (PATHAN, Sultan Ismail *et al*., 2020).

Natural products containing oxygenated heterocyclic compounds are considered highly attractive due to their biological activity. This has driven the development of synthetic strategies and methodologies for their production. Among these, benzofurans have emerged as one of the most extensively studied heterocycles due to their notable biological profile (SHAMSUZZAMAN, Hena Khanam 2015).

Structurally, benzofuran compound is characterized by the fusion of a benzene ring with a furan ring, a five-membered heterocyclic ring. This class of heterocyclic compounds comprises two isomeric heterocycles: 1-benzofuran (**31**) (commonly

referred to as benzofuran) and 2-benzofuran (**32**) (also known as isobenzofuran) (**Figure 5**) (FARHAT, Joviana *et al*., 2022).

Figure 5. Chemical structure of benzofurans.

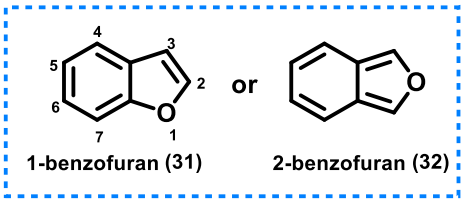

Studies have shown that benzofuran and its derivatives are widely distributed among both natural and synthetic compounds. Natural products containing these moieties are predominantly isolated from plant species belonging to the families Rutaceae, Asteraceae, Cyperaceae, Fabaceae and Liliaceae. (MIAO, Yu Hang *et al*., 2019). Examples of benzofurans extracted from plants with biological activity are shown in **Figure 6**.

Figure 6. Benzofurans extracted from plants with biological activities.

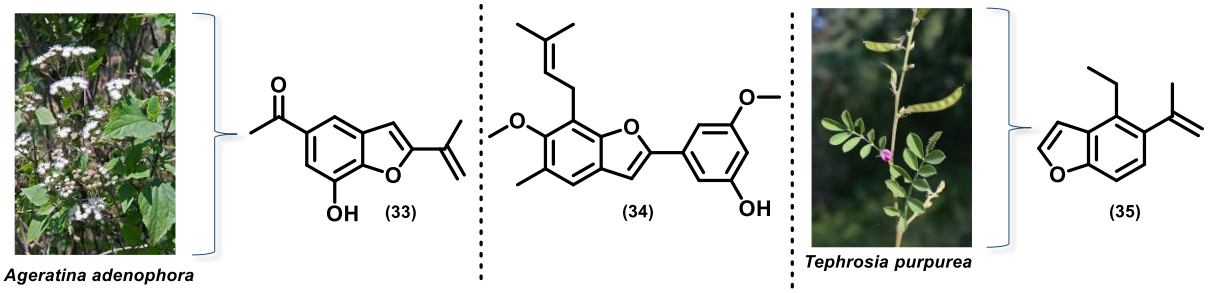

Benzofuran **33** was isolated from *Ageratina adenophora* (Asteraceae) and exhibits antifungal activity against four different pathogenic fungal species (ZHENG, Guowei *et al*., 2018). Compound **34**, isolated from the stem bark of *Calpocalyx dinklagei* (Fabaceae), shows excellent anti-inflammatory activity (KAPCHE, Deccaux W.F.G *et al*., 2017) and benzofuran (**35**), obtained from *Tephrosia purpurea* (Fabaceae), displays notable anti-allergic activity (SHILL, Manik Chandra *et al*., 2015).

These oxygenated heterocycles are also present in various polymers and pharmaceuticals (NEVAGI; DIGHE & DIGHE, 2015). Moreover, a wide range of synthetic analogs feautiring the benzofuran scaffold have been reported, and several clinically used drugs incorporating this structural motif are available for the treatment of various pathological conditions, as illustrated in **Figure 7** (WANG, Bingqiao *et al*., 2019; LUMB & TRAUNER, 2005).

Figure 7. Drugs on the market containing the benzofuran scaffold.

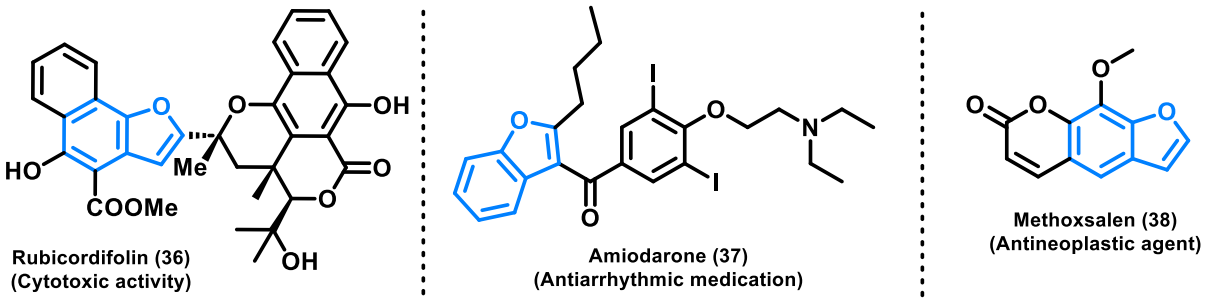

As shown in **Scheme 9**, benzofurans were first synthesized by W. H. PERKIN in 1890 from coumarins (**39**). Since then, a wide range of synthetic routes has been investigated (MORE, Kishor R., 2017). A novel metal-free cyclization of *o*-hydroxystilbenes (**40**) using hypervalent iodine reagents was later developed, yielding 2-arylbenzofurans (SINGH & WIRTH, 2012). Another efficient one-pot method involves the palladium-catalyzed cyclization of 2-chloroaryl alkynes (**41**) to produce substituted benzofurans (ANDERSON, Kevin W. *et al*., 2006). Additionally, a one-pot sequence combining Sonogashira coupling of dichlorophenols (**42**) with terminal alkynes, followed by intramolecular cyclization and a Suzuki–Miyaura coupling, affords disubstituted benzo[*b*]furans using a palladium–dihydroxyterphenylphosphine catalyst (YAMAGUCHI, Miyuki *et al*., 2016).

Scheme 9. Different approaches to the synthesis of benzofurans.

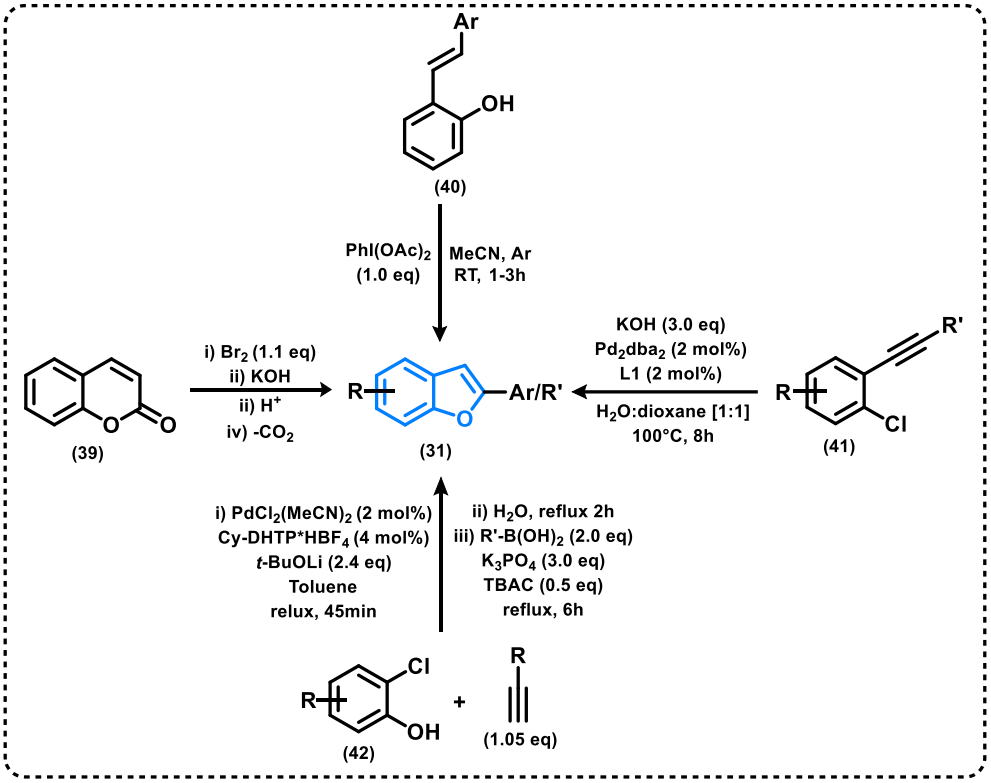

Among oxygenated compounds, ether moieties are noteworthy for their structural simplicity combined with a wide occurrence in complex molecular architectures (HU, Die *et al*., 2023; DEMMAK, Rym Gouta *et al*., 2021). They are commonly found in nature, often as integral components of natural products or larger molecular frameworks (ZHU, Junjie *et al*., 2021).

Ethers are generally more chemically stable and less reactive than benzofurans. Nevertheless, they deserve particular attention, as ether-containing oxygenated compounds have demonstrated a remarkable diversity of biological activities (LIU, Wentao *et al*., 2021). The continued study of their synthesis and biological properties is therefore important for the discovery and development of new therapeutic agents (CHEN, Xiaofang *et al*., 2017; KRAUS, George A. *et al*., 2008; WEI, Meng-Xue *et al*., 2021).

1.2 RESEARCH PURPOSE

The main goal of this research is to synthesize oxygenated heterocyclic derivatives of paeonol. The aim is to obtain a diverse set of novel derivatives with

different scaffolds in order to evaluate their biological activity and potential contribution to drug discovery.

This work will employ a methodology that has already been optimized and successfully used in our research group to generate diverse derivatives of natural products. The approach is simple, provides easy access to the target compounds, and allows for straightforward purification.

1.2.1 General Objective:

The general objective of this research is to synthesize oxygenated heterocyclic compounds—specifically ethers and benzofurans derived from paeonol—through alkylation *via* nucleophilic substitution reactions between paeonol and benzyl or phenacyl bromides, and to evaluate their cytotoxic activity.

1.2.2 Specific Objectives:

- Synthesis of novel paeonol-derived ethers and benzofurans bearing diverse substituents, using different phenacyl and phenyl bromides.
- Purification of the synthesized compounds employing the most appropriate purification techniques according to their physicochemical properties.
- Characterization and structural elucidation of all synthesized compounds through spectrometric and spectroscopic methods.
- Evaluation of the cytotoxic activity of the obtained derivatives in collaboration with Letícia V. Costa-Lotufo laboratory at the Department of Pharmacology, Institute of Biomedical Sciences, University of São Paulo.

The general idea of the research proposal is illustrated in **Scheme 10**:

Scheme 10. General Research Purpose.

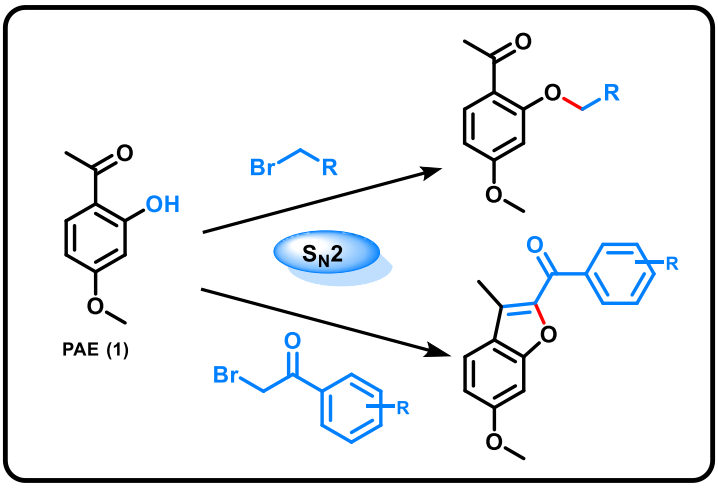

1.3 RESULTS AND DISCUSSION

1.3.1 Synthesis of paeonol Derivatives:

The synthesis of the ether and benzofuran derivatives was carried out using the natural product paeonol (PAE) as the starting material for a bimolecular nucleophilic substitution reaction, a methodological strategy previously employed by our research group (FIGUEROA, Laura Patricia *et al*., 2023). Since this previous work yielded excellent results, we decided to expand the study of ether derivatives by employing additional benzyl bromides and testing phenacyl bromides.

To obtain all derivatives, an excess of potassium carbonate was used as a base to deprotonate the phenolic hydroxyl group of PAE. The resulting phenoxide ion is stabilized by resonance with the aromatic ring, while the negative charge localized on the oxygen atom enhances its nucleophilic character, promoting nucleophilic attack on the electron-deficient carbon atom of the bromide *via* an S_N2 mechanism.

All synthetized derivatives were fully characterized by spectrometric and spectroscopic methods such as uni and two-dimensional ^{1}H, ^{13}C NMR, heteronuclear single quantum coherence (HSQC), heteronuclear multiple bond correlation (HMBC), high resolution electrospray ionization mass spectrometry and Fourier-transform infrared spectroscopy (FTIR). We also determined the crystal structure of one of these ether derivatives (**43a**) and of five benzofuran derivatives (**44a**, **44b**, **44c**, **44f** and **44g**) using single crystal X-ray diffraction analyses. The corresponding spectra and analytical data are provided in the Appendix and detailed in the Experimental Part.

1.3.2 Ether Derivatives:

In order to complete the series of previously synthesized PAE ether derivatives developed by our research group, reactions were carried out with different bromides, affording the four expected products (**43a-d**, **Table 1**) in excellent yields ranging from 80% to 100%. All compounds were purified by column chromatography on silica gel (^{n}Hexane/EtOAc), using solvent systems of varying polarity depending on each case. These derivatives include compounds bearing electron-donating groups (EDGs), electron-withdrawing groups (EWGs), as well as aliphatic substituents.

Table 1. Ether Derivatives synthesized from paeonol.

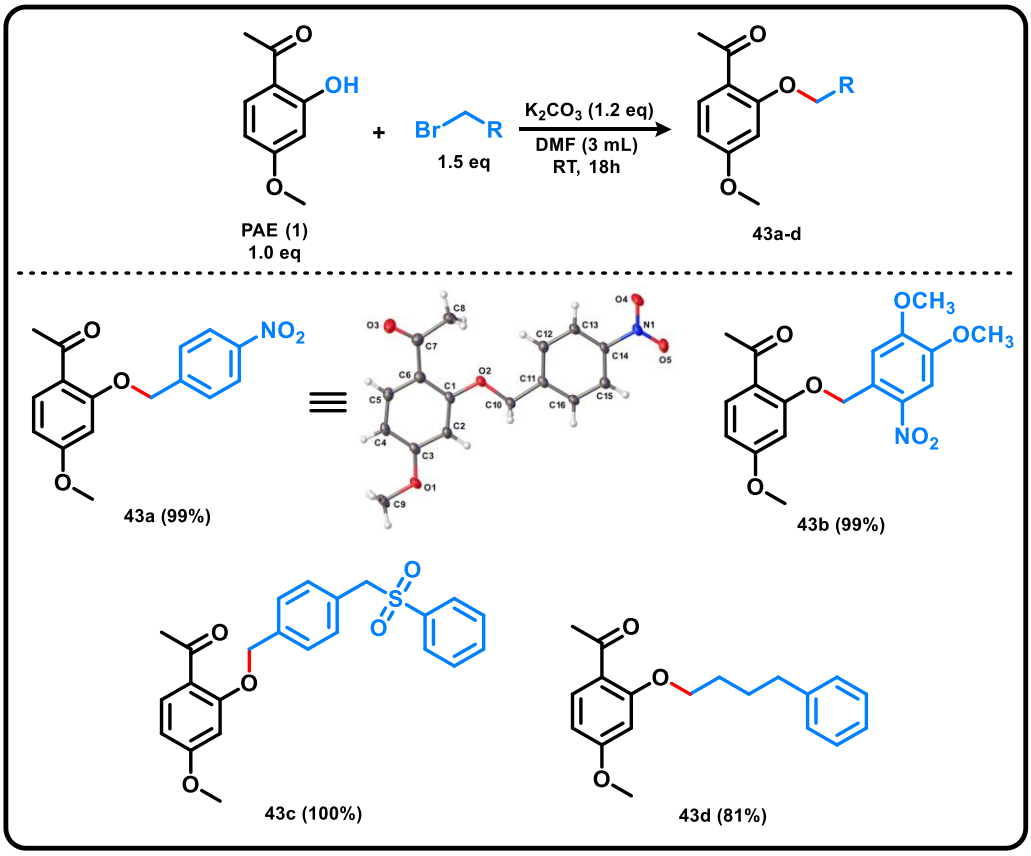

In the case of compound **43a**, the NMR spectrum displayed, in addition to the characteristic signals of the PAE core, a methylene group with proton signals at 5.24 ppm (s, 2H) and a corresponding carbon signal at 69.6 ppm (CH_2). The aromatic region showed signals typical of a 1,4-disubstituted benzene ring at 8.27 (d, *J* = 8.7 Hz, 2H) and 7.64 ppm (d, *J* = 8.7 Hz, 2H). This substitution pattern was further supported by HMBC correlations between these aromatic protons and their corresponding carbons, confirming the presence of a *para*-nitro substituent.

Regarding compound **43b**, the spectrum exhibited, besides the methylene group signals characteristic of the ether derivatives, two aromatic proton signals at 7.78 (s, 1H) and 7.70 ppm (s, 1H), which confirmed the presence of a tetrasubstituted aromatic ring. Additionally, the proton signals at 4.06 (s, 3H) and 3.97 ppm (s, 3H), together with the corresponding carbon signals at 57.9 (CH_3) and 56.5 ppm (CH_3) attributed to the methoxy groups, and the quaternary carbon signal at 139.0 ppm (C_q) assigned to the carbon bearing the nitro group, supported the substitution pattern of the aromatic ring in the molecular structure.

As for compound **43c**, several aromatic proton signals were observed, consistent with the presence of two new aromatic rings, exhibiting mono- and disubstitution patterns, respectively. Moreover, two methylene groups were identified: one linked to the PAE moiety at 5.15 ppm (s, 2H) with a corresponding carbon signal at 68.8 ppm (CH_2), and another connected to the phenylsulfonyl group and the disubstituted aromatic ring at 4.50 ppm (s, 2H) with a corresponding carbon signal at 59.8 ppm (CH_2).

Finally, in the spectrum of compound **43d**, carbon and proton signals corresponding to a four-carbon aliphatic chain were identified, together with aromatic signals consistent with the ring attached to this aliphatic chain in the molecular structure.

To illustrate the characterization process, compound **43a**, bearing a nitro group at the *para* position, was selected as a representative example. In the ^{1}H and ^{13}C NMR spectra, slight downfield shifts were observed, which could be attributed to the electron-withdrawing effect of the nitro group.

In the ^{1}H NMR spectrum (400 MHz, $CDCl_3$) (**Figure 8**), two singlets at 2.57 (s, 3H) and 3.83 ppm (s, 3H) were observed, corresponding to the methyl and methoxy groups of the PAE moiety. In the aromatic region, two doublets at 6.46 and 7.85 ppm, assigned to **H-3** and **H-6** of PAE, and a double doublet at 6.57 ppm completed the characteristic aromatic proton pattern of the PAE core. Additionally, a methylene group appeared at 5.24 ppm (s, 2H), assigned to **H-10**, along with further aromatic doublets at 8.27 and 7.64 ppm (**H-12**, **H-12′**, **H-13**, and **H-13′**), typical of a 1,4-disubstituted benzene ring.

Figure 8. ^{1}H NMR spectrum of compound **43a**.

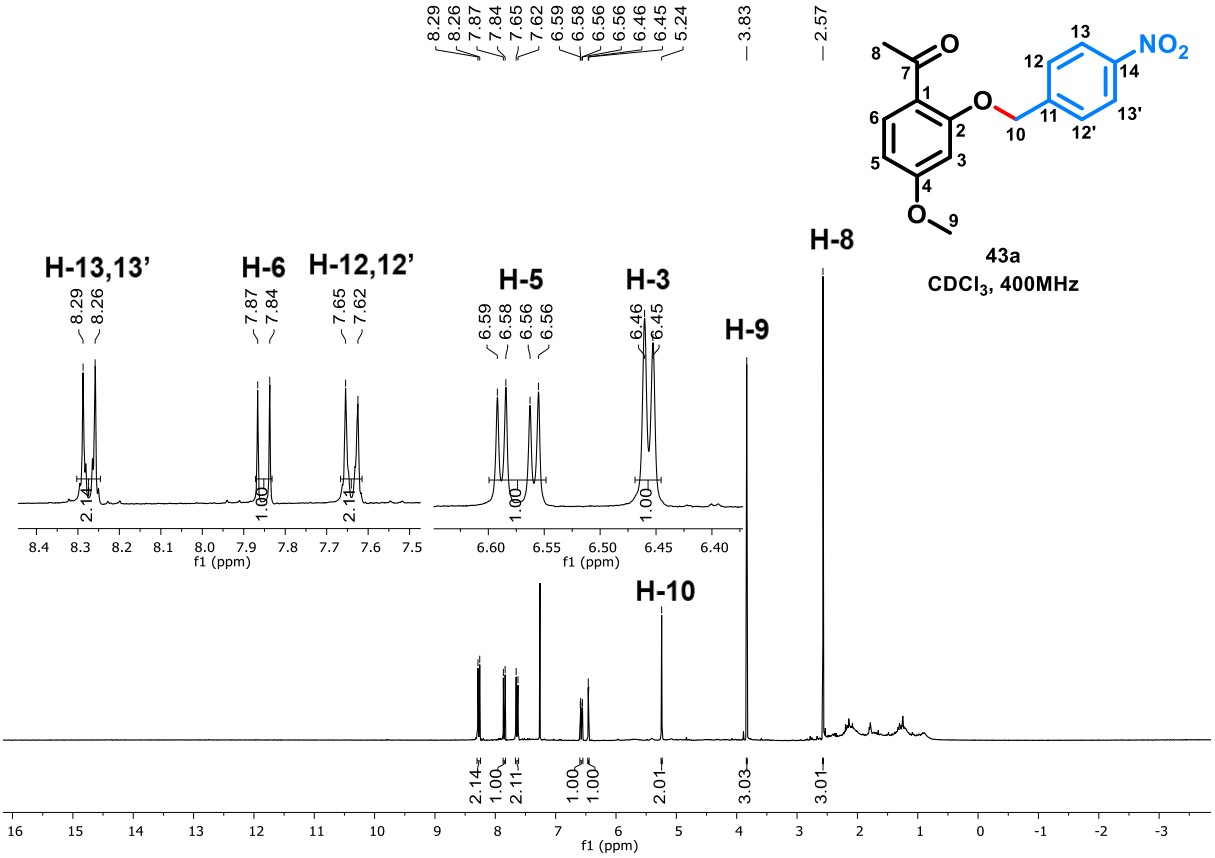

In the ^{13}C NMR spectrum (100 MHz, $CDCl_3$) (**Figure 9**), all characteristic carbon signals of the PAE framework were identified, together with an additional resonance at 69.6 ppm (CH_2), corresponding to the methylene group. Further aromatic carbon signals at 143.5, 128.0, 124.2, and 147.9 ppm were attributed to the carbons of the new aromatic ring in the molecule (**C-11**, **C-12**, **C-12′**, **C-13**, **C-13′**, and **C-14**).

Figure 9. ^{13}C NMR spectrum of compound **43a**.

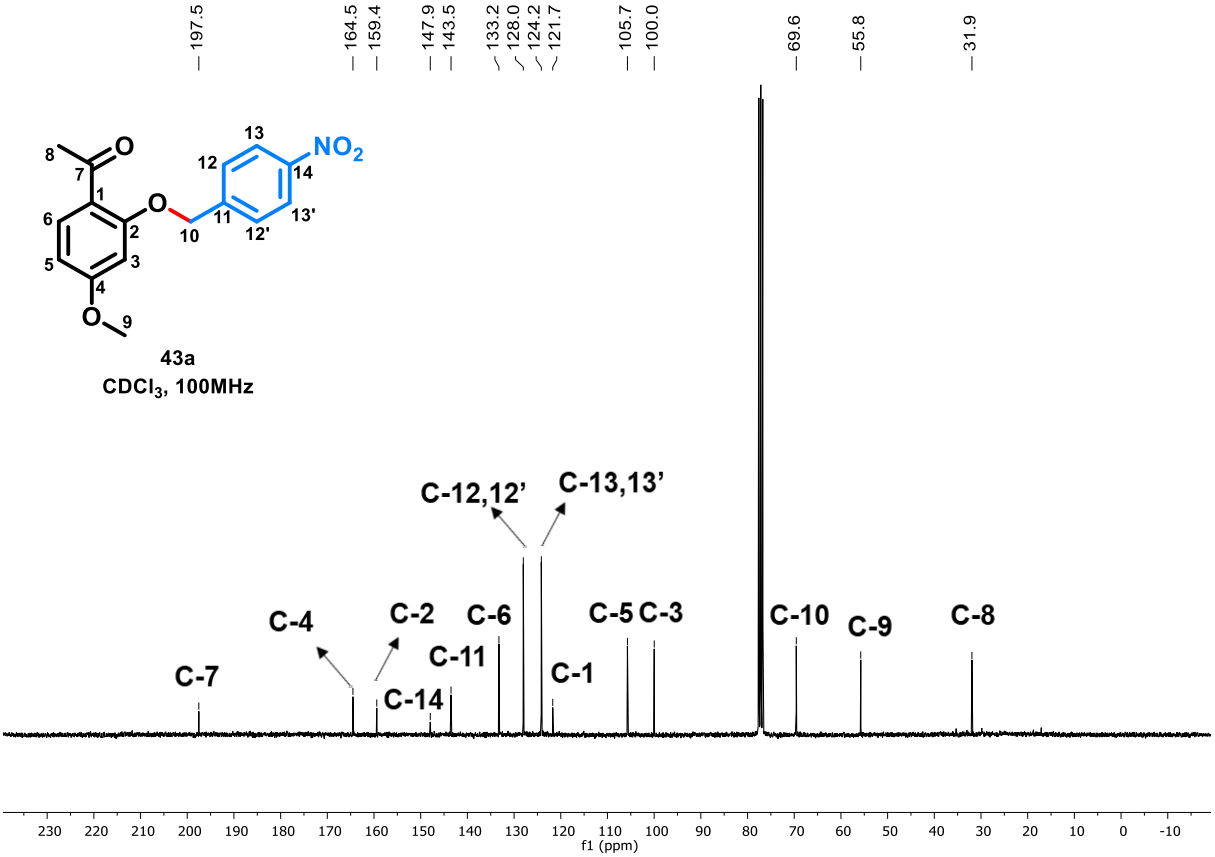

A single crystal suitable for X-ray diffraction analysis was obtained for compound **43a**, enabling the determination of its molecular structure. The results confirmed the proposed structure, and the corresponding ORTEP representation is shown in **Figure 10**.

Figure 10. ORTEP representation of compound **43a**. Color code: grey, carbon; red, oxygen; blue, nitrogen; white, hydrogen atoms.

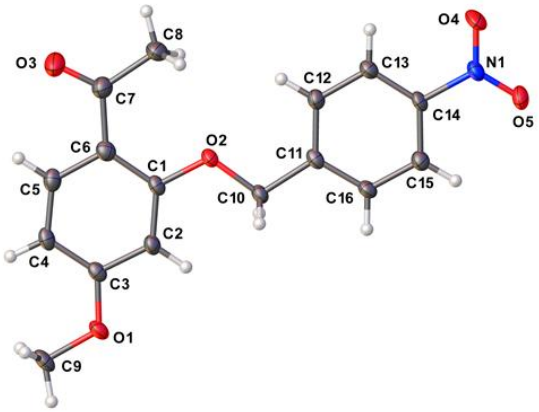

With all compounds fully characterized, the proposed mechanism for the synthesis of the PAE ether derivatives is shown in **Scheme 11**. It corresponds to a

bimolecular nucleophilic substitution (S_N2) reaction, in which potassium carbonate deprotonates the phenolic hydroxyl group, generating the corresponding phenoxide ion. The resulting phenoxide then attacks the electron-deficient carbon atom of the alkyl bromide, leading to the formation of the desired ether product. This proposed mechanism is consistent with the experimental results and aligns well with previously reported reactions of similar systems.

Scheme 11. Proposed S_N2 Reaction Mechanism.

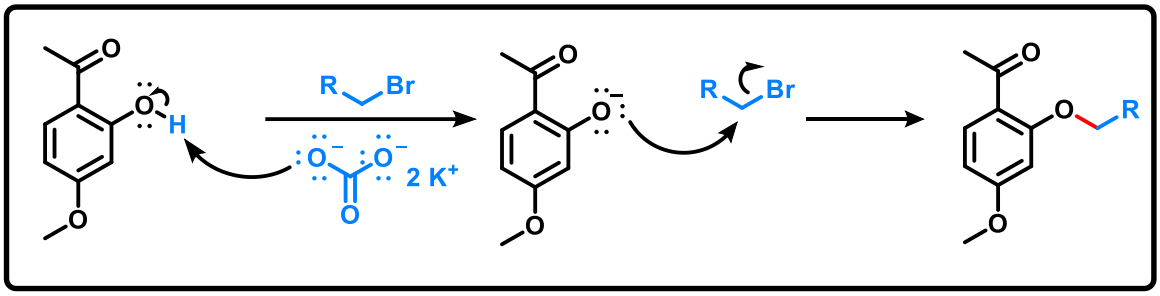

1.3.3 Benzofuran Derivatives:

Since all previously synthesized PAE derivatives obtained through this methodology showed excellent results, we decided to test different bromides. Using phenacyl bromides, we successfully obtained seven benzofuran derivatives (**44a–g**). These derivatives include compounds bearing electron-donating groups (EDGs) and electron-withdrawing groups (EWGs). Derivatives **44a–f** were obtained in good yields ranging from 66% to 92%, while derivative **44g** showed the lowest yield (29%) (**Table 2**). All compounds were purified by column chromatography on silica gel (^{n}Hexane/EtOAc), using solvent systems of varying polarity depending on each case.

Table 2. Benzofuran Derivatives Synthesized from paeonol.

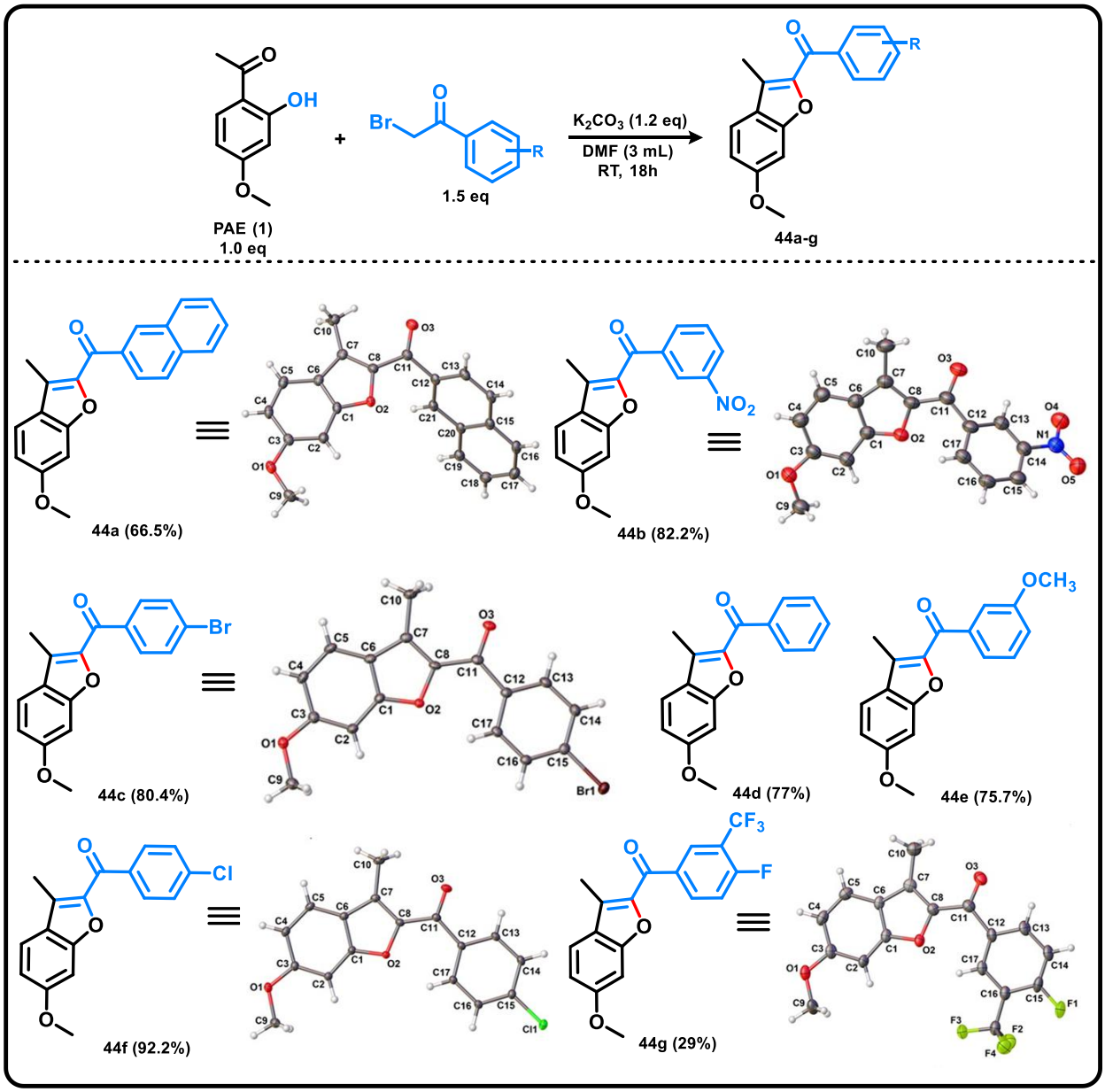

The formation of benzofuran derivatives, rather than ether derivatives, was confirmed through detailed NMR analysis. The main criteria used to verify cyclization involved identifying the absence of methylene group signals (characteristic of ether derivatives) and the presence of the corresponding aromatic carbon and proton signals of the furan ring. None of the synthesized benzofurans exhibited methylene signals; instead, all showed the characteristic resonances of the furan carbons, confirming successful ring closure.

Compound **44a** displayed, in addition to the typical PAE NMR pattern, signals corresponding to seven aromatic protons at 8.64, 8.10, 8.01, 7.91, 7.61, 7.58, and 7.56 ppm, consistent with a naphthalene moiety in the structure. The ^{13}C NMR spectrum also revealed resonances at 156.0 (C_q) and 148.5 ppm (C_q), assigned to the quaternary carbons bonded to the oxygen atoms of the furan ring. HMBC correlations further supported these assignments.

For compound **44b**, aromatic proton signals were observed at 7.72 (t, *J* = 7.8 Hz, 1H), 8.41 (ddd, *J* = 7.8, 1.9, 1.2 Hz, 1H), 8.44 (ddd, *J* = 7.8, 1.9, 1.2 Hz, 1H), and 8.99 ppm (t, *J* = 1.9 Hz, 1H), corresponding to the four aromatic hydrogens of the newly introduced ring. A resonance at 148.1 ppm (C_q) was attributed to the quaternary carbon bearing the nitro group.

The **44c** derivative exhibited aromatic proton signals at 7.96 (d, *J* = 8.4 Hz, 2H) and 7.66 ppm (d, *J* = 8.4 Hz, 2H), characteristic of a 1,4-disubstituted aromatic ring incorporated into the PAE structure. This pattern was corroborated by a quaternary carbon signal at 137.0 ppm (C_q), assigned to the carbon bonded to the bromine atom, as confirmed by HMBC correlations. Additional signals at 155.9 (C_q) and 148.0 ppm (C_q) were consistent with the furan ring carbons, confirming the benzofuran framework.

Derivative **44d** presented aromatic proton resonances at 8.06 (m, 2H), 7.59 (tt, *J* = 1.5, 7.4 Hz, 1H), and 7.52 ppm (m, 2H), together with ^{13}C signals at 138.3 (C_q), 132.4 (CH), 129.7 (CH), and 128.4 ppm (CH), consistent with a monosubstituted aromatic ring attached to the structure.

For compound **44e**, aromatic proton signals appeared at 7.68 (br d, *J* = 7.4 Hz, 1H), 7.58–7.57 (m, 1H), 7.42 (t, *J* = 7.8 Hz, 1H), and 7.14 ppm (brd, *J* = 1.9, 8.2 Hz, 1H), corresponding to the newly introduced aromatic ring. Additional resonances at 3.88 (s, 3H) and 55.6 ppm (CH_3) confirmed the presence of a methoxy substituent in the *meta* position. Signals at 156.0 (C_q) and 148.3 ppm (C_q) were assigned to the furan ring carbons, supporting the formation of the benzofuran core.

Derivative **44f** showed aromatic proton signals at 8.05 (d, *J* = 8.5 Hz, 2H) and 7.49 ppm (d, *J* = 8.5 Hz, 2H), consistent with a *para*-substituted aromatic ring. The crystal structures of compounds **44c** and **44f** further confirmed the 1,4-disubstitution patterns, revealing bromine and chlorine substituents, respectively.

Finally, compound **44g** exhibited aromatic resonances at 7.35 (t, *J* = 9.0 Hz, 1H), 8.36 (m, 1H), and 8.44 ppm (dd, *J* = 1.9, 7.0 Hz, 1H), corresponding to a

trisubstituted aromatic ring. A quaternary carbon signal at 134.3 ppm (C_q) was attributed to the carbon attached to the trifluoromethyl group, confirming its presence in the structure.

As well as in ether derivatives, to illustrate the characterization process compound **44a**, bearing a naphthalene group, was selected as a representative example.

In the ^{1}H NMR spectrum (400MHz, $CDCl_3$) (**Figure 11**), all characteristic protons of the PAE core were observed, including the methyl group at 2.61 ppm (s, 3H) and the methoxy group at 3.89 ppm(s, 3H). In the aromatic region, the PAE protons were identified as two doublets at 7.96 (d, *J* = 2.2 Hz, 1H) and 7.04 ppm (d, *J* = 8.7 Hz, 1H), and a double doublet at 6.99 ppm (dd, *J* = 2.2, 8.8 Hz, 1H). Additional signals corresponding to the naphthalene moiety (**H-13** to **H-19**) were observed at 8.64 (brs, 1H), 8.10 (dd, *J* = 1.5, 8.6 Hz, 1H), 8.01 (brd, *J* = 7.8 Hz, 1H), 7.91 (brd, *J* = 7.8 Hz, 1H), 7.61 (td, *J* = 1.5, 7.8 Hz, 1H), 7.58 (d, *J* = 8.6 Hz, 1H), and 7.56 ppm (td, *J* = 1.5, 7.8 Hz, 1H).

Figure 11. ^{1}H NMR spectrum of compound **44a**.

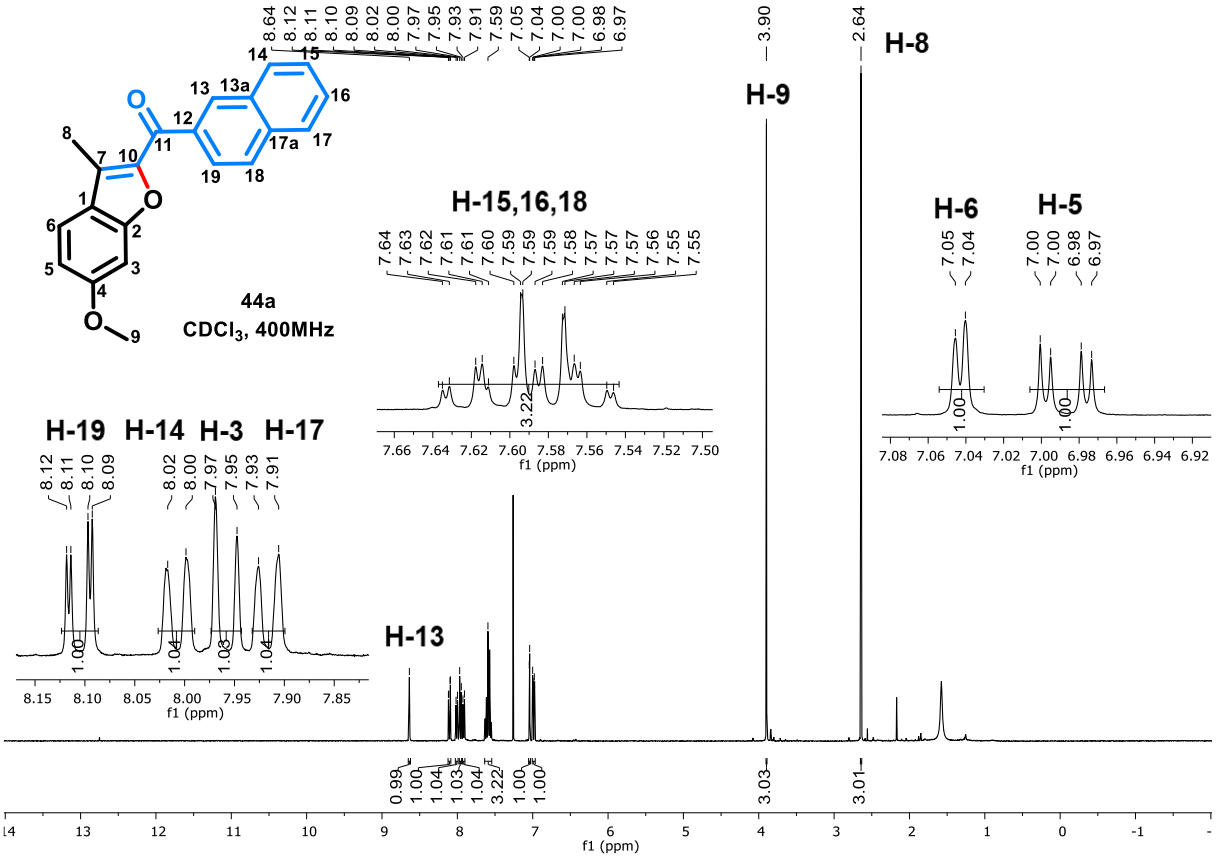

In the ^{13}C NMR spectrum (100MHz, $CDCl_3$) (**Figure 12**), all characteristic PAE carbons were identified, along with the quaternary carbons of the benzofuran ring bonded to oxygen at 156.0 and 148.5 ppm (**C-2** and **C-10**). The carbonyl carbon of the phenacyl group appeared at 185.4 ppm (**C-11**). Additional signals at 135.6, 135.4, 131.4, 129.8, 128.3, 127.9, 126.7, 125.6, 122.9, and 122.0 ppm were assigned to the naphthalene carbons (**C-12** to **C-19**) of the compound.

Figure 12. ^{13}C NMR spectrum of compound **44a**.

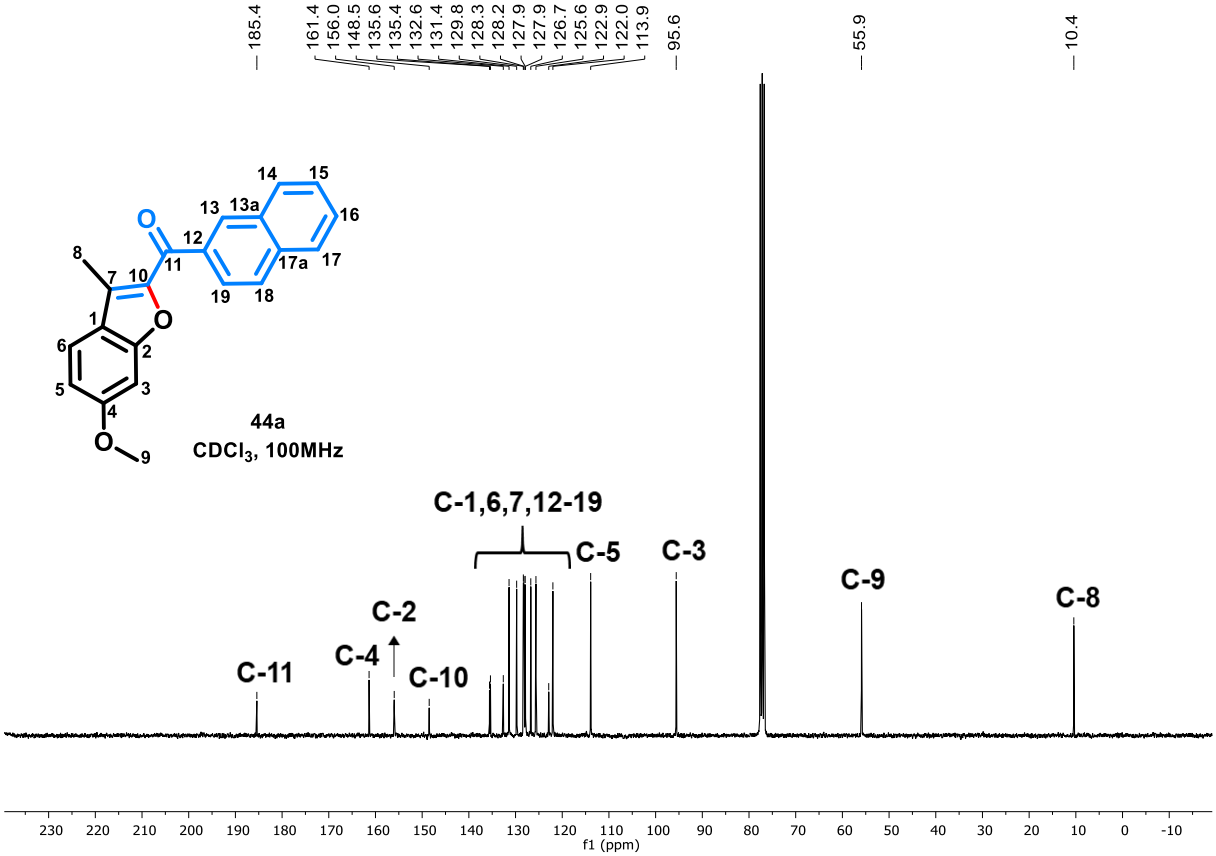

Single-crystal X-ray diffraction analysis of compound **44a** was performed using a crystal suitable for this purpose, which allowed unambiguous determination of its molecular structure. The results confirmed the proposed structure, with the corresponding ORTEP representation shown in **Figure 13**.

Figure 13. ORTEP representation of compound **44a**. Color code: grey, carbon; red, oxygen; white, hydrogen atoms.

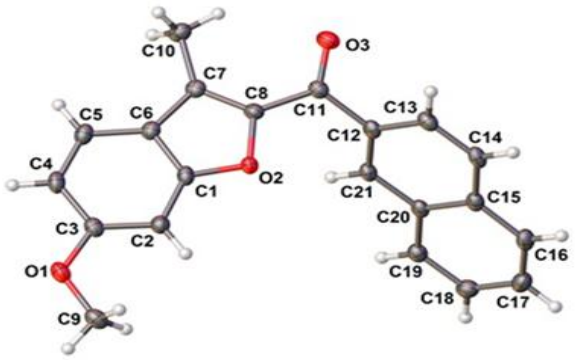

With all compounds fully characterized, the proposed mechanism for these derivatives suggests that the carbonyl group in the phenacyl bromide plays a crucial role in facilitating the cyclization process. The reaction begins with the deprotonation of the hydroxyl group by potassium carbonate, generating the corresponding alkoxide ion. This nucleophilic species then attacks the electrophilic carbonyl carbon within the PAE moiety, initiating an intramolecular cyclization. Proton transfers and water elimination restore aromaticity through resonance, driving the formation of the benzofuran derivative, as shown in **Scheme 12**.

Scheme 12. Proposed Intramolecular Cyclization Mechanism.

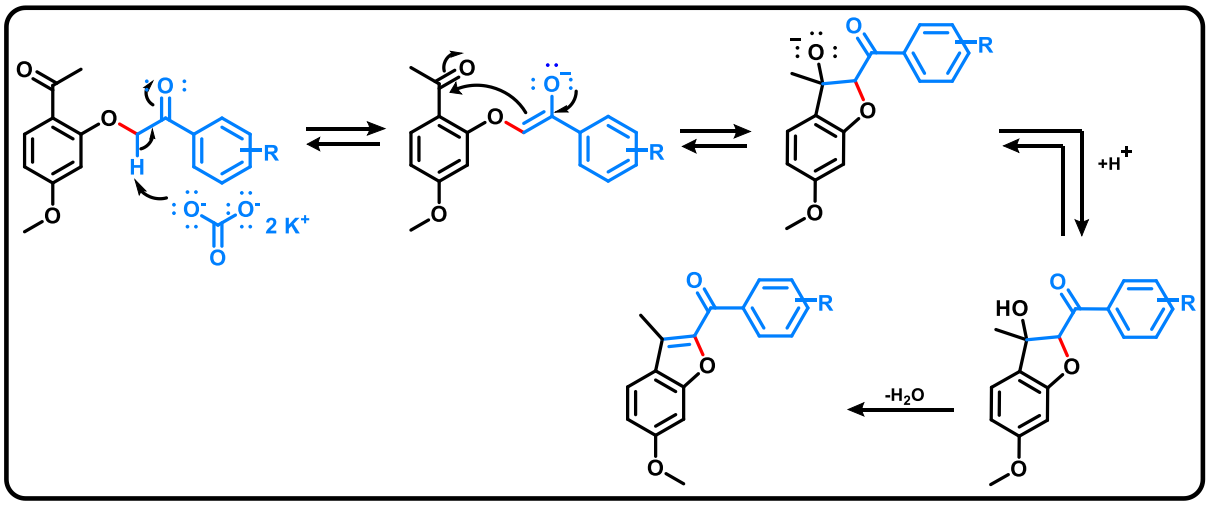

1.3.4 Cytotoxic Analysis:

This study evaluated compounds **43a**–**43d** and **44a**–**44g** for their cytotoxic activity against two cancer cell lines, HCT116 (colorectal adenocarcinoma) and MCF-7 (breast carcinoma), at a concentration of 10 μM after 72 hours of incubation using

the MTT assay. In this preliminary screening, compounds **44b**, **44e**, and **44g** showed significant activity against HCT116 cells, with growth inhibition exceeding 60%, whereas no compounds were active against MCF-7 cells (**Figure 14A**).

A follow-up assay was performed to determine the IC_{50} values by treating the cells with increasing concentrations (0.006–10 μM) of the active compounds and the positive control, doxorubicin (**Figure 14B**). Compound **44e** showed the highest potency, with an IC_{50} of 0.2 μM, followed by **44g** and **44b**, with IC_{50} values of 0.5 and 1.1 μM, respectively. Doxorubicin displayed an IC_{50} of 0.1 μM under the same conditions.

Figure 14. Cytotoxicity of paeonol derivatives evaluated through MTT assay after 72 h incubation. **A.** Compounds **43a**–**43d** and **44a**–**44g** were tested at10 μM in two cell lines: adenocarcinoma colorectal cells HCT-116 and breast carcinoma cells MCF-7. **B.** Compounds **44b**, **44e** and **44g** were tested in HCT- 116 at increasing concentrations to obtain the IC_{50} values. Doxorubicin was used as positive control. Data correspond to mean ± standard error of the mean from two (A) or three (B) independent experiments performed in duplicate.

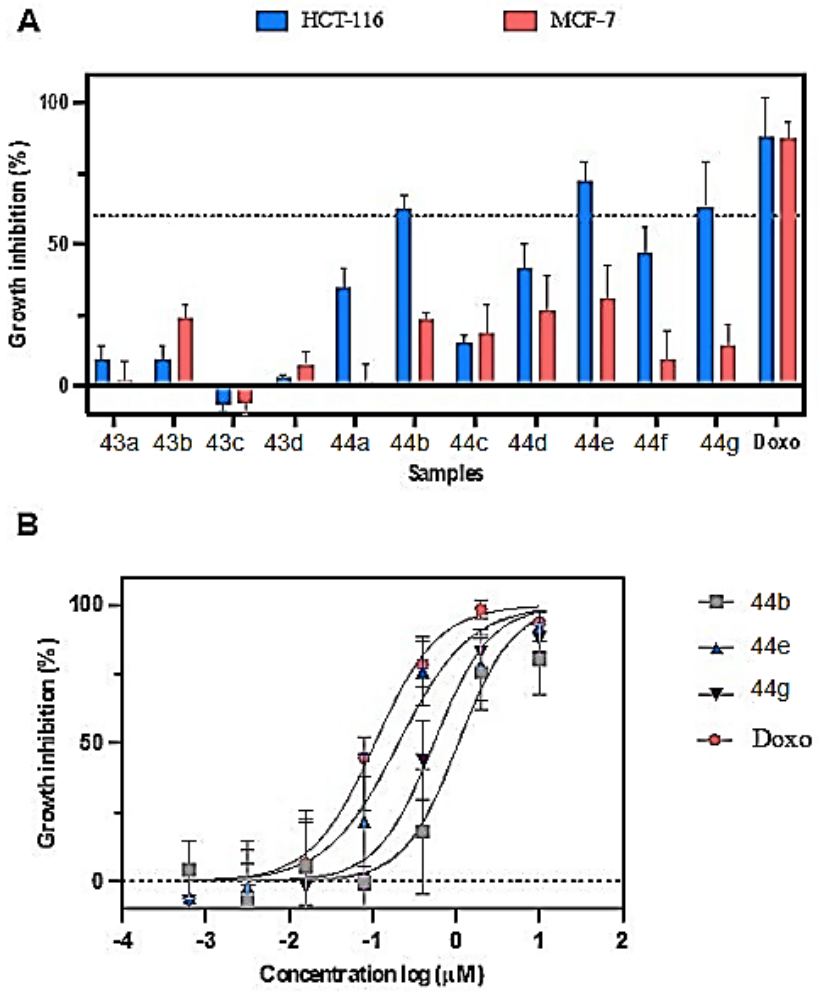

Compounds **44b**, **44e**, and **44g** contain substituents in the *meta* position of the newly introduced aromatic ring fused to the paeonol core. This suggests that substitution at this position may be critical for the biological activity of the tested benzofuran derivatives. Among these, compounds **44b** and **44g**, which were less active than **44e**, feature electron-withdrawing groups, while compound **44e** carries an electron-donating substituent. These results indicate that electron-donating groups at the *meta* position of the newly introduced ring enhance the cytotoxic activity of the benzofuran scaffold against colorectal adenocarcinoma HCT116 cells.

Based on these findings, compound **44e** was selected for further analysis. Its cytotoxicity was evaluated using the MTT assay after shorter incubation periods (24 and 48 hours) to assess the time dependency of its activity (**Figure 15A**). Notably, reducing the incubation time to 24 hours significantly increased the IC_{50} value to 5.6 μM, which is 28 times higher than the IC_{50} observed after 72 hours. Extending the incubation to 48 hours reduced the IC_{50} to 0.5 μM, highlighting a strong time-dependent effect. To assess the compound's ability to inhibit clonogenic potential, HCT116 cells were treated with 0.14 and 0.07 μM of **44e** for 24 hours, then replated at low density and allowed to grow for seven days. Compound **44e** markedly reduced both the number and size of colonies, supporting its anticancer potential (**Figure 15B**).

As previously noted, paeonol has traditionally been used in China to treat conditions related to pain and inflammation, and evidence supports its neuroprotective, antitumor, and cardioprotective effects (ZHANG; LI & LIU, 2019). However, the molecular mechanisms underlying these effects and the specific targets involved remain poorly understood. Paeonol has shown activity against tumor cells of various origins, including HCT116 colorectal carcinoma, as studied here. Nevertheless, previous studies have shown that its cytotoxic effect occurs at significantly higher concentrations than those observed for derivative **44e.** For instance, after 72 hours of treatment, paeonol reduced cell viability by 50% only at a concentration of 30 mg/L (180 μM) (LI, TAN & WANG, 2014), while compound **44e** achieved a comparable effect with an IC_{50} of just 0.2 μM, suggesting that the structural modifications introduced substantially improved its cytotoxic activity.

Figure 15. A. Compound **44e** was tested in HCT-116 at increasing concentrations to obtain the IC_{50} values after 24 and 48 h of incubation using an MTT assay. **B.** Colony formation after doxorubicin or compound **44e** treatment for 24 h, followed by replating in a drug-free media for seven days. Representative images illustrate colony formation in HCT-116 after control (DMSO 0.5%), doxorubicin (0.1 μM), and compound **44e** (0.07 and 0.14 μM) treatment. Data correspond to mean ± standard error of the mean from three independent experiments in duplicates.

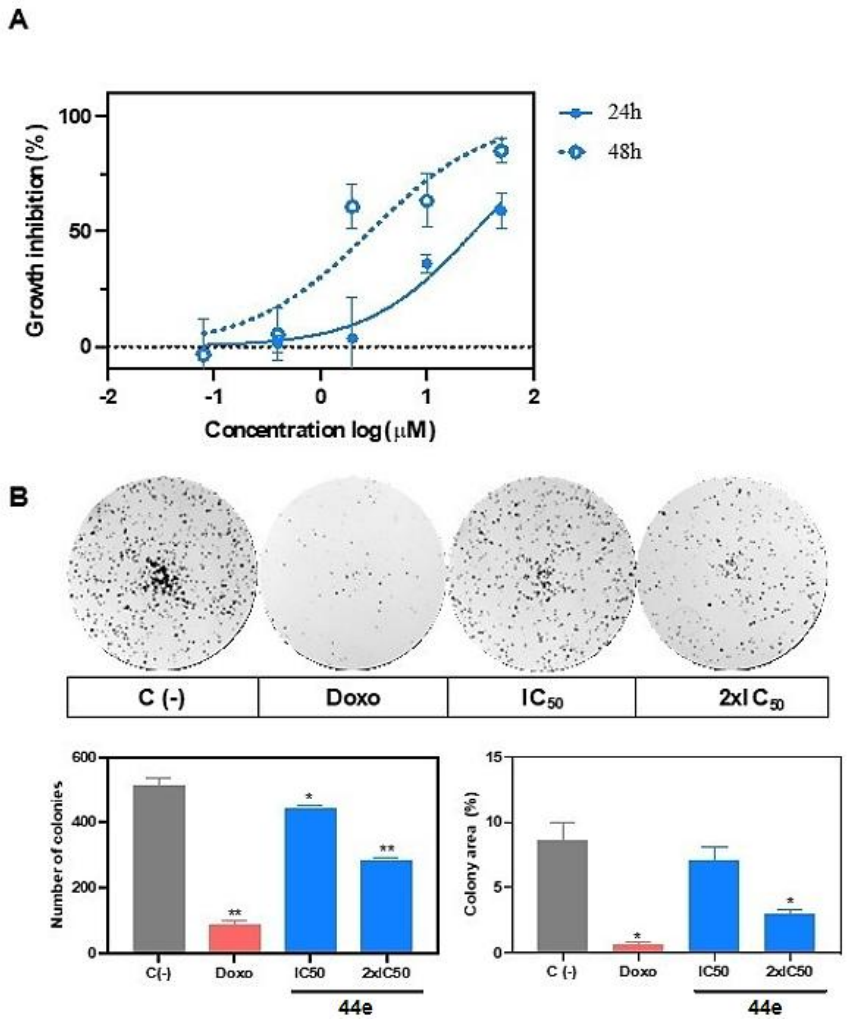

1.4 CONCLUSIONS

This work successfully reports the synthesis of four novel ether and seven benzofuran derivatives of paeonol, three of which are newly described, using a straightforward methodology, with yields ranging from 29% to 100%. Among the synthesized compounds, **43a–d**, **44b**, **44c**, and **44f** exhibited excellent yields above 80%.

The cytotoxic activity of these compounds was evaluated against two cancer cell lines: HCT116 (colorectal adenocarcinoma) and MCF-7 (breast carcinoma). Compounds **44b**, **44e**, and **44g** were considered active against HCT116 cells, showing

growth inhibition greater than 60%. Notably, compound **44e** exhibited a IC_{50} value of 0.2 μM and was selected for further biological analysis. These results reinforce its potential as an anticancer candidate.

Overall, this research not only provides a practical and efficient approach to synthesizing oxygen-containing paeonol derivatives but also highlights their promise as anticancer agents.

The findings presented in this study have been published in Chemistry & Biodiversity.

Laura P. R. Figueroa, Helori V. Domingos, Jennifer B. Pardo, Pedro H. O. Santiago, Javier Ellena,Valdemar Lacerda Junior, Letícia V. Costa-Lotufo,* and Warley de S. Borges*. Synthesis of Cytotoxic Benzofurans and Ethers Derivatives of Paeonol. **2024**, 21, e202400943. doi.org/10.1002/cbdv.202400943.

1.5 EXPERIMENTAL PART

1.5.1 General Remarks:

Starting materials obtained from commercial suppliers were used as received unless otherwise stated. Thin layer chromatography (TLC) was performed using aluminum-backed 60 F254 silica plates (20 x 20 cm). Visualization was achieved by UV fluorescence (250 and 300nm). Flash column chromatography (FCC) was performed using silica gel (Aldrich 40-63 μm, 230-400 mesh). ^{1}H and ^{13}C nuclear magnetic resonance (NMR) spectra were recorded on a Varian 400 MHz spectrometer (Palo Alto, USA) using deuterated chloroform ($CDCl_3$) as the solvent and tetramethylsilane (TMS) as the internal standard. Chemical shifts (δ) are reported in parts per million (ppm), and coupling constants (J) are expressed in Hertz (Hz). High-resolution mass (HRMS) spectra were obtained on a Bruker Daltonics micrOTOF QII / ESI-TOF instrument (Billerica, USA) by direct injection of the compound dissolved in methanol (CH_3OH), providing unambiguous molecular formula assignments for singly charged molecular ions, such as $[M - H]^-$ or $[M + H]^+$. Infrared (IR) spectra were recorded on a Bruker Tensor 27 FT-IR spectrometer (Bremen, Germany) within the wavelength range of 4000–500 cm^{-1}. The names of the compounds were generated using ChemDraw software.

1.5.2 General Procedure for the Synthesis of paeonol Ether Derivatives:

In a 10 mL round-bottom flask, paeonol (0.050 g, 1.0 mmol) was dissolved in dimethylformamide (DMF, 3 mL) under stirring in an ice bath, followed by the addition of potassium carbonate (0.089 g, 1.2 mmol). The reaction mixture was stirred under these conditions for 1 hour. Subsequently, the corresponding benzyl bromide (1.5 mmol) was added, and the system was maintained at room temperature under continuous stirring for 18 hours (**Scheme 13**). All compounds were purified by column chromatography.

Scheme 13. General Synthesis of PAE Ether Derivatives **43a-d**.

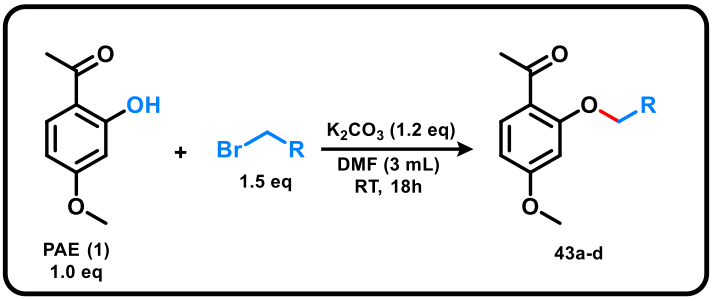

Characterization Data: Products 43a-d

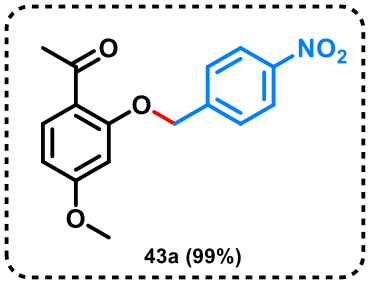

1-(4-methoxy-2-((4-nitrobenzyl)oxy)phenyl)ethan-1-one (compound **43a**) was obtained as a yellow solid (99%) and purified by column chromatography on silica gel (*n*-hexane/EtOAc [7:3]). **^{1}H NMR (400 MHz, $CDCl_3$)** δ=8.27 (d, *J*=8.7 Hz, 2H), 7.85 (d, *J*=8.7 Hz, 1H), 7.64 (d, *J*=8.7 Hz, 2H), 6.57 (dd, *J*=2.3, 8.7 Hz, 1H), 6.46 (d, *J*=2.3 Hz, 1H), 5.24 (s, 2H), 3.83 (s, 3H), 2.57 (s, 3H). **^{13}C NMR (100 MHz, $CDCl_3$)** δ=197.4 (C_q), 164.4 (C_q), 159.2 (C_q), 147.8 (C_q), 143.3 (C_q), 133.1 (CH), 127.9 (CH), 127.9 (CH), 124.0 (CH), 124.0 (CH), 121.6 (C_q), 105.6 (CH), 99.8 (CH), 69.4 (CH_2), 55.6 (CH_3), 31.8 (CH_3). **FTIR (ATR)$_{vmax}$** cm^{-1} 3057, 2845, 1519, 1342, 1267, 1038, 829. **ESI (+)**

FT-ICR MS calcd. for $C_{16}H_{16}NO_5^+$ $[M+H]^+$: 302.10230; found: 302.10199; calcd. for $C_{16}H_{15}NO_5Na^+$ $[M+Na]^+$: 324.08424; found: 324.08318. **m.p.** (°C) = 109.3.

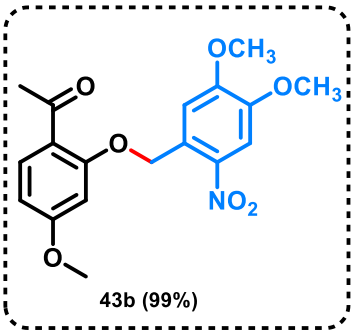

43b (99%)

1-(2-((4,5-dimethoxy-2-nitrobenzyl)oxy)-4-methoxyphenyl)ethan-1-one (compound **43b**) was obtained as a red solid (99%) and purified by column chromatography on silica gel (*n*-hexane/EtOAc [3:2]). **^{1}H NMR (400 MHz, $CDCl_3$)** δ=7.82 (d, *J*=8,7 Hz, 1H), 7.78 (s, 1H), 7.70 (s, 1H), 6.58 (d, *J*=2.3 Hz, 1H), 6.57 (dd, *J*=2.3, 8.7 Hz, 1H), 5.55 (s, 2H), 4.06 (s, 3H), 3.97 (s, 3H), 3.86 (s, 3H), 2.60 (s, 3H). **^{13}C NMR (100 MHz, $CDCl_3$)** δ=197.1 (C_q), 164.4 (C_q), 159.2 (C_q), 154.3 (C_q), 148.0 (C_q), 138.8 (C_q), 133.2 (CH), 128.6 (C_q), 121.1 (C_q), 110.2 (CH), 108.0 (CH), 105.3 (CH), 100.0 (CH), 67.7 (CH_2), 56.8 (CH_3), 56.4 (CH_3), 55.6 (CH_3), 30.7 (CH_3). **FTIR (ATR)$_{vmax}$** cm^{-1} 2971, 2938, 1600, 1509, 1466, 1320, 1256, 1022, 885, 840. **ESI (+) FT-ICR MS** calcd. for $C_{18}H_{20}NO_7Na^+$ $[M+Na]^+$: 384.10537; found: 384.10507. **m.p.** (°C) = 163.8.

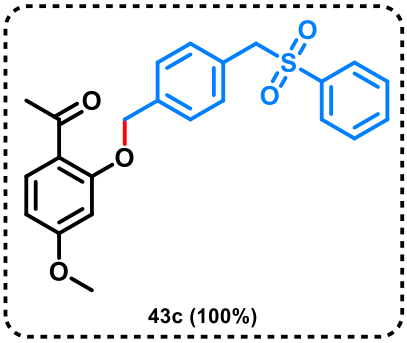

43c (100%)

1-(4-methoxy-2-((2-((phenylsulfonyl)methyl)benzyl)oxy)phenyl)ethan-1-one (compound **43c**) was obtained as a white solid (100%) and purified by column chromatography on silica gel (*n*-hexane/EtOAc [3:2]). **^{1}H NMR (400 MHz, $CDCl_3$)** δ=7.82 (d, *J*=8.7 Hz, 1H), 7.69 (dd, *J*=1.2, 7.4 Hz, 2H), 7.64 (tt, *J*=1.2, 7.4 Hz, 1H), 7.50 (brt, *J*=7.4 Hz, 2H), 7.46 (dd, *J*=1.3, 7.4 Hz, 1H), 7.37 (td, *J*=1.3, 7.4 Hz, 1H), 7.25

(td, *J*=1.4, 7.4 Hz, 1H), 7.00 (dd, *J*=1.3, 7.8 Hz, 1H), 6.56 (dd, *J*=2.3, 8.7 Hz, 1H), 6.53 (d, *J*=2.3 Hz, 1H), 5.15 (s, 2H), 4.50 (s, 2H), 3.86 (s, 3H), 2.41 (s, 3H). **^{13}C NMR (100 MHz, $CDCl_3$)** δ=197.4 (C_q), 164.5 (C_q), 159.8 (C_q), 138.1 (C_q), 136.3 (C_q), 134.0 (CH), 132.8 (CH), 132.9 (CH), 129.7 (CH), 129.5 (CH), 129.2 (CH), 129.2 (CH), 128.6 (CH), 128.6 (CH), 128.6 (CH), 126.5 (C_q), 121.4 (C_q), 105.9 (CH), 99.5 (CH), 68.7 (CH_2), 59.6 (CH_2), 55.6 (CH_3), 31.8 (CH_3). **FTIR (ATR)$_{vmax}$** cm^{-1}: 3003, 2839, 1301, 1136, 893, 855, 790, 763, 717. **ESI (+) FT-ICR MS** calcd. for $C_{23}H_{22}O_5SNa^+$ $[M+Na]^+$: 433.10802; found: 433.10770; calcd. for $C_{23}H_{22}O_5SK^+$ $[M+K]^+$: 449.08195; found: 449.08151; calcd. for $C_{46}H_{44}O_{10}S_2K^+$ $[2M+K]^+$: 859.20075; found: 859.19928. **m.p.** (°C) = 137.5.

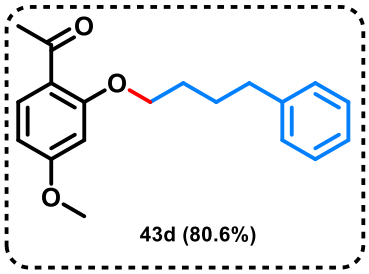

1-(4-methoxy-2-(4-phenylbutooxy)phenyl)ethan-1-one (compound **43d**) was obtained as a yellow oil (80,6%) and purified by column chromatography on silica gel (*n*-hexane/EtOAc [9:1]). **^{1}H NMR (400 MHz, $CDCl_3$)** δ=7.83 (d, *J*=8.7 Hz, 1H), 7.27–7.32 (m, 2H), 7.16–7.22 (m, 3H), 6.51 (dd, *J*=2.3, 8.7 Hz, 1H), 6.41 (d, *J*=2.3 Hz, 1H), 4.04 (t, *J*=5.8 Hz, 2H), 3.84 (s, 3H), 2.70 (t, *J*=7.0 Hz, 2H), 2.57 (s, 3H), 1.80–1.90 (m, 4H). **^{13}C NMR (100 MHz, $CDCl_3$)** δ=197.9 (C_q), 164.5 (C_q), 160.5 (C_q), 141.8 (C_q), 132.7 (CH), 128.4 (CH), 128.4 (CH), 125.9 (CH), 125.9 (CH), 125.9 (CH), 121.2 (C_q), 105.0 (CH), 99.8 (CH), 68.3 (CH_2), 55.8 (CH_3), 35.5 (CH_2), 32.1 (CH_3), 28.7 (CH_2), 28.0 (CH_2). **FTIR (ATR)$_{vmax}$** cm^{-1} 2938, 2867, 1596, 1497, 1257, 1034, 749, 702**. ESI (+) FT-ICR MS** calcd. for $C_{19}H_{23}O_3^+$ $[M+H]^+$: 299.1641; found: 299.16412; calcd. for $C_{19}H_{22}O_3Na^+$ $[M+Na]^+$: 321.14612; found: 321.14606; calcd. for $C_{19}H_{22}O_3K^+$ $[M+K]^+$: 337.12005; found: 337.12003.

1.5.3 General Procedure for the Synthesis of paeonol Benzofuran Derivatives:

In a 10 mL round-bottom flask, paeonol (0.050 g, 1.0 mmol) was dissolved in dimethylformamide (DMF, 3 mL) under stirring in an ice bath, followed by the addition

of potassium carbonate (0.089 g, 1.2 mmol). The reaction mixture was stirred under these conditions for 1 hour. Subsequently, the corresponding phenacyl bromide (1.5 mmol) was added, and the system was maintained at room temperature under continuous stirring for 18 hours (**Scheme 14**). All compounds were purified by column chromatography.

Scheme 14. General Synthesis of PAE Benzofuran Derivatives 44a-d.

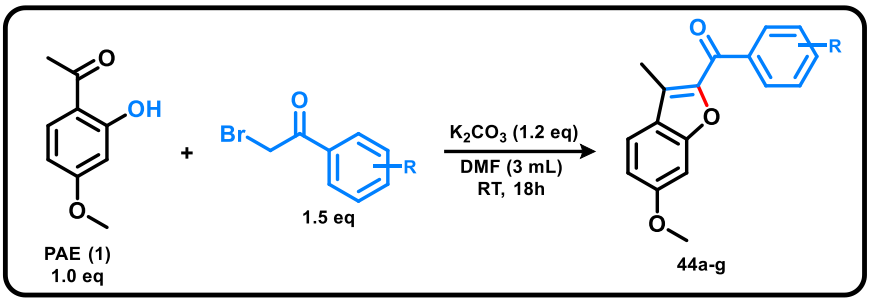

Characterization Data: Products 44a-g

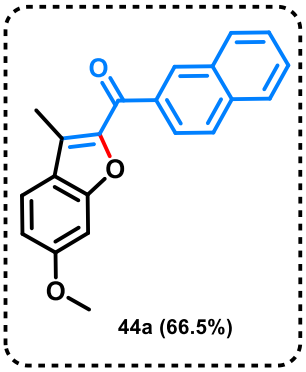

(6-methoxy-3-methylbenzofuran-2-yl)(naphtalen-2-yl)methanone (compound **44a**) was obtained as a yellow solid (66.5%) and purified by column chromatography on silica gel (*n*-hexane/EtOAc [4:1]). **^{1}H NMR (400 MHz, $CDCl_3$)** δ=8.64 (brs, 1H), 8.10 (dd, *J*=1.5, 8.6 Hz, 1H), 8.01 (brd, *J*=7.8 Hz, 1H), 7.96 (d, *J*=2.2 Hz, 1H), 7.91 (brd, *J*=7.8 Hz, 1H), 7.61 (td, *J*=1.5, 7.8 Hz, 1H), 7.58 (d, *J*=8.6 Hz, 1H), 7.56 (td, *J*=1.5, 7.8 Hz, 1H), 7.04 (d, *J*=8.7 Hz, 1H), 6.99 (dd, *J*=2.2, 8.7 Hz, 1H), 3.89 (s, 3H), 2.64 (s, 3H). **^{13}C NMR (100 MHz, $CDCl_3$)** δ=185.2 (C_q), 161.2 (C_q), 155.8 (C_q), 148.3 (C_q), 135.4 (C_q), 135.2 (C_q), 132.5 (C_q), 131.2 (CH), 129.6 (CH), 128.2 (CH), 128.0 (CH), 127.8 (C_q), 127.7 (CH), 126.6 (CH), 125.5 (CH), 122.7 (C_q), 121.8 (CH), 113.8 (CH), 95.4 (CH), 55.7 (CH_3), 10.3 (CH_3). **FTIR (ATR)$_{vmax}$** cm^{-1} 3003, 2841, 1596, 1460, 1136, 891, 854, 762. **ESI (+) FT-ICR MS** calcd. for $C_{21}H_{17}O_3^+$ $[M+H]^+$: 317.11722; found:

317.20892; calcd. for $C_{42}H_{32}O_6K^+$ $[2M+K]^+$: 671.18305; found: 671.48633. **m.p.** (°C) = 125.2.

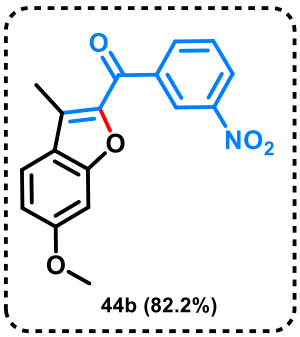

(6-methoxy-3-methylbenzofuran-2-yl)(3-nitrophenyl)methanone (compound **44b**) was obtained as a yellow solid (82.2%) and purified by column chromatography on silica gel (*n*-hexane/EtOAc 3:2). **^{1}H NMR (400 MHz, $CDCl_3$)** δ=8.99 (t, *J*=1.9 Hz, 1H), 8.44 (ddd, *J*=1.2, 1.9, 7.8 Hz, 1H), 8.41 (ddd, *J*=1.2, 1.9, 7.8 Hz, 1H), 7.72 (t, *J*=7.8 Hz, 1H), 7.60 (dd, *J*=2.3, 8.6 Hz, 1H), 7.02 (m, 1H), 6.99 (d, *J*=2.3 Hz, 1H), 3.90 (s, 3H), 2.69 (s, 3H). **^{13}C NMR (100 MHz, $CDCl_3$)** δ=182.2 (C_q), 161.8 (C_q), 156.1 (C_q), 148.1 (C_q), 147.4 (C_q), 139.3 (C_q), 135.3 (CH), 129.9 (CH), 129.4 (CH), 126.5 (CH), 124.7 (CH), 122.1 (CH), 114.4 (CH), 95.3 (CH), 55.8 (CH_3), 10.3 (CH_3). **FTIR (ATR)$_{vmax}$** cm^{-1} 3002, 2841, 1596, 1488, 1571, 1314, 1135, 855, 763, 718, 690. **ESI (+) FT-ICR MS** calcd. for $C_{17}H_{13}NO_5^+$ $[M+H]^+$: 312.08665; found: 312.08667; calcd. for $C_{17}H_{13}NO_5Na^+$ $[M+Na]^+$: 334.06859; found: 334,06860; calcd. for $C_{34}H_{26}N_2O_{10}Na^+$ $[2M+Na]^+$: 645.14797; found: 645.14801. **m.p. (°C)** = 119.3.

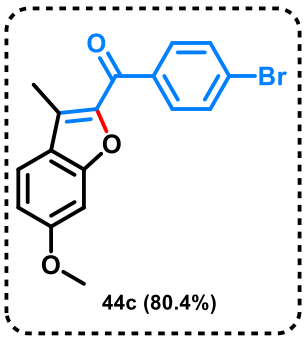

(4-bromophenyl)(6-methoxy-3-methylbenzofuran-2-yl)methanone (compound **44c**) was obtained as a yellow solid (80.4%) and purified by column chromatography on silica gel (*n*-hexane/ EtOAc [9:1]). **^{1}H NMR (400 MHz, $CDCl_3$)** δ = 7.96 (d, *J*=8.4

Hz, 2H), 7.66 (d, *J*=8.4 Hz, 2H), 7.58 (d, *J*=8.6 Hz, 1H), 7.00 (d, *J*=2.2 Hz, 1H), 6.97 (dd, *J*=2.2, 8.6 Hz, 1H), 3.88 (s, 3H), 2.62 (s, 3H). **^{13}C NMR (100 MHz, $CDCl_3$)** δ = 184.0 (C_q), 161.4 (C_q), 155.8 (C_q), 147.8 (C_q), 136.8 (C_q), 131.5 (CH), 131.5 (CH), 131.2 (CH), 131.2 (CH), 128.4 (C_q), 127.3 (C_q), 122.6 (C_q), 121.9 (CH), 113.9 (CH), 95.3 (CH), 55.7 (CH_3), 10.2 (CH_3). **FTIR (ATR)$_{vmax}$** cm^{-1}: 3002, 2841, 1595, 1491, 1131, 1026, 856, 790, 761. **ESI (+) FT-ICR MS** calcd. for $C_{17}H_{13}BrO_3Na^+$ $[M+Na]^+$: 366.99405; found: 366.99403; calcd. for $C_{17}H_{13}BrO_3K^+$ $[M+K]^+$: 382.96797; found: 382.96802; calcd. for $C_{34}H_{26}Br_2O_6Na^+$ $[2M+Na]^+$: 710.99883; found: 710,99890. **m.p.** (°C) = 123.8.

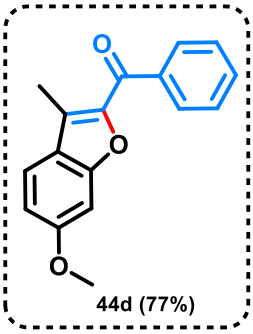

44d (77%)

(6-methoxy-3-methylbenzofuran-2-yl)(phenyl)methanone (compound **44d**) was obtained as a yellow solid (77%) and purified by column chromatography on silica gel (*n*-hexane/ EtOAc [4:1]). **^{1}H NMR (400 MHz, $CDCl_3$)** δ = 8.07–8.04 (m, 2H), 7.59 (td, *J*=1.5, 7.4 Hz, 1H), 7.53–7.49 (m, 2H), 7.56 (d, *J*=8.7 Hz, 1H), 7.01 (d, *J*=2.2 Hz, 1H), 6.97 (dd, *J*=2.2, 8.7 Hz, 1H), 3.88 (s, 3H), 2.61 (s, 3H). **^{13}C NMR (100 MHz, $CDCl_3$)** δ = 185.4 (C_q), 161.2 (C_q), 155.8 (C_q), 148.1 (C_q), 138.2 (C_q), 132.3 (CH), 129.6 (CH), 129.6 (CH), 128.2 (CH), 128.2 (CH), 127.8 (C_q), 122.7 (C_q), 121.8 (C_q), 113.7 (CH), 95.4 (CH), 55.7 (CH_3), 10.2 (CH_3). **FTIR (ATR)$_{vmax}$** cm^{-1}: 3002, 2841, 1660, 1597, 1491, 1137, 893, 855, 790, 761, 718. **ESI (+) FT-ICR MS** calcd. for $C_{34}H_{28}O_6^+$ $[2M+H]^+$: 533.19587; found: 533.36615. **m.p.** (°C) = 75.7.

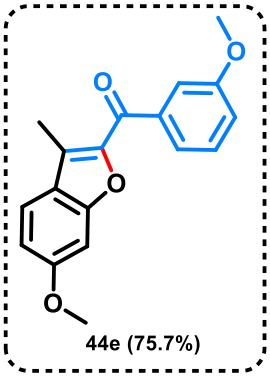

(6-methoxy-3-methylbenzofuran-2-yl)(3-methoxyphenyl)methanone (compound **44e**) was obtained as a yellow oil (75.7%) and purified by column chromatography on silica gel (*n*-hexane/EtOAc [7:3]). **^{1}H NMR (400 MHz, $CDCl_3$)** δ = 7.68 (brd, *J*=7.4 Hz, 1H), 7.57 (brs, 1H), 7.56 (d, *J*=8.7 Hz, 1H), 7.42 (t, *J*=7.8 Hz, 1H), 7.14 (brdd, *J*=1.9, 8.2 Hz, 1H), 7.01 (d, *J*=2.2 Hz, 1H), 6.97 (dd, *J*=2.2, 8.7 Hz, 1H), 3.88 (s, 3H), 3.88 (s, 3H), 2.60 (s, 3H). **^{13}C NMR (100 MHz, $CDCl_3$)** δ = 185.1 (C_q), 161.2 (C_q), 159.5 (C_q), 155.8 (C_q), 148.1 (C_q), 139.4 (C_q), 129.2 (CH), 127.9 (C_q), 122.7 (C_q), 122.3 (CH), 121.8 (CH), 118.7 (CH), 114.1 (CH), 113.8 (CH), 95.4 (CH), 55.7 (CH_3), 55.5 (CH_3), 10.3 (CH_3). **FTIR (ATR)$_{vmax}$** cm^{-1}: 2939, 2835, 1551, 1484, 1268, 851, 787. **ESI (+) FT-ICR MS** calcd. for $C_{18}H_{16}O_4Na^+$ $[M+Na]^+$: 319.09408; found: 319,09402; calcd. for $C_{18}H_{16}O_4K^+$ $[M+K]^+$: 335.06802; found: 335.06799; calcd. for $C_{36}H_{32}O_8Na^+$ $[2M+Na]^+$: 615.19894; found: 615.19885.

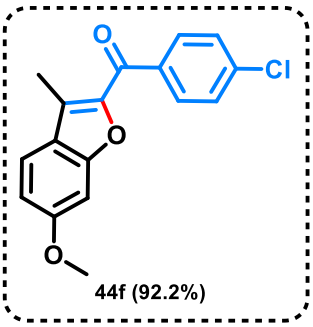

(4-chlorophenyl)(6-methoxy-3-methylbenzofuran-2-yl)methanone (compound **44f**) was obtained as a yellow solid (92.2%) and purified by column chromatography on silica gel (*n*-hexane/ EtOAc [9:1]). **^{1}H NMR (400 MHz, $CDCl_3$)** δ = 8.05 (d, *J*=8.5 Hz, 2H), 7.57 (d, *J*=8.6 Hz, 1H), 7.49 (d, *J*=8.5 Hz, 2H), 7.00 (d, *J*=2.1 Hz, 1H), 6.98 (dd, *J*=2.1, 8.6 Hz, 1H), 3.89 (s, 3H), 2.63 (s, 3H). **^{13}C NMR (100 MHz, $CDCl_3$)** δ = 183.8 (C_q), 161.4 (C_q), 155.8 (C_q), 147.9 (C_q), 138.7 (C_q), 136.4 (C_q), 131.1 (CH), 131.1 (CH),

128.5 (CH), 128.5 (CH), 128.4 (C_q), 122.6 (C_q), 121.9 (CH), 113.9 (CH), 95.3 (CH), 55.7 (CH_3), 10.2 (CH_3). **FTIR (ATR)$_{vmax}$** cm^{-1}: 3002, 2840, 1135, 1084, 890, 854, 791, 763**. ESI (+) FT-ICR MS** calcd. for $C_{17}H_{13}ClO_3Na^+$ $[M+Na]^+$: 323.04454; found: 323.04459; calcd. for $C_{34}H_{26}Cl_2O_6Na^+$ $[2M+Na]^+$: 623.09987; found: 623.10016. **m.p.** (°C) = 112.1.

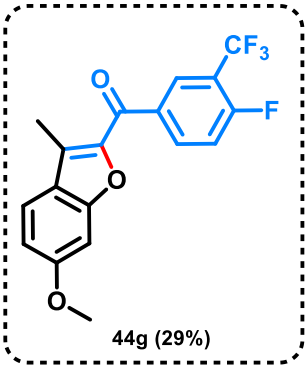

(4-fluoro-3-(trifluoromethyl)phenyl)(6-methoxy-3-methylbenzo-furan-2-yl)methanone (compound **44g**) was obtained as a yellow solid (29%) and purified by column chromatography on silica gel (*n*-hexane/EtOAc [9:1]). **^{1}H NMR (400 MHz, $CDCl_3$)** δ = 8.44 (dd, *J*=1.9, 7.0 Hz, 1H), 8.38–8.33 (m, 1H), 7.58 (d, *J*=8.7 Hz, 1H), 7.35 (t, *J*=9.0 Hz, 1H), 7.00 (d, *J*=2.2 Hz, 1H), 6.99 (dd, *J*=2.2, 8.7 Hz, 1H), 3.90 (s, 3H), 2.66 (s, 3H). **^{13}C NMR (100 MHz, $CDCl_3$)** δ = 181.9 (C_q), 163.0 (C_q), 161.7 (C_q), 155.9 (C_q), 147.5 (C_q), 135.7 (CH), 135.6 (C_q), 134.3 (C_q), 129.5 (C_q), 129.4 (CH), 122.5 (C_q), 122.1 (CH), 117.0 (CH), 116.9 (C_q), 114.2 (CH), 95.3 (CH), 55.8 (CH_3), 10.3 (CH_3). **FTIR (ATR)$_{vmax}$** cm^{-1} 3003, 2841, 1270, 1157, 1138, 892, 856, 761. **ESI (+) FT-ICR MS** calcd, for $C_{18}H_{12}F_4O_3Na^+$ $[M+Na]^+$: 375.06148; found: 375.06155; calcd. for $C_{36}H_{24}F_8O_6Na^+$ $[2M+Na]^+$: 727.13373; found: 727.13373. **m.p.** (°C) = 149.0.

1.5.4 Single Crystal X-ray Diffraction:

Single-crystal X-ray diffraction measurements for compounds **43a**, **44a**, **44b**, **44c**, **44f**, and **44g** were performed on a Rigaku XtaLAB Synergy-S Dualflex diffractometer equipped with a HyPix-6000HE detector system, using Mo Kα (λ = 0.71073 Å) or Cu Kα (λ = 1.54184 Å) radiation, with data collected at 100 K. The software CrysAlisPro (Agilent Technologies Ltd., Yarnton, Oxfordshire, England, 2022) was used for cell refinement, data collection and reduction, and absorption correction. The structures were solved by the intrinsic phasing method using the SHELXT-2018/2

program, and refined by the least-squares method using the SHELXL-2019/2 (SHELDRICK, George M., 2015), both included in the Olex2 software (DOLOMANOV, Oleg V. *et al*., 2009).The non-hydrogen atoms had their positions determined with Fourier maps analyses and refined anisotropically, whereas the hydrogen atoms were located in calculated positions and refined using the riding model (CHANG & CHEN, 2021). The CIF files of the structures **43a**, **44a**, **44b**, **44c**, **44f** and **44g** were deposited in the Cambridge Structural Database under CCDC number 2260249 (**43a**), 2260250 (**44a**), 2260251 (**44b**), 2260252 (**44c**), 2260253 (**44f**) and 2260254 (**44g**). Tables A1 to A7 in the appendices material summarize the crystallographic data.

1.5.5 Cytotoxic Analysis:

MTT assay. Cytotoxicity was measured by a 3-[4,5-dimethylthiazol-2-yl]-2,5-diphenyltetrazolium bromide (MTT) (Thermo Fisher Scientific) assay. In the first set of experiments, compounds **43a**–**43d** and **44a**–**44g** were tested in two human cancer cell lines: HCT-116 (adenocarcinoma colorectal cells) and MCF-7 (carcinoma breast cells) at 10 μM after a 72 h incubation. Doxorubicin and DMSO were used as positive and negative controls, respectively. In a second set of experiments, compounds **44b**, **44e**, **44g** and doxorubicin were evaluated at increasing concentrations (0.0032–10 μM) to obtain the mean inhibitory concentration (IC_{50}) after 72 h of incubation. Compound **44e** was also evaluated after shorter incubations, 24 h and 48 h.

For all experiments cells (1×104 cells/well) were cultured in a 96-well plate in a DMEM medium, containing 10% FBS and 1% penicillin-streptomycin. After 24h, evaluated compounds were added to the plates and kept at 37°C in a CO_2 incubator. After the exposure period, the culture media were replaced with fresh media containing MTT solution (0.5 mg mL^{-1}) and incubated for three hours. The MTT solution was then removed, and plates were dried at 50°C for 30 min. The formazan product was solubilized with 150 μL of DMSO and the absorbance was obtained at 570 nm. In total two or three independent experiments were performed in duplicates. Data were analyzed as mean and standard error of the mean. IC_{50} values were obtained by nonlinear regression using GraphPad Prism 10 (GraphPad Software, Inc., San Diego, CA, USA).

Clonogenic Assay. HCT-116 cells (1×104 mL^{-1}) cells were seeded on 60 mm plate dishes in a total volume of 5 mL and, 24 h later, treated with Compound 44e (0.07

μM and 0.14 μM) for 24 h. Doxorubicin (Doxo;0.1 μM) was used as the positive control and 0.5% DMSO as negative control. Concentrations were based on IC_{50} values at 72h.

After the cells were subjected to treatment, cells were collected, plated at 1×103 cell/plate on 35-mm plates and maintained in culture for seven days in a drug-free medium. The medium was replaced every two days. Cells were then fixed and stained with a solution of 20% MeOH (Synth, Diadema, São Paulo, Brazil) and 0.5 g crystal violet (Sigma-Aldrich, St. Louis, MO, USA). Images were acquired using G:BOX Chemi XRQ (Syngene, Cambridge, UK) and quantified using the ImageJ software (ColonyArea; US National Institutes of Health, Bethesda, MD, USA).

1.6 REFERENCES

ADKI, Kaveri M.; KULKARNI, Yogesh A. Chemistry, pharmacokinetics, pharmacology and recent novel drug delivery systems of paeonol. **Life Sciences**, v. 250, n. January, p. 117544, 2020. Available at: <https://doi.org/10.1016/j.lfs.2020.117544>.

ADKI, Kaveri M.; KULKARNI, Yogesh A. Neuroprotective effect of paeonol in streptozotocin-induced diabetes in rats. **Life Sciences**, v. 271, n. December 2020, p. 119202, 2021. Available at: <https://doi.org/10.1016/j.lfs.2021.119202>.

AL-MULLA, Abbas. A Review : Biological Importance of Heterocyclic Compounds Abbas Al-Mulla. **Der Pharma Chemica**, v. 9, n. 13, p. 141–147, 2017.

ANDERSON, Kevin W. *et al*. The Selective Reaction of Aryl Halides with KOH: Syhthesis of Phenols, Aromatic Ethers, and Benzofurans**. Journal of the American Chemical Society**, v. 128, n. 128, p. 10694-10695, 2006. Available at: <http://doi.org/10.1021/ja0639719>.

CHANG, Meng-Yang; CHEN, Kuan-Ting. Bi(OTf)3-Mediated (4+1) Annulation of α-Sulfonyl o-Hydroxyacetophenones with α-Hydroxy Arylketones to Access Sulfonyl 2-Aroylbenzofurans. **Advanced Synthesis & Catalysis**, v. 363, p. 1-17, 2021. Available at: <http://doi.org/10.1002/adsc.202100143>.

CHE, Zhiping *et al*. Synthesis of paeonol ester derivatives and their insecticidal, nematicidal, and anti-oomycete activities. **Pest Management Science**, v. 78, p. 3442-3455, 2022. Available at: <http://doi.org/10.1002/ps.6985>.

CHEN, Bendong; NING, Mingliang; YANG, Guangshun. Effect of paeonol on antioxidant and immune regulatory activity in hepatocellular carcinoma rats. **Molecules**, v. 17, n. 4, p. 4672–4683, 2012. Available at: <http://doi.org/10.3390/molecules17044672>.

CHEN, Xiaofang *et al*. Synthesis and in vitro activity of dicationic indolyl diphenyl ethers as novel potent antibiotic agents against drug-resistant bacteria. **Bioorganic & Medicinal Chemistry Letters**, v. 27, p. 841-844, 2017. Available at: <http://dx.doi.org/10.1016/j.bmcl.2017.01.019>.

CHEN, Z.X. *et al*. Evaluation of paeonol-loaded transethosomes as transdermal delivery carriers. **European Journal of Pharmaceutical Sciences**, v. 99, p. 240-245, 2017. Available at: < http://dx.doi.org/10.1016/j.ejps.2016.12.026>.

CHOU, Tz Chong. Anti-inflammatory and analgesic effects of paeonol in carrageenan-evoked thermal hyperalgesia. **British Journal of Pharmacology**, v. 139, n. 6, p. 1146–1152, 2003. Available at: <https://doi.org/10.1038/sj.bjp.0705360>.

DEMMAK, Rym Gouta *et al*. Antibacterial and antioxidant activities of a novel enol ether nor-sesquiterpene isolated from *Myrtus nivellei* Batt. & Trab. **Fitoterapia**, v. 153, n. April, p. 104987, 2021. Available at: <https://doi.org/10.1016/j.fitote.2021.104987>.

DOLOMANOV, Oleg V. *et al*. OLEX2: a complete structure solution, refinement and analysis program. **Journal of Applied Crystallography**, v. 42, p. 339-341, 2009. Available at: <https://doi.org/10.1107/S0021889808042726>.

DWARAKANATH, Review Deepika; GAONKAR, Santosh L. Advances in Synthetic Strategies and Medicinal Importance of Benzofurans : A Review. **Asian Jornal of Organic Chemistry**. v. 11. e202200282, 2022. Available at: <http:// doi.org/10.1002/ajoc.202200282>.

FARHAT, Joviana *et al*. Structure – Activity Relationship of Benzofuran Derivatives with Potential Anticancer Activity. **Cancers**. v. 14. 2196, p. 1–22, 2022. Available at: <https://doi.org/ 10.3390/cancers14092196>.

FIGUEROA, Laura Patricia R. *et al*. Synthesis and Evaluation of Antibacterial Activity of 1,2,3-Triazole and Ether Derivatives of Paeonol. **Journal of the Brazilian Chemical Society**, v. 34, n. 1, p. 25–35, 2023. Available at: <https://dx.doi.org/10.21577/0103-5053.20220085>.

FU, Pin-Kuei *et al*. Evaluation of LPS-Induced Acute Lung Injury Attenuation in Rats by Aminothiazole-Paeonol Derivatives. **Molecules**, v. 22, p. 1605, 2017. Available at: <https://doi.org/10.3390/molecules22101605>.

GUPTA, KUMAR & GUPTA. Heterocyclic Chemistry I. Principles, Three- and Four-Membered Heterocycles. Edi, **Springer**, 1985. Available at: <https://doi.org/10.1007/978-3-642-72276-9>.

HARADA & YAMASHITA. Pharmacological Studies on the Root Bark of Paeonia Moutan. I. Central Effects of Paeonol. **Yakugaku Zasshi,** v. 89, p. 1205–1211, 1969. Available at: < https://doi.org/10.1248/yakushi1947.89.9_1205>.

HU, Die *et al*. Synthesis and biological activities of novel chalcone derivatives containing pyrazole oxime ethers. **Fitoterapia**, v. 166, 2023. Available at: <https://doi.org/10.1016/j.fitote.2023.105458>.

HU, Yang Sheng *et al*. Novel paeonol derivatives: Design, synthesis and anti-inflammatory activity in vitro and in vivo. **Bioorganic Chemistry**, v. 98, n. January, p. 103735, 2020. Available at: <https://doi.org/10.1016/j.bioorg.2020.103735>.

HUANG, Ligua *et al*. Synthesis and anti-inflammatory activity of paeonol analogues in the murine model of complete Freund's adjuvant induced arthritis. **Bioorganic and Medicinal Chemistry Letters**, v. 26, n. 21, p. 5218–5221, 2016. Available at: <http://dx.doi.org/10.1016/j.bmcl.2016.09.060>.

JIANG, Yuqin *et al*. Design, synthesis, and antilung adenocarcinoma activity research of novel paeonol Schiff base derivatives containing a 1,2,3-triazole moiety. **Journal of the Chinese Chemical Society**, v. 67, n. 1, p. 165–171, 2020. Available at: <http://doi.org/10.1002/jccs.201800491>.

KAPCHE, Deccaux W.F.G *et al*. Aryl benzofuran derivatives from the stem bark of *Calpocalyx dinklagei* attenuate inflammation. **Phytochemistry**, v. 141, p. 70-79, 2017. Available at: <http://dx.doi.org/10.1016/j.phytochem.2017.05.007>.

KRAUS, George A. et al. Synthesis and antibacterial activity of littorachalcone and related diphenyl ethers. **Bioorganic & Medicinal Chemistry Letters**, v. 18, p. 2329-2332, 2008. Available at: <http://doi.org/10.1016/j.bmcl.2008.02.082>.

KUMAR, Sarvesh et al. Arylalkyl Ketones, Benzophenones, Desoxybenzoins and Chalcones Inhibit TNF-a Induced Expression of ICAM-1: Structure-Activity Analysis. **Archiv der Pharmazie – Chemistry in Life Sciences**, v. 345, p. 368-377, 2012. Available at: <http://doi.org/10.1002/ardp.201100279>.

LAU, C. H. *et al*. Pharmacological investigations of the anti-diabetic effect of Cortex Moutan and its active component paeonol**. Phytomedicine**, v. 14, n. 11, p. 778–784, 2007. Available at: <http://doi.org/10.1016/j.phymed.2007.01.007>.

LEE, Bomi *et al*. Antiallergic effect of the root of Paeonia lactiflora and its constituents paeoniflorin and paeonol. **Archives of Pharmacal Research**, v. 31, n. 4, p. 445–450, 2008. Available at: <http://doi.org/10.1007/s12272-001-1177-6>.

LI, Qian *et al*. Antifungal efficacy of paeonol on *Aspergillus flavus* and its mode of action on cell walls and cell membranes**. Lwt,** v. 149, n. June, p. 111985, 2021. Available at: <https://doi.org/10.1016/j.lwt.2021.111985>.

LI, TANG & WANG. Paeonol exerts an anticancer effect on human colorectal cancer cells through inhibition of PGE_2 synthesis and COX-2 expression. **Oncology Reports**, v. 32, p. 2845-2853, 2014. Available at: <https://doi.org/10.3892/or.2014.3543>.

LIU, WANG & ZHANG. Dietary Chinese Herbs. Chemistry, Pharmacology and Clinical Evidence. Edi, **Springer**, 2015. Available at: <https://doi.org/10.1007/978-3-211-99448-1>.

LIU, Wentao *et al*. Surface chemical modification of poly(phthalazinone ether nitrile ketone) through rhBMP-2 and antimicrobial peptide conjugation for enhanced osteogenic and antibacterial activities *in vitro* and *in vivo*. **Chemical Engineering Journal**, v. 424, p. 130321, 2021. Available at: <https://doi.org/10.1016/j.cej.2021.130321>.

LUMB & TRAUNER. Biomimetic Synthesis and Structure Elucidation of Rubicordifolin, a Cytotoxic Natural Product from *Rubia cordifolia*. **Journal of the American Chemical Society**, v. 127, n. 9, p. 2870-2871, 2005. Available at: <https://doi.org/10.1021/ja042375g>.

McGRATH, BRICHACEK & NJARDARSON. A Graphical Journey of Innovative Organic Architectures That Have Improved Our Lives. **Journal of Chemical Education**, v. 87, n. 12, 2010. Available at: <https://doi.org/10.1021/ed1003806>.

MIAO, Yu Hang *et al*. Natural source, bioactivity and synthesis of benzofuran derivatives. **RSC Advances**, v. 9, n. 47, p. 27510–27540, 2019. Available at: <http://doi.org/10.1039/c9ra04917g>.

MORE, Kishor R. Review on Synthetic Routes for Synthesis of Benzofuran-Based Compounds. **Journal of Chemical and Pharmaceutical Research**, v. 9, n. 5, p. 210-220, 2017.

NEVAGI, Reshma J; DIGHE, Santosh N; DIGHE, Satish N. Biological and medicinal significance of benzofuran. **European Journal of Medicinal Chemistry**. v. 97, p. 561-581, 2015. Available at: <http://dx.doi.org/10.1016/j.ejmech.2014.10.085>.

PATHAN, Sultan Ismail *et al*. A review on synthetic approaches of heterocycles via insertion-cyclization reaction. **Synthetic Communications**, v. 50, n. 9, p. 1251–1285, 2020. Available at: <https://doi.org/10.1080/00397911.2020.1712609>.

QIN, Dong Dong *et al*. Crystal structure and biological activities of water-soluble nickel(II) and copper(II) complexes of a Schiff-base derived from paeonol. **Transition Metal Chemistry**, v. 34, n. 5, p. 499–505, 2009. Available at: <http://doi.org/10.1007/s11243-009-9222-z>.

QIN, Dong Dong *et al*. Evaluation of the antioxidant, DNA interaction and tumor cell cytotoxicity activities of Copper(II) complexes with Paeonol Schiff-base. **Inorganic Chemistry Communications**, v. 13, n. 6, p. 727–729, 2010. Available at: <http://dx.doi.org/10.1016/j.inoche.2010.03.030>.

ROMAGNA, Rodrigo de Alemeida et al. Synthesis of Chalcones, Screening *In silico* and *In vitro* and Evaluation of *Helicobacter pylori* Adhesion by Molecular Docking. **Current Pharmaceutical Design**, v. 30, p. 3350-3366, 2024. Available at: <http://dx.doi.org/10.2174/0113816128327090240821101355>.

SON, Minky *et al*. Tryptamine–Triazole Hybrid Compounds for Selective Butyrylcholinesterase Inhibition. **Bulletin of the Korean Chemical Society**, v. 40, n. 6, p. 544–553, 2019. Available at: <http://doi.org/10.1002/bkcs.11729>.

SHAMSUZZAMAN, Hena Khanam. Bioactive Benzofuran derivatives: A review. **European Journal of Medicinal Chemistry**, v. 97, p. 483-504, 2015. Available at: http://dx.doi.org/10.1016/j.ejmech.2014.11.039>.

SHELDRICK, George M. Crystal structure refinement with SHELXL. **Acta Crystallographica Section C. Structural Chemistry**, C. 71, p. 3-8, 2015. Available at: <http://doi.org/10.1107/S2053229614024218>.

SHILL, Manik Chandra et al. The isolation and synthesis of a novel benzofuran compound from *Tephrosia purpurea*, and the synthesis of several related derivatives, which suppress histamine H_1 receptor gene expression. **Bioorganic & Medicinal Chemistry**, v. 23, p. 6869-6874, 2015. Available at: <http://dx.doi.org/10.1016/j.bmc.2015.09.049>.

SINGH & WIRTH. Hpecyiapl teopricvalent Iodine Mediated Oxidative Cyclization of *o*-Hydroxystilbenes into Benzo- and Naphthofurans. **Synthesis**, v. 44, p. 1171-1177, 2012. Available at: <http://dx.doi.org/10.1055/s-0031-1290588>.

TIAN, Mingfa *et al*. Preparation of Paeonol Ethosomes by Microfluidic Technology Combined with Gaussians and Evaluation of Biological Activity by Zebrafish. **ACS Omega**, v. 9, p. 44425-44435, 2024. Available at: <https://doi.org/10.1021/acsomega.4c05830>.

TSAI, Chia Ying *et al*. Synthesis and evaluation of aminothiazole-paeonol derivatives as potential anticancer agents. **Molecules**, v. 21, n. 2, p. 1–9, 2016. Available at: <http:// doi.org/10.3390/molecules21020145>.

WANG, Bingqiao *et al*. One-Step Regioselective Synthesis of Benzofurans from Phenols and α–Haloketones. **Molecules**, v. 24, p. 2187, 2019. Available at: <http://doi.org/10.3390/molecules24112187>.

WANG, Jilei *et al*. Paeonol Derivatives and Pharmacological Activities: A Review of Recent Progress. **Mini-Reviews in Medicinal Chemistry**, v. 20, n. 6, p. 466–482, 2019. Available at: <http://doi.org/10.2174/1389557519666191015204223>.

W.H. PERKIN, F.R.S. XXIX.-On some new bromine derivatives of coumarin**. Journal of the Chemical Society**, v. 23, p. 368-371. Available at: <https://doi.org/10.1039/JS8702300368>.

WEI, Meng-Xue *et al*. Synthesis of artemisinin-piperazine-furan ether hybrids and evaluation of *in vitro* cytotoxic activity. **European Journal of Medicinal Chemistry**, v. 215, p. 113295, 2021. Available at: <https://doi.org/10.1016/j.ejmech.2021.113295>.

YAMAGUCHI, Miyuki *et al*. One-Pot Synthesis of Substituted Benzo[*b*]furans and Indoles from Dichlorophenols/Dichloroanilines Using a Palladium−Dihydroxyterphenylphosphine Catalyst. **The Journal of Organic Chemistry**, v. 81, p. 5450-5463, 2016. Available at: <https://doi.org/10.1021/acs.joc.6b00824>.

YAN, Binjun *et al*. Advancement in the chemical analysis of *Paeoniae Radix* (*Shaoyao*). **Journal of Pharmaceutical and Biomedical Analysis**, v. 160, p. 276–288, 2018. Available at: <https://doi.org/10.1016/j.jpba.2018.08.009>.

YANG, Tingting *et al*. Design, synthesis, and antitumor activity of novel paeonol derivatives containing the 1,4-benzoxazinone and 1,2,3-triazole moieties. **Journal of Chemical Research**, v. 48, n. 7–8, p. 241–247, 2019. Available at: <https://doi.org/10.1177/1747519819857479>.

YIN, Juan *et al*. Paeonol induces apoptosis in human ovarian cancer cells. **Acta Histochemica**, v. 115, n. 8, p. 835–839, 2013. Available at: <http://dx.doi.org/10.1016/j.acthis.2013.04.004>.

YIN, Wanying *et al*. Synthesis, anti-oomycete and anti-fungal activities of aminoguanidine derivatives of paeonol sulfonate. **Journal of Molecular Structure**, v. 1321, P. 4, p. 140085, 2024. Available at: <https://doi.org/10.1016/j.molstruc.2024.140085>.

YU, Lijuan *et al*. Synthesis and evaluation of acetylferulic paeonol ester and ferulic paeonol ester as potential antioxidants to inhibit fish oil oxidation. **Food Chemistry**, v. 365, n. June, p. 130384, 2021. Available at: <https://doi.org/10.1016/j.foodchem.2021.130384>.

ZHANG, Famin *et al*. Novel paeonol derivatives: Design, synthesis, and their activity in relieving idiopathic pulmonary fibrosis *via* the PIM1/p65 pathway. **Bioorganic Chemistry**, v. 163, p. 108731, 2025. Available at: <https://doi.org/10.1016/j.bioorg.2025.108731>.

ZHANG, Liang; LI, Deng chang; LIU, Li fang. Paeonol: pharmacological effects and mechanisms of action. **International Immunopharmacology**, v. 72, n. January, p. 413–421, 2019. Available at: <https://doi.org/10.1177/1747519819857479>.

ZHAO, Jin Feng *et al*. Novel effect of paeonol on the formation of foam cells: Promotion of LXRα-ABCA1 dependent cholesterol efflux in macrophages**. American Journal of Chinese Medicine**, v. 41, n. 5, p. 1079–1096, 2013. Available at: <https://doi.org/10.1142/S0192415X13500730>.

ZHENG, Guowei *et al*. Specialized metabolites from *Ageratina adenophora* and their inhibitory activities against pathogenic fungi. **Phytochemistry**, v. 148, p. 57-62, 2018. Available at: <https://doi.org/10.1016/j.phytochem.2018.01.013>.

ZHOU, An *et al*. Synthesis and Evaluation of Paeonol Derivatives as Potential Multifunctional Agents for the Treatment of Alzheimer's Disease. **Molecules**, v. 20, p. 1304-1318, 2015. Available at: <https://doi.org/10.3390/molecules20011304>.

ZHU, Junjie *et al*. New diphenyl ethers from a fungus *Epicoccum sorghinum* L28 and their antifungal activity against phytopathogens. **Bioorganic Chemistry**, v. 115, p. 105232, 2021. Available at: <https://doi.org/10.1016/j.bioorg.2021.105232>.

ZONG, Shi-yu *et al*. Study on the physicochemical properties and anti-inflammatory effects of paeonol in rats with TNBS-induced ulcerative colitis. **International Immunopharmacology**, v. 42, p. 32-38, 2017. Available at: <http://dx.doi.org/10.1016/j.intimp.2016.11.010>.

CHAPTER 2

Naphthoquinonynes in the development of trypanocidal quinones

2.1 INTROUCTION

2.1.1 Quinones:

Quinones constitute a class of compounds distinguished by their fully conjugated cyclic dione structures. As defined by the IUPAC, quinones are derived from aromatic compounds through the transformation of an even number of –CH= groups into carbonyl groups, accompanied by any requisite rearrangement of double bonds. This classification also encompasses polycyclic and heterocyclic analogs (IUPAC, 2012).

Quinones are further categorized based on the type of cyclic system from which their respective hydrocarbon precursors are derived. These include benzoquinones, naphthoquinones, anthraquinones, and phenanthraquinones (**Figure 16**), which are structurally related to benzene, naphthalene, anthracene, and phenanthrene ring systems, respectively (ASCHE, C. 2005; THOMSON, R.H. 1996).

Figure 16. Classification of quinones based on their hydrocarbon analogues.

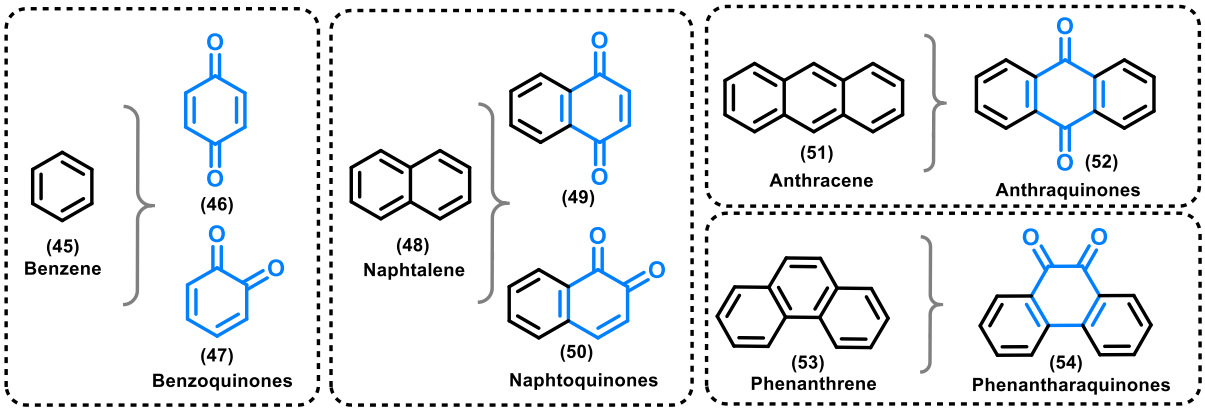

Although their definition and classification are straightforward, quinones represent a vast and diverse group of compounds found widely in nature. They are present in various sources, including plant species, bacteria, and marine organisms, among others. Quinones constitute an extensive series of natural products that play critical roles in biological processes of great importance (MORTON, R. A. 1966). Notable examples include Lawsone (JELLY, Renne *et al*., 2008), Juglone (SODERQUIST, Charles J. 1973), Lapachol, *α*-lapachone, and *β*-lapachone (DA SILVA JÚNIOR, Eufrânio N. *et al*., 2008), Thiaplidiaquinone A and B (AIELLO, Anna *et al*., 2005), Streptonigrin (NASIR, Naurah Nabihah *et al*., 2023), Doxorubicin (BLUM & CARTER, 1974), and Vitamin K1 (Phylloquinone) (BINKLEY, S. B. *et al*., 1939).

Figure 17 illustrates these examples, highlighting each quinone alongside representative natural sources where they can be found. Many of these quinones exhibit significant biological activity.

Figure 17. Examples of quinones and their representative natural sources.

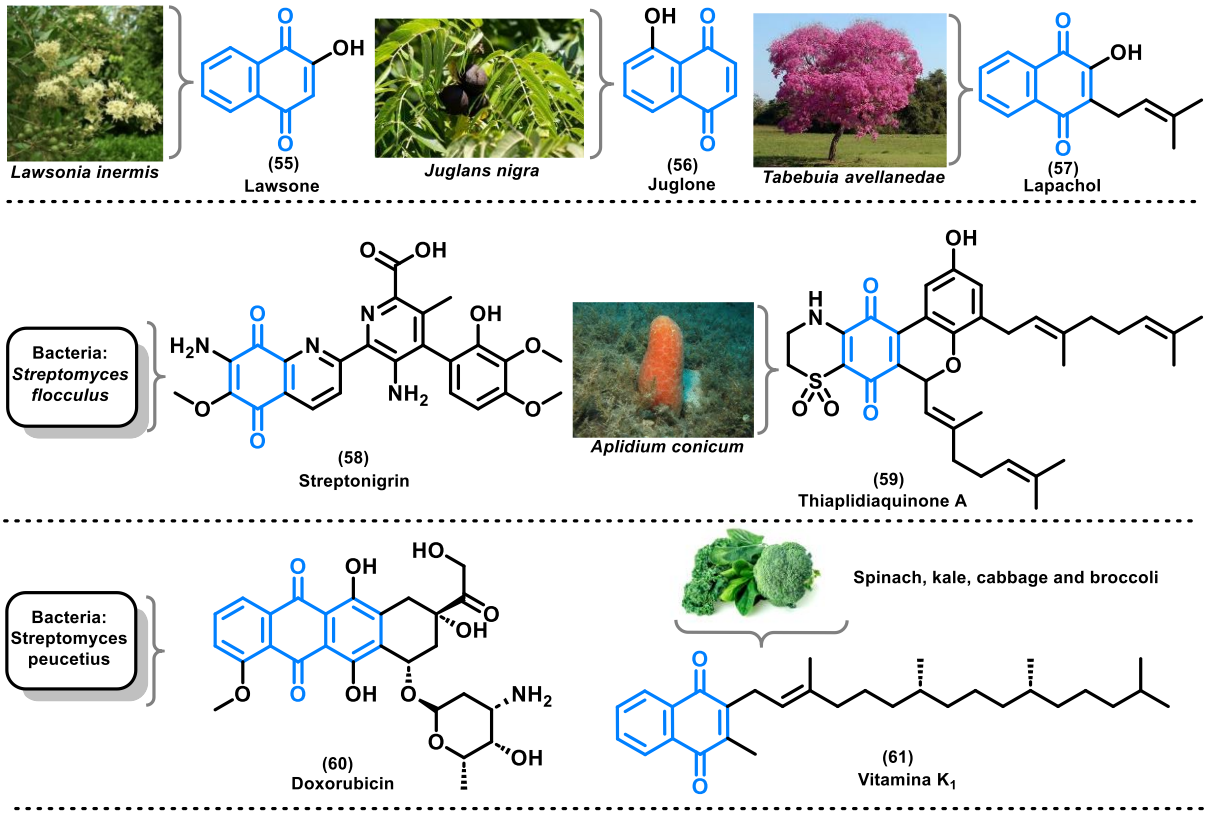

Owing to their distinctive electronic properties, particularly their capacity for electron and proton transfer (PRICE & DRIESSEN, 2010), the quinone moiety is a fundamental component in diverse scientific fields, including organic chemistry (THOMSON, R. H. 1996), materials science (JESIONOWSKI, KLAPISZEWSKI & MILCZAREK, 2014), redox-flow battery and energy applications (JONES, Alexandra E. *et al*., 2022), fluorescence (KERN, Dóra *et al*., 2024) and chemiluminescence fields (EL-MAGHRABEY, Mahmoud *et al*., 2021), and medicine (KOYAMA, Junko 2006), among others.

Quinones are mainly significant due to their diverse biological activities. These compounds demonstrate a broad spectrum of pharmacological effects, such as antifungal and antibacterial (GAFNER, Stefan *et al*., 1996), antitumor (COELHO-CERQUEIRA, Eduardo *et al*., 2014), trypanocidal (DA SILVA JÚNIOR, Eufrânio N. *et al*., 2008), antiparasitic (GUIMARÃES, Tiago T. *et al*., 2013), anti-inflammatory (DE

ALMEIDA, Edvaldo R. *et al*., 1990), and anti-HIV (STAGLIANO, Kenneth W. *et al*., 2006) properties, to highlight some relevant properties.

Among the diverse derivatives derived from quinones, naphthoquinones stand out due to their notable biological potential. These compounds are widely distributed in nature, primarily functioning as pigments (LÓPEZ LÓPEZ, Lluvia Itzel *et al*., 2014). Their pronounced reactivity, combined with their inherent synthetic versatility, has positioned them as a focus of considerable interest in scientific research (DA SILVA JÚNIOR, Eufrânio N. *et al*., 2019).

Within the various naphthoquinones, beyond those previously discussed, Atovaquone, Parvaquone and Buparvaquone are notable for their clinical relevance. These compounds are of particular importance, as they are commercially available for the treatment of malaria (CHEN, Anan *et al*., 2024) and bovine theileriosis (RASHID, Muhammad *et al*., 2024), respectively (**Figure 18**).

Figure 18. Notable Examples of naphthoquinones: Atovaquone, Parvaquone, and Buparvaquone, along with their Biological tpplications.

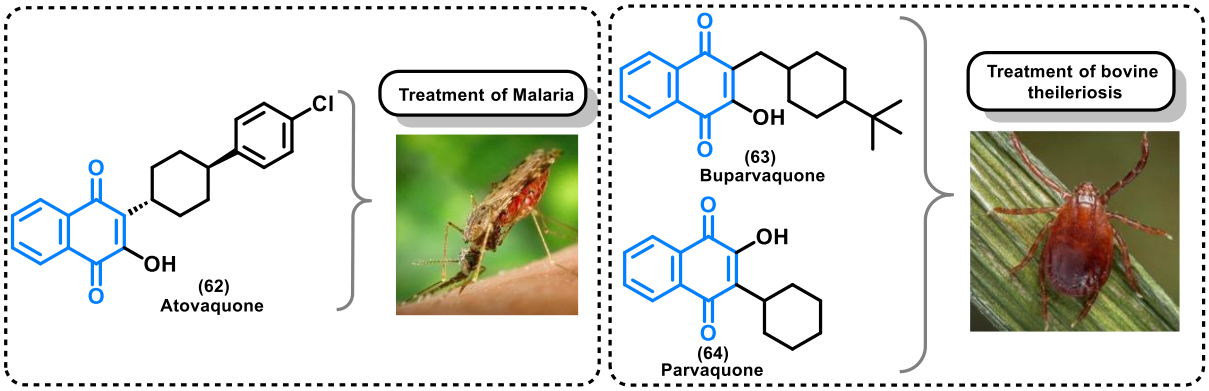

2.1.2 Naphthoquinone Derivatives:

The remarkable properties of naphthoquinones, combined with their facility for structural modifications and reactivity, highlight this class of compounds as a promising foundation for developing new derivatives with significant biological activities (DIAS, Gleiston G. *et al*., 2018).

As previously described, naphthoquinoidal compounds feature planar structures derived from naphthalene, consisting of an aryl group (**A-ring**) fused with a quinoidal unit (**B-ring**) and exhibiting diverse substitution patterns (GAULTIER & HAUW, 1965). More complex molecules based on naphthoquinones can be

synthesized from 1,4-naphthoquinone by introducing modifications to either the A-ring or the B-ring (**Scheme 15**) (JARDIM, Guilherme A.M. *et al*., 2017).

The B-ring of 1,4-naphthoquinone derivatives allows a wide range of modifications, including halogenation (SU, Jinling *et al*., 2019), methylation and alkylation (NASIRI, Hamid Reza *et al*., 2013), and acylation (DUMANSKA, Yuliia *et al*., 2013). Similarly, functionalization of the A-ring encompasses transformations such as C–H iodination (JARDIM, DA SILVA & BOWER, 2016), hydroxylation (DIAS, Gleiston G. *et al*., 2018), organothiolation (JARDIM, Guilherme A. M. *et al*., 2018), selenation (JARDIM, Guilherme A. M. *et al*., 2019), and alkenylation (DIAS, Gleiston G. *et al*., 2018) *et al*., 2019). **Scheme 15** highlights the most notable examples of these transformations and functionalizations derived from simple 1,4-naphthoquinone.

Scheme 15. Notable Examples of Distinguished Derivatives of 1,4-naphthoquinone.

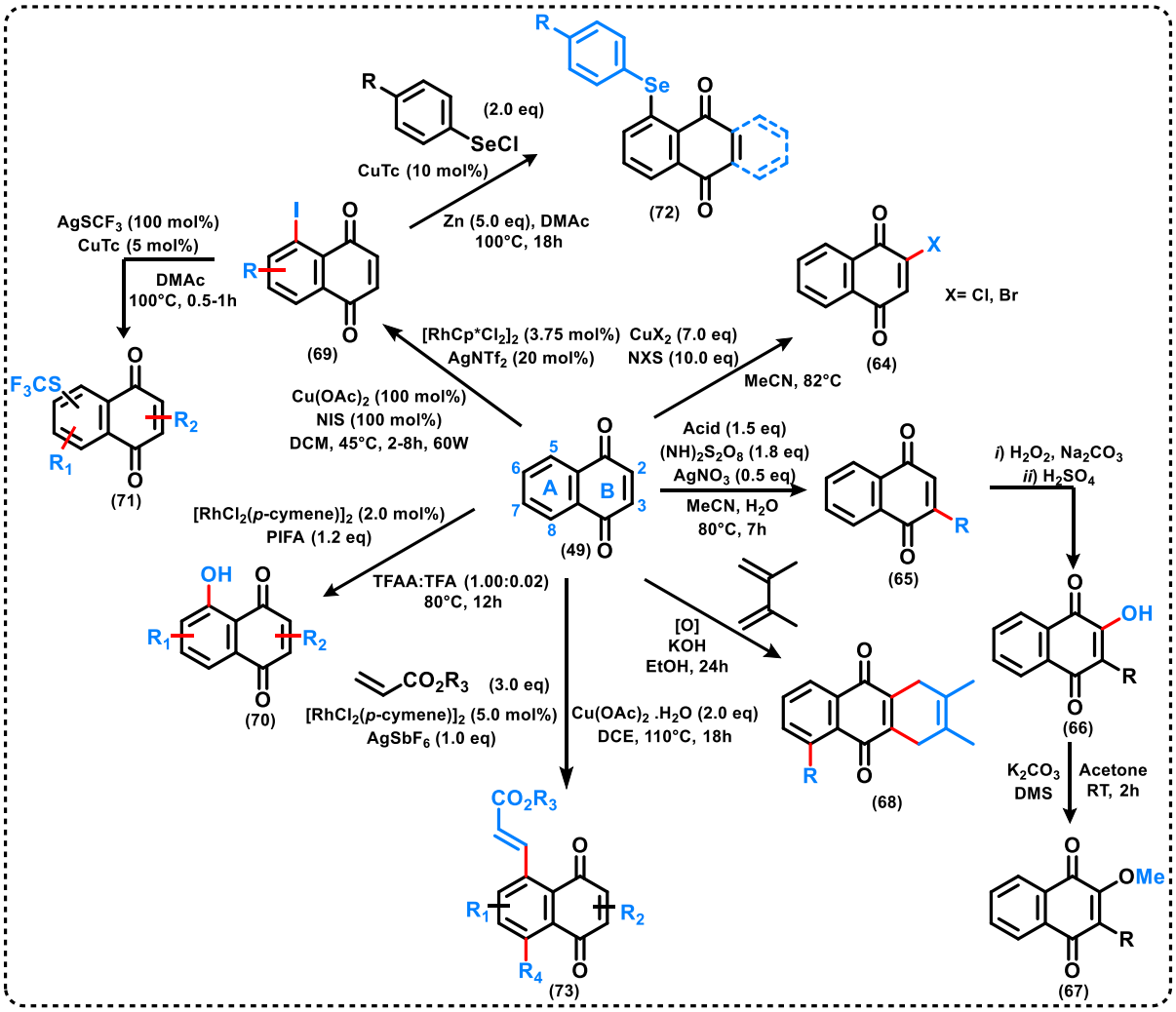

Da Silva Júnior Research Group has developed several strategies for the selective functionalization of the benzenoid A-ring at the C-5 position. While numerous well-established methods exist for functionalizing the naphthoquinoidal B-ring, further exploration of approaches targeting the A-ring remains a significant area of interest. In this context, recent advancements include the Ru-catalyzed C–H alkenylation reported by DE OLIVEIRA, Joyce *et al*., 2024 and methods for the generation and *in situ* capture of naphthoquinonynes described by DE CARVALHO, Renato *et al*., 2024. These methodologies enable polyfunctionalization at the C-5, C-6, and C-7 positions, as illustrated in **Scheme 16**.

Scheme 16. Latest Advances in A-Ring Functionalization of 1,4-Naphthoquinones.

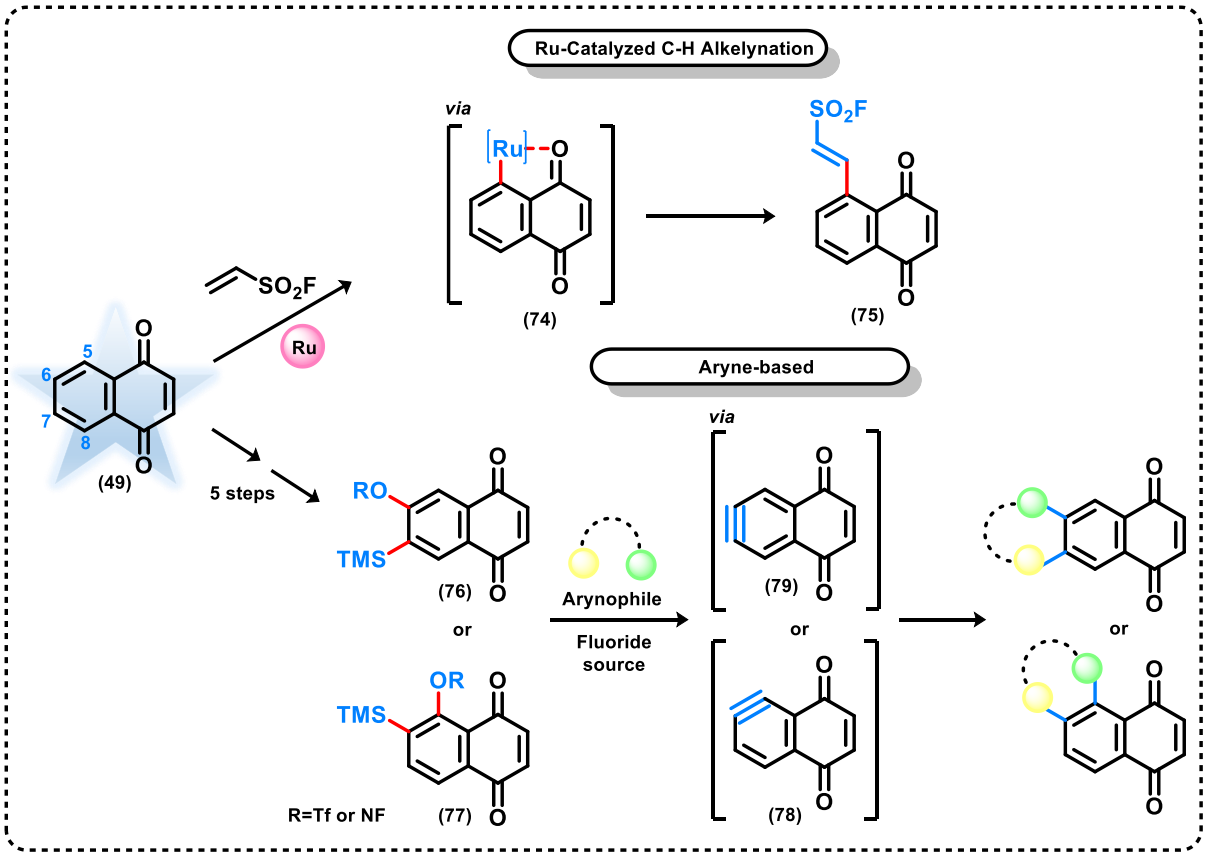

The search for highly bioactive molecules has driven the exploration of less-studied substitutions, particularly at positions 6 and 7 on A-ring. Investigating these substitutions remains crucial, as it expands the potential for novel functionalizations and broadens the scope of possibilities in molecular design.

2.1.3 Chagas Disease and the Role of Quinones in its Therapy:

Neglected tropical diseases (NTDs) encompass a group of 20 illnesses that disproportionately impact the poorest populations in tropical and subtropical regions (BELTRAN-HORTELANO, Iván *et al*., 2020). Among these is Chagas disease (CD), also referred to as American trypanosomiasis. This century-old disease was first described in 1909 and named in honor of Carlos Chagas, a Brazilian physician and researcher who discovered it (CHAGAS, Carlos, 1909).

CD is a parasitic infection and potentially life-threatening illness caused by the protozoan *Trypanosoma cruzi* (*T. cruzi*), which belongs to the class *Kinetoplastida* and the family *Trypanosomatidae* (FREIRE, Elainne Silva *et al*., 2025). The primary mode of transmission is through the feces of infected insects from the subfamily *Triatominae*. Endemic to 21 countries in Latin America, it places 70 million people at risk, resulting in approximately 30,000 new cases and 12,000 deaths annually (BÁRCENAS-IRABIÉN, Alejandra Gabriela *et al*., 2024). Globally, an estimated six to seven million people are currently infected (PEREIRA & NAVARRO, 2013).

Throughout its complex life cycle, *T. cruzi* transitions through three main stages: the epimastigote (the proliferative form in insect vectors), the amastigote (the proliferative form within vertebrate host cells), and the trypomastigote (the infective form) (BELTRAN-HORTELANO, Iván *et al*., 2020). **Figure 19** provides a detailed depiction of the parasite's life cycle.

CD typically progresses through two distinct stages: an acute phase lasting approximately two months following infection and a chronic phase that can persist throughout the patient’s lifetime (BEZERRA & NETO, 2010). The acute phase is characterized by high parasitemia and is often asymptomatic or presents with a range of nonspecific clinical manifestations. The most common symptoms include viral-like signs such as fever, malaise, and lymphadenopathy. During this phase, the high concentration of parasites circulating in the bloodstream allows for their detection using various diagnostic methods (NUNES, Maria Carmo P. *et al*., 2024). If left untreated, the disease progresses to a silent chronic phase, which may remain asymptomatic for years or decades before leading to severe complications involving the heart, digestive system, or nervous system (CÓRDOVA, Ezequiel *et al*., 2010). Chronic phase of CD is therefore considered a major contributor to the significant morbidity and mortality associated with the infection (BELTRAN-HORTELANO, Iván *et al*., 2020).

Figure 19. Life Cycle of *T. cruzi*: The Vector Phase (Red) and Host Phase (Blue).

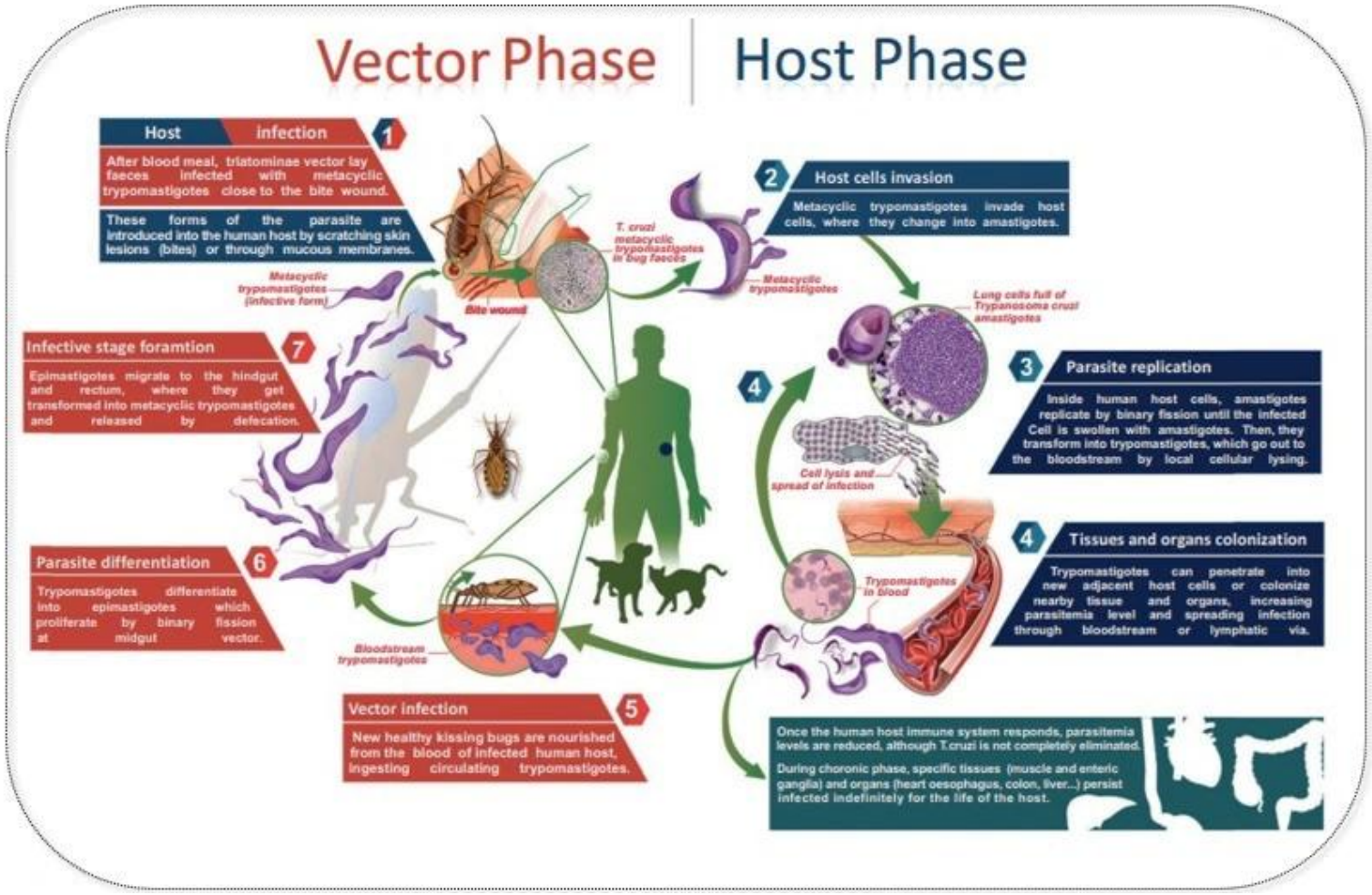

Reproduced from BELTRAN-HORTELANO, Ivan; PEREZ-SILANES & GALIANO, 2017.

Since the 1970s, several new compounds have been introduced for the treatment of Chagas disease. Two of the most notable are nitrofurfurylidene [(*R,S*)-3-methyl-N-[(1*E*)-(5-nitro-2-furyl)methylene]thiomorpholin-4-amine 1,1-dioxide], known as Nifurtimox (NF), and the nitroimidazole derivative *N*-benzyl-2-nitro-1-imidazoleacetamide, known as Benznidazole (BNZ) (RIBEIRO, Vanessa *et al*., 2020) (**Figure 20**).

Figure 20. Timeline showing the history of Chagas disease treatment.

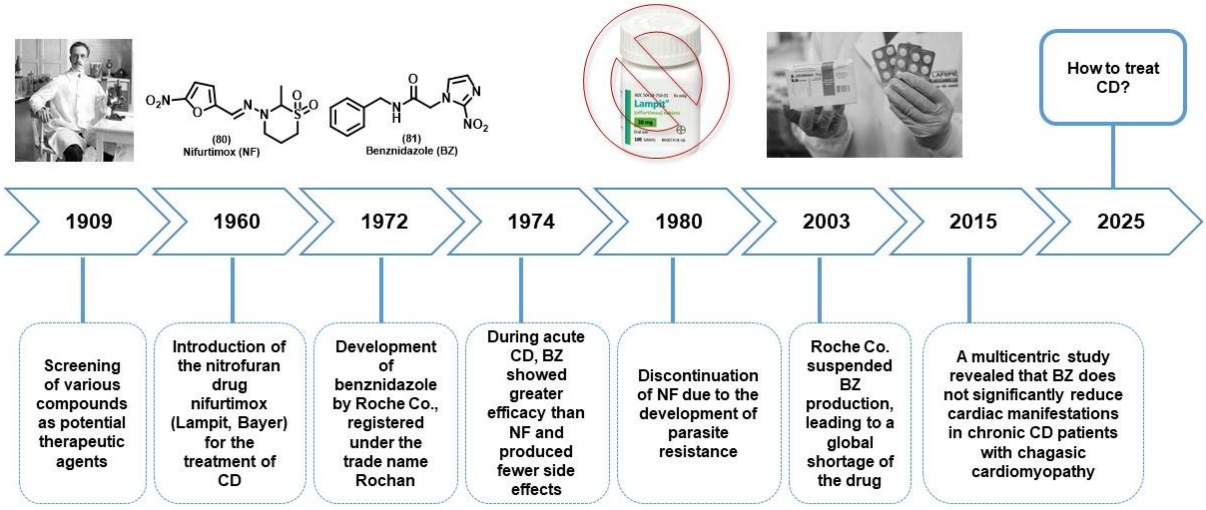

NF and BNZ are most effective during the acute phase of CD (CALDAS, Ivo Santana *et al*., 2008) (**Figure 21**). However, their use is associated with several disadvantages, including prolonged treatment durations, significant side effects, and variable efficacy (PINAZO, Maria Jesus *et al*., 2024).

Figure 21. Antiparasitic Agents Used in the Treatment of CD.

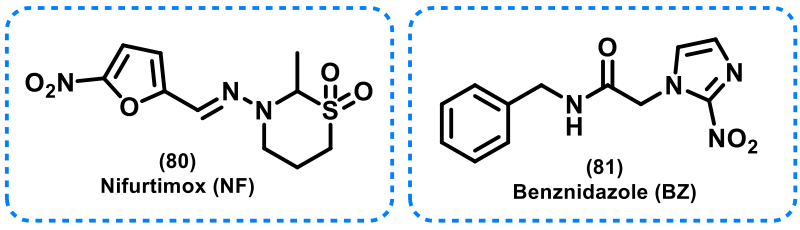

The primary challenge in developing new treatments for *T. cruzi* lies in its nature as an intracellular parasite. It depends on the host cell's metabolism to replicate, producing hundreds of new parasites that are released upon cellular rupture, subsequently infecting surrounding tissues (ALVES & COLLI, 2007).

Recent advances in the development of novel classes of anti-trypanosomal agents are highly promising. Within this framework, natural products represent a vital

resource for the discovery of new pharmacologically active compounds for the treatment of parasitic diseases (SUTO, Yutaka *et al*., 2015).

Within this framework, quinoidal compounds are among one of the most promising classes of molecules with trypanocidal activity (COURA & DE CASTRO, 2002). As previously discussed, quinones function as electron transfer agents in bio-oxidation-reduction reactions. Consequently, quinonoid substances are expected to interfere with and disrupt the mitochondrial electron transport chain of *T. cruzi* parasites. This mechanism likely underlies the broad-spectrum antiprotozoal activity of these compounds, as respiratory inhibition alone can result in parasite death (HUDSON, A.T. 1993).

Scheme 17 illustrates the redox cycling of quinones. The process begins with the enzymatic reduction of quinones, leading to the formation of reactive semiquinone radicals. Enzymes such as NADPH–cytochrome P450 reductase, NADPH–cytochrome b5 reductase, and NADPH–ubiquinone oxidoreductase catalyze this reduction by facilitating electron transfer and driving the overall process (BANDYOPADHYAY, DAS, & BANERJEE, 1999). The resulting semiquinone radical anions can be particularly harmful to cells because of their ability to catalytically generate hydrogen peroxide within biological environments through continuous redox cycling (SOUZA & ANDRADE, 2016).

Scheme 17. Schematic Representation of 1,4-Naphthoquinone Metabolism, Redox Cycle, and Reactive Species Production.

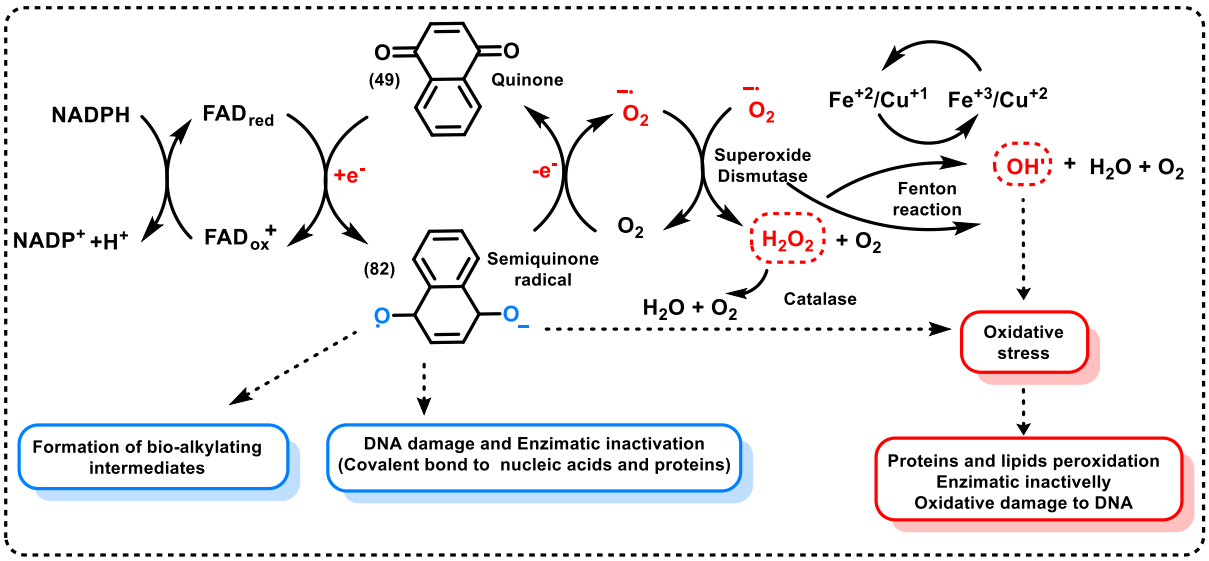

Own elaboration based on SOUZA & ANDRADE, 2016.

During this cycle, reactive oxygen species (ROS) are generated following the reduction of molecular oxygen (O_2) to form superoxide anions ($O_2^{\bullet -}$). These ROS also produce free radicals, such as hydroxyl radicals (OH•), which interact with the mitochondrial respiratory chain and contribute to oxidative stress. The resulting oxidative damage affects essential cellular components, including DNA, proteins, and lipids, further exacerbating cellular dysfunction (SIES & JONES, 2020).

As mentioned, the growing interest in naphthoquinones arises from their ability to form covalent bonds with biological targets and function as electron transfer agents in bio-oxidation-reduction reactions and their capacity to induce oxidative stress in cells through the generation of reactive oxygen species (KUMAGAI, Yoshito *et al*., 2012).

Most of the naphthoquinone derivatives discussed here have been evaluated for their trypanocidal activity, with numerous recent studies highlighting their potential. For instance, a structure–activity relationship study on quinone compounds with trypanocidal properties was conducted by MOLFETTA, F.A. *et al*., 2005 (**Figure 22**).

Figure 22. Chemical structure of the quinone compounds studied in MOLFETTA, F. A. *et al*., 2005 study.

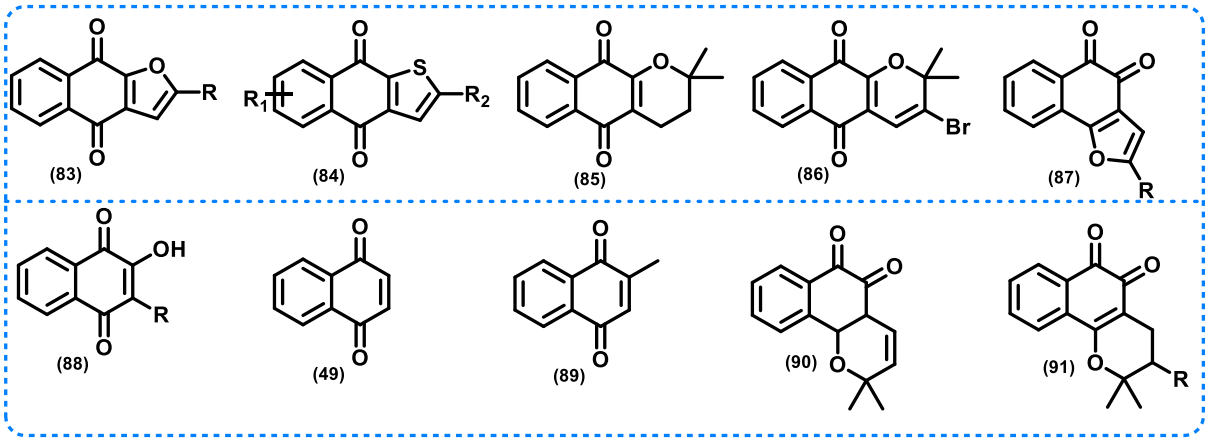

Additionally, quinone derivatives have been extensively investigated as inhibitors of multiple *T. cruzi* targets (BELTRAN-HORTELANO, Iván *et al*., 2022). A particularly notable example is the study by SUTO, Yutaka *et al*., 2015, which evaluated komaroviquinone as an anti-*Trypanosoma cruzi* agent and reported promising results. The study determined that the quinone moiety of komaroviquinone plays a crucial role in its antitrypanosomal activity, whereas the complex fused cyclic structure is not necessarily required for its biological effect.

2.1.4 Aryne Chemistry:

Arynes are a class of transient species widely regarded as some of the most reactive intermediates in organic chemistry (SHI, LI & LI, 2021). First proposed over a century ago (STOERMER & KAHLERT, 1902), these highly strained and short-lived unsaturated hydrocarbons have become indispensable tools in the field due to their exceptional reactivity and versatility (YOSHIDA & TAKAKI, 2012) (BIJU, Akkattu T. 2021).

The exploration of arynes as reactive intermediates has been particularly valuable for the synthesis of 1,2-disubstituted benzene derivatives, as well as various benzo-fused carbocycles and heterocycles. This approach has demonstrated notable advantages, especially for the preparation of compounds whise synthesis is challenging and inefficient through conventional methods (GAMPE & CARREIRA, 2012).

Over the past seven decades, arynes have attracted considerable attention from chemists, leading to an extensive body of literature dedicated to their study. In recent years, several novel reactions involving arynes have been reported, providing new opportunities for the synthesis of structurally complex and diverse compounds (HOFFMANN & SUZUKI, 2013). **Figure 23** presents an overview of the number of studies on arynes published every half-decade since 1960. Notably, the data reveal a sharp increase in the number of publications over the past years, underscoring the growing interest and advancements in aryne chemistry (YOSHIDA & HOSOYA, 2015).

Figure 23. Number of Publications on Arynes Published per Half-Decade Since 1960.

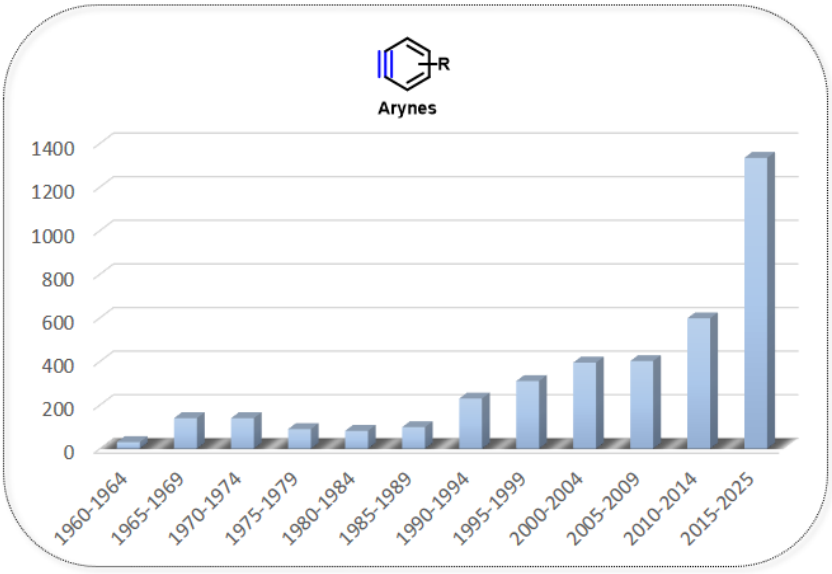

Due to their inherent instability, arynes cannot be directly isolated and must instead be generated *in situ* from appropriate precursors (YOSHIDA & HOSOYA, 2015). The historical development of benzyne precursors, from the earliest reports to the end of the 20th century, is summarized in **Figure 24**. This timeline begins with the structural assignment of benzyne by Roberts and Huisgen in 1953 (ROBERTS *et al*, 1953) (HUISGEN & RIST, 1954), followed by the exploitation of organic reactions by Wittig in 1956 (WITTIG & POHMER, 1956). Subsequent key advancements include the introduction of *o*-silylaryl triflates by Kobayashi in 1983 (HIMESHIMA, SONODA & KOBAYASHI, 1983) and *o*-iodoaryl triflates by Suzuki in 1991 (MATSUMOTO, Takashi *et al*., 1991), both of which remain among the most widely recognized and utilized benzyne precursors.

Figure 24. Chronological Overview of Representative Benzyne Precursors.

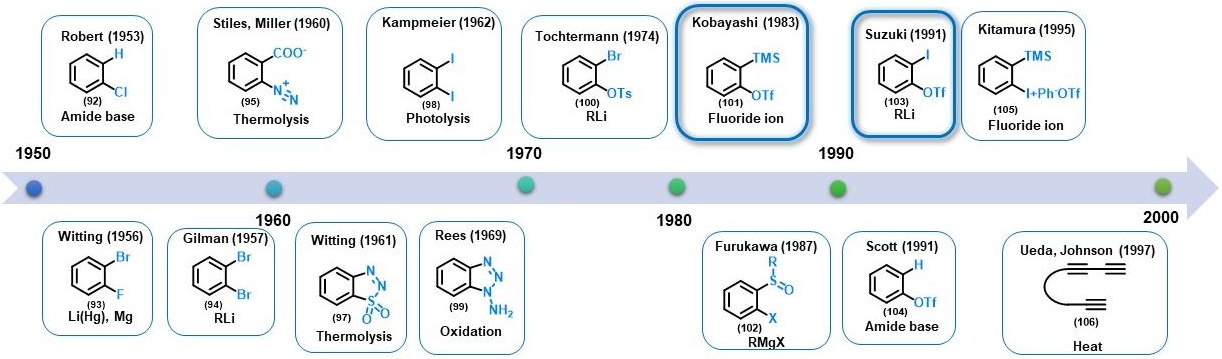

Diverse strategies have been developed for the synthesis of arynes. Among the most prominent are those that involve the generation of aryl anion species, which can be achieved through several distinct pathways (**Scheme 18**) (TAKIKAWA, Hiroshi *et al*., 2018):

a) *β*-elimination of aryl halides in the presence of a base;
b) halogen–metal exchange, followed by elimination from aryl halides bearing *o*-leaving groups;
c) fluoride-promoted desilylation of aryl trimethylsilanes, accompanied by elimination of an *o*-leaving group;
d) thermal decomposition of benzenediazonium-2-carboxylates;
e) reactions relying on thermally induced retro-cycloaddition processes;
f) intramolecular hexadehydro-Diels–Alder (HDDA) reaction of triyne precursors.

Scheme 18. Most Significant Approaches to Aryne Generation.

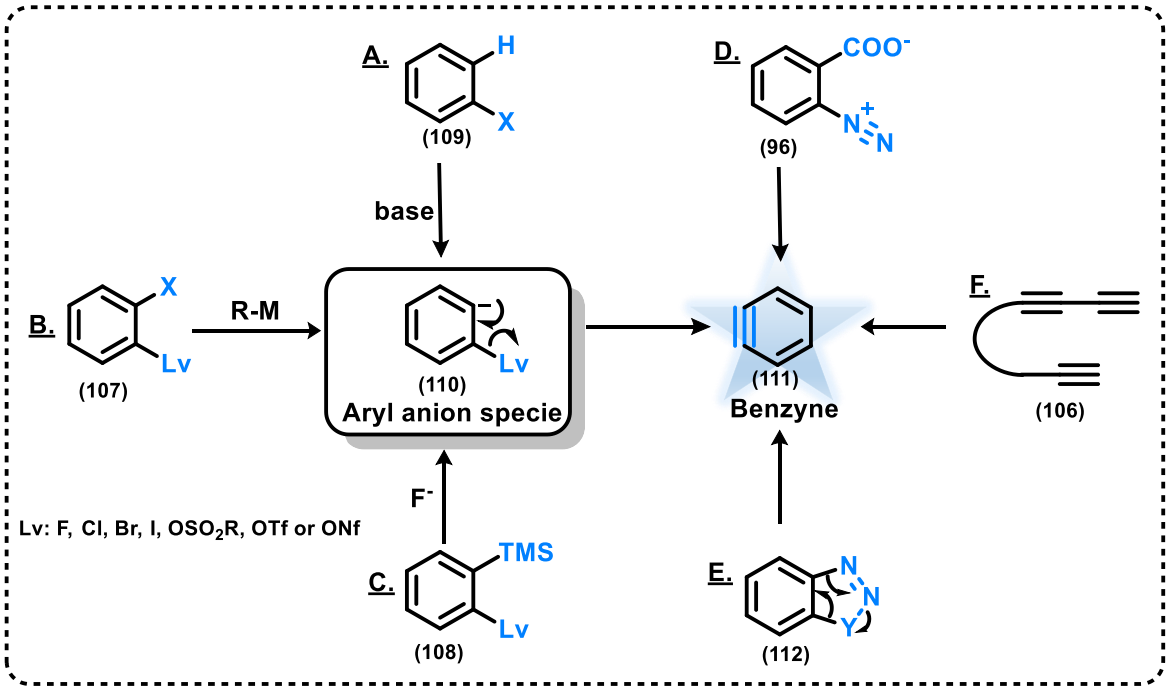

Arynes can be classified through various approaches, with one of the most common being based on their chemical structure. They can be categorized based on the position of the dehydrogenation, including *o*-arynes (e.g., *o*-benzynes, which may be substituted, annelated, or heterocyclic), *m*-arynes (e.g., *m*-benzynes, substituted or annelated *m*-pyridynes, and didehydroaryl cations), *p*-arynes (e.g., *p*-benzynes and enediynes), and other related species (e.g., benzdiynes and tridehydrobenzenes) (WENK, WINKLER & SANDER, 2003). **Figure 25** illustrates the most studied examples to date.

Figure 25. Key Structural Patterns of Arynes.

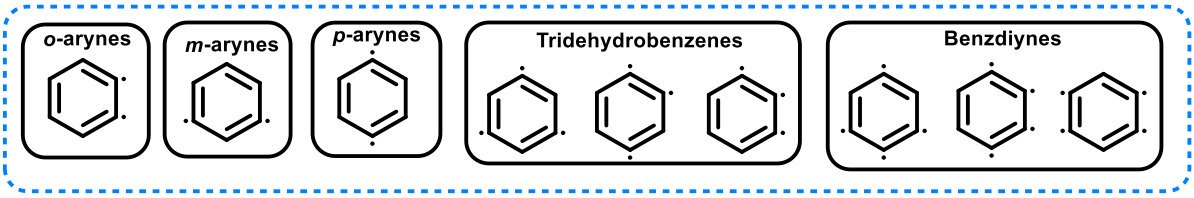

The most widely studied aryne intermediates are benzynes; however, other aryne species display diverse and unique reactivities (**Figure 26**). Notable examples include cycloalkynes, such as cyclohexyne, cyclopentyne, as well as naphthalynes, piperidyne and pyridynes derivatives (BROWN & BUSZEK, 2012). Additionally, heteroarynes derived from five-membered heterocyclic systems, including 3,4-

pyrrolyne and indolyne derivatives (BRONNER, BAHNCK & GARG, 2009) (GAMPE & CARREIRA, 2012).

Figure 26. Various Types of Aryne Intermediates.

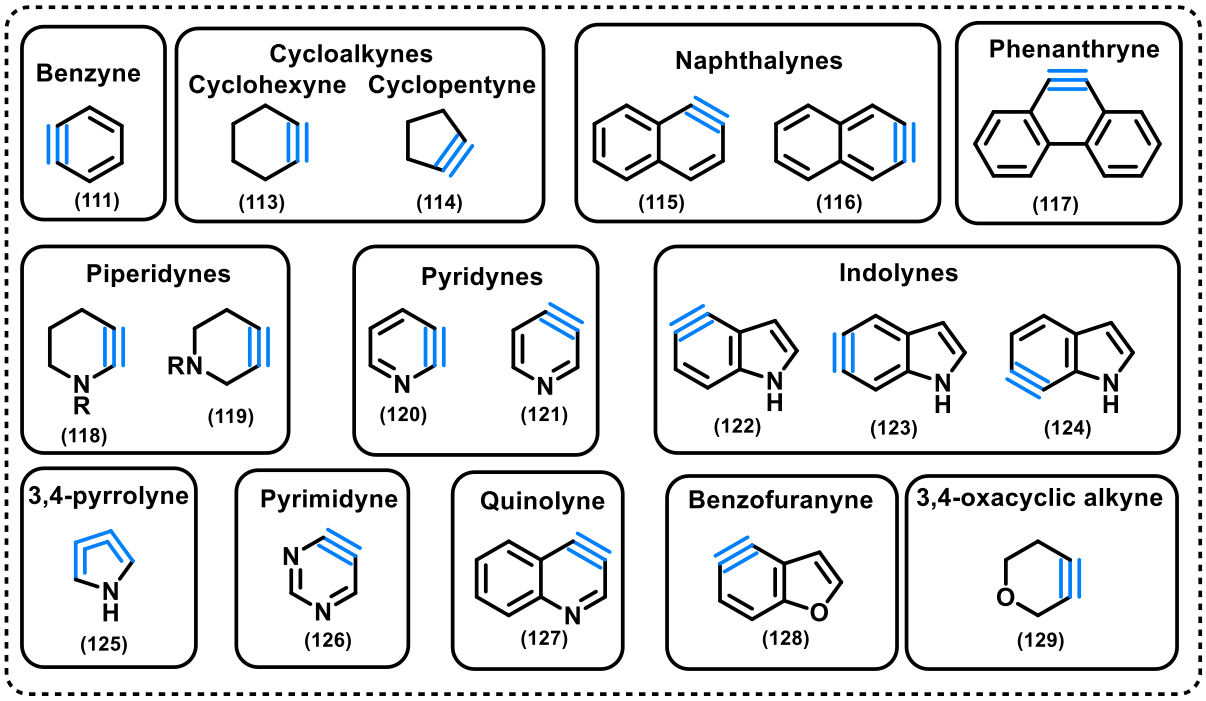

Historically, arynes were considered merely reactive intermediates; however, what was once a scientific curiosity has now evolved into a powerful tool for synthetic chemistry (WU & SHI, 2013). Arynes have proven to be highly versatile reagents, enabling the synthesis of numerous privileged heterocycles. Their exceptional reactivity has also led to an increasing number of strategic applications in total synthesis (PELLIESER & SANTELLI, 2003). **Scheme 19** illustrates these reactions.

Reactions involving arynes can be broadly categorized into three main groups:

- Pericyclic reactions, which include Diels–Alder reactions (both inter- and intramolecular), [2+2] cycloadditions, dipolar cycloadditions, and ene reactions.
- Nucleophilic additions to arynes occur when arynes readily react with a broad spectrum of nucleophiles, resulting in the formation of an aryl anion intermediate. This intermediate can then be captured by a proton, an external electrophile, or an internal electrophile. Some examples of such reactions include: arylation (LIU & LAROCK, 2005), multicomponent reactions (YOSHIDA, Hiroto *et al*., 2004), and molecular rearrangements (CANT, Alastair A. *et al*., 2009).

- Transition metal-catalyzed reactions, with palladium-catalyzed transformations being the most extensively studied and widely utilized.

Scheme 19. Reactivity Patterns of Arynes: A Generalized Framework.

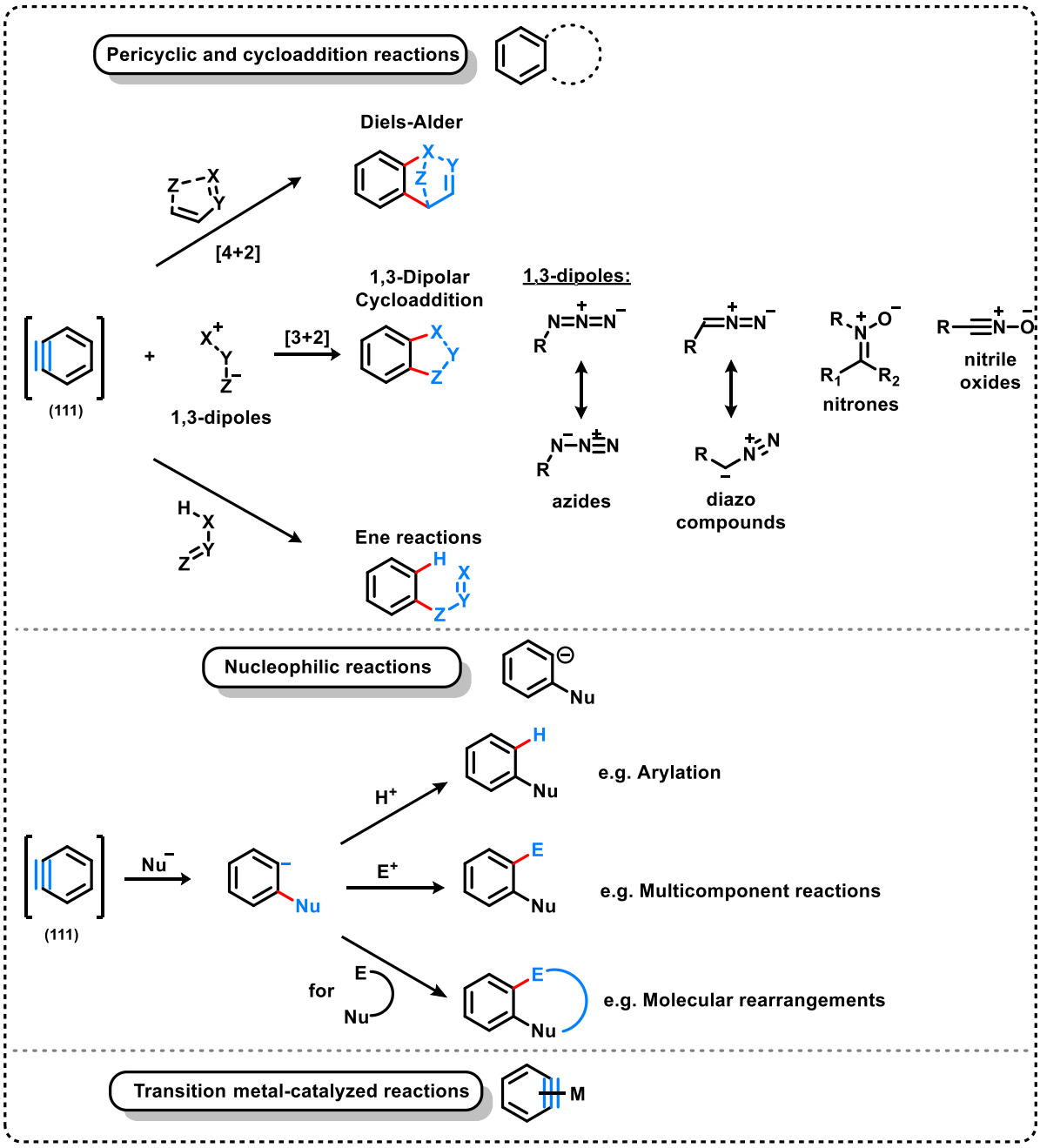

As previously demonstrated, varieties of aryne precursors have been reported. Among these, Kobayashi-type precursors (*o*-(trimethylsilyl)aryl triflates) have become the most widely used due to their straightforward synthesis from phenol derivatives and the mild conditions required for aryne generation, which do not necessitate low temperatures (IKAWA, Takashi et al., 2011). A comparison with Suzuki-type

precursors (*o*-iodoaryl triflates) highlights their significantly greater adoption, as evidenced by a higher number of studies published from 1980 to 2014 (YOSHIDA & HOSOYA, 2015) (**Figure 27**).

Figure 27. Number of Publications: A Comparison of Kobayashi-type precursor (blue) and Suzuki-type precursors (orange).

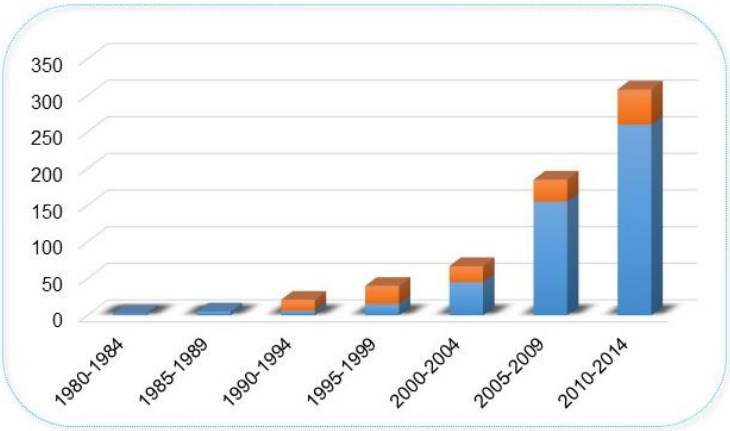

The Kobayashi method stands out from other approaches to aryne generation by leveraging the high affinity of fluoride ions for silicon and the ease with which the aryl anion is formed *in situ*. This process concludes when the aryl anion formed intramolecularly eliminates the leaving group, which can be triflate (Tf), imidazolylsulfonates (SO_2Im) (KOVÁCS, Szabolcs *et al*., 2012), iodine (I_2) (CROSSLEY, James A. *et al*., 2010), or nonafluorobutanesulfonyl (Nf) (IKAWA, Takashi *et al*., 2011), among others (**Scheme 20**). A major advantage of the Kobayashi route is its ability to control the rate of benzyne generation by adjusting the concentration of fluoride ions in the reaction solution (DUBROVSKIY, MARKINA & LAROCK, 2013).

Scheme 20. Benzyne Generation *via* the Kobayashi Method.

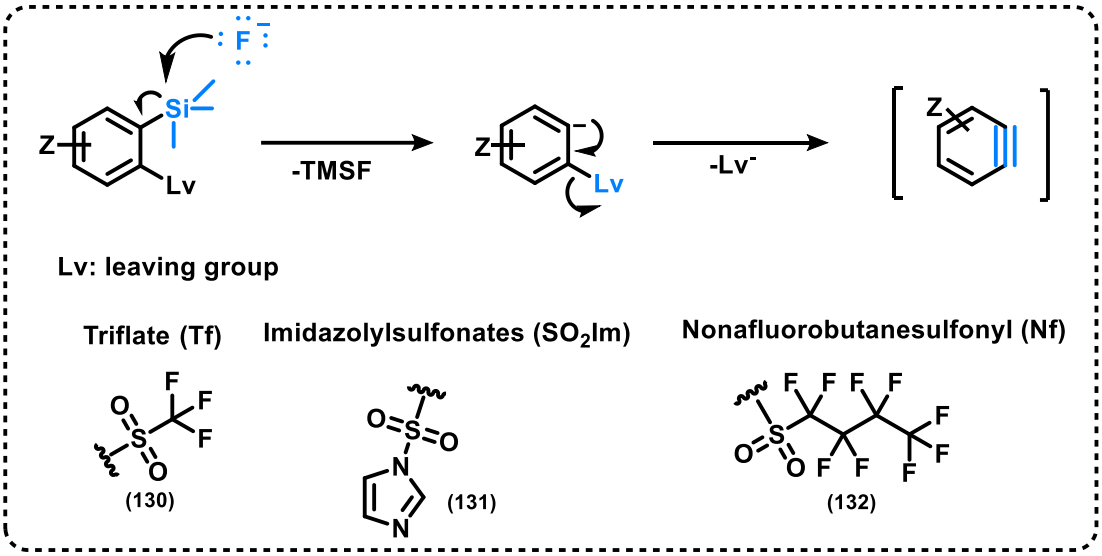

An important aspect to consider in aryne chemistry is regioselectivity. Achieving a high degree of regioselectivity in aryne reactions is crucial for their practical application. To date, various rules and protocols have been developed to control regioselectivity in intermolecular aryne transformations, including steric effects, ring strain, and electronic factors. Conversely, intramolecular aryne reactions typically exhibit *o*-selectivity in annulation processes (**Figure 28**) (SHI, LI & LI, 2021). Recently, Garg, Houk, and their collaborators introduced a distortion/interaction model for aryne transformations, which provides valuable insights into how electronic factors influence the regioselective control of these reactions (BICKELHAUPT & HOUK, 2017).

Figure 28. Factors Influencing Regioselectivity: Arrow Denotes the Preferred Site of Attack.

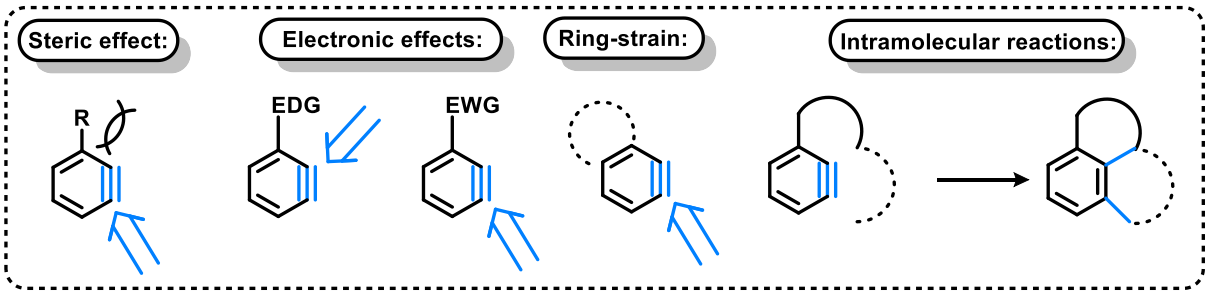

The application of aryne chemistry expands the scope for synthesizing a wide variety of compounds, offering potential utility in areas such as natural product synthesis (TADROSS & STOLTZ, 2012) (GAMPE & CARREIRA, 2012), heterocycle construction (GOETZ; GARG, 2014), and materials science (DARZI, BARBER &

GARG, 2019). This versatility is exemplified by the synthetic examples illustrated in **Figure 29** (MCVEIGH, Matthew S. *et al*., 2020).

Figure 29. Compounds synthesized using aryne chemistry. Aryne derived moieties are shown in blue.

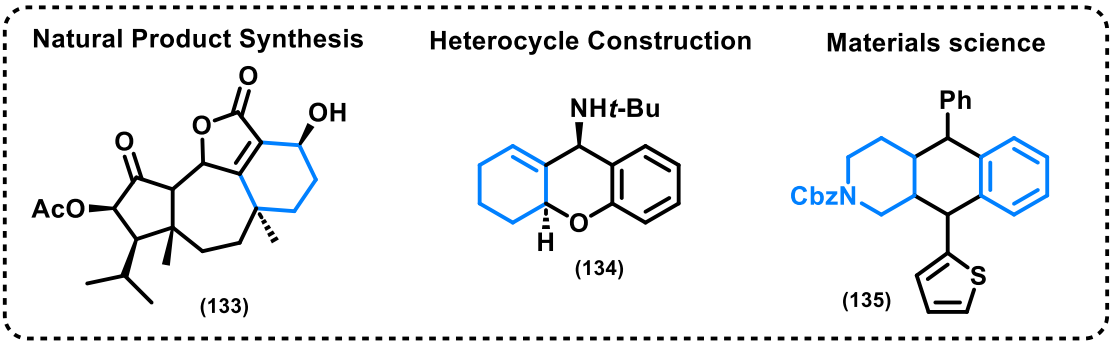

Regarding the background of aryne chemistry and its connection to quinones, one notable compound is 2,3-didehydro-1,4-benzoquinone, a quinoid didehydrobenzene analogue. This molecule has been investigated both theoretically by Cramer *et al*. (CRAMER, Christopher J. 1999), and experimentally using negative-ion photoelectron spectroscopy (NIPES) by Davico *et al* (DAVICO, Gustavo E. *et al*., 1999). Additionally, it is important to highlight the use of anthraquinone bisketene in the first observation of *p*-benzyne, reported by Chapman *et al*. in 1976 (CHAPMAN, CHANG & KOLC, 1976). These two quinones are depicted in **Figure 30** (WENK, WINKLER & SANDER, 2003).

Figure 30. Exploring the Background of Aryne Chemistry: Two Cases Linking It to Quinones.

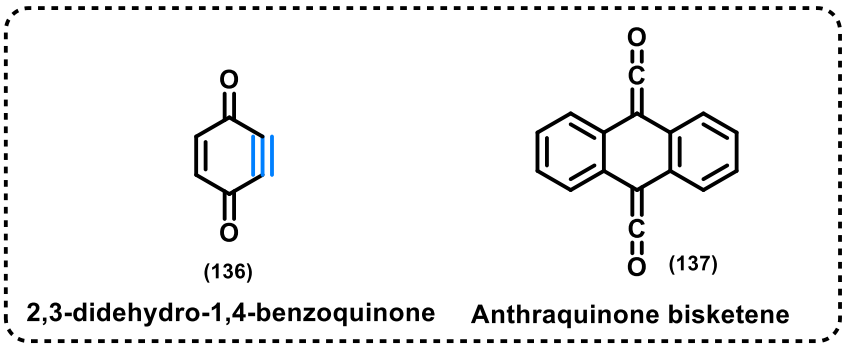

Thus far, only one study has been reported on the development and application of aryne chemistry in naphthoquinones to generate and trap quinonyl intermediates. This research, conducted by our group, represents the first systematic exploration of the synthesis and reactivity of naphthoquinonynes (DE CARVALHO, Renato *et al*.,

2024). This work underscores the importance of further investigating the potential of naphthoquinonynes.

2.2 RESEARCH PURPOSE

The purpose of this research is to implement a robust aryne-based methodology to enable the direct functionalization of the benzenoid ring of 1,4-benzoquinones at the C6–C7 positions by generating and trapping aryne intermediates *in situ*. The resulting library of functionalized benzoquinones will be subjected to biological evaluation against *Trypanosoma cruzi*, with the aim of identifying compounds with promising pharmacological profiles and contributing to ongoing efforts in Chagas disease drug discovery.

This work will employ a methodology that has already been optimized and successfully applied within the Eufrânio Lab research group. The approach is simple, provides efficient access to the target compounds, and allows for straightforward purificatio

2.2.1 General Objective:

The general objective of this research is to develop an innovative methodology for the direct functionalization of the benzenoid ring (ring A) of 1,4-benzoquinones at the 6- and 7-positions *via in situ* generation and subsequent trapping of aryne intermediates with a broad range of arynophiles. Furthermore, the project seeks to assess the medicinal potential of the newly synthesized derivatives as promising candidates for the treatment of Chagas disease.

2.2.2 Specific Objectives:

- Development of a synthetic route for the introduction of aryne precursor into the 6- and 7-positions of the 1,4-naphthoquinone framework.
- Synthesize a series of 1,4-benzoquinone derivatives selectively functionalized at C5–C7 *via* aryne precursor capture, introducing diverse substituents, including *N*-nucleophiles and pyridine *N*-oxide groups.
- Purifiy of all synthesized compounds using the most suitable chromatographic or crystallization techniques, according to their physical properties.

- Characterize and identification of all compounds through comprehensive spectroscopic and spectrometric analysis.
- Evaluate of the biological activity of the newly obtained derivatives against *Trypanosoma cruzi*, aiming at potential applications in Chagas disease therapy in collaboration with Rubem F. S. Menna-Barreto Laboratory of Cellular Biology, IOC, FIOCRUZ, Rio de Janeiro.

The general idea of the research proposal is illustrated in **Scheme 21**:

Scheme 21. General Research Purpose.

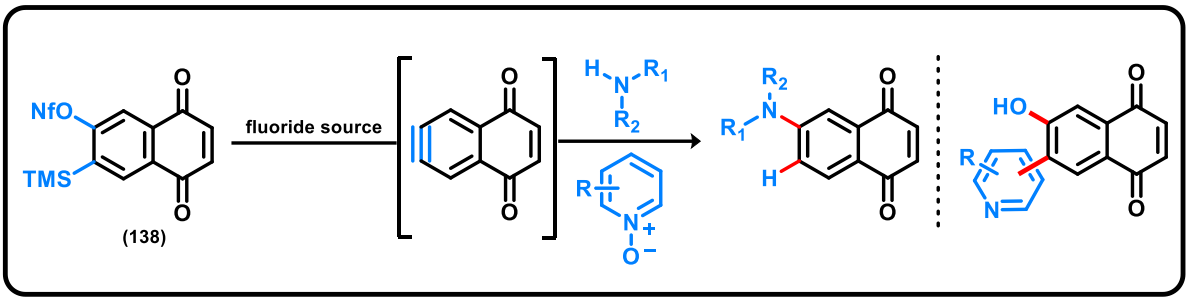

2.3 RESULTS AND DISCUSSION

2.3.1 Synthesis of the 6,7-Aryne Precursor:

This Kobayashi-type precursor was obtained in a high-yielding, six-step, five-pot sequence starting from 1,4-dimethoxynaphthalene (**139**), following a method previously developed in the Da Silva Júnior Lab Research group (DE CARVALHO, Renato *et al*., 2024). The synthesis begins with an iridium-catalyzed C–H borylation/oxidation at the C6 position of 1,4-dimethoxynaphthalene (**139**) to afford naphthol (**140**) with complete regioselectivity. Subsequent conversion to carbamate **141** enabled the introduction of a C7 trimethylsilyl group *via* directed lithiation. Upon completion of this step, $LiAlH_4$ reduction effected the removal of the carbamate, providing compound **142** in a one-pot process. Reaction of **142** with NfF yielded intermediate **143**, which was then oxidized using CAN to generate the target naphthoquinone **144**. This compound was found to be unstable upon prolonged storage and was therefore prepared as needed from the bench-stable precursor **143**. **Scheme 22** illustrates the complete synthetic route.

All compounds obtained throughout this synthetic sequence were fully characterized, and their spectroscopic data were consistent with those reported by DE

CARVALHO, Renato *et al*. (2024). The corresponding spectra and analytical data are provided in the Appendix and detailed in the Experimental Part. Using the 6,7-aryne precursor **138**, aryne capture reactions were subsequently carried out to synthesize a series of 1,4-benzoquinone derivatives bearing various substituents, including *N*-nucleophiles and pyridine *N*-oxide groups.

Scheme 22. Synthesis of 6,7-Aryne Precursor **138**.

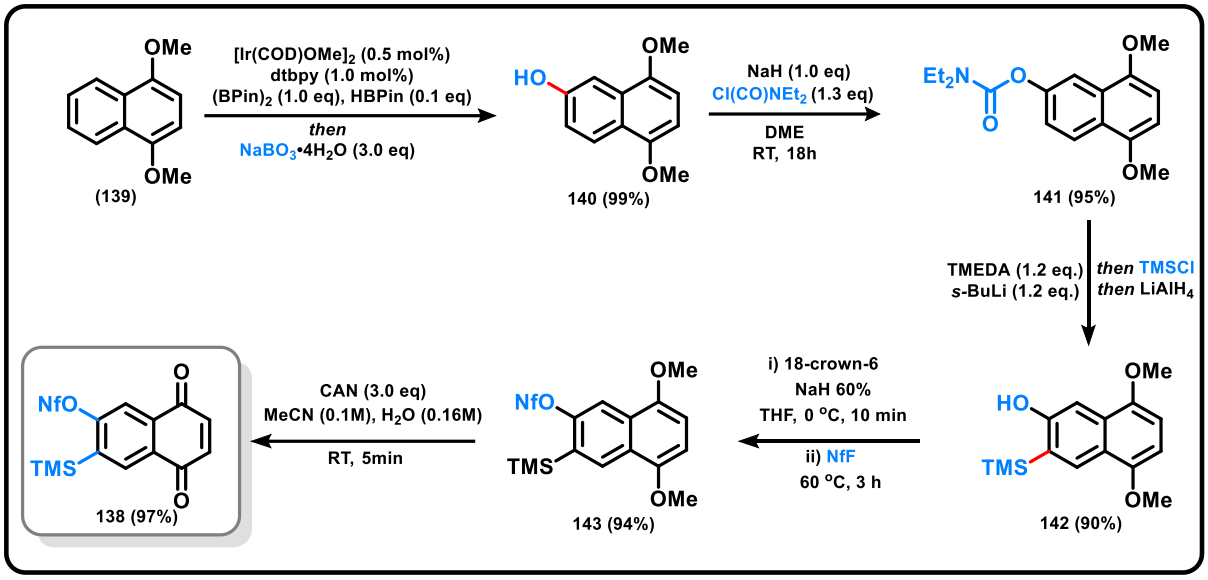

2.3.2 Aryne Capture for the Synthesis of 1,4-Benzoquinone Derivatives:

A series of 6-mono- and 6,7-difunctionalized 1,4-naphthoquinones were prepared using recently reported conditions (DE CARVALHO, Renato *et al*., 2024) for the generation and trapping of 6,7-naphthoquinonyne (**138'**) from the corresponding *ortho*-silyl nonaflate **138** (**Scheme 23**). The generation of naphthoquinonyne from *ortho*-silyl nonaflate **138** using KF and 18-crown-6 proved to be compatible with the sensitive quinone moiety, thereby enabling the exploration of a wide range of aryne-capture reactions previously reported in other contexts employing the Kobayashi approach. Since the naphthoquinonyne generation–capture sequence is highly sensitive to water, all reactions were carried out under strictly anhydrous conditions in a glovebox.

Scheme 23. *In situ* generation of aryne intermediate.

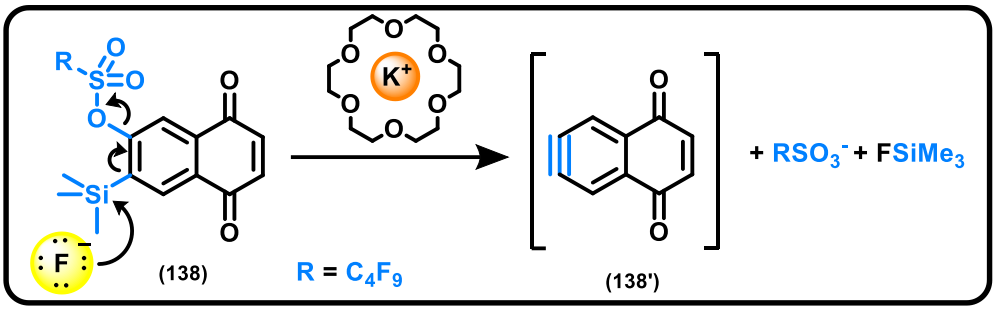

Using the optimized method, two classes of aryne-capture processes were further explored: (1) nucleophilic additions of amines and related *N*-nucleophiles, and (2) (3+2) cycloaddition/rearrangement reactions with pyridine *N*-oxides.

In the former case, efficient reactivity was observed with both primary and secondary anilines, providing access to compounds **144a–d** (**Table 3**). 1-Naphthylamine and 4-aminobenzonitrile afforded lower yields of **144e** and **144f**, respectively, the latter likely due to the reduced nucleophilicity of the nitrogen center. Pyrazole proved to be an effective nucleophile, and its reaction with **138** delivered **144g** in 67% yield.

Secondary alkylamines also served as competent reaction partners. Interestingly, diisopropylamine and dicyclohexylamine—the most sterically demanding amines evaluated—afforded **144k** and **144l** in 53% and 57% yield, respectively, whereas the smaller diethylamine was less efficient, giving **144j** in 47% yield.

Certain *N*-nucleophiles were found to be incompatible under the optimized conditions, including *N*-ethyl-*N*-methylamine, cyclic secondary amines, and electronically activated anilines (**Table 3**). The structures of naphthoquinones **144a**, **144b**, and **144j** were confirmed by single-crystal X-ray diffraction, while ^{1}H, ^{13}C NMR and HRMS analyses supported the structural assignments of the remaining products.

Table 3 summarizes the results obtained for the synthesis of amine-derived and related *N*-nucleophilic 1,4-naphthoquinone derivatives using benzyne chemistry. Notably, derivatives **144a, 144b**, **144e**, **133f**, **144i**, and **144j** are reported here for the first time. The table also highlights the amines that either failed to produce the expected products or resulted in mixtures of compounds.

Table 3. Naphthoquinonyne capture with *N*-nucleophiles.

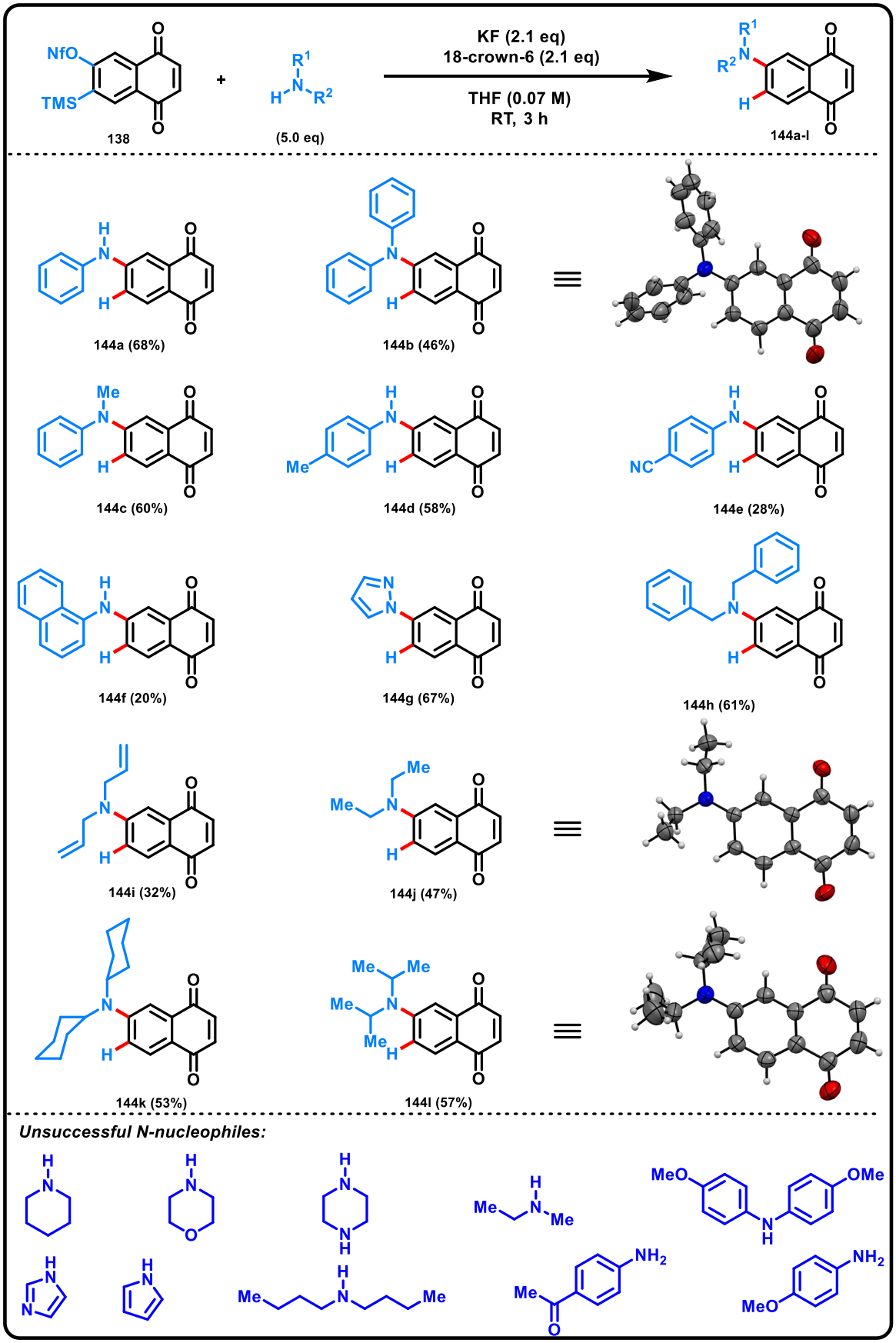

All synthetized derivatives were fully characterized by spectrometric and spectroscopic methods. The corresponding spectra and analytical data are provided in the Appendix and detailed in the Experimental Part. To exemplify the characterization procedure, compound **144b**, bearing a diphenylamine group at the C-6 position, was selected as a representative example. In the ^{1}H and ^{13}C NMR spectra, characteristic signals corresponding to the 1,4-naphthoquinone core, the aromatic protons of the diphenyl group, and the C–N bond were observed.

In the ^{1}H NMR spectrum (400 MHz, $CDCl_3$) (**Figure 31**), characteristic signals of the 1,4-naphthoquinone core were identified at 6.89 (d, *J* = 10.3 Hz, 1H, **H-2**) and 6.84 ppm (d, *J* = 10.2 Hz, 1H, **H-3**). The remaining aromatic protons appeared at 7.88 (d, *J* = 8.7 Hz, 1H), 7.55 (d, *J* = 2.5 Hz, 1H), 7.38–7.33 (m, 4H), 7.22–7.20 (m, 2H), and 7.18–7.15 ppm (m, 5H).

Figure 31. ^{1}H NMR spectrum of compound **144b.**

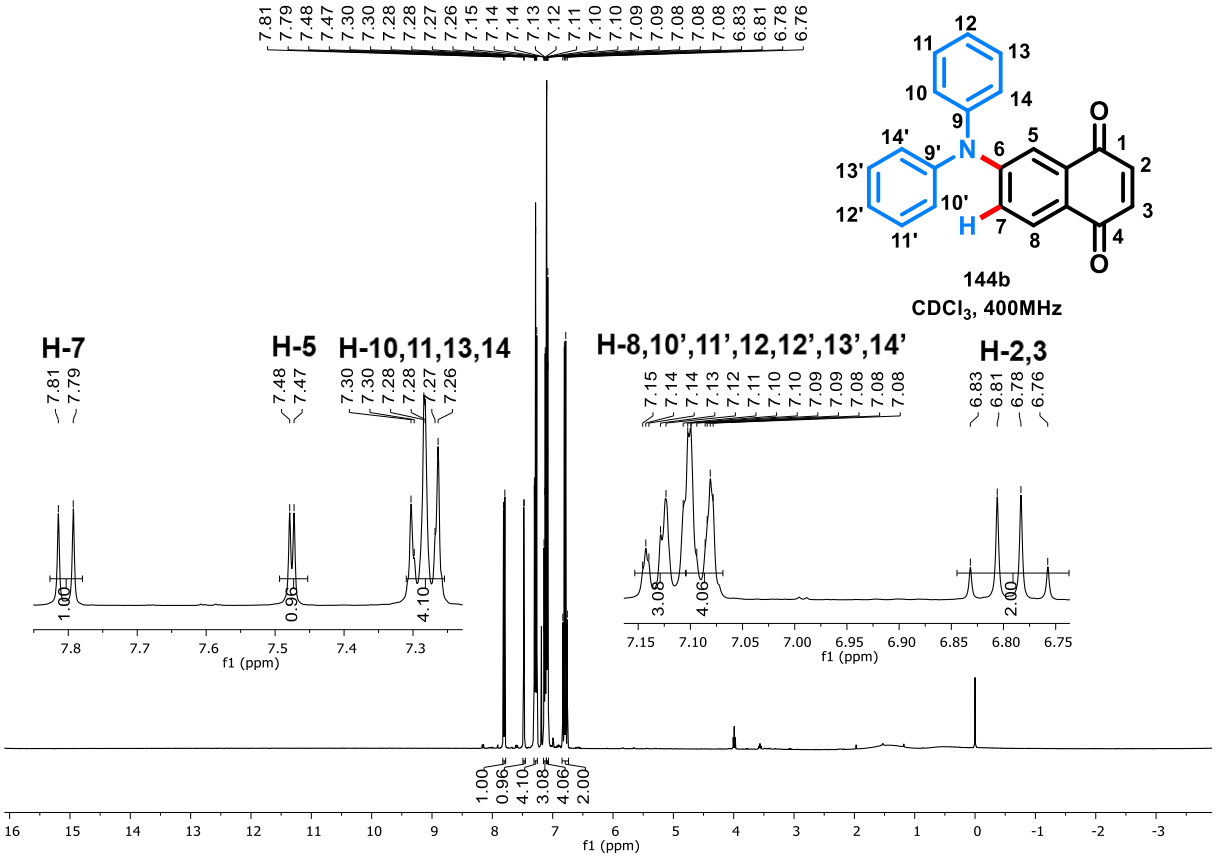

In the ^{13}C NMR spectrum (100 MHz, $CDCl_3$) (**Figure 32**), the carbonyl carbons were observed at 185.6 (C_q) and 183.8 ppm (C_q). The signal corresponding to the C–N bond was detected at 153.1 ppm (C_q). Additional quaternary carbons resonated at 145.9 ppm (2 × C_q), while aromatic carbons were observed at 139.6 (CH), 138.1 (CH),

133.5 (C), 130.1 (4 × CH), 128.5 (CH), 126.4 (4 × CH), 125.7 (2 × CH), 124.3 (C), 123.4 (CH), and 116.2 ppm (CH).

Figure 32. ^{13}C NMR spectrum of compound **144b**.

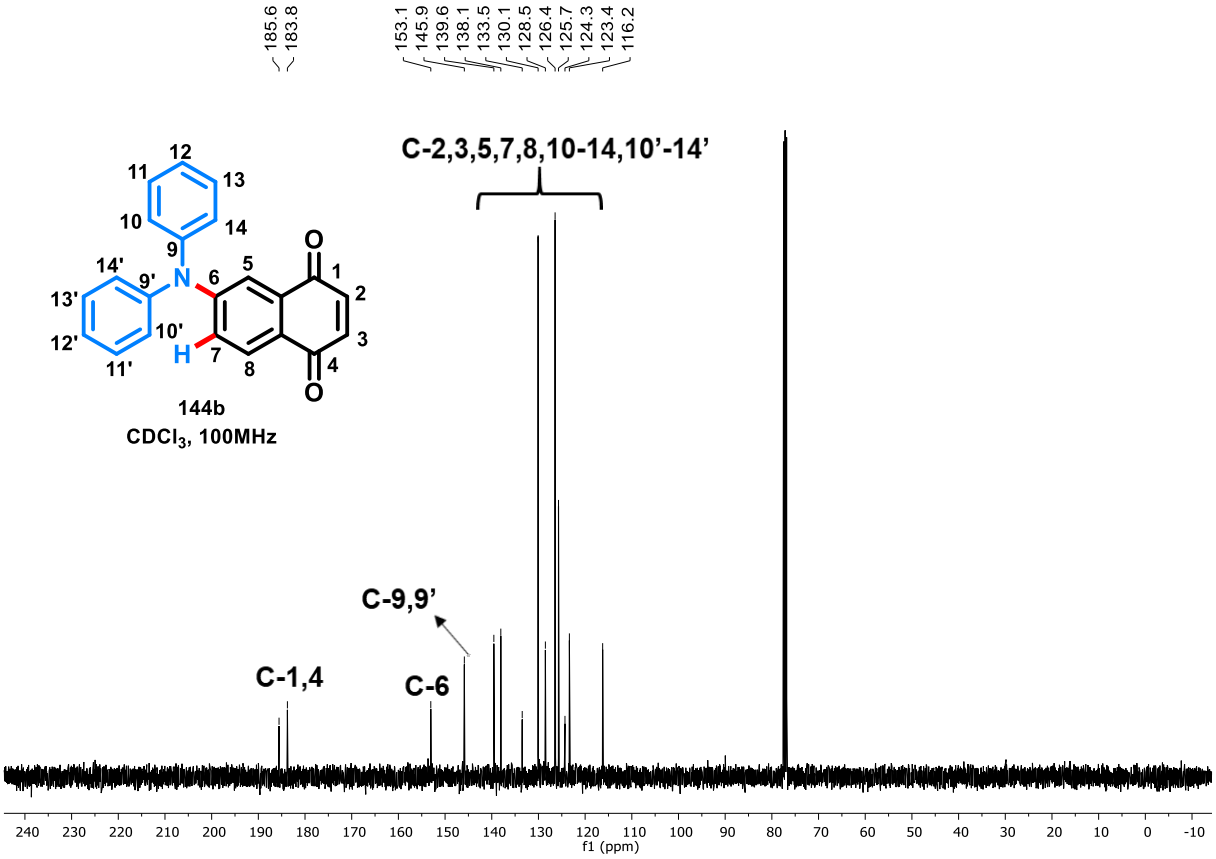

Also, the single-crystal X-ray diffraction analysis of compound **144b** was performed using a crystal suitable for this purpose, which allowed unambiguous determination of its molecular structure (**Figure 33**).

Figure 33. Mercury projections of **144b,** with displacement ellipsoids at the 50% probability level. Color code: grey, carbon; red, oxygen; white, hydrogen; blue, nitrogen atoms.

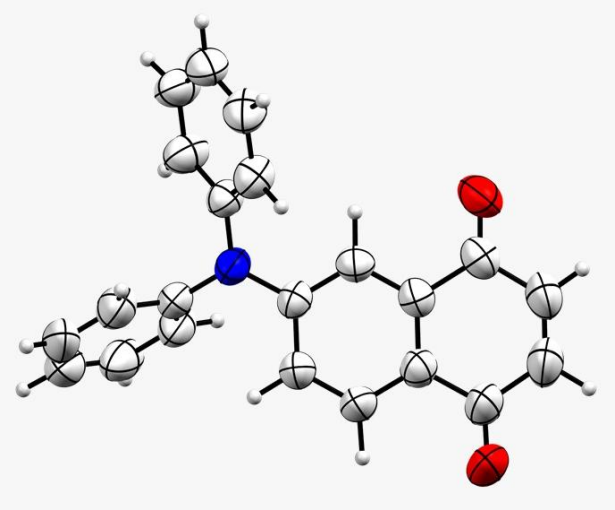

Following the identification of all compounds, a nucleophilic addition mechanism was proposed for the synthesis of these molecules (**Scheme 24**) (BIJU, Akkattu T. 2021). In this process, the aryne intermediate is attacked by the *N*-nucleophile at one of the triple-bond carbons, forming an σ-adduct intermediate. Subsequent protonation and rearomatization lead to the formation of the final C–N bonded naphthoquinone derivative.

Scheme 24. Proposed general mechanism for the formation of *N*-nucleophilic derivatives.

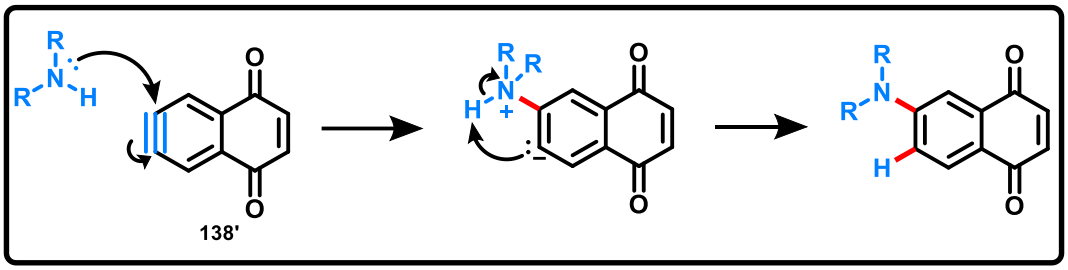

The scope of the (3+2) cycloaddition/rearrangement reactions with pyridine *N*-oxides was further explored, as summarized in **Table 4**. The pyridine *N*-oxides were prepared by oxidation of the corresponding pyridines, and their reactions with **138** provided a useful range of *ortho*-hydroxy pyridyl adducts in yields from 14 to 74%. In most cases, high selectivity was observed for C–C bond formation at the C3 position of the heteroaromatic unit.

Table 4. Naphthoquinonyne capture with pyridine *N*-oxides.

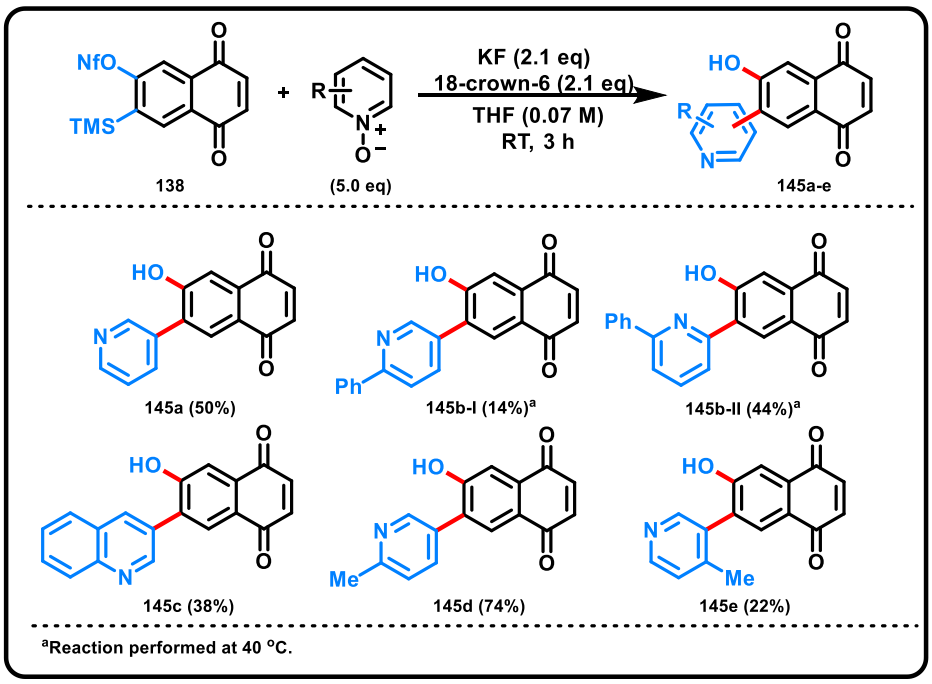

In the case of 2-phenylpyridine *N*-oxide, no identifiable products were obtained when the reaction was carried out at room temperature. However, increasing the temperature to 40 °C resulted in a mixture of regioisomers, with the C2-substituted adduct **145b-II** being favored over the C3-regioisomer **145b-I** (3:1 ratio). These results are consistent with previous reports for analogous transformations involving other arynes (RAMINELLI, LIU & LAROCK, 2006) and can be rationalized by two divergent mechanistic pathways (**Scheme 25**).

Following the initial (3+2) cycloaddition to form intermediate **145-A**, a rearrangement process leads to cyclopropane intermediate **145-B**, which then undergoes elimination-induced rearomatization to yield the C3-pyridyl adduct **145b-I**. Alternatively, direct rearomatization from intermediate **145-A** gives the C2-pyridyl adduct **145b-II**. The origin of the preference for the latter pathway in this system remains unclear.

Scheme 25. Proposed mechanistic pathways for the formation of **145b-I** and **145b-II**.

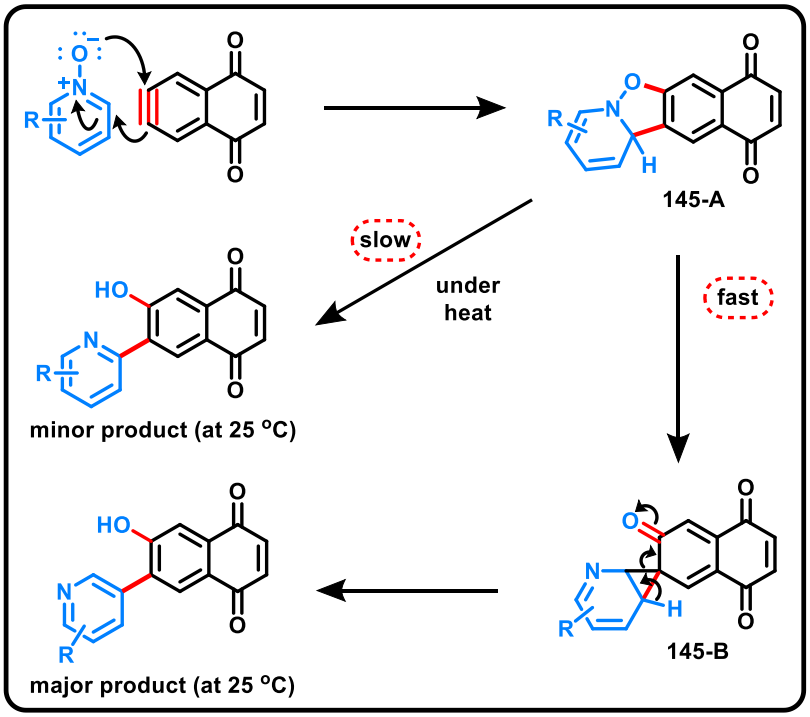

Among the synthesized compounds, five of the the pyridine *N*-oxide derivatives (**145b-I**, **145b-II**, **145c**, **145d**, and **145e**) constitute a new class of molecules not previously reported in the literature. To exemplify their structural characterization,

compound **145b-I**, featuring a *para*-substituted phenyl group, was chosen as a representative case.

In the ^{1}H NMR spectrum (400 MHz, $CDCl_3$) (**Figure 34**), the characteristic quinonoid protons **H-2** and **H-3** were observed at 6.95 (s, 2H) ppm. The aromatic protons appeared at 8.63 (s, 1H), 8.10 (d, *J* = 7.7 Hz, 1H), 8.03 (t, *J* = 7.8 Hz, 1H), 7.93–7.91 (m, 2H), 7.78 (dd, *J* = 7.8, 0.8 Hz, 1H), 7.62 (s, 1H), and 7.58–7.51 ppm (m, 3H). In addition, the hydroxyl proton at position **6** was detected at 15.97 ppm (br s, 1H).

Figure 34. ^{1}H NMR spectrum of compound **145b-I**.

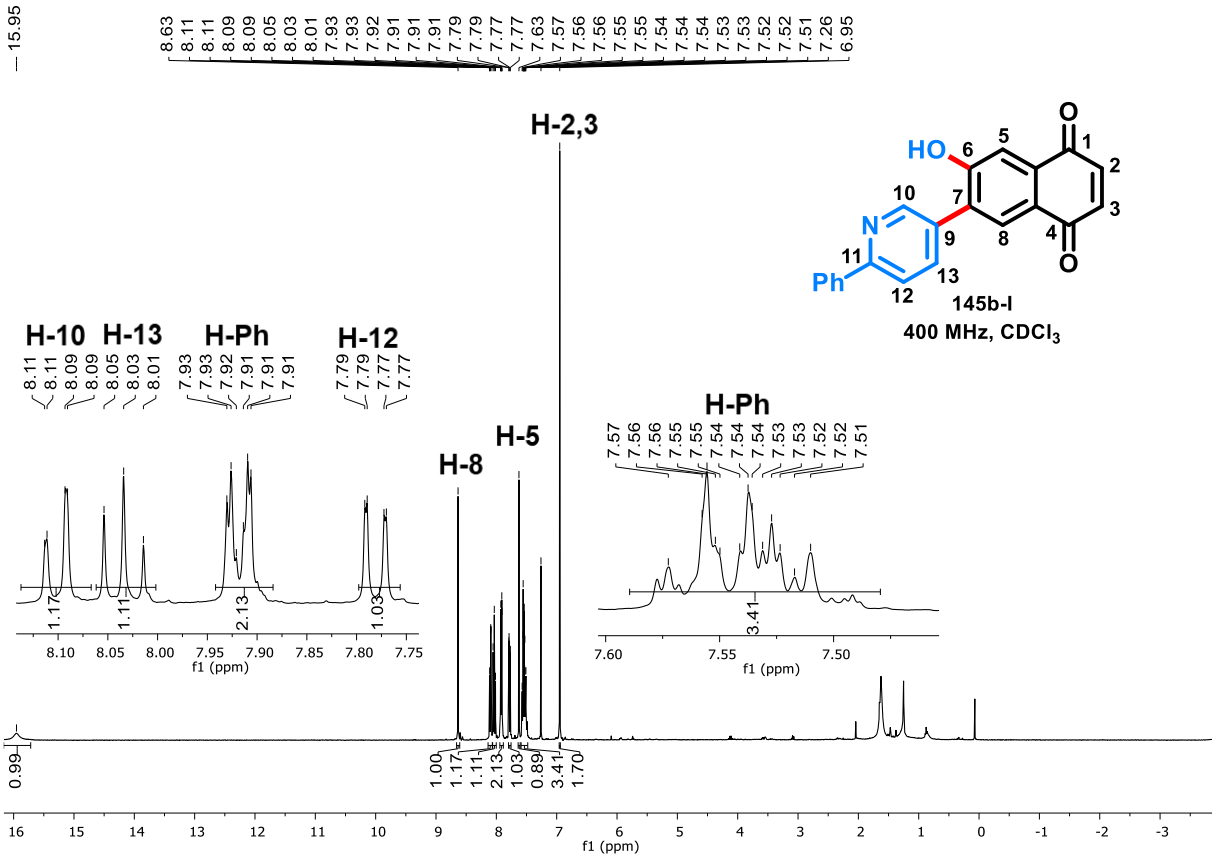

In the ^{13}C NMR spectrum (100 MHz, $CDCl_3$) (**Figure 35**), the carbonyl carbons were observed at 184.9 (C_q) and 184.1 ppm (C_q). The quaternary carbon at the **C-6** position, linked to the hydroxyl group, appeared at 165.5 ppm (C_q). The remaining aromatic carbons resonated at 156.0 (C_q), 155.2 (C_q), 139.5 (CH), 138.8 (CH), 137.4 (C), 134.4 (C_q), 130.3 (CH), 129.5 (2 × CH), 127.1 (2 × CH), 126.4 (CH), 123.5 (C_q), 123.0 (C_q), 120.7 (CH), 118.8 (CH), and 116.6 ppm (CH).

Figure 35. ^{13}C NMR spectrum of compound **145b-l**.

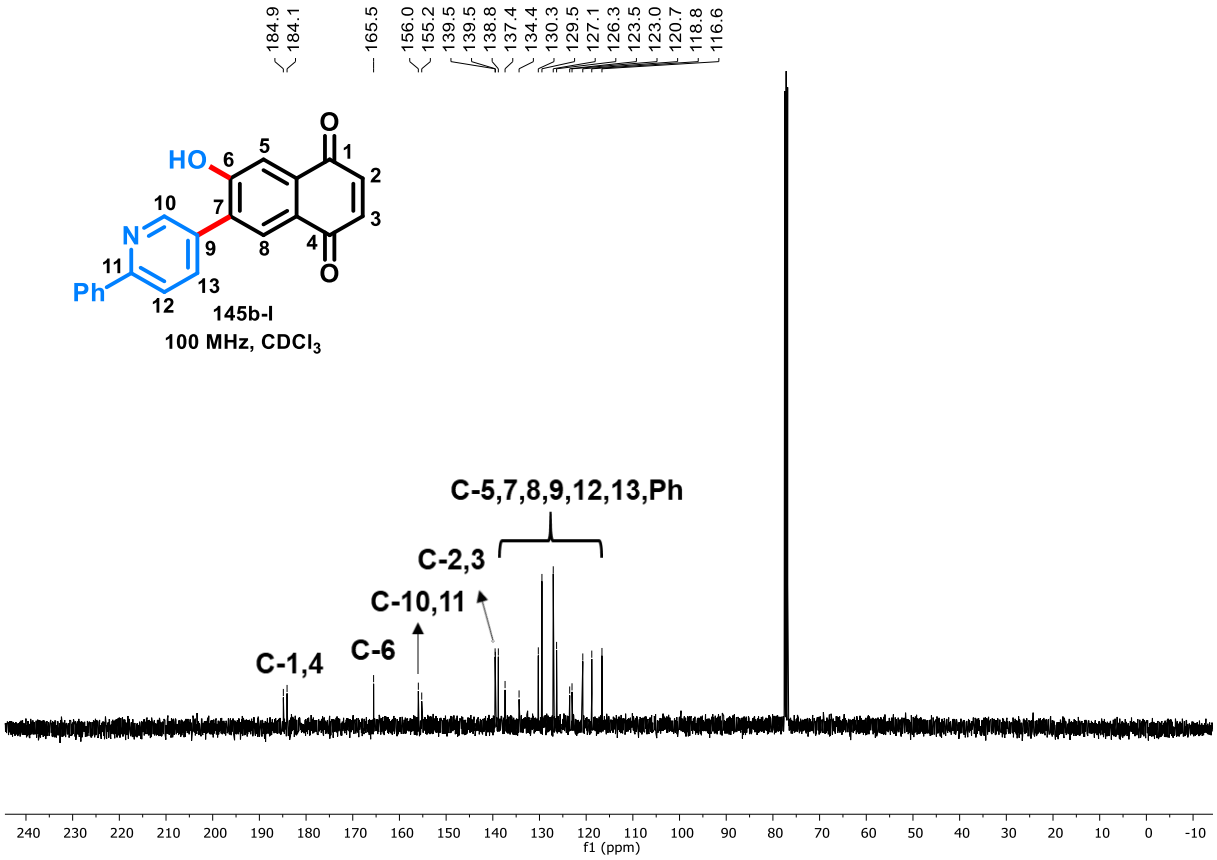

Finally, after the identification of all compounds, a (3+2) cycloaddition/rearrangement mechanism with pyridine *N*-oxides was proposed (**Scheme 26**). In this pathway, the aryne intermediate reacts with the pyridine *N*-oxide through a (3+2) cycloaddition to form a transient five-membered cycloadduct. This intermediate subsequently undergoes N–O bond cleavage and rearrangement, resulting in the transfer of oxygen to the naphthoquinone framework. The process concludes with fragmentation and rearomatization, furnishing the oxygenated naphthoquinone while retaining the pyridine moiety in the final structure.

Scheme 26. Proposed mechanism for the (3+2) cycloaddition/rearrangement of naphthoquinonyne with pyridine *N*-oxides.

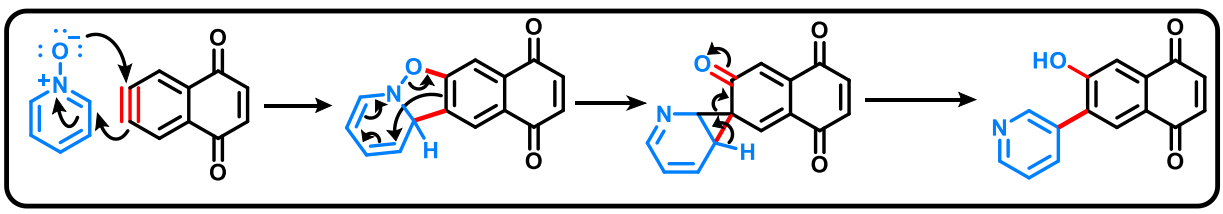

2.3.3 Biological studies: Tripanocidal Activity

We evaluated the trypanocidal activity of all compounds synthesized in this study against the trypomastigote form of *Trypanosoma cruzi* (**Table 5**). In addition, synthetic intermediates along the route to the naphthoquinonyne precursor **138** were also tested. Unfortunately, compound **138** was too unstable to be evaluated, and compound **143** was insoluble under the assay conditions. However, intermediate **142** displayed higher activity than benznidazole, with an IC_{50}/24 h value of 69.3 µM.

Table 5. IC_{50}/24 h (µM) of quinones derivatives against the trypomastigote form of *T. cruzi*[a]. [a]Mean ± SD of at least three independent experiments, 5% of blood at 4 °C. IC_{50}/24 h for benznidazole = 108.2 (± 0.4).

Compound	IC_{50}/24 h	Compound	IC_{50}/24 h
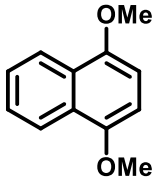 **139**	>500.0	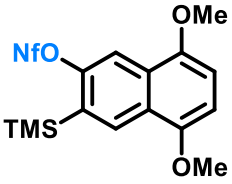 **143**	not soluble
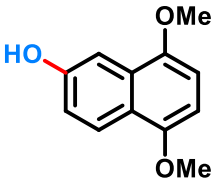 **140**	379.2 (± 87.5)	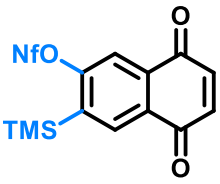 **138**	unstable
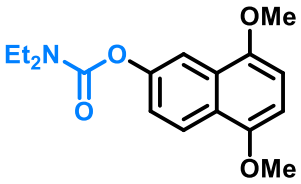 **141**	>800.0	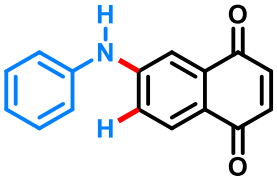 **144a**	39.2 (± 5.3)
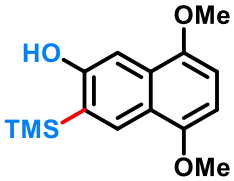 **142**	69.3 (± 3.9)	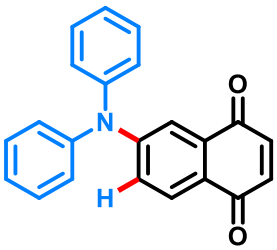 **144b**	133.8 (± 15.7)

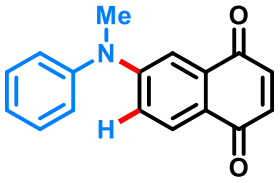

29.5 (± 2.0)

144c

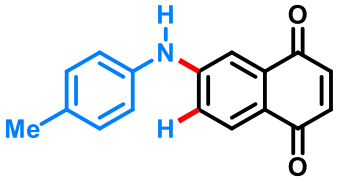

137.9 (± 20.8)

144d

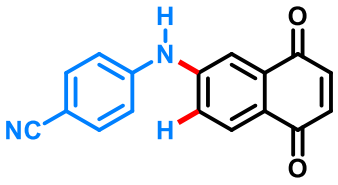

94.8 (± 6.7)

144e

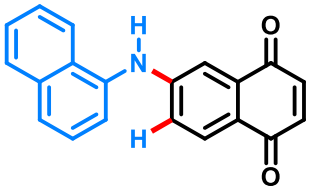

185.6 (± 7.7)

144f

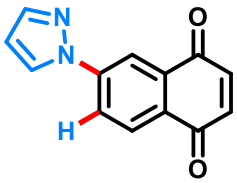

74.4 (± 2.2)

144g

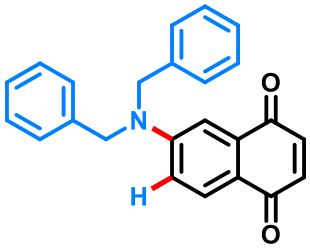

>400.0

144h

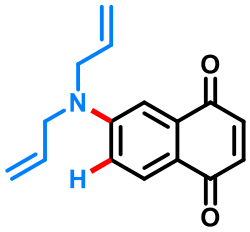

110.8 (± 5.2)

144i

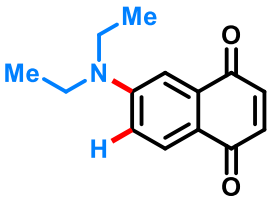

96.2 (± 2.5)

144j

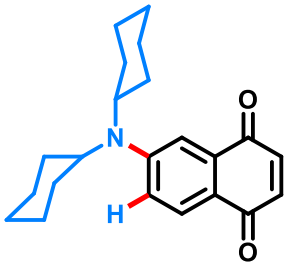

54.2 (± 12.9)

144k

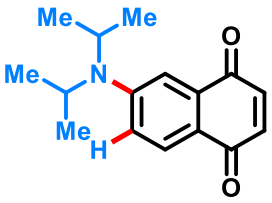

18.0 (± 1.4)

144l

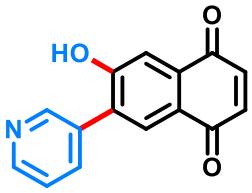

not soluble

145a

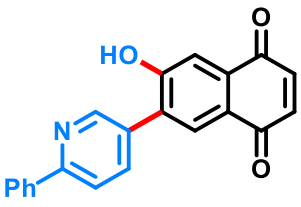

10.5 (± 2.6)

145b-l

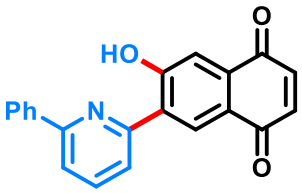

30.1 (± 7.6)

145b-II

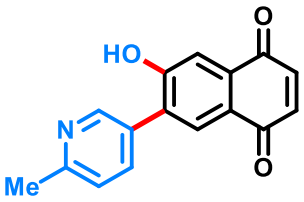

24.2 (± 2.5)

145d

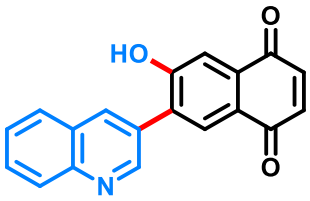

46.6 (± 7.4)

145c

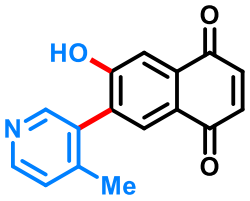

180.9 (± 12.1)

145e

Each family of derivatives accessed *via* naphthoquinonyne **138′** included at least one representative exhibiting remarkable trypanocidal potency (**Table 5**). Among the *N*-nucleophile-derived products, the highest activity was observed for compounds **144c** and **144l,** with IC_{50}/24 h values of 29.5 and 18.0 µM, respectively—corresponding to potencies 3.5- and 5.7-fold greater than that of benznidazole. These results indicate that both *N*-aryl and *N*-alkyl substituents can enhance trypanocidal activity. Nevertheless, no clear structure–activity relationship (SAR) could be established. Indeed, other *N*-alkyl or *N*-aryl derivatives showed much weaker activity; for instance, compounds **144b** and **144j** exhibited IC_{50}/24 h values of 133.8 and 96.2 µM, respectively.

Regarding the pyridine *N*-oxide–derived series, compounds **145b-I** and **145b-II** displayed the strongest activity against the parasite, with IC_{50}/24 h values of 10.5 and 30.1 µM, corresponding to potencies 9.9- and 3.4-fold higher than benznidazole. In these cases, the presence of a phenyl substituent on the pyridine ring may play an important role in modulating the redox properties of the molecules, thereby facilitating reactive oxygen species (ROS) generation. This substituent also appears to improve solubility—note that compound **145a** was insufficiently soluble to be tested under the assay conditions.

The potential contribution of an extended π-system may also account for the comparable activity of compound **145c** (IC_{50}/24 h = 46.6 µM, 2.2-fold more potent than benznidazole). Interestingly, structurally similar compounds **145d** and **145e** exhibited contrasting activities, with IC_{50}/24 h values of 24.2 and 180.9 µM, respectively. A

plausible explanation is that the 4-methyl substituent in **145e** may induce conformational misalignment between the π-systems of the pyridyl and naphthoquinonoid moieties, thereby reducing electronic communication and activity.

Figure 36 provides an overview of the most active synthesized derivatives evaluated against *T. cruzi*, highlighting the comparison between *N*-nucleophile and pyridine *N*-oxide derivatives and the reference drug benznidazole (Bz).

Figure 36. Summary of the Most Active Synthesized Derivatives against *T. cruzi*.

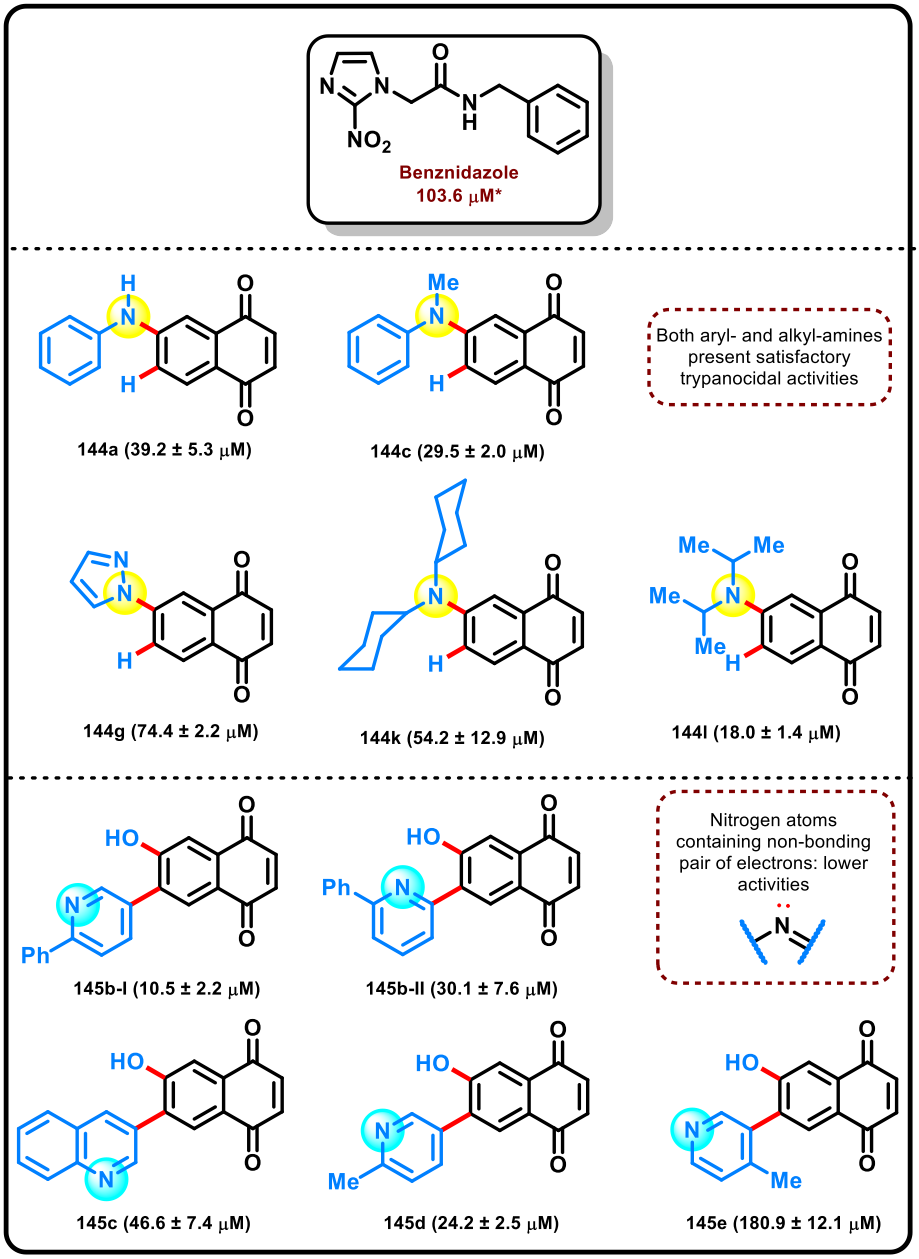

2.4 CONCLUSIONS

In this study, an efficient aryne-based methodology was successfully developed for the synthesis of a series of functionalized naphthoquinones, exploiting the intermediacy of naphthoquinonynes. Through this strategy, 12 amines and 6 pyridine *N*-oxides were employed as reaction partners, enabling the regioselective preparation of a diverse set of A-ring functionalized naphthoquinones, including nine novel compounds.

The synthesized compounds were evaluated for their trypanocidal activity, yielding highly promising results. Fourteen of the naphthoquinones exhibited greater activity than benznidazole, the drug currently used to treat Chagas disease, and notably, two of them showed approximately tenfold higher potency.

These results represent a significant contribution to the search for new trypanocidal agents and underscore the potential of this synthetic approach for drug discovery. The findings from this study have been published in RSC Medicinal Chemistry.

Laura P. R. Figueroa, Renato L. de Carvalho, Renata G. Almeida, Esther R. S. Paz, Emilay B. T. Diogo, Maria H. Araujo, Warley S. Borges, Victor F. S. Ramos, Rubem F. S. Menna-Barreto, James M. Wood, John F. Bower and Eufrânio N. da Silva Júnior. 2025, 16, 694, doi: 10.1039/d4md00558a.

2.5 EXPERIMENTAL PART

2.5.1 General remarks:

All commercially sourced compounds were used as received, unless otherwise stated. Reactions requiring anhydrous conditions were run under an atmosphere of dry nitrogen or argon; glassware was either flame dried immediately prior to use or placed in an oven (200 °C) for at least 2 h and allowed to cool either in a desiccator or under an atmosphere of nitrogen or argon; except in the cases of reactions set up in a glovebox, liquid reagents, solutions or solvents were added via syringe through rubber septa; solid reagents were added via Schlenk type adapters. Melting points were determined using a Reichert melting point table and temperature controller or a Stuart SMP30 melting point apparatus, and are uncorrected. Infrared spectra were recorded in the range 4000-600 cm^{-1} on a Perkin Elmer Spectrum either as neat films or solids

compressed onto a diamond window. Abbreviations used are: w (weak), m (medium) or s (strong). NMR spectra were recorded using either a Varian 400-MR, Bruker Nano 400 or Bruker UltrashieldTM Plus 500. Chemical shifts (δ) are quoted in parts per million (ppm), coupling constants (J) are given in Hz. Other abbreviations used are s (singlet), d (doublet), t (triplet), m (multiplet) and br. (broad). ^{1}H and ^{13}C NMR spectra were referenced to the appropriate residual solvent peak or the carbon resonance of the NMR solvent, respectively. ^{19}F spectra were referenced to CCl_3F as an external standard. Interpretation of ^{1}H NMR and ^{13}C NMR spectra was aided by COSY, HSQC and HMBC experiments. Mass spectra were determined by the University of Bristol mass spectrometry service using a Shimadzu GCMS QP2010+ (EI+ mode), Brüker Daltonics FT-ICR-MS Apex 4e 7.0T FT-MS (ESI+ mode), Thermo Scientific Orbitrap Elite (APCI mode), or by the University of Liverpool mass spectrometry service using an Agilent CI-GCMS-QTOF (CI+ mode).

2.5.2 Synthesis of the 6,7-Aryne Precursor from 1,4-Benzoquinone:

The compounds **138**, **140**, **141**, **142** and **143** were prepared following the previously reported procedure by Eufrânio Lab Research Group, and their spectroscopic data were consistent with those described in the literature (DE CARVALHO, Renato *et al*., 2024).

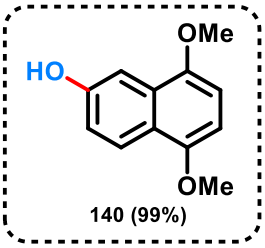

5,8-Dimethoxynaphthalen-2-ol (Compound **140**)**:** A Schlenk flask was charged with 1,4-dimethoxynaphthalene (**139**) (12.6 g, 67.0 mmol), $(Bpin)_2$ (17.1 g, 67.0 mmol), $[Ir(cod)OMe]_2$ (223 mg, 0.336 mmol) and 4,4′-di-*tert*-butyl-2,2′-dipyridyl (180 mg, 0.670 mmol). The flask was placed under an atmosphere of N_2, then THF (40 mL) was added. To this solution was added HBpin (0.98 mL, 6.70 mmol) and the reaction mixture was heated to 80 °C for 18 h, then cooled to 0 °C and quenched carefully by addition of MeOH until evolution of H_2 ceased. The reaction mixture was concentrated *in vacuo* to give the crude boronate ester, which was dissolved in THF (440 mL). To this solution was added $NaBO_3{\cdot}4H_2O$ (30.9 g, 201 mmol), then H_2O (220 mL). The resultant

suspension was stirred at room temperature for 4 h, after which TLC analysis showed the reaction was complete. The purple reaction mixture was quenched by addition Na_2SO_3 (15 g) and stirred for 1 h, then acidified to < pH 6 with conc HCl upon which it turned yellow. The aqueous layer was extracted with EtOAc (3 × 150 mL), then the combined organic layers were washed with brine (100 mL), dried over anhydrous Na_2SO_4, filtered and concentrated *in vacuo*. Purification by flash column chromatography (15%–20% EtOAc/Hex) on silica gel afforded the title compound **140** (13.5 g, 99%) as a colourless oil; **^{1}H NMR (400 MHz, $CDCl_3$)** δ 8.05 (d, J = 9.0 Hz, 1H), 7.42 (d, J = 2.6 Hz, 1H), 7.03 (dd, J = 9.0, 2.6 Hz, 1H), 6.61 (d, J = 8.2 Hz, 1H), 6.48 (d, J = 8.4 Hz, 1H), 5.06 (br s, 1H), 3.86 (s, 3H), 3.86 (s, 3H); **^{13}C NMR (100 MHz, $CDCl_3$)** δ 154.0 (C_q), 149.9 (C_q), 148.6 (C_q), 127.8 (C_q), 124.3 (CH), 121.7 (C_q), 117.1 (CH), 104.5 (CH), 104.3 (CH), 101.0 (CH), 55.9 (CH_3), 55.8 (CH_3).

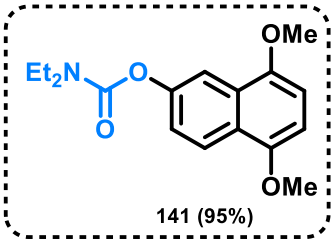

141 (95%)

5,8-Dimethoxynaphthalen-2-yl-*N*,*N*-diethylcarbamate (Compound **141**)**:** To a suspension of NaH (60% *w/w* dispersion in mineral oil, 2.80 g, 69.9 mmol) in 1,2-dimethoxyethane (200 mL) at 0 °C was added a solution of naphthol **140** (11.9 g, 58.2 mmol) in 1,2-dimethoxyethane (30 mL) dropwise. The reaction mixture was warmed to room temperature and stirred for 10 min, then cooled back down to 0 °C and treated with *N*,*N*-diethylcarbamoyl chloride (8.9 mL, 70.2 mmol). The reaction was allowed to warm to room temperature slowly and stirred for 18 h, then quenched by addition of H_2O (1 mL). The reaction solvent was removed *in vacuo* and the residue obtained partitioned between H_2O (200 mL) and Et_2O (200 mL). The aqueous layer was extracted with Et_2O (2 × 200 mL), then the combined organic layers were washed with 1 M KOH (50 mL), H_2O (50 mL) and brine (50 mL), dried over anhydrous Na_2SO_4, filtered and concentrated *in vacuo*. Purification by flash column chromatography (20%–25% EtOAc/Hex) on silica gel afforded the title compound **141** (16.8 g, 95%) as a colourless oil; **^{1}H NMR (500 MHz, $CDCl_3$)** δ 8.23 (d, J = 9.0 Hz, 1H), 7.95 (d, J = 2.4 Hz, 1H), 7.34 (dd, J = 9.0, 2.4 Hz, 1H), 6.70 (d, J = 8.4 Hz, 1H), 6.66 (d, J = 8.4 Hz, 1H), 3.96 (s, 3H), 3.95 (s, 3H), 3.50 (q, J = 7.0 Hz, 2H), 3.44 (q, J = 7.3 Hz, 2H), 1.32

(t, *J* = 7.3 Hz, 3H), 1.25 (t, *J* = 7.3 Hz, 3H); **^{13}C NMR (125 MHz, $CDCl_3$)** *δ* 154.4 (C_q), 149.8 (C_q), 149.6 (C_q), 149.2 (C_q), 127.2 (C_q), 124.1 (C_q), 123.4 (CH), 121.4 (CH), 113.2 (CH), 103.9 (CH), 102.7 (CH), 55.8 (CH_3), 55.7 (CH_3), 42.3 (CH_2), 42.0 (CH_2), 14.4 (CH_3), 13.5 (CH_3).

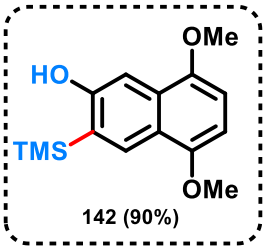

142 (90%)

5,8-Dimethoxy-3-(trimethylsilyl)naphthalen-2-ol (Compound **142**)**:** To a solution of carbamate **141** (7.36 g, 24.3 mmol) and TMEDA (4.48 mL, 29.1 mmol) in THF (121 mL) at −78 °C was added *s*-BuLi (1.25 M in cyclohexane, 23.3 mL, 29.1 mmol) dropwise over 10 min. The reaction mixture was stirred at −78 °C for 30 min, then TMSCl (4.56 mL, 36.4 mmol) was added dropwise. The reaction mixture was allowed to warm to room temperature and stirred for a further 30 min. The mixture was then cooled down to 0 ºC, and $LiAlH_4$ (4.6 g, 121.4 mmol) was added portionwise. The reaction mixture was heated under reflux for 16 h, then cooled to 0 ºC and diluted with Et_2O (200 mL). The reaction was quenched by dropwise addition of H_2O (8.1 mL), 15% *w/w* aq NaOH (8.1 mL) and H_2O (24.2 mL) sequentially. The mixture was warmed to room temperature and stirred for 30 min, then anhydrous $MgSO_4$ (100 g) was added and the suspension stirred a further 10 min. The suspension was filtered through a pad of Celite®, washing with EtOAc (4 × 50 mL). The filtrate was concentrated *in vacuo* and then purified by flash column chromatography (20% EtOAc/Hex) on silica gel to afford the title compound **142** (6.0 g, 90%) as a colourless solid; **mp** 100–102 ºC; **^{1}H NMR (400 MHz, $CDCl_3$)** *δ* 8.34 (s, 1H), 7.38 (s, 1H), 6.71 (d, *J* = 8.3 Hz, 1H), 6.56 (d, *J* = 8.3 Hz, 1H), 5.36 (s, 1H), 3.98 (s, 3H), 3.95 (s, 3H), 0.44 (s, 9H); **^{13}C NMR (100 MHz, $CDCl_3$)** *δ* 158.6 (C), 150.2 (C), 148.3 (C), 130.3 (CH), 128.6 (C), 128.1 (C), 121.3 (C), 104.8 (CH), 103.1 (CH), 100.8 (CH), 56.0 (CH_3), 55.7 (CH_3), −0.7 (CH_3).

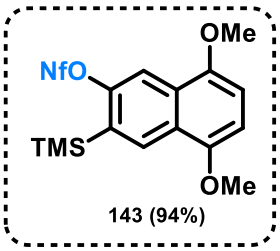

143 (94%)

5,8-Dimethoxy-3-(trimethylsilyl)naphthalen-2-yl 1,1,2,2,3,3,4,4,4-nonafluorobutane-1-sulfonate (Compound **143**): To a solution of naphthol **142** (8.36 g, 30.2 mmol) and 18-crown-6 (7.99 g, 30.2 mmol) in THF (302 mL) at 0 ºC was added NaH (60% *w/w* dispersion in mineral oil, 1.81 g, 45.4 mmol) portionwise, and the resulting suspension was stirred for 10 min. Perfluorobutanesulfonyl fluoride (8.2 mL, 45.4 mmol) was added, then the reaction mixture was stirred at 60 ºC for 3 h. The reaction was cooled to room temperature, then quenched with H_2O (250 mL). The aqueous layer was extracted with EtOAc (3 × 150 mL), then the combined organic layers were washed with 2 M aq HCl (100 mL), brine (100 mL), dried over anhydrous Na_2SO_4, filtered and concentrated *in vacuo*. Purification by flash column chromatography (10% EtOAc/Hex) on silica gel afforded the title compound **143** (16.7 g, 94%) as a pale yellow solid; **mp** 79–81 ºC (CH_2Cl_2/petrol); **^{1}H NMR (400 MHz, $CDCl_3$)** δ 8.41 (s, 1H), 8.14 (s, 1H), 6.77 (d, J = 8.4 Hz, 1H), 6.73 (d, J = 8.4 Hz, 1H), 3.97 (s, 3H), 3.96 (s, 3H), 0.45 (s, 9H); **^{13}C NMR (100 MHz, $CDCl_3$)** δ 153.6 (C), 149.5 (C), 149.2 (C), 131.6 (CH), 130.8 (C), 127.6 (C), 124.6 (C), 111.8 (CH), 105.4 (CH), 104.3 (CH), 56.0 (CH_3), 55.9 (CH_3), −0.5. (CH_3), $SO_2C_4F_9$ signals present as a complex range of multiplets; **^{19}F NMR (376 MHz, $CDCl_3$)** δ −80.57 (t, J = 9.7 Hz), −109.40 (t, J =13.9 Hz), −120.79 (m), −125.64 (m).

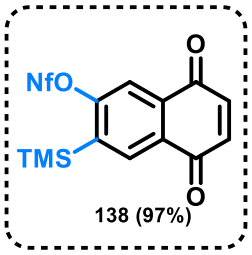

138 (97%)

5,8-Dioxo-3-(trimethylsilyl)-5,8-dihydronaphthalen-2-yl 1,1,2,2,3,3,4,4,4-nonafluorobutane-1-sulfonate (Compound **138**): To a solution of 1,4-dimethoxynaphthalene **143** (546 mg, 0.979 mmol) in MeCN (10 mL, 0.1 M) at room temperature was added a solution of CAN (1.61 g, 2.94 mmol) in H_2O (6 mL, 0.16 M) dropwise. The reaction mixture was stirred for 5 min, then diluted with H_2O (20 mL). The aqueous layer was extracted with EtOAc (3 × 20 mL), then the combined organic layers were washed with sat aq $NaHCO_3$ (15 mL) and brine (15 mL), dried over anhydrous Na_2SO_4, filtered and concentrated *in vacuo*. The crude product thus obtained was purified by flash column chromatography (10% EtOAc/Hex) on silica gel to afford the title compound **138** (502 mg, 97%) as a yellow oil; **^{1}H NMR (400 MHz,**

$CDCl_3$) δ 8.27 (s, 1H), 7.97 (s, 1H), 7.03 (d, J = 10.4 Hz, 1H), 7.00 (d, J = 10.4 Hz, 1H), 0.43 (s, 9H); **^{13}C NMR (100 MHz, $CDCl_3$)** δ 183.9 (C), 183.5 (C), 158.7 (C), 140.8 (C), 138.9 (2 × CH), 135.5 (CH), 134.7 (C), 129.7 (C), 116.9 (CH), −1.0 (CH_3), $SO_2C_4F_9$ ^{13}C signals present as a complex range of multiplets; **^{19}F NMR (376 MHz, $CDCl_3$)** δ −80.56 (t, J = 9.6 Hz), −109.00 (t, J = 13.4 Hz), −120.75 (m), −125.67 (m).

2.5.3 General procedure for Aryne Capture:

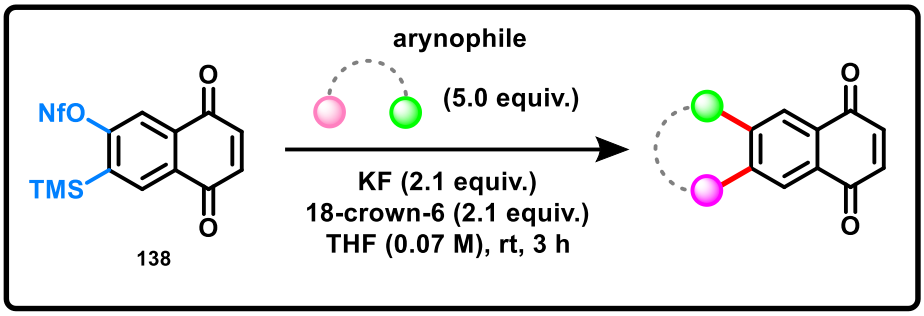

All aryne capture procedures followed the same standard general procedure as follows (DE CARVALHO, Renato *et al*., 2024).

In a glovebox, a 10 mL flame-dried reaction tube was charged with the respective freshly prepared aryne precursor (0.2 mmol, 1.0 equiv), arynophile (1.0 mmol, 5.0 equiv), anhydrous KF (24.5 mg, 0.42 mmol, 2.1 equiv), and 18-crown-6 (112 mg, 0.42 mmol, 2.1 equiv), which were then dissolved in dry and degassed THF (2.0 mL, 0.1 M). Additional THF (0.8 mL, 0.25 M) was used to rinse the walls of the reaction tube, giving a final reaction concentration of 0.07 M with respect to the aryne precursor. Once tightly closed, the tube containing the resulting mixture was then removed from the glovebox. The resulting mixture was stirred for 3 h at room temperature, then diluted with H_2O (10 mL) and extracted with CH_2Cl_2 (3 × 10 mL). The combined organic layers were dried over anhydrous Na_2SO_4, filtered and concentrated *in vacuo*. Purification by flash column chromathography (10% EtOAc/Hex) on silica gel afforded the respective product.

Characterization Data: Products 144a-l

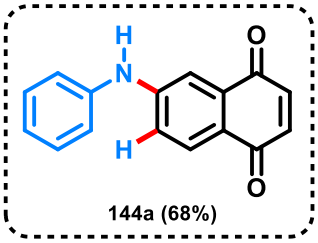

6-(Phenylamino)naphthalene-1,4-dione (Compound **144a**): Purification by flash column chromatography (10% EtOAc/Hex) afforded the title compound **144a** (34 mg, 68%) as a dark purple solid; **mp** 177-179 ºC; **^{1}H NMR (400 MHz, CDCl$_3$)** δ 7.96 (d, *J* = 7.0 Hz, 1H), 7.55 (d, *J* = 2.1 Hz, 1H), 7.40 (t, *J* = 6.4 Hz, 2H), 7.23 (d, *J* = 6.7 Hz, 3H), 7.16 (t, *J* = 6.2 Hz, 1H), 6.90 (d, *J* = 8.6 Hz, 1H), 6.87 (d, *J* = 8.3 Hz, 1H), 6.46 (br s, 1H); **^{13}C NMR (100 MHz, CDCl$_3$)** δ 185.7 (C_q), 183.7 (C_q), 149.6 (C_q), 139.7 (C_q), 139.7 (CH), 137.9 (CH), 134.0 (C_q), 129.9 (2 × CH), 129.2 (CH), 124.6 (CH), 123.9 (C_q), 121.8 (2 × CH), 118.6 (CH), 111.6 (CH). The spectroscopic properties were consistent with the data available in the literature (DE CARVALHO, Renato *et al*., 2024).

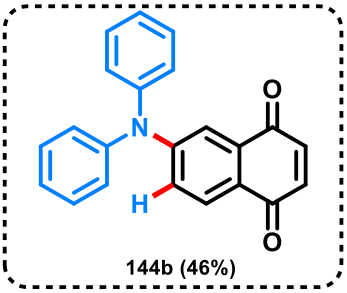

144b (46%)

6-(Diphenylamino)naphthalene-1,4-dione (Compound **144b**): Purification by flash column chromatography (10% EtOAc/Hex) afforded the title compound **144b** (30 mg, 46%) as red crystals; **mp** 128–130 ºC; **ν_{max}/cm^{-1}**: 1653 (s), 1559 (s), 1312 (s), 833 (m); **^{1}H NMR (400 MHz, CDCl$_3$)** δ 7.88 (d, *J* = 8.7 Hz, 1H), 7.55 (d, *J* = 2.5 Hz, 1H), 7.38–7.33 (m, 4H), 7.22–7.20 (m, 2H), 7.18–7.15 (m, 5H), 6.89 (d, *J* = 10.3 Hz, 1H), 6.84 (d, *J* = 10.2, 1H); **^{13}C NMR (100 MHz, CDCl$_3$)** δ 185.6 (C_q), 183.8 (C_q), 153.1 (C_q), 145.9 (2 × C_q), 139.6 (CH), 138.1 (CH), 133.5 (C_q), 130.1 (4 × CH), 128.5 (CH), 126.4 (4 × CH), 125.7 (2 × CH), 124.3 (C_q), 123.4 (CH), 116.2 (CH); **HRMS (ESI+):** Calculated for $C_{22}H_{16}NO_2$: 326.1181. Found $[M + H]^+$: 326.1021. The structure of the product was also confirmed by X-ray diffraction (CCDC number = 2352788).

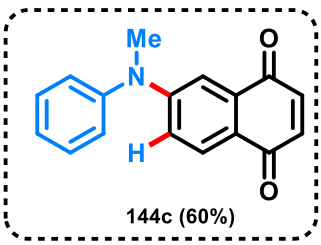

144c (60%)

6-(Methyl(phenyl)amino)naphthalene-1,4-dione (Compound **144c**): Purification by flash column chromatography (10% EtOAc/Hex) afforded the title compound **144c** (31

mg, 60%) as a dark red solid; **mp** 128–129 ºC; **^{1}H NMR (500 MHz, $CDCl_3$) δ** 7.86 (d, *J* = 8.7 Hz, 1H), 7.45 (t, *J* = 7.7 Hz, 2H), 7.34 (d, *J* = 2.8 Hz, 1H), 7.30 (t, *J* = 7.5 Hz, 1H), 7.24 (d, *J* = 7.5 Hz, 2H), 6.93 (dd, *J* = 8.8, 2.9 Hz, 1H), 6.87 (d, *J* = 10.2 Hz, 1H), 6.84 (d, *J* = 10.2 Hz, 1H), 3.46 (s, 3H); **^{13}C NMR (125 MHz, $CDCl_3$)** δ 186.1 (C_q), 183.8 (C_q), 153.2 (C_q), 146.6 (C_q), 139.7 (CH), 137.8 (CH), 133.5 (C_q), 130.3 (2 × CH), 128.6 (CH), 126.7 (CH), 126.6 (2 × CH), 122.0 (C_q), 117.7 (CH), 110.1 (CH), 40.7 (CH_3). The spectroscopic properties were consistent with the data available in the literature (DE CARVALHO, Renato *et al*., 2024).

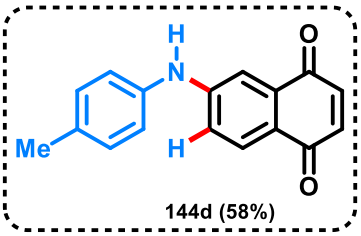

144d (58%)

6-(*p*-Tolylamino)naphthalene-1,4-dione (Compound **144d**): Purification by flash column chromatography (10% EtOAc/Hex) afforded the title compound **144d** (31 mg, 58%) as a purple solid; **mp** 126–128 ºC; **ν_{max}/cm^{-1}**: 2923 (m), 1653 (s), 1541 (s), 1051 (m), 810 (m); **^{1}H NMR (400 MHz, $CDCl_3$)** δ 7.83 (d, *J* = 8.6 Hz, 1H), 7.37 (d, *J* = 2.5 Hz, 1H), 7.10 (d, *J* = 8.1 Hz, 2H), 7.04–7.00 (m, 3H), 6.79 (d, *J* = 10.3 Hz, 1H), 6..75 (d, *J* = 10.4 Hz, 1H), 6.15 (br s, 1H), 2.26 (s, 3H); **^{13}C NMR (100 MHz, $CDCl_3$)** δ 185.8 (C_q), 183.7 (C_q), 150.2 (C_q), 139.7 (CH), 137.9 (CH), 137.0 (C_q), 134.8 (C_q), 134.0 (C_q), 130.5 (2 × CH), 129.2 (CH), 123.5 (C_q), 122.6 (2 × CH), 118.1 (CH), 111.1 (CH), 21.1 (CH_3); **HRMS (ESI-):** Calculated for $C_{17}H_{12}NO_2$: 262.0868. Found $[M - H]^-$: 262.0773.

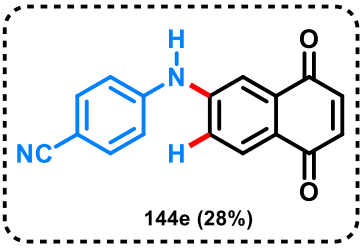

144e (28%)

4-((5,8-Dioxo-5,8-dihydronaphthalen-2-yl)amino)benzonitrile (Compound **144e**): Purification by flash column chromatography (10% EtOAc/Hex) afforded the title compound **144e** (15 mg, 28%) as a purple solid; **mp** 129–132 ºC; **ν_{max}/cm^{-1}**: 3364 (m), 2221 (m), 1654 (s), 1540 (s), 1356 (m), 1058 (m), 825 (s); **^{1}H NMR (400 MHz, $CDCl_3$)** δ 7.95 (d, *J* = 8.4 Hz, 1H), 7.62 (d, *J* = 2.4 Hz, 1H), 7.53 (dt, *J* = 8.7, 2.4 Hz, 2H), 7.28 (dd, *J* = 8.5, 2.4 Hz, 1H), 7.12 (dt, *J* = 8.8, 2.2 Hz, 2H), 6.86 (d, *J* = 10.4 Hz, 1H), 6.83

(d, *J* = 10.4 Hz, 1H), 6.45 (br s, 1H); **^{13}C NMR (100 MHz, CDCl$_3$)** *δ* 185.1 (C_q), 183.7 (C_q), 146.5 (C_q), 144.7 (C_q), 139.5 (CH), 138.2 (CH), 134.2 (2 × CH), 133.9 (C_q), 129.2 (CH), 126.0 (C_q), 121.5 (CH), 119.1 (C_q), 118.5 (2 × CH), 114.0 (CH), 105.6 (C_q); **HRMS (ESI-)**: Calculated for $C_{17}H_{10}N_2O_2$: 273.0664. Found $[M - H]^-$: 273.0568.

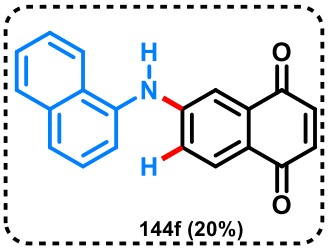

144f (20%)

6-(Naphthalen-1-ylamino)naphthalene-1,4-dione (Compound **144f**): Purification by flash column chromatography (10% EtOAc/Hex) afforded the title compound **144f** (16 mg, 32%) as a purple solid; **mp** 160–162 ºC; **ν_{max}/cm^{-1}**: 1654 (s), 1541 (s), 1339 (m), 1261 (s), 824 (m); **^{1}H NMR (400 MHz, CDCl$_3$)** *δ* 7.88 (d, *J* = 8.8 Hz, 1H), 7.77 (d, *J* = 8.7 Hz, 1H), 7.73 (d, *J* = 8.0 Hz, 1H), 7.66 (d, *J* = 8.0 Hz, 1H), 7.53 (d, *J* = 1.8 Hz, 1H), 7.51 (d, *J* = 2.5 Hz, 1H), 7.39 (td, *J* = 8.1, 1.1 Hz, 1H), 7.33 (td, *J* = 8.1, 1.2 Hz, 1H), 7.24 (dd, *J* = 8.7, 2.2 Hz, 1H), 7.20 (dd, *J* = 8.6, 2.5 Hz, 1H), 6.81 (d, *J* = 10.3 Hz, 1H), 6.78 (d, *J* = 10.3 Hz, 1H), 6.39 (br s, 1H); **^{13}C NMR (100 MHz, CDCl$_3$)** *δ* 185.7 (C_q), 183.7 (C_q), 149.5 (C_q), 139.7 (CH), 138.0 (CH), 137.3 (C_q), 134.3 (C_q), 134.0 (C_q), 130.9 (C_q), 129.9 (CH), 129.3 (CH), 127.9 (CH), 127.3 (CH), 127.0 (CH), 125.4 (CH), 124.2 (C_q), 121.8 (CH), 118.8 (CH), 117.8 (CH), 111.9 (CH); **HRMS (ESI-):** Calculated for $C_{20}H_{13}NO_2$: 298.0868. Found $[M + H]^+$: 298.0760.

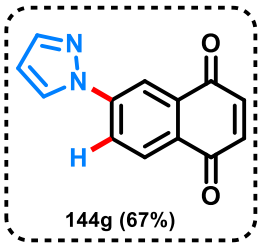

144g (67%)

6-(1*H*-Pyrazol-1-yl)naphthalene-1,4-dione (Compound **144g**): Purification by flash column chromatography (10% EtOAc/Hex) afforded the title compound **144g** (30 mg, 67%) as a yellow solid; **mp** 124–126 ºC; **^{1}H NMR (500 MHz, CDCl$_3$)** *δ* 8.31 (d, *J* = 1.6 Hz, 1H), 8.23–8.19 (m, 2H), 8.13 (d, *J* = 2.6 Hz, 1H), 7.82 (d, *J* = 1.5 Hz, 1H), 7.03–7.00 (m, 2H), 6.58–6.57 (m, 1H); **^{13}C NMR (125 MHz, CDCl$_3$)** *δ* 184.5 (C_q), 184.1 (C_q), 144.2 (C_q), 142.8 (CH), 139.2 (CH), 138.7 (CH), 133.4 (C_q), 129.4 (C_q), 128.8 (CH), 127.2 (CH), 123.5 (CH), 115.3 (CH), 109.4 (CH). The spectroscopic properties were

consistent with the data available in the literature (DE CARVALHO, Renato *et al*., 2024).

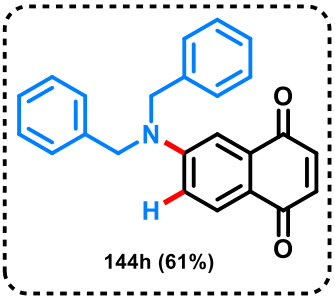

6-(Dibenzylamino)naphthalene-1,4-dione (Compound **144h**): Purification by flash column chromatography (10% EtOAc/Hex) afforded the title compound **144h** (43 mg, 61%) as a dark red oil; **^{1}H NMR (500 MHz, $CDCl_3$)** δ 7.89 (d, *J* = 8.8 Hz, 1H), 7.41 (d, *J* = 2.9 Hz, 1H), 7.35 (t, *J* = 7.2 Hz, 4H), 7.30 (d, *J* = 5.8 Hz, 2H), 7.21 (d, *J* = 7.0 Hz, 4H), 6.94 (dd, *J* = 8.8, 2.9 Hz, 1H), 6.84 (d, *J* = 10.2 Hz, 1H), 6.80 (d, *J* = 10.3 Hz, 1H), 4.79 (s, 4H); **^{13}C NMR (125 MHz, $CDCl_3$)** δ 186.1 (C_q), 183.6 (C_q), 153.3 (C_q), 139.8 (CH), 137.7 (CH), 136.6 (2 × C_q), 133.8 (C_q), 129.3 (CH), 129.1 (4 × CH), 127.7 (2 × CH), 126.6 (4 × CH), 121.5 (C_q), 115.9 (CH), 108.7 (CH), 54.1 (2 × CH_2). The spectroscopic properties were consistent with the data available in the literature (DE CARVALHO, Renato *et al*., 2024).

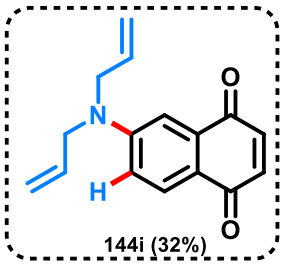

6-(Diallylamino)naphthalene-1,4-dione (Compound **144i**): Purification by flash column chromatography (10% EtOAc/Hex) afforded the title compound **144i** (16 mg, 32%) as a purple solid; **mp** 132–134 ºC; **ν_{max}/cm^{-1}**: 1700 (s), 1541 (s), 1049 (m); **^{1}H NMR (400 MHz, $CDCl_3$)** δ 7.81 (d, *J* = 8.8 Hz, 1H), 7.16 (s, 1H), 6.78 (dd, *J* = 8.8, 2.8 Hz, 1H), 6.76 (d, *J* = 10.1 Hz, 1H), 6.72 (d, *J* = 10.3 Hz, 1H), 5.81–5.72 (m, 2H), 5.13 (dq, *J* = 10.4, 1.4 Hz, 2H), 5.07 (dq, *J* = 17.1, 1.5 Hz, 2H), 3.98–3.96 (m, 4H); **^{13}C NMR (100 MHz, $CDCl_3$)** δ 186.3 (C), 183.7 (C), 152.7 (C), 139.9 (CH), 137.7 (CH), 133.7 (C), 132.1 (2 × CH), 129.1 (CH), 121.0 (C), 117.1 (2 × CH_2), 115.7 (CH), 108.7 (CH), 52.9 (2 × CH_2); **HRMS (ESI+):** Calculated for $C_{16}H_{16}NO_2$: 254.1181. Found $[M + H]^+$: 254.1135.

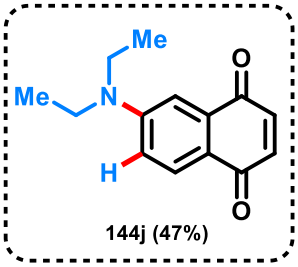

144j (47%)

6-(Diethylamino)naphthalene-1,4-dione (Compound **144j**): Purification by flash column chromatography (10% EtOAc/Hex) afforded the title compound **144j** (22 mg, 47%) as purple crystals; **mp** 138–141 ºC; **ν_{max}/cm^{-1}:** 2926 (m), 1653 (s), 1559 (s), 1319 (s), 820 (s); **^{1}H NMR (600 MHz, $CDCl_3$)** δ 7.91 (d, J = 8.8 Hz, 1H), 7.21 (d, J = 2.8 Hz, 1H), 6.85–6.79 (m, 3H), 3.53 (q, J = 7.1 Hz, 4H), 1.27 (t, J = 7.2 Hz, 6H); **^{13}C NMR (150 MHz, $CDCl_3$)** δ 186.6 (C_q), 183.5 (C_q), 151.7 (C_q), 140.1 (CH), 137.5 (CH), 133.9 (C_q), 129.3 (CH), 120.0 (C_q), 114.7 (CH), 108.0 (CH), 44.9 (2 × CH_2), 12.7 (2 × CH_3); **HRMS** (ESI+): Calculated for $C_{14}H_{16}NO_2$: 230.1181. Found $[M + H]^+$: 230.1138. The structure of the product was also confirmed by X-ray diffraction (CCDC number = 2352787).

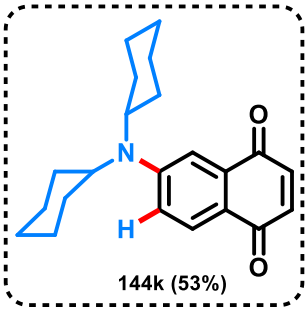

144k (53%)

6-(Dicyclohexylamino)naphthalene-1,4-dione (Compound **144k**): Purification by flash column chromatography (10% EtOAc/Hex) afforded the title compound **144k** (36 mg, 53%) as a dark red solid; **mp** 129–130 ºC; **^{1}H NMR (500 MHz, $CDCl_3$)** δ 7.86 (d, J = 8.8 Hz, 1H), 7.43 (d, J = 2.9 Hz, 1H), 7.05 (dd, J = 9.0, 2.9 Hz, 1H), 6.85 (d, J = 10.2 Hz, 1H), 6.81 (d, J = 10.2 Hz, 1H), 3.55–3.49 (m, 2H), 1.90–1.85 (m, 8H), 1.77–1.73 (m, 6H), 1.44–1.37 (m, 4H), 1.26–1.21 (m, 2H); **^{13}C NMR (125 MHz, $CDCl_3$)** δ 186.5 (C_q), 183.5 (C_q), 153.1 (C_q), 140.0 (CH), 137.5 (CH), 133.1 (C_q), 128.3 (CH), 120.2 (C_q), 118.5 (CH), 111.8 (CH), 58.5 (2 × CH), 31.3 (4 × CH_2), 26.5 (4 × CH_2), 25.7 (2 × CH_2). The spectroscopic properties were consistent with the data available in the literature (DE CARVALHO, Renato *et al*., 2024).

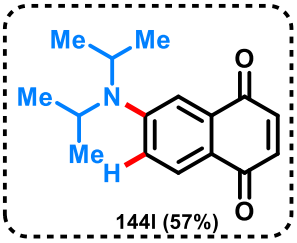

6-(Diisopropylamino)naphthalene-1,4-dione (Compound **144l**): Purification by flash column chromatography (10% EtOAc/Hex) afforded the title compound **144l** (29 mg, 57%) as a dark red solid; **mp** 133–134 ºC; **^{1}H NMR (500 MHz, CDCl$_3$)** *δ* 7.88 (d, *J* = 8.8 Hz, 1H), 7.39 (d, *J* = 2.9 Hz, 1H), 7.02 (dd, *J* = 9.0, 2.9 Hz, 1H), 6.85 (d, *J* = 10.4 Hz, 1H), 6.82 (d, *J* = 10.2 Hz, 1H), 4.11–4.03 (m, 2H), 1.38 (d, *J* = 6.9 Hz, 12H); **^{13}C NMR (125 MHz, CDCl$_3$)** δ 186.5 (C$_q$), 183.6 (C$_q$), 152.3 (C$_q$), 140.0 (CH), 137.5 (CH), 133.3 (C$_q$), 128.5 (CH), 120.1 (C$_q$), 118.0 (CH), 111.2 (CH), 48.0 (2 × CH), 21.0 (4 × CH$_3$). The spectroscopic properties were consistent with the data available in the literature (DE CARVALHO, Renato *et al*., 2024). The structure of the product **144l** was confirmed by X-ray diffraction (CCDC number = 2352789).

Characterization Data: Products 145a-e

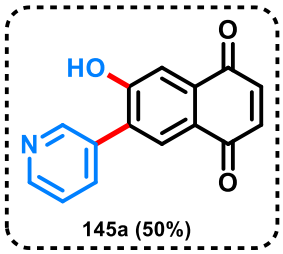

6-Hydroxy-7-(pyridin-3-yl)naphthalene-1,4-dione (Compound **145a**): Purification by flash column chromatography (10% EtOAc/Hex) afforded the title compound **145a** (25 mg, 50%) as an orange solid; **mp** 209–211 ºC; **^{1}H NMR (500 MHz, CDCl$_3$)** *δ* 15.51 (br s, 1H), 8.61 (s, 1H), 8.59 (d, *J* = 4.4 Hz, 1H), 8.17 (d, *J* = 8.3 Hz, 1H), 7.98 (td, *J* = 8.3, 1.8 Hz, 1H), 7.63 (s, 1H), 7.43–7.40 (m, 1H), 6.95 (s, 2H); **^{13}C NMR (125 MHz, CDCl$_3$)** *δ* 184.9 (C$_q$), 184.1 (C$_q$), 165.5 (C$_q$), 156.1 (C$_q$), 145.9 (CH), 139.5 (CH), 138.8 (CH), 138.7 (CH), 134.4 (C$_q$), 126.1 (CH), 123.5 (CH), 122.9 (C$_q$), 120.5 (CH), 116.7 (CH). The spectroscopic properties were consistent with the data available in the literature (DE CARVALHO, Renato *et al*., 2024).

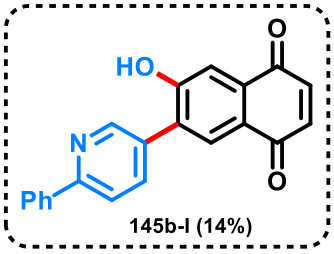

145b-I (14%)

6-Hydroxy-7-(6-phenylpyridin-3-yl)naphthalene-1,4-dione (Compound **145b-I**): Purification by flash column chromatography (10% EtOAc/Hex) afforded the title compound **145b-I** (9 mg, 14%) as a purple solid, as well as compound **145b-II** (29 mg, 44%) as dark red crystals; **mp** 194–195 ºC (decompose); **ν_{max}/cm^{-1}**: 3415 (m), 1666 (s), 1595 (s), 1587 (s), 1312 (m); **^{1}H NMR (400 MHz, $CDCl_3$)** δ 15.97 (br s, 1H), 8.63 (s, 1H), 8.10 (d, J = 7.7 Hz, 1H), 8.03 (t, J = 7.8 Hz, 1H), 7.93–7.91 (m, 2H), 7.78 (dd, *J* = 7.8, 0.8 Hz, 1H), 7.62 (s, 1H), 7.58-7.51 (m, 3H), 6.95 (s, 2H); **^{13}C NMR (100 MHz, $CDCl_3$)** *δ* 184.9 (C_q), 184.1 (C_q), 165.5 (C_q), 156.0 (C_q), 155.2 (C_q), 139.5 (CH), 139.5 (CH), 138.8 (CH), 137.4 (C_q), 134.4 (C_q), 130.3 (CH), 129.5 (2 × CH), 127.1 (2 × CH), 126.4 (CH), 123.5 (C_q), 123.0 (C_q), 120.7 (CH), 118.8 (CH), 116.6 (CH); **HRMS (ESI-):** Calculated for $C_{21}H_{13}NO_3$: 327.1. Found $[M + H]^-$: 327.1.

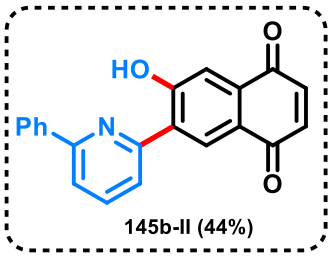

145b-II (44%)

6-hydroxy-7-(6-phenylpyridin-2-yl)naphthalene-1,4-dione (Compound **145b-II**): Purification by flash column chromatography (10% EtOAc/Hex) afforded the title compound **145b-II** (29 mg, 44%) as a purple solid, as well as compound **145b-I** (9 mg, 14%) as a dark orange solid; **mp** 154–155 ºC (decompose); **ν_{max}/cm^{-1}**: 3416 (m), 1672 (s), 1661 (s), 1588 (s), 1327 (m), 841 (m); **^{1}H NMR (400 MHz, $CDCl_3$)** *δ* 8.60 (s, 1H), 8.33 (d, *J* = 7.8 Hz, 1H), 8.15 (t, *J* = 8.0 Hz, 1H), 8.05 (d, *J* = 7.7 Hz, 1H), 8.02–8.00 (m, 2H), 7.62–7.58 (m, 2H), 7.56–7.53 (m, 1H), 7.39 (s, 1H), 7.03 (s, 2H); **^{13}C NMR (100 MHz, $CDCl_3$)** *δ* 184.6 (C_q), 183.5 (C_q), 163.6 (C_q), 154.3 (C_q), 154.3 (C_q), 139.9 (CH), 139.5 (CH), 138.6 (CH), 137.2 (C_q), 133.7 (C_q), 130.0 (CH), 129.4 (2 × CH), 126.9 (CH), 126.7 (2 × CH), 124.5 (C_q), 123.4 (C_q), 120.9 (CH), 120.7 (CH), 114.6 (CH); **HRMS (ESI-):** Calculated for $C_{21}H_{13}NO_3$: 327.1. Found $[M + H]^-$: 327.1.

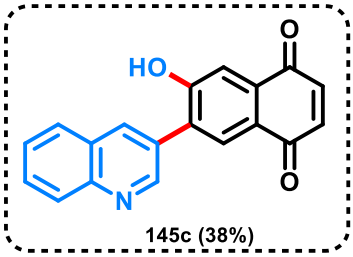

145c (38%)

6-Hydroxy-7-(quinolin-3-yl)naphthalene-1,4-dione (Compound **145c**): Purification by flash column chromatography (10% EtOAc/Hex) afforded the title compound **145c** (23 mg, 38%) as an orange solid; **mp** 262–263 ºC (decompose); **ν_{max}/cm^{-1}**: 3314 (w), 2848 (m), 1665 (s), 1577 (s), 1312 (m), 1233(m), 1056 (m), 836 (s); **^{1}H NMR (600 MHz, $CDCl_3$)** δ 8.74 (s, 1H), 8.40 (d, *J* = 8.9 Hz, 1H), 8.25 (d, *J* = 8.9 Hz, 1H), 8.07 (d, *J* = 8.6 Hz, 1H), 7.89 (d, *J* = 7.9 Hz, 1H), 7.81 (t, *J* = 7.2 Hz, 1H), 8.07 (d, *J* = 8.6 Hz, 1H), 7.67 (s, 1H), 7.64 (t, *J* = 7.1 Hz, 1H), 6.98–6.94 (m, 2H); **^{13}C NMR (100 MHz, DMSO-d_6)** δ 184.9 (C_q), 183.8 (C_q), 155.9 (C_q), 139.9 (CH), 139.4 (CH), 139.1 (CH), 139.0 (C_q), 139.0 (C_q), 134.6 (C_q), 131.7 (CH), 131.7 (C_q), 128.5 (CH), 128.3 (CH), 127.8 (CH), 127.7 (CH), 127.5 (CH), 123.7 (C_q), 119.5 (C_q), 115.2 (CH); **HRMS (ESI-):** Calculated for $C_{19}H_{12}NO_3$: 302.1. Found [M + H]$^{-}$: 302.1.

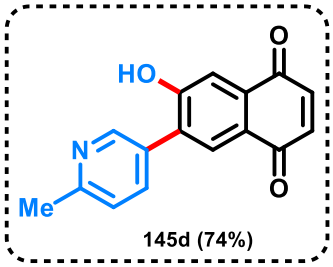

145d (74%)

6-Hydroxy-7-(6-methylpyridin-3-yl)naphthalene-1,4-dione (Compound **145d**): Purification by flash column chromatography (10% EtOAc/Hex) afforded the title compound **145d** (39 mg, 74%) as red crystals; **mp** 128–129 ºC (decompose); **ν_{max}/cm^{-1}**: 1666 (s), 1558 (s), 1585 (s), 1312 (m), 842 (s); **^{1}H NMR (600 MHz, $CDCl_3$)** δ 15.90 (br s, 1H), 8.58 (s, 1H), 7.97 (d, *J* = 8.1 Hz, 1H), 7.86 (t, *J* = 7.9 Hz, 1H), 7.60 (s, 1H), 7.24 (d, *J* = 7.6 Hz, 1H), 6.94–6.91 (m, 2H); **^{13}C NMR (150 MHz, $CDCl_3$)** δ 185.0 (C_q), 184.1 (C_q), 165.8 (C_q), 155.5 (C_q), 139.5 (CH), 139.3 (C_q), 138.9 (CH), 138.8 (CH), 134.2 (C_q), 126.2 (CH), 123.4 (C_q), 123.2 (CH), 123.0 (C_q), 117.5 (CH), 116.7 (CH), 23.8 (CH_3); **HRMS (ESI-):** Calculated for $C_{16}H_{12}NO_3$: 266.1. Found [M + H]$^{-}$: 266.1.

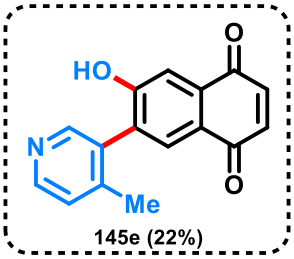

145e (22%)

6-Hydroxy-7-(4-methylpyridin-3-yl)naphthalene-1,4-dione (Compound **145e**): Purification by flash column chromatography (10% EtOAc/Hex) afforded the title compound **145e** (12 mg, 22%) as a purple solid; **mp** 129–130 ºC (decompose); **ν_{max}/cm^{-1}**: 1667 (s), 1613 (s), 1582 (s), 1315 (m), 843 (m), 827 (m); **^{1}H NMR (600 MHz, CDCl$_3$)** δ 15.57 (br s, 1H), 8.57 (s, 1H), 8.41 (d, *J* = 5.2 Hz, 1H), 7.97 (s, 1H), 7.60 (s, 1H), 7.21 (d, *J* = 5.1 Hz, 1H), 6.94-6.90 (m, 2H), 2.52 (s, 3H); **^{13}C NMR (150 MHz, CDCl$_3$)** δ 184.9 (C_q), 184.2 (C_q), 165.8 (C_q), 155.7 (C_q), 150.4 (C_q), 145.4 (CH), 139.5 (CH), 138.8 (CH), 134.2 (C_q), 125.9 (CH), 124.5 (CH), 123.3 (C_q), 122.9 (C_q), 121.0 (CH), 116.7 (CH), 21.8 (CH_3); **HRMS (ESI-):** Calculated for $C_{16}H_{12}NO_3$: 266.1. Found [M + H]$^{-}$: 266.1.

2.5.4 Trypanocidal Assay:

In vitro activity of compounds against bloodstream trypomastigotes of *T. cruzi*: For all the experiments stock solutions of the compounds were prepared in dimethyl sulfoxide, with the final concentration of the solvent never exceeding 0.5 %, concentration known to exert no toxicity to the parasite or host cells (SALOMÃO K, *et al*. 2010). Bloodstream trypomastigotes of Y strain (DA SILVA & NUSSENSZWEIG, 1953) were obtained from infected Swiss Webster mice at the peak of parasitaemia by differential centrifugation process. The parasites (5 × 10^6 parasites/mL) plus 5 % of blood were incubated at 4 °C for 24 h in 5 % CO_2 atmosphere in absence or presence of the compounds. Parasites counts were performed by light microscopy and the activity of the compounds was expressed as IC_{50}/24 h, corresponding to the concentration that led to 50 % lysis of the parasites. At least three independent experiments were performed, and the mean and standard deviation were calculated. The standard drug Bz was used as control.

2.6 REFERENCES

AIELLO, Anna *et al*. Antitumor effects of two novel naturally occurring terpene quinones isolated from the mediterranean ascidian Aplidium conicum. **Journal of Medicinal Chemistry**, v. 48, n. 9, p. 3410–3416, 2005. Available at: <http://doi.org/10.1021/jm0489915>.

ALVES, Maria Júlia M.; COLLI, Walter. Trypanosoma cruzi: Adhesion to the host cell and intracellular survival. **IUBMB Life**, v. 59, n. 4–5, p. 274–279, 2007. Available at: <http://doi.org/10.1080/15216540701200084>.

ASCHE, C. Antitumour Quinones. **Mini-Reviews in Medicinal Chemistry**, v. 5, n. 5, p. 449–467, 2005. Available at: <https://doi.org/10.2174/1389557053765556>.

BANDYOPADHYAY, Uday.; DAS, Dipark.; BANERJEE, Ranajit, K. Reactive Oxygen Species: Oxidative Damage and Pathogenesis. **Current Science**, v. 77, n. 5, p. 658–666, 1999.

BÁRCENAS-IRABIÉN, Alejandra Gabriela *et al*. Educational intervention to raise awareness and foster responsibility for Chagas disease risk factors in the rural community of Texca, Guerrero, Mexico. **Clinical Epidemiology and Global Health**, v. 30, n. 101831, 2024. Available at: <https://doi.org/10.1016/j.cegh.2024.101831>.

BELTRAN-HORTELANO, Iván *et al*. Examination of multiple *Trypanosoma cruzi* targets in a new drug discovery approach for Chagas disease. **Bioorganic and Medicinal Chemistry**, v. 58, n. 116577, 2022. Available at: <https://doi.org/10.1016/j.bmc.2021.116577>.

BELTRAN-HORTELANO, Iván *et al*. The role of imidazole and benzimidazole heterocycles in Chagas disease: A review. **European Journal of Medicinal Chemistry**, v. 206, n. 112692, 2020. Available at: <https://doi.org/10.1016/j.ejmech.2020.112692>.

BELTRAN-HORTELANO, Ivan; PEREZ-SILANES, Silvia; GALIANO, Silvia. Trypanothione Reductase and Superoxide Dismutase as Current Drug Targets for *Trypanosoma cruzi*: An Overview of Compounds with Activity against Chagas Disease. **Current Medicinal Chemistry**, v. 24, n. 11, p. 1066–1138, 2017. Available at: <https://doi.org/10.2174/0929867323666161227094049>.

BEZERRA, Rita Cristina. *Trypanosoma cruzi*, hemocultura: uma abordagem prática. **Revista da Sociedade Brasileira de Clínica Médica**, v. 8, n. 3, p. 205–207, 2010.

BICKELHAUPT, F. Matthias; HOUK, Kendall N. Analyzing Reaction Rates with the Distortion/Interaction-Activation Strain Model. **Angewandte Chemie** - International Edition, v. 56, n. 34, p. 10070–10086, 2017. Available at: <https://doi.org/10.1002/anie.201701486>.

BIJU, Akkattu, T. Modern Aryne Chemistry. **WILLEY-VCH**, 2021. Chapter. 1, p. 1-15. Available at: <https://doi.org/10.1002/9783527823086>.

BINKLEY, S.B. *et al*. the Isolation of Vitamin K1. **Journal of Biological Chemistry**, v. 130, n. 1, p. 219–234, 1939. Available at: <http://dx.doi.org/10.1016/S0021-9258(18)73574-6>.

BLUM, Ronald, H.; CARTER, Stephen. A new anticancer drug with significant clinical activity. **Annals of Internal Medicine**, v. 80, p. 249-259, 1974. Available at: <https:doi.org/10.7326/0003-4819-80-2-249>.

BRONNER, Sarah M.; BAHNCK, Kevin B.; GARG, Neil K. Indolynes as electrophilic indole surrogates: Fundamental reactivity and synthetic applications. **Organic Letters**, v. 11, n. 4, p. 1007–1010, 2009. Available at: <https://doi.org/10.1021/ol802958a>.

BROWN, Neil; BUSZEK, Keith R. Regioselectivity of Diels-Alder reactions between 6,7-dehydrobenzofuran and 2-substituted furans. **Tetrahedron Letters**, v. 53, n. 31, p. 4022–4025, 2012. Available at: <http://dx.doi.org/10.1016/j.tetlet.2012.05.118>.

CALDAS, Ivo Santana *et al*. Benznidazole therapy during acute phase of Chagas disease reduces parasite load but does not prevent chronic cardiac lesions. **Parasitology Research**, v. 103, n. 2, p. 413–421, 2008. Available at: <https://doi.org/10.1007/s00436-008-0992-6>.

CANT, Alastair A. *et al*. The benzyne aza-claisen reaction. **Angewandte Chemie** - International Edition, v. 48, n. 28, p. 5199–5202, 2009. Available at: https://doi.org/10.1002/anie.200901410>.

CHAGAS, Carlos. Nova tripanozomiaze humana: estudos sobre a morfolojia e o ciclo evolutivo do *Schizotrypanum cruzi* n. gen., n. sp., ajente etiolojico de nova entidade morbida do homem. **Memórias do Instituto Oswaldo Cruz**. Tomo I, p. 168-218,1909. Avaliable at: <https://doi.org/10.1590/S0074-02761909000200008>.

CHAPMAN, O. L.; CHANG, C. C.; KOLC, J. 9,10-Dehydroanthracene. A Derivative of 1,4-Dehydrobenzene. **Journal of the American Chemical Society**, v. 98, n. 18, p. 5703–5705, 1976. Available at: <9,10-Dehydroanthracene. A Derivative of 1,4-Dehydrobenzene>.

CHEN, Anan *et al*. Atovaquone enhances antitumor efficacy of TCR-T therapy by augmentation of ROS-induced ferroptosis in hepatocellular carcinoma. **Cancer Immunology, Immunotherapy**, v. 73, n. 3, 2024. Available at: <https://doi.org/10.1007/s00262-024-03628-2>.

COELHO-CERQUEIRA, Eduardo *et al*. Beyond topoisomerase inhibition: Antitumor 1,4-naphthoquinones as potential inhibitors of human monoamine oxidase. **Chemical Biology and Drug Design**, v. 83, n. 4, p. 401–410, 2014. Available at: <https://doi.org/10.1111/cbdd.12255>.

CÓRDOVA, Ezequiel *et al*. Neurological manifestations of Chagas' disease. **Neurological Research**, v. 32, n. 3, p. 238–244, 2010. Available at: <https://doi.org/10.1179/016164110X12644252260637>.

COURA, José Rodrigues; DE CASTRO, Solange L. A critical review on chagas disease chemotherapy**. Memorias do Instituto Oswaldo Cruz**, v. 97, n. 1, p. 3–24, 2002. Available at: <https://doi.org/10.1590/S0074-02762002000100001>.

COURA, José Rodrigues; DIAS, João Carlos Pinto. Epidemiology, control and surveillance of Chagas disease - 100 years after its discovery. **Memorias do Instituto Oswaldo Cruz**, v. 104, n. SUPPL. 1, p. 31–40, 2009. Available at: <https://doi.org/10.1590/S0074-02762009000900006>.

CRAMER, Christopher J. 2,3-Didehydro-1,4-benzoquinone. A quantum thermochemical study. **Journal of the Chemical Society, Perkin Transactions 2**. n. 2, p. 2273–2283, 1999. Available at: <https://doi.org/10.1039/A903116B>.

CROSSLEY, James A. *et al*. On the use of 2-(trimethylsilyl)iodobenzene as a benzyne precursor. **Tetrahedron Letters**, v. 51, n. 50, p. 6608–6610, 2010. Available at: <http://dx.doi.org/10.1016/j.tetlet.2010.10.052>.

DA SILVA, Eufrânio N. *et al*. Naphthoquinoidal [1,2,3]-triazole, a new structural moiety active against Trypanosoma cruzi. **European Journal of Medicinal Chemistry**, v. 43, n. 8, p. 1774–1780, 2008. Available at: <https://doi.org/10.1016/j.ejmech.2007.10.015>.

DA SILVA JÚNIOR, Eufrânio N. *et al*. Synthesis of quinones with highlighted biological applications: A critical update on the strategies towards bioactive compounds with emphasis on lapachones. **European Journal of Medicinal Chemistry**, v. 179, p. 863–915, 2019. Available at: < https://doi.org/10.1016/j.ejmech.2019.06.056>.

DA SILVA & NUSSENSZWEIG. A Strain of *Trypanosoma cruzi* Highly Virulent for Mice. **Folia Clinical Biology**, v.20, p. 191–207, 1953.

DARZI, Evan R.; BARBER, Joyann S.; GARG, Neil K. Cyclic Alkyne Approach to Heteroatom-Containing Polycyclic Aromatic Hydrocarbon Scaffolds. **Angewandte Chemie** - International Edition, v. 58, n. 28, p. 9419–9424, 2019. Available at: <https://doi.org/10.1002/anie.201903060>.

DAVICO, Gustavo E. *et al*. Photoelectron spectroscopy of benzoquinonide and dehydrobenzoquinone anions. **Journal of the American Chemical Society**, v. 121, n. 25, p. 6047–6054, 1999. Available at: https://doi.org/10.1021/ja990479z>.

DE ALMEIDA, Edvaldo Rodrigues *et al*. Antiinflammatory action of lapachol. **Journal of Ethnopharmacology**, v. 29, n. 2, p. 239–241, 1990. Available at: <https://doi.org/10.1016/0378-8741(90)90061-w>.

DE CARVALHO, Renato L. *et al*. The Synthesis and Reactivity of Naphthoquinonynes. **Angewandte Chemie** - International Edition, v. 63, n. 18, 2024. Available at: <https://doi.org/10.1002/anie.202400188>.

DE OLIVEIRA, Joyce C. *et al*. SuFEx-Functionalized Quinones via Ruthenium-Catalyzed C–H Alkenylation: A Potential Building Block for Bioactivity Valorization. **Chemistry – An Asian Journal**, v. 19, p. 1–7, 2024. Available at: <https://doi.org/10.1002/asia.202400757>.

DIAS, Gleiston G. *et al*. Ruthenium-catalyzed C-H oxygenation of quinones by weak O-coordination for potent trypanocidal agents. **Chemical Communications**, v. 54, n. 91, p. 12840–12843, 2018. Available at: <https://doi.org/10.1039/c8cc07572g>.

DIAS, Gleiston G. *et al*. Ruthenium(II)-Catalyzed C–H Alkenylation of Quinones: Diversity-Oriented Strategy for Trypanocidal Compounds. **European Journal of Organic Chemistry**, v. 2019, n. 13, p. 2344–2353, 2019. Available at: <https://doi.org/10.1002/ejoc.201900004>.

DUBROVSKIY, Anton V.; MARKINA, Nataliya A.; LAROCK, Richard C. Use of benzynes for the synthesis of heterocycles. **Organic and Biomolecular Chemistry**, v. 11, n. 2, p. 191–218, 2013. Available at: <https://doir.org/10.1039/c2ob26673c>.

DUMANSKA, Yuliia *et al*. Synthesis of New Fused Tricyclic Quinoid Systems and Studying of Their Biological Activity *In-Silico*. **Research Journal of Pharmaceutical, Biological and Chemical Sciences**. v. 4, n. 4, p. 1471–1479, 2013.

EL-MAGHRABEY, Mahmoud *et al*. Design of a dual functionalized chemiluminescence ultrasensitive probe for quinones based on their redox cycle. Application to the determination of doxorubicin in lyophilized powder and human serum. **Sensors and Actuators, B: Chemical**, v. 329, p. 129226, 2021. Available at: <https://doi.org/10.1016/j.snb.2020.129226>.

FREIRE, Elainne Silva *et al*. New Drugs and Promising Drug Combinations in the Treatment of Chagas Disease in Brazil: A Systematic Review and Meta-Analysis. **Archives of Medical Research**, v. 56, n. 1, p. 103084, 2025. Available at: <https://doi.org/10.1016/j.arcmed.2024.103084>.

GAFNER, Stefan *et al*. Antifungal and antibacterial naphthoquinones from Newbouldia laevis roots. **Phytochemistry**, v. 42, n. 5, p. 1315–1320, 1996. Available at: <https://doi.org/10.1016/0031-9422(96)00135-5>.

GAMPE, Christian M.; CARREIRA, Erick M. Arynes and cyclohexyne in natural product synthesis. **Angewandte Chemie** - International Edition, v. 51, n. 16, p. 3766–3778, 2012. Available at: <https://doi.org/10.1002/anie.201107485>.

GAULTIER, J.; HAUW, C. Structure de 1'α-naphtoquinone. **Acta Crystallographica**, v. 18, n. 2, p. 179–183, 1965. Available at: < https://doi.org/10.1107/S0365110X65000439>.

GOETZ, Adam E.; GARG, Neil K. Enabling the use of heterocyclic arynes in chemical synthesis. **Journal of Organic Chemistry**, v. 79, n. 3, p. 846–851, 2014. Available at: <https://dx.doi.org/10.1021/jo402723e>.

GUIMARÃES, Tiago T. *et al*. Potent naphthoquinones against antimony-sensitive and -resistant Leishmania parasites: Synthesis of novel α- And nor-α-lapachone-based 1,2,3-triazoles by copper-catalyzed azide-alkyne cycloaddition. **European Journal of Medicinal Chemistry**, v. 63, p. 523–530, 2013. Available at: <http://dx.doi.org/10.1016/j.ejmech.2013.02.038>.

HIMESHIMA, Yoshio; SONODA, Takaaki; KOBAYASHI, Hiroshi. Fluoride-induced 1,2-elimination of *o*-trimethylsilyl-phenyl triflateto benzyne under mild conditions. **Chem. Lett**., v. 12, issue. 8, p. 1211–1214, 1983. Available at: <https://doi.org/10.1246/cl.1983.1211>.

HOFFMANN, Reinhard W.; SUZUKI, Keisuke. A “hot, energized” benzyne. **Angewandte Chemie** - International Edition, v. 52, n. 10, p. 2655–2656, 2013. Available at: <https://doi.org/10.1002/anie.201209041>.

HUDSON, A. T. Atovaquone - a novel broad-spectrum anti-infective drug. **Parasitology Today**, v. 9, n. 2, p. 66–68, 1993. Available at: <https://doi.org/10.1016/0169-4758(93)90040-m>.

HUISGEN, Rolf; RIST, Herbert. Über Umlagerungen bei nucleophilen Substitutionen in der aromatischen Reihe und ihre Deutung. **Die Naturwissenschaften**, v. 41, n. 15, p. 358–359, 1954. Available at: <https://doi.org/10.1007/BF00643284>.

IKAWA, Takashi *et al*. A domino process for benzyne preparation: Dual activation of o-(trimethylsilyl)phenols by nonafluorobutanesulfonyl fluoride. **Organic Letters**, v. 13, n. 7, p. 1730–1733, 2011. Available at: <https://doi.org/10.1021/ol200252c r2011>.

IUPAC, International Union of Pure and Applied Chemistry, Compendium of chemical terminology. **Gold Book**. Version 2.3.1, p. 1220, 2012.

JARDIM, Guilherme A.M. *et al*. Copper complexes and carbon nanotube-copper ferrite-catalyzed benzenoid A-ring selenation of quinones: An efficient method for the synthesis of trypanocidal agents. **New Journal of Chemistry**, v. 43, n. 35, p. 13751–13763, 2019. Available at: <https://doi.org/10.1039/C9NJ02026H>.

JARDIM, Guilherme A.M. *et al*. Direct sequential C-H iodination/organoyl-thiolation for the benzenoid A-ring modification of quinonoid deactivated systems: A new protocol for potent trypanocidal quinones. **Organic and Biomolecular Chemistry**, v. 16, n. 10, p. 1686–1691, 2018. Available at: <https://doi.org/10.1039/c8ob00196k>.

JARDIM, Guilherme A.M. *et al*. Rhodium-catalyzed C-H bond activation for the synthesis of quinonoid compounds: Significant Anti-Trypanosoma cruzi activities and electrochemical studies of functionalized quinones. **European Journal of Medicinal Chemistry**, v. 136, p. 406–419, 2017. Available at: <http://dx.doi.org/10.1016/j.ejmech.2017.05.011>.

JARDIM, Guilherme A.M.; DA SILVA, Eufranio N.; BOWER, John F. Overcoming naphthoquinone deactivation: Rhodium-catalyzed C-5 selective C-H iodination as a gateway to functionalized derivatives. **Chemical Science**, v. 7, n. 6, p. 3780–3784, 2016. Available at: <https://doi.org/10.1039/c6sc00302h>.

JELLY, Renee *et al*. Lawsone: A novel reagent for the detection of latent fingermarks on paper surfaces. **Chemical Communications**, n. 30, p. 3513–3515, 2008. Available at: <http://doir.org/10.1039/B808424F>.

JESIONOWSKI, Teofil; KLAPISZEWSKI, Łukasz; MILCZAREK, Grzegorz. Kraft lignin and silica as precursors of advanced composite materials and electroactive blends. **Journal of Materials Science**, v. 49, n. 3, p. 1376–1385, 2014. Available at: <https://doi.org/10.1007/s10853-013-7822-7>.

JONES, Alexandra E. *et al*. Quinone voltammetry for redox-flow battery applications. **Journal of Electroanalytical Chemistry**, v. 920, n. June, p. 116572, 2022. Available at: <https://doi.org/10.1016/j.jelechem.2022.116572>.

KERN, Dóra *et al*. I Bind It That Way – Bioorthogonal Unmasking of Pro-Fluorescent Quinone Methides. **European Journal of Organic Chemistry**, v. 202400541, p. 1–7, 2024. Available at: <https://doi.org/10.1002/ejoc.202400541>.

KOVÁCS, Szabolcs *et al*. Design and application of new imidazolylsulfonate-based benzyne precursor: An efficient triflate alternative. **Organic Letters**, v. 14, n. 8, p. 2022–2025, 2012. Available at: <https://doi.org/10.1021/ol300529j>.

KOYAMA, Junko. Anti-Infective Quinone Derivatives of Recent Patents. **Recent Pat Antiinfect Drug Discov.** p. 113–125, n. 1, 2006. Available at: <https://doir.org/10.2174/157489106775244073>.

KUMAGAI, Yoshito *et al*. The chemical biology of naphthoquinones and its environmental implications. **Annual Review of Pharmacology and Toxicology**, v. 52, p. 221–247, 2012. Available at: <https://doir.org/10.1146/annurev-pharmtox-010611-134517>.

LIU, Zhijian; LAROCK, Richard C. Intermolecular C-N addition of amides and S-N addition of sulfinamides to arynes. **Journal of the American Chemical Society**, v. 127, n. 38, p. 13112–13113, 2005. Available at: <https://doir.org/10.1021/ja054079p>.

LÓPEZ LÓPEZ, Lluvia Itzel *et al*. Naphthoquinones: Biological properties and synthesis of lawsone and derivatives — a structured review. **Vitae**, v. 21, n. 3, p. 248–258, 2014. Available at: <https://doi.org/10.17533/udea.vitae.17322>.

MATSUMOTO, Takashi *et al*. New efficient protocol for aryne generation. Selective synthesis of differentially protected 1,4,5-naphthalenetriols. **Tetrahedron Letters**, v. 32, n. 46, p. 6735–6736, 1991. Available at: <https://doi.org/10.1016/S0040-4039(00)93589-5>.

MCVEIGH, Matthew S. *et al*. Silyl Tosylate Precursors to Cyclohexyne, 1,2-Cyclohexadiene, and 1,2-Cycloheptadiene. **Organic Letters**, v. 22, n. 11, p. 4500–4504, 2020. Available at: <https://dx.doi.org/10.1021/acs.orglett.0c01510>.

MOLFETTA, F. A. *et al*. A structure-activity relationship study of quinone compounds with trypanocidal activity. **European Journal of Medicinal Chemistry**, v. 40, n. 4, p. 329–338, 2005. Available at: <https://doi.org/10.1016/j.ejmech.2004.10.009>.

MORTON, R A. Biochemistry of Quinones. **Angew. Chem**, v. 78, n. 12, p. 651, 1966. Available at: <https://doi.org/10.1002/ange.19660781223>.

NASIR, Naurah Nabihah *et al*. Chemistry, Biosynthesis and Pharmacology of Streptonigrin: An Old Molecule with Future Prospects for New Drug Design, Development and Therapy. **Drug Design, Development and Therapy**, v. 17, p. 1065–1078, 2023. Available at: <https://doi.org/10.2147/DDDT.S388490>.

NASIRI, Hamid Reza *et al*. Design, synthesis, and biological testing of novel naphthoquinones as substrate-based inhibitors of the quinol/fumarate reductase from *Wolinella succinogenes*. **Journal of Medicinal Chemistry**, v. 56, n. 23, p. 9530–9541, 2013. Available at: <https://doi.org/10.1021/jm400978u>.

NUNES, Maria Carmo P. *et al*. Clinical features of Chagas disease progression and severity. **The Lancet Regional Health - Americas**, v. 37, p. 100832, 2024. Available at: <https://doi.org/10.1016/j.lana.2024.100832>.

PELLIESER, Hélene.; SANTELLI, Maurice. The Use of Arynes in Organic Synthesis. **Tetrahedron**, v. 59, n. 6, p. 701-703, 2003. Available at: <https://doi.org/ 10.1016/S0040-4020(02)01563-6>.

PEREIRA, Paulo Câmara Marques; NAVARRO, Elaine Cristina. Challenges and perspectives of Chagas disease: A review. **Journal of Venomous Animals and Toxins Including Tropical Diseases**, v. 19, n. 1, p. 1–8, 2013. Available at: <https://doi.org/10.1186/1678-9199-19-34>.

PINAZO, Maria Jesus *et al*. Challenges and advancements in the development of vaccines and therapies against Chagas disease**. The Lancet Microbe**, v. 5, n. October, p. 1–12, 2024. Available at: <https://doi.org/10.1016/ j.lanmic.2024.100972>.

PRICE, Claire E.; DRIESSEN, Arnold J.M. Biogenesis of membrane bound respiratory complexes in *Escherichia coli*. **Biochimica et Biophysica Acta - Molecular Cell Research,** v. 1803, n. 6, p. 748–766, 2010. Available at: <http://dx.doi.org/10.1016/j.bbamcr.2010.01.019>.

RAMINELLI, LIU & LAROCK. Regioselective Synthesis of 3-(2-Hydroxyaryl)pyridine via Arynes and Pyridine *N*-Oxides. **Journal of Organic Chemistry**, v. 71, n. 12, p. 4689-4691, 2006. Available at: <https://doi.org/10.1021/jo060523a>.

RASHID, Muhammad *et al*. Systematic review on buparvaquone resistance associated with non-synonymous mutation in drug binding genes site of *Theileria annulate*.

Veterinary Parasitology, v. 332, n. October, p. 110321, 2024. Available at: <https://doi.org/10.1016/j.vetpar.2024.110321>.

RIBEIRO, Vanessa *et al*. Current trends in the pharmacological management of Chagas disease. **International Journal for Parasitology: Drugs and Drug Resistance**, v. 12, n. August 2019, p. 7–17, 2020. Available at: <https://doi.org/10.1016/j.ijpddr.2019.11.004>.

ROBERTS, Jhon D *et al*. Rearrangement in the reaction of chlorobenzene-1-C^{14} with potassium amide. **Journal of the American Chemical Society**. v. 75, no. 13, p. 3290–3291, 1953. Available at: <https://doi.org/10.1021/ja01109a523>.

SALOMÃO K, *et al*. *In Vitro* and In *Vivo* Activities of 1,3,4-Thiadiazole-2-Arylhydrazone Derivatives of Megazol against *Trypanosoma cruzi*. **Antimicrobial Agents and Chemother**. V. 54, p. 2023–2031, 2010. Available at: <https://doi.org/10.1128/AAC.01241-09>.

SHI, Jiarong; LI, Lianggui; LI, Yang. *O*-Silylaryl Triflates: A Journey of Kobayashi Aryne Precursors. **Chemical Reviews**, v. 121, n. 7, p. 3892–4044, 2021. Available at: <https://dx.doi.org/10.1021/acs.chemrev.0c01011>.

SIES, Helmut; JONES, Dean P. Reactive oxygen species (ROS) as pleiotropic physiological signalling agents. **Nature Reviews Molecular Cell Biology**, v. 21, n. 7, p. 363–383, 2020. Available at: <http://dx.doi.org/10.1038/s41580-020-0230-3>.

SODERQUIST, C. J. Juglone and allelopathy. **Journal of chemical education**, v. 50, n. 11, p. 782–783, 1973. Available at: <https://doi.org/10.1021/ed050p782>.

SOUZA, LOPES & DE ANDRADE. Fontes, formação, reatividade e determinação de quinonas na atmosfera. **Química Nova**, v. 39, n. 40, p, 486-495, 2016. Available at: < http://dx.doi.org/10.5935/0100-4042.20160034>.

STAGLIANO, Kenneth W. *et al*. Regiocontrolled synthesis and HIV inhibitory activity of unsymmetrical binaphthoquinone and trimeric naphthoquinone derivatives of conocurvone. **Bioorganic and Medicinal Chemistry**, v. 14, n. 16, p. 5651–5665, 2006. Available at: <https://doi.org/10.1016/j.bmc.2006.04.034>.

STOERMER & KAHLERT. Ueber das 1- und 2-Brom-cumaron. **Deutschen Chemischen Gesellschaft**. v. 35, p. 1633–1640, 1902. Available at: <https://doi.org/10.1002/cber.19020350286>.

SU, Jinling *et al*. A Copper Halide Promoted Regioselective Halogenation of Coumarins Using N-Halosuccinimide as Halide Source. **Synlett**, v. 30, n. 5, p. 630–634, 2019. Available at: <https://doi.org/10.1055/s-0037-1612080>.

SUTO, Yutaka *et al*. Synthesis and biological evaluation of quinones derived from natural product komaroviquinone as anti-*Trypanosoma cruzi* agents. **Bioorganic and Medicinal Chemistry Letters**, v. 25, n. 15, p. 2967–2971, 2015. Available at: <http://dx.doi.org/10.1016/j.bmcl.2015.05.022>.

TADROSS, Pamela M.; STOLTZ, Brian M. A comprehensive history of arynes in natural product total synthesis. **Chemical Reviews**, v. 112, n. 6, p. 3550–3577, 2012. Available at: <https://dx.doi.org/10.1021/cr200478h>.

TAKIKAWA, Hiroshi *et al*. Aryne-based strategy in the total synthesis of naturally occurring polycyclic compounds. **Chemical Society Reviews**, v. 47, n. 21, p. 8030–8056, 2018. Available at: <https://doi.org/10.1039/c8cs00350e>.

THOMSON, R. H. Naturally Occurring Quinones IV. Recent advances. Fourth Edition. **Blackie Academic & Professional**. Ed, Chapman & Hall. 1996. Chapter. 2, p. 112-123. Available at: <https://doi.org/10.1007/978-94-009-1551-0>.

WENK, Hans Henning; WINKLER, Michael; SANDER, Wolfram. One century of aryne chemistry. **Angewandte Chemie** - International Edition, v. 42, n. 5, p. 502–528, 2003. Available at: <https://doi/10.1002/anie.200390151>.

WITTIG, Georg; POHMER, Liselotte. Über das intermediäre Auftreten von Dehydrobenzol. **Chemische Berichte**, v. 89, n. 5, p. 1334–1351, 1956. Available at: <https://doi.org/10.1002/CBER.19560890539>.

WU, Chunrui; SHI, Feng. A Closer look at aryne chemistry: Details that remain mysterious. **Asian Journal of Organic Chemistry**, v. 2, n. 2, p. 116–125, 2013. Available at: <https://doi.org/10.1002/ajoc.201200142>.

YOSHIDA, Hiroto *et al*. Arynes in a three-component coupling reaction: Straightforward synthesis of benzoannulated iminofurans. **Angewandte Chemie** - International Edition, v. 43, n. 30, p. 3935–3938, 2004. Available at: <https://doi.org/10.1002/anie.200460009>.

YOSHIDA, Hiroto; TAKAKI, Ken. Aryne insertion reactions into carbon-carbon σ-bonds. **Synlett**, v. 23, n. 12, p. 1725–1732, 2012. Available at: https://doi.org/10.1055/s-0031-1290401>.

YOSHIDA, Suguru; HOSOYA, Takamitsu. The renaissance and bright future of synthetic aryne chemistry. **Chemistry Letters**, v. 44, n. 11, p. 1450–1460, 2015. Available at: <https://doi.org/10.1246/cl.150839>.

CHAPTER 3

BODIPY-Based Fluorescent Molecules

This chapter of the thesis was developed during a six-month Ph.D. exchange program carried out in collaboration with Prof. Dr. Daniel Werz at the Albert-Ludwigs-Universität Freiburg, Germany. The project was coordinated and prepared on the Brazilian side by Prof. Eufrânio N. da Silva Junior from the Federal University of Minas Geral, from April to September 2024, as part of EDITAL 01/2024, PDSE – CAPES PrInt.

3.1 INTROUCTION

3.1.1 BODIPY Chemistry:

The family of compounds known as 4,4-difluoro-4-bora-3a,4a-diaza-s-indacene or boron-dipyrromethene (BODIPY) is considered one of the most important classes of organic chromophores today, owing to their remarkable photophysical properties and high versatility, which enable a wide range of applications (SQUEO, Benedetta Maria *et al*., 2021; LOUDET & BURGESS, 2007).

The characteristic structure of BODIPY compounds, as depicted in **Figure 37**, comprises a dipyrromethene ligand coordinated to a disubstituted boron atom, giving rise to the BODIPY core. The IUPAC numbering system for BODIPY dyes differs from that of dipyrromethenes, which may lead to some ambiguity. Nevertheless, the designations *α*-, *β*-, and *meso*- are consistently used across both systems (Dixon, H. B. F. *et al*., 1987).

Figure 37. Naming and numbering of Dipyrrin and BODIPY core.

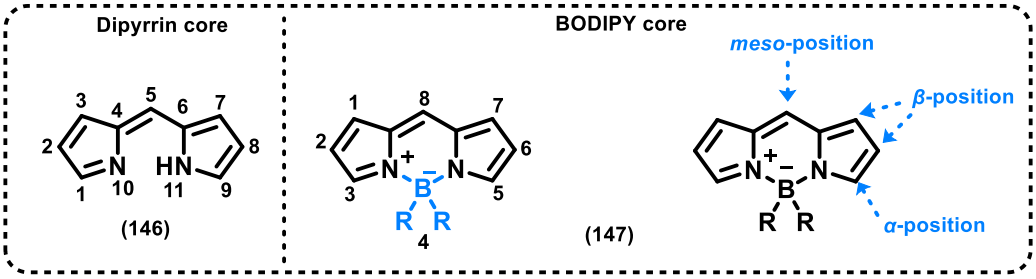

BODIPY dyes constitute a versatile family of organoboron compounds widely recognized for their exceptional photophysical and chemical properties. They display strong and narrow absorption and emission bands, small Stokes shifts, high molar absorption coefficients (up to 1.2 × 10^5 M^{-1} cm^{-1}), and outstanding fluorescence quantum yields (ULRICH, ZIESSEL & HARRIMAN, 2008; BASSAN, Elena *et al*., 2021).

In addition, BODIPY fluorophores are remarkably photostable and thermally stable, showing minimal sensitivity to environmental factors such as polarity or pH (ZHANG, Wangquan *et al*., 2021; KOLEMEN, Safacan. *et al*., 2015; HUANG, GAO & HAN, 2017). Structurally, the molecule adopts a nearly planar configuration, which ensures effective π-conjugation throughout the fluorophore core (NI & WU, 2014).

Because of this combination of desirable optical and chemical features, BODIPY compounds have emerged as one of the most extensively studied classes of fluorescent dyes. Ongoing research efforts are focused on the design and synthesis of new BODIPY derivatives with tunable absorption and emission wavelengths, enabling their application across a broad range of fields, from materials science to bioimaging (FRATH, Denis *et al.*, 2014).

At the beginning of the 21st century, fundamental studies on the chemical reactivity and photophysical properties of BODIPY dyes began to emerge at an accelerated pace. Since then, the number of research publications has continued to grow steadily, reflecting the remarkable versatility of this class of fluorophores (**Figure 38**). In 2024 alone, 1,083 journal articles reported diverse applications of BODIPY-based dyes, and to date, 2,429 patents related to BODIPY technologies have been filed (CAS SciFinder, 2025).

Figure 38. Annual number of scientific publications describing BODIPY dyes (CAS SciFinder).

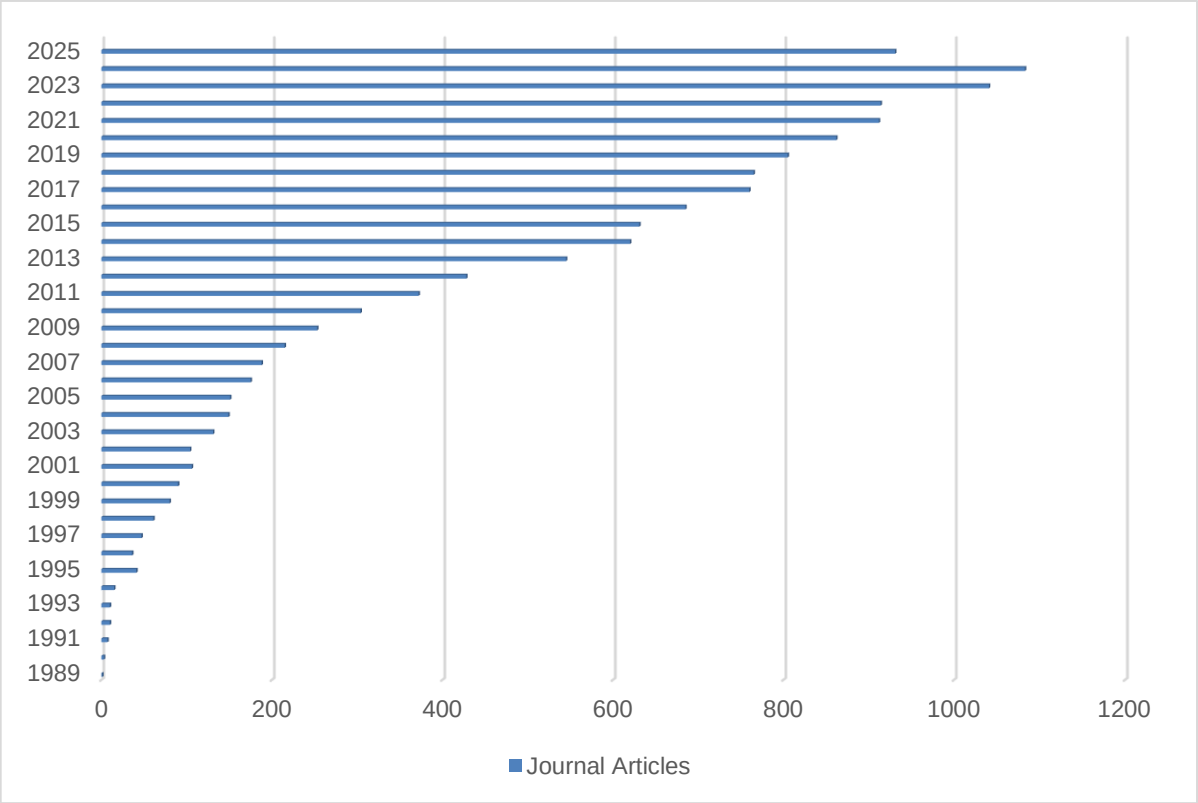

BODIPY dyes were first reported in 1968 by Treibs and Kreuzer (TREIBS & KREUZER, 1968), who synthesized mono- and di-substituted BODIPY derivatives from 2,4-dimethylpyrrole in the presence of acetic anhydride and boron trifluoride

diethyl etherate ($BF_3 \cdot OEt_2$), yielding compounds with characteristic green fluorescence (**Scheme 27**) (TREIBS & KREUZER, 1968).

Scheme 27. Preparation of the first reported BODIPY dyes in 1968 by Treibs and Kreuzer.

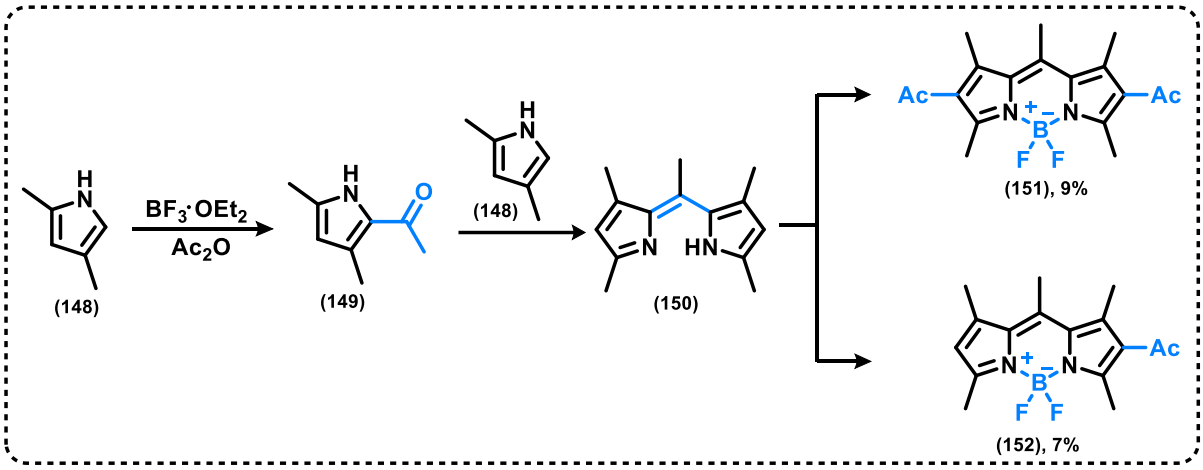

Since then, the synthesis of BODIPY core has become well established and can generally be categorized into two main approaches (**Scheme 28**) (ULRICH, ZIESSEL & HARRIMAN, 2008; LOUDET & BURGESS, 2007). The first approach typically leads to symmetric BODIPYs. It involves the formation of a dipyrromethene intermediate through the condensation of two pyrrole units with a highly electrophilic carbonyl compound—such as an acyl chloride, acid anhydride, or aldehyde—to generate the methane bridge. Subsequent complexation with $BF_3 \cdot OEt_2$ in the presence of a base, commonly a tertiary amine, affords the BODIPY core (BOYER, Joseph H. *et al*., 1993; LI, MINTZER & BITTMAN, 2006, WAGNER & LINDSEY, 1996).

The second approach proceeds through the formation of ketopyrrole intermediates. In this case, a Lewis acid–mediated condensation between a carbonyl-containing pyrrole and another pyrrole molecule, were typically yields asymmetric BODIPYs. **Scheme 28** illustrates a general synthetic outline for both symmetric and asymmetric BODIPY dyes, along with representative examples of each (TAHTAOUI, Chouaib, *et al* 2006).

Scheme 28.Typical synthesis of symmetric (A) and asymmetric (B) BODIPY dyes and examples.

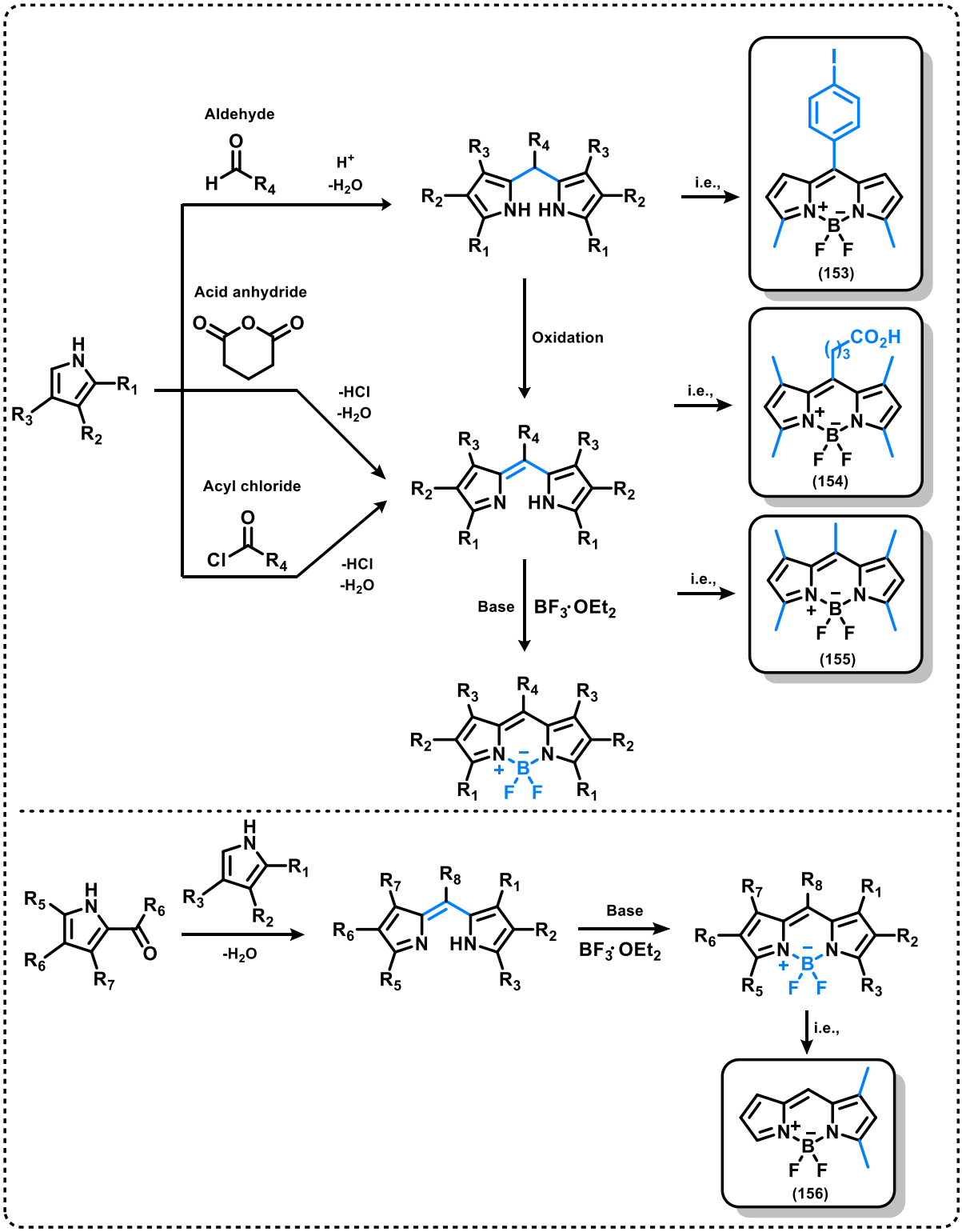

3.1.2 Derivatives and Functionalization of BODIPY dyes:

Among the many families of fluorescent dyes, boron-dipyrromethene (BODIPY) derivatives occupy a prominent position due to their excellent photophysical properties, discussed in the previous section, and, the remarkable chemical versatility of their boron-dipyrromethene core, which can be modified through a wide range of synthetic strategies (**Figure 39**) (BENSTEAD, MEHL & BOYLE, 2011).

The BODIPY framework contains eight reactive positions that allow precise modulation of its optical and electronic properties (**Figure 39**): two boron positions, two *α*-positions, four *β*-positions, and the *meso*-position. The *α* and *β* positions exert the strongest influence on the π-electronic delocalization, whereas the *meso* and boron positions play a smaller role in the electronic distribution but significantly affect the steric environment of the molecule (LLANO, Rebeca Sola, *et al*, 2018; LITTLER, Benjamin J. *et al,* 1999).

Such structural flexibility enables exhaustive and selective functionalization of BODIPY dyes with a wide variety of substituents. The resulting substitution patterns not only determine the fundamental photophysical characteristics of the dyes but can also lead to new photochemical behaviors, including charge or electron transfer, energy transfer, and triplet-state population (ZIESSEL, ULRICH & HARRIMAN, 2007; BOENS, VERBELEN & DEHAEN, 2015; LAKSHMI, SHARMA & RAVIKANTH, 2016).

Figure 39. Schematic view of structural modifications and example chemical reactions on the BODIPY core.

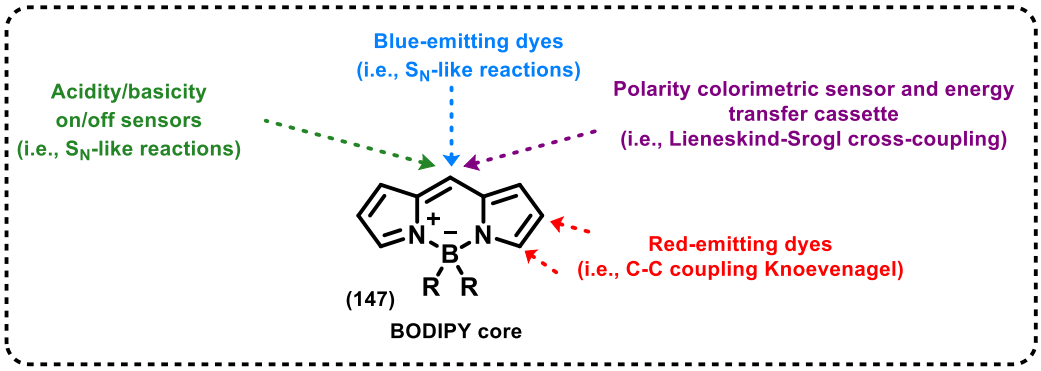

When comparing pre- and post-functionalization strategies for modifying the BODIPY core, these approaches can sometimes compete with each other, whereas in other cases they are complementary. For instance, compound **159** is more conveniently synthesized by starting from appropriately substituted pyrroles, which makes a pre-functionalization route the most efficient option (BOENS, Noël *et al*.,

2012). In contrast, derivatives such as compound **160**, which contain electron-donating heteroatoms at the 3-position of the BODIPY core, are more easily obtained through post-functionalization. In this case, nucleophilic substitution (**A**) (ROHAND, Taoufik *et al*., 2006) or oxidative nucleophilic hydrogen substitution (**B**) provides practical and efficient access to the target structures, as shown in **Scheme 29** (LEEN, Volker *et al*., 2010).

Scheme 29. Comparison of Pre- and Post-Functionalization (A: nucleophilic substitution, B: oxidative nucleophilic hydrogen substitution) Strategies for BODIPY Core Modification.

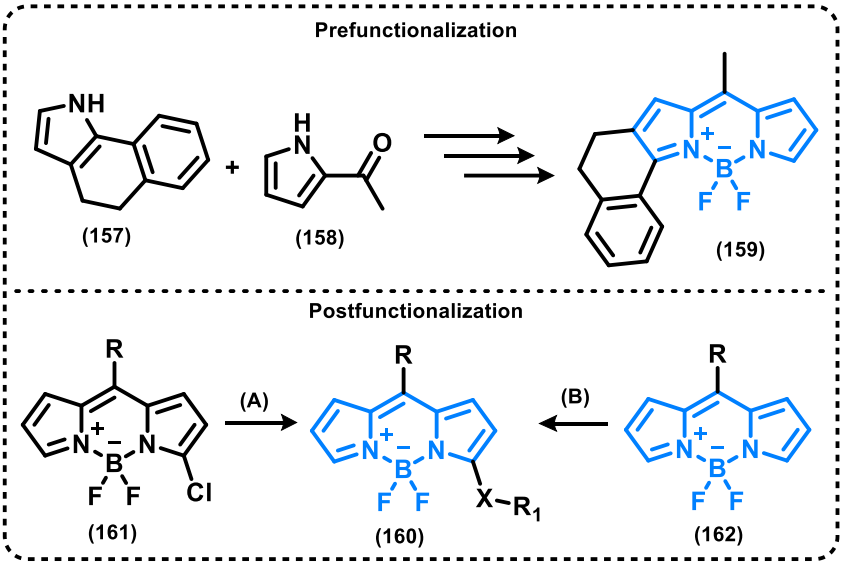

There are cases in which the BODIPY core can be functionalized through both strategy, and the choice between pre- and post-functionalization depends on the synthetic efficiency and accessibility of the desired target. Below, some of the most extensively studied examples of functionalized BODIPY derivatives are presented. For clarity, they are classified according to the substitution position on the BODIPY scaffold, as previously discussed.

- ***Meso*-functionalized BODIPYs:**

One of the most desirable families of BODIPY fluorophores are those bearing functionalized **aryl groups** at the *meso*-position. These derivatives are straightforward to obtain from functionalized aromatic aldehydes, and can be readily prepared through the well-established Lindsey approach (compound **163**) (LAKSHMI, RAO & RAVIKANTH, 2015).

Another relevant modification involves **8-thiomethyl BODIPYs** (compound **164**), which can be synthesized in only a few steps. The thiomethyl (–SCH_3) group at

the *meso*-position exhibits excellent reactivity, making it a key synthon for the preparation of diverse *meso*-substituted BODIPYs *via* Liebeskind–Srogl cross-coupling. In addition, it can act as a leaving group in nucleophilic substitution processes, enabling access to N- and O-nucleophile substituted analogues through S_NAr-type reactions (GOUD, TUTAR & BIELLMANN, 2006).

***Meso*-halogenated BODIPYs** have also been extensively investigated due to their versatility (compound **165**). These compounds serve as valuable intermediates for the construction of more complex *meso*-substituted derivatives, either through S_NAr reactions or transition-metal-catalyzed cross-coupling transformations, including Suzuki, Stille, Heck, Negishi, and Sonogashira reactions (LEEN, Volker *et al*., 2010).

Scheme 30 summarizes representative examples of these *meso*-functionalized BODIPY derivatives.

- **Pyrrole functionalized BODIPYs:**

The BODIPY core can be mono-functionalized at either the 2- or 3-position, allowing the introduction of substituents such as halogens, formyl (compound **166**), nitro (compound **167)**, amino, cyano, sulfonyl, among others, through various synthetic routes (JIAO, Lijuan *et al*., 2009; ESNAL, Ixone *et al*., 2013).

Di-functionalization is also common. The 2,6-positions bear the lowest positive charge density and are therefore susceptible to electrophilic attack, enabling transformations such as dihalogenation (compound **168**), diformylation *via* the Vilsmeier–Haack reaction, dinitration, dicyanation, and disulfonylation (compound **169** and **170**). In the case of 3,5-difunctionalization, halogenated, formyl, and cyano derivatives are frequently observed. The 1,7-positions of the BODIPY core are electron-poor, and direct halogenation at these sites is generally not feasible unless other positions are blocked beforehand. Additionally, 1,2- or 2,3-difunctionalized BODIPYs have been obtained through dihalogenation when the second pyrrole ring carbons are sterically or electronically protected (KIM & KIM, 2014; WANG, Liang *et al*., 2013).

Tri- and tetra-substitution are also possible, with most reported examples involving halogenation. In some cases, even penta- and hexa-substituted BODIPYs have been synthesized for specific applications (ORTIZ, Maria J. *et al*, 2012). **Scheme 31** illustrates representative examples of these pyrrole-functionalized derivatives.

Scheme 30. Representative examples of *Meso*-Functionalized BODIPYs.

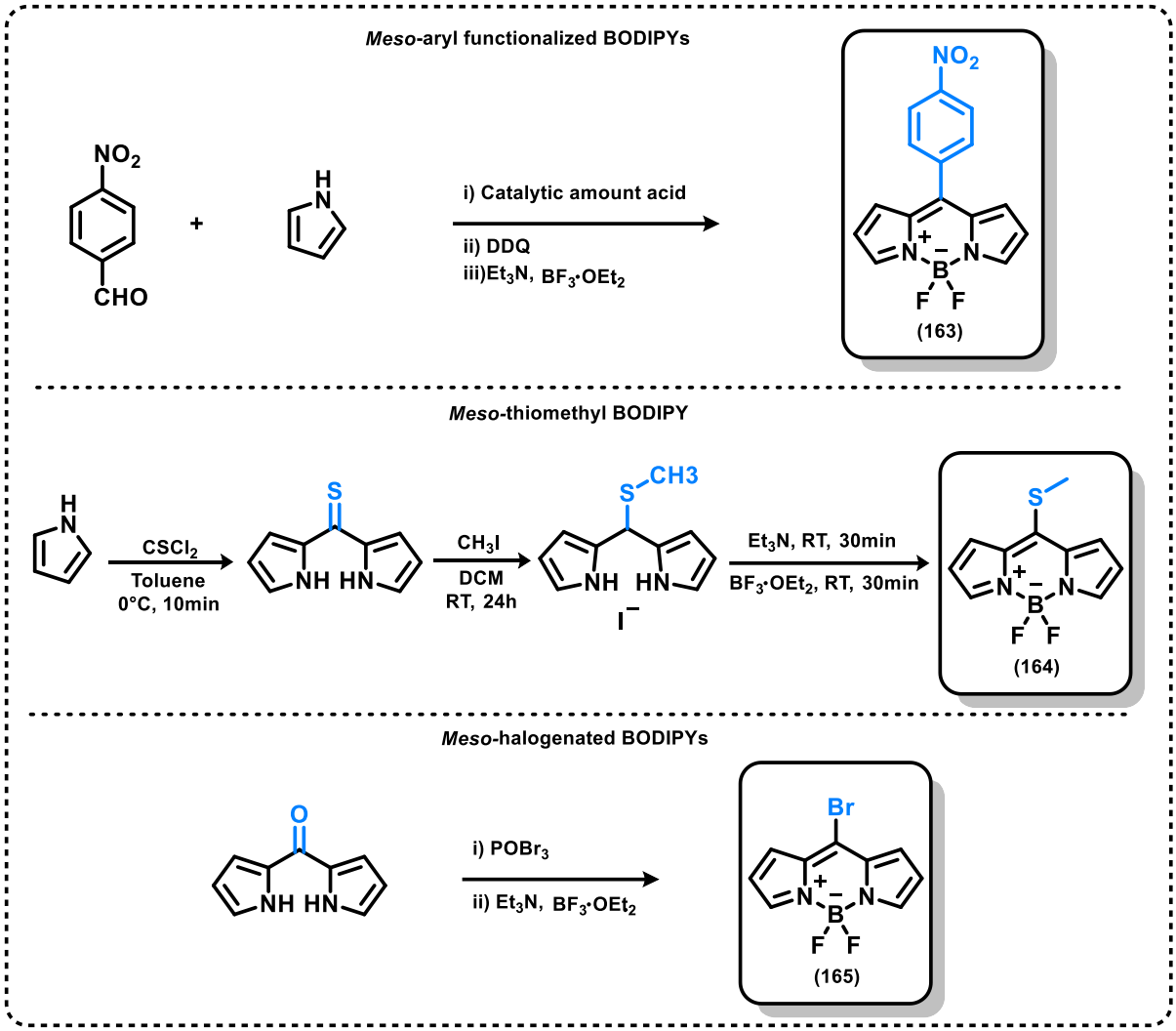

After discussing classical functionalization strategies on the BODIPY core, it is pertinent to highlight the most recent developments in this field. **Figure 40** illustrates representative examples, including the **AZA-BODIPY** class, characterized by the substitution of the meso-carbon by a nitrogen atom (SHIMIZU, Soji *et al*., 2013). It also features the **BOIMPY** motif (bis(borondifluoride)-8-imidazodipyrromethene), a red-emissive and highly fluorescent scaffold that constitutes a promising structural extension of the well-established BODIPY family (PATALAG, JONES & WERZ, 2016). Additionally, Compound **176** presents a case of B(III)-center functionalization, where fluorine atoms are replaced by ethynylarenes (ULRICH, Gilles *et al*., 2005).

Scheme 31. Representative examples of Pyrrole-Functionalized BODIPYs.

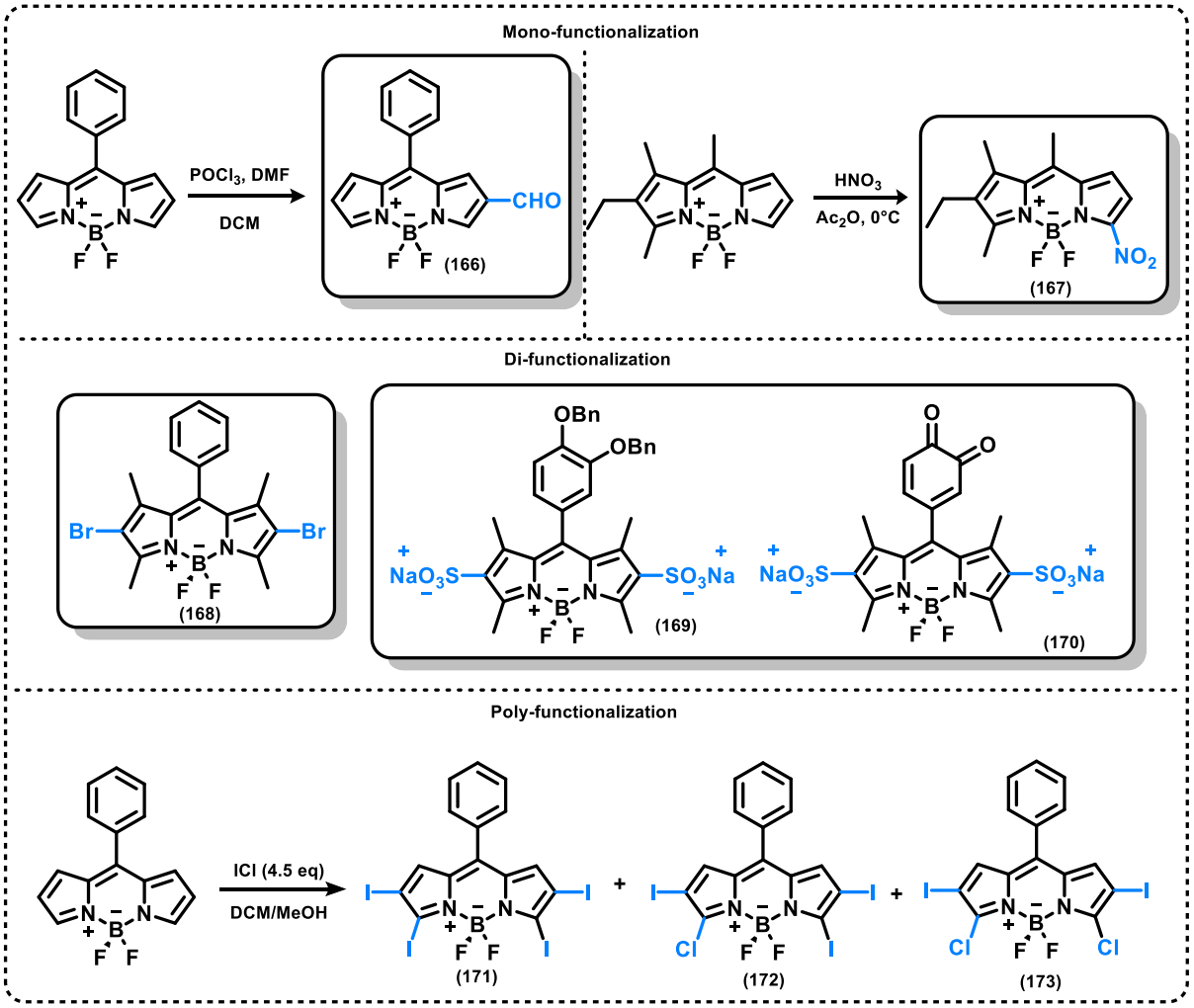

Figure 40. Representative examples of recent BODIPY core modifications.

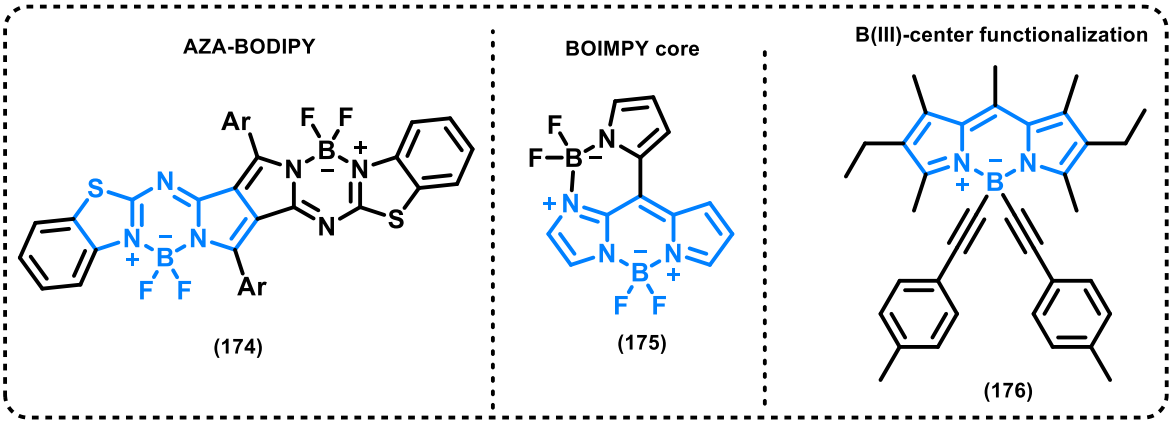

3.1.3 BODIPY Applications and Future Perspectives:

From a historical perspective, the first reported application of a BODIPY dye dates back to 1989, when it was employed as a fluorescent probe for bioactive ligands (MONSMA, Frederick J. *et al*., 1989). Since then, an extensive range of applications has been developed for fluorescent BODIPYs (**Figure 41**).

Following this early breakthrough, the practical utility of BODIPY dyes diversified rapidly. In recent years, they have been applied as fluorescent indicators (BOENS, LEEN & DEHAEN, 2012), biological and biomolecular labels (GONÇALVES, M. Sameiro T, 2009), probes for bioimaging (KOWADA, MAEDA & KIKUCHI, 2015), chromogenic probes and cation sensors (BEER, Gerhard *et al*., 2000), tunable laser dyes (ARBELOA, F. López *et al*., 2005), drug-delivery agents (MCCUSKER, CARROLL & ROTELLO, 2005), fluorescent switches (GOLOVKOVA, KOZLOV & NECKERS, 2005), potential photodynamic therapy agents (AWUAH & YOU, 2012), electroluminescent films (HEPP, A. *et al*., 2004), light-harvesters (LI & LINDSEY, 1999), and solar-cell sensitizers (HATTORI, Shigeki *et al*., 2005), among many others.

Figure 41. Historical timeline of key developments in BODIPY chemistry and applications.

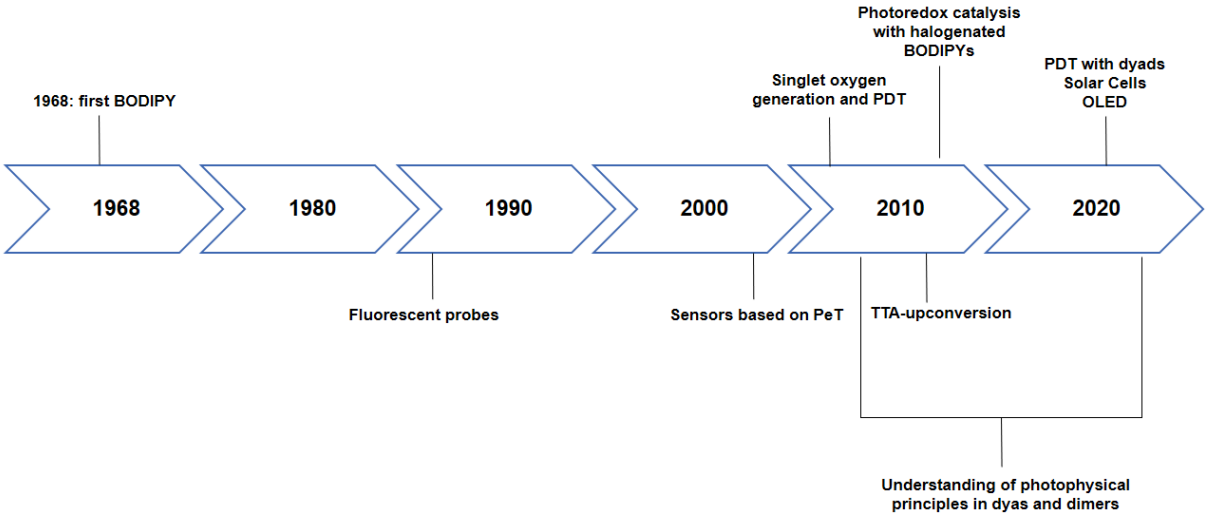

In summary, BODIPY dyes have transitioned from simple fluorescent probes to highly versatile molecular platforms with applications in chemistry, biology and materials science. Their tunable photophysical properties and structural flexibility continue to drive new developments, ensuring their relevance in current and future research (NAKASHIMA, Mika *et al*., 2018).

3.2 RESEARCH PURPOSE

The main goal of this research is to develop and optimize the synthesis of a series of BODIPY derivatives molecules exhibiting outstanding fluorescent properties for a wide range of applications. To develop an efficient synthetic approach that provides facile access to the desired compounds and allows for straightforward purification.

3.2.1 General Objectives:

The general objective of this research is to develop an efficient synthetic strategy for the preparation of novel kripto-BODIPY and *meso*-phenyl-BODIPY derivative chromophores *via* different reaction pathways, aiming at diverse potential applications.

3.2.2 Specific Objectives:

- Development, optimization, and execution of the synthesis of krypto-BODIPY and *meso*-phenyl-BODIPY derivative chromophores with diverse scaffolds.
- Purify all obtained BODIPY compounds using the most appropriate chromatographic or crystallization techniques according to their physical properties.
- Characterize and identify all BODIPY compounds through comprehensive spectroscopic and spectrometric analyses.

The general idea of the research proposal is illustrated in **Scheme 32**.

Scheme 32. General Research Purpose.

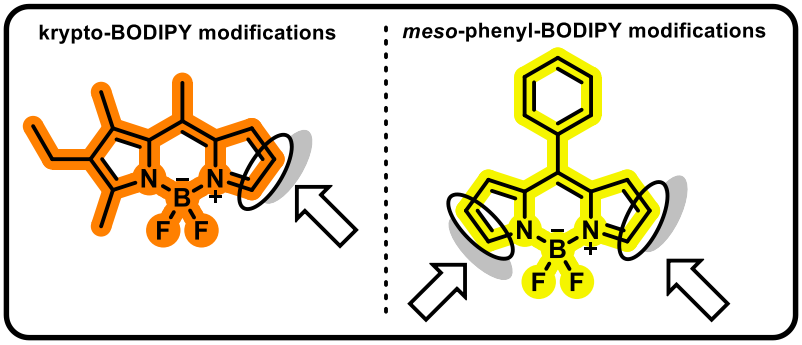

3.3 RESULTS AND DISCUSSION

3.3.1 Synthesis of krypto-BODIPY derivatives:

A series of Krypto-BODIPYs was synthesized through different methodologies. **Scheme 33** illustrates the synthetics strategies, from the preparation of BODIPY **177** and followed by regioselective acetylation, halogenation, and chlorination steps to afford the new derivatives **178**–**181**.

Scheme 33. Synthetic route toward Krypto-BODIPY derivatives **177**–**181**.

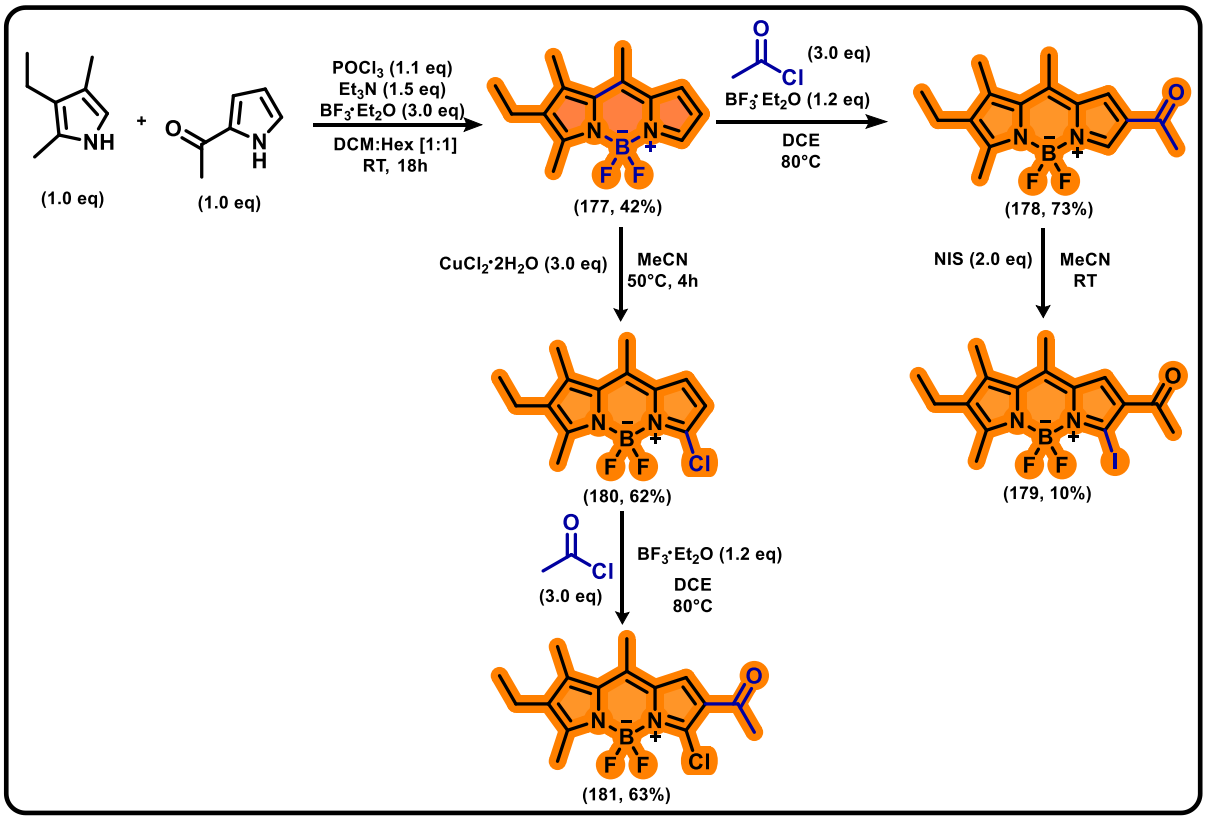

As a starting point, BODIPY **177** was prepared following the procedure reported by BAÑUELOS-PRIETO, Jorge *et al.*, 2010, consisting of the condensation of 2-acetylpyrrole with 3-ethyl-2,4-dimethylpyrrole. This reaction afforded the target BODIPY in 42% yield.

The NMR spectrum of BODIPY **177** displayed all the characteristic signals, and the spectroscopic data were consistent with those reported in the literature (BAÑUELOS-PRIETO, Jorge *et al.*, 2010). For the purpose of analysis and discussion, the key ^{1}H NMR signals are described. Three methyl groups appeared at 2.34 (s, 3H) and 2.56 ppm (s, 6H), corresponding to the methyl substituents at the 1,3-positions of the pyrrole and the *meso*-position of the BODIPY core. The ethyl group at the 2-

position of the pyrrole was observed at 1.06 ppm (t, J = 7.6 Hz, 3H) for the methyl protons and 2.42 ppm (q, J = 7.6 Hz, 2H) for the methylene protons. The three protons of the unsubstituted pyrrole ring appeared at 7.56 (d, J = 2.2 Hz, 1H) (*α*-position), 6.40 (dd, J = 4.0, 2.2 Hz, 1H), and 7.03 ppm (d, J = 4.0 Hz, 1H) (*β*-positions). In addition, ^{11}B and ^{19}F NMR spectra showed a typical triplet in ^{11}B NMR and a characteristic quartet in ^{19}F NMR due to ^{11}B–^{19}F coupling ($^{1}J_{B,F}$ = 31 Hz).

As shown in **Scheme 34**, the synthesis of BODIPY **177** proceeds through a mechanism adapted from BAÑUELOS-PRIETO, Jorge *et al*., 2010. Treatment of 2-acetylpyrrole with $POCl_3$ generates an electrophilic chloroiminium species *via* activation of the carbonyl group, yielding intermediate (**A**). This intermediate is susceptible to nucleophilic attack by kryptopyrrole, forming the coupled adduct (**B**). Subsequent rearrangement, proton transfer, and elimination of chloride result in the formation of the dipyrromethene framework (**C**). This dipyrromethene intermediate is a key precursor that, upon coordination with boron reagents, furnishes the final BODIPY **177**.

Scheme 34. Proposed mechanism for the synthesis of BODIPY **177**.

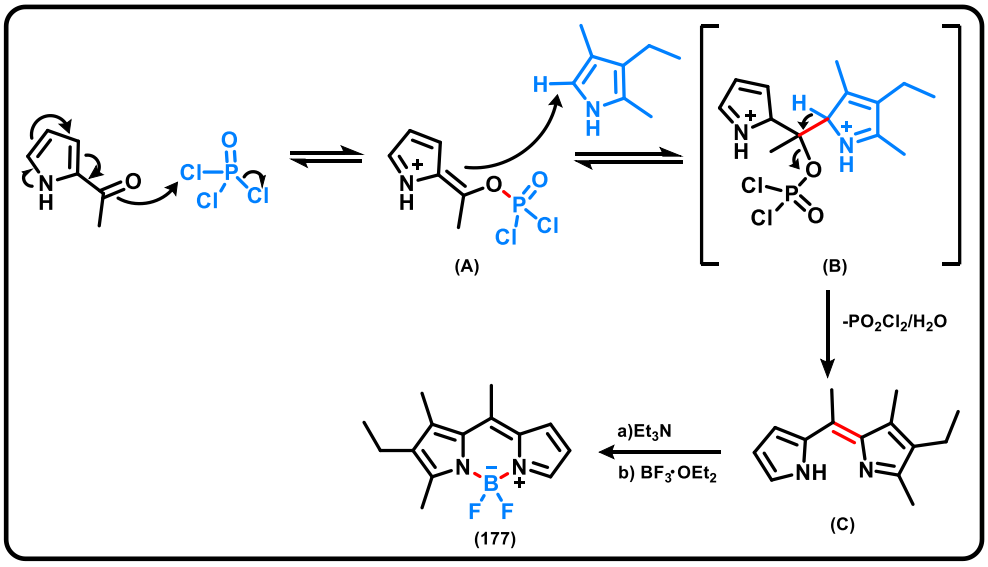

Subsequently, BODIPY **177** was regioselectively acetylated with acetyl chloride and $BF_3{\cdot}OEt_2$ *via* a Friedel–Crafts electrophilic aromatic substitution, affording the *β*-acylated BODIPY **178** in 73% yield. The procedure was adapted from GONZÁLEZ-VERA, Juan A. *et al*., 2020, and the reaction was optimized by adjusting solvent concentration and reaction time. The ^{1}H NMR data confirmed the absence of the *β*-

proton and showed a singlet at 2.45 ppm (s, 3H) corresponding to the new methyl group, while the ^{13}C NMR spectrum displayed the carbonyl carbon at 193.1 ppm (C_q).

After protection of the *β*-position, halogenation at the *α*-position was achieved using NIS, yielding the 3-iodinated BODIPY **179**. The NMR data confirmed the absence of the *α*-proton, and HRMS supported the presence of the iodine atom. Both derivatives (**178** and **179**) constitute novel compounds.

BODIPY **177** was also subjected to direct *α*-chlorination using $CuCl_2 \cdot 2H_2O$, affording BODIPY **180** in 62% yield. This transformation was carried out following the methodology recently reported by ZHOU, Xin *et al*., 2015, and the reaction was optimized by adjusting the equivalents of Cu(II) and the reaction time.The NMR spectrum and the spectroscopic data were fully consistent with those reported in the literature.

Based on the findings reported by Zhou and co-workers, a plausible mechanism for this *α*-chlorination is proposed in **Scheme 35**. The reaction proceeds through a single-electron transfer (SET) process from the free pyrrole unit of BODIPY **177** to $CuCl_2$, generating the cation radical H. This *in situ*-formed cation radical then undergoes rapid electrophilic attack by a chloride anion at the *α*-position (bearing the highest positive charge), leading to the formation of radical intermediate **A**. Finally, the target *α*-chloro BODIPY **180** is obtained through a second SET process from intermediate **A** (ZHOU, Xin *et al*., 2015).

Scheme 35. Proposed mechanism for the synthesis of *α*-chloro BODIPY **180**.

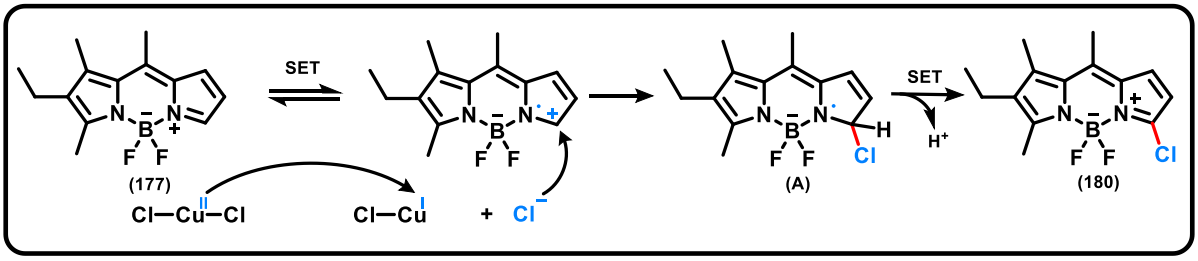

Subsequently, the same regioselective acetylation methodology described above was applied to afford BODIPY **181** in 63% yield, which represents a novel derivative. The ^{1}H NMR spectrum confirmed the presence of a single aromatic proton at 7.40 ppm (s, 1H) and a singlet at 2.62 ppm (s, 3H) corresponding to the new methyl group, while the ^{13}C NMR spectrum showed the carbonyl carbon at 192.2 ppm (C_q).

Scheme 36 summarizes a second synthetic sequence that employs BODIPY **177** for halogenation, Sonogashira couplings, and the final construction of the

symmetric bis-BODIPY **186**. With the exception of the mono-iodinated precursor, all derivatives obtained in this sequence are novel compounds.

Scheme 36. Synthetic sequence to obtain halogenated and novel alkynyl-substituted Krypto-BODIPYs **182-186**.

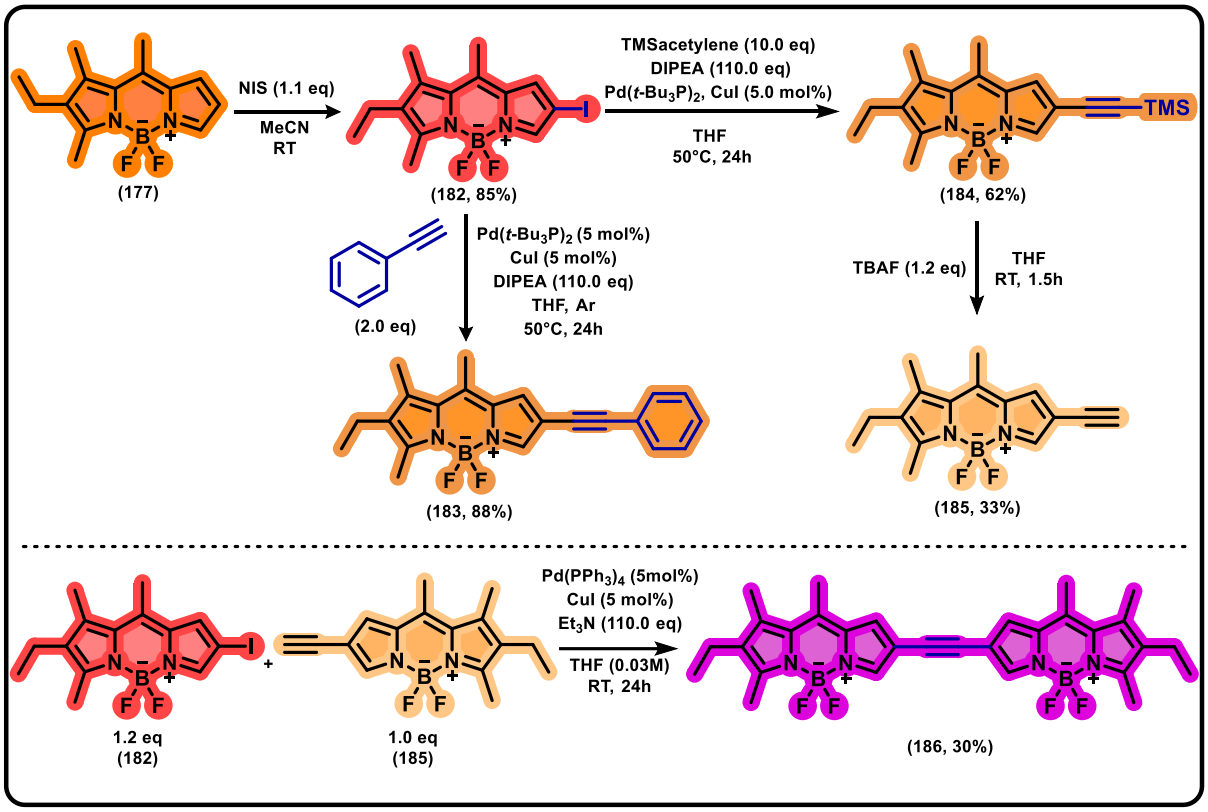

A direct halogenation was performed to obtain the 2-iodinated BODIPY **182** from BODIPY **177** in 85% yield. Since the 2,6-positions of the BODIPY core bear the lowest positive charge according to its electronic structure, they are the most susceptible to electrophilic substitution. Based on this principle, a methodology developed in the WerzLab research group employs NIS in acetonitrile at room temperature. The reaction conditions were optimized, and the best results were achieved using 1.1 equivalents of NIS and a reaction time of 24 h. The ^{1}H NMR spectrum confirmed the disappearance of the corresponding *β*-proton, and HRMS analysis supported the incorporation of the iodine atom.

The 2-iodinated BODIPY **182** was then subjected to two different Sonogashira cross-coupling reactions, using a methodology specifically developed in the WerzLab for BODIPY derivatives. The procedure employs 5 mol% Pd catalyst, CuI as co-catalyst, DIPEA as base, and dry THF under an argon atmosphere. In the first reaction,

phenylacetylene was used as coupling partner. After optimization, the best conditions were obtained using 2 equivalents of alkyne and heating to 50 °C, affording the novel BODIPY **183** in 88% yield. The ^{1}H NMR spectrum displayed the expected aromatic signals at 7.32 (m, 3H) and 7.48 ppm (m, 2H), confirming the formation of the coupled product.

The second Sonogashira reaction was carried out using trimethylsilylacetylene under the same optimized conditions, affording BODIPY **184** in 62% yield. The presence of the TMS group was confirmed by the ^{1}H NMR signal at 0.23ppm (s, 9H) and the corresponding ^{13}C NMR signal at 0.2 ppm, attributed to the three equivalent methyl groups.

After BODIPY **184** was successfully synthesized, the TMS protecting group was removed. Several deprotection methodologies previously used in the WerzLab were tested, and the best results were obtained by adding TBAF (1.2 equiv) dropwise under an argon atmosphere, affording BODIPY **185** in 33% yield. The disappearance of the TMS signals in the NMR spectra and the appearance of the terminal alkyne proton at 3.03 ppm (s, 1H) confirmed the successful deprotection.

Finally, a Sonogashira cross-coupling was performed using 1.2 equivalents of the 2-iodinated BODIPY **182** and 1.0 equivalent of the terminal alkyne BODIPY **185**. The reaction proceeded at room temperature for 24 h, leading to complete consumption of BODIPY **185** and affording the bis-BODIPY internal alkyne **186** in 30% yield. Notably, the incorporation of an internal alkyne linker produced a striking change in the photophysical behavior: while the remaining compounds display orange-to-red fluorescence, compound **186** exhibits an intense purple emission. The symmetrical structure of **186** simplified its NMR spectra, and HRMS unambiguously confirmed the formation of the final product.

As a representative example of the Sonogashira coupling, the catalytic cycle involved in the functionalization of BODIPY **182** is depicted in **Scheme 37**, based on the mechanism proposed by Amna and co-workers (AMNA, ATEŞ & OZTURK, 2023). The Sonogashira reaction is a well-established cross-coupling methodology that proceeds through a palladium-catalyzed cycle involving oxidative addition, transmetallation, and reductive elimination. In this process, oxidative addition of the halogenated BODIPY **182** substrate to a Pd(0) species generates the corresponding Pd(II) intermediate (**A**). Subsequent transmetallation with the copper acetylide affords

a Pd(II)–alkynyl complex (**B**), which then undergoes reductive elimination to form the desired alkynylated BODIPY **184** product while regenerating the Pd(0) catalyst.

Scheme 37. Proposed mechanism for the Sonogashira coupling of BODIPY **182**.

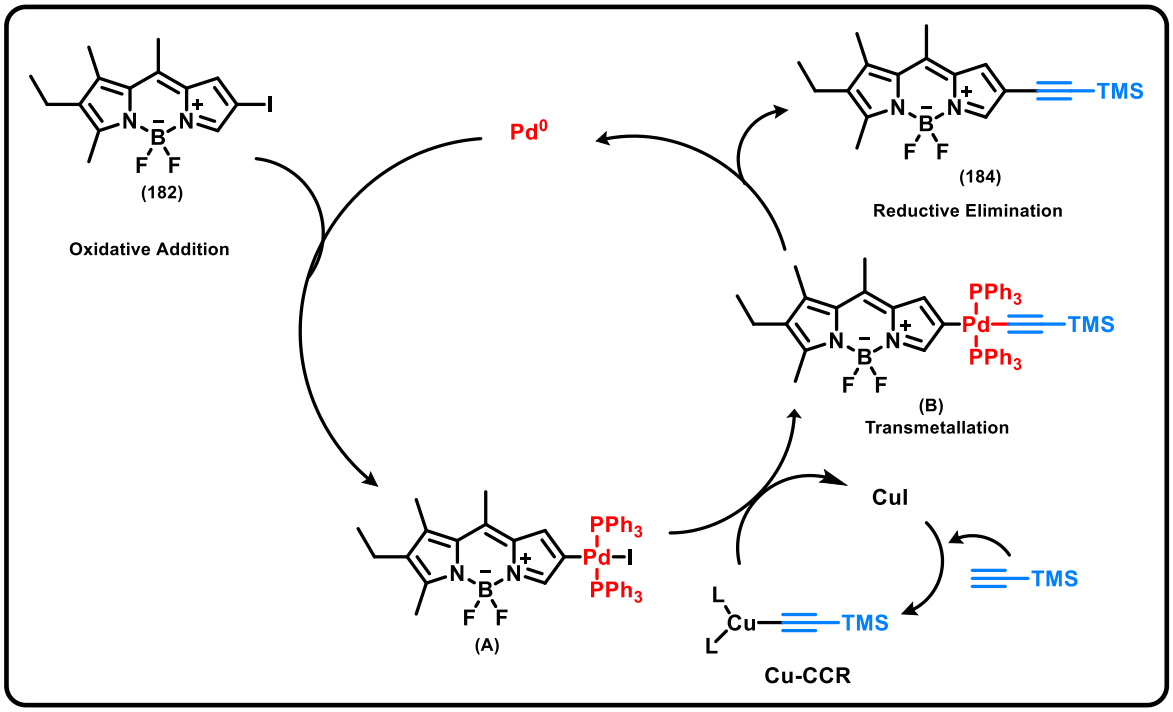

All synthesized BODIPYs were fully characterized using spectrometric and spectroscopic techniques. The corresponding spectra and analytical data are provided in the Appendix and described in detail in the Experimental Section. Physical characteristics, such as color and physical state, are also reported and are illustrated in **Figure 42**.

Figure 42. Synthesized BODIPYs **177**-**183** under visible and UV light 365nm.

To illustrate the characterization procedure, BODIPY **184**, bearing an alkyne substituent at the *β*-position and a TMS group, was selected as a representative example. The ^{1}H and ^{13}C NMR spectra display the characteristic signals of the BODIPY **177** core, the TMS group, and the C–N bond.

In the ^{1}H NMR spectrum (400 MHz, $CDCl_3$) (**Figure 43**), two methyl singlets at 2.57 (s, 3H) and 2.51 ppm (s, 3H) were assigned to the methyl substituents at the 1,3-positions of the pyrrole ring. The ethyl group at the 2-position of the pyrrole was observed at 1.06 ppm (t, *J* = 7.6 Hz, 3H) for the methyl protons and at 2.42 ppm (q, *J* = 7.6 Hz, 2H) for the methylene protons. In addition, a singlet at 2.53 ppm (s, 3H) corresponds to the methyl group at the *meso*-position of the BODIPY core. The two protons of the unsubstituted pyrrole ring appeared as singlets at 7.04 (*α*-position) and 7.63 ppm (*β*-position). Finally, the TMS group was observed as a singlet at 0.23 ppm (s, 9H).

Figure 43. ^{1}H NMR spectrum of BODIPY **184**.

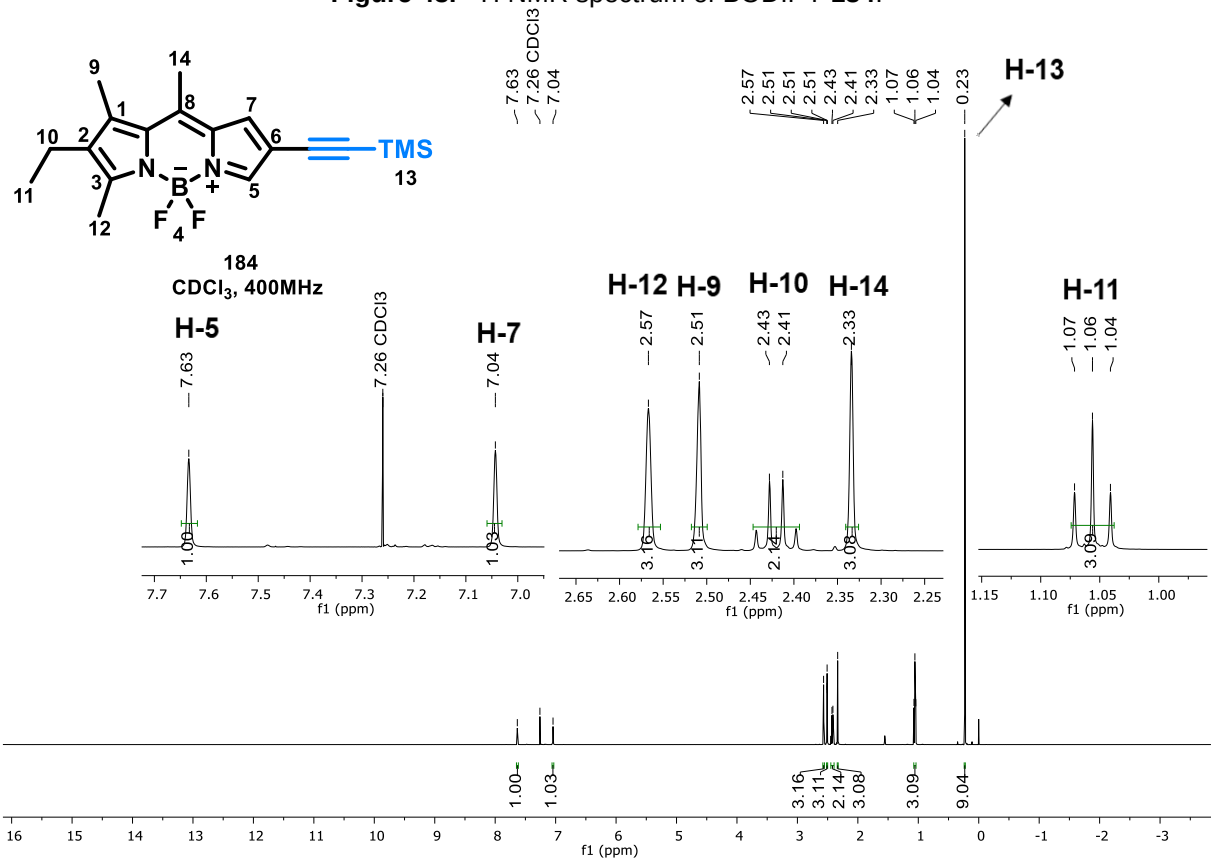

In addition, the expected signals corresponding to the boron atom in the ^{11}B NMR spectrum and the fluorine atoms in the ^{19}F NMR spectrum were observed for all synthesized BODIPYs, confirming the presence of the characteristic BF_2 moiety. The ^{11}B NMR spectrum displayed a typical triplet (**Figure 44**), while the19F NMR spectrum showed a characteristic quartet (**Figure 45**) arising from ^{11}B–^{19}F coupling (1*J*B,F = 31 Hz).

Figure 44. ^{11}B NMR spectrum of compound **184**.

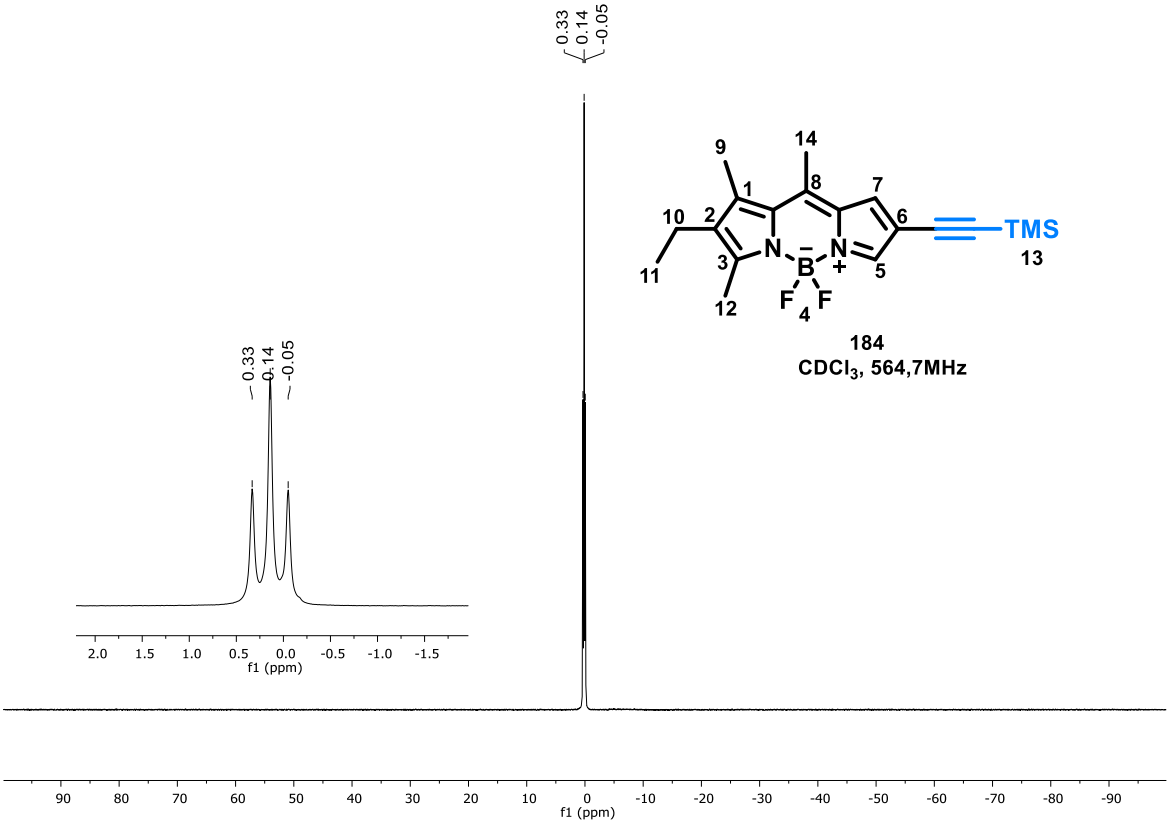

Figure 45. ^{19}F NMR spectrum of compound **184**.

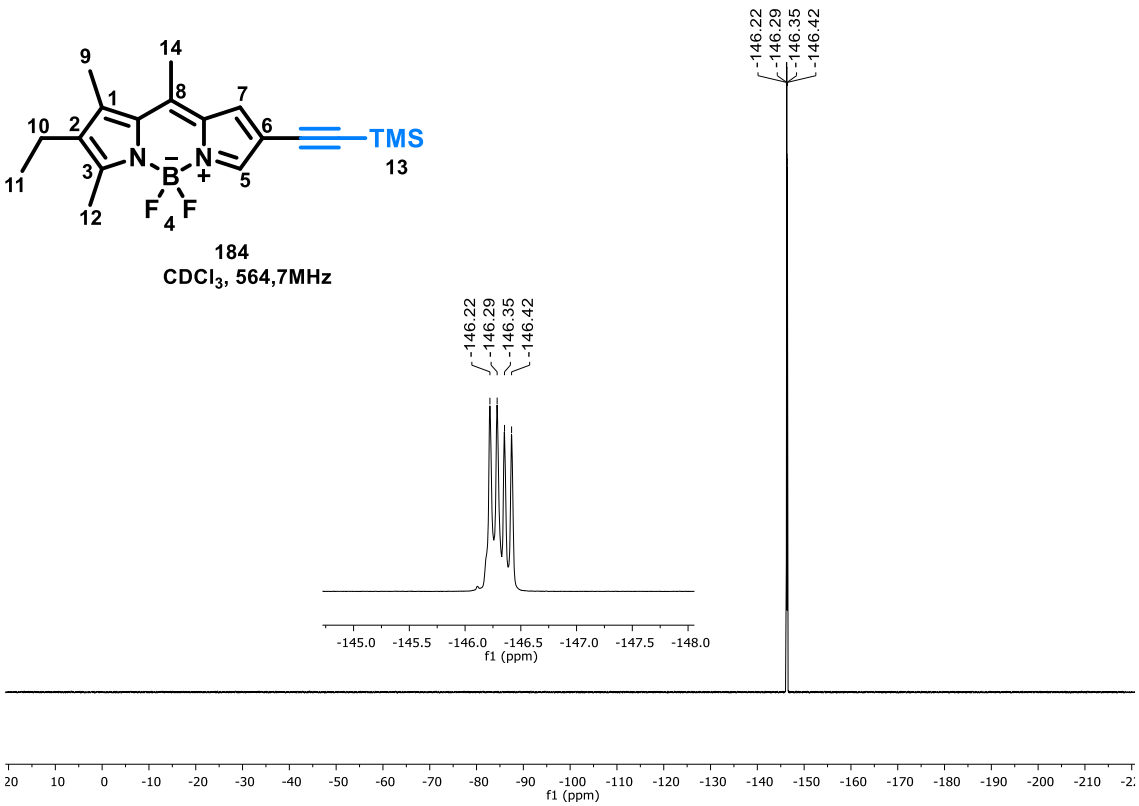

3.3.2 Synthesis of *meso*-phenyl BODIPY derivatives:

For the *meso*-phenyl series, **Scheme 38** outlines the synthetic sequence leading to BODIPYs **187**–**189**, including the formation of BODIPY **187**, copper-catalyzed α-diacylation to afford BODIPY **188**, and final 2,6-diiodination yielding the novel BODIPY **189**.

BODIPY **187** was synthesized as the precursor using a procedure followed the methodology reported by FARFÁN-PAREDES, Mónica *et al.*, 2020, in which benzaldehyde and pyrrole react in the presence of a catalytic amount of trifluoroacetic acid to form the dipyrromethene intermediate, followed by oxidation with DDQ and complexation with $BF_3{\cdot}Et_2O$, affording the product in 40% yield. The NMR spectrum of BODIPY **187** displayed all characteristic signals, and the spectroscopic data were consistent with those reported in the literature. The ^1H NMR showed resonances for the pyrrolic protons at 6.94 ppm (d, J = 4.3 Hz, 2H) for positions 1,7, 6.55 ppm (d, J = 4.3 Hz, 2H) for positions 2,6, and 7.95 ppm (m, 2H) for positions 3,5, along with the aromatic protons of the phenyl substituent at 7.56 ppm (m, 5H).

Scheme 38. Synthesis of *meso*-phenyl-BODIPY derivatives.

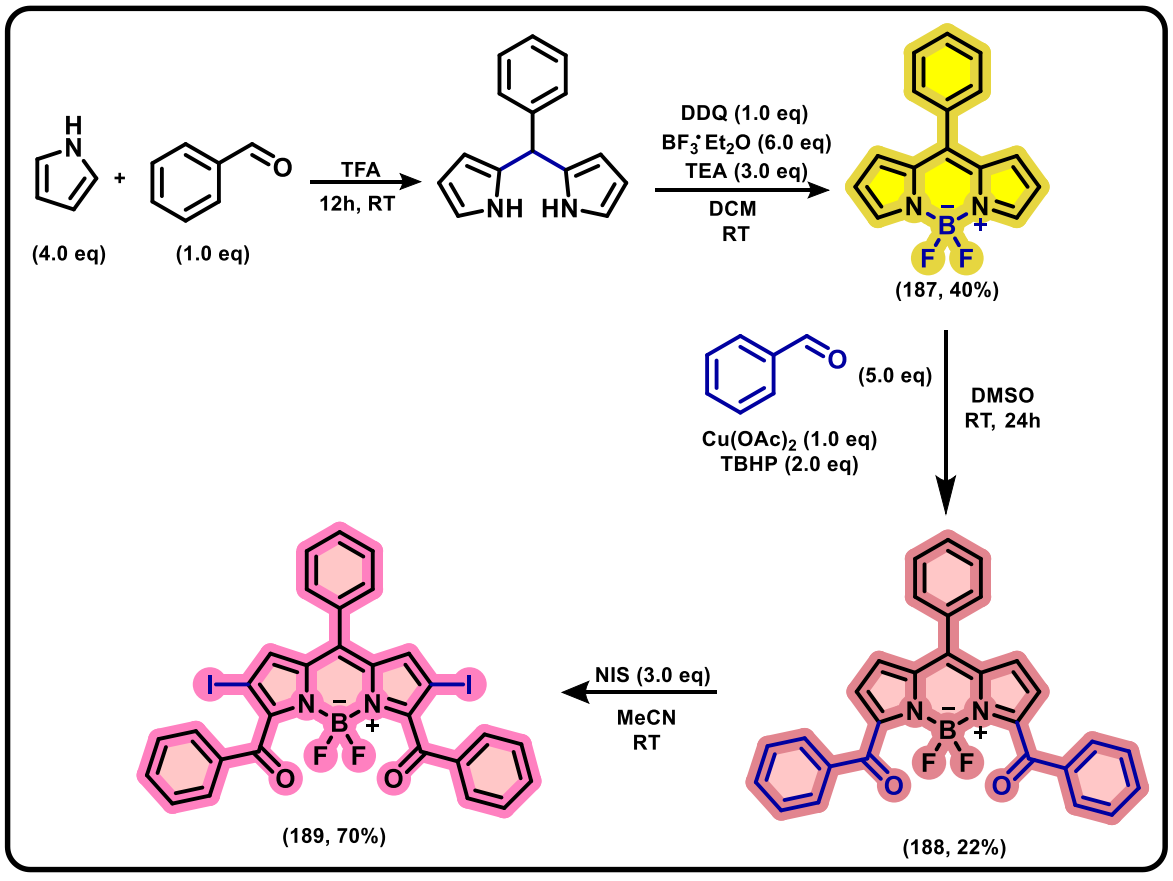

A copper-catalyzed direct *α*-diacylation of BODIPY **187** with benzaldehyde *via* C–H bond activation was then carried out following the methodology reported by LV, Fan *et al*., 2023. The best results were obtained when the reaction was performed at room temperature for 24 h, affording BODIPY **188** in 22% yield. The NMR spectrum of BODIPY **188** displayed the expected characteristic signals, and the spectroscopic data were consistent with those reported in the literature. The absence of *α*-protons in the ^{1}H NMR spectrum, together with the appearance of ten additional aromatic signals, confirmed the formation of the diacylated product.

Finally, a direct 2,6-halogenation was carried out using 3 equivalents of NIS at 50 °C for 24 h, yielding the novel BODIPY **189** in 70% yield. In the ^{1}H NMR spectrum, besides the aromatic protons of the phenyl substituent, only the 1,7-protons of the BODIPY core were observed at 7.23 ppm (s, 2H), shifted due to the presence of the iodine atoms. The structure was also confirmed by HRMS.

All synthetized BODIPY derivatives were fully characterized by spectrometric and spectroscopic methods such as uni dimensional ^{1}H, ^{13}C NMR, high resolution electrospray ionization mass spectrometry (HRMS) and Fourier-transform infrared spectroscopy (FTIR). The corresponding spectra and analytical data are provided in the Appendix and detailed in the Experimental Part.

These transformations demonstrate that the *meso*-phenyl BODIPY is compatible with both C–H activation and electrophilic iodination, enabling efficient access to structurally diverse and previously unreported derivatives. Together with the alkyl-substituted and krypto-BODIPY series synthesized in this work, these compounds provide a robust platform for further functionalization and for comparative studies of how structural modifications influence electronic distribution, photophysical behavior, and potential applications in sensing and bioimaging.

3.4 CONCLUSIONS

A series of novel krypto-BODIPY and *meso*-phenyl-BODIPY derivatives was successfully synthesized, comprising eight previously unreported compounds, including mono- and di-halogenated scaffolds, acetylated analogues, Sonogashira coupling products, and a symmetric bis-BODIPY internal alkyne. These results demonstrate that both kryptopyrrole and *meso*-phenyl frameworks are compatible with

electrophilic substitution, C–H activation, and palladium-catalyzed cross-coupling, enabling efficient diversification of the BODIPY core.

Given their structural and electronic features, these compounds are expected to exhibit distinct photophysical and bioluminescent properties, especially those incorporating heavy atoms or extended π-conjugation. Therefore, the synthesized derivatives represent valuable precursors for future functional studies.

It is important to continue with the photophysical characterization and application-oriented evaluation of these systems, as such studies may reveal relevant behavior for sensing, imaging, or light-driven processes. Overall, this synthetic work establishes a solid platform for the development of advanced BODIPY-based materials.

3.5 EXPERIMENTAL PART

3.5.1 General Remarks:

All commercially sourced compounds were used as received, unless otherwise stated. Reactions requiring anhydrous conditions were run under an atmosphere of dry nitrogen or argon. Melting points were determined using a Reichert melting point table and temperature controller or a Stuart SMP30 melting point apparatus, and are uncorrected. Infrared spectra were recorded in the range 4000-600 cm-1 on a Perkin Elmer Spectrum either as neat films or solids compressed onto a diamond window. NMR spectra were recorded using either a Varian 400-MR, Bruker Nano 400 or Bruker UltrashieldTM Plus 500. Chemical shifts (δ) are quoted in parts per million (ppm), coupling constants (J) are given in Hz. Other abbreviations used are s (singlet), d (doublet), t (triplet) and m (multiplet). ^{1}H, ^{13}C and ^{11}B NMR spectra were referenced to the appropriate residual solvent peak or the carbon resonance of the NMR solvent, respectively. ^{19}F spectra were referenced to CCl_3F as an external standard. Mass spectra were determined by the mass spectrometry service using a Shimadzu GCMS QP2010+ (EI+ mode), Brüker Daltonics FT-ICR-MS Apex 4e 7.0T FT-MS (ESI+ mode), Thermo Scientific Orbitrap Elite (APCI mode). All this measures were performed in the University of Freiburg.

3.5.1 Synthesis of krypto-BODIPY precursors:

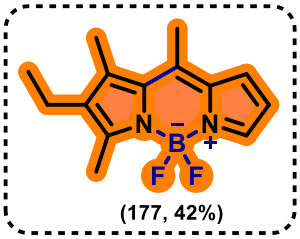

(177, 42%)

2-ethyl-4,4-difluoro-1,3,8-trimethyl-4-bora-3a,4a-diaza-s-indacene (compound **177**): To a solution of 2-acetylpyrrole (1 equiv) in DCM/hexane (1:1) was added $POCl_3$ (1.1 equiv), and the mixture was stirred at room temperature for 30 min. Then, a solution of 3-ethyl-2,4-dimethylpyrrole (1 equiv) in DCM/hexane (1:1) was added, and the reaction mixture was stirred for 12 h at room temperature. Triethylamine (1.5 equiv) was added and the mixture was stirred for 30 min, followed by the addition of $BF_3{\cdot}Et_2O$ (3.0 equiv). Stirring was continued for 3–4 h, after which the reaction was quenched with saturated $NaHCO_3$ and extracted with DCM. The organic layer was washed with water, dried over Na_2SO_4, filtered, and concentrated under reduced pressure. The product was obtained as an orange solid (42%) and purified by column chromatography on silica gel (Toluene). **^{1}H NMR (400 MHz, $CDCl_3$)** δ=7.56 (d, *J*=2.2 Hz, 1H), 7.03 (d, *J*=4.0 Hz, 1H), 6.40 (dd, *J*=4.0, 2.2 Hz, 1H), 2.56 (s, 6H), 2.42 (q, *J*=7.6 Hz, 2H), 2.34 (s, 3H), 1.06 (t, *J*=7.6 Hz, 3H). **^{13}C NMR (100 MHz, $CDCl_3$)** δ=160.5 (C=N), 140.9 (C_q), 140.4 ($2C_q$), 136.8 (CH), 135.3 (C_q), 134.2 (C_q), 122.8 (CH), 115.1 (CH), 17.2 (CH_2), 16.7 (CH_3), 14.7 (CH_3), 14.2 (CH_3), 13.2 (CH_3). **FTIR (ATR)$_{vmax}$** cm^{-1} 2972, 1561 (C=N), 1455 (C=C), 1371. **ESI (+) FT-ICR MS** calcd. for $C_{14}H_{18}N_2BF_2^+$ $[M+H]^+$: 263.1531; found: 263.1526; calcd. for $C_{14}H_{17}N_2BF_2Na^+$ $[M+Na]^+$: 285.1347; found: 285.1345. **m.p.** (°C) = 169.1. The spectroscopic properties were consistent with the data available in the literature (BAÑUELOS-PRIETO, Jorge *et al*., 2010).

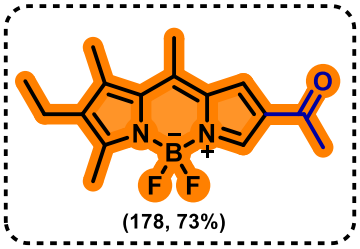

(178, 73%)

1-[2-ethyl-4,4-difluoro-1,3,8-trimethyl-4-bora-3a,4a-diaza-s-indacene]ethan-1one (compound **178**): BODIPY **177** (1 equiv), acetyl chloride (3 equiv), and $BF_3{\cdot}Et_2O$ (1.2

equiv) were dissolved in 1,2-dichloroethane (3 mL). The reaction mixture was stirred at 80 °C and monitored by TLC. Upon completion, the mixture was cooled to room temperature, poured into CH_2Cl_2 (100 mL), washed with water (3 × 100 mL), dried over Na_2SO4, filtered, and concentrated under reduced pressure. The product was obtained as an orange solid (73%) and purified by column chromatography on silica gel (*n*-pentane/EtAcO [9:1]). **^{1}H NMR (400 MHz, $CDCl_3$)** *δ*=7.95 (s, 1H), 7.37 (s,1H), 2.60 (m, 6H), 2.45 (s, 3H), 2.42 (q, *J*=7.6 Hz, 2H), 2.38 (s, 3H), 1.08 (t, *J*=7.6 Hz, 3H). **^{13}C NMR (100 MHz, $CDCl_3$)** *δ*= 193.1 (C=O), 165.2 (C=N), 142.7 (C_q), 140.5 ($2C_q$), 137.5 (CH), 137.1 (C_q), 136.3 (C_q), 134.4 (C_q), 120.3 (CH), 27.4 (CH_3), 17.2 (CH_2), 16.4 (CH_3), 14.4 (CH_3), 14.4 (CH_3), 13.6 (CH_3). **FTIR (ATR)$_{vmax}$** cm^{-1} 1660 (C=O), 1570 (C=N), 1452 (C=C), 1254. **ESI (+) FT-ICR MS** calcd. for $C_{16}H_{19}ON_2BF_2Na^+$ $[M+Na]^+$: 327.1454; found: 327.1451. **m.p.** (°C) = 193.5.

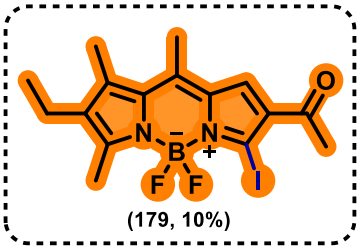

(179, 10%)

1-[2-ethyl-4,4-difluoro-5-iodo-1,3,8-trimethyl-4-bora-3a,4a-diaza-s-indacene]ethan-1one (compound **179**): To a solution of BODIPY **178** (1 equiv) in acetonitrile (0.03 M), NIS (2 equiv) was added. The reaction mixture was stirred at room temperature for 3 h and monitored by TLC. Upon completion, the solvent was removed under reduced pressure. The product was obtained as an orange solid (10%) and purified by column chromatography on silica gel using *n*-pentane/EtOAc (9:1) as eluent.. **^{1}H NMR (400 MHz, $CDCl_3$)** *δ*=7.32 (s, 1H), 3.05 (s, 3H), 2.56 (s, 3H), 2.49 (s, 3H), 2.47 (q, *J*=7.6 Hz, 2H), 2.40 (s, 3H), 1.08 (t, *J*=7.6 Hz, 3H). **^{13}C NMR (100 MHz, $CDCl_3$)** *δ*= 192.3 (C=O), 165.4 (C=N), 143.6 (C_q), 142.7 ($2C_q$), 138.3 (CH), 137.7 (C_q), 136.3 (C_q), 132.6 (C_q), 129.7 (CH), 28.8 (CH_3), 19.6 (CH_2), 17.4 (CH_3), 15.6 (CH_3), 14.3 (CH_3), 13.8 (CH_3). **FTIR (ATR)$_{vmax}$** cm^{-1} 1671 (C=O), 1573 (C=N), 1432 (C=C). **ESI (+) FT-ICR MS** calcd. for $C_{16}H_{19}ON_2BF_2I^+$ $[M+H]^+$: 431.0600; found: 431.0598. **m.p.** (°C) = 189.1.

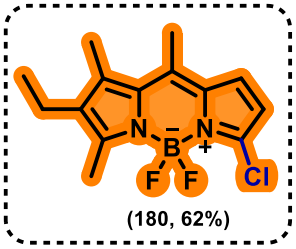

(180, 62%)

5-chloro-2-ethyl-4,4-difluoro-1,3,8-trimethyl-4-bora-3a,4a-diaza-s-indacene (compound **180**): A mixture of BODIPY **177** (1 equiv) and $CuCl_2 \cdot 2H_2O$ (3 equiv) in acetonitrile (15 mL) was stirred under air at 50 °C for 4 h and monitored by TLC. After cooling to room temperature, the reaction mixture was poured into dichloromethane (30 mL), washed with water (3 × 50 mL), dried over anhydrous Na_2SO_4, filtered, and concentrated under reduced pressure. The product was obtained as an orange solid (62%) and purified by column chromatography on silica gel using *n*-pentane/EtOAc (9.5:0.5) as eluent. **^{1}H NMR (400 MHz, $CDCl_3$)** δ=6.97 (d, *J*=4.1 Hz, 1H), 6.27 (dd, *J*=4.1, 1.2 Hz, 1H), 2.58 (s, 3H), 2.51 (s, 3H), 2.42 (q, *J*=7.6 Hz, 2H), 2.34 (s, 3H), 1.06 (t, *J*=7.6 Hz, 3H). **^{13}C NMR (100 MHz, $CDCl_3$)** δ= 161.2 (C=N), 140.8 (C_q), 138.7 ($2C_q$), 135.9 (CH), 134.2 (C_q), 133.2 (C_q), 122.9 (C_q), 114.6 (CH), 17.2 (CH_2), 16.0 (CH_3), 14.6 (CH_3), 14.2 (CH_3), 13.3 (CH_3). **FTIR (ATR)$_{vmax}$** cm^{-1} 1571 (C=N), 1445 (C=C), 762 (C-Cl). **ESI (+) FT-ICR MS** calcd. for $C_{14}H_{17}N_2BClF_2^+$ $[M+H]^+$: 297.1137; found: 297.1136, calcd. for $C_{14}H_{16}N_2BClF_2Na^+$ $[M+Na]^+$: 319.0957; found: 319.0955. **m.p.** (°C) = 208.9. The spectroscopic properties were consistent with the data available in the literature (ZHOU, Xin *et al*., 2015).

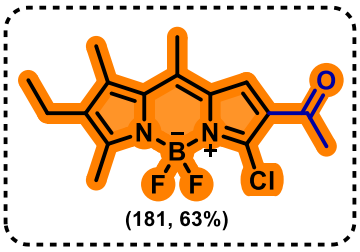

(181, 63%)

1-[2-ethyl-4,4-difluoro-1,3,8-trimethyl-4-bora-3a,4a-diaza-s-indacene]ethan-1one (compound **181**): BODIPY **180** (1 equiv), acetyl chloride (3 equiv), and $BF_3 \cdot Et_2O$ (1.2 equiv) were dissolved in 1,2-dichloroethane (4.4 mL). The reaction mixture was stirred at 80 °C and monitored by TLC. Upon completion, the mixture was cooled to room temperature, poured into CH_2Cl_2 (100 mL), washed with water (3 × 100 mL), dried over Na_2SO4, filtered, and concentrated under reduced pressure. The product was obtained as an orange solid (63%) and purified by column chromatography on silica gel (*n*-

pentane/EtAcO [8:2]). **^{1}H NMR (400 MHz, $CDCl_3$)** δ=7.40 (s, 1H), 2.62 (s, 3H), 2.54 (s, 6H), 2.54 (q, *J*=7.6 Hz, 2H), 2.37 (s, 3H), 1.08 (t, *J*=7.6 Hz, 3H). **^{13}C NMR (100 MHz, $CDCl_3$)** δ= 192.2 (C=O), 165.6 (C=N), 142.4 (C_q), 138.6 ($2C_q$), 137.9 (CH), 136.1 (C_q), 131.8 (C_q), 126.2 (C_q), 122.1 (CH), 29.5 (CH_3), 17.3 (CH_2), 15.8 (CH_3), 14.4 (CH_3), 14.4 (CH_3), 13.7 (CH_3). **FTIR (ATR)$_{vmax}$** cm^{-1} 2923, 1772 (C=O), 1565 (C=N), 1449 (C=C), 728 (C-Cl). **ESI (+) FT-ICR MS** calcd. for $C_{16}H_{18}ON_2BClF_2Na^+$ $[M+Na]^+$: 361.1059; found: 361.1061. **m.p.** (°C) = 150.0.

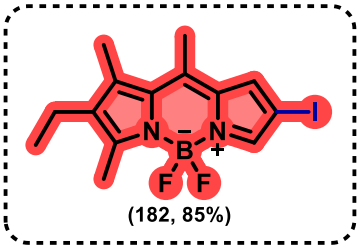

(182, 85%)

2-ethyl-4,4-difluoro-6-iodo-1,3,8-trimethyl-4-bora-3a,4a-diaza-s-indacene (compound **182**): To a solution of BODIPY **177** (1 equiv) in MeCN, NIS (1.1 equiv) was added. The reaction mixture was stirred at room temperature for 24 h and monitored by TLC. Upon completion, the solvent was removed under reduced pressure. The product was obtained as a red solid (85%) and purified by column chromatography on silica gel using toluene as eluent. **^{1}H NMR (400 MHz, $CDCl_3$)** δ=7.48 (s, 1H), 7.05 (s, 1H) , 2.57 (s, 3H), 2.51 (s. 3H), 2.42 (q, *J*=7.6 Hz, 2H), 2.34 (s, 3H), 1.06 (t, *J*=7.6 Hz, 3H). **^{13}C NMR (100 MHz, $CDCl_3$)** δ=162.9 (C=N), 142.1 (C_q), 139.9 (CH), 139.0 (C_q), 136.4 (C_q), 135.4 (C_q), 134.8 (C_q), 127.7 (CH), 66.8 (C-I), 17.2 (CH_2), 16.5 (CH_3), 14.5 (CH_3), 14.3 (CH_3), 13.4 (CH_3). **FTIR (ATR)$_{vmax}$** cm^{-1} 1570 (C=N), 1451 (C=C), 1168. **ESI (+) FT-ICR MS** calcd. for $C_{14}H_{16}N_2BF_2INa^+$ $[M+Na]^+$: 411.0313; found: 411.0311. **m.p.** (°C) = 220.0. The spectroscopic properties were consistent with the data available in the literature (ORTIZ, Maria J. *et al*., 2012).

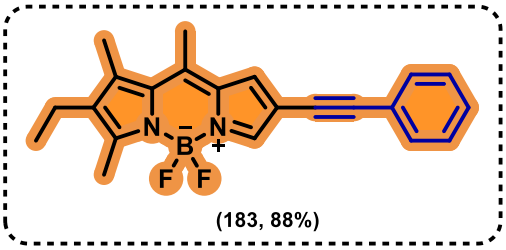

(183, 88%)

2-ethyl-4,4-difluoro-1,3,8-trimethyl-6-(phenylethynyl)-4-bora-3a,4a-diaza-s-indacene (compound **183**): To a round-bottom flask, BODIPY **182** (1 equiv), Pd(*t*-

$Bu_3P)_2$ (5 mol%), CuI (5 mol%), DIPEA (110 equiv) and dry THF (0.03 M) were added under an argon atmosphere. Then, phenylacetylene (2 equiv) was added dropwise. The reaction mixture was stirred at 50°C for 24 h and monitored by TLC. Upon completion, the mixture was poured into cold distilled water (20 mL) and extracted with DCM (3 × 10 mL). The combined organic layers were washed with water (3 × 15 mL), dried over Na_2SO_4, filtered, and concentrated under reduced pressure. The product was obtained as an orange solid (85%) and purified by column chromatography on silica gel using chloroform as eluent. **^{1}H NMR (400 MHz, $CDCl_3$)** δ=7.70 (s, 1H), 7.51 – 7.45 (m, 2H), 7.35-7.39 (m, 3H). 7.09 (s, 1H), 2.58 (s, 3H), 2.53 (s. 3H), 2.42 (q, *J*=7.6 Hz, 2H), 2.34 (s, 3H), 1.06 (t, *J*=7.6 Hz, 3H). **FTIR (ATR)$_{vmax}$** cm^{-1} 3121, 1567 (C=N), 1448 (C=C). **ESI (+) FT-ICR MS** calcd. for $C_{22}H_{22}N_2BF_2^+$ $[M+H]^+$: 363.1843; found: 363.1839. **m.p.** (°C) = 148.9.

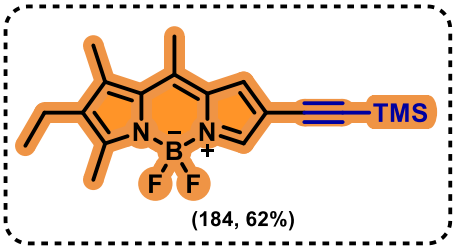

(184, 62%)

2-ethyl-4,4-difluoro-1,3,8-trimethyl-6-((trimethylsilyl)ethynyl)-4-bora-3a,4a-diaza-s-indacene (compound **184**): To a round-bottom flask, BODIPY **182** (1 equiv), Pd(*t*-$Bu_3P)_2$ (5 mol%), CuI (5 mol%), DIPEA (110 equiv), TMS-acetylene (10 equiv) and dry THF (0.03 M) were added under an argon atmosphere. The reaction mixture was stirred at 50 °C for 24 h and monitored by TLC. After completion, the mixture was poured into cold distilled water (20 mL) and extracted with DCM (3 × 10 mL). The combined organic layers were washed with water (3 × 15 mL), dried over anhydrous Na_2SO_4, filtered, and concentrated under reduced pressure. The product was obtained as an orange solid (62%) and purified by column chromatography on silica gel using toluene as eluent. **^{1}H NMR (400 MHz, $CDCl_3$)** δ=7.63 (s, 1H), 7.04 (s, 1H), 2.57 (s, 3H), 2.51 (s. 3H), 2.42 (q, *J*=7.6 Hz, 2H), 2.33 (s, 3H), 1.06 (t, *J*=7.6 Hz, 3H), 0.23 (s, 9H). **^{13}C NMR (100 MHz, $CDCl_3$)** δ=162.7 (C=N), 141.8 (C_q), 139.9 (CH), 139.3 (C_q), 136.2 (C_q), 135.3 (C_q), 133.3 (C_q), 124.2 (CH), 110.5 (C_q), 99.1 (C_q), 94.9 (C_q), 17.2 (CH_2), 16.5 (CH_3), 14.6 (CH_3), 14.3 (CH_3), 13.4 (CH_3), 0.2 ($3CH_3$). **FTIR (ATR)$_{vmax}$** cm^{-1} 2952, 2155, 1566 (C=N), 1447 (C=C). **ESI (+) FT-ICR MS** calcd. for $C_{19}H_{26}N_2BF_2Si^+$ $[M+H]^+$: 359.1919; found: 359.1921. **m.p.** (°C) = 208.4.

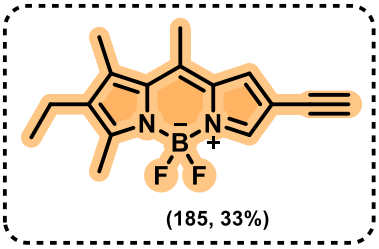

2-ethyl-6-ethynyl-4,4-difluoro-1,3,8-trimethyl-4-bora-3a,4a-diaza-s-indacene (compound **185**): To a solution of BODIPY **184** (1 equiv) in dry THF, TBAF (1.2 equiv) was added dropwise under an argon atmosphere. The reaction mixture was stirred at room temperature until completion (TLC monitoring). The solvent was removed under reduced pressure. The product was obtained as an orange solid (33%) and purified by column chromatography on silica gel using DCM/*n*-pentane (2:1) as eluent. **^{1}H NMR (400 MHz, $CDCl_3$)** δ=7.65 (s, 1H), 7.07 (s, 1H), 3.03 (s, 1H), 2.58 (s, 3H), 2.55 (s. 3H), 2.43 (q, *J*=7.6 Hz, 2H), 2.36 (s, 3H), 1.01 (t, *J*=7.6 Hz, 3H), 0.23 (s, 9H). **^{13}C NMR (100 MHz, $CDCl_3$)** δ=163.1 (C=N), 142.0 (C_q), 139.9 (CH), 139.0 (C_q), 136.4 (C_q), 136.4 (C_q), 135.4 (C_q), 133.3 (CH), 124.4 (CH), 109.2 (C_q), 77.9 (CH), 17.2 (CH_2), 16.5 (CH_3), 14.5 (CH_3), 14.3 (CH_3), 13.4 (CH_3). **FTIR (ATR)$_{vmax}$** cm^{-1} 3280, 2940, 2105, 1570 (C=N), 1452 (C=C). **ESI (+) FT-ICR MS** calcd. for $C_{16}H_{18}N_2BF_2^+$ $[M+H]^+$: 287.1531; found: 287.1526. **m.p.** (°C) = 103.1.

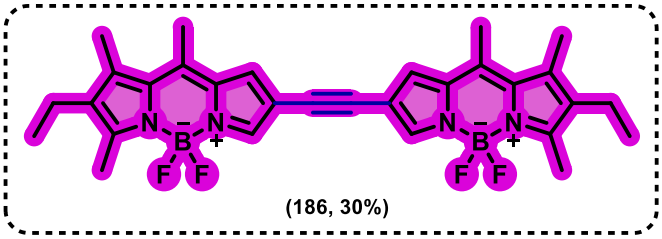

1,2-bis[6-(2-ethyl)-4,4-difluoro-1,3,8-trimethyl-4-bora-3a,4a-diaza-s-indacen-6-yl]ethyne (compound **186**): To a round-bottom flask, BODIPY **182** (1.2 equiv), Pd(*t*-$Bu_3P)_2$ (5 mol%), CuI (5 mol%), DIPEA (110 equiv) and dry THF (0.03 M) were added under an argon atmosphere. Then, BODIPY **185** (1 equiv) was added. The reaction mixture was stirred at room temperature for 24 h and monitored by TLC. After completion, the mixture was poured into cold distilled water (20 mL) and extracted with DCM (3 × 10 mL). The combined organic layers were washed with water (3 × 15 mL), dried over anhydrous Na_2SO_4, filtered and concentrated under reduced pressure. The product was obtained as an purple solid (30%) and purified by column chromatography on silica gel using chloroform as eluent. **^{1}H NMR (400 MHz, $CDCl_3$)** δ=7.68 (s, 2H),

7.08 (s, 2H), 2.58 (s, 6H), 2.56 (s. 6H), 2.43 (q, *J*=7.6 Hz, 4H), 2.36 (s, 6H), 1.06 (t, *J*=7.6 Hz, 6H). **FTIR (ATR)$_{vmax}$** cm^{-1} 2919, 1565 (C=N), 1445 (C=C). **ESI (+) FT-ICR MS** calcd. for $C_{30}H_{33}N_4B_2F_4^+$ $[M+H]^+$: 547.2824; found: 547.2822. **m.p.** (°C) = >360.

3.5.2 Synthesis of *meso*-phenyl-BODIPY precursors:

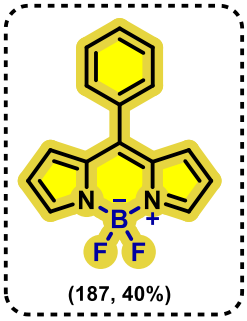

(187, 40%)

4,4-Difluoro-8-phenyl-4-bora-3a,4a-diaza-s-indacene (compound **187**): To a solution of the aldehyde (1.0 equiv) in pyrrole (4.0 equiv), a catalytic amount of trifluoroacetic acid (TFA) was added. The reaction mixture was stirred at room temperature until complete consumption of the aldehyde. The mixture was washed with brine, extracted with CH_2Cl_2, dried over anhydrous Na_2SO_4, filtered, and concentrated under reduced pressure. The crude product was purified by column chromatography on silica gel (*n*-hexane/ethyl acetate) to afford the corresponding dipyrromethene. The purified dipyrromethene was dissolved in CH_2Cl_2, and DDQ (1.0 equiv) was added. The mixture was stirred at room temperature for 1 h. Then, $BF_3{\cdot}Et_2O$ (6.0 equiv) was added under a nitrogen atmosphere and stirred for 15 min, followed by dropwise addition of triethylamine (3.0 equiv). Stirring was continued until completion of the reaction, as monitored by TLC. The reaction mixture was washed with brine, extracted with CH_2Cl_2, and the combined organic layers were dried over Na_2SO_4, filtered, and concentrated under reduced pressure to afford the crude product. The product was obtained as an yellow solid (40%) and purified by column chromatography on silica gel using *n*-hexane/ethyl acetate (8:2) as eluent. **^{1}H NMR (400 MHz, $CDCl_3$)** *δ*=7.95 (s, 2H), 7.62-7.49 (m, 5H), 6.94 (d, *J*=4.3 Hz, 2H), 6.55 (d, *J*=4.3 Hz, 2H). **FTIR (ATR)$_{vmax}$** cm^{-1} 2651, 1575 (C=N), 1475 (C=C). **ESI (+) FT-ICR MS** calcd. for $C_{15}H_{11}N_2BF^+$ $[M+H]^+$: 249.0996; found: 249.0994. **m.p.** (°C) = 110.0. The spectroscopic properties were consistent with the data available in the literature (FARFÁN-PAREDES, Mónica *et al*., 2020).

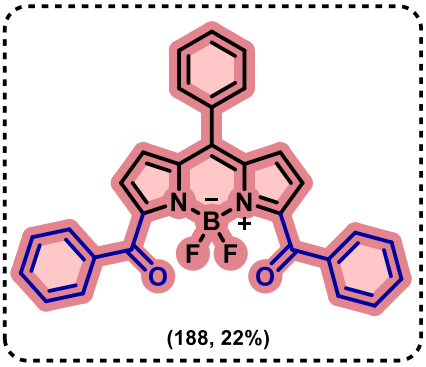

4,4-Difluoro-8-phenyl-3,5-diphenylmethanone-4-bora-3a,4a-diaza-s-indacene (compound **188**): BODIPY **187** (92 mg, 0.34 mmol), benzaldehyde (0.17 mL, 1.7 mmol), $Cu(OAc)_2$ (6 mg, 0.034 mmol), and tert-butyl hydroperoxide (TBHP, 0.066 mL, 0.68 mmol) were dissolved in DMSO (3 mL). The reaction mixture was stirred at room temperature for 24 h. Upon completion, the mixture was poured into dichloromethane (100 mL), washed three times with water (100 mL), dried over Na_2SO_4, filtered, and concentrated under reduced pressure to afford the crude product. The product was obtained as an pink solid (22%) and purified by column chromatography on silica gel using DCM as eluent. **^{1}H NMR (400 MHz, $CDCl_3$)** δ=7.92-7.86 (m, 4H), 7.66-7.59 (m, 3H), 7.59-7.54 (m, 4H), 7.48-7.39 (m, 4H), 7.03 (d, *J*=4.3 Hz, 2H), 6.69 (d, *J*=4.3 Hz, 2H). **ESI (+) FT-ICR MS** calcd. for $C_{29}H_{19}O_2N_2BF_2Na^+$ $[M+Na]^+$: 499.1410; found: 499.1400. The spectroscopic properties were consistent with the data available in the literature (LV, Fan *et al*., 2023).

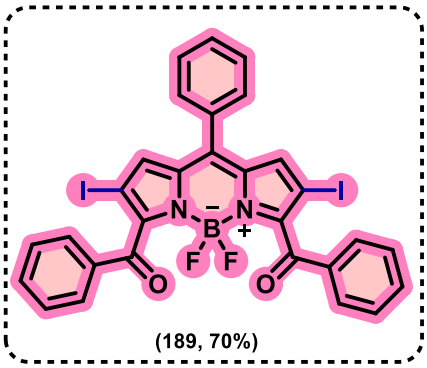

4,4-Difluoro-2,6-diiodo-8-phenyl-3,5-diphenylmethanone-4-bora-3a,4a-diaza-s-indacene (compound **189**): To a solution of **188** (1.0 equi) in MeCN (0.03 M), NIS (3.0 equi) was added. The reaction mixture was stirred at 50 °C for 24 h until completion. The solvent was removed under reduced pressure. The product was obtained as an

pink solid (70%) and purified by column chromatography on silica gel using DCM as eluent. **^{1}H NMR (400 MHz, $CDCl_3$)** δ=7.84-7.80 (m, 4H), 7.65-7.62 (m, 3H), 7.61-7.57 (m, 4H), 7.48-7.41 (m, 4H), 7.23 (s, 2H). **FTIR (ATR)$_{vmax}$** cm^{-1} 2910, 1538 (C=N), 14212, 1057. **ESI (+) FT-ICR MS** calcd. for $C_{29}H_{18}O_2N_2BF_2I_2^+$ $[M+H]^+$: 728.9518; found: 728.9513.

3.6 REFERENCES

AMNA, ATEŞ & OZTURK. Pd/Cu-catalyzed sonogashira cross-coupling polycondensation: A promising approach for synthesizing conjugated polymers with useful applications. **European Polymer Journal**, v. 196, n. 11, p. 112275, 2023. . Available at: <https://doi.org/10.1016/j.eurpolymj.2023.112275>.

ARBELOA, F. López *et al*. Structural, photophysical and lasing properties of pyrromethene dyes. **International Reviews in Physical Chemistry**, v. 24, n. 2, p. 339-374, 2005. Available at: <https://doi.org/10.1080/01442350500270551>.

AWUAH & YOU. Boron dipyrromethene (BODIPY)-based photosensitizers for photodynamic therapy. **RSC Advances**, v. 2, p. 11169-11183, 2012. Available at: <https://doi.org/10.1039/c2ra21404k>.

BAÑUELOS-PRIETO, Jorge *et al*. Controlling Optical Properties and Function of BODIPY by Using Asymmetric Substitution Effects. **Chemistry a European Journal**, v. 16, p. 14094-14105, 2010. Available at: <https://doi.org/10.1002/chem.201002095>.

BASSAN, Elena *et al*. Design of BODIPY dyes as triplet photosensitizers: electronic properties tailored for solar energy conversion, photoredox catalysis and photodynamic therapy. **Chemical Science**, v. 12, p. 6607-6628, 2021. Available at: <https://doi.org/10.1039/d1sc00732g>.

BEER, Gerhard *et al*. Redox Switches with Chiroptical Signal Expression Based on Binaphthyl Boron Dipyrromethene Conjugates. **Angewandte Chemie - International Edition**, v. 39, n. 18, p. 3252-3255, 2000. Available at: <https://doi.org/10.1002/1521-3773(20000915)39:18<3252::AID-ANIE3252>3.0.CO;2-P>.

BENSTEAD, MEHL & BOYLE. 4,4'-Difluoro-4-bora-3a,4a-diaza-s-indacenes (BODIPYs) as components of novel light active materials. **Tetrahedron**, v. 67, p. 3573-3601, 2011. Available at: <https://doi.org/10.1016/j.tet.2011.03.028>.

BOENS, LEEN & DEHAEN. Fluorescent indicators based on BODIPY. **Chemical Society Reviews**, v. 41, p. 1130-1172, 2012. Available at: <https://doi.org/ 10.1039/c1cs15132k>.

BOENS, Noël *et al*. Visible Absorption and Fluorescence Spectroscopy of Conformationally Constrained, Annulated BODIPY Dyes. **Journal of Physical Chemistry**, v. 116, n. 39, p. 9621-9631, 2012. Available at: <https://doi.org/10.1021/jp305551w>.

BOENS, VERBELEN & DEHAEN. Postfunctionalization of the BODIPY Core: Synthesis and Spectroscopy. **European Journal of Organic Chemistry**, v. 2015, n.30, p. 6577-6595, 2015. Available at: <https://doi.org/10.1002/ejoc.201500682>.

BOYER, Joseh H. *et al*. Pyrromethene-BF_2 Complexes as Laser Dyes: 2. **Heteroatom Chemistry**, v. 4, n. 1, p. 39-49, 1993. Available at: <https://doi.org/10.1002/hc.520040107>.

DIXON, H. B. F *et al*. Nomenclature of Tetrapyrroles. **Pure and Applied Chemistry**, v. 59, n. 6, p. 779-832, 1987. Available at: <http://dx.doi.org/10.1351/pac198759060779>.

ESNAL, Ixone et al. Nitro and amino BODIPYS: crucial substituents to modulate their photonic behavior. **RSC Advances**, v.3 p. 1547-1556, 2013. Available at: <http://dx.doi.org/10.1039/c2ra22916a>.

FARFÁN-PAREDES Mónica *et al*. Physicochemical and computational insight of 19F NMR and emission properties of meso-(o-aryl)-BODIPYs. **New Journal of Chemistry**, v. 44, p. 19459, 2020. Available at: <https://doi.org/10.1039/d0nj02576c>.

FRATH, Denis *et al*. Luminescent Materials: Locking π-Conjugated and Heterocyclic Ligands with Boron(III). **Angewandte Chemie - International Edition**, v. 53, n. 9, p. 2290–2310, 2014. Available at: <https://doi.org/10.1002/anie.201305554>.

GOLOVKOVA, KOZLOV & NECKERS. Synthesis and Properties of Novel Fluorescent Switches. **Journal of Organic Chemistry**, v. 70, n. 14, p.5545-5549, 2005. Available at: <https://doi.org/10.1021/jo050540k>.

GONÇALVES, M. Sameiro T. Fluorescent Labeling of Biomolecules with Organic Probes. **Chemical Reviews**, v. 109, n. 1, p. 190-212, 2009. Available at: <https://doi.org/10.1021/cr0783840>.

GONZÁLEZ-VERA, Juan A. *et al*. Unusual spectroscopic and photophysical properties of solvatochromic BODIPY analogues of Prodan. **Dyes and Pigments**, v. 182, p. 108510, 2020. Available at: <https://doi.org/10.1016/j.dyepig.2020.108510>.

GOUD, TUTAR & BIELLMANN. Synthesis of 8-heteroatom-substituted 4,4-difluoro-4-bora-3a, 4a-diaza-s-indacene dyes (BODIPY). **Tetrahedron**, v. 62, p. 5084-5091, 2006. Available at: <https://doi.org/10.1016/j.tet.2006.03.036>.

HATTORI, Shigeki *et al*. Charge Separation in a Nonfluorescent Donor-Acceptor Dyad Derived from Boron Dipyrromethene Dye, Leading to Photocurrent Generation. **Journal of Physical Chemistry B,** v. 109, n. 32, p. 15368-15375, 2005. Available at: <https://doi.org/10.1021/jp050952x>.

HEPP, A *et al*. Highly efficient energy transfer to a novel organic dye in OLED devices. **Synthetic Metals**, v. 146, p. 11-15, 2004. Available at: <https://doi.org/ 10.1016/j.synthmet.2004.06.016>.

HUANG, GAO & HAN. Photoswitchable Near-Infrared-Emitting Borondipyrromethene (BODIPY) Nanoparticles. **Particle & Particle Systems Characterization**, v. 34, n. 11, p. 1700223, 2017. Available at: <https://doi.org/10.1002/ppsc.201700223>.

JIAO, Lijuan *et al*. *β*-Formyl-BODIPYs from the Vilsmeier-Haack Reaction. **Journal of Organic Chemistry**, v. 74, p. 7525-7528, 2009. Available at: <https://doi.org/10.1021/jo901407h>.

KIM J. & KIM, Y. A water-soluble sulfonate-BODIPY based fluorescent probe for selective detection of HOCl/OCl^- in aqueous media. **Analyst**. v. 139, p. 2986, 2014. Available at: <https://doi.org/10.1039/C4AN00466C>.

KOLEMEN, Safacan et al. Intracellular Modulation of Excited-State Dynamics in a Chromophore Dyad: Differential Enhancement of Photocytotoxicity Targeting Cancer Cells. **Angewandte Chemie - International Edition**, v. 54, p. 1-6, 2015. Available at: <https://doi.org/10.1002/anie.201411962>.

KOWADA, MAEDA & KIKUCHI. BODIPY-based probes for the fluorescence imaging of biomolecules in living cells. **Chemical Society Reviews**, v. 44, p. 4953-4972, 2015. Available at: <https://doi.org/10.1039/c5cs00030k>.

LAKSHMI, RAO & RAVIKANTH. Halogenated Boron-Dipyrromethenes: Synthesis, Properties and Applications. **Organic & Biomolecular Chemistry**, v. 13, p. 2501-2517, 2015. Available at: <https://doi.org/10.1039/C4OB02293A>.

LAKSHMI, SHARMA & RAVIKANTH. Functionalized boron-dipyrromethenes and their applications. **Reports in Organic Chemistry**, v. 6, p. 1-24, 2016. Available at: <http://dx.doi.org/10.2147/ROC.S60504>.

LEEN, Volker *et al*. Direct functionalization of BODIPY dyes by oxidative nucleophilic hydrogen substitution at the 3- or 3,5-positionsw. **Chemical Communications**, v. 46, p. 4908-4910, 2010. Available at: <http://dx.doi.org/10.1039/c0cc00568a>.

LI & LINDSEY. Efficient Synthesis of Light-Harvesting Arrays Composed of Eight Porphyrins and One Phthalocyanine. **Journal of Organic Chemistry**, v. 64, n. 25, p. 9109-9108, 1999. Available at: <https://doi.org/10.1021/jo991102e>.

LI, MINTZER & BITTMAN. First Synthesis of Free Cholesterol-BODIPY Conjugates. **Journal of Organic Chemistry**, v. 71, n. 4, p. 1718-1721, 2006. Available at: <https://doi.org/10.1021/jo052029x>.

LITTLER, J. Benjamin *et al*. Refined Synthesis of 5-Substituted Dipyrromethanes. **Journal of Organic Chemistry**, v. 64, n. 4, p. 1391-1396, 1999. Available at: <https://doi.org/10.1021/jo982015+>.

LLANO, Rebeca Sola *et al*. Tailoring the Photophysical Signatures of BODIPY Dyes: Toward Fluorescence Standards across the Visible Spectral Region. **Photochemistry and Photophysics - Fundamentals to Applications**, Chapter 2, 2018. Available at: <http://dx.doi.org/10.5772/intechopen.74848>.

LOUDET, A & BURGUESS, K; BODIPY. Dyes and Their Derivatives: Syntheses and . Spectroscopic Properties. **Chemical Reviews**. v. 107, p. 4891-4932, 2007. Available at: <https://doi.org/10.1021/cr078381n>.

LV, Fan *et al*. Copper-catalyzed α-selective cross-dehydrogenative coupling of BODIPY dyes with aldehydes: A new route to acylated BODIPYs and dipyrromethenes. **Dyes and Pigments**, v. 210, p. 111030, 2023. Available at: <https://doi.org/10.1016/j.dyepig.2022.111030>.

McCUSKER, CARROLL & ROTELLO. Cationic polyhedral oligomeric silsesquioxane (POSS) units as carriers for drug delivery processes. **Chemical Communications**, n. 8, p. 996-998, 2005. Available at: <https://doi.org/10.1039/b416266h>.

MONSMA, Frederick J. Jr. *et al*. Characterization of Novel Fluorescent Ligands with High Affinity for D_1 and D_2 Dopaminergic Receptors. **Journal of Neurochemistry**, v. 52, n. 5, p. 1641-1644, 1989. Available at: <https://doi.org/10.1111/j.1471-4159.1989.tb09220.x>.

NAKASHIMA, Mika, *et al*. Selenium-containing BODIPY dyes as photosensitizers for triplet-triplet annihilation upconversion. **Journal of Materials Chemistry C.** v. 6, p. 6208, 2018. Available at: <https://doi.org/10.1039/C8TC00944A>.

NI, T & WU, J. Far-red and near infrared BODIPY dyes: synthesis and applications for fluorescent pH probes and bio-imaging. **Organic & Biomolecular Chemistry.** v. 12, p. 3774, 2014. Available at: <https://doi.org/10.1039/C3OB42554A>.

ORTIZ, Maria J. *et al*. Synthesis and functionalization of new polyhalogenated BODIPY dyes. Study of their photophysical properties and singlet oxygen generation. **Tetrahedron**, v. 68, p. 1153-1162, 2012. Available at: <https://doi.org/10.1016/j.tet.2011.11.070>.

PALAO, SLANINA & KLÁN. Construction of the carbon–chalcogen (S, Se, Te) bond at the 2,6-positions of BODIPY *via* Stille cross-coupling reaction. **Chemical Communications**, v. 52, 11951, 2016. Available at: <https://doi.org/10.1039/C6CC06923A>.

PATAG, JONES & WERZ. BOIMPYs: Rapid Access to a Family of Red-Emissive Fluorophores and NIR Dyes. **Angewandte Chemie - International Edition**, v. 55, p. 13340-13344, 2016. Available at: <http://dx.doi.org/10.1002/anie.201606883>.

ROHAN, Taoufik *et al*. Functionalisation of fluorescent BODIPY dyes by nucleophilic Substitution. **Chemical Communications**, p. 266-268, 2006. Available at: <https://doi.org/10.1039/b512756d>.

SHIMIZU, Soji *et al*. Pyrrolopyrrole aza-BODIPY analogues: a facile synthesis and intense fluorescence. **Chemical Communications**, v. 49, p. 1621-1623, 2013. Available at: <https://doi.org/10.1039/c3cc38452g>.

SQUEO, Benedetta Maria *et al*. BODIPY-Based Molecules, a Platform for Photonic and Solar Cells. **Molecules**. v. 26, p. 153, 2021. Available at:

<https://doi.org/10.3390/molecules26010153>.

TAHTAOUI, Chouaib *et al*. Convenient Method To Access New 4,4-Dialkoxyand 4,4-Diaryloxy-diaza-s-indacene Dyes: Synthesis and Spectroscopic Evaluation. **Journal of Organic Chemistry**, v. 72, p. 269-272, 2007. Available at: <https://doi.org/10.1021/jo061567m>.

TREIBS & KREUZER. Dufluorboryl-Komplexe von Di- und Tripyrrylmethen. **Justus Liebigs Annalen der Chemie**, v. 718, p. 208-223, 1968. Available at: <https://doi.org/10.1002/JLAC.19687180119>.

ULRICH, Gilles *et al*. Pyrromethene Dialkynyl Borane Complexes for “Cascatelle” Energy Transfer and Protein Labeling. **Angewandte Chemie - International Edition**, v. 44, n. 24, p. 3694-3698, 2005. Available at: <https://doi.org/10.1002/anie.200500808>.

ULRICH, ZIESSEL & HARRIMAN, A. The chemistry of fluorescent bodipy dyes: versatility unsurpassed. **Angewandte Chemie - International Edition,** v. 47, p. 1184, 2008. Available at: <https://doi.org/10.1002/anie.200702070>.

WAGNER & LINDSAY. Boron-dipyrromethene dyes for incorporation in synthetic multi-pigment light-harvesting arrays. **Pure and Applied Chemistry**, v. 68, n. 7, p. 1373-1380. Available at: <http://dx.doi.org/10.1351/pac199668071373>.

WANG, Liang *et al*. Regioselective 2,6-dihalogenation of BODIPYs in 1,1,1,3,3,3-hexafluoro-2-propanol and preparation of novel *meso*-alkyl polymeric BODIPY dyes. **RSC Advances**. v. 3, p. 9219, 2013. Available at: <https://doi.org/10.1039/C3RA41298A>.

ZIESSEL, ULRICH & HARRIMAN. The chemistry of Bodipy: A new *El Dorado* for fluorescence tools. **New Journal of Chemistry**, v. 31, p. 496-501, 2007. Available at: <https://doi.org/10.1039/b617972j>.

ZHANG, Wangquan, *et al*. Application of multifunctional BODIPY in photodynamic therapy. **Dyes and Pigments**. v. 185, p. 108937, 2021. Available at: <https://doi.org/10.1016/j.dyepig.2020.108937>.

ZHOU, Xin *et al*. Highly Regioselective *α*-Chlorination of the BODIPY Chromophore with Copper(II) Chloride. **Organic Letters**, v. 17, p. 4632-4635, 2015. Available at: <https://doi.org/10.1021/acs.orglett.5b02383>.

GENERAL CONCLUSIONS

The work presented in this thesis enabled the development and application of a broad range of methodologies and competencies in organic synthesis, encompassing the preparation of natural product derivatives, total synthesis approaches, and fluorescent molecular systems, all within the context of fine chemical techniques. The interdisciplinary nature of the research, together with collaborative work across different research groups, contributed significantly to expanding the scientific perspective of the researcher and strengthening experimental and analytical skills. Collectively, the results highlight the successful design of efficient synthetic strategies for the construction of biologically relevant and fluorescent molecular scaffolds, providing new compounds and methodological approaches with potential impact in medicinal chemistry and chemical biology.

APPENDICES A - Characterization of the compounds Chapter 1

Figure A1. ^{1}H NMR spectrum of compound **43a** (400 MHz, $CDCl_3$).

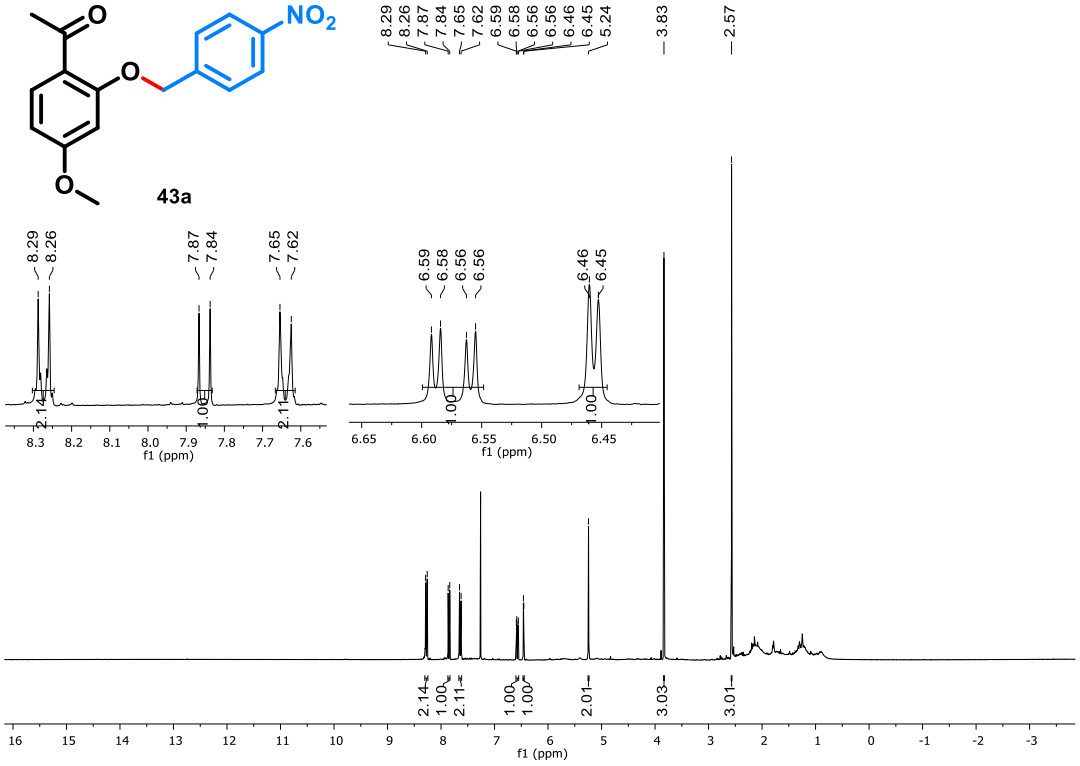

Figure A2. ^{13}C NMR spectrum of compound **43a** (100 MHz, $CDCl_3$).

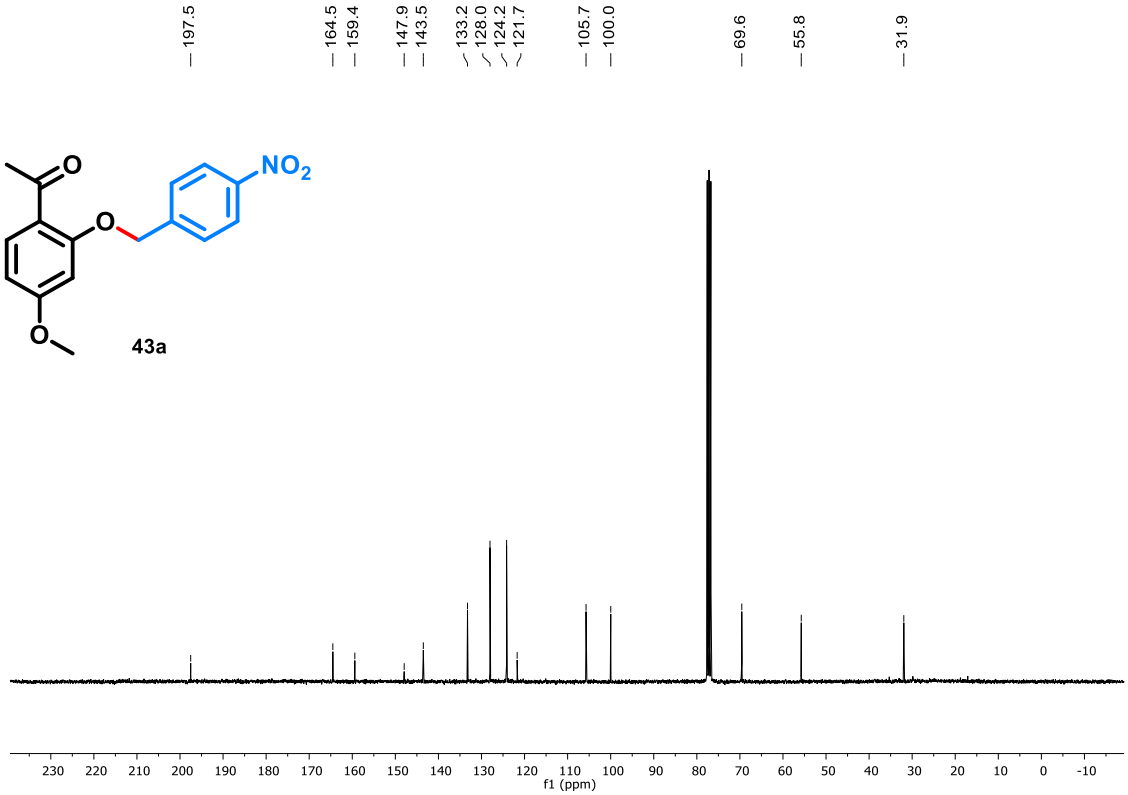

Figure A3. FT-IR (Attenuated total reflection – ATR) ν_{max} / cm^{-1} of compound **43a**.

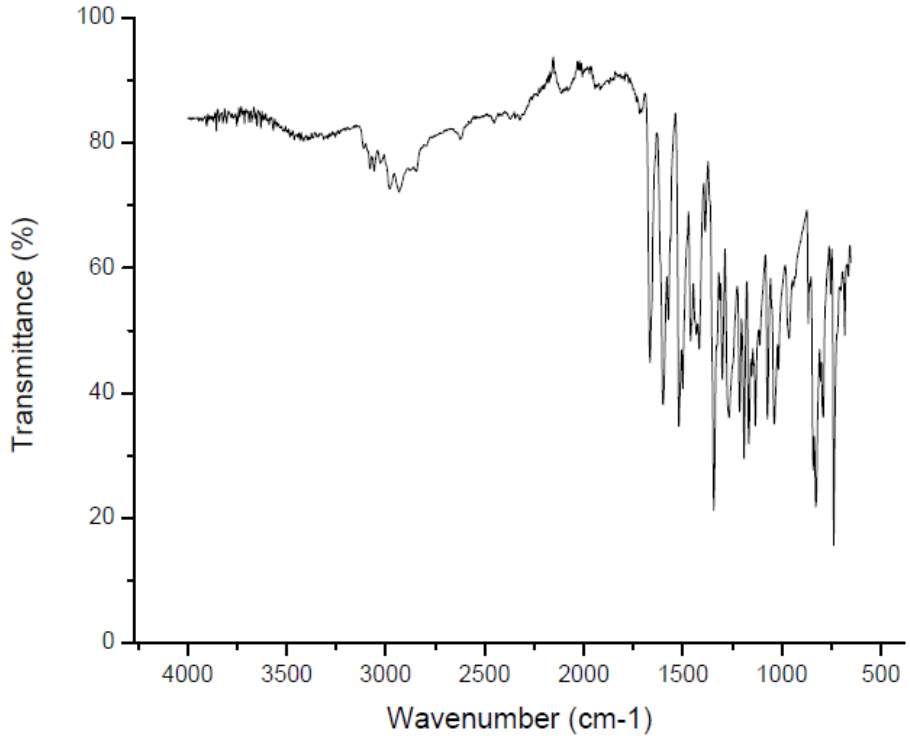

Figure A4. ESI (+) FT-ICR MS Spectra of compound **43a**.

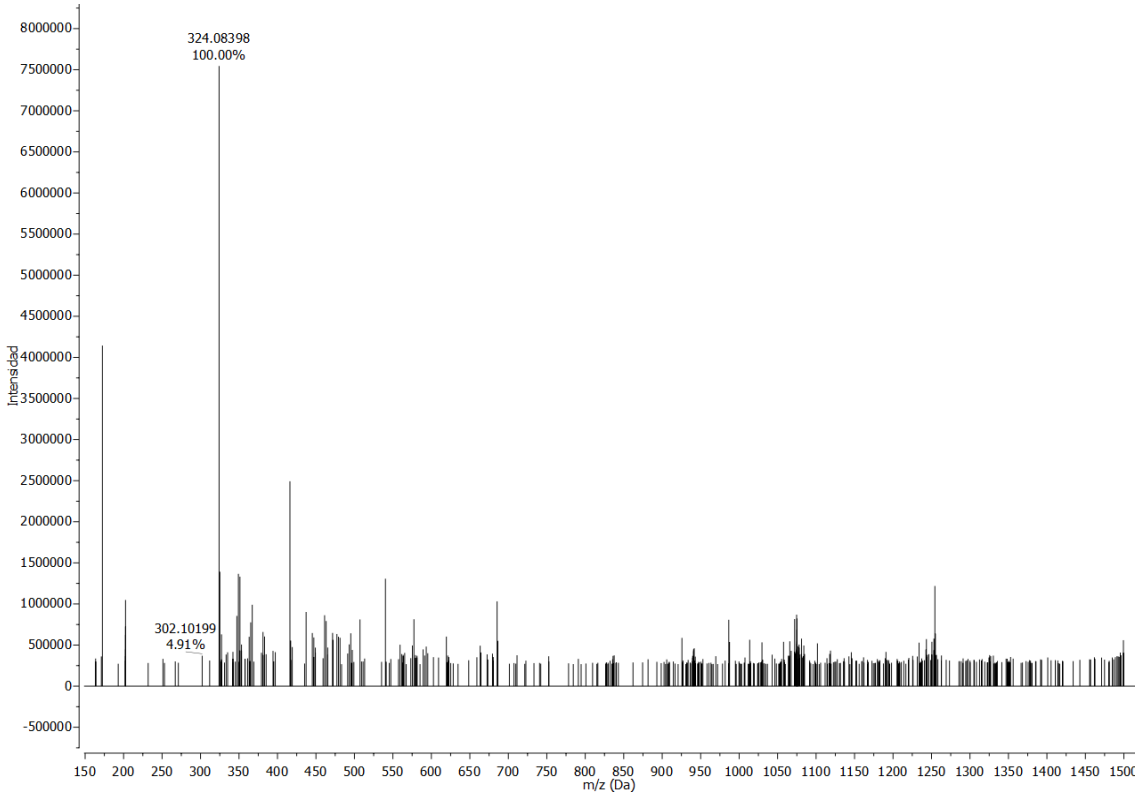

Table A1. X-ray data collection and refinement parameters for **43a**.

Compound 43a	
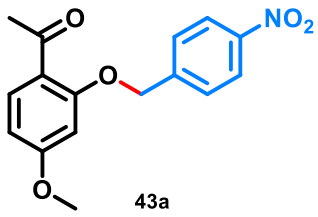 **43a** **Chemical Formula:** $C_{16}H_{15}NO_5$	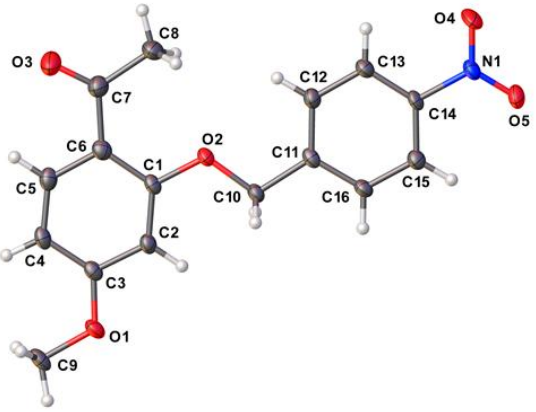
Chemical formula	$C_{16}H_{15}NO_5$
M (g mol^{-1})	301.29
Radiation	Cu Kα
Crystal system	Orthorhombic
Space group	*Fdd2*
a (Å)	49.0718(9)
b (Å)	28.8688(3)
c (Å)	3.8662(1)
α (º)	90
β (º)	90
γ (º)	90
V ($Å^3$)	5477.03(18)
Z	16
Density /g cm^{-3}	1.462
θ_{min} /º	7.106
θ_{max} /º	159.004
μ /mm^{-1}	0.918
Absorption correction	Multi-scan
Max./min. transmission	1.000/0.717
Measured reflections	23186
Independent reflections / Rint	2900/0.0669
Refined parameters	201
R_1	0.0422
wR_2	0.1129
GooF	1.078
Largest diff. peak and hole ($eÅ^{-3}$)	0.36/-0.34

Figure A5. ^{1}H NMR spectrum of compound **43b** (400 MHz, $CDCl_3$).

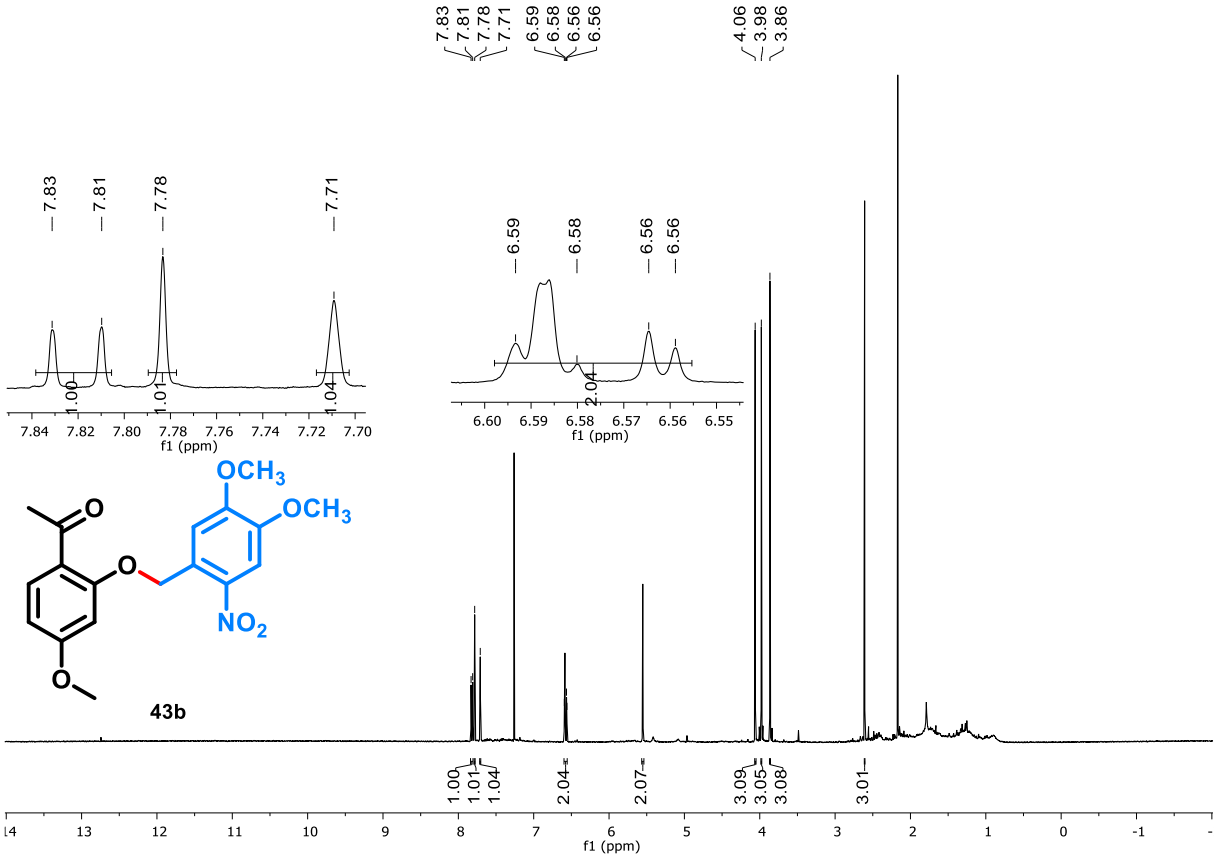

Figure A6. ^{13}C NMR spectrum of compound **43b** (100 MHz, $CDCl_3$).

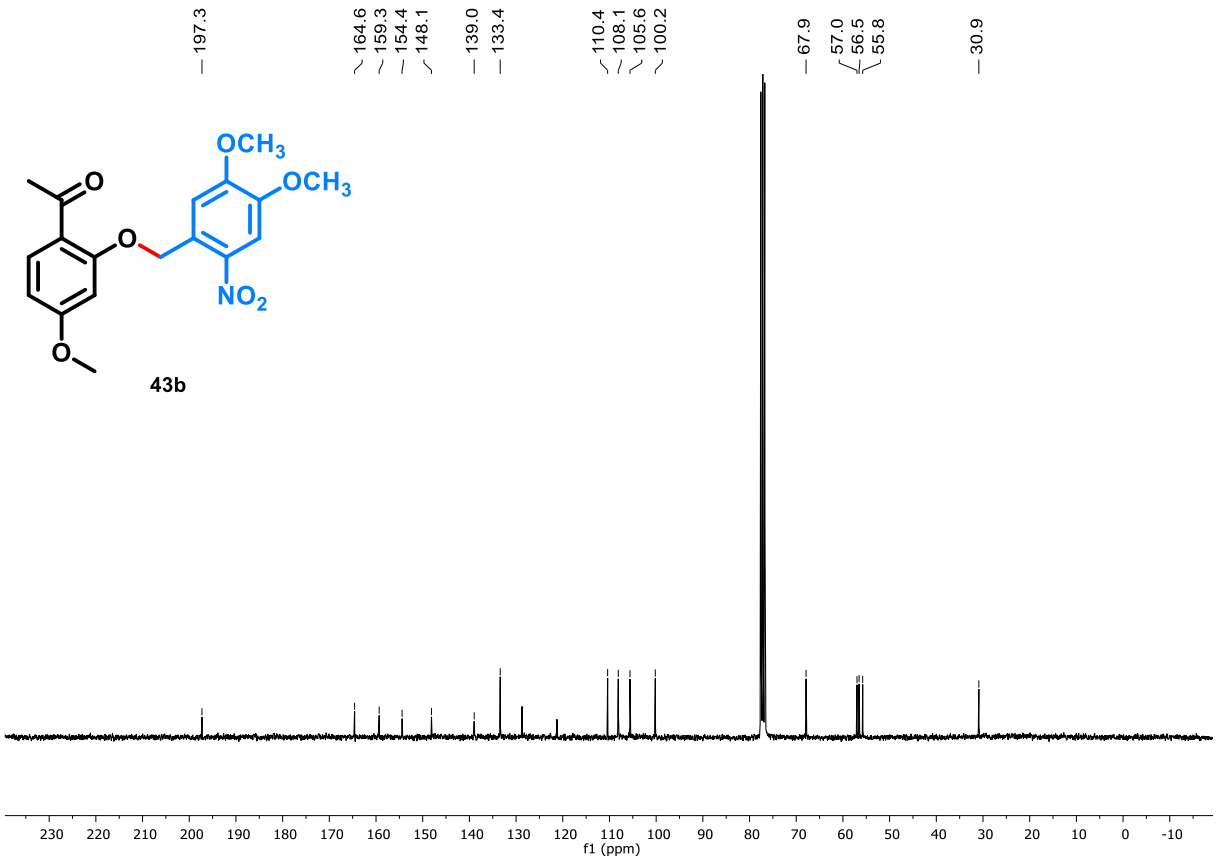

Figure A7. FT-IR (Attenuated total reflection – ATR) ν_{max} / cm^{-1} of compound **43b**.

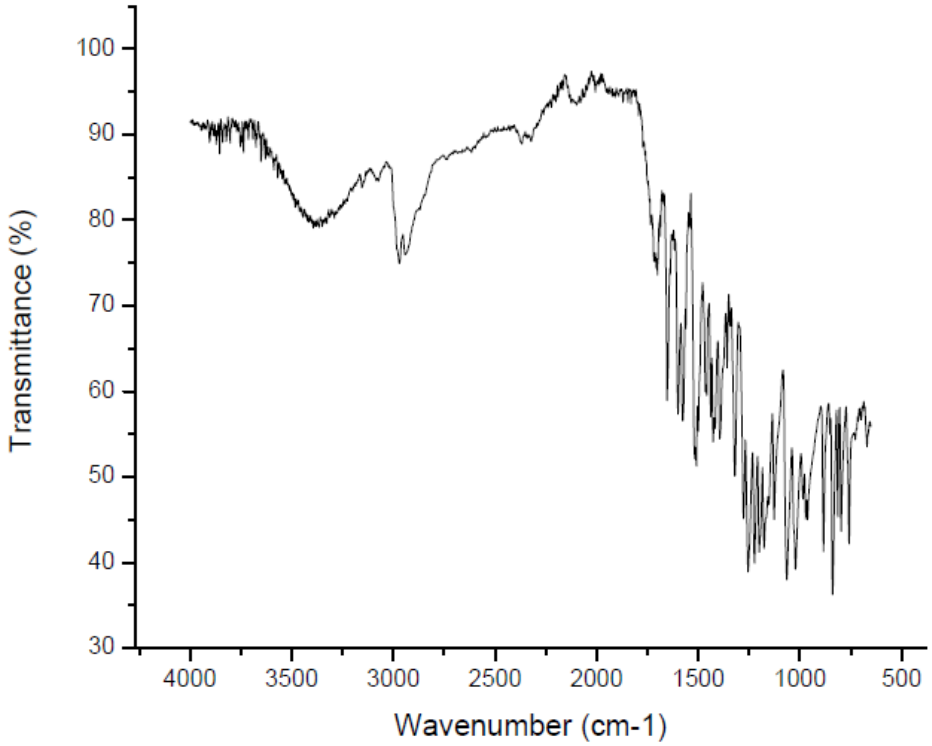

Figure A8. Figure A4. ESI (+) FT-ICR MS Spectra of compound **43b**.

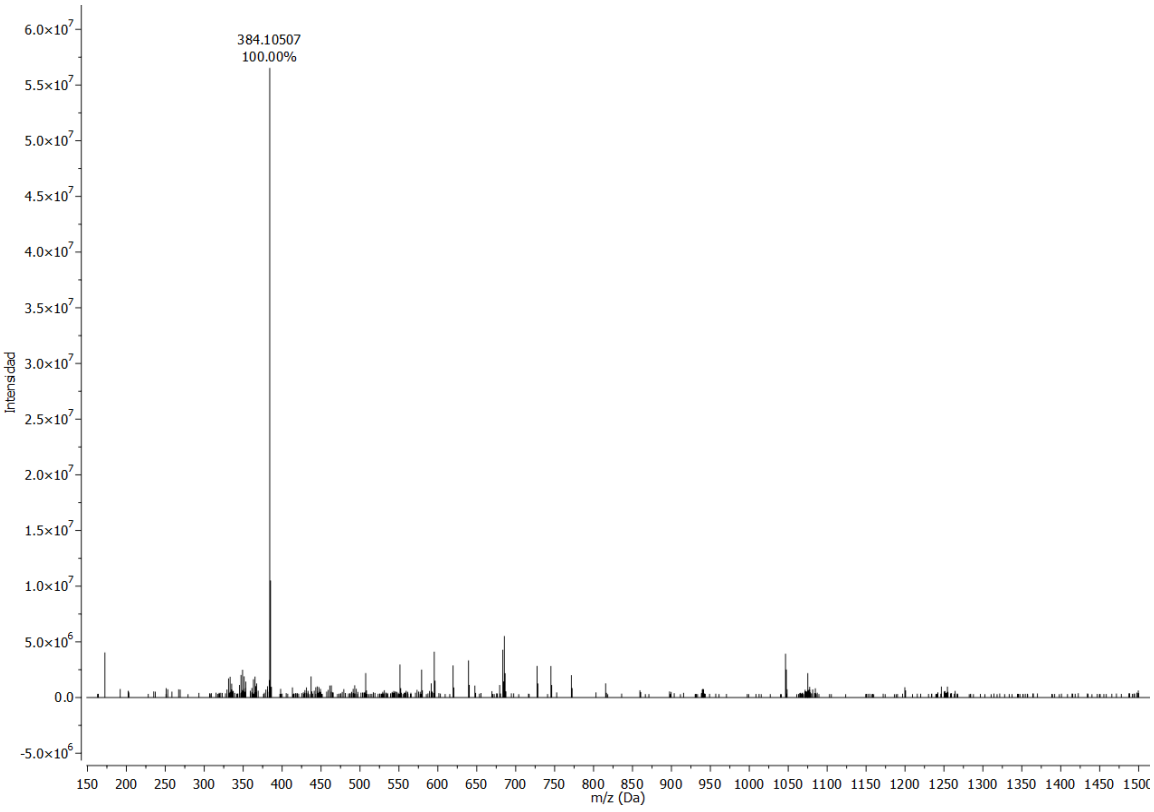

Figure A9. ^{1}H NMR spectrum of compound **43c** (400 MHz, $CDCl_3$).

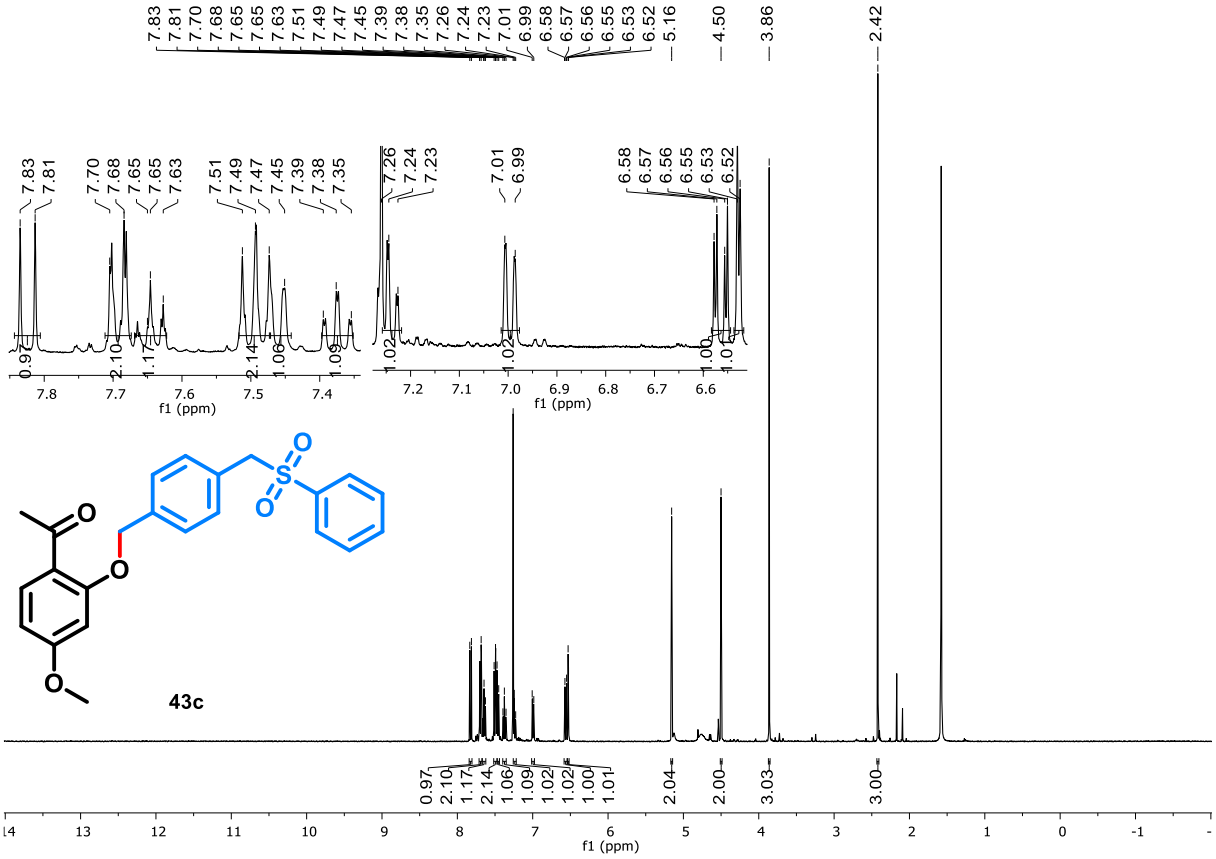

Figure A10. ^{13}C NMR spectrum of compound **43c** (100 MHz, $CDCl_3$).

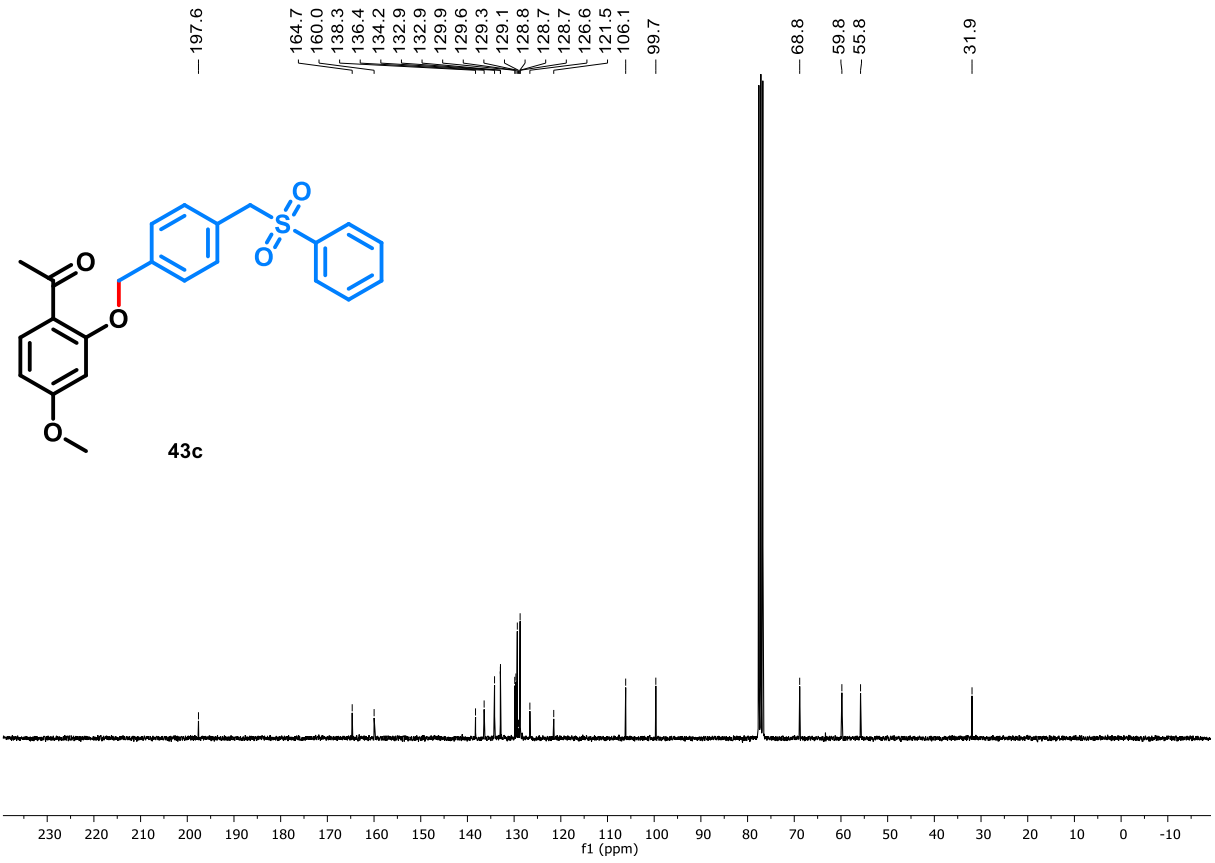

Figure A11. FT-IR (Attenuated total reflection – ATR) $_{vmax}$ / cm^{-1} of compound **43c**.

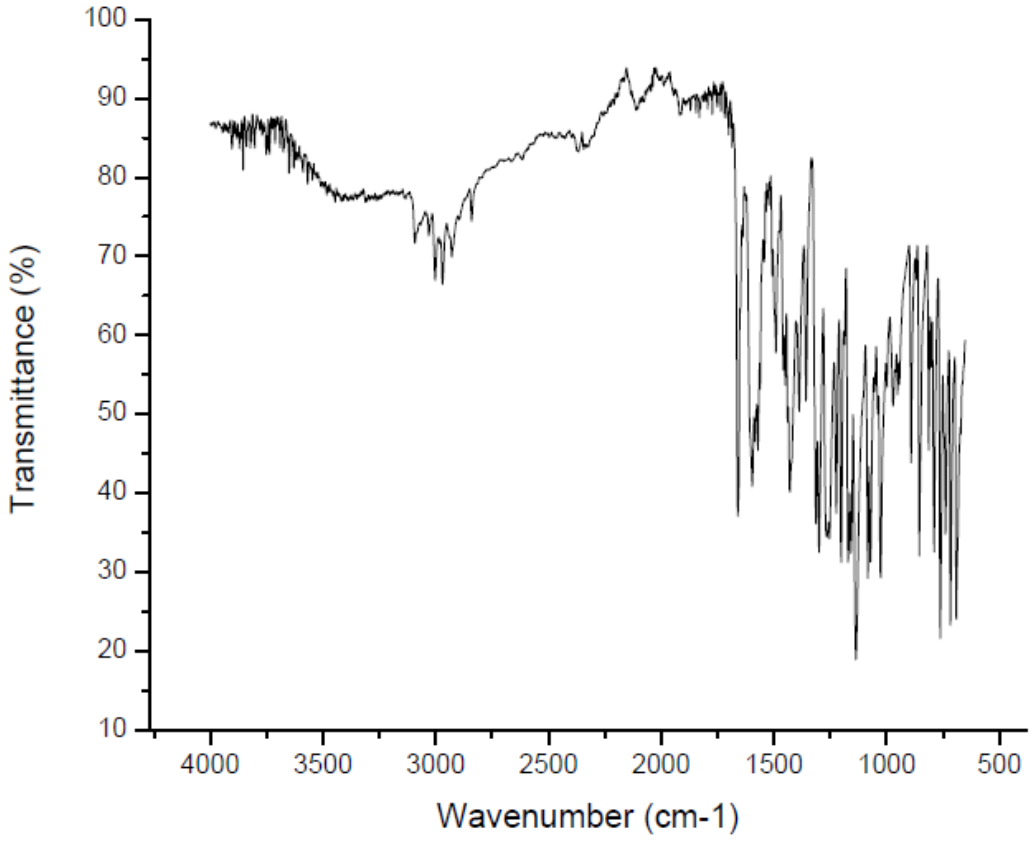

Figure A12. ESI (+) FT-ICR MS Spectra of compound **43c**.

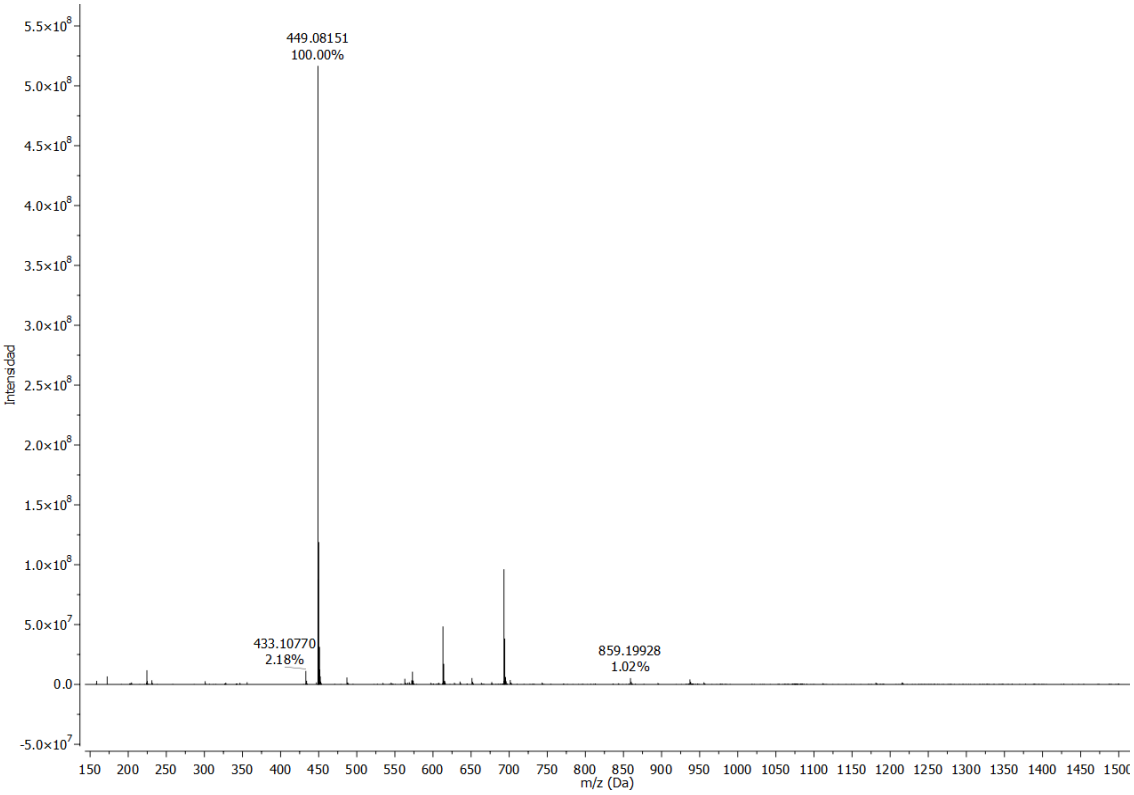

Figure A13. ^{1}H NMR spectrum of compound **43d** (400 MHz, $CDCl_3$).

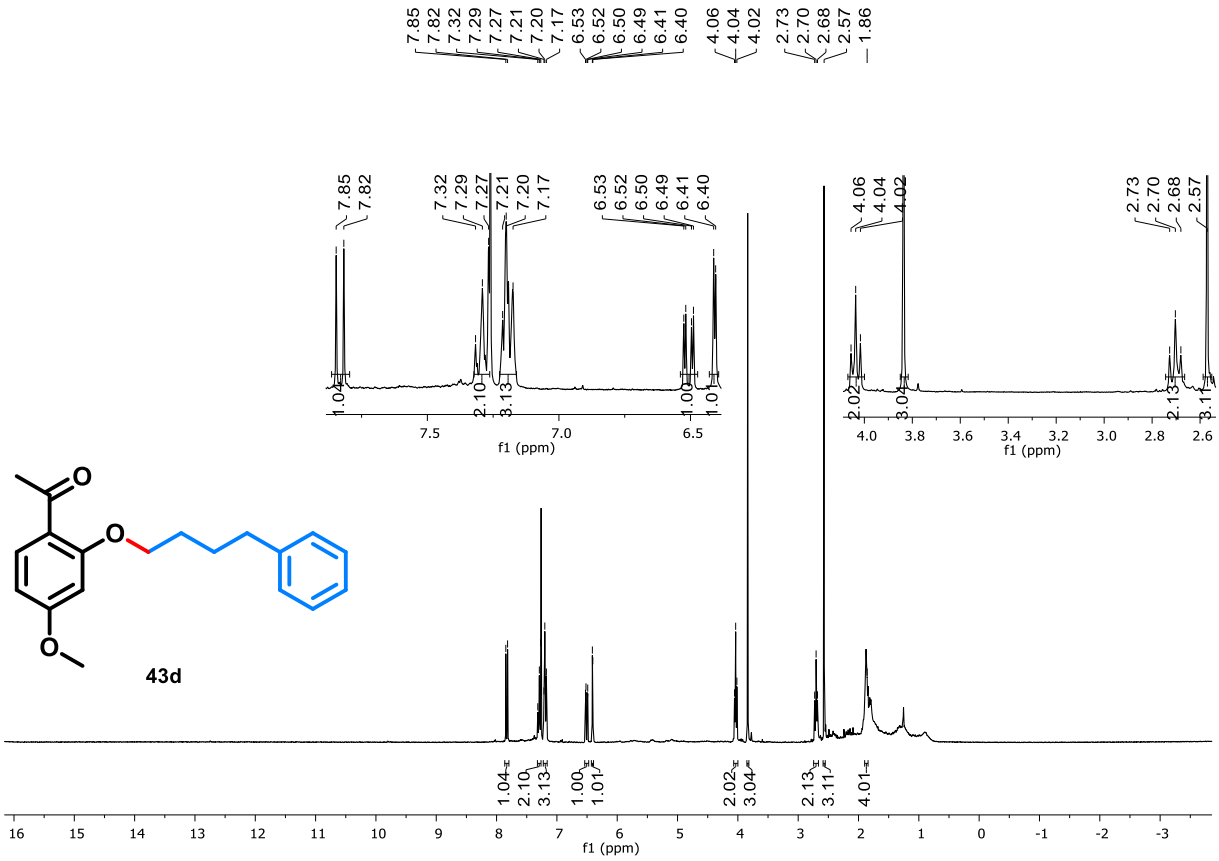

Figure A14. ^{13}C NMR spectrum of compound **43d** (100 MHz, $CDCl_3$).

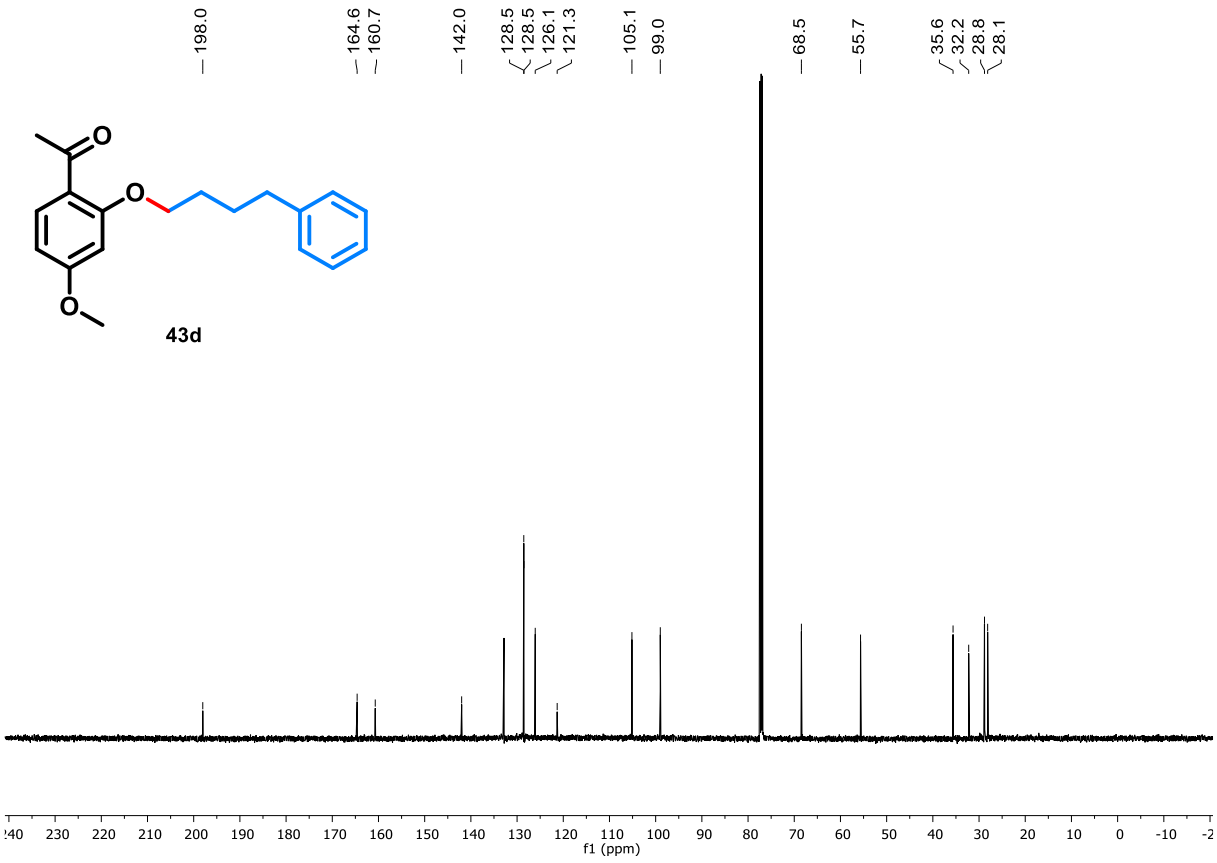

Figure A15. FT-IR (Attenuated total reflection – ATR) $_{vmax}$ / cm^{-1} of compound **43d**.

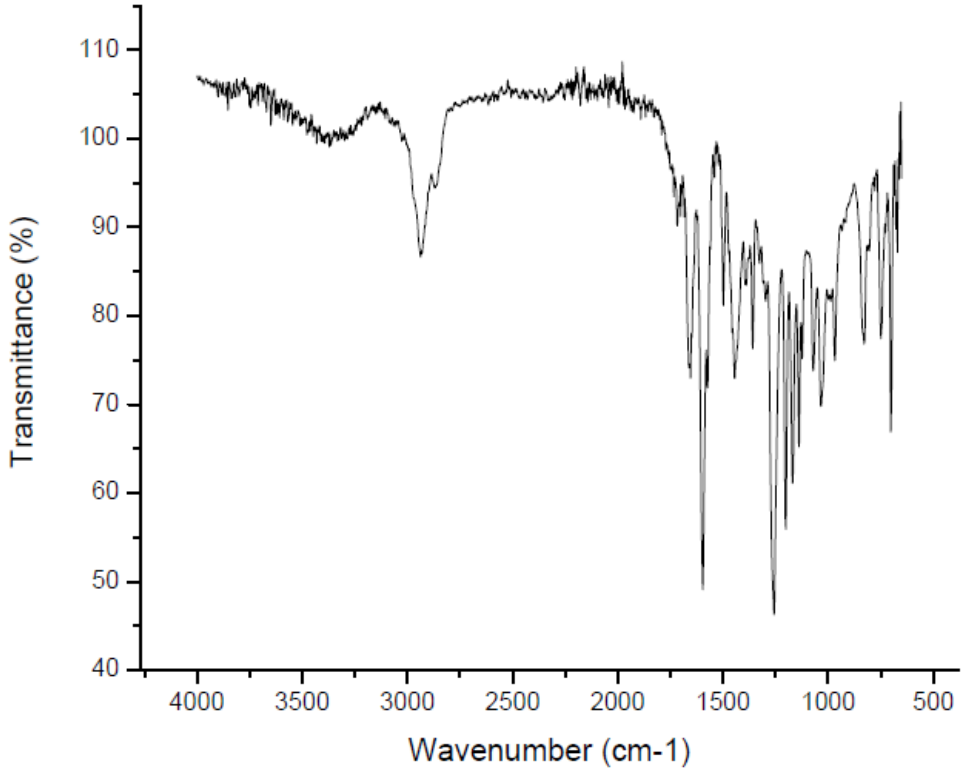

Figure A16. ESI (+) FT-ICR MS Spectra of compound **43d**.

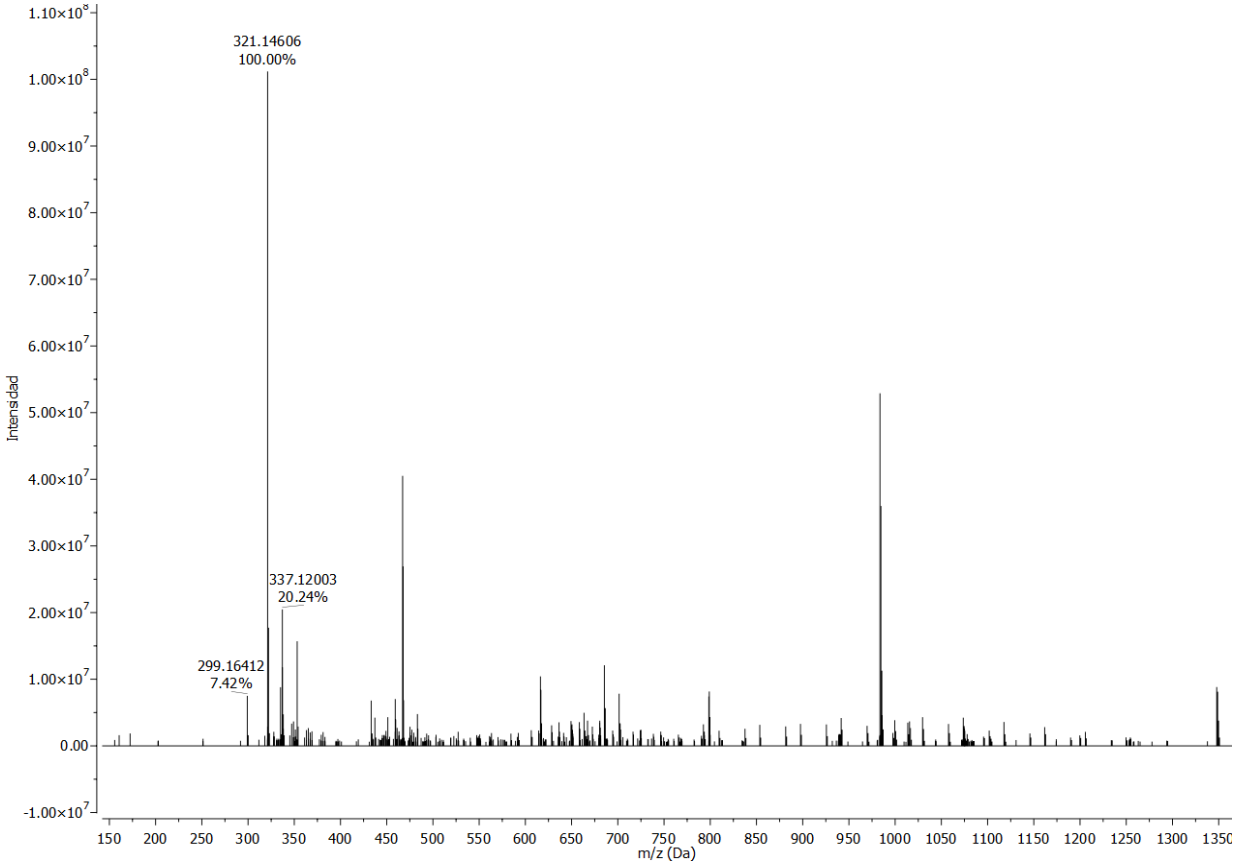

Figure A17. ^{1}H NMR spectrum of compound **44a** (400 MHz, $CDCl_3$).

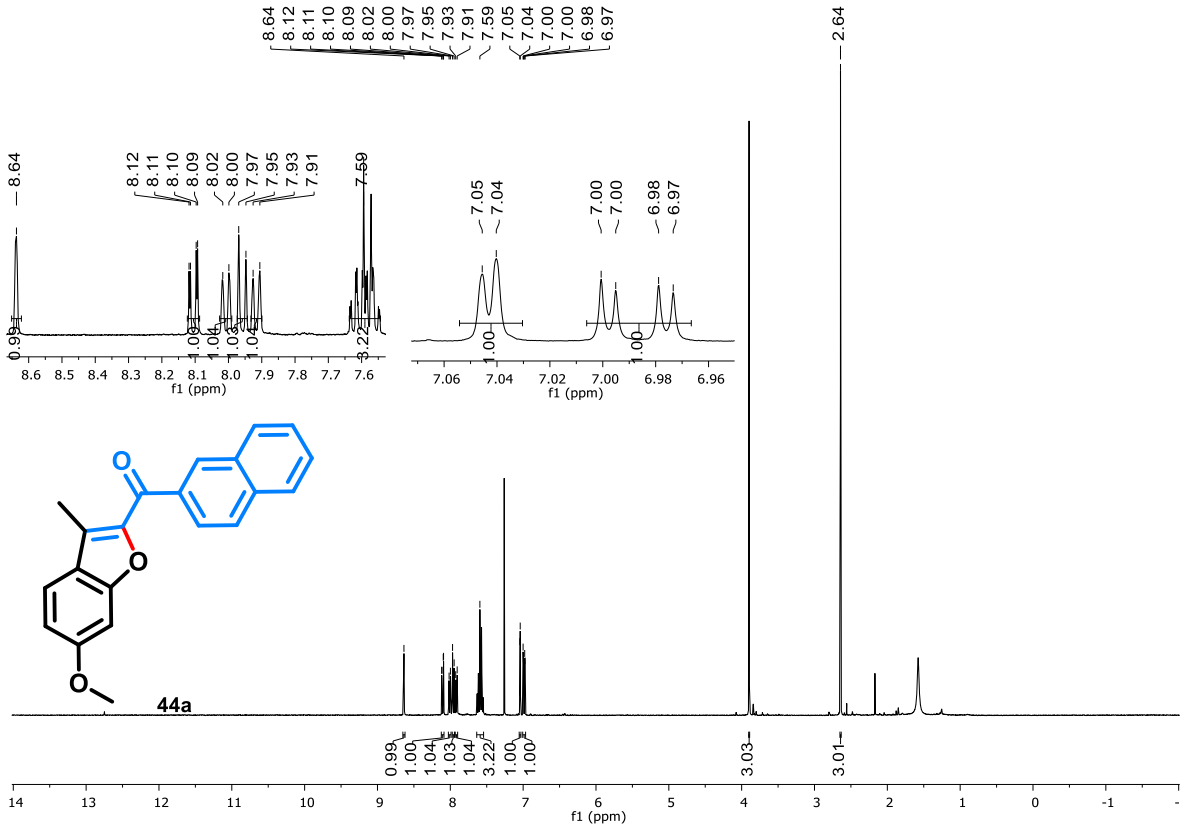

Figure A18. ^{13}C NMR spectrum of compound **44a** (100 MHz, $CDCl_3$).

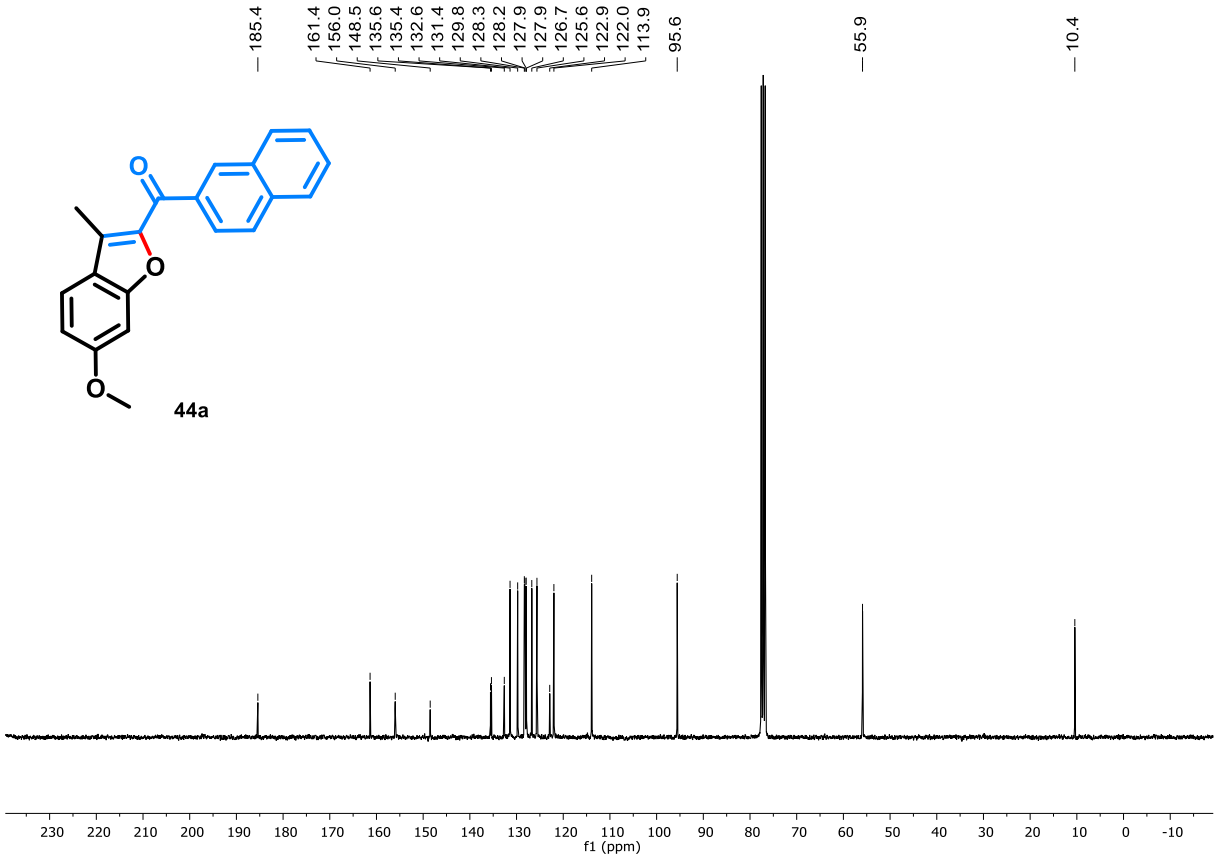

Figure A19. FT-IR (Attenuated total reflection – ATR) ν_{max} / cm^{-1} of compound **44a**.

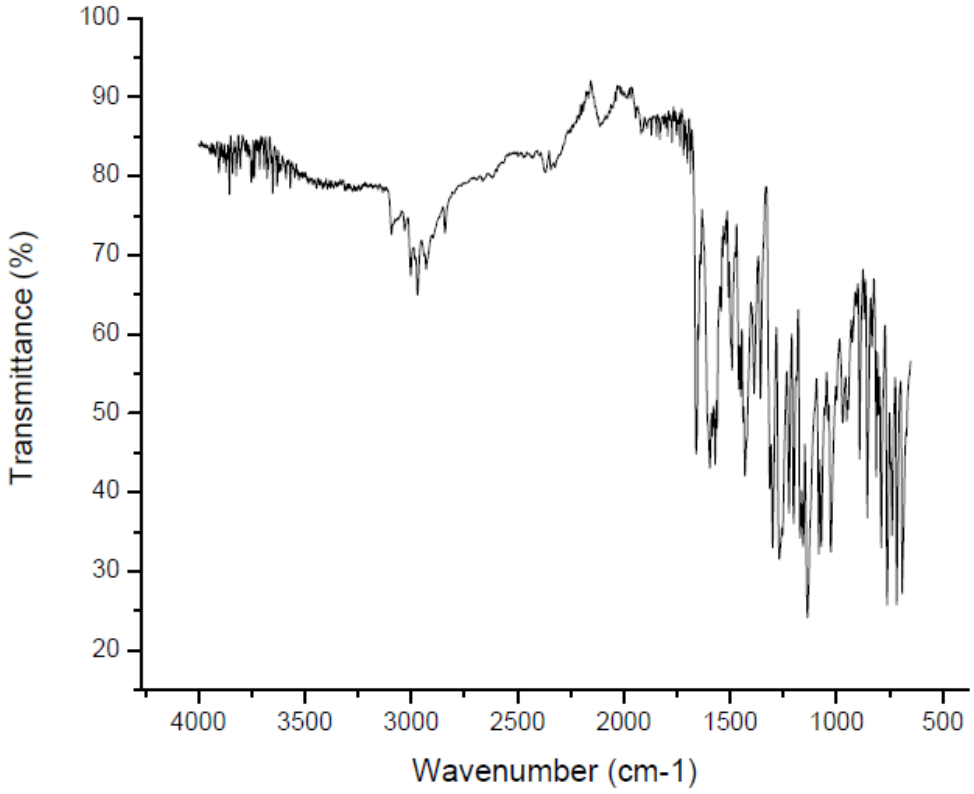

Figure A20. ESI (+) FT-ICR MS Spectra of compound **44a**.

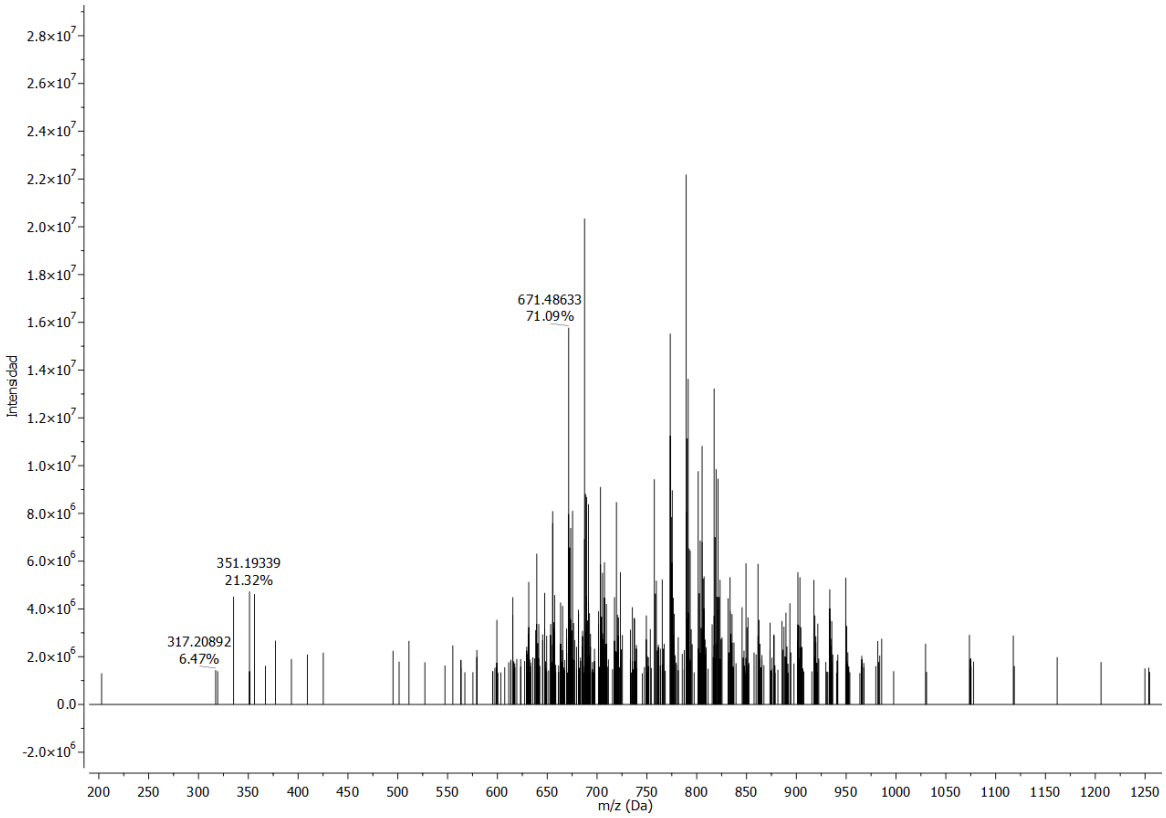

Table A2. X-ray data collection and refinement parameters for **44a**.

Compound 44a	
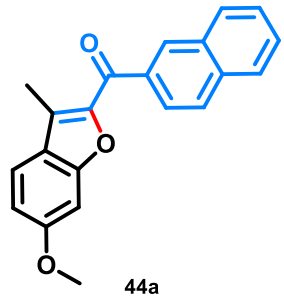 **44a** **Chemical Formula:** $C_{21}H_{16}O_3$	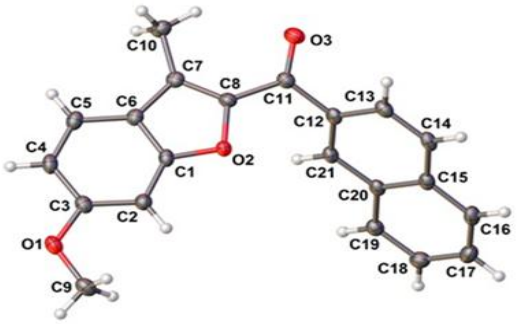
Chemical formula	$C_{21}H_{16}O_3$
M (g mol^{-1})	316.34
Radiation	Cu Kα
Crystal system	Monoclinic
Space group	*P2$_1$/c*
a (Å)	5.6813(1)
b (Å)	16.9465(2)
c (Å)	16.1191(2)
α (º)	90
β (º)	91.5729(10)
γ (º)	90
V (Å^3)	1551.33(3)
Z	4
Density /g cm^{-3}	1.354
θ_{min} /º	10.44
θ_{max} /º	140.122
μ /mm^{-1}	0.725
Absorption correction	Multi-scan
Max./min. transmission	1.000/0.475
Measured reflections	10354
Independent reflections / Rint	2907/0.0454
Refined parameters	220
R_1	0.0375
wR_2	0.0989
GooF	1.054
Largest diff. peak and hole (eÅ^{-3})	0.24/-0.20

Figure A21. ^{1}H NMR spectrum of compound **44b** (400 MHz, $CDCl_3$).

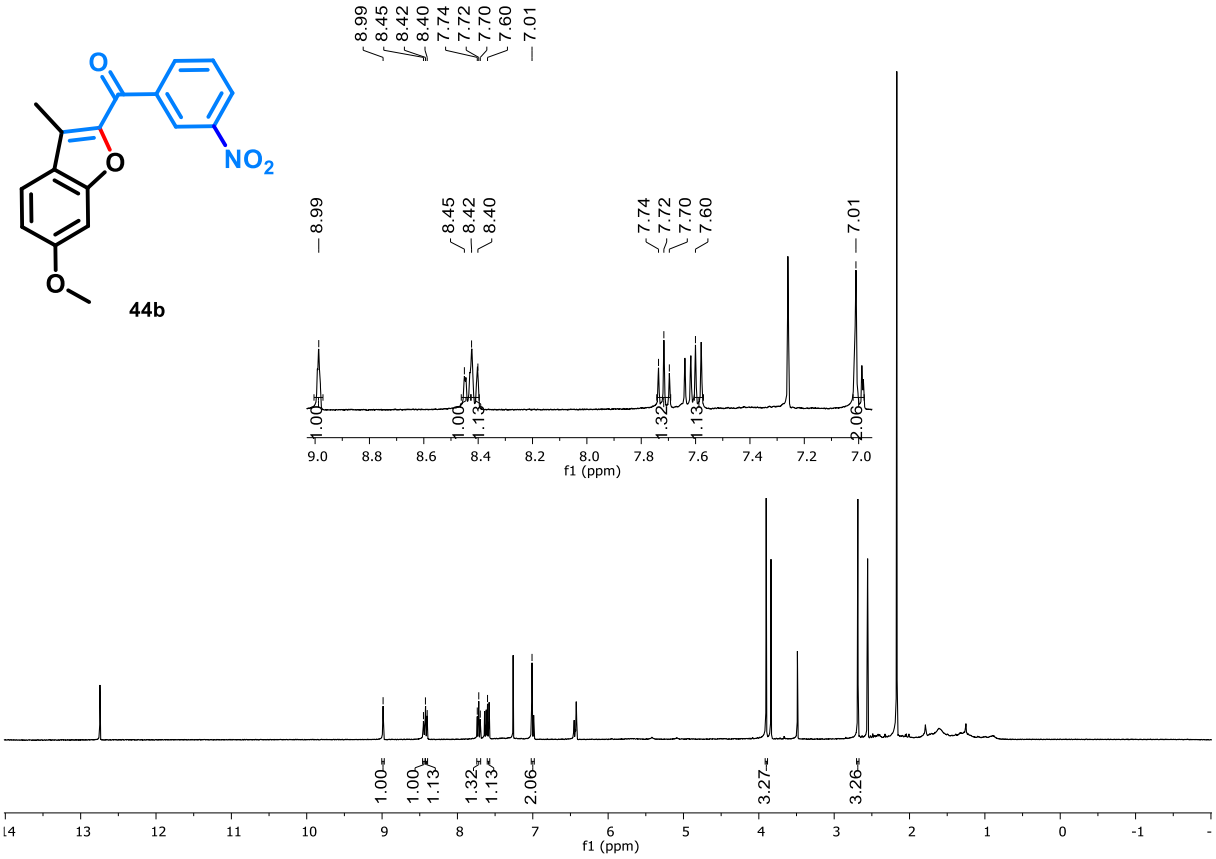

Figure A22. ^{13}C NMR spectrum of compound **44b** (100 MHz, $CDCl_3$).

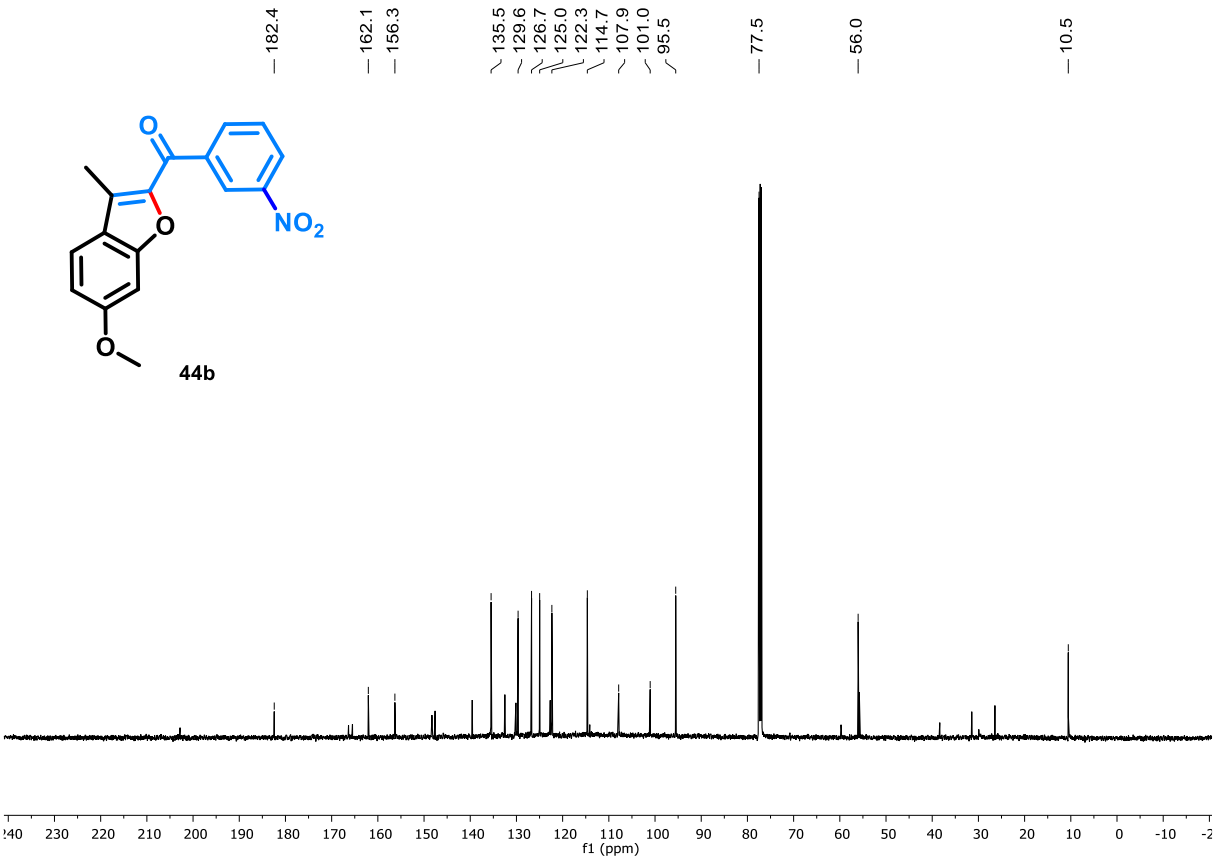

Figure A23. FT-IR (Attenuated total reflection – ATR) $_{vmax}$ / cm^{-1} of compound **44b**.

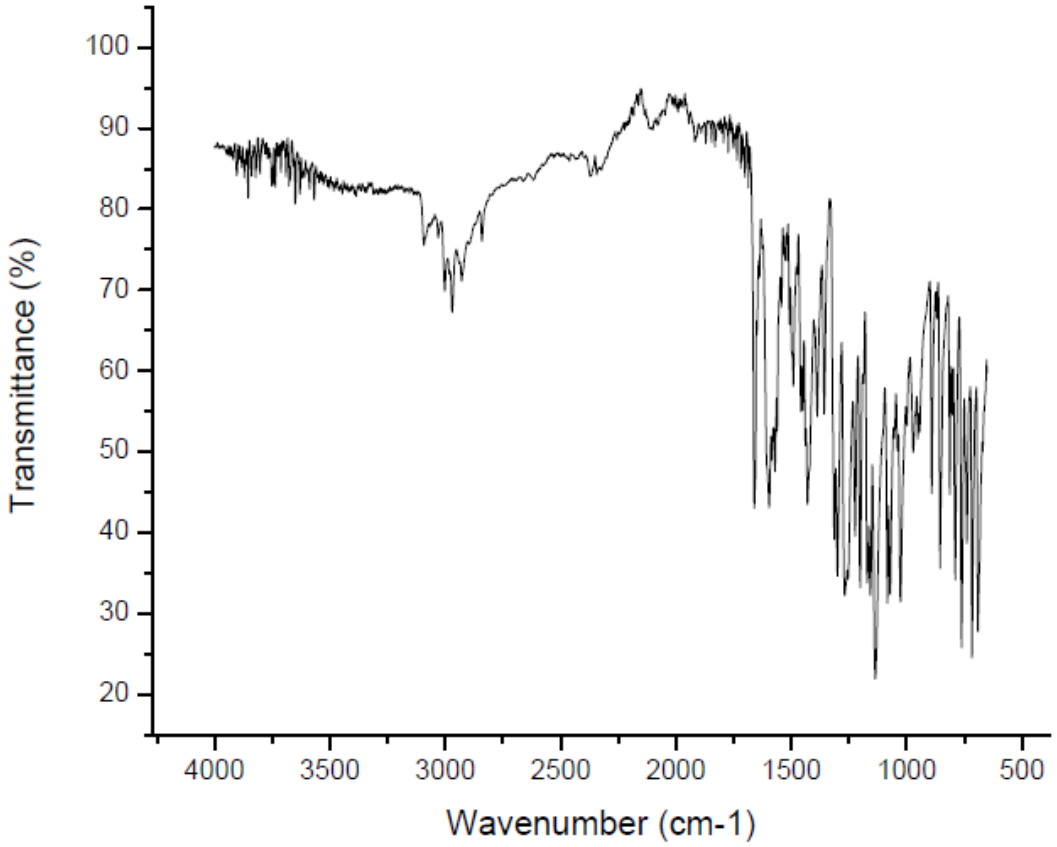

Figure A24. ESI (+) FT-ICR MS Spectra of compound **44b**.

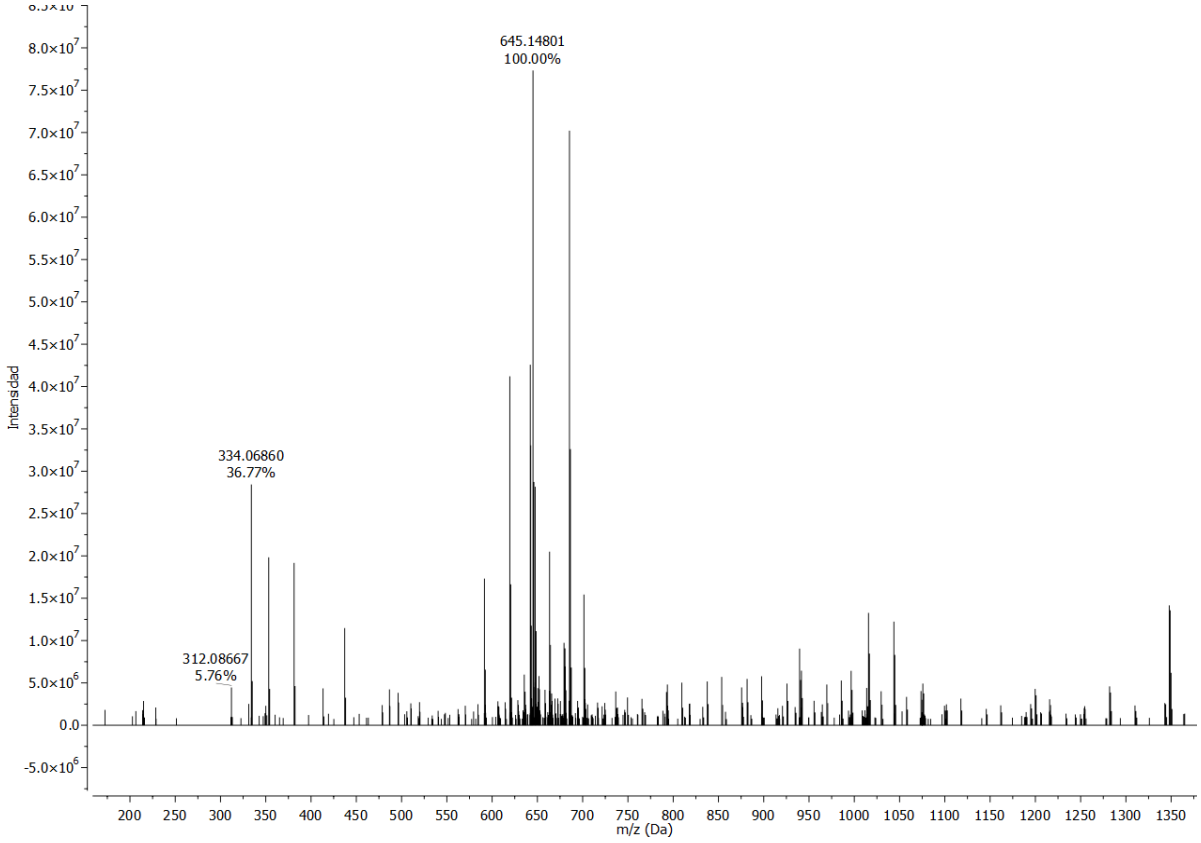

Table A3. X-ray data collection and refinement parameters for **44b**.

Compound 44b	
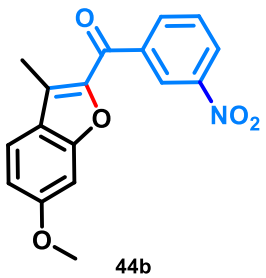 **44b** **Chemical Formula:** $C_{17}H_{13}NO_5$	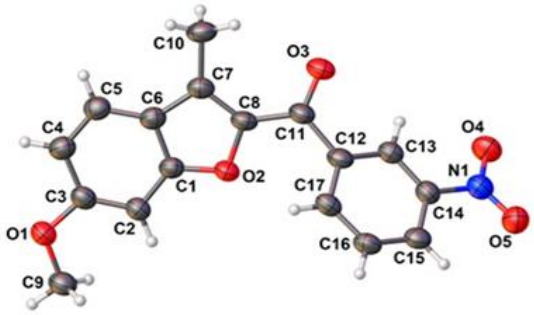
Chemical formula	$C_{17}H_{13}NO_5$
M (g mol^{-1})	311.28
Radiation	Cu Kα
Crystal system	Orthorhombic
Space group	*Pca2$_1$*
a (Å)	32.4730(30)
b (Å)	3.8109(4)
c (Å)	11.5390(7)
α (º)	90
β (º)	90
γ (º)	90
V (Å^3)	1428.00(20)
Z	4
Density /g cm^{-3}	1.448
θ_{min} /º	9.402
θ_{max} /º	140.112
μ /mm^{-1}	0.905
Absorption correction	Gaussian
Max./min. transmission	1.000/0.603
Measured reflections	21044
Independent reflections / Rint	2672/0.1193
Refined parameters	210
R_1	0.0543
wR_2	0.1205
GooF	1.109
Largest diff. peak and hole (eÅ^{-3})	0.21/-0.26

Figure A25. ^{1}H NMR spectrum of compound **44c** (400 MHz, $CDCl_3$).

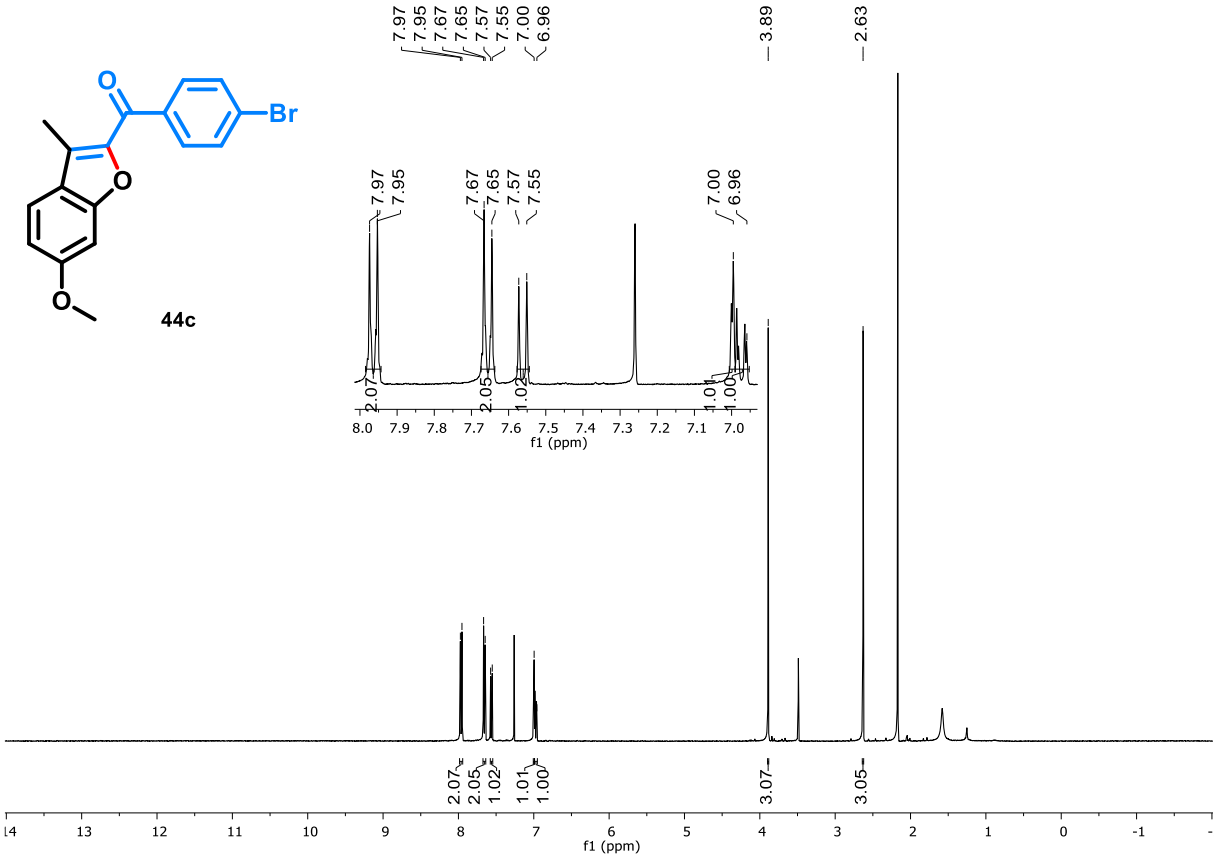

Figure A26. ^{13}C NMR spectrum of compound **44c** (100 MHz, $CDCl_3$).

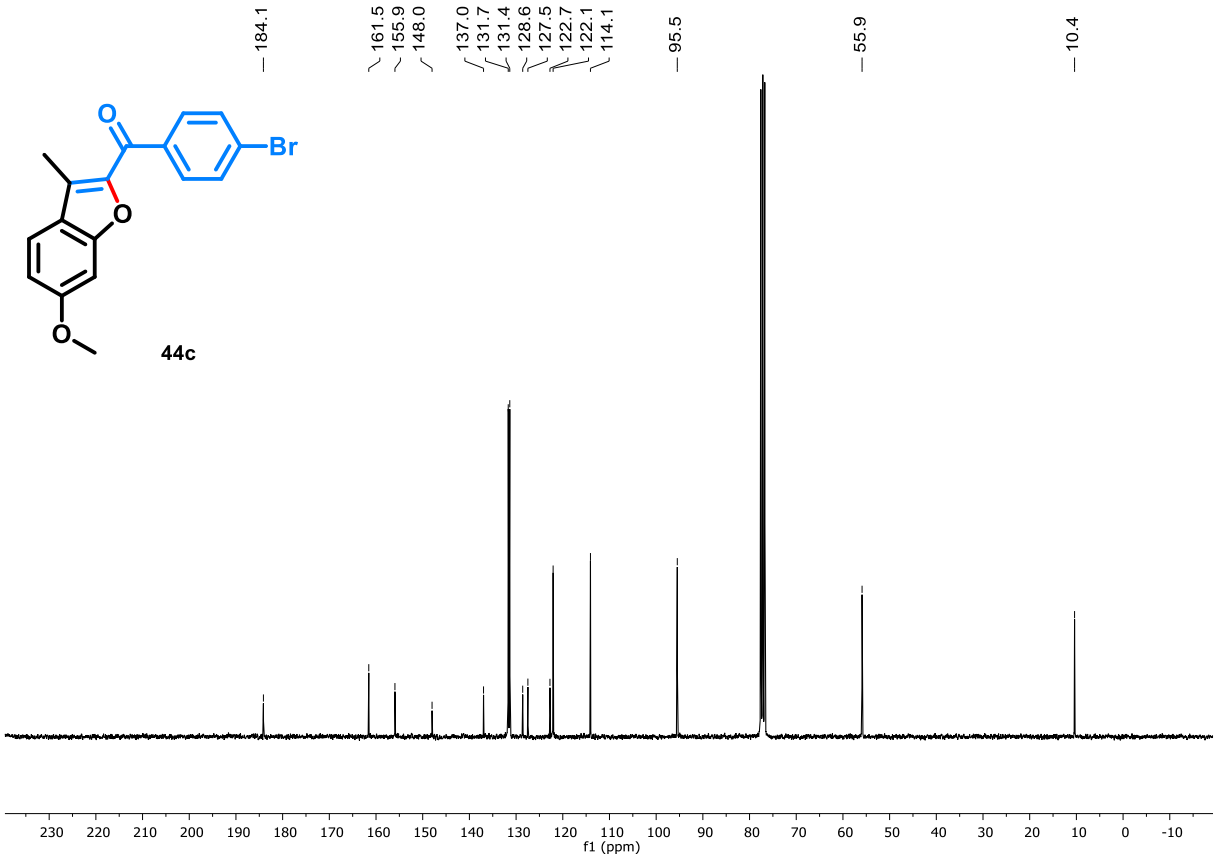

Figure A27. FT-IR (Attenuated total reflection – ATR) $_{vmax}$ / cm^{-1} of compound **44c**.

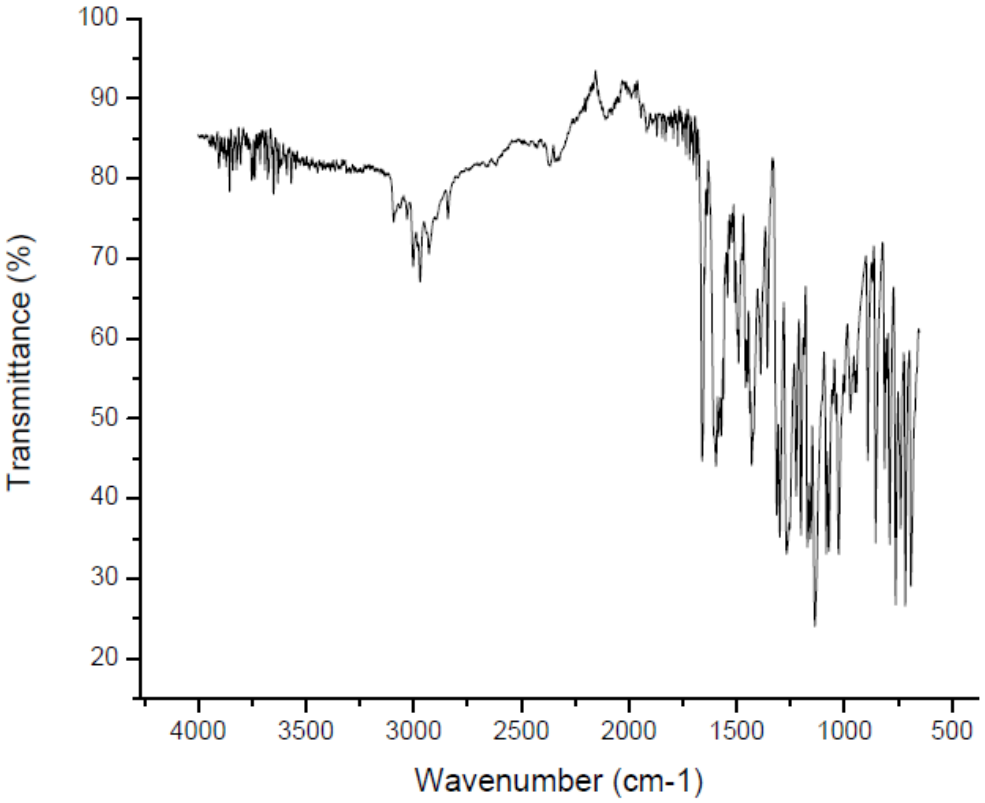

Figure A28. ESI (+) FT-ICR MS Spectra of compound **44c**.

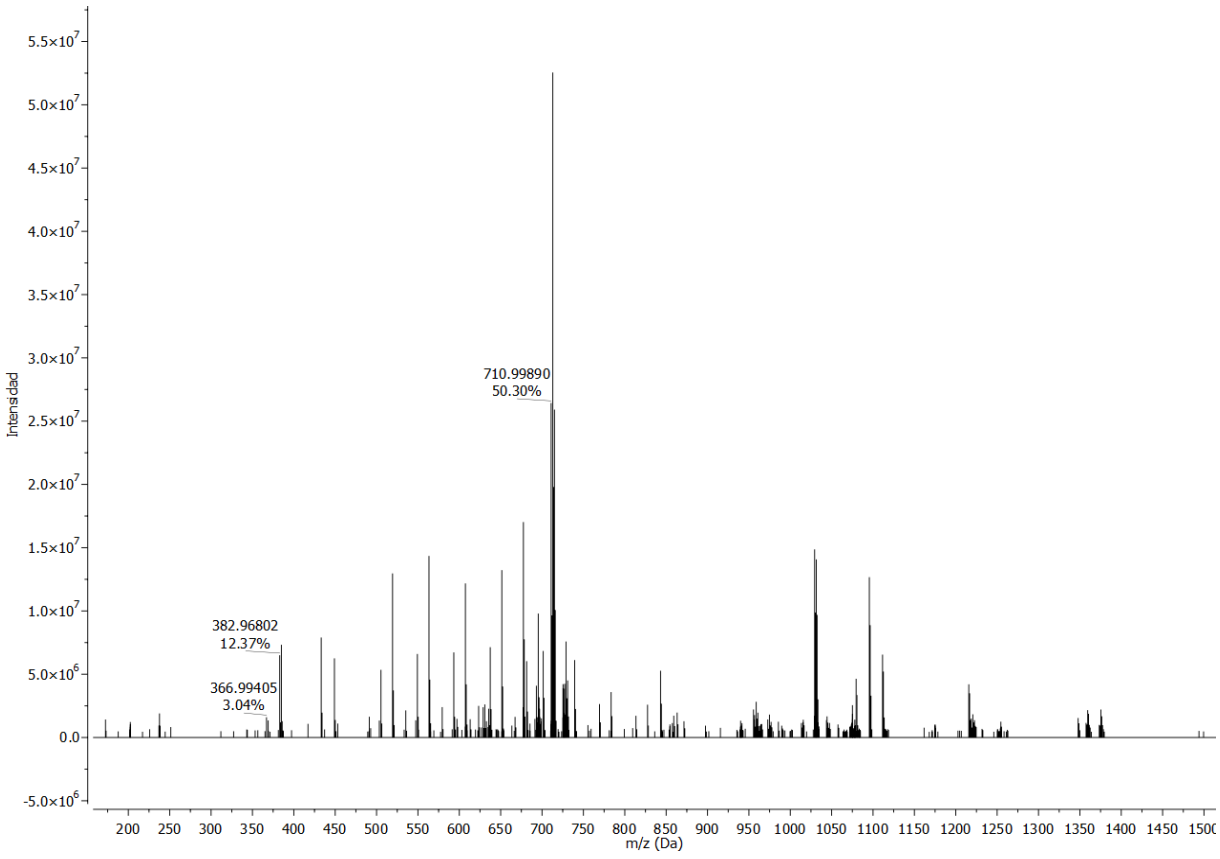

Table A4. X-ray data collection and refinement parameters for **44c**.

Compound 44c 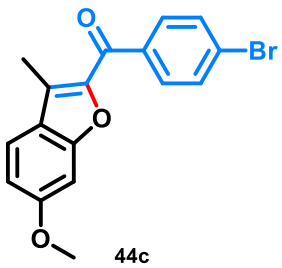 **44c** **Chemical Formula:** $C_{17}H_{13}BrO_3$	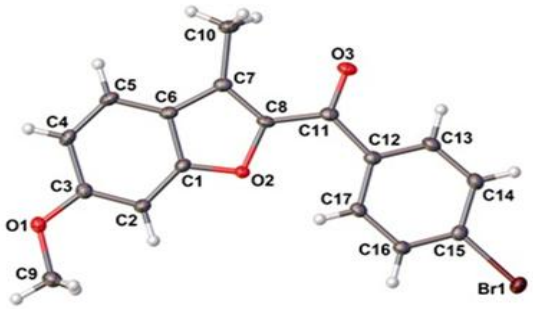
Chemical formula	$C_{17}H_{13}BrO_3$
M (g mol^{-1})	345.18
Radiation	Cu Kα
Crystal system	Orthorhombic
Space group	*Pbca*
a (Å)	7.5455(1)
b (Å)	13.8244(1)
c (Å)	26.8962(2)
α (º)	90
β (º)	90
γ (º)	90
V (Å^3)	2805.61(3)
Z	8
Density /g cm^{-3}	1.634
θ_{min} /º	12.808
θ_{max} /º	140.106
μ /mm^{-1}	4.063
Absorption correction	Multi-scan
Max./min. transmission	1.000/0.380
Measured reflections	34593
Independent reflections / Rint	2653/0.0729
Refined parameters	192
R_1	0.0300
wR_2	0.0808
GooF	1.082
Largest diff. peak and hole (eÅ^{-3})	0.59/-0.71

Figure A29. ^{1}H NMR spectrum of compound **44d** (400 MHz, $CDCl_3$).

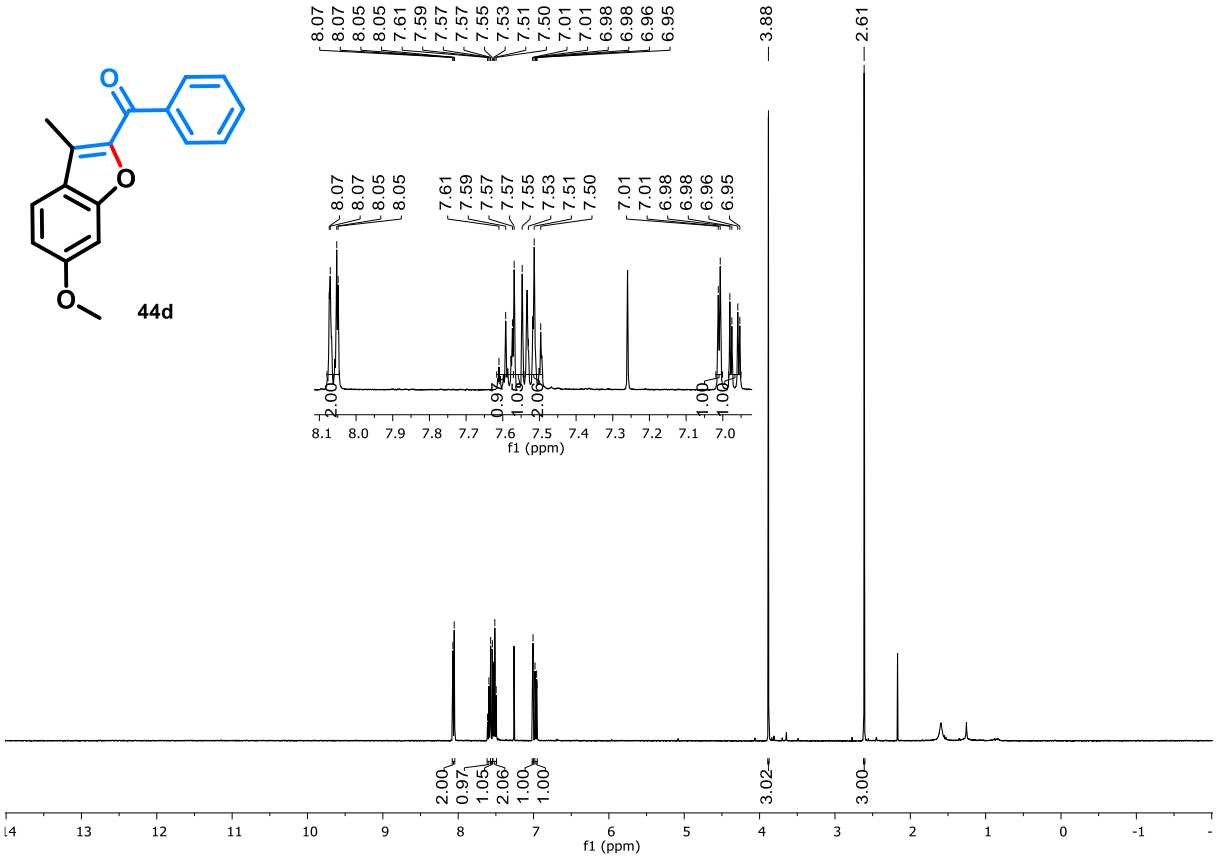

Figure A30. ^{13}C NMR spectrum of compound **44d** (100 MHz, $CDCl_3$).

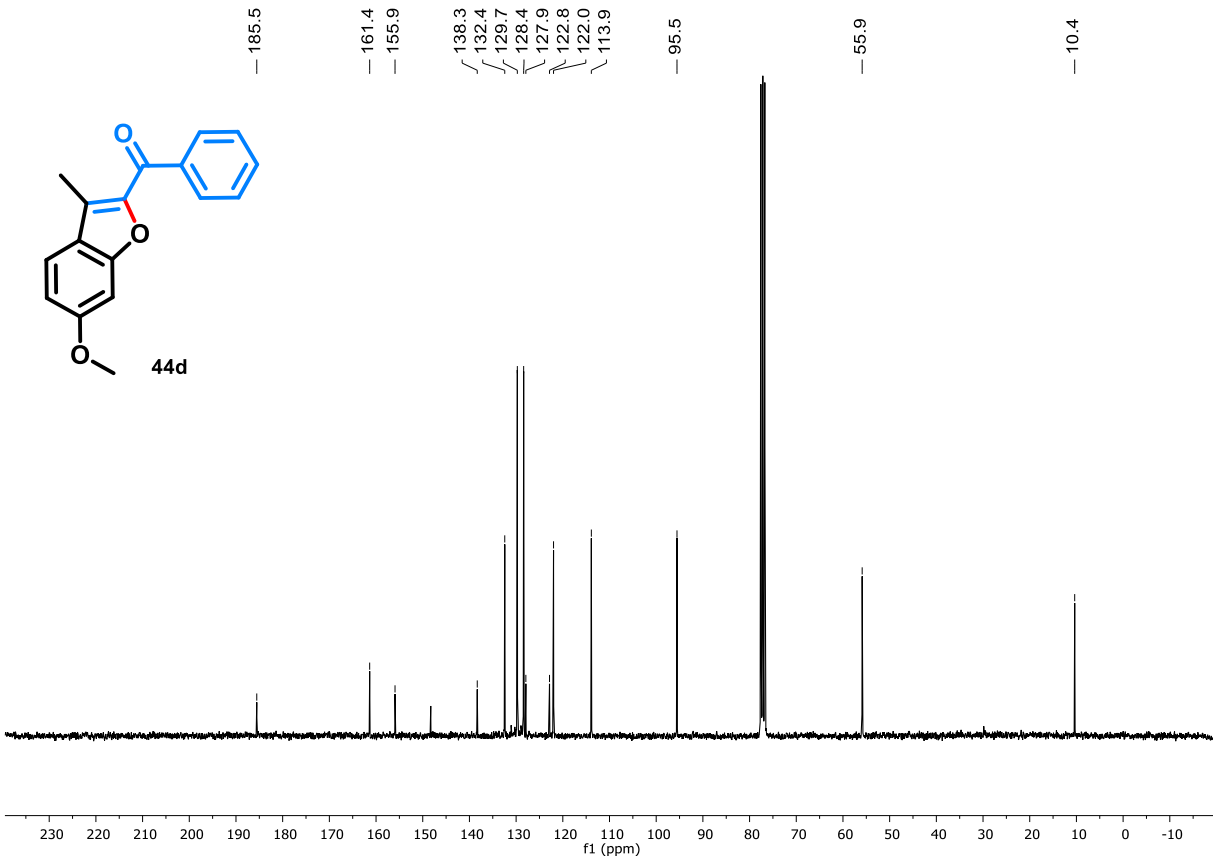

Figure A31. FT-IR (Attenuated total reflection – ATR) $_{vmax}$ / cm^{-1} of compound **44d**.

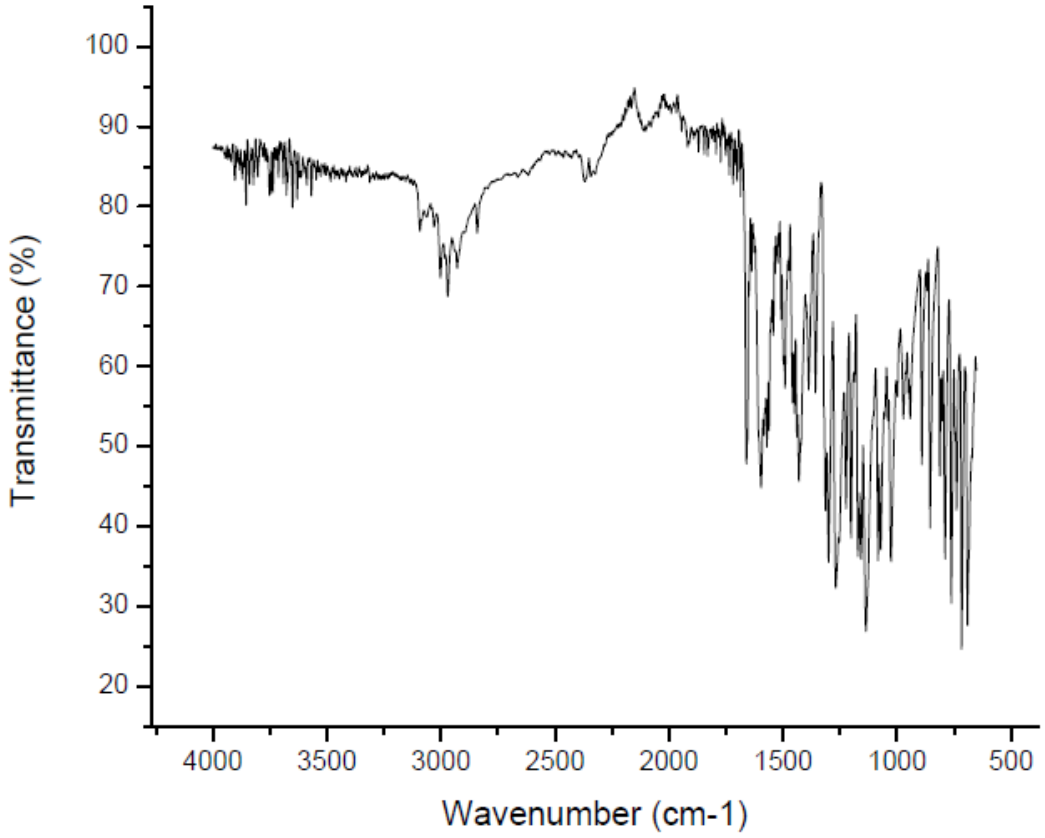

Figure A32. ESI (+) FT-ICR MS Spectra of compound **44d**.

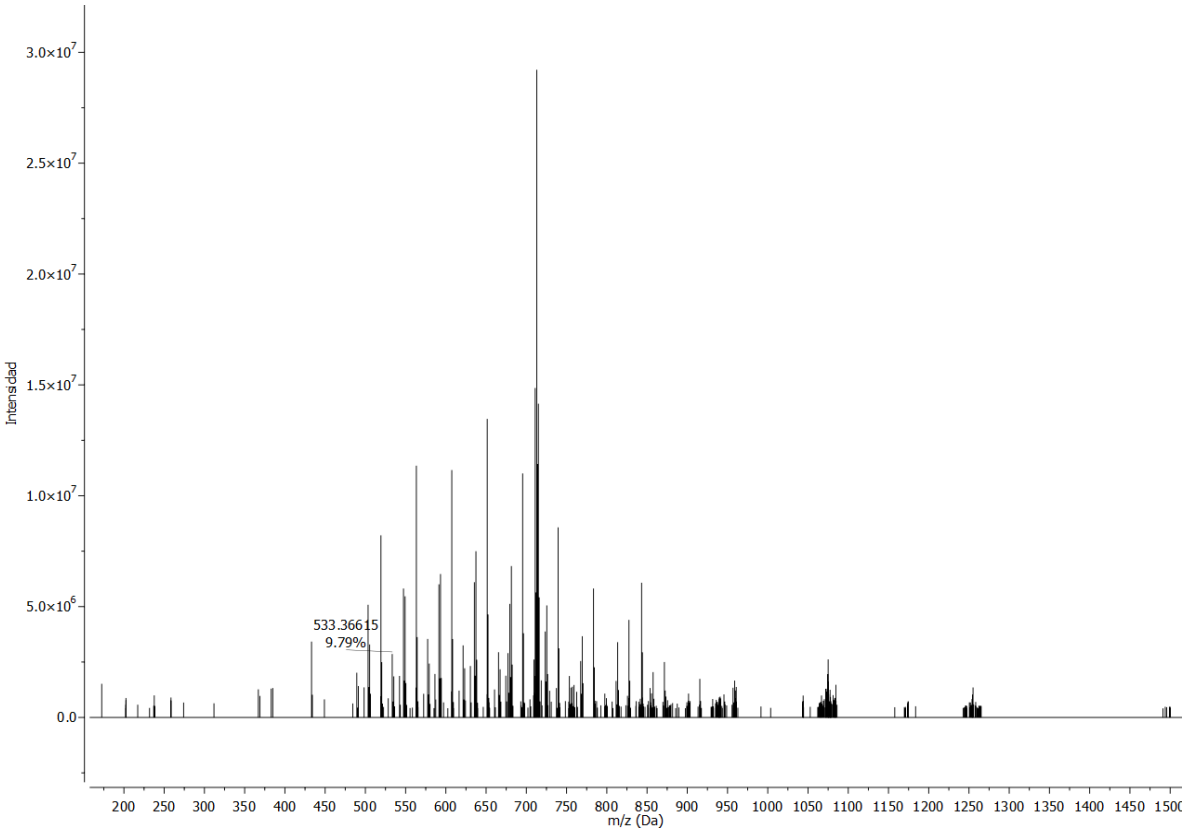

Figure A33. ^{1}H NMR spectrum of compound **44e** (400 MHz, $CDCl_3$).

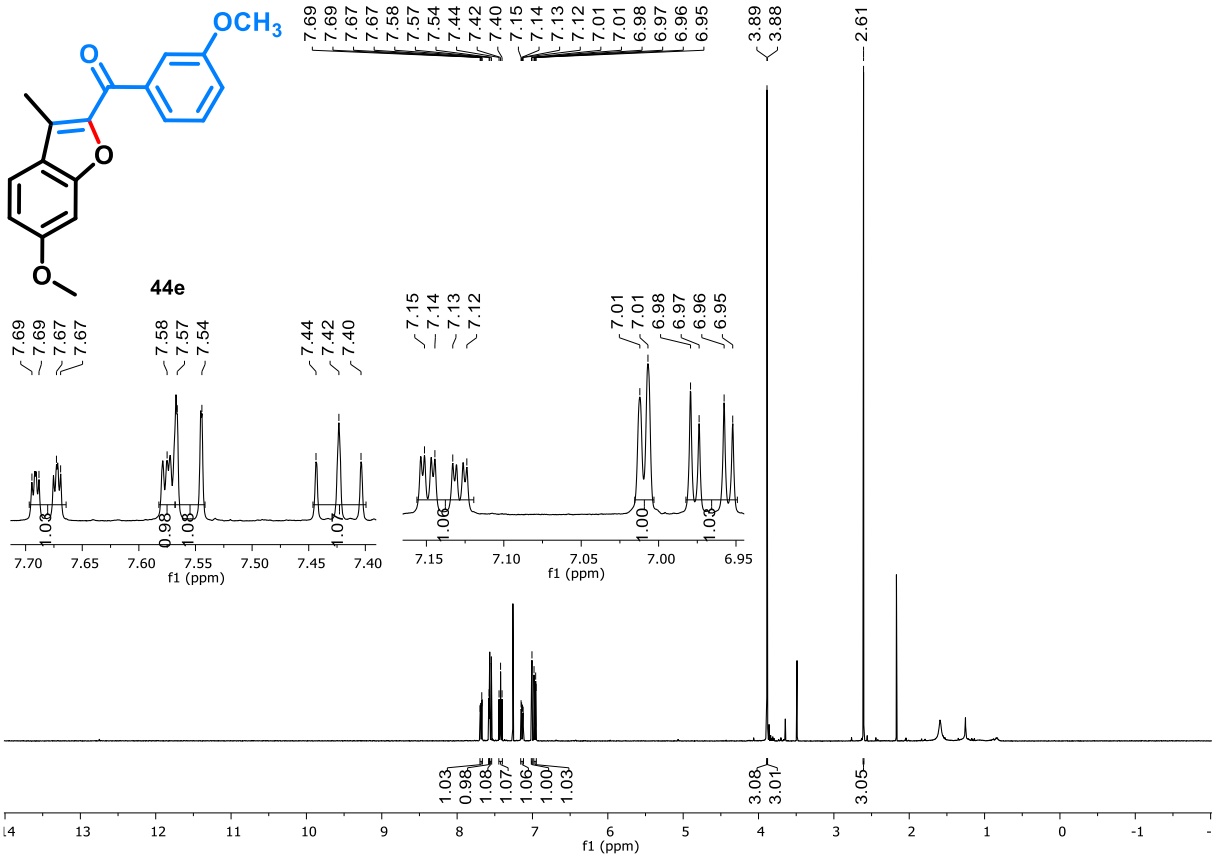

Figure A34. ^{13}C NMR spectrum of compound **44e** (100 MHz, $CDCl_3$).

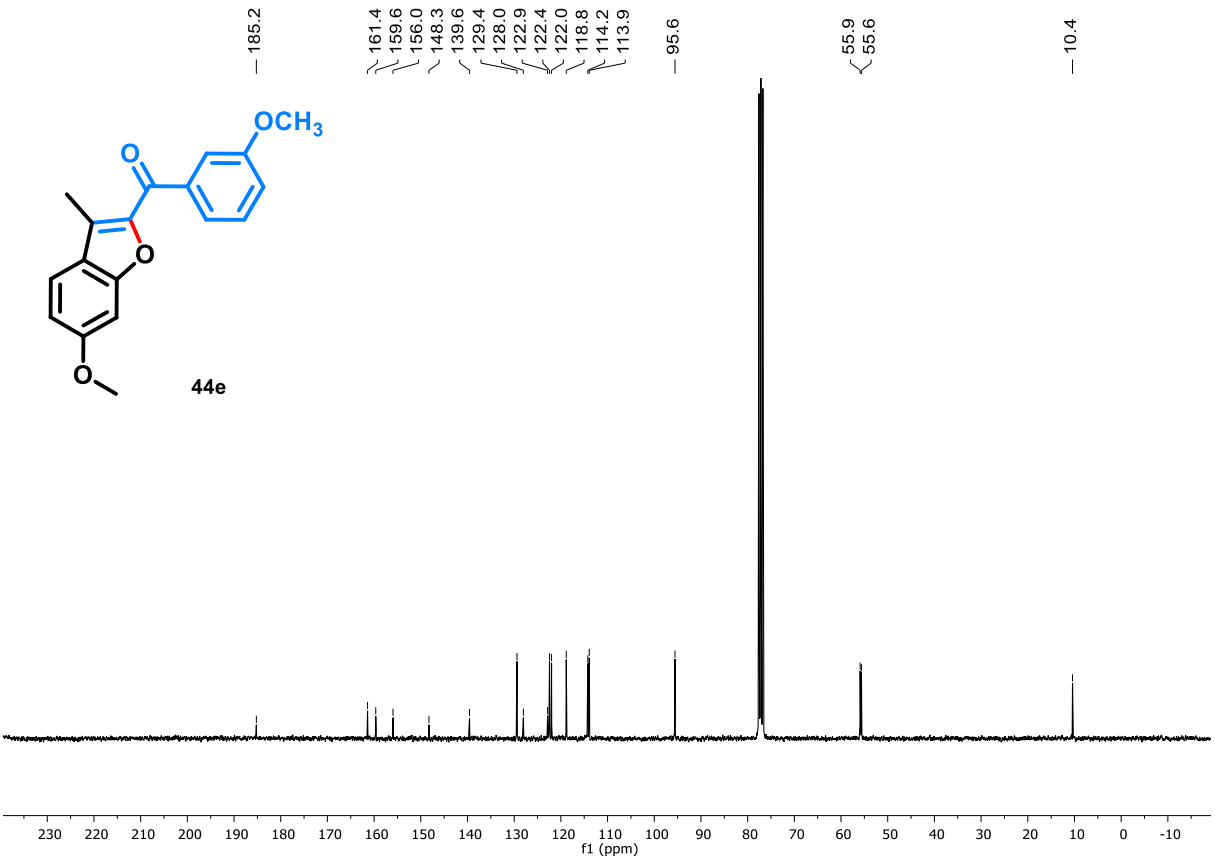

Figure A35. FT-IR (Attenuated total reflection – ATR) $_{vmax}$ / cm^{-1} of compound **44e**.

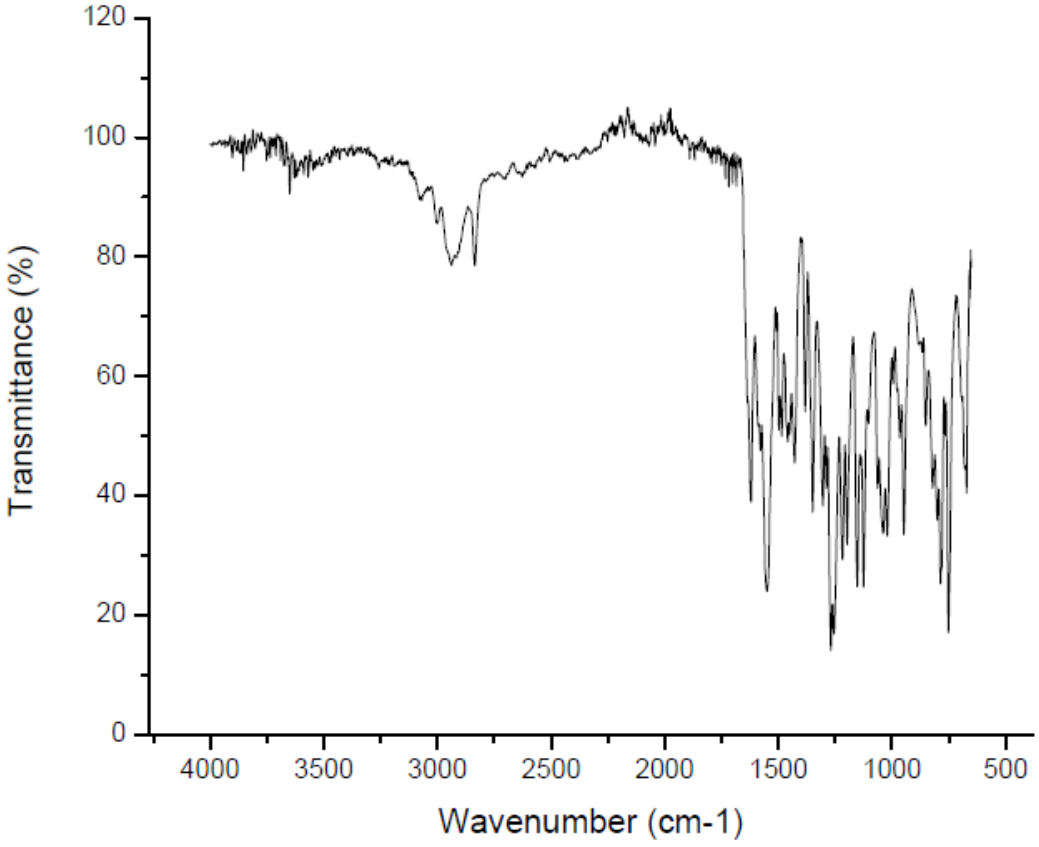

Figure A36. ESI (+) FT-ICR MS Spectra of compound **44e**.

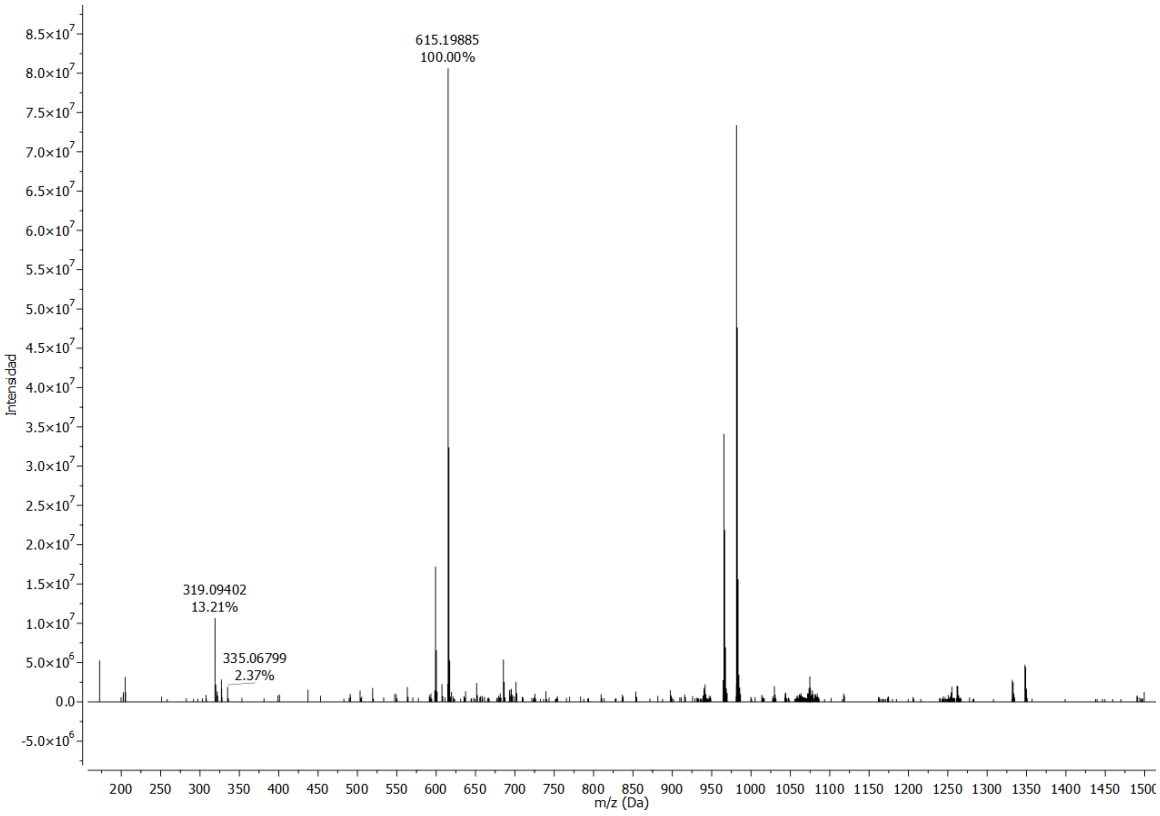

Figure A37. ^{1}H NMR spectrum of compound **44f** (400 MHz, $CDCl_3$).

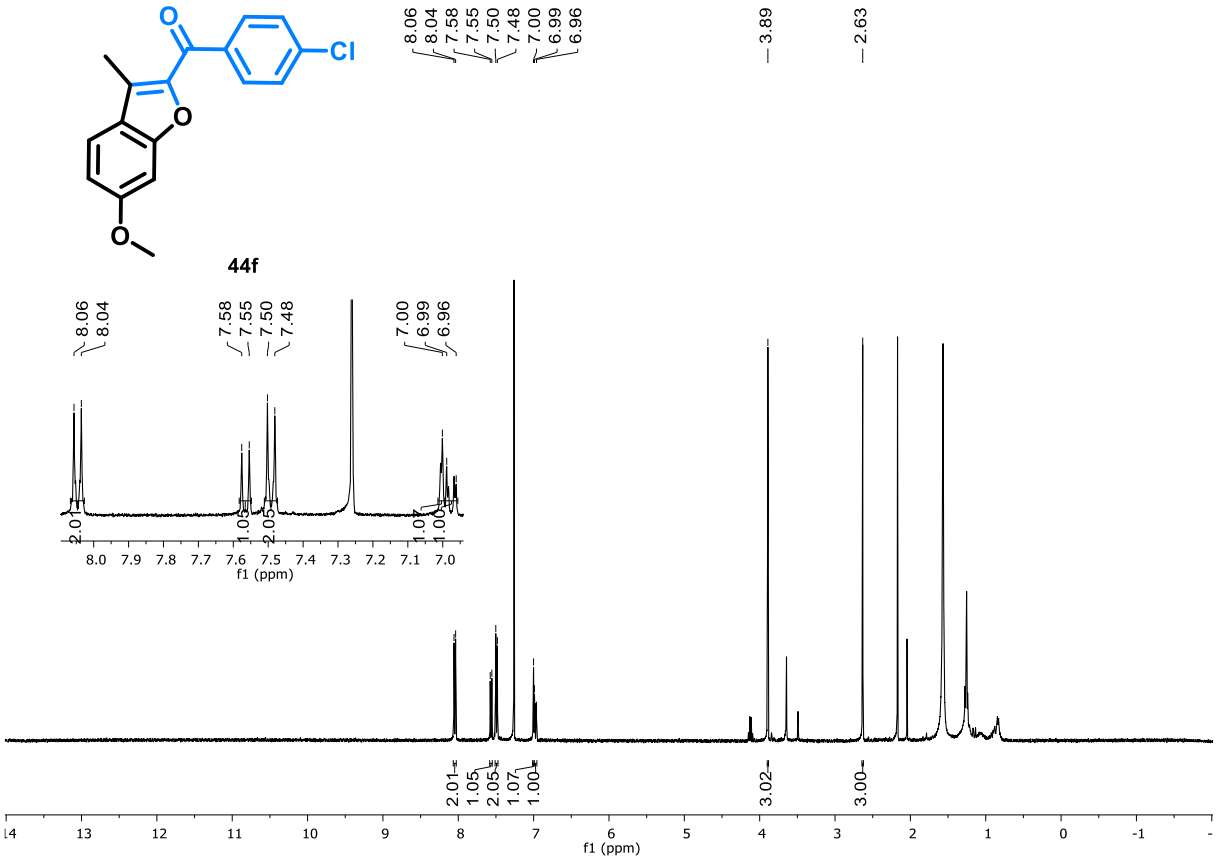

Figure A38. ^{13}C NMR spectrum of compound **44f** (100 MHz, $CDCl_3$).

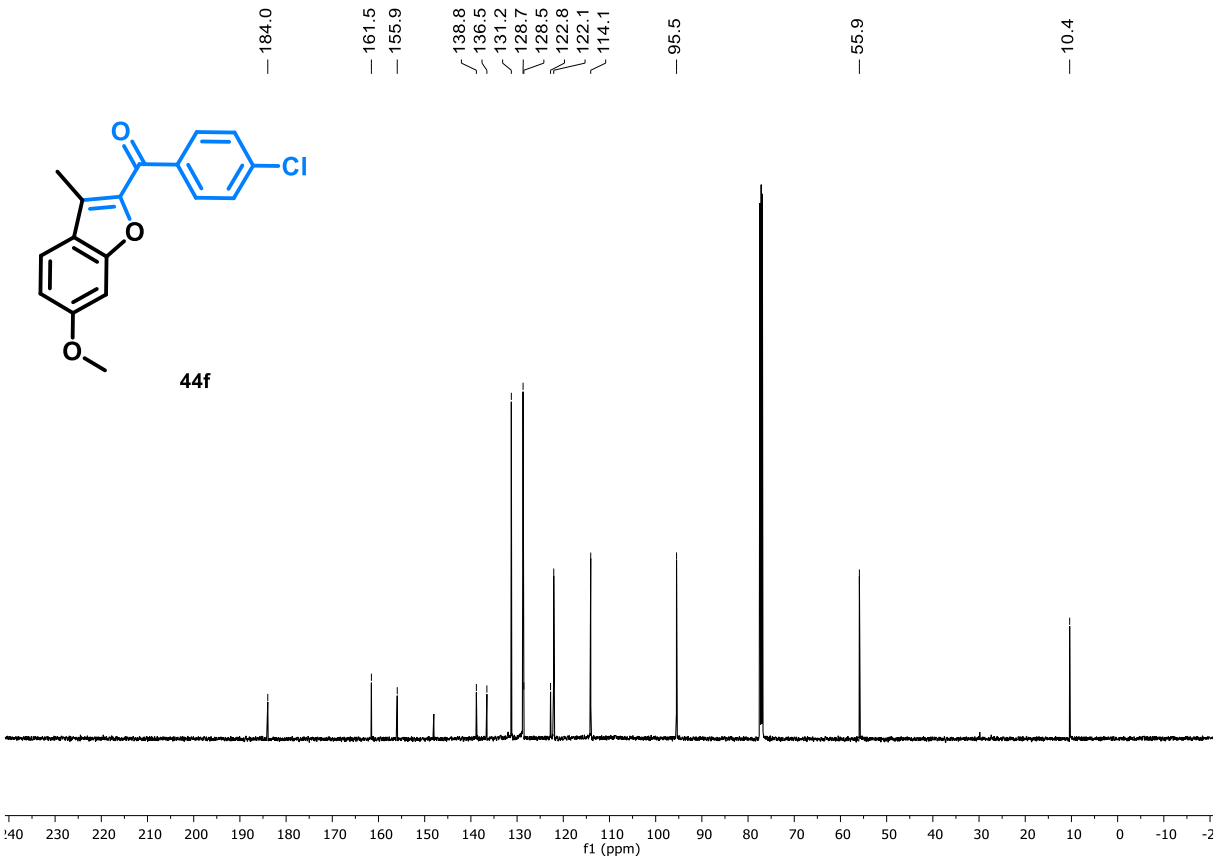

Figure A39. FT-IR (Attenuated total reflection – ATR) ν_{max} / cm^{-1} of compound **44f.**

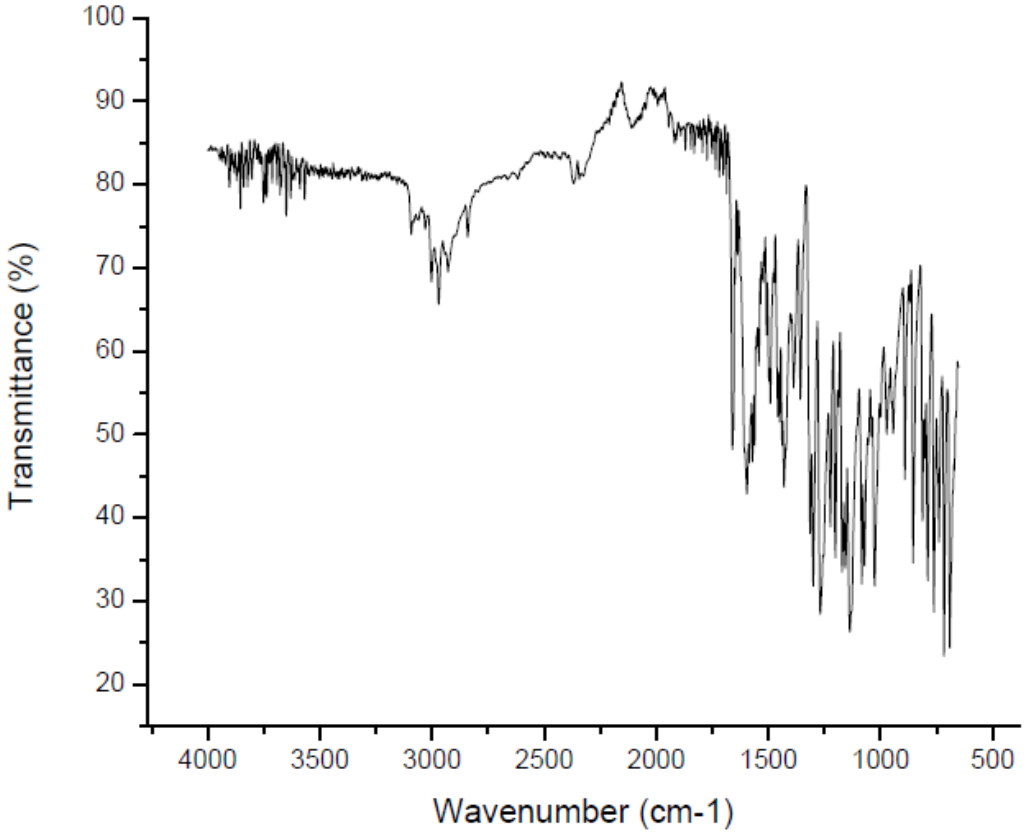

Figure A40. ESI (+) FT-ICR MS Spectra of compound **44f**.

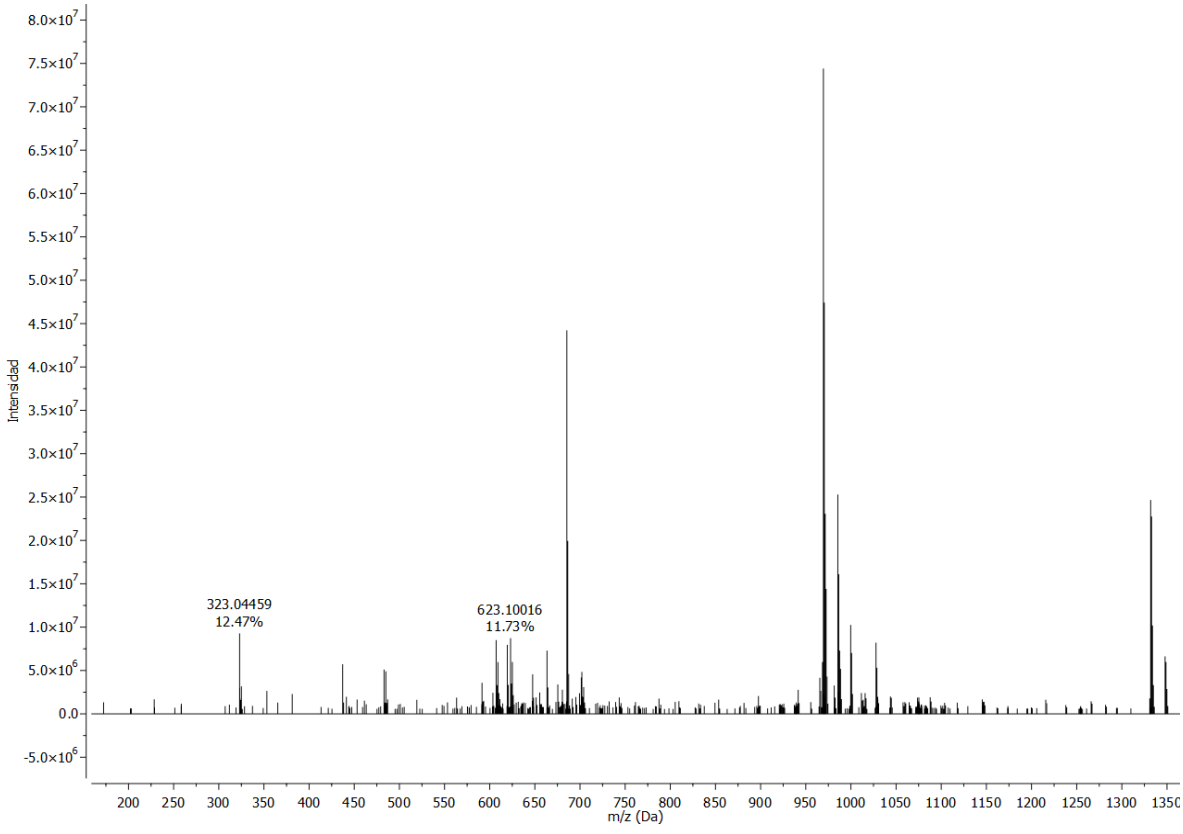

Table A5. X-ray data collection and refinement parameters for **44f**.

Compound 44f **Chemical Formula:** $C_{17}H_{13}ClO_3$ 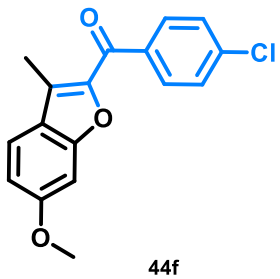 **44f**	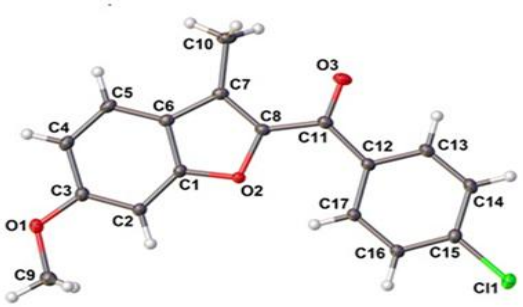
Chemical formula	$C_{17}H_{13}ClO_3$
M (g mol^{-1})	300.72
Radiation	Mo Kα
Crystal system	Monoclinic
Space group	*P2$_1$/c*
a (Å)	7.8256(3)
b (Å)	26.4325(6)
c (Å)	7.5205(3)
α (º)	90
β (º)	118.6720(50)
γ (º)	90
V (Å^3)	1364.87(10)
Z	4
Density /g cm^{-3}	1.463
θ_{min} /º	5.934
θ_{max} /º	67.84
μ /mm^{-1}	0.287
Absorption correction	Multi-scan
Max./min. transmission	1.000/0.968
Measured reflections	22525
Independent reflections / Rint	4749/0.0299
Refined parameters	193
R_1	0.0338
wR_2	0.0921
GooF	1.045
Largest diff. peak and hole (eÅ^{-3})	0.47/-0.24

Figure A41. ^{1}H NMR spectrum of compound **44g** (400 MHz, $CDCl_3$).

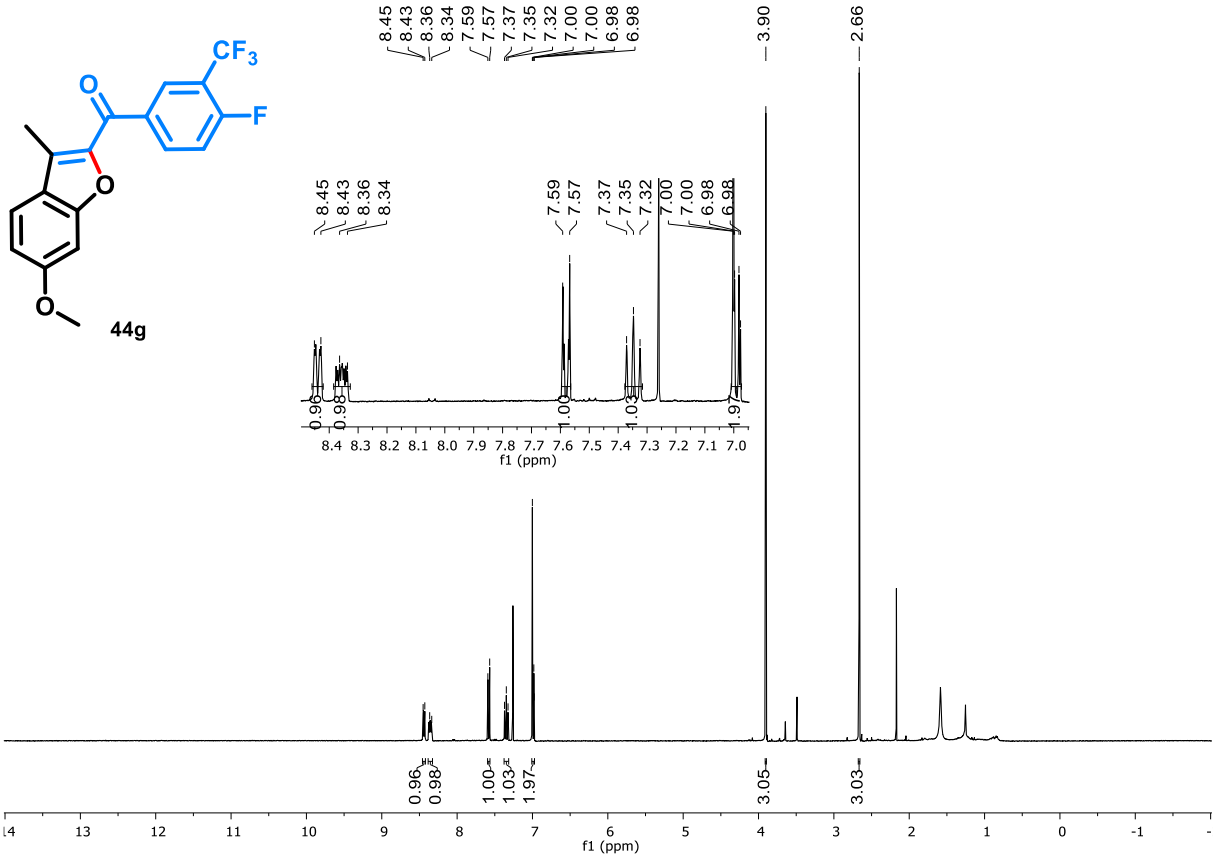

Figure A42. ^{13}C NMR spectrum of compound **44g** (100 MHz, $CDCl_3$).

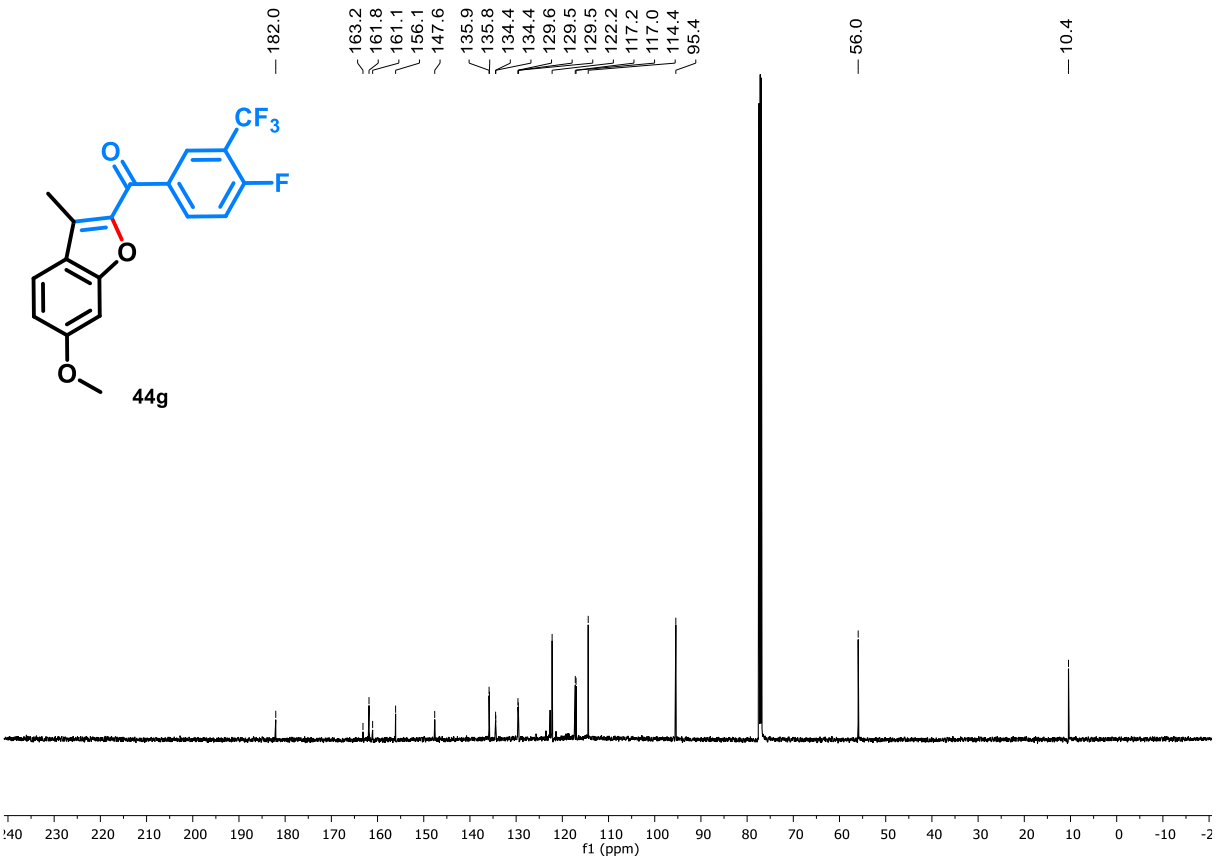

Figure A43. FT-IR (Attenuated total reflection – ATR) $_{vmax}$ / cm^{-1} of compound **44g**.

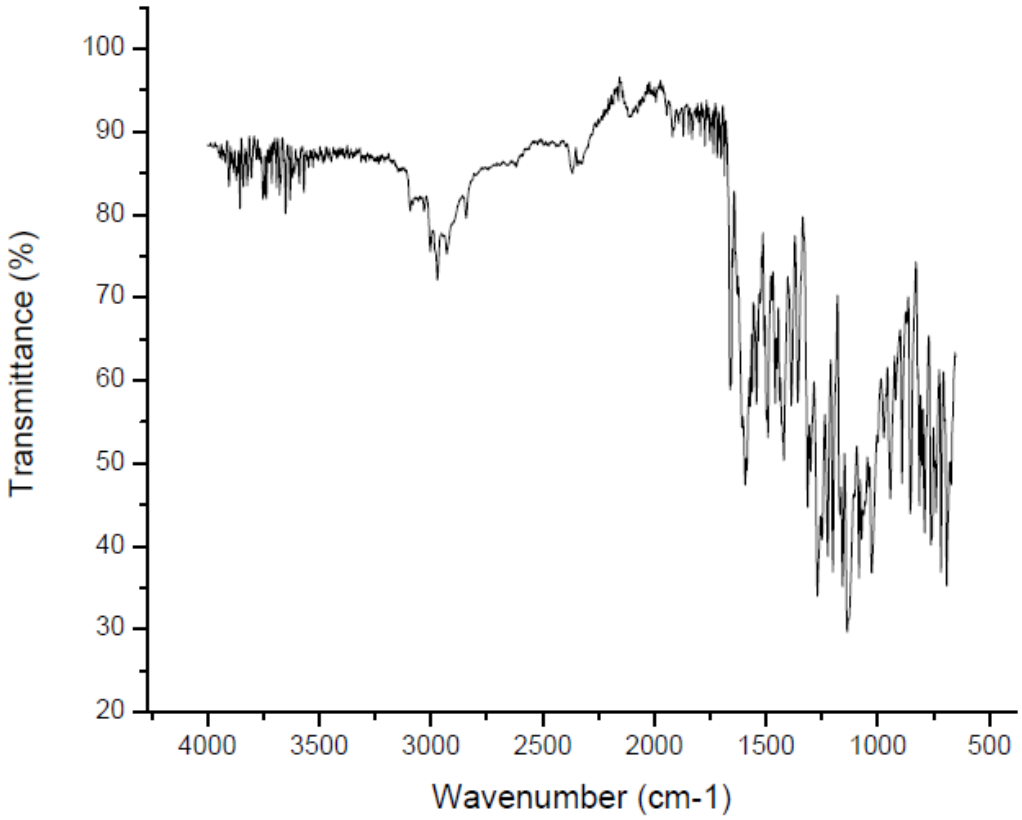

Figure A44. ESI (+) FT-ICR MS Spectra of compound **44g**.

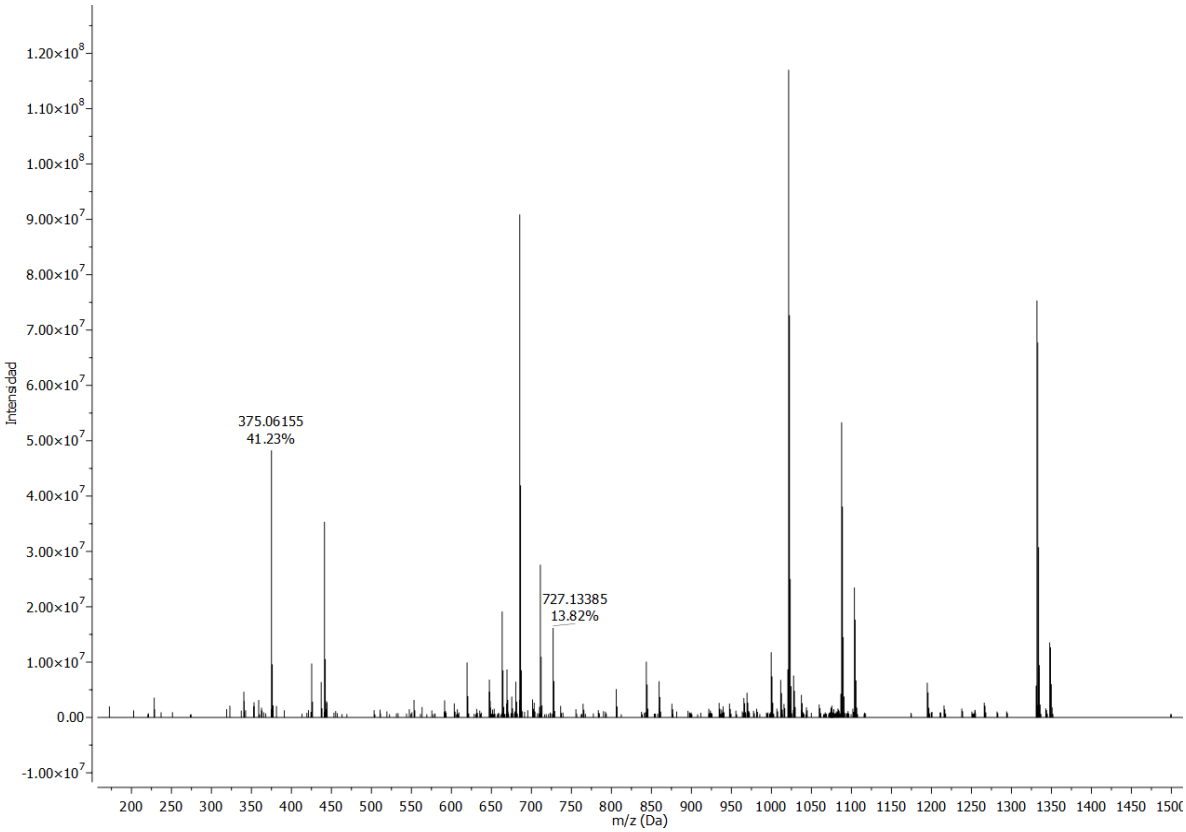

Table A6. X-ray data collection and refinement parameters for **44g**.

Compound 44g	
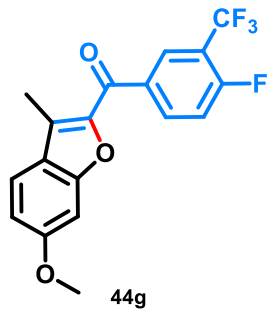 44g **Chemical Formula:** $C_{18}H_{12}F_4O_3$	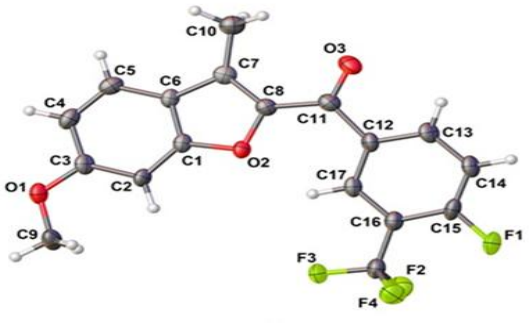
Chemical formula	$C_{18}H_{12}F_4O_3$
M (g mol^{-1})	352.28
Radiation	Mo Kα
Crystal system	Orthorhombic
Space group	*Pca2₁*
a (Å)	33.7881(16)
b (Å)	4.9835(3)
c (Å)	8.8615(4)
α (º)	90
β (º)	90
γ (º)	90
V (Å³)	1492.13(13)
Z	4
Density /g cm^{-3}	1.568
θ_{min} /º	5.19
θ_{max} /º	55.732
μ /mm^{-1}	0.139
Absorption correction	Multi-scan
Max./min. transmission	1.000/0.401
Measured reflections	19739
Independent reflections / Rint	3492/0.0967
Refined parameters	228
R_1	0.0710
wR_2	0.1423
GooF	1.091
Largest diff. peak and hole (e$Å^{-3}$)	0.35/-0.25

Table A7. Non-classical hydrogen bonds parameters for 43a, 44b, 44c, 44f and 44g.

Compound	D–H···A	d(D–H)/Å	d(H–A)/Å	d(D–A)/Å	D–H···A/º
43a	C10–H10···O5[1]	0.99	2.60	3.321(3)	130.0
	C15–H15···O1[2]	0.95	2.54	3.434(3)	157.4
	C13–H13···O3[3]	0.95	2.57	3.477(3)	160.4
	C9–H9c···O4[4]	0.98	2.57	3.210(4)	123.0
44b	C15–H15···O3[5]	0.95	2.57	3.183(7)	122.7
44c	C17–H17···O2	0.95	2.18	2.853(2)	126.7
	C16–H16···O3[6]	0.95	2.35	3.302(2)	157.7
	C14–H14···O1[7]	0.95	2.54	3.439(2)	157.7
44f	C17–H17···O2	0.95	2.19	2.868(1)	127.3
	C16–H16···O3[8]	0.95	2.39	3.319(1)	166.1
	C14–H14···O1[9]	0.95	2.56	3.470(1)	159.9
44g	C17–H17···O2	0.95	2.10	2.785(6)	127.5
	C9–H9a···F1[10]	0.98	2.44	3.289(7)	144.1
	C5–H5···O3[11]	0.95	2.44	3.383(7)	171.2
	C14–H14···O1[12]	0.95	2.56	3.434(7)	152.2

Figure A45. Two-dimensional arrangement formed in **43a** with the hydrogen bonds, viewed in the *ab* plane.

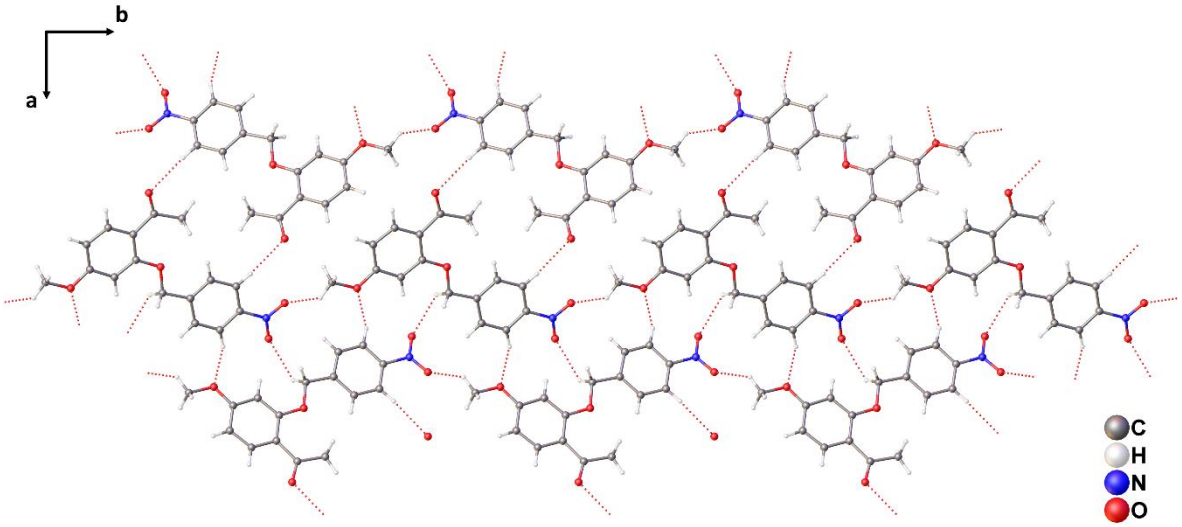

Figure A46. Column-like structure obtained for **43a** with the π···π stacking interactions along the *c* axis.

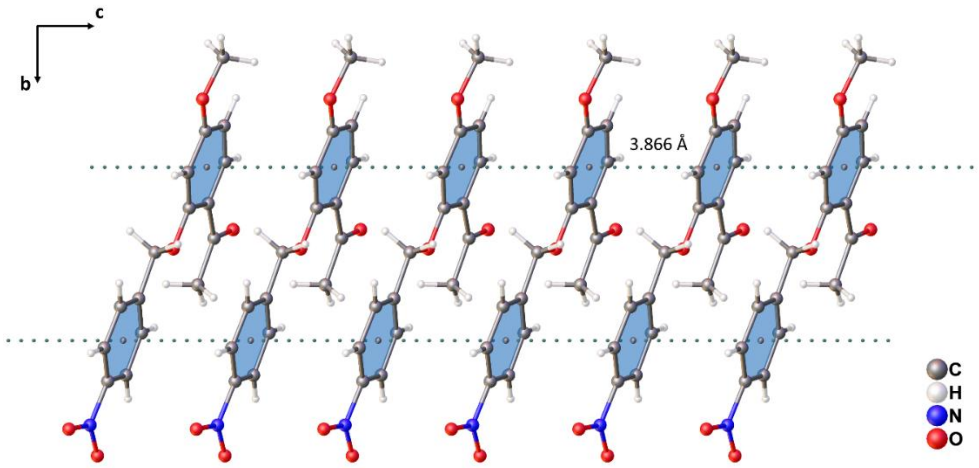

Figure A47. One-dimensional chain formed in **44b** with the hydrogen bonds along the *c* axis.

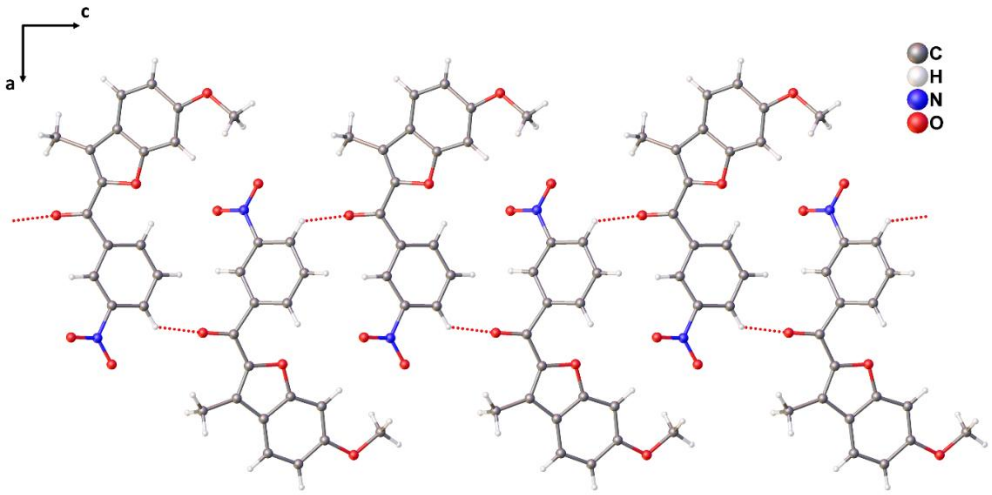

Figure A48. Column-like structure obtained for **44b** with the π···π stacking interactions along the *b* axis.

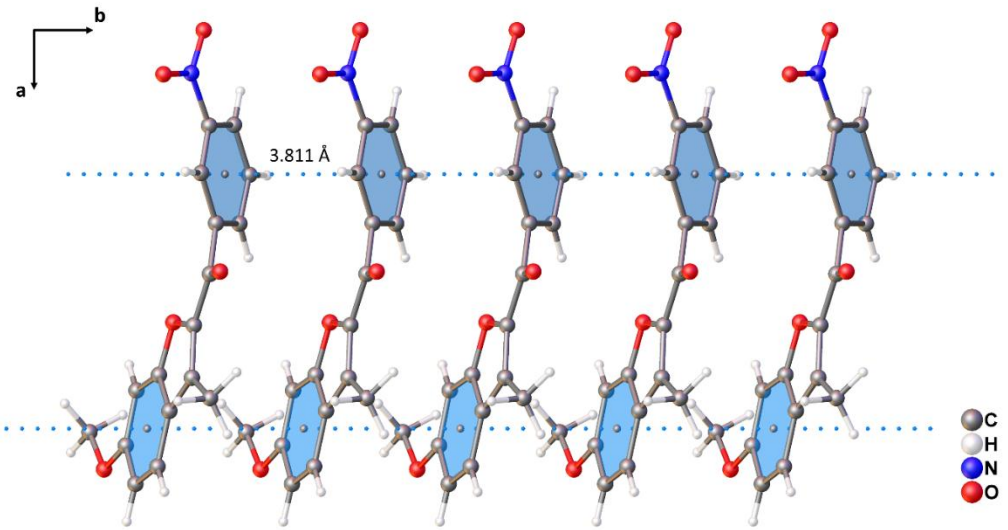

Figure A49. Two-dimensional arrangement formed in **44c** with the hydrogen bonds along the *bc* plane.

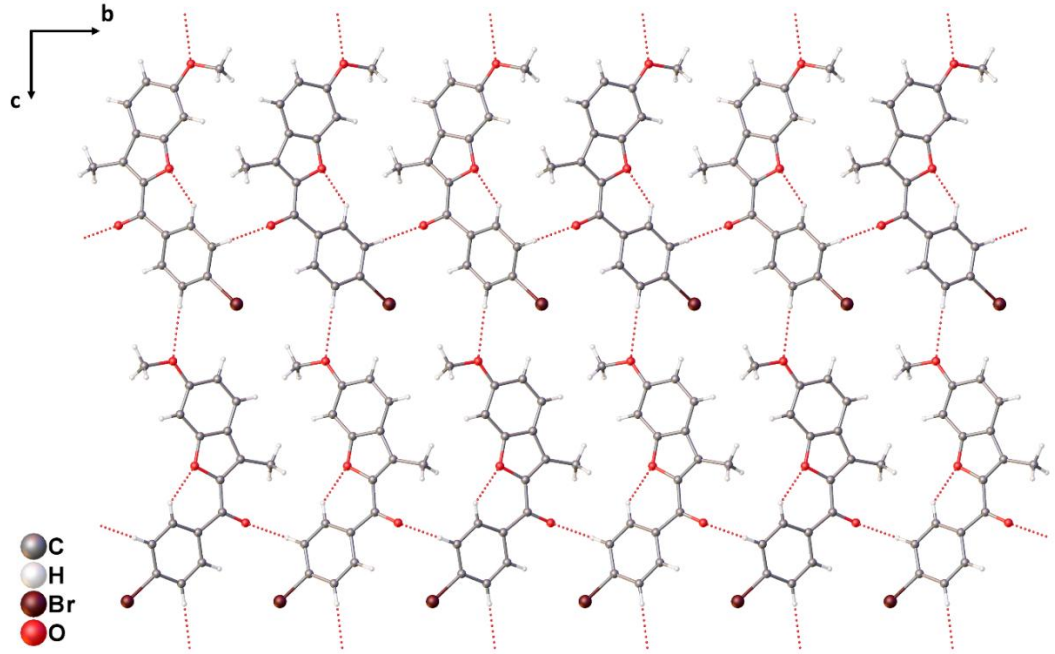

Figure A50. One-dimensional chain formed in 44c with the π···π stacking interactions along the *a* axis.

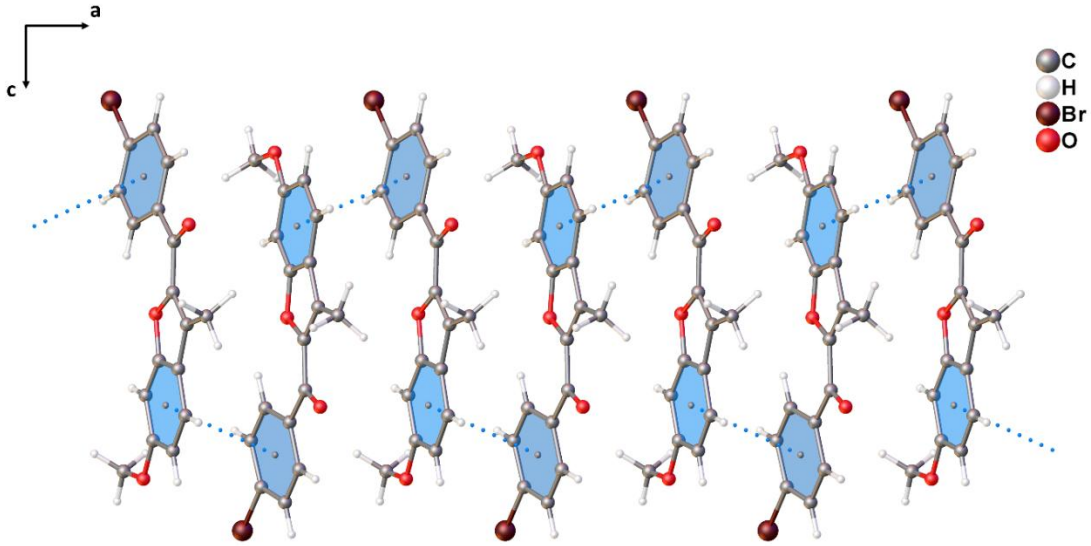

Figure A51. Two-dimensional arrangement formed in **44f** with the hydrogen bonds along the *ab* plane.

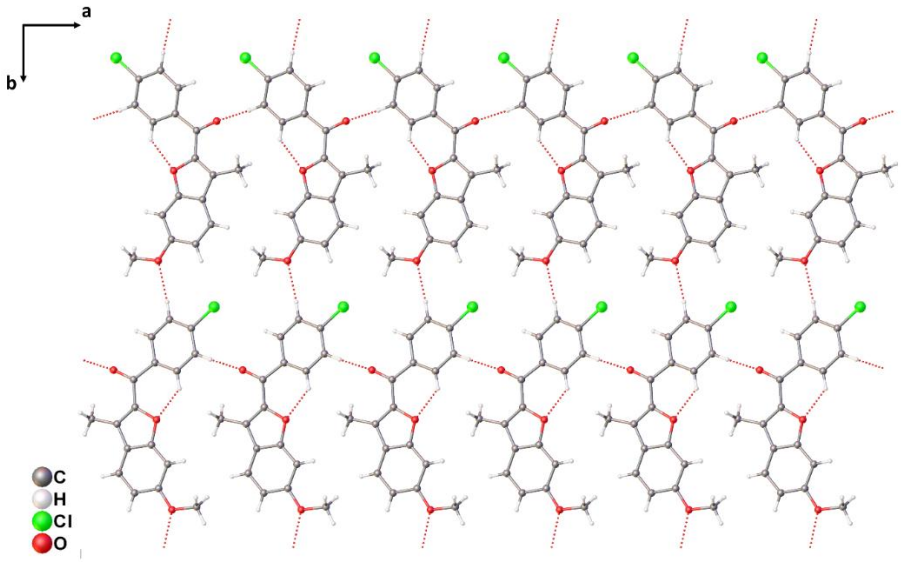

Figure A52. One-dimensional chain formed in 44f with the π···π stacking interactions along the *c* axis.

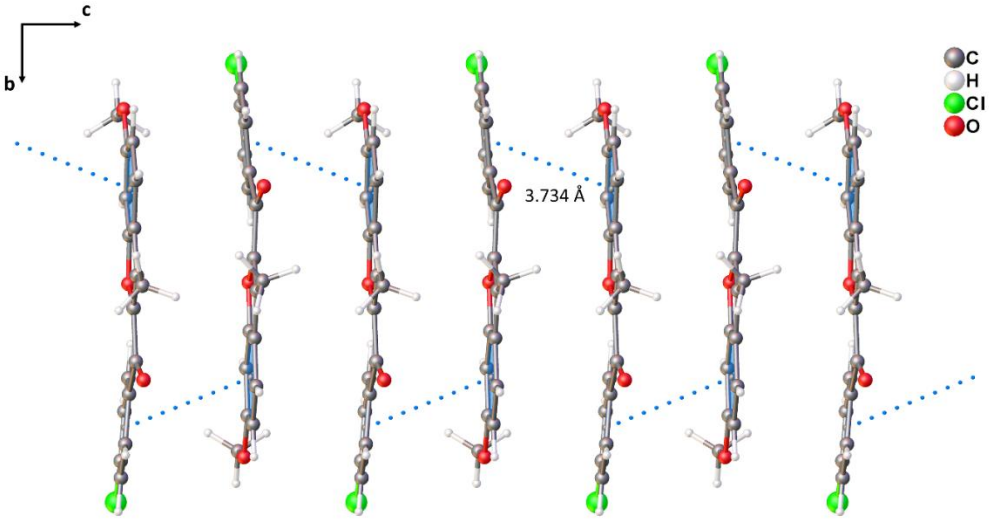

Figure A53. One-dimensional arrangement for **44g** with the hydrogen bonds.

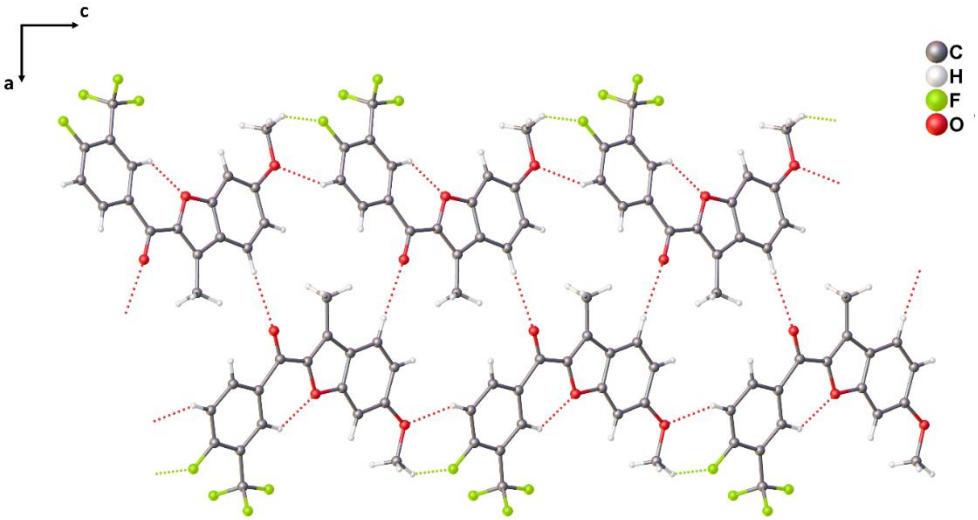

APPENDICES B - Characterization of the compounds Chapter 2

Figure B1. ^{1}H NMR spectrum of compound **140** (500 MHz, $CDCl_3$).

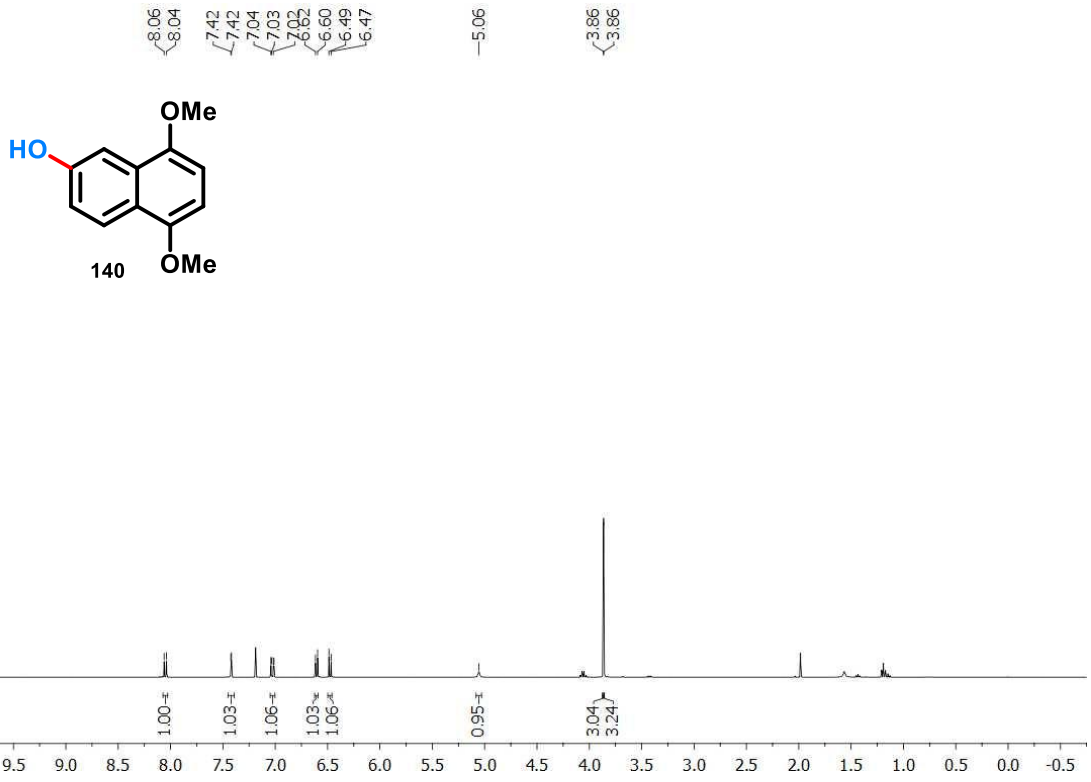

Figure B2. ^{13}C NMR spectrum of compound **140** (125 MHz, $CDCl_3$).

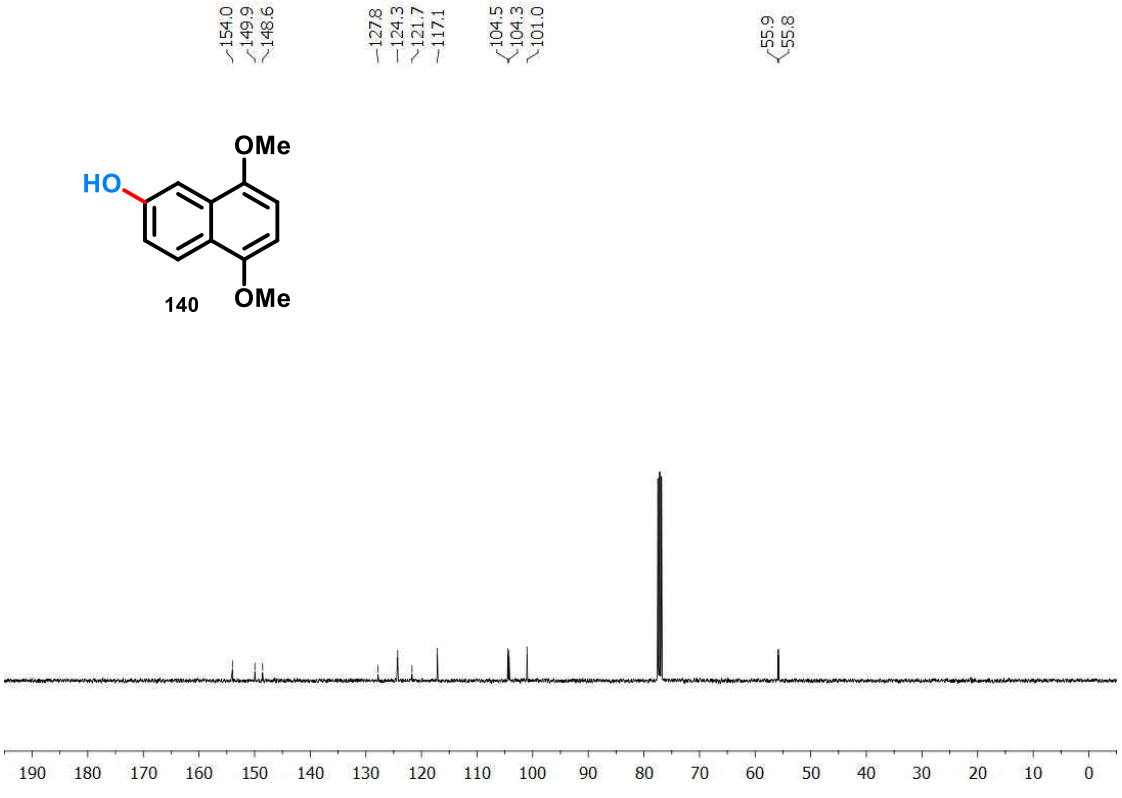

Figure B3. ^{1}H NMR spectrum of compound **141** (500 MHz, $CDCl_3$).

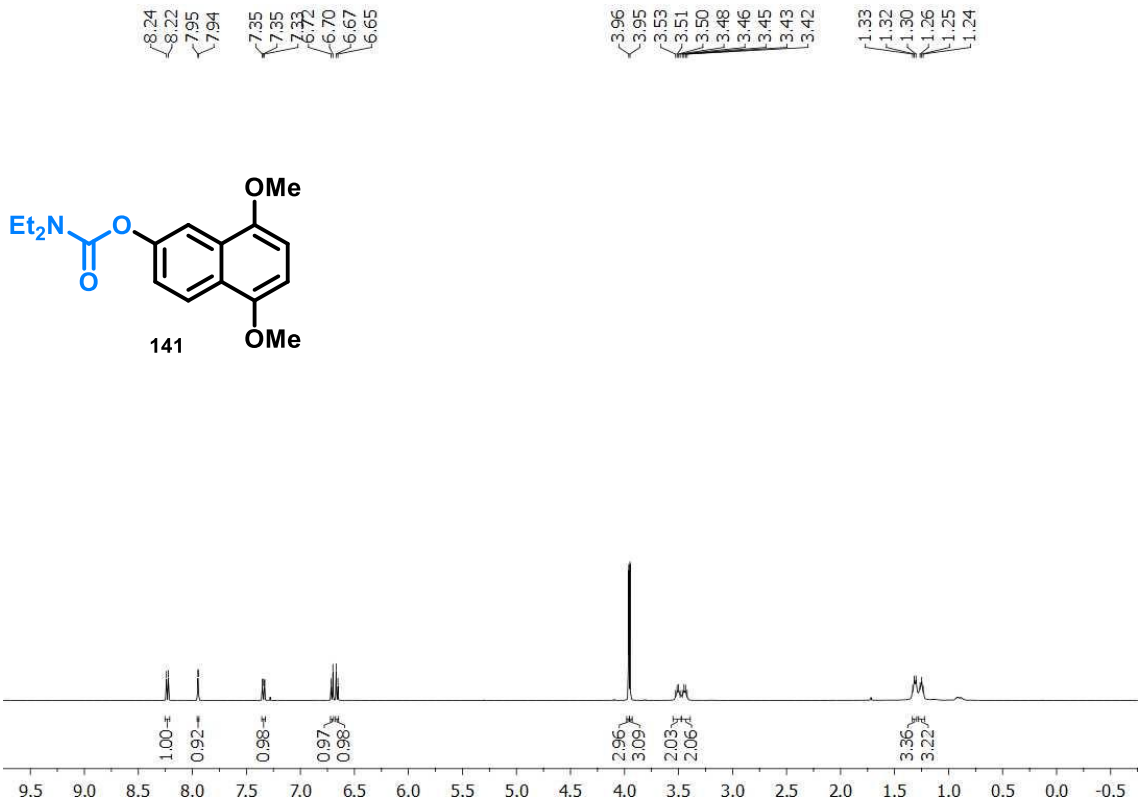

Figure B4. ^{13}C NMR spectrum of compound **141** (125 MHz, $CDCl_3$).

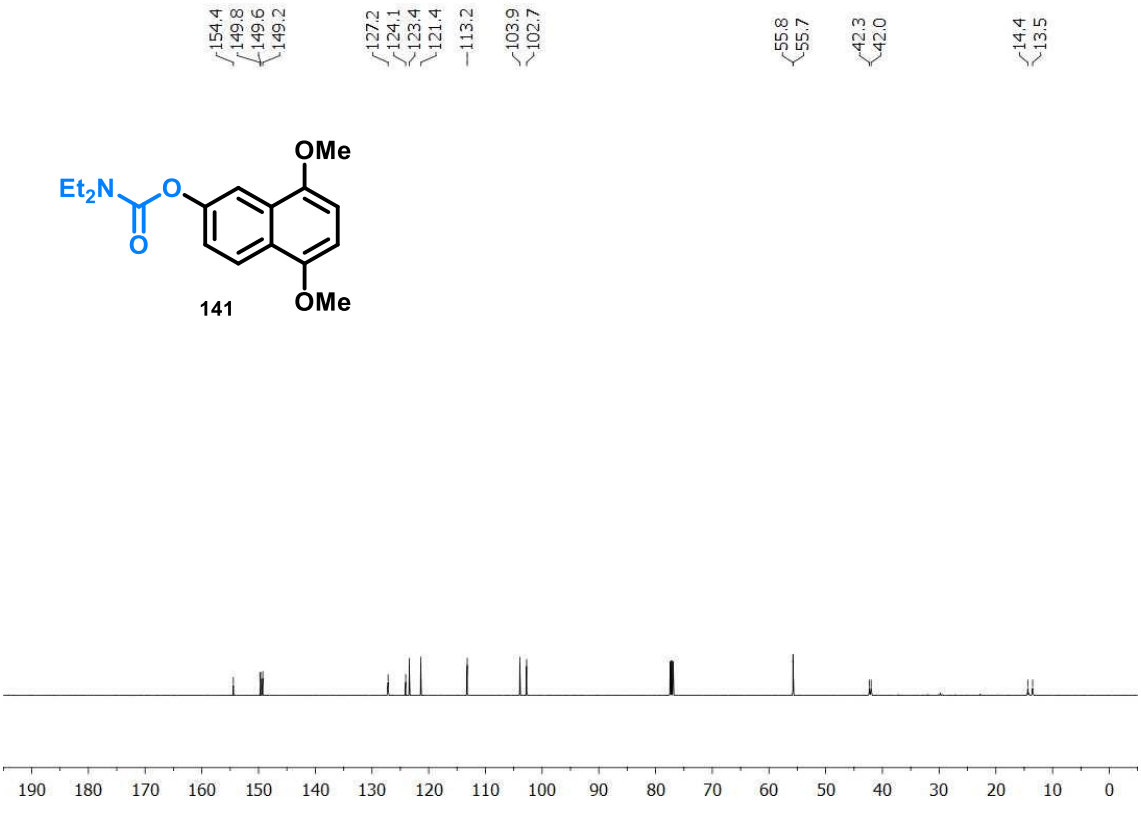

Figure B5. ^{1}H NMR spectrum of compound **142** (400 MHz, $CDCl_3$).

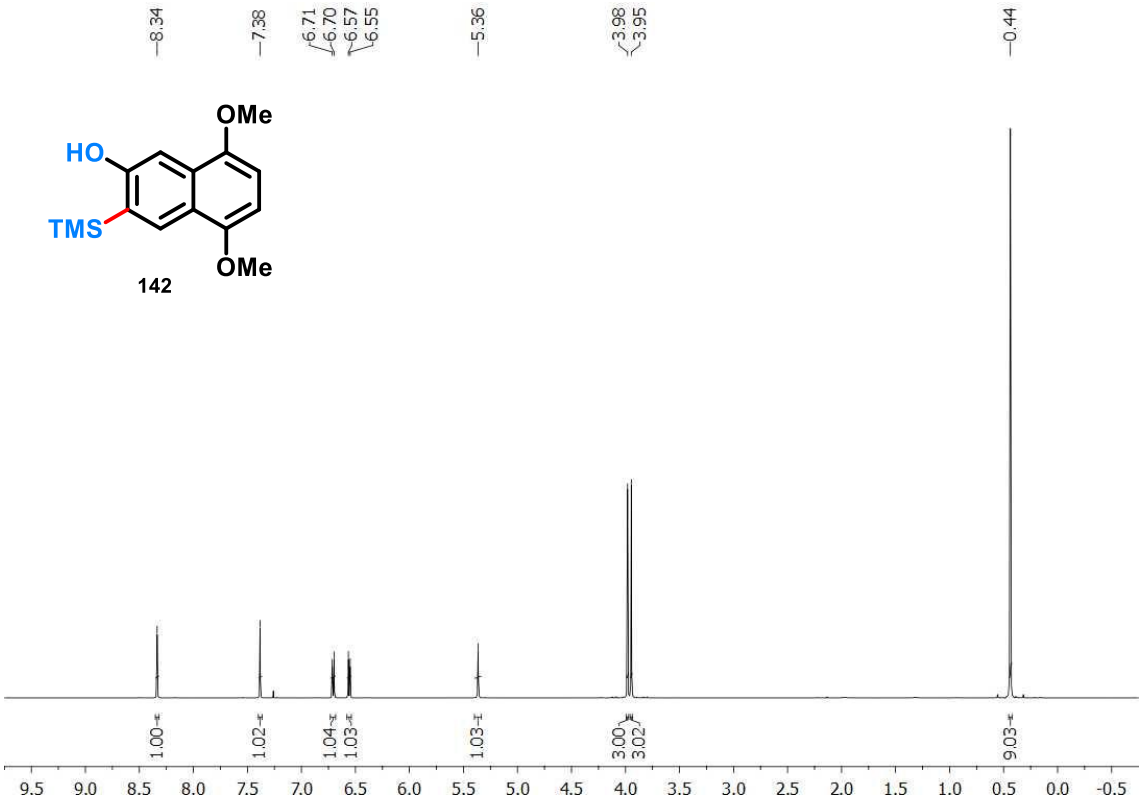

Figure B6. ^{13}C NMR spectrum of compound **142** (100 MHz, $CDCl_3$).

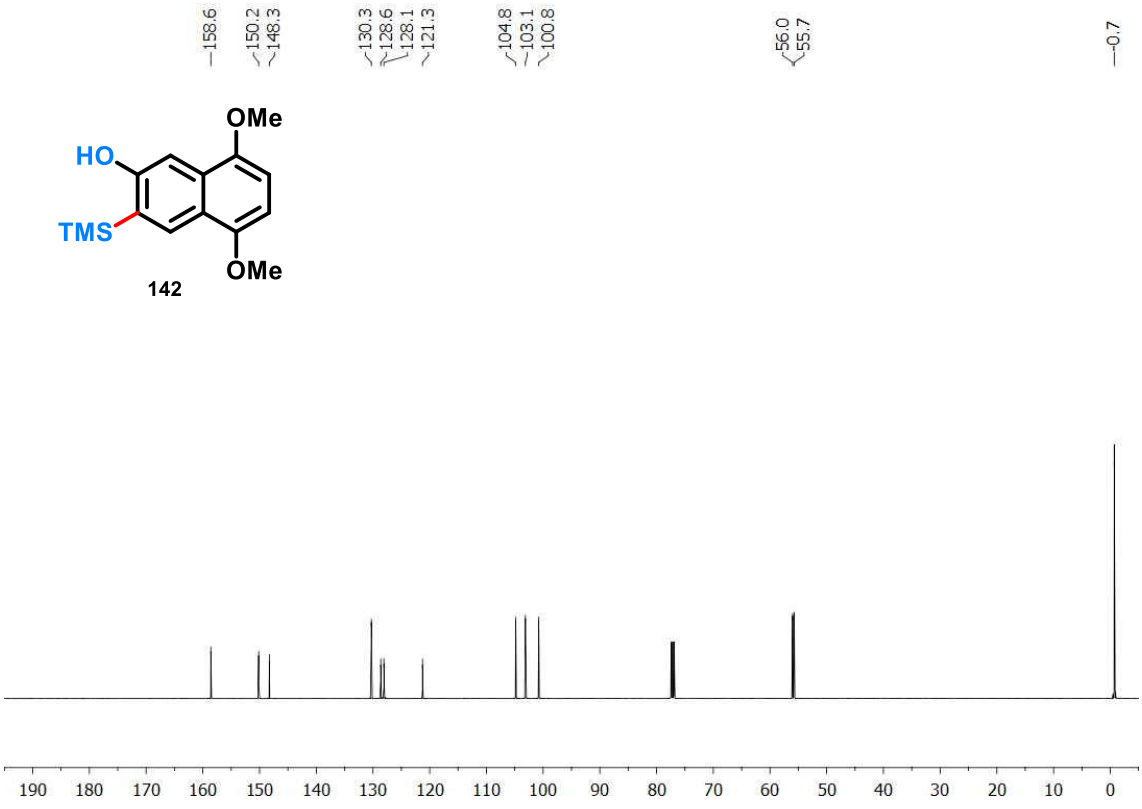

Figure B7. ^{1}H NMR spectrum of compound **143** (400 MHz, $CDCl_3$).

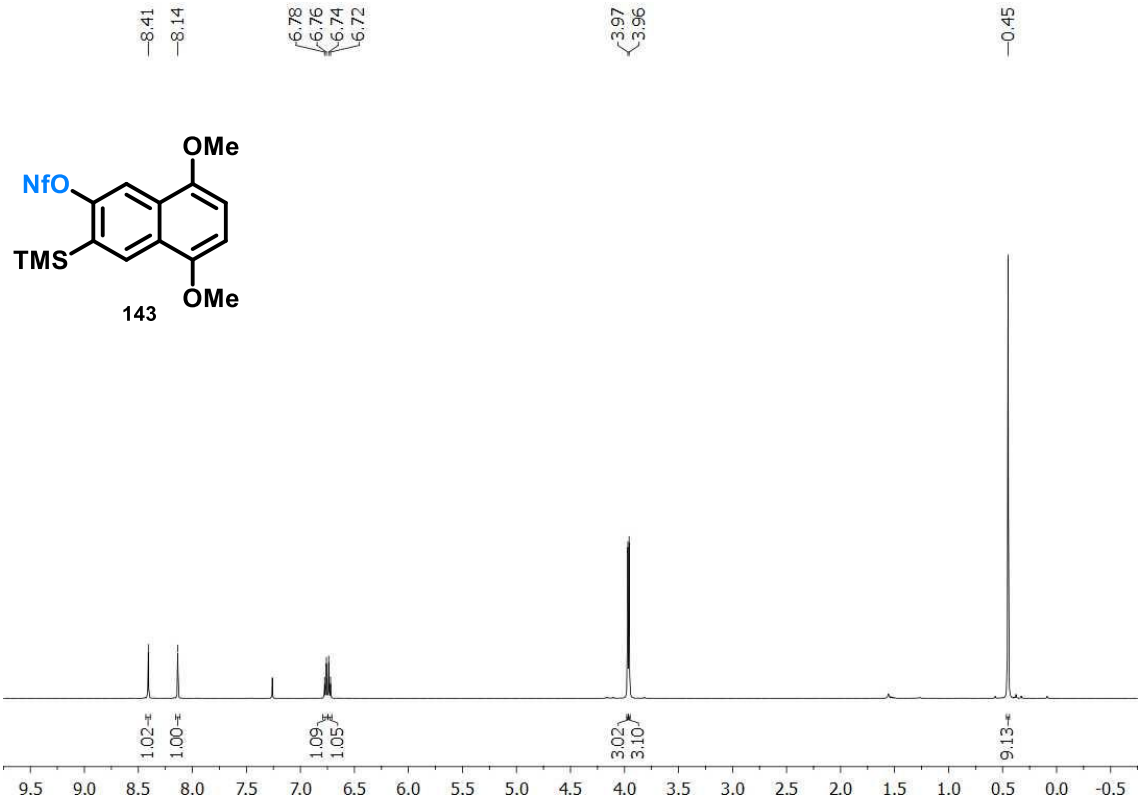

Figure B8. ^{13}C NMR spectrum of compound **143** (100 MHz, $CDCl_3$).

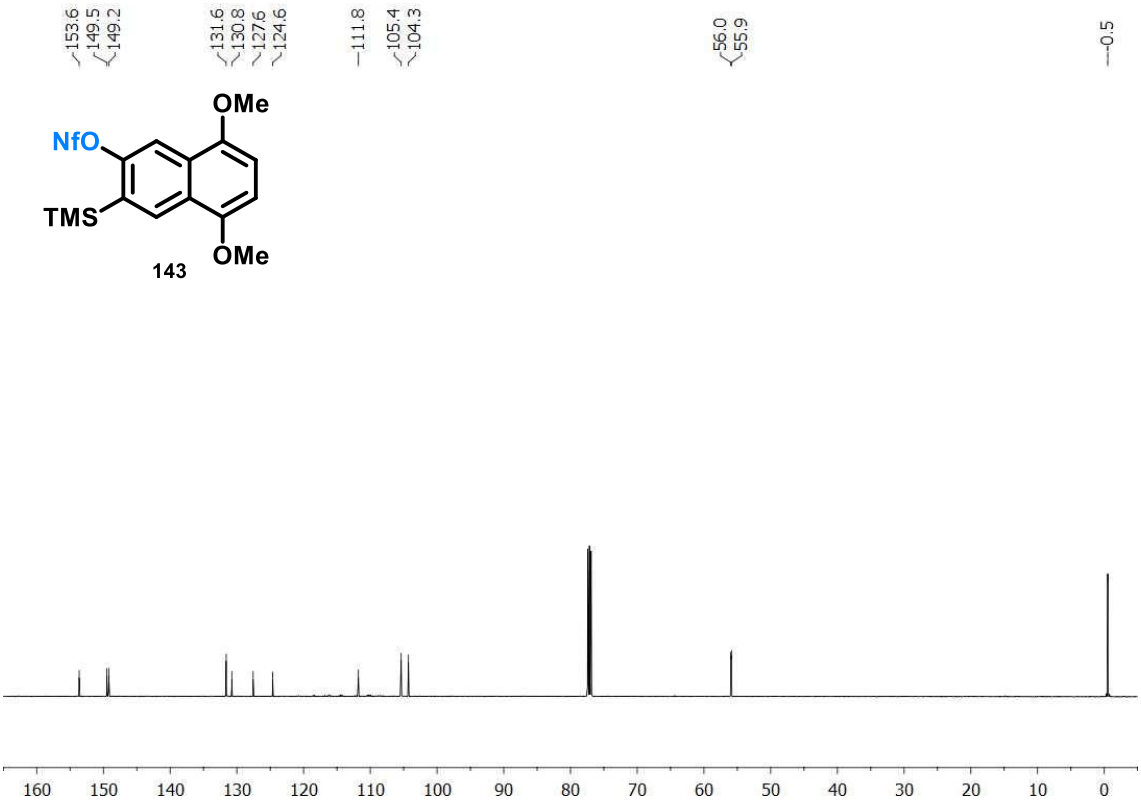

Figure B9. ^{19}F NMR of compound **143** (377 MHz, $CDCl_3$).

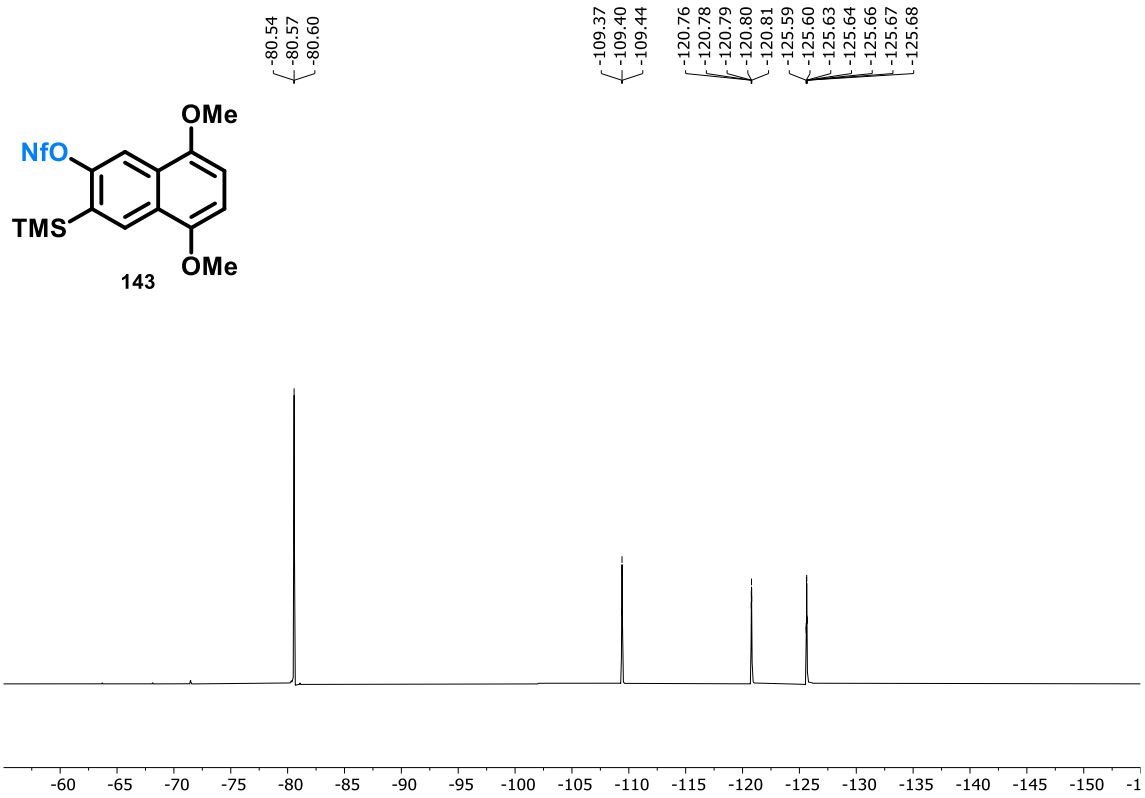

Figure B10. ^{1}H NMR spectrum of compound **138** (400 MHz, $CDCl_3$).

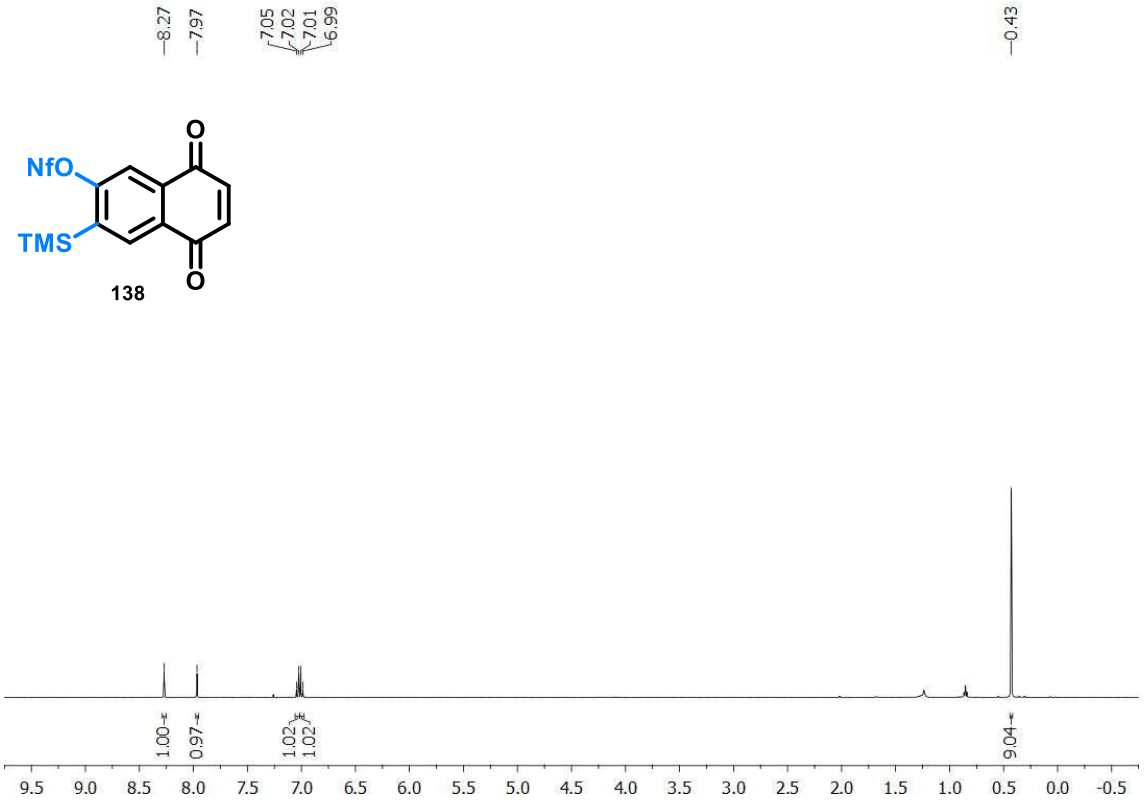

Figure B11. ^{13}C NMR spectrum of compound **138** (100 MHz, $CDCl_3$).

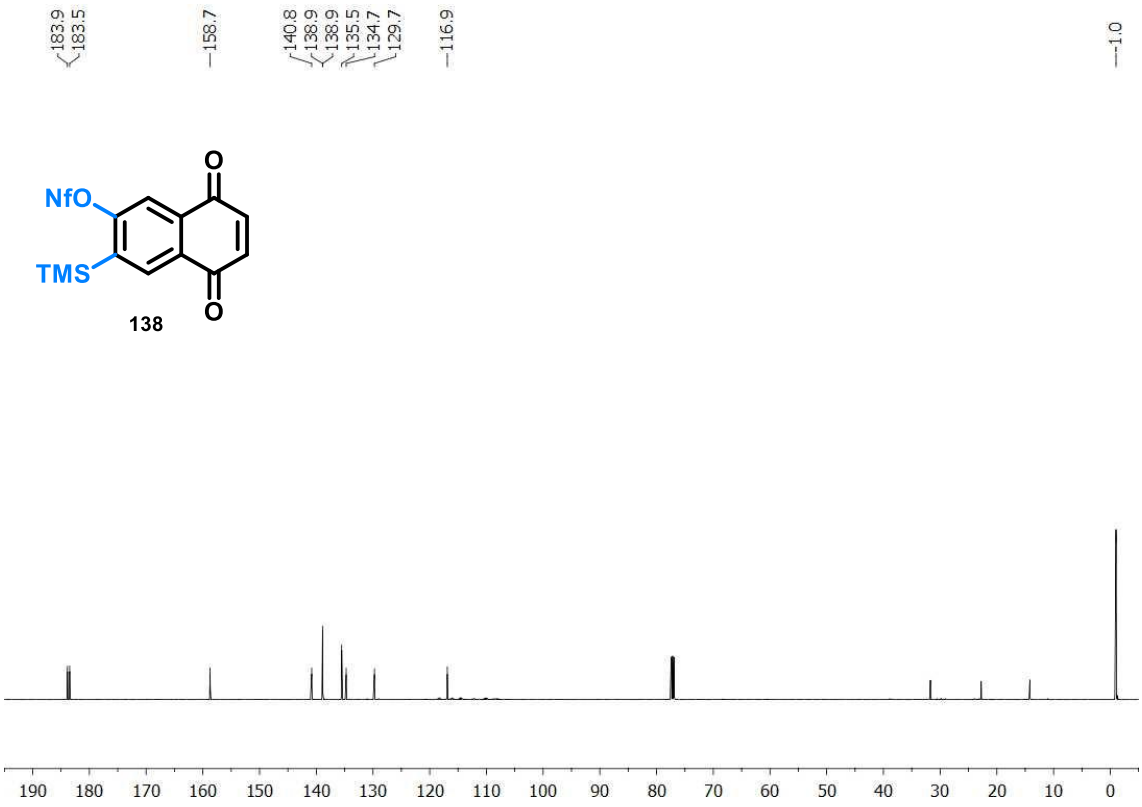

Figure B12. ^{19}F NMR of compound **138** (377 MHz, $CDCl_3$).

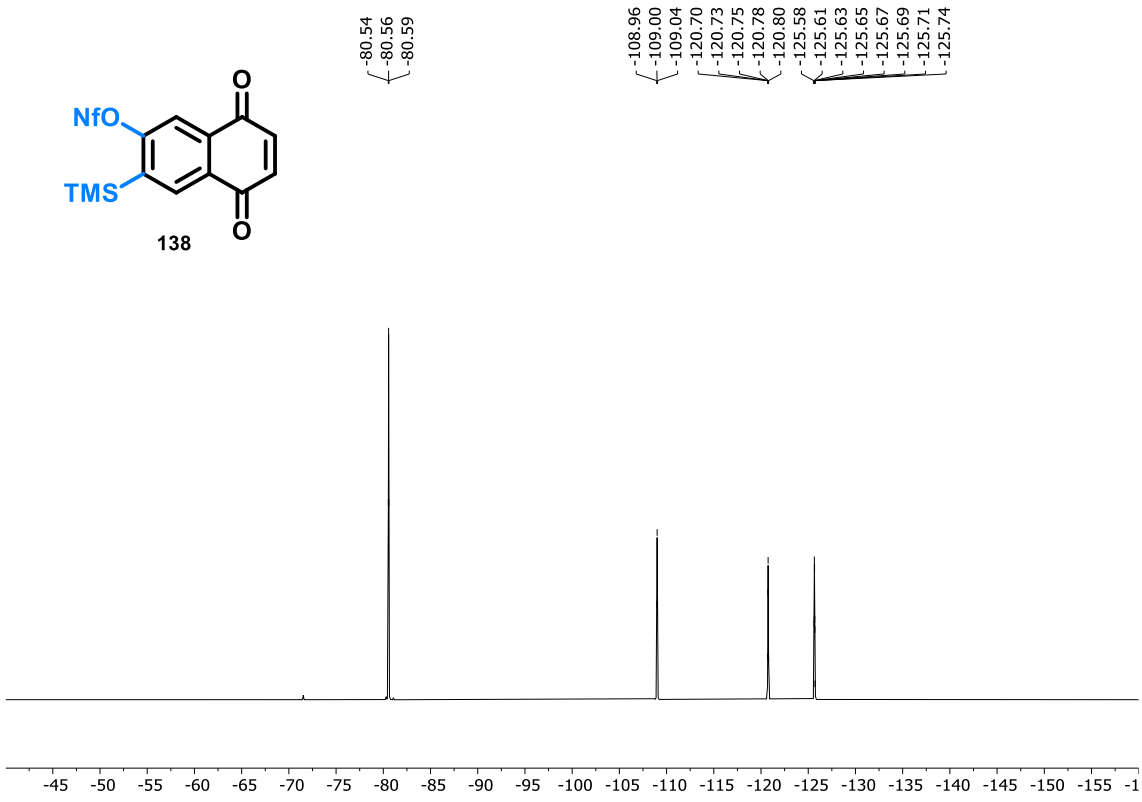

Figure B13. ^{1}H NMR spectrum of compound **144a** (400 MHz, $CDCl_3$).

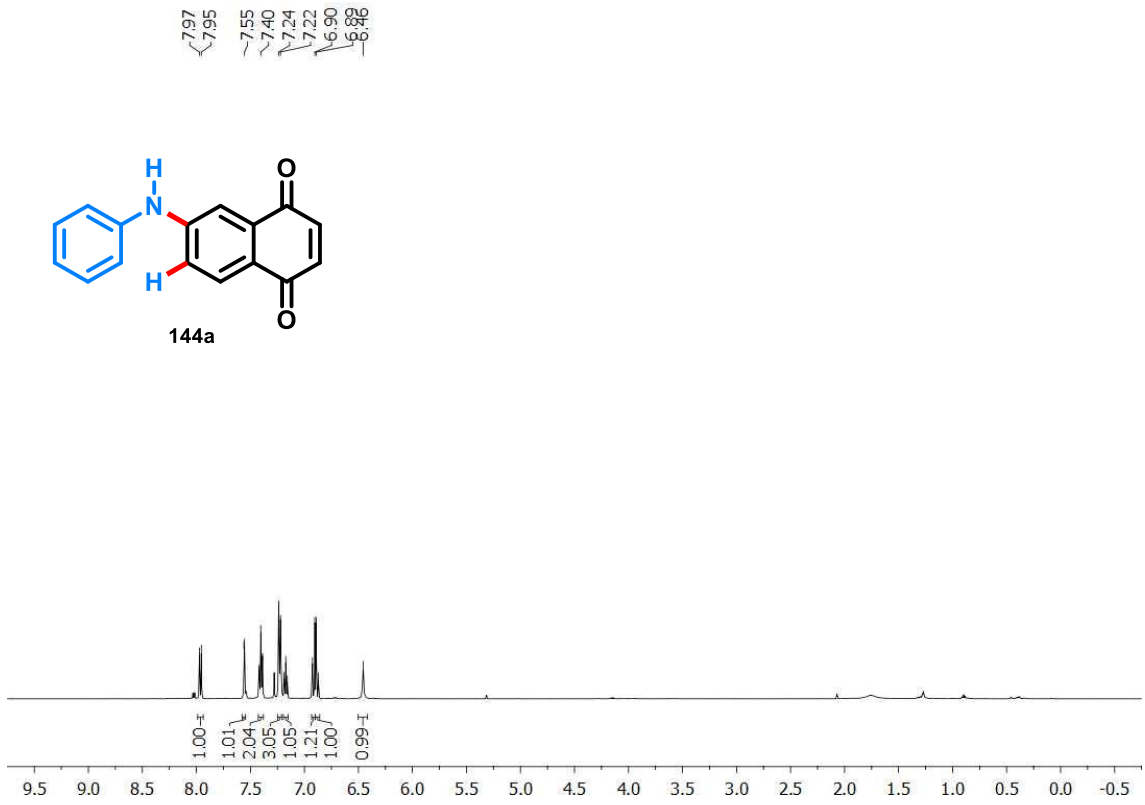

Figure B14. ^{13}C NMR spectrum of compound **144a** (100 MHz, $CDCl_3$).

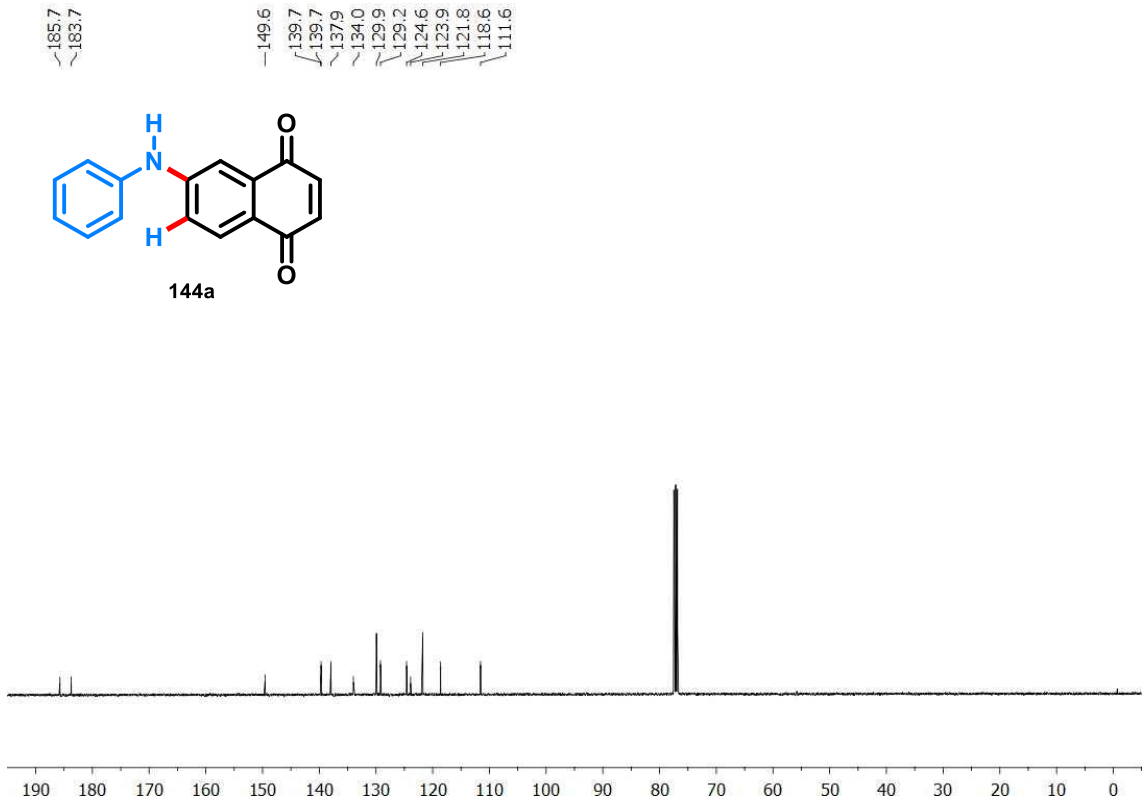

Figure B15. ^{1}H NMR spectrum of compound **144b** (400 MHz, $CDCl_3$).

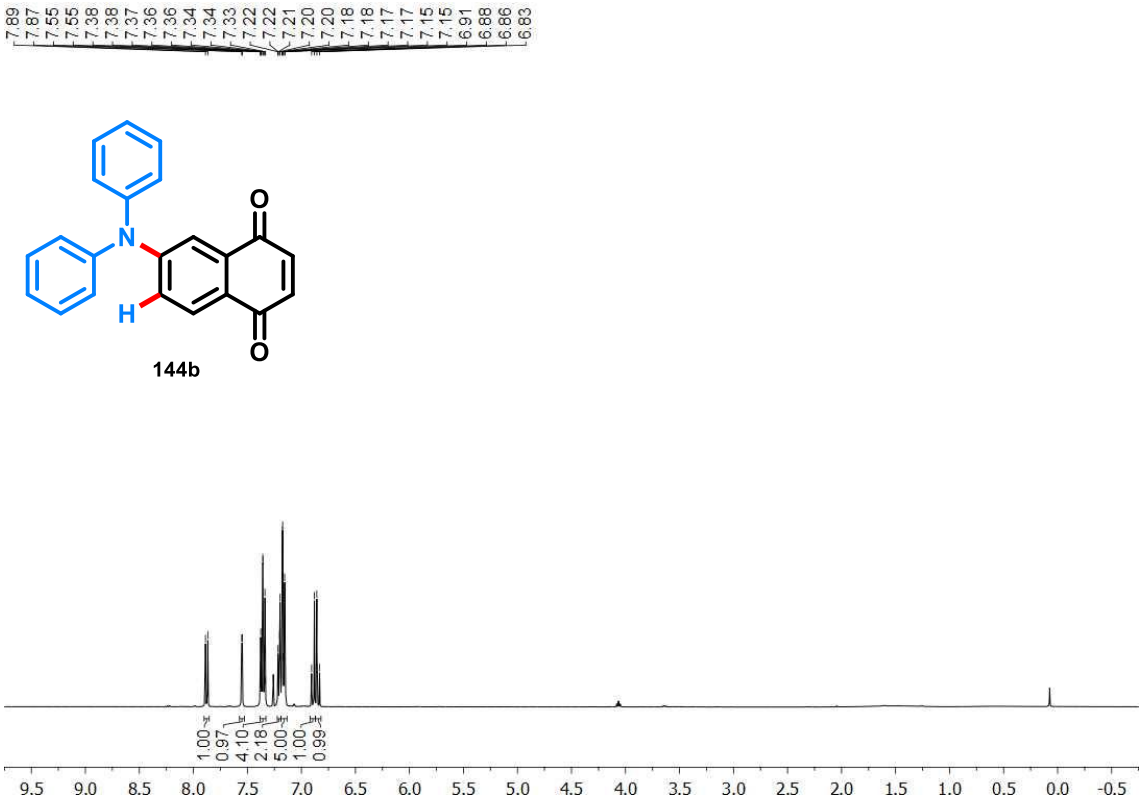

Figure B16. ^{13}C NMR spectrum of compound **144b** (100 MHz, $CDCl_3$).

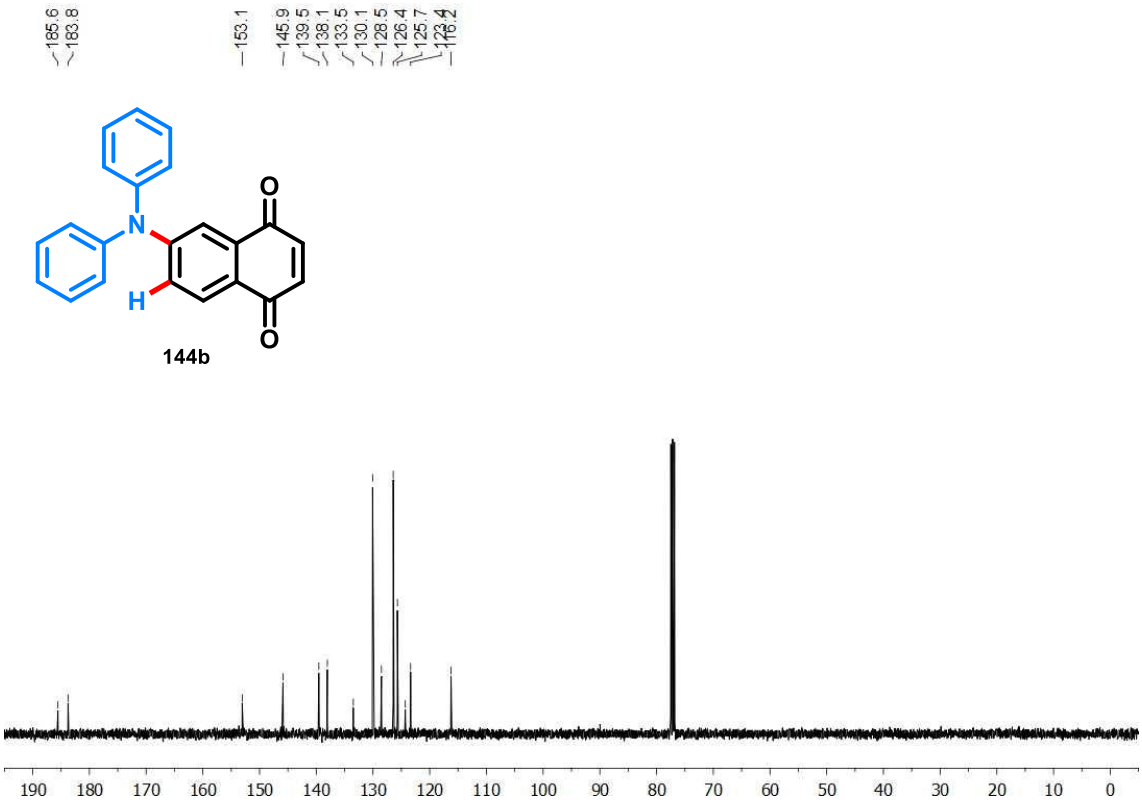

Figure B17. HRMS (ESI +) of compound **144b**.

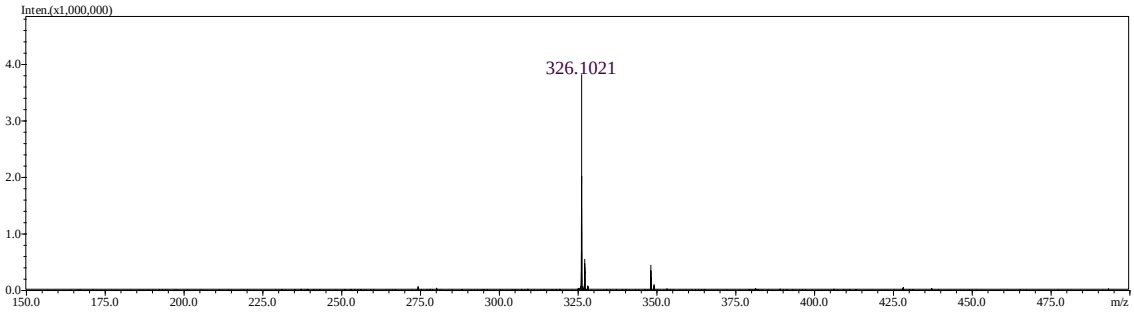

Table B1. Crystal Data and structure refinement for **144b**.

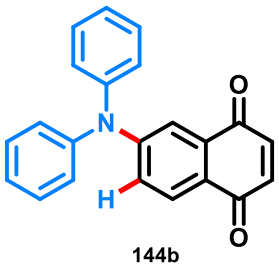 144b	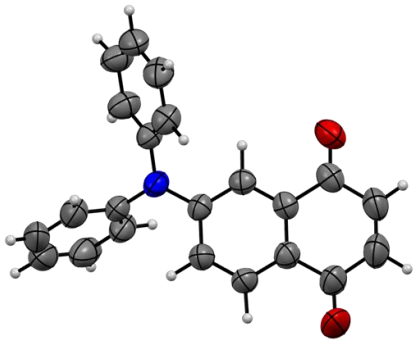
CCDC number	2352788
Identification code	**144b**
Empirical formula	$C_{22}H_{15}NO_2$
Formula weight	325.35
Temperature/K	299.05(10)
Crystal system	orthorhombic
Space group	Fdd2
a/Å	35.2203(12)
b/Å	20.9152(7)
c/Å	9.2515(3)
α/°	90
β/°	90
γ/°	90
Volume/Å^3	6815.0(4)
Z	16
ρ_{calc}g/cm^3	1.268
μ/mm^{-1}	0.650
F(000)	2720.0
Crystal size/mm^3	0.34 × 0.15 × 0.09
Radiation	CuKα (λ = 1.54184)
2Θ range for data collection/°	9.836 to 136.48
Index ranges	-42 ≤ h ≤ 32, -24 ≤ k ≤ 24, -11 ≤ l ≤ 10
Reflections collected	8924
Independent reflections	2825 [R_{int} = 0.0325, R_{sigma} = 0.0307]
Data/restraints/parameters	2825/1/287
Goodness-of-fit on F^2	1.132
Final R indexes [I>=2σ (I)]	R_1 = 0.0343, wR_2 = 0.0876
Final R indexes [all data]	R_1 = 0.0441, wR_2 = 0.1004
Largest diff. peak/hole / e Å^{-3}	0.10/-0.09

Figure B18. ^{1}H NMR spectrum of compound **144c** (400 MHz, $CDCl_3$).

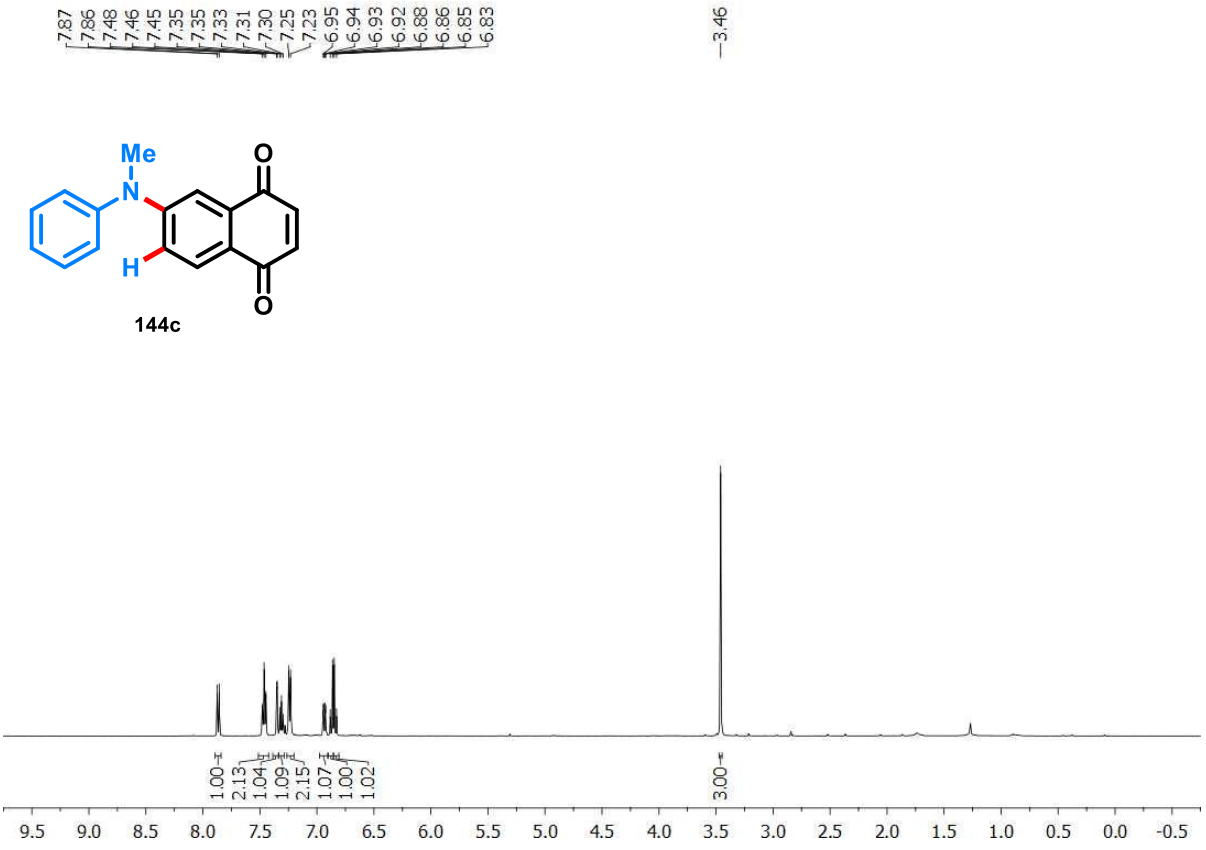

Figure B19. ^{13}C NMR spectrum of compound **144c** (100 MHz, $CDCl_3$).

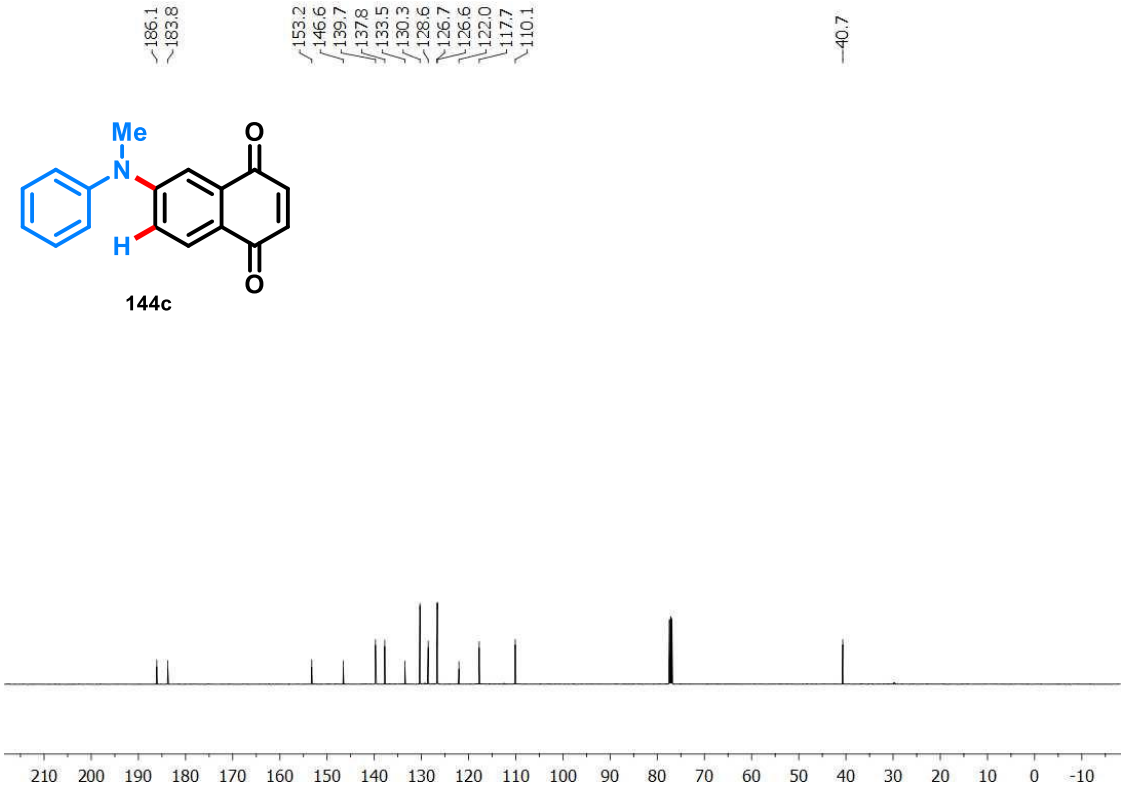

Figure B20. ^{1}H NMR spectrum of compound **144d** (400 MHz, $CDCl_3$).

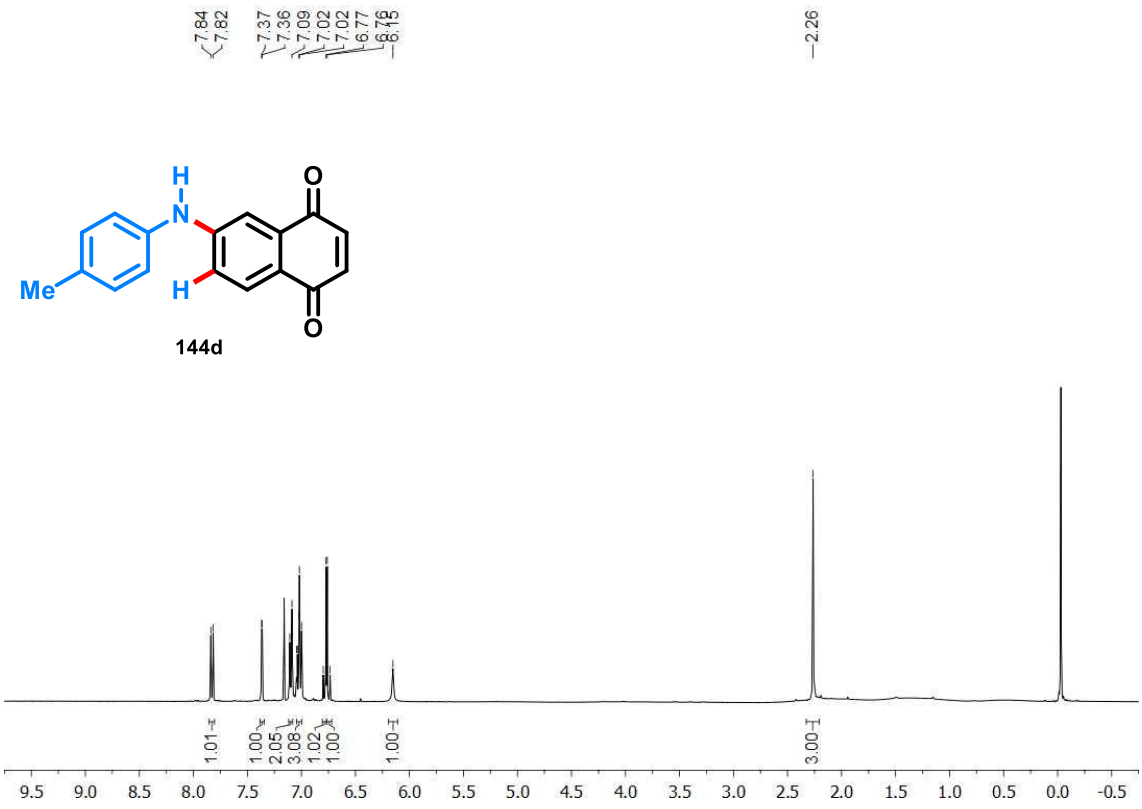

Figure B21. ^{13}C NMR spectrum of compound **144d** (100 MHz, $CDCl_3$).

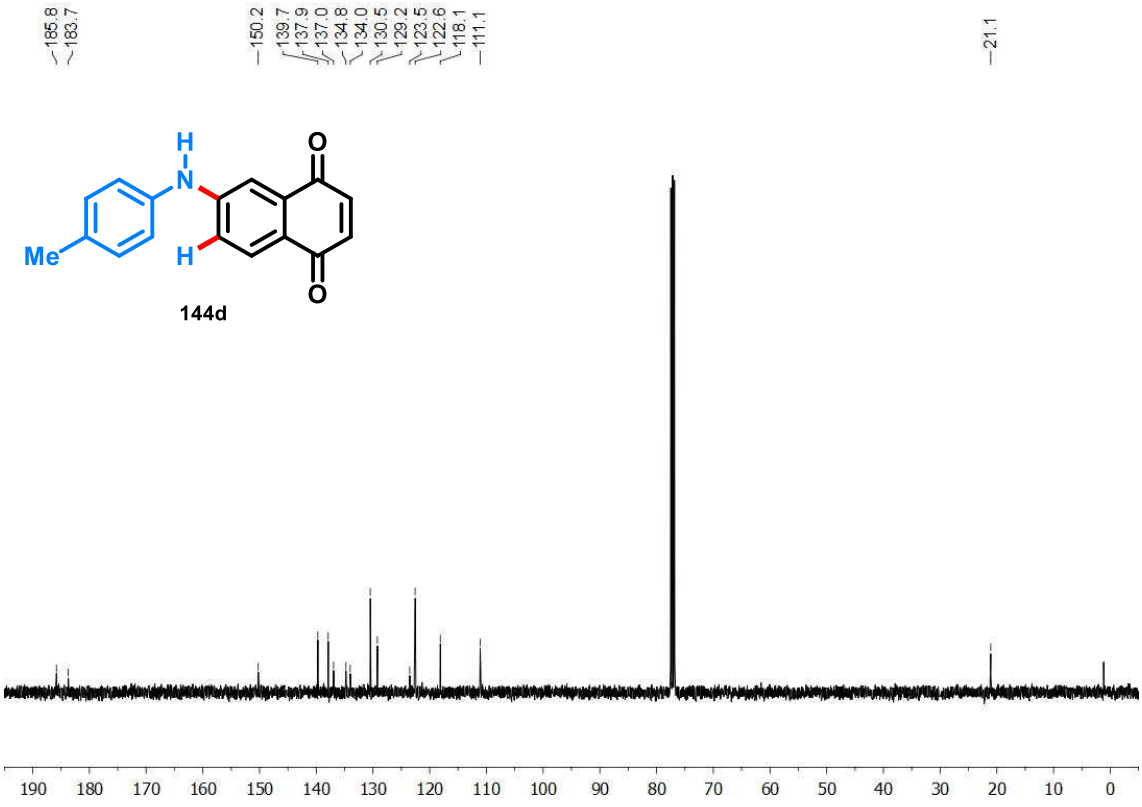

Figure B22. HRMS (ESI -) of compound **144d**.

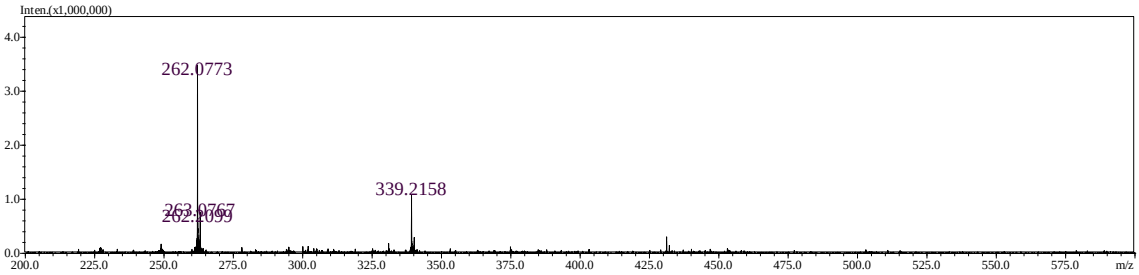

Figure B23. ^{1}H NMR spectrum of compound **144e** (400 MHz, $CDCl_3$).

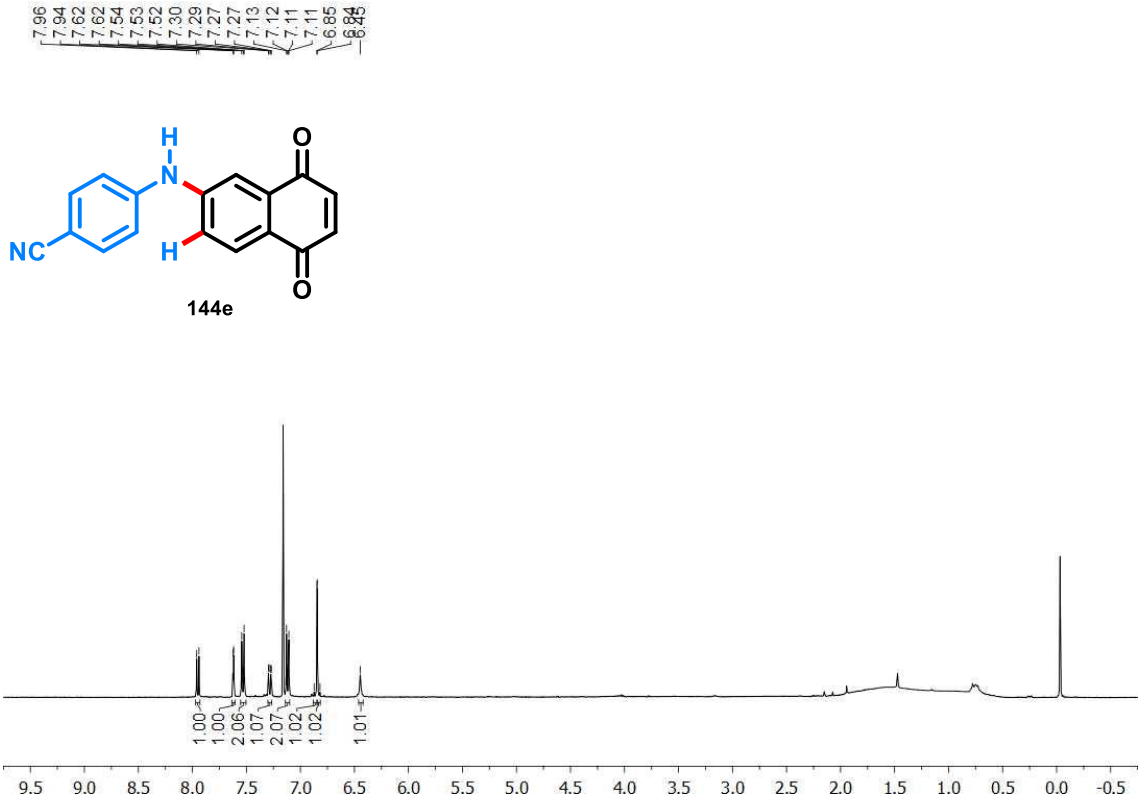

Figure B24. ^{13}C NMR spectrum of compound **144e** (100 MHz, $CDCl_3$).

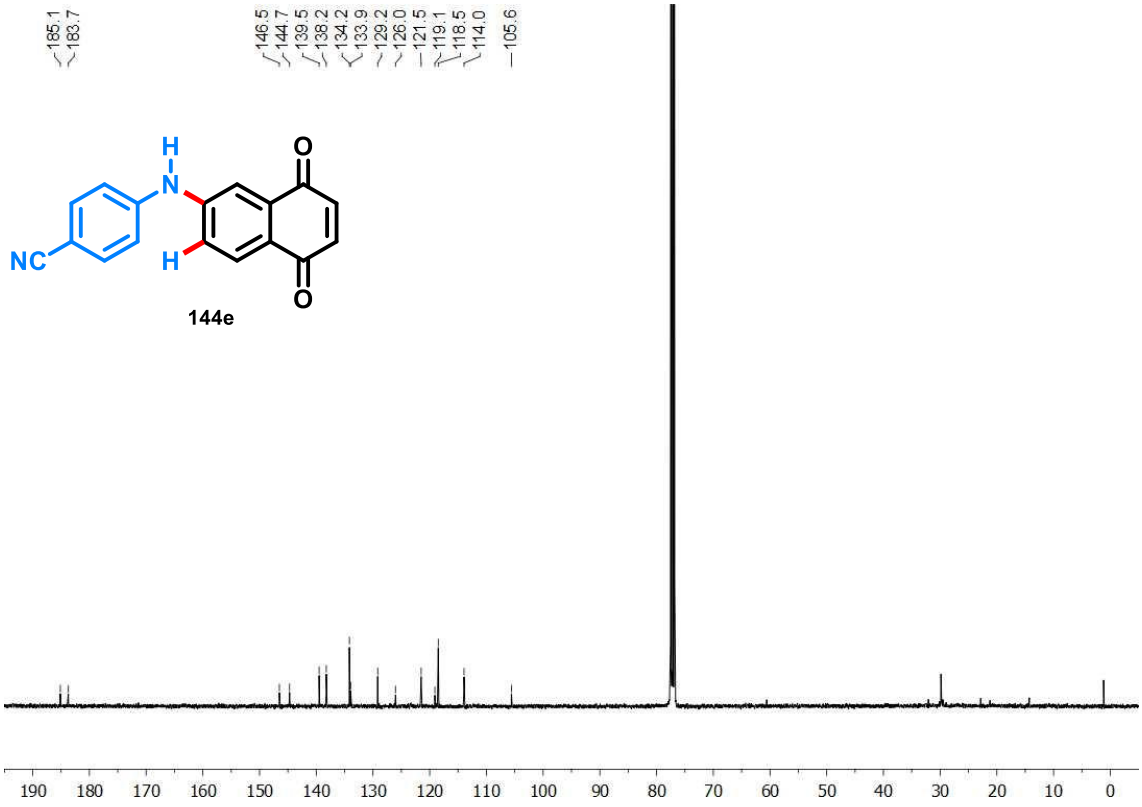

Figure B25. HRMS (ESI -) of compound **144e**.

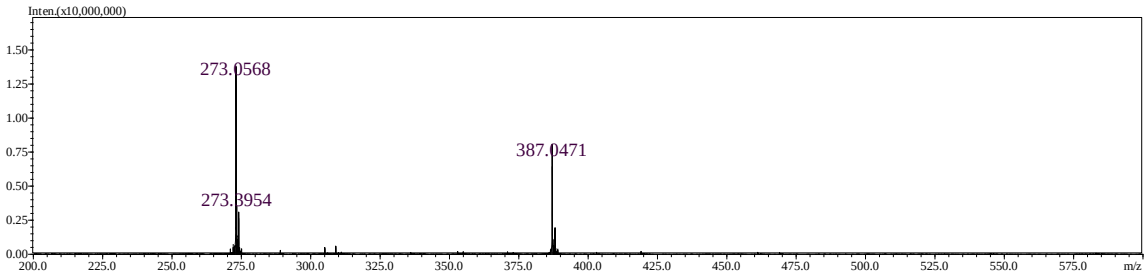

Figure B26. ^{1}H NMR spectrum of compound **144f** (400 MHz, $CDCl_3$).

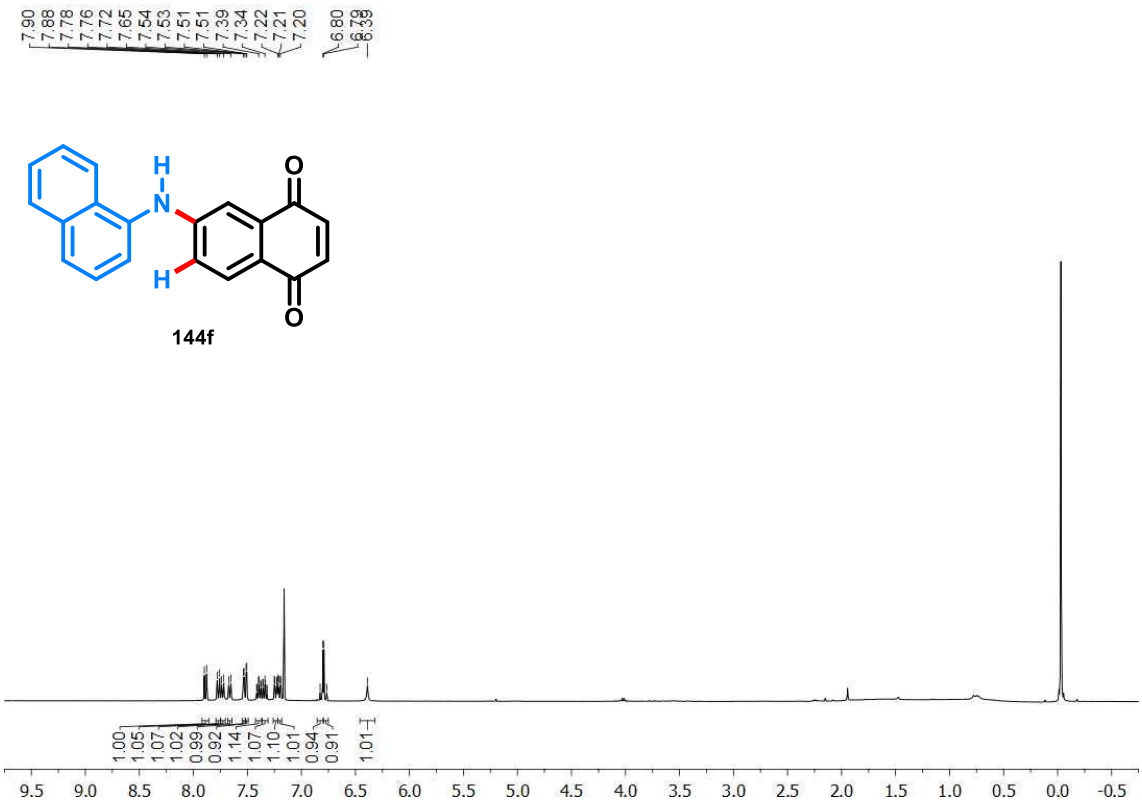

Figure B27. ^{13}C NMR spectrum of compound **144f** (100 MHz, $CDCl_3$).

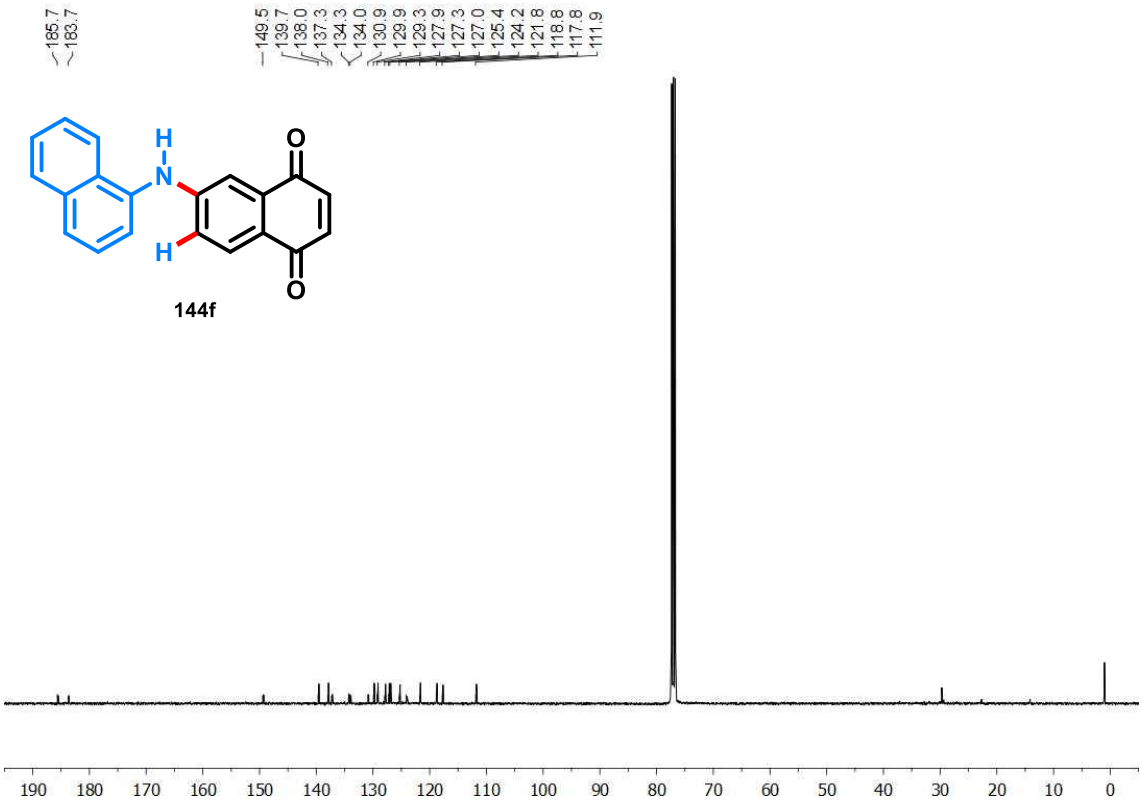

Figure B28. HRMS (ESI +) of compound **144f**.

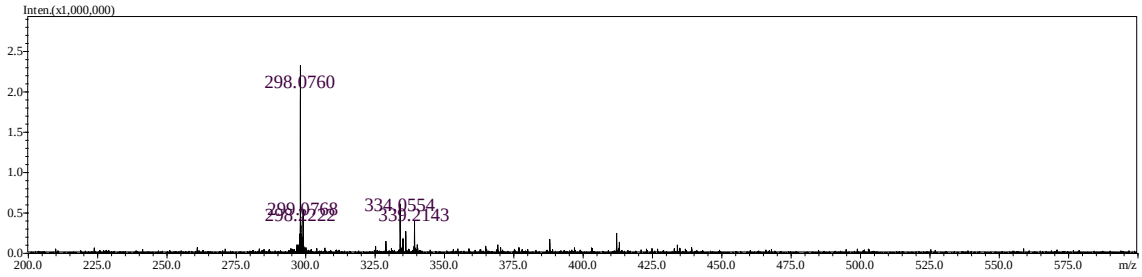

Figure B29. ^{1}H NMR spectrum of compound **144g** (400 MHz, $CDCl_3$).

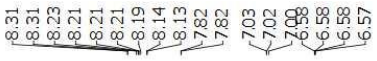

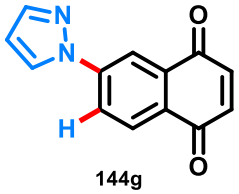

144g

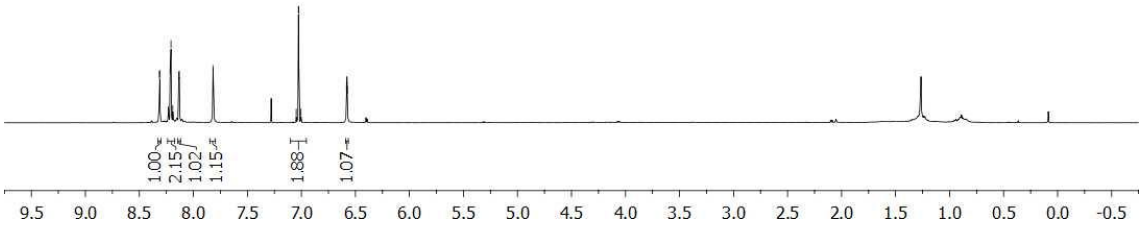

Figure B30. ^{13}C NMR spectrum of compound **144g** (100 MHz, $CDCl_3$).

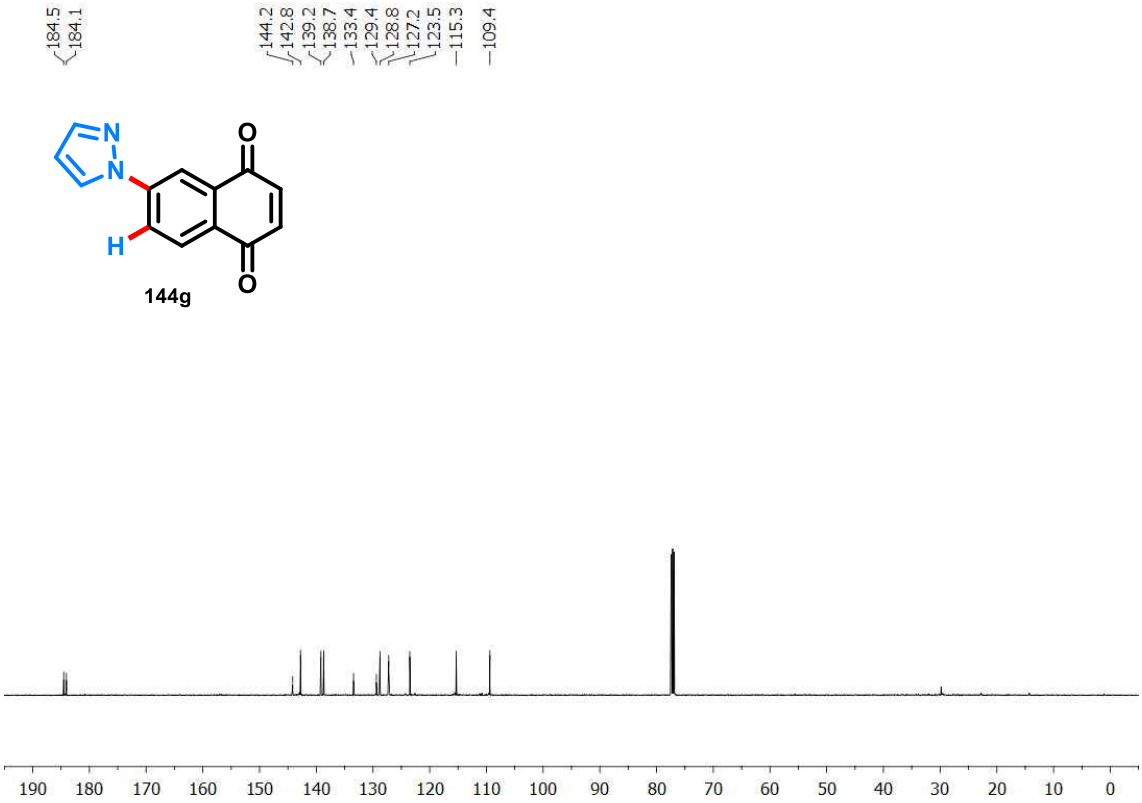

Figure B31. ^{1}H NMR spectrum of compound **144h** (400 MHz, $CDCl_3$).

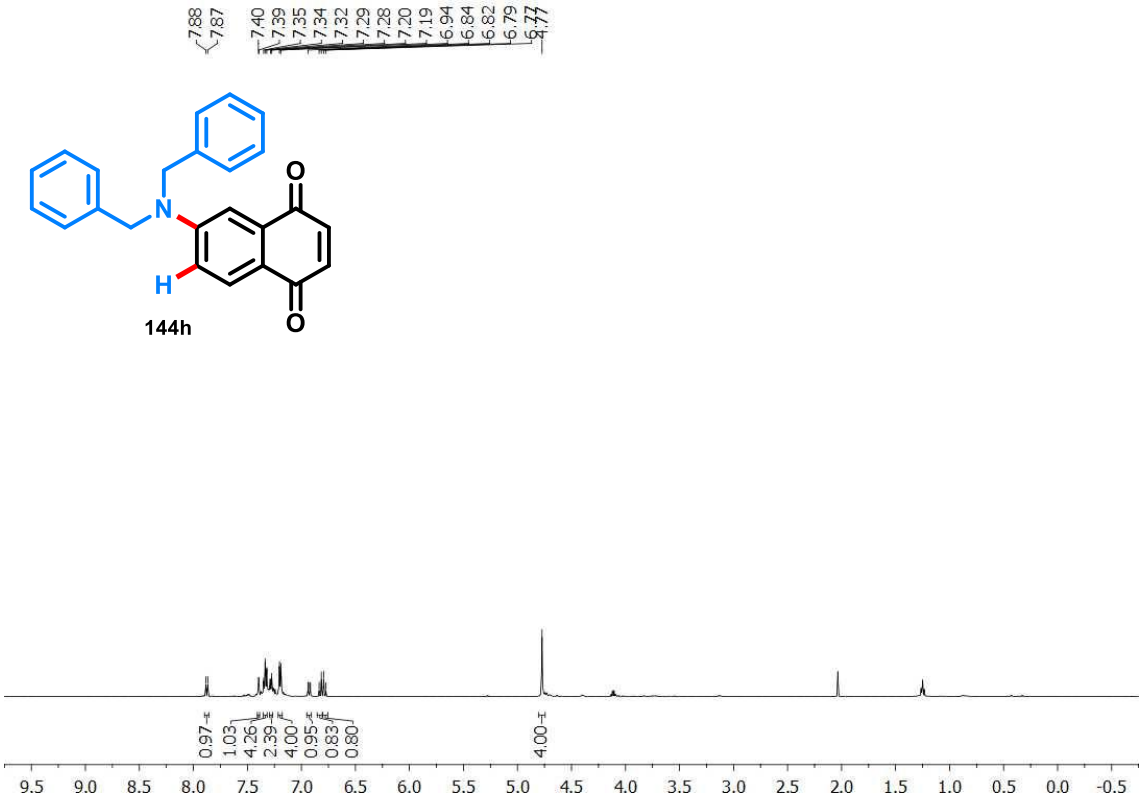

Figure B32. ^{13}C NMR spectrum of compound **144h** (100 MHz, $CDCl_3$).

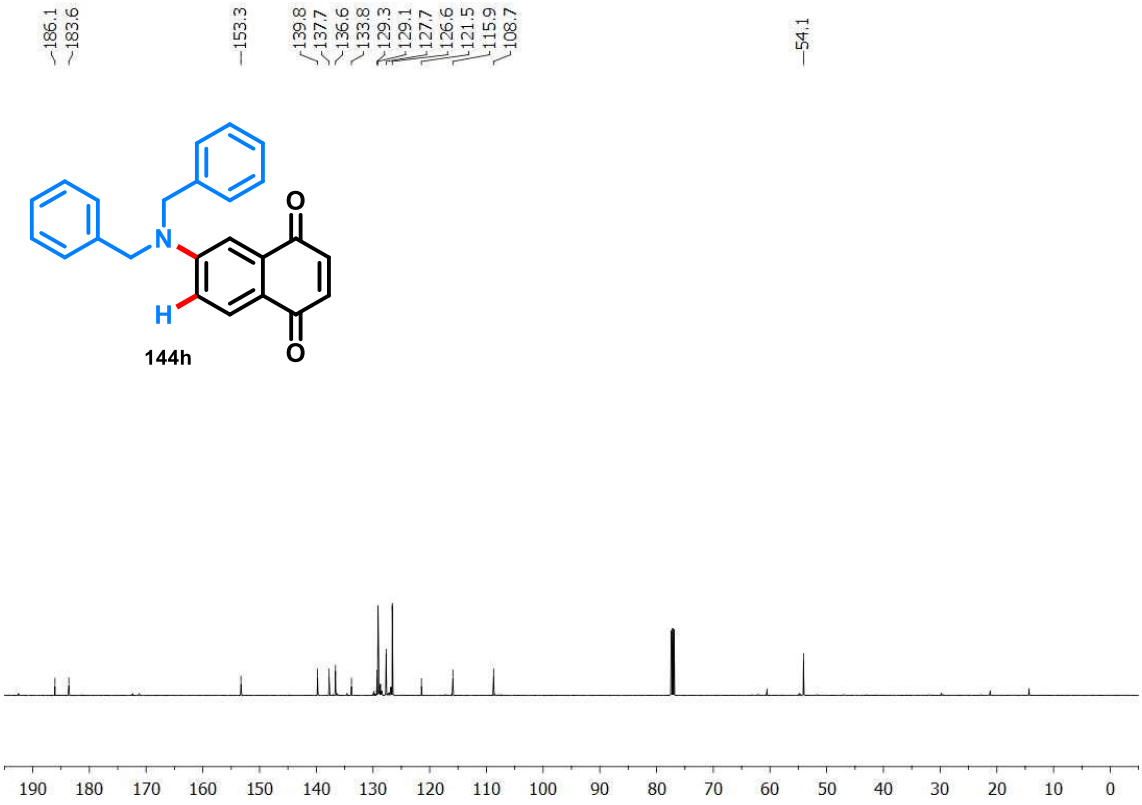

Figure B33. ^{1}H NMR spectrum of compound **144i** (400 MHz, $CDCl_3$).

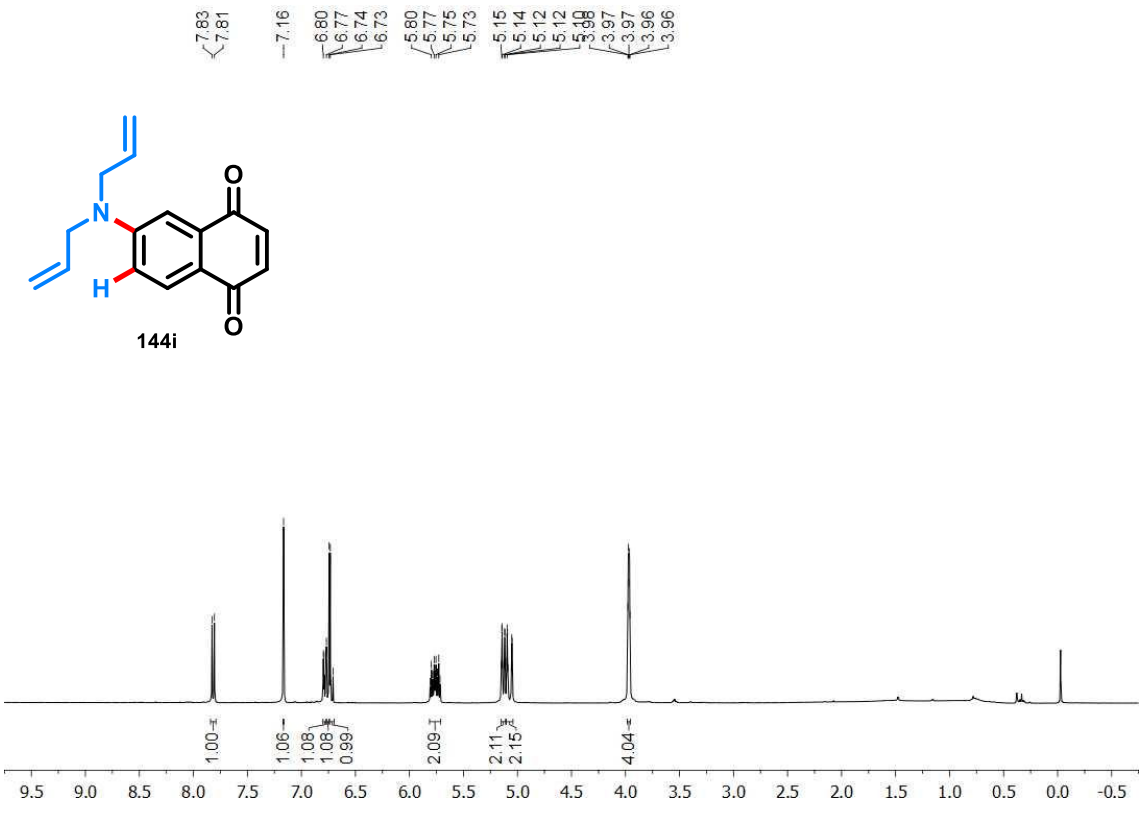

Figure B34. ^{13}C NMR spectrum of compound **144i** (100 MHz, $CDCl_3$).

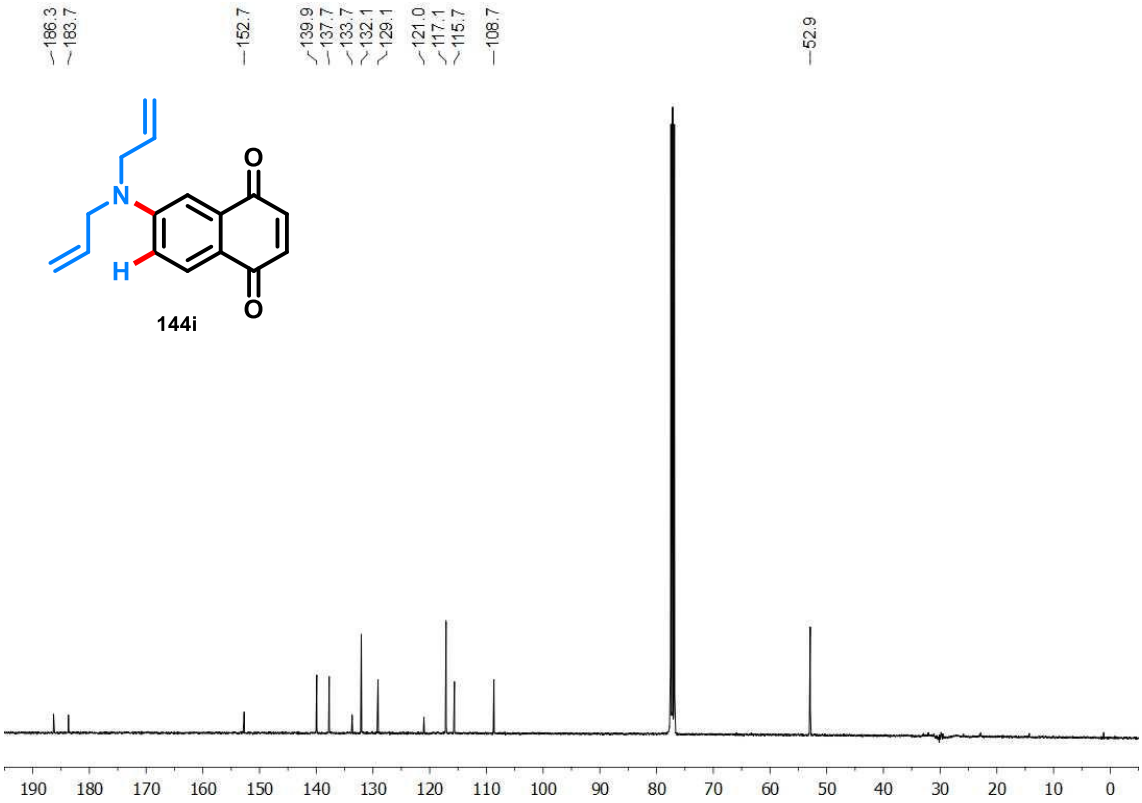

Figure B35. HRMS (ESI +) of compound **144i**.

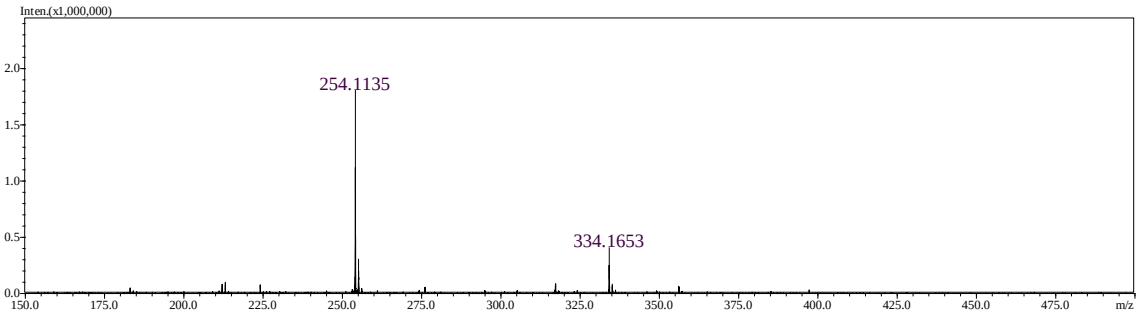

Figure B36. ^{1}H NMR spectrum of compound **144j** (400 MHz, $CDCl_3$).

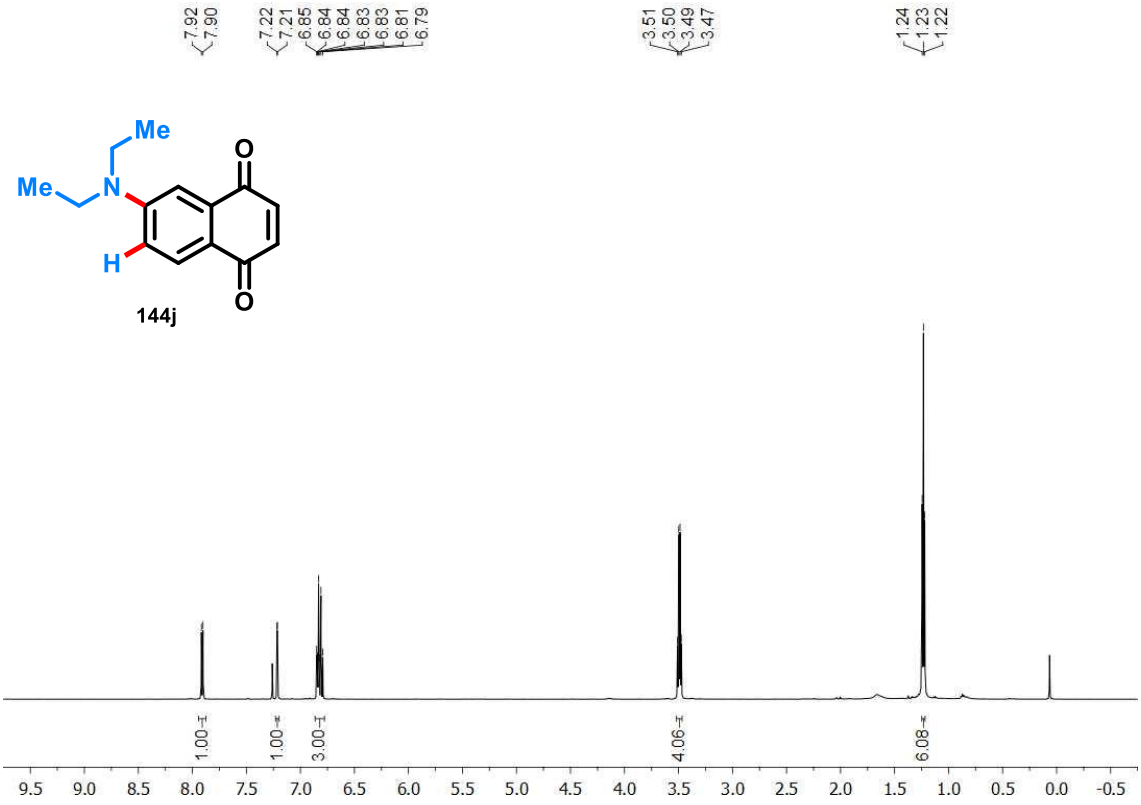

Figure B37. ^{13}C NMR spectrum of compound **144j** (100 MHz, $CDCl_3$).

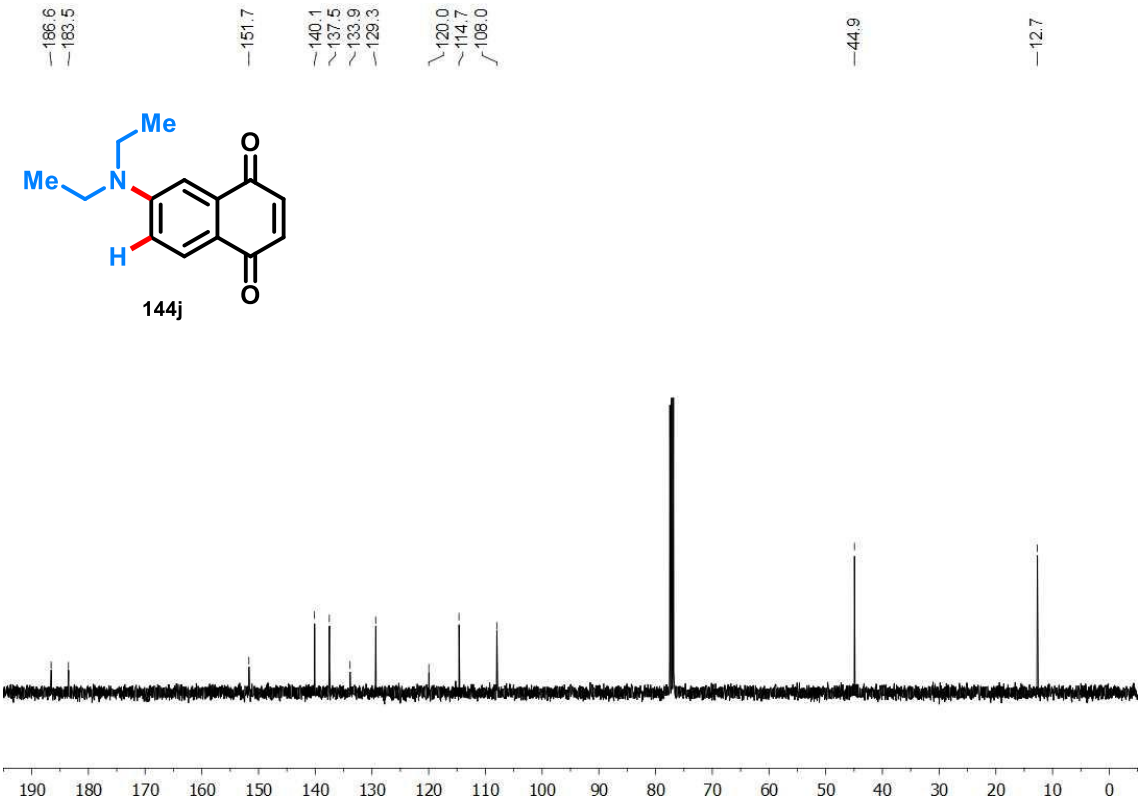

Figure B38. HRMS (ESI +) of compound **144j**.

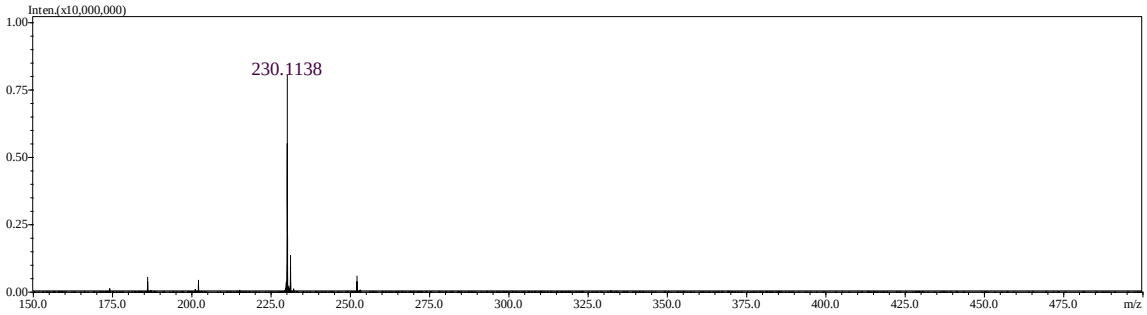

Table B2. Crystal Data and structure refinement for **144j**.

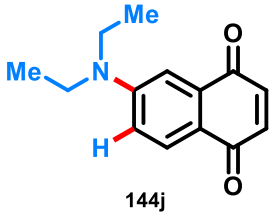	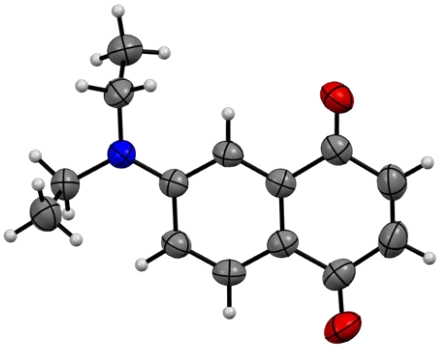
144j	
CCDC number	2352787
Identification code	**144j**
Empirical formula	$C_{14}H_{15}NO_2$
Formula weight	229.27
Temperature/K	299,05 (10)
Crystal system	monoclinic
Space group	C2/c
a/Å	15.4613(3)
b/Å	7.7422(2)
c/Å	20.6904(4)
α/°	90
β/°	102.765(2)
γ/°	90
Volume/Å^3	2415.52(9)
Z	8
ρ_{calc}g/cm^3	1.261
μ/mm^{-1}	0.679
F(000)	976.0
Crystal size/mm^3	0.17 × 0.11 × 0.09
Radiation	CuKα (λ = 1.54184)
2Θ range for data collection/°	8.764 to 157.986
Index ranges	-18 ≤ h ≤ 19, -9 ≤ k ≤ 8, -26 ≤ l ≤ 25
Reflections collected	12062
Independent reflections	2472 [R_{int} = 0.0292, R_{sigma} = 0.0200]
Data/restraints/parameters	2472/0/157
Goodness-of-fit on F^2	1.045
Final R indexes [I>=2σ (I)]	R_1 = 0.0380, wR_2 = 0.1053
Final R indexes [all data]	R_1 = 0.0471, wR_2 = 0.1126
Largest diff. peak/hole / e Å^{-3}	0.17/-0.12

Figure B39. ^{1}H NMR spectrum of compound **144k** (400 MHz, $CDCl_3$).

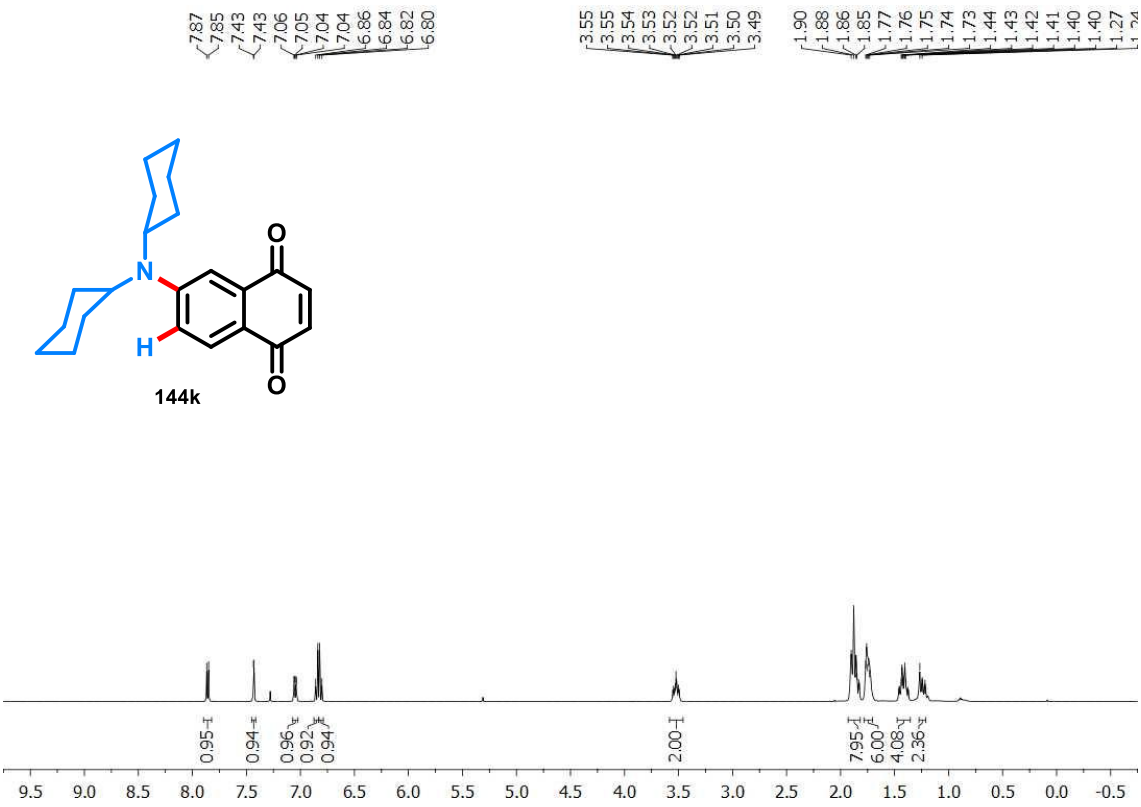

Figure B40. ^{13}C NMR spectrum of compound **144k** (100 MHz, $CDCl_3$).

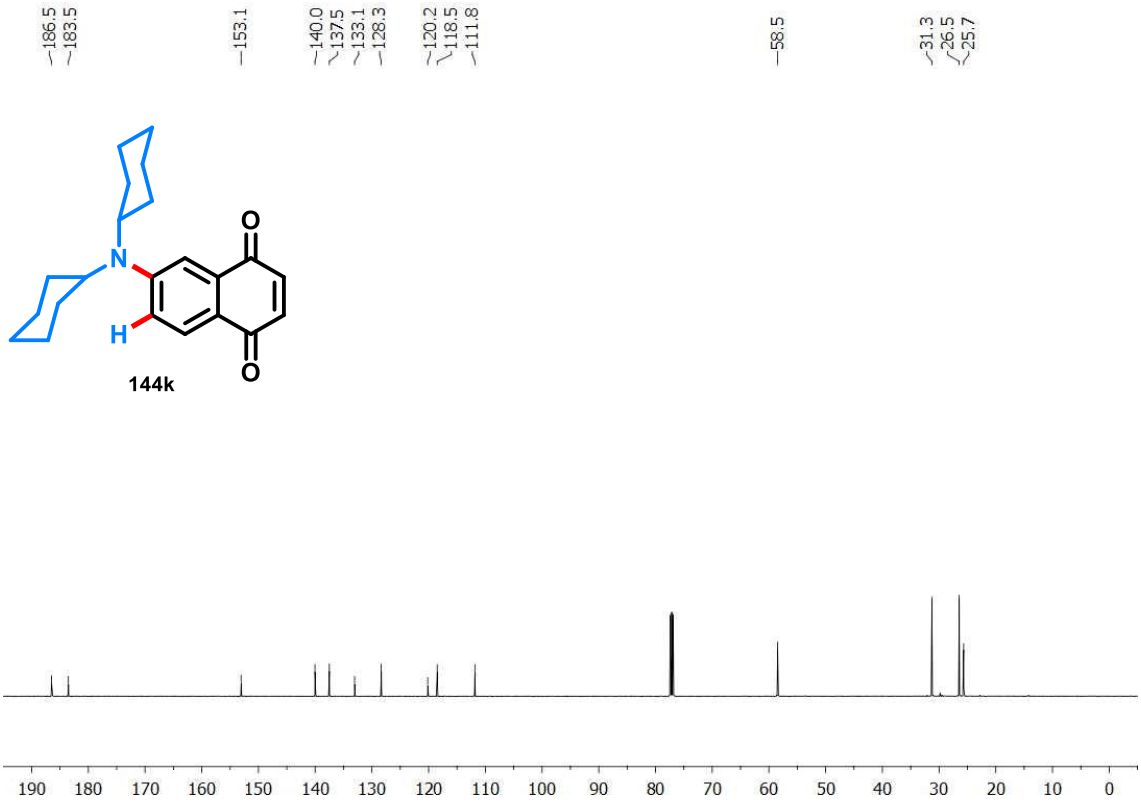

Figure B41. ^{1}H NMR spectrum of compound **144l** (400 MHz, $CDCl_3$).

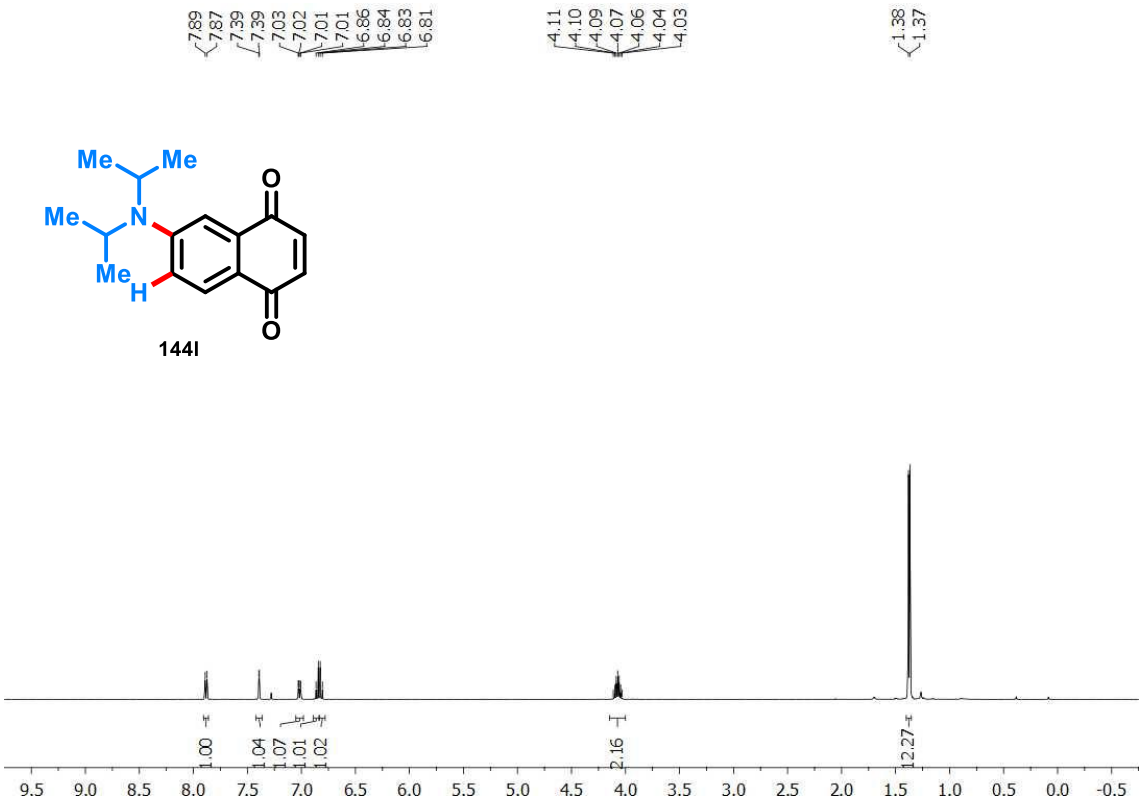

Figure B42. ^{13}C NMR spectrum of compound **144l** (100 MHz, $CDCl_3$).

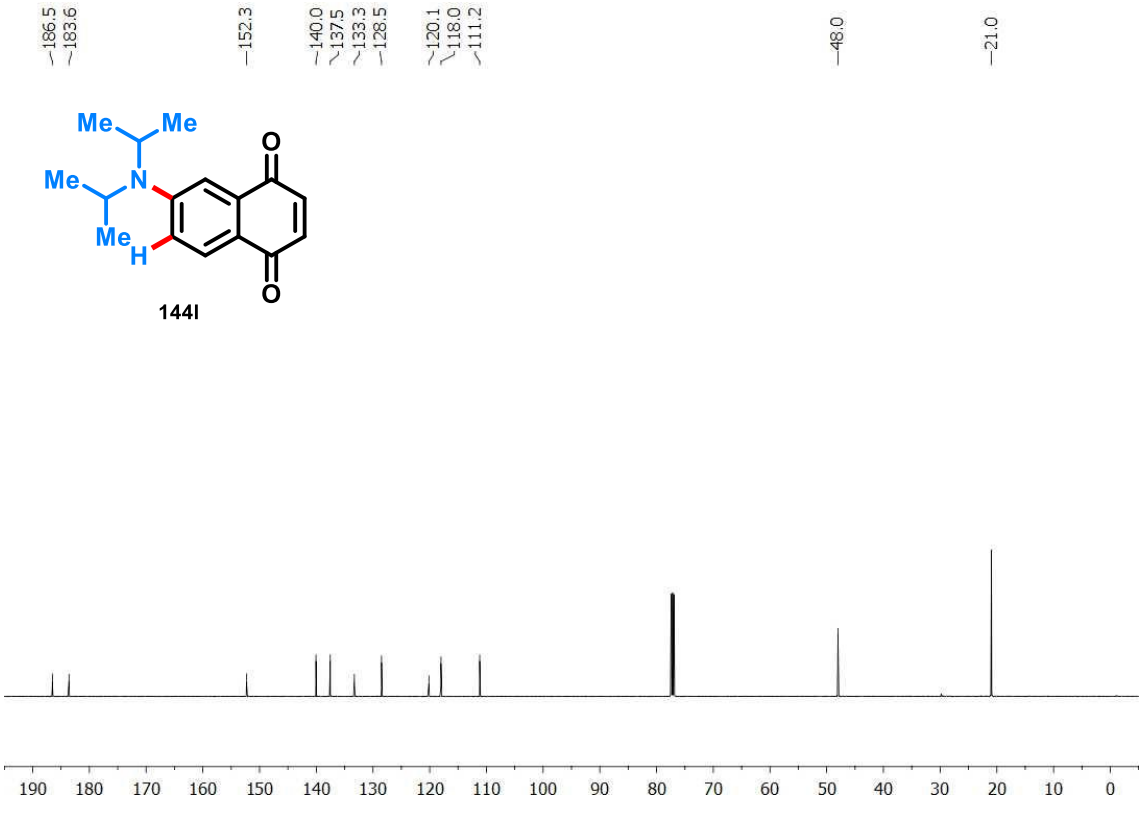

Table B3. Crystal Data and structure refinement for **144l**.

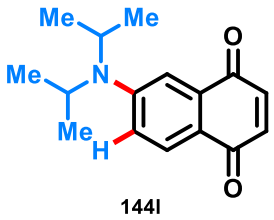 144l	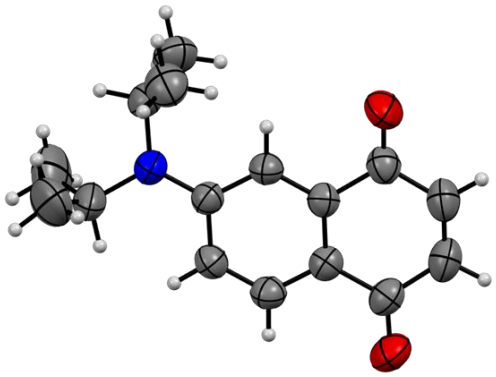
CCDC number	2352789
Identification code	**144l**
Empirical formula	$C_{16}H_{19}NO_2$
Formula weight	257.32
Temperature/K	299.05(10)
Crystal system	monoclinic
Space group	$P2_1/n$
a/Å	8.12310(10)
b/Å	9.1098(2)
c/Å	19.3288(3)
α/°	90
β/°	94.209(2)
γ/°	90
Volume/Å^3	1426.47(4)
Z	4
ρ_{calc}g/cm^3	1.198
μ/mm^{-1}	0.626
F(000)	552.0
Crystal size/mm^3	0.43 × 0.20 × 0.11
Radiation	CuKα (λ = 1.54184)
2Θ range for data collection/°	9.176 to 157.29
Index ranges	-7 ≤ h ≤ 10, -10 ≤ k ≤ 11, -24 ≤ l ≤ 24
Reflections collected	14058
Independent reflections	2929 [R_{int} = 0.0270, R_{sigma} = 0.0195]
Data/restraints/parameters	2929/0/177
Goodness-of-fit on F^2	1.113
Final R indexes [I>=2σ (I)]	R_1 = 0.0442, wR_2 = 0.1274
Final R indexes [all data]	R_1 = 0.0520, wR_2 = 0.1330
Largest diff. peak/hole / e Å^{-3}	0.14/-0.15

Figure B43. ^{1}H NMR spectrum of compound **145a** (400 MHz, $CDCl_3$).

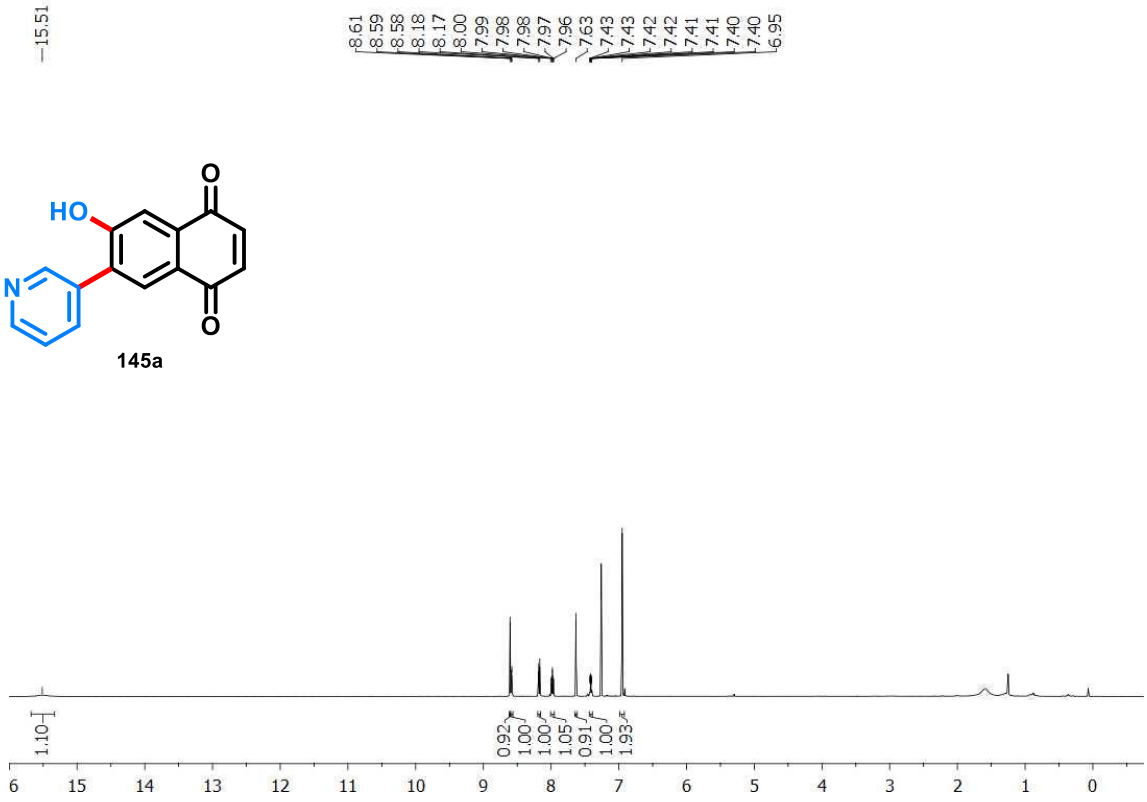

Figure B44. ^{13}C NMR spectrum of compound **145a** (100 MHz, $CDCl_3$).

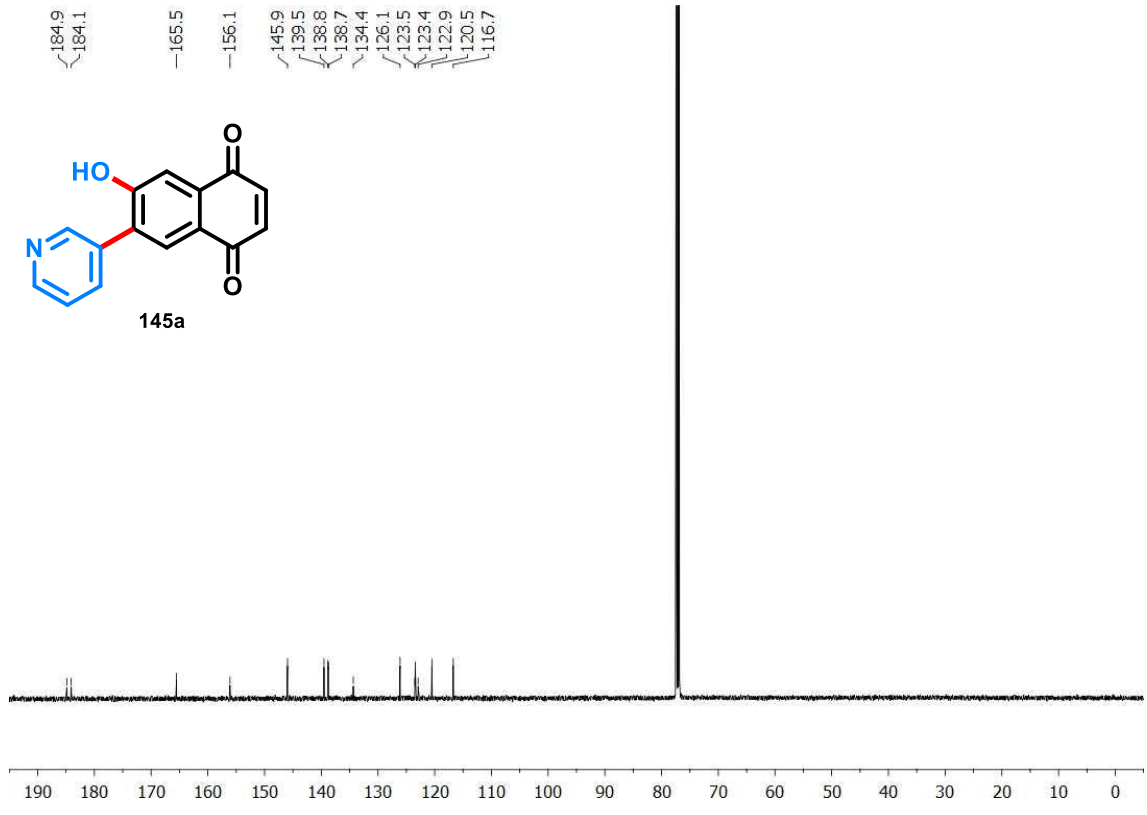

Figure B45. ^{1}H NMR spectrum of compound **145b-l** (400 MHz, $CDCl_3$).

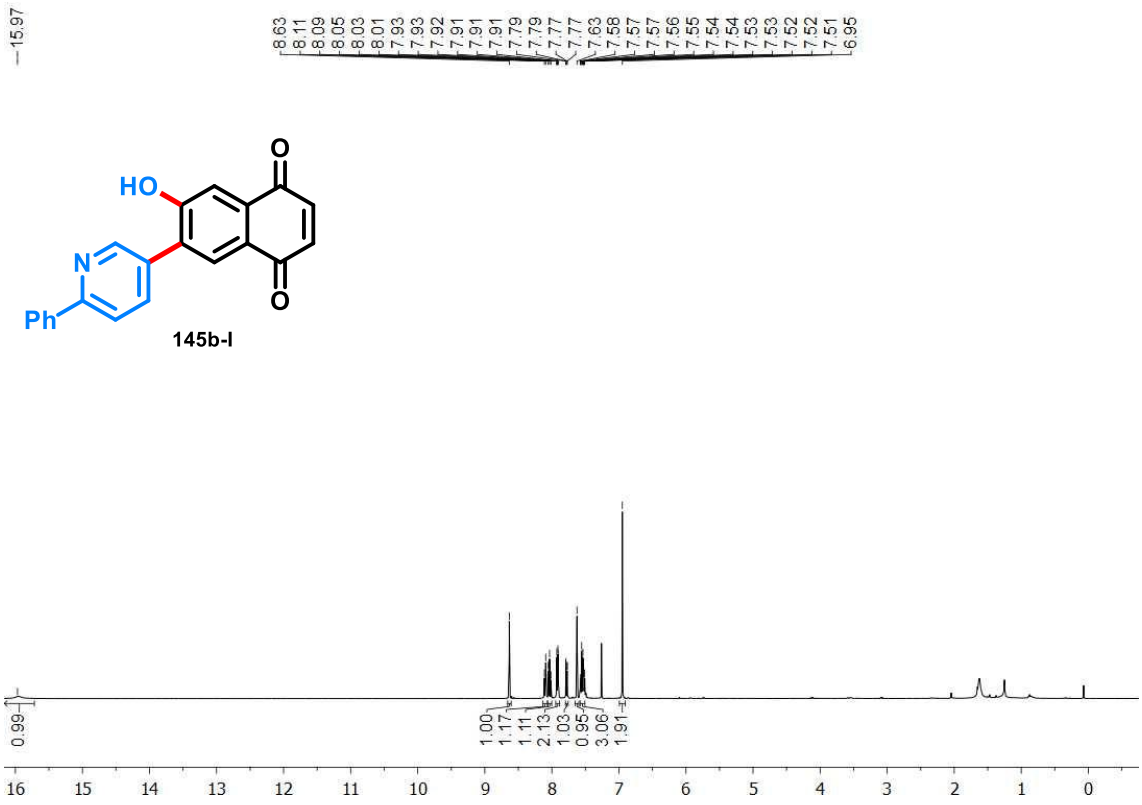

Figure B46. ^{13}C NMR spectrum of compound **145b-l** (100 MHz, $CDCl_3$).

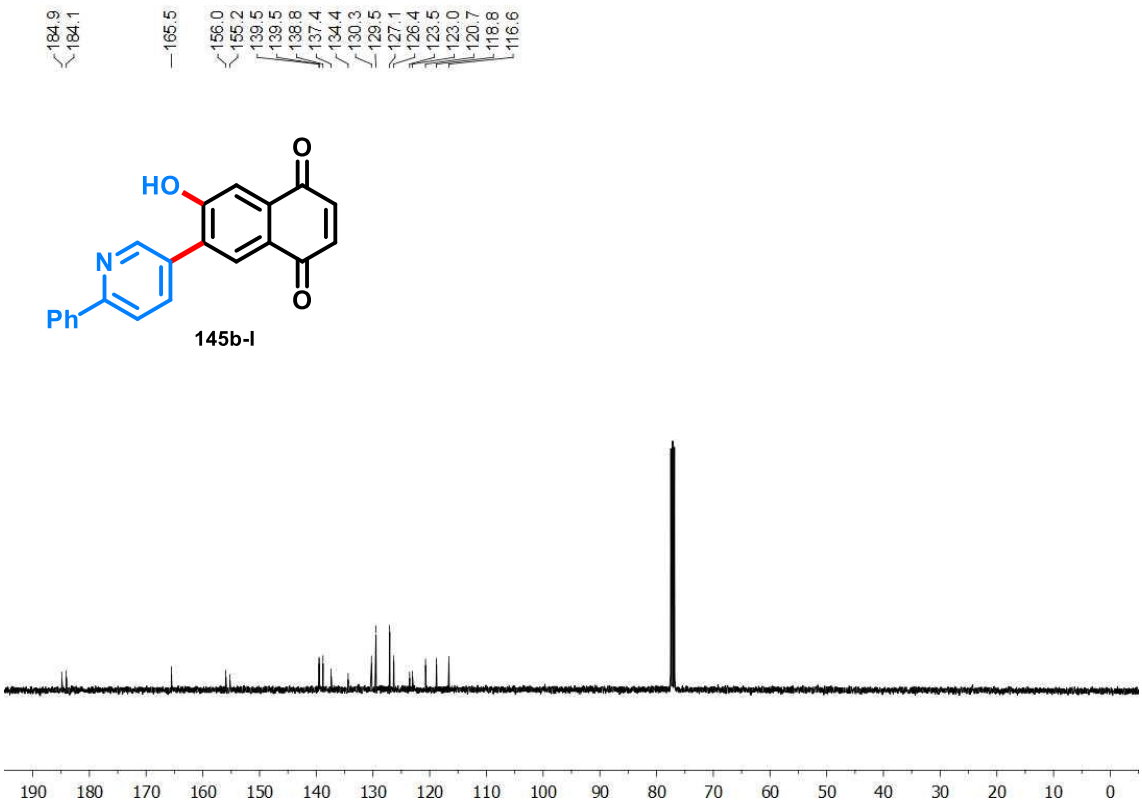

Figure B47. ^{1}H NMR spectrum of compound **145b**-II (400 MHz, $CDCl_3$).

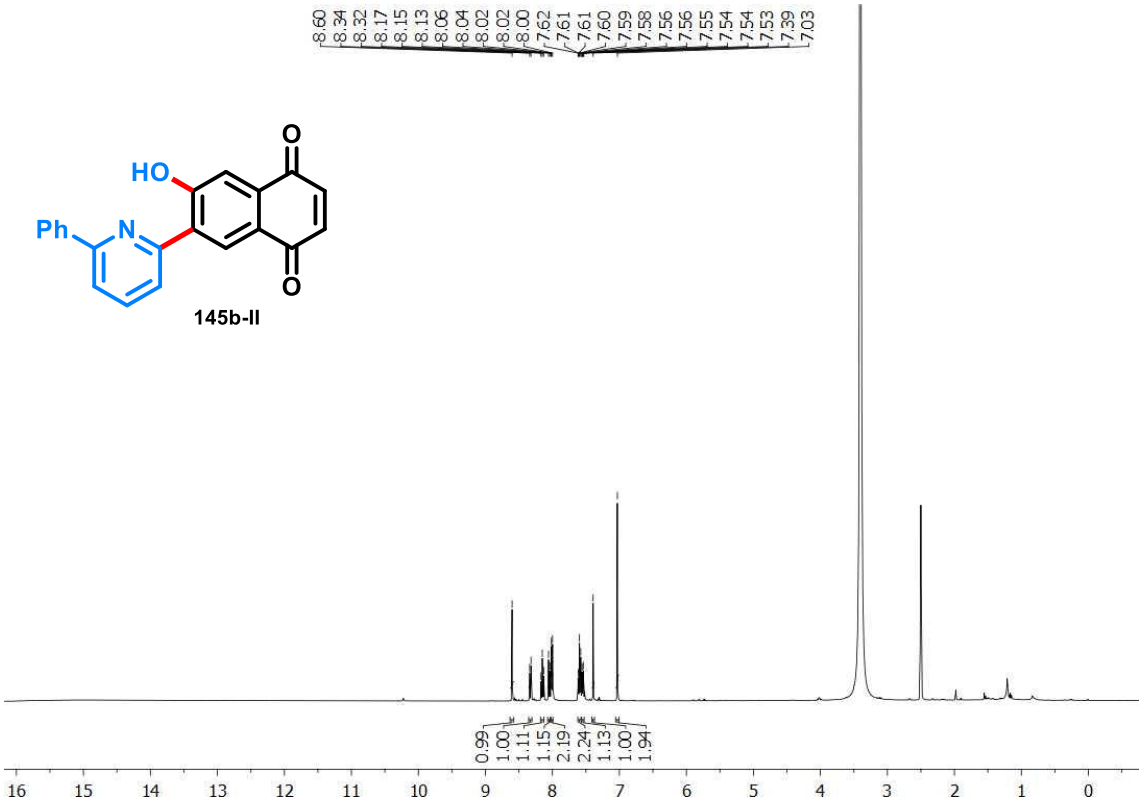

Figure B48. ^{13}C NMR spectrum of compound **145b-II** (100 MHz, $CDCl_3$).

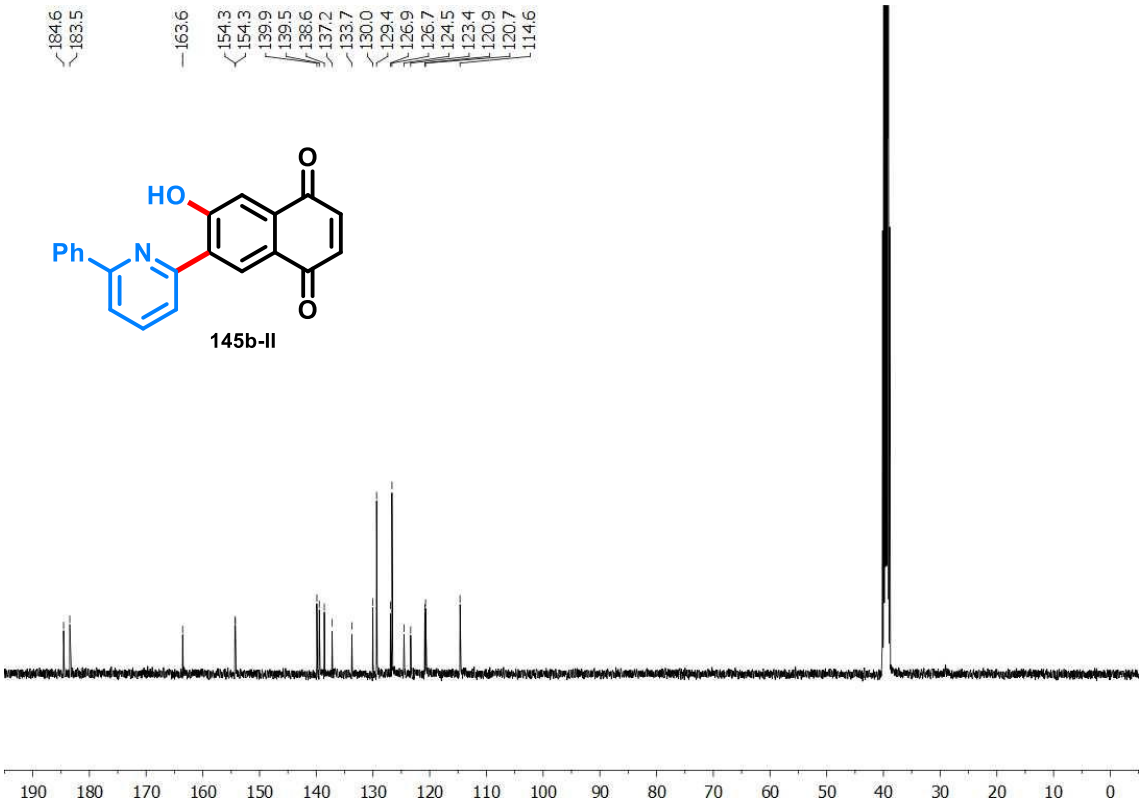

Figure B49. ^{1}H NMR spectrum of compound **145c** (400 MHz, $CDCl_3$).

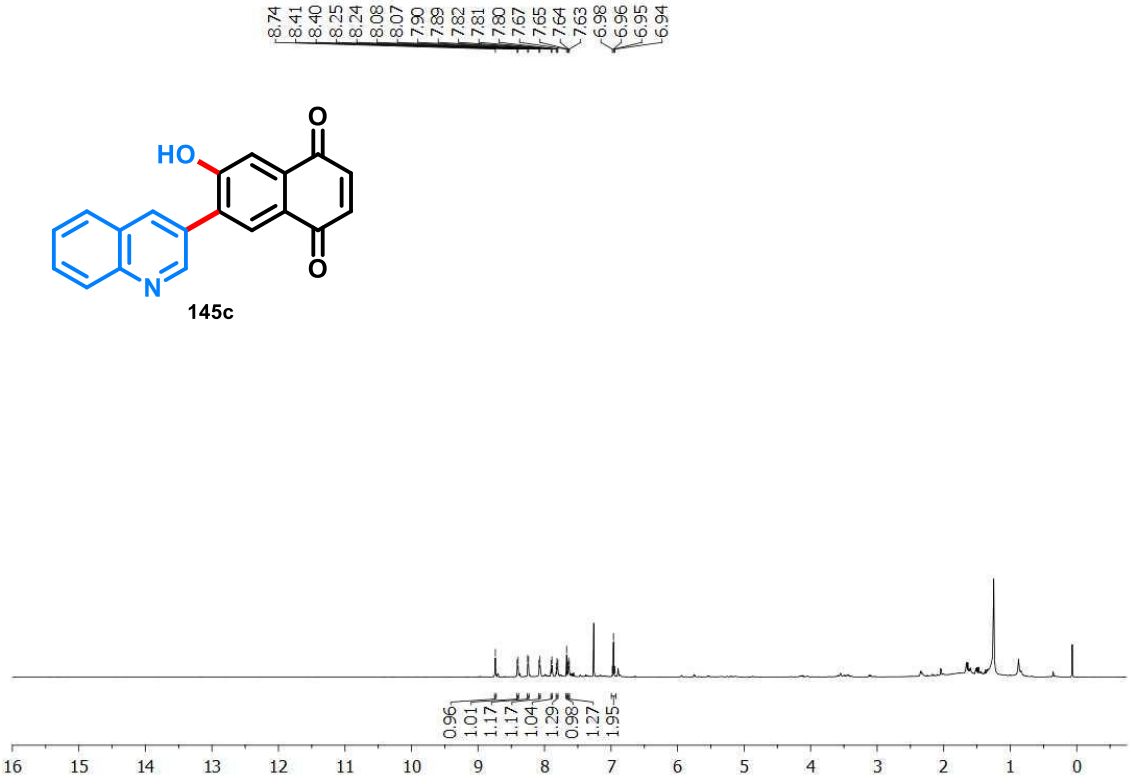

Figure B50. ^{13}C NMR spectrum of compound **145c** (100 MHz, $CDCl_3$).

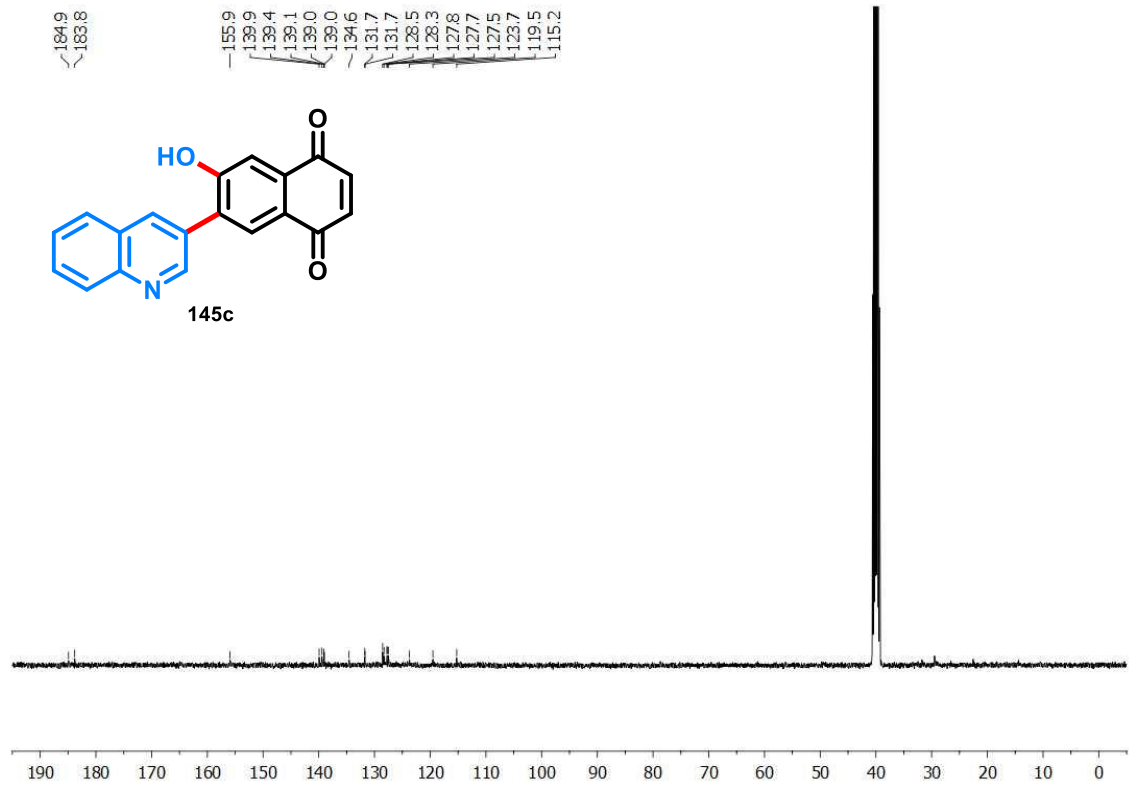

Figure B51. ^{1}H NMR spectrum of compound **145d** (400 MHz, $CDCl_3$).

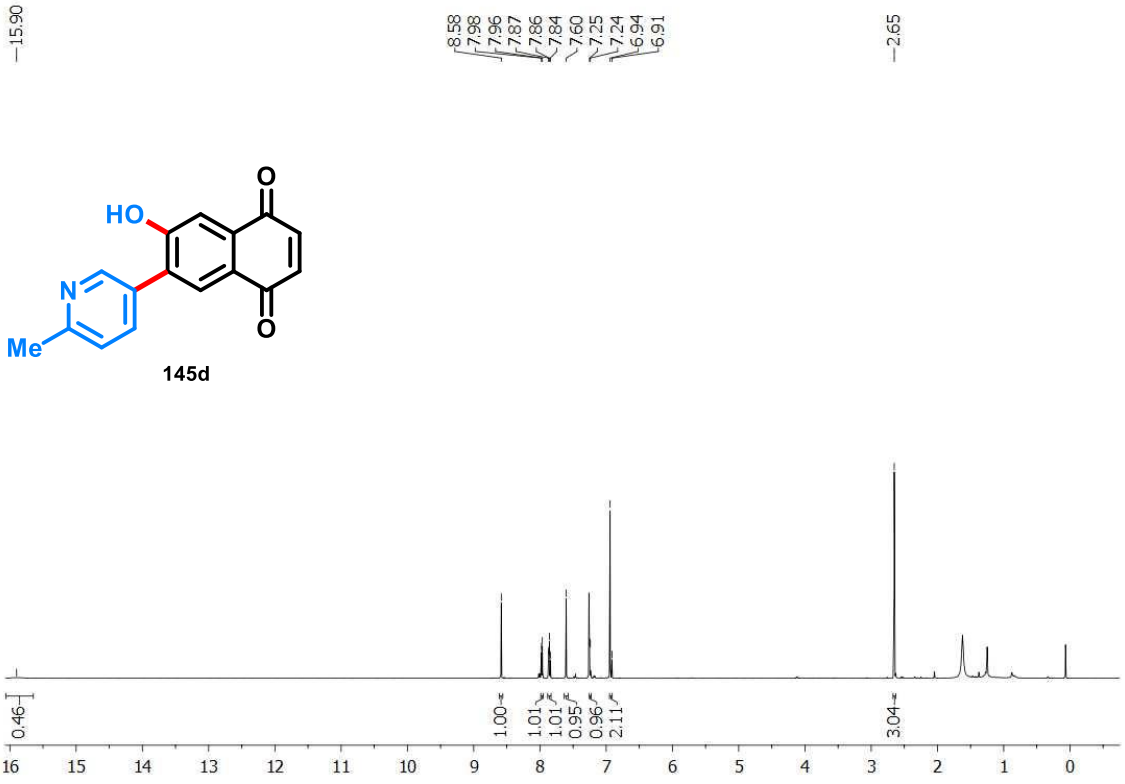

Figure B52. ^{13}C NMR spectrum of compound **145d** (100 MHz, $CDCl_3$).

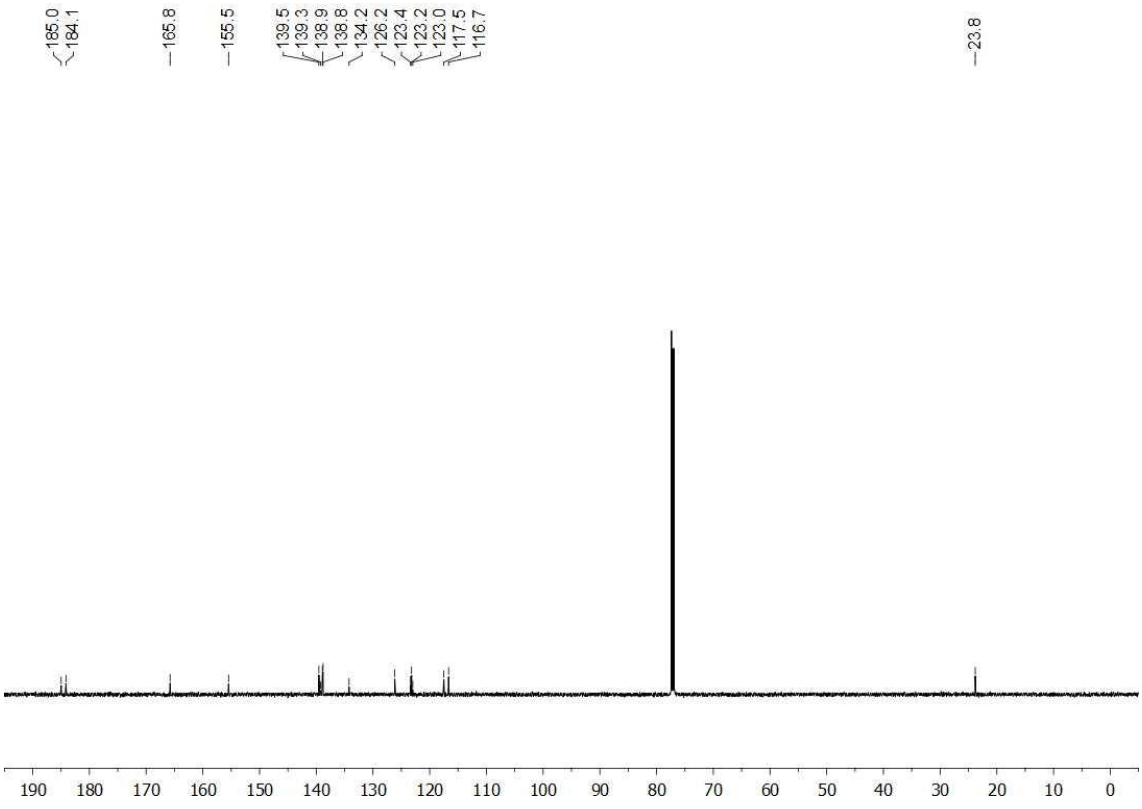

Figure B53. ^{1}H NMR spectrum of compound **145e** (400 MHz, $CDCl_3$).

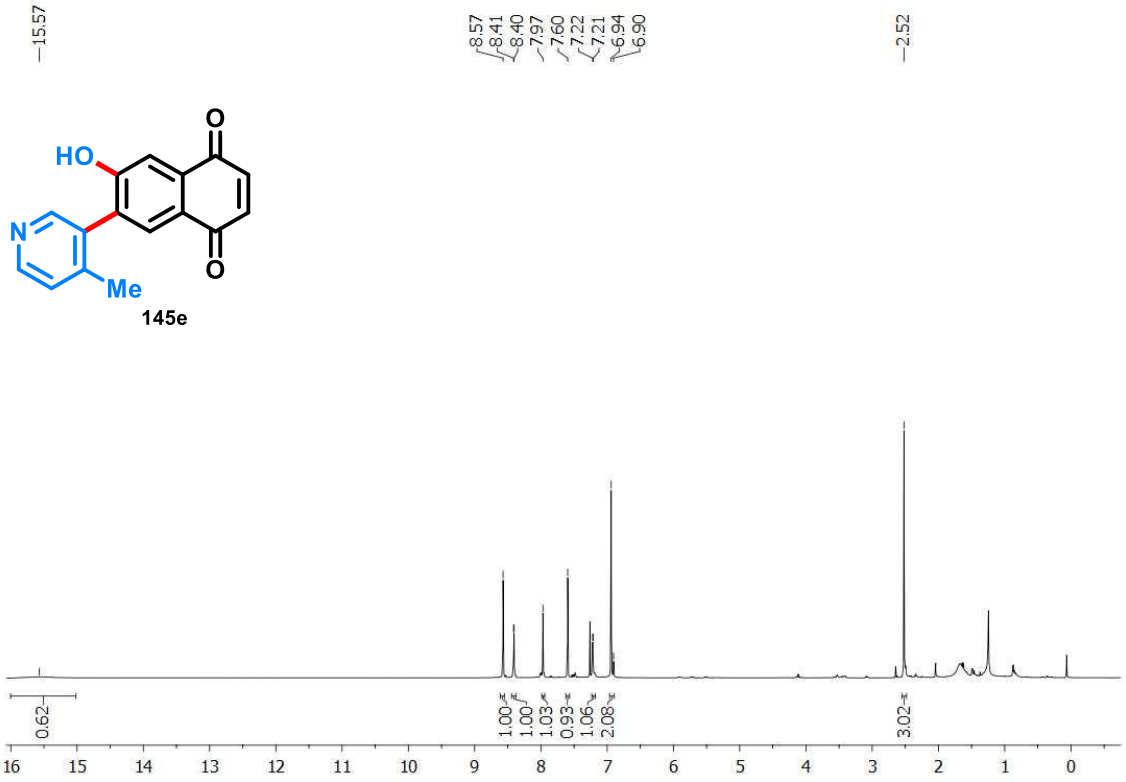

Figure B54. ^{13}C NMR spectrum of compound **145e** (100 MHz, $CDCl_3$).

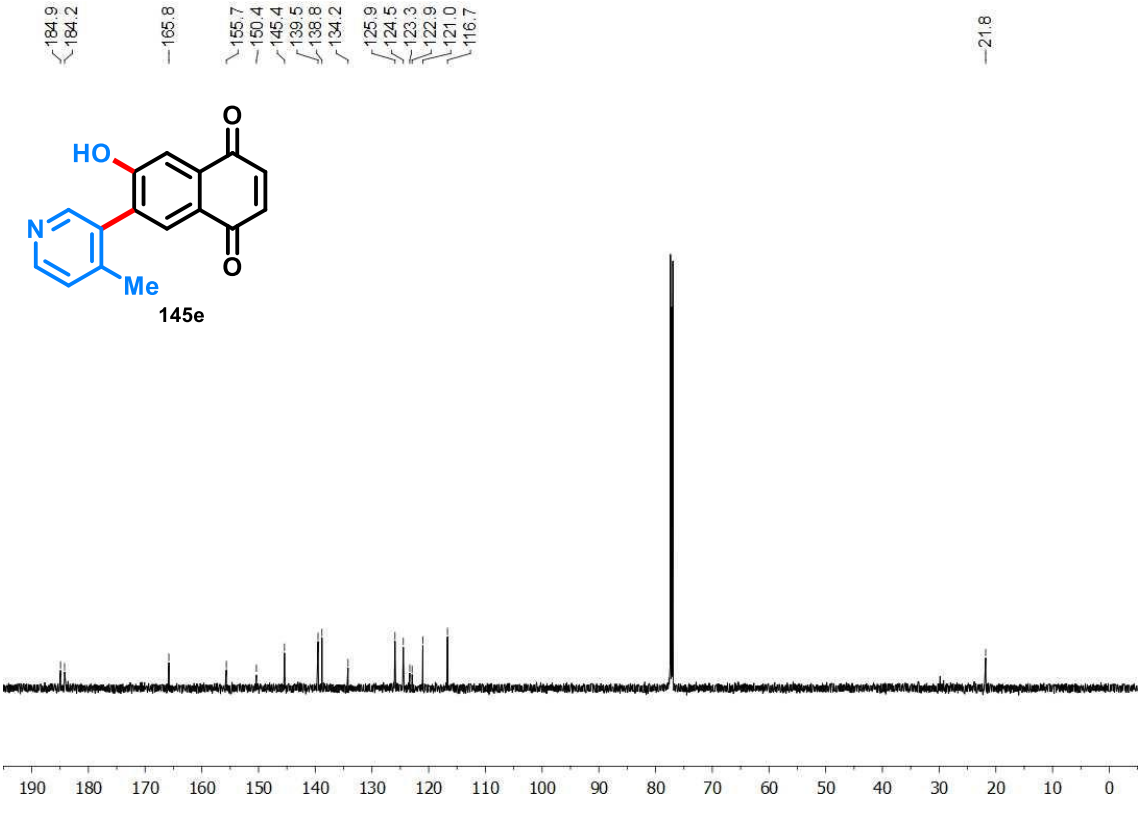

APPENDICES C - Characterization of the compounds Chapter 3

Figure C1. ^{1}H NMR spectrum of compound **177** (400 MHz, $CDCl_3$).

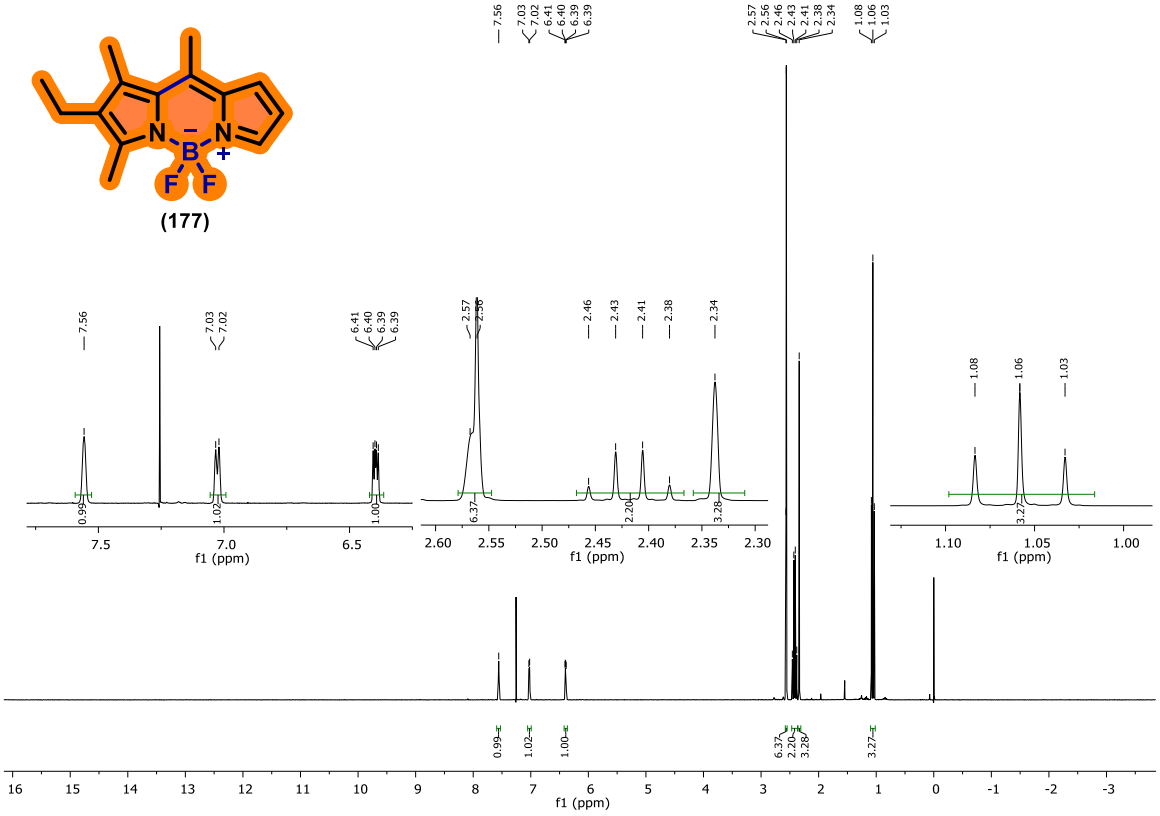

Figure C2. ^{13}C NMR spectrum of compound **177** (100 MHz, $CDCl_3$).

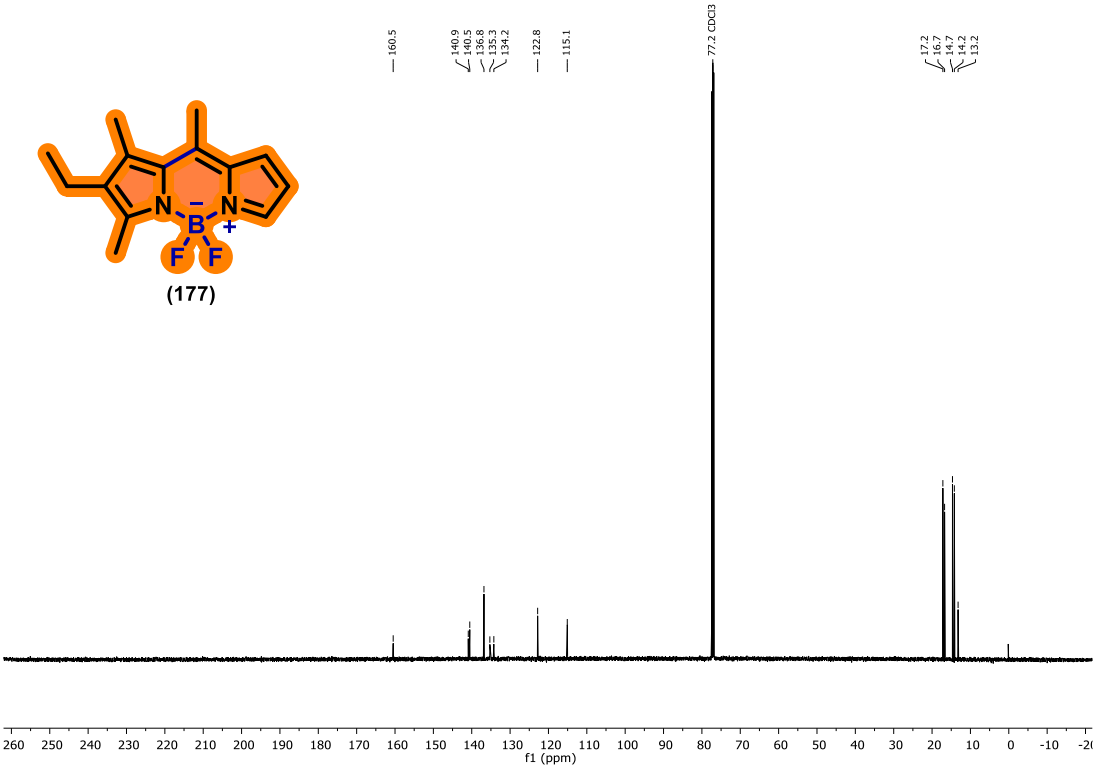

Figure C3. ^{11}B NMR spectrum of compound **177** (564.7MHz, $CDCl_3$).

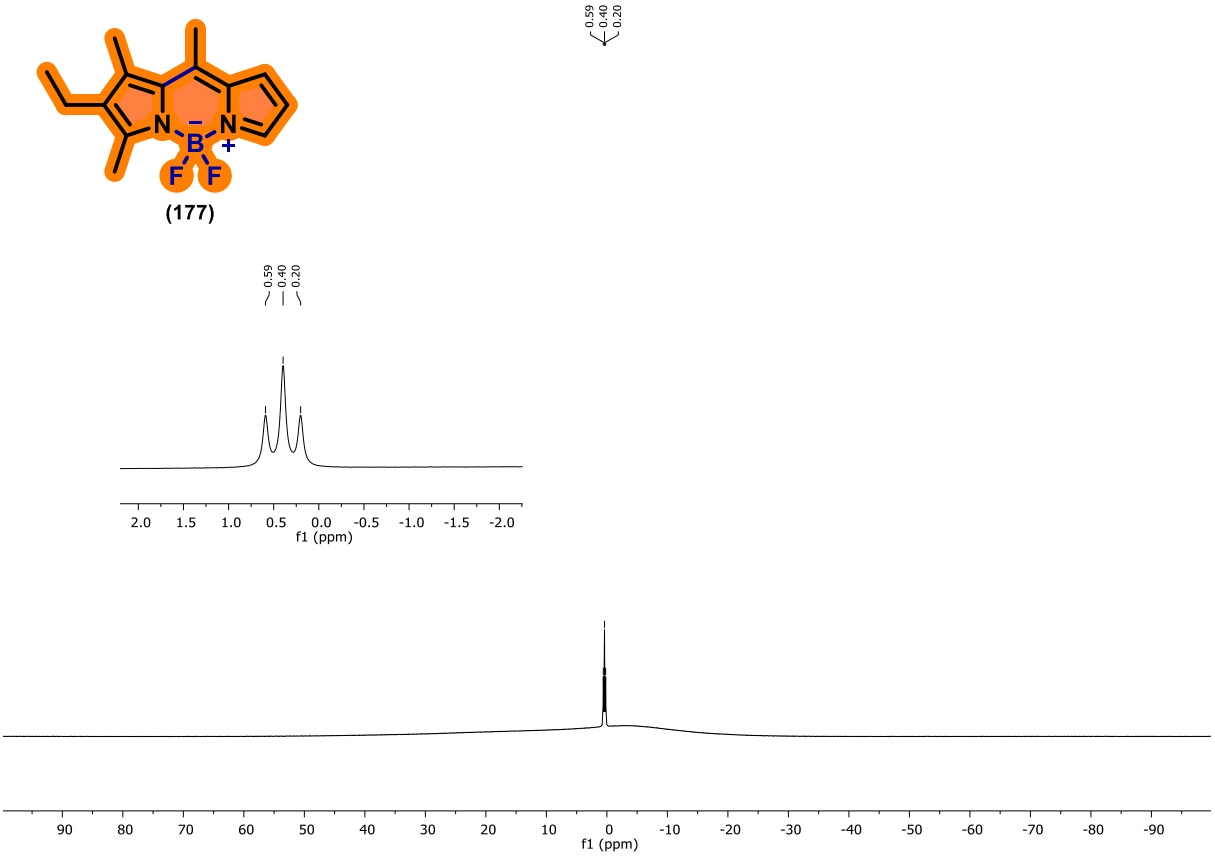

Figure C4. ^{19}F NMR spectrum of compound **177** (564.7MHz, $CDCl_3$).

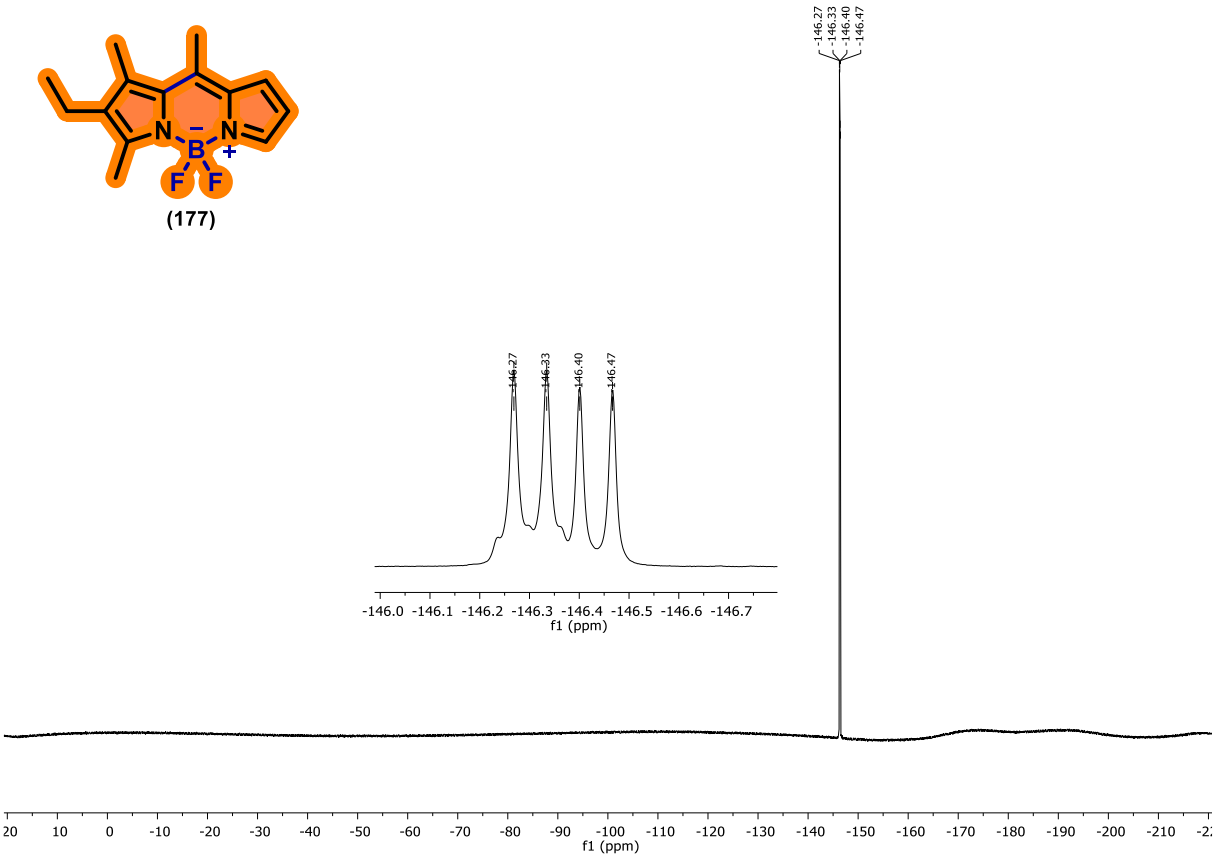

Figure C5. FTIR Spectrum of compound **177**.

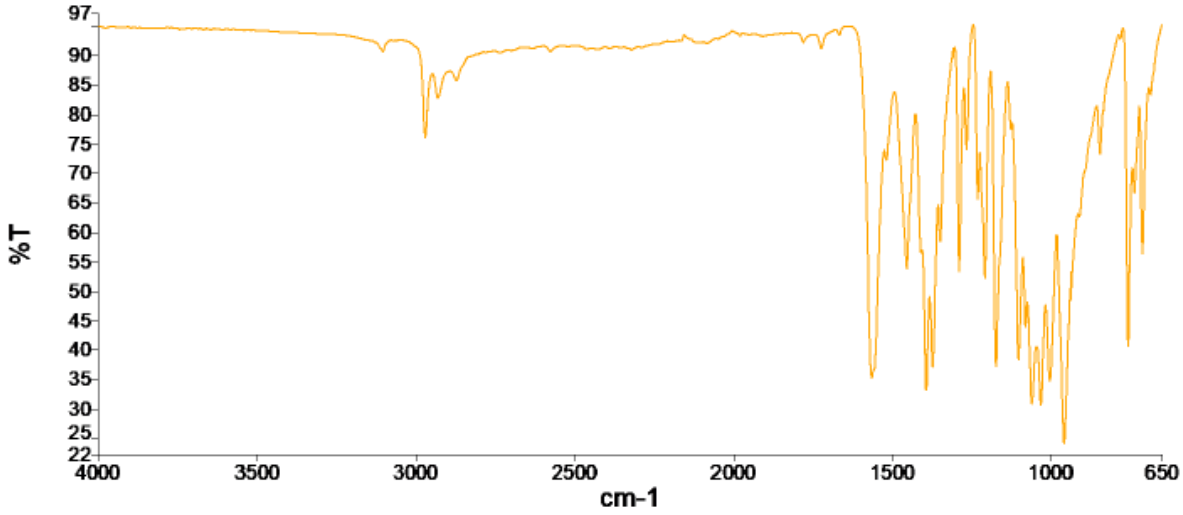

Figure C6. HRMS (ESI +) of compound **177**.

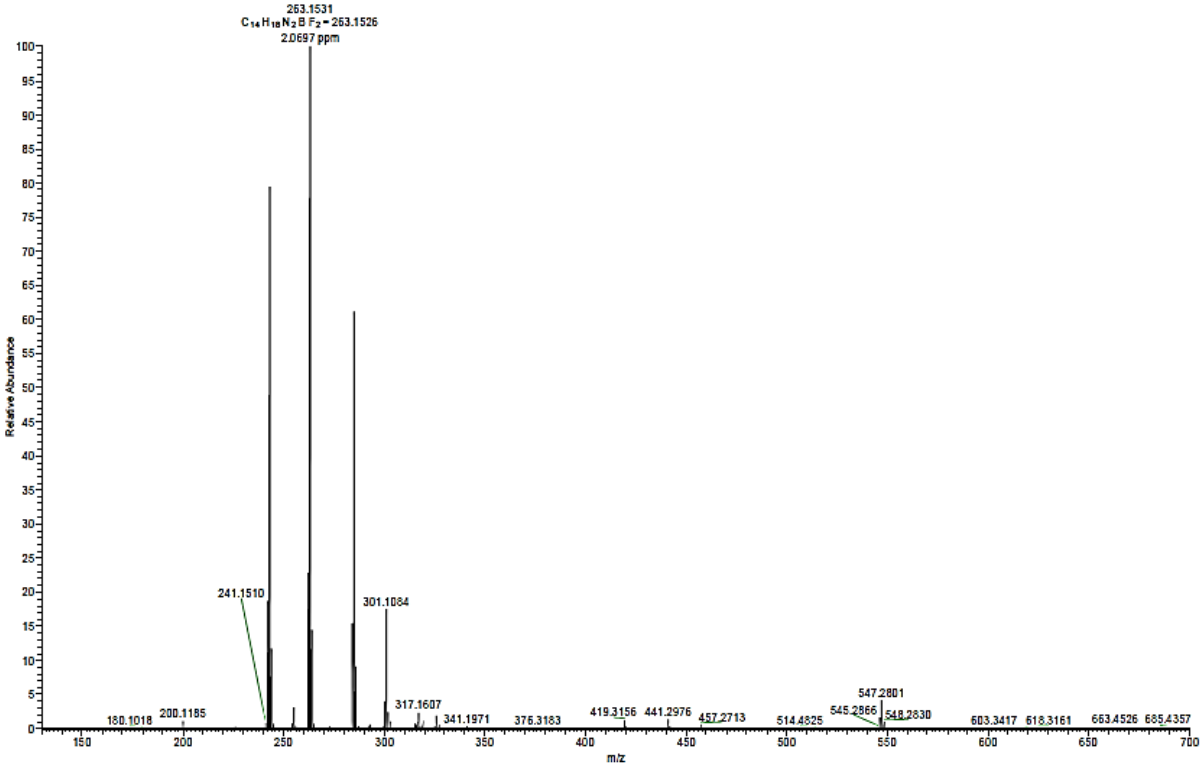

Figure C7. ^{1}H NMR spectrum of compound **178** (400 MHz, $CDCl_3$).

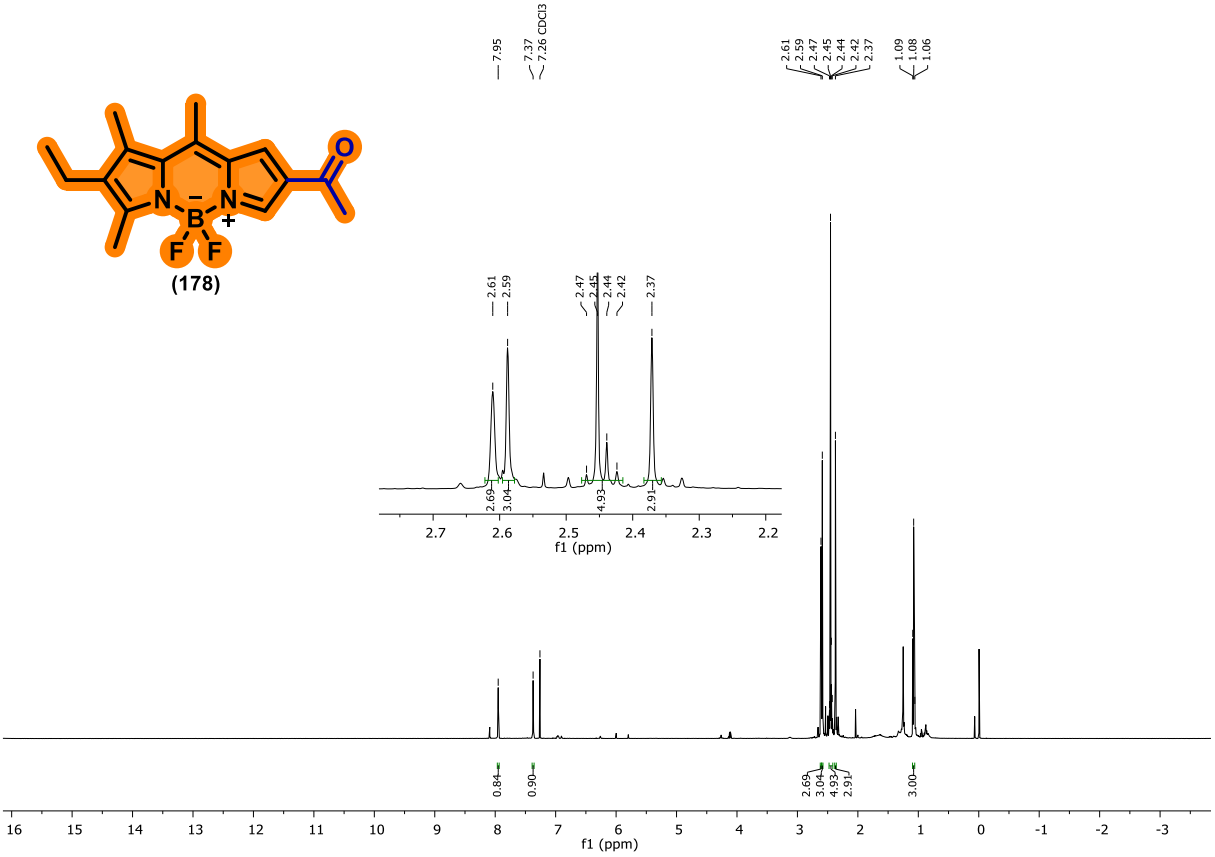

Figure C8. ^{13}C NMR spectrum of compound **178** (100 MHz, CDCl3).

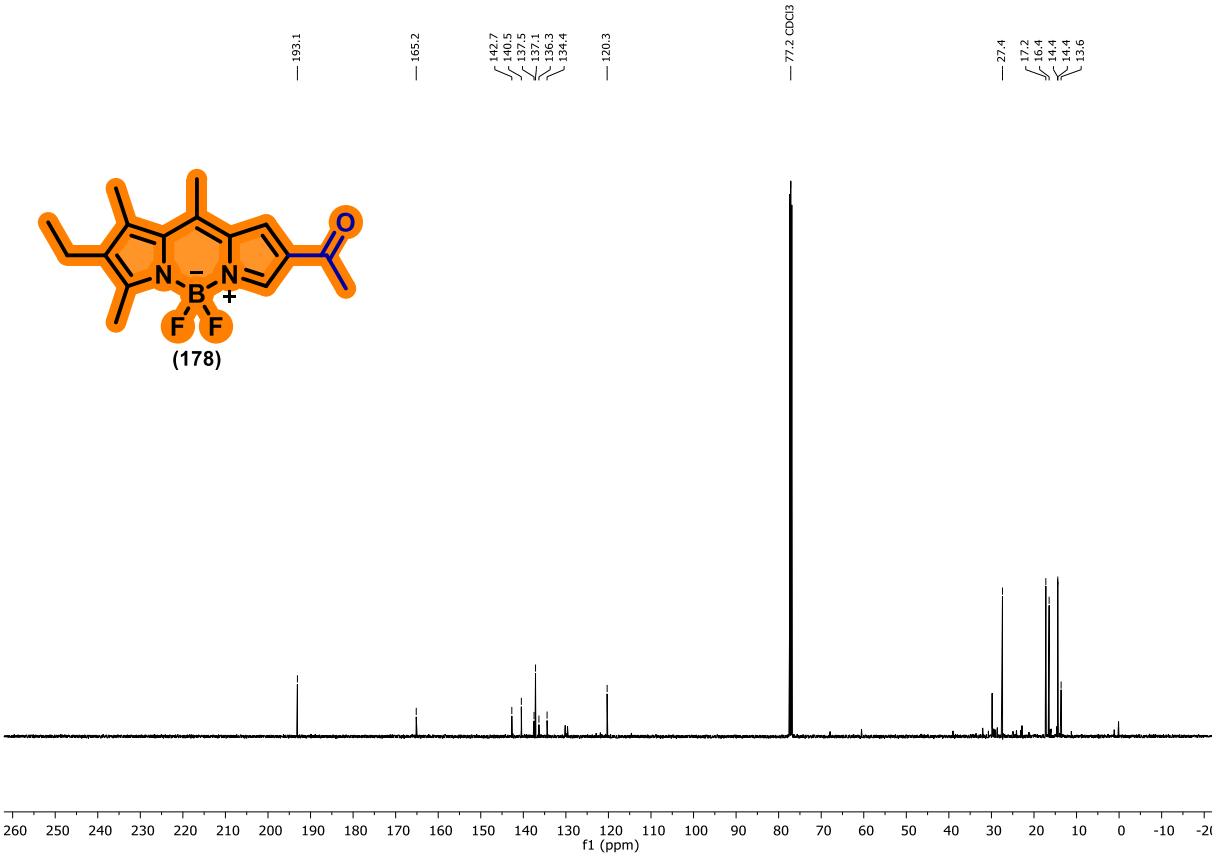

Figure C9. ^{11}B NMR spectrum of compound **178** (564.7MHz, $CDCl_3$).

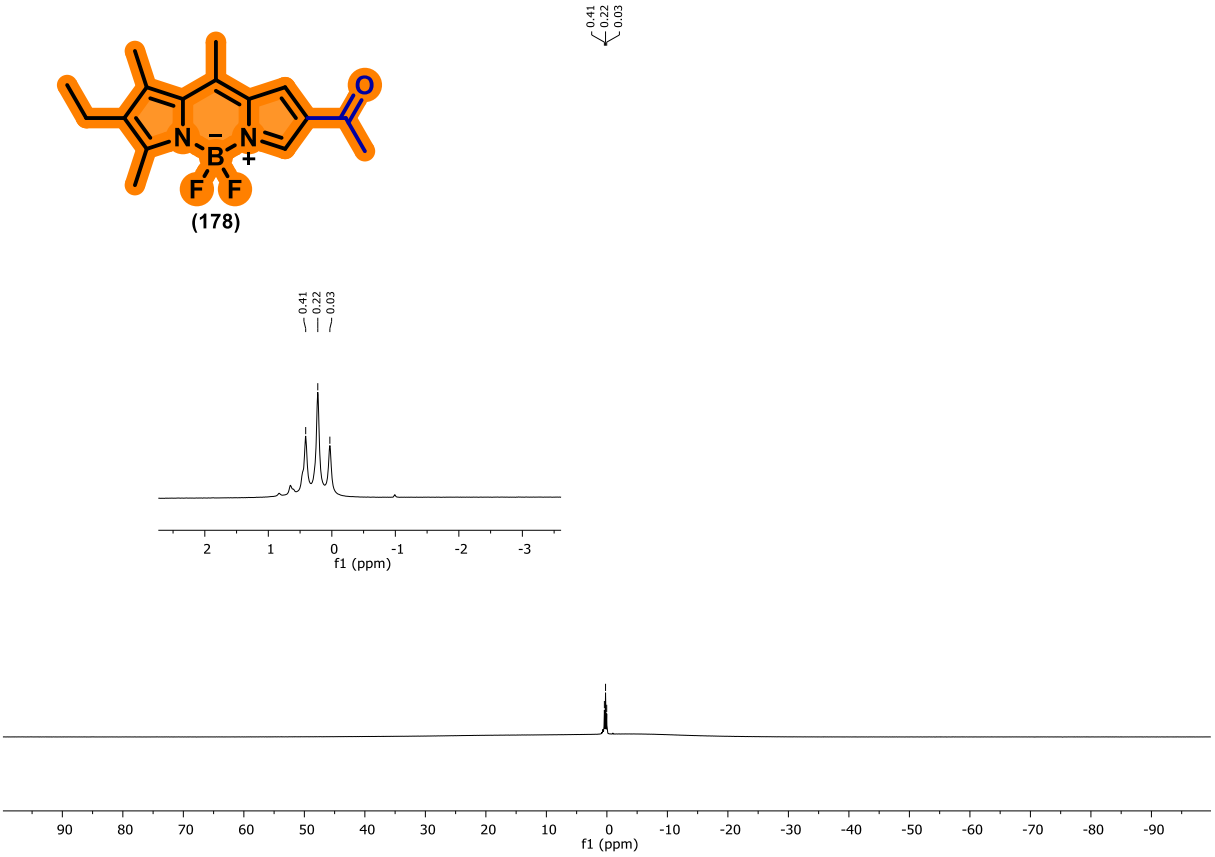

Figure C10. ^{19}F NMR spectrum of compound **178** (564.7MHz, $CDCl_3$).

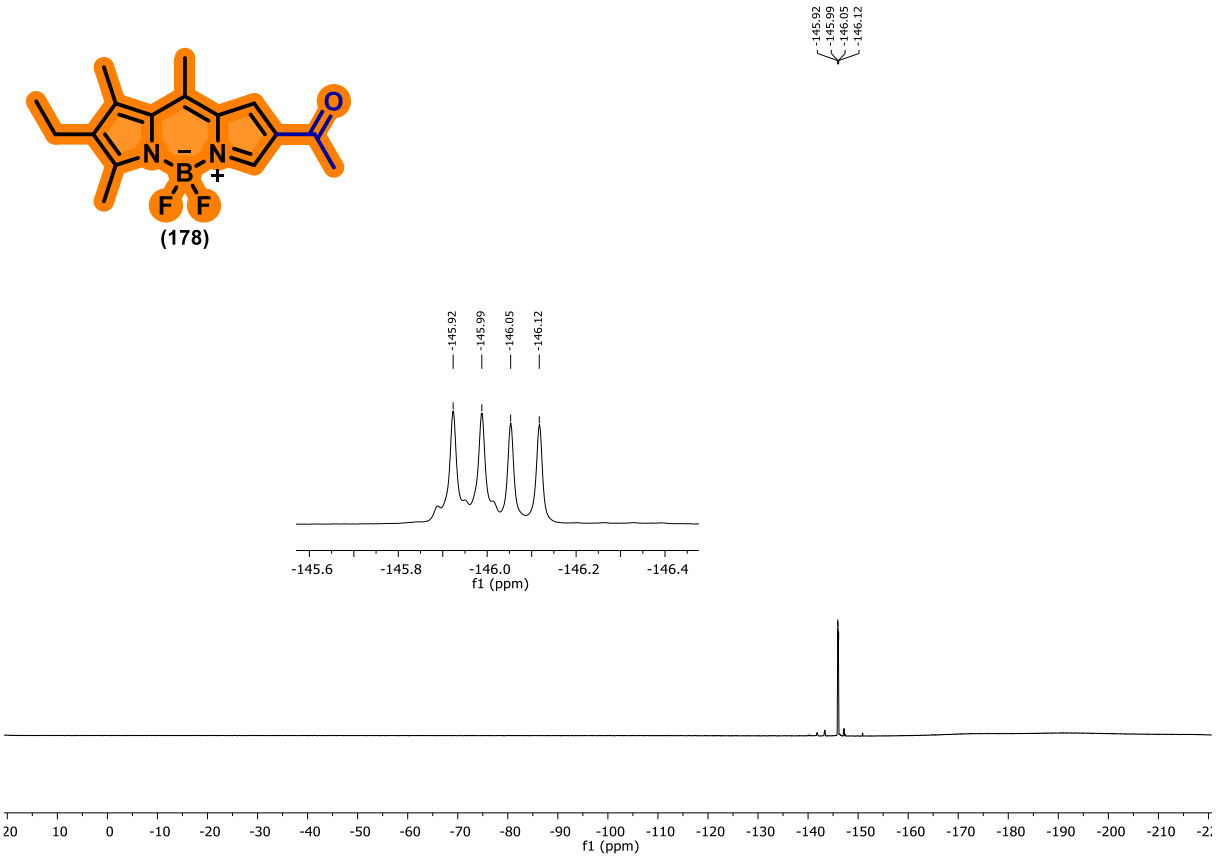

Figure C11. FTIR Spectrum of compound **178**.

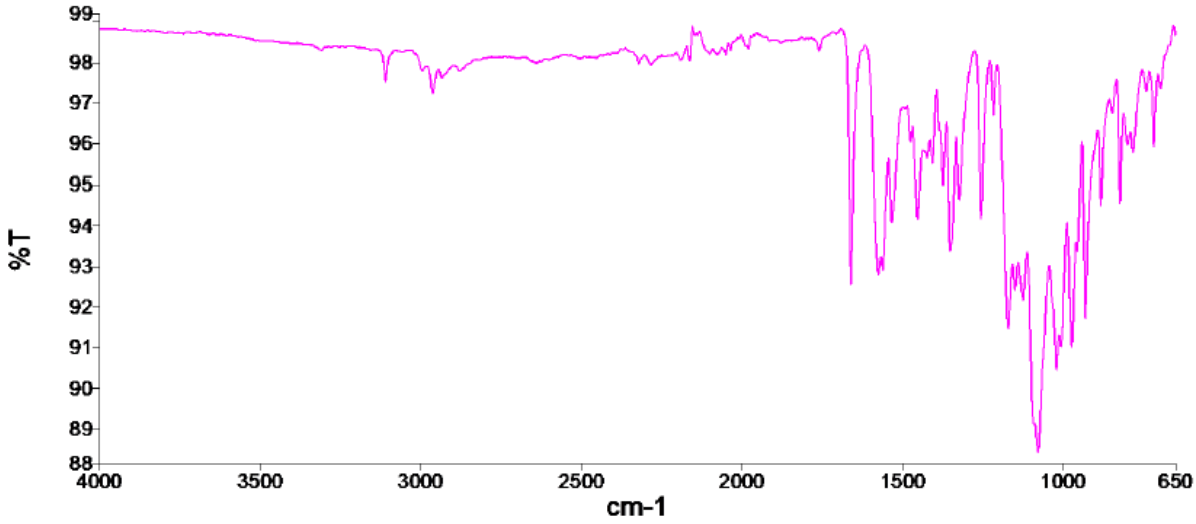

Figure C12. HRMS (ESI +) of compound **178**.

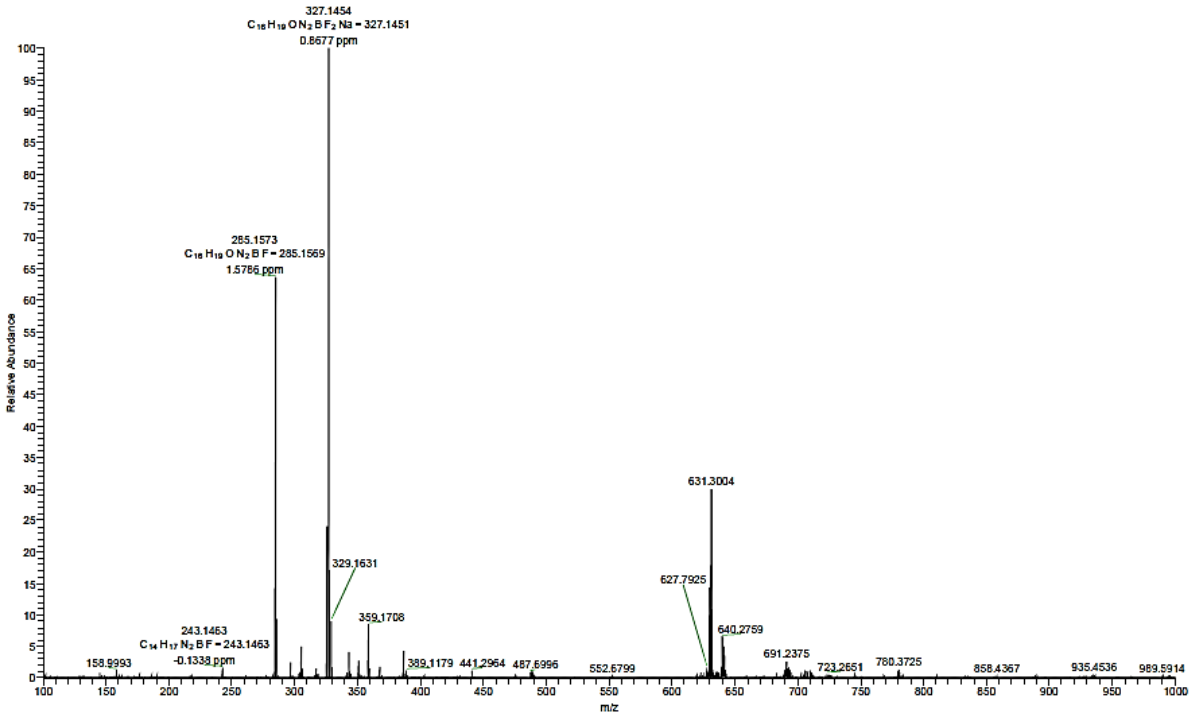

Figure C13. ^{1}H NMR spectrum of compound **179** (400 MHz, $CDCl_3$).

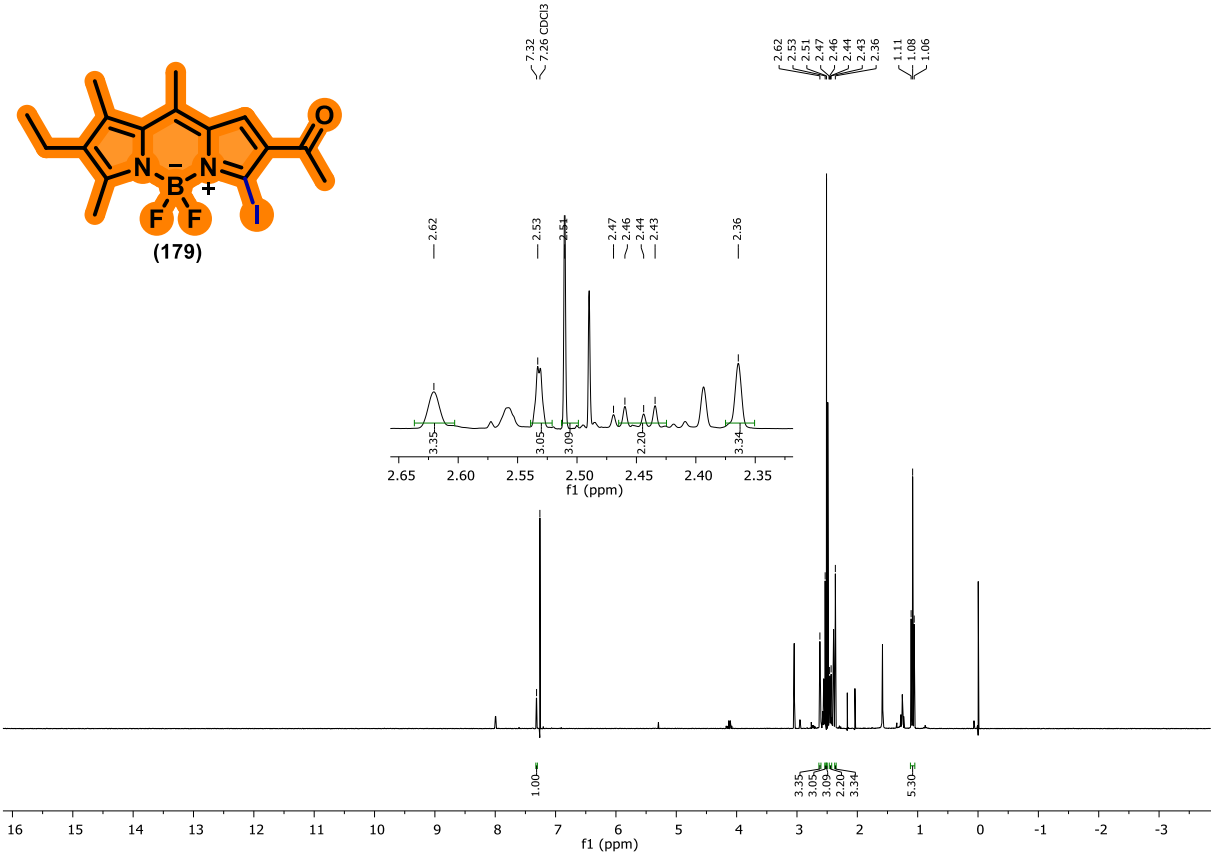

Figure C14. ^{13}C NMR spectrum of compound **179** (100 MHz, $CDCl_3$).

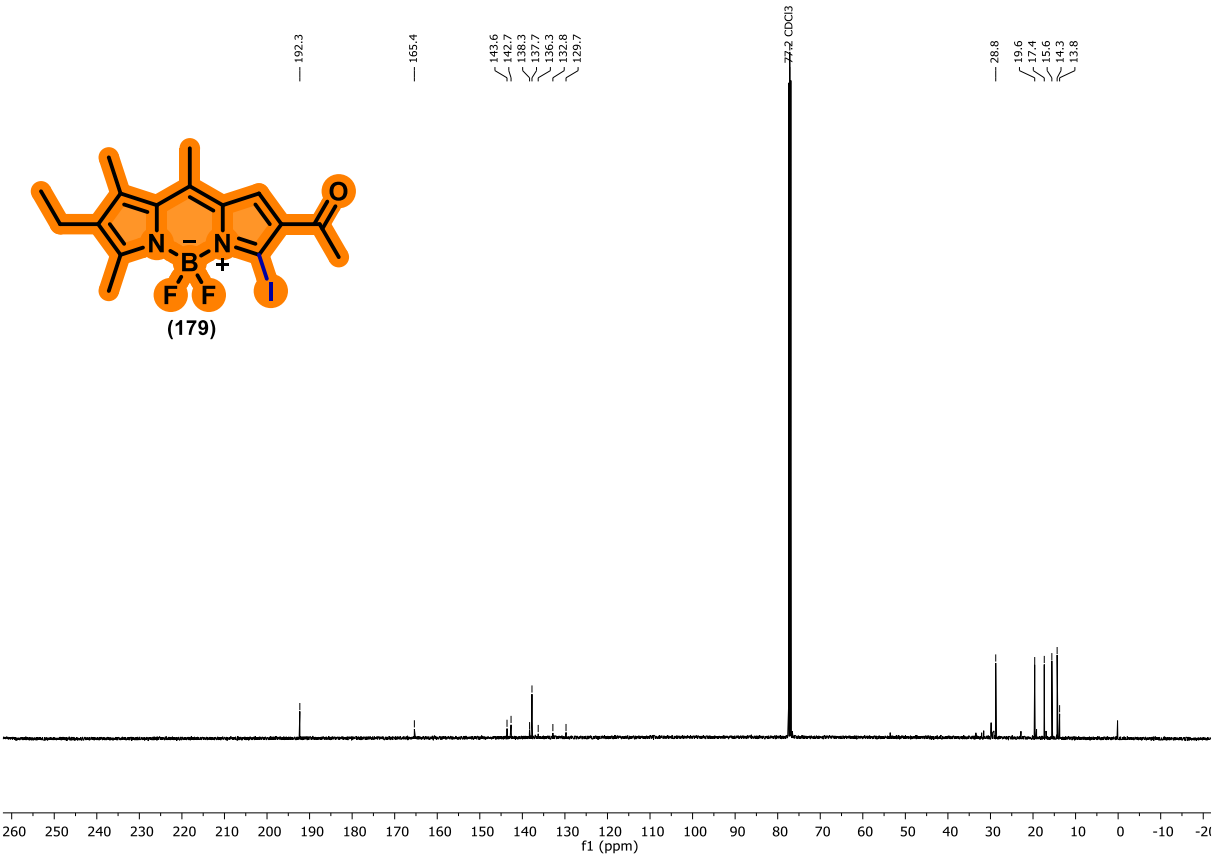

Figure C15. ^{11}B NMR spectrum of compound **179** (564.7MHz, $CDCl_3$).

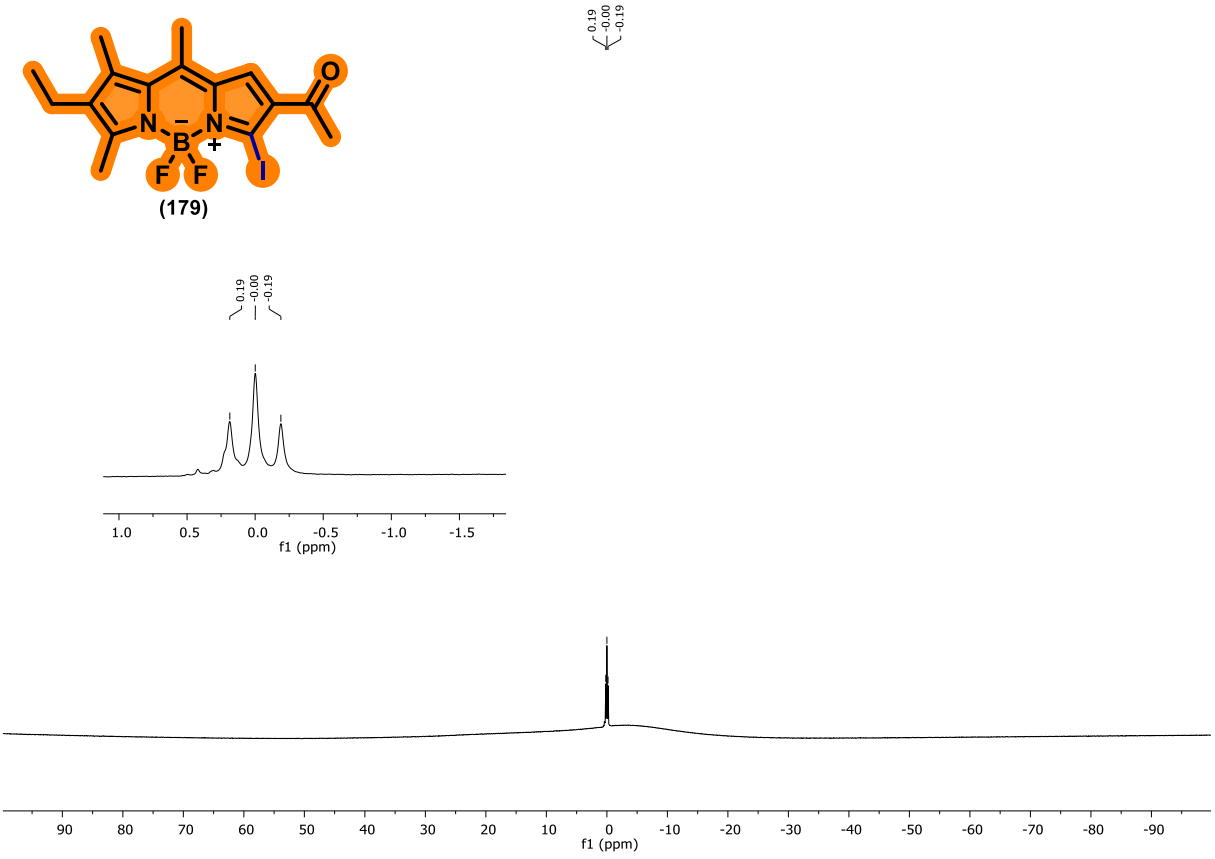

Figure C16. ^{19}F NMR spectrum of compound **179** (564.7MHz, $CDCl_3$).

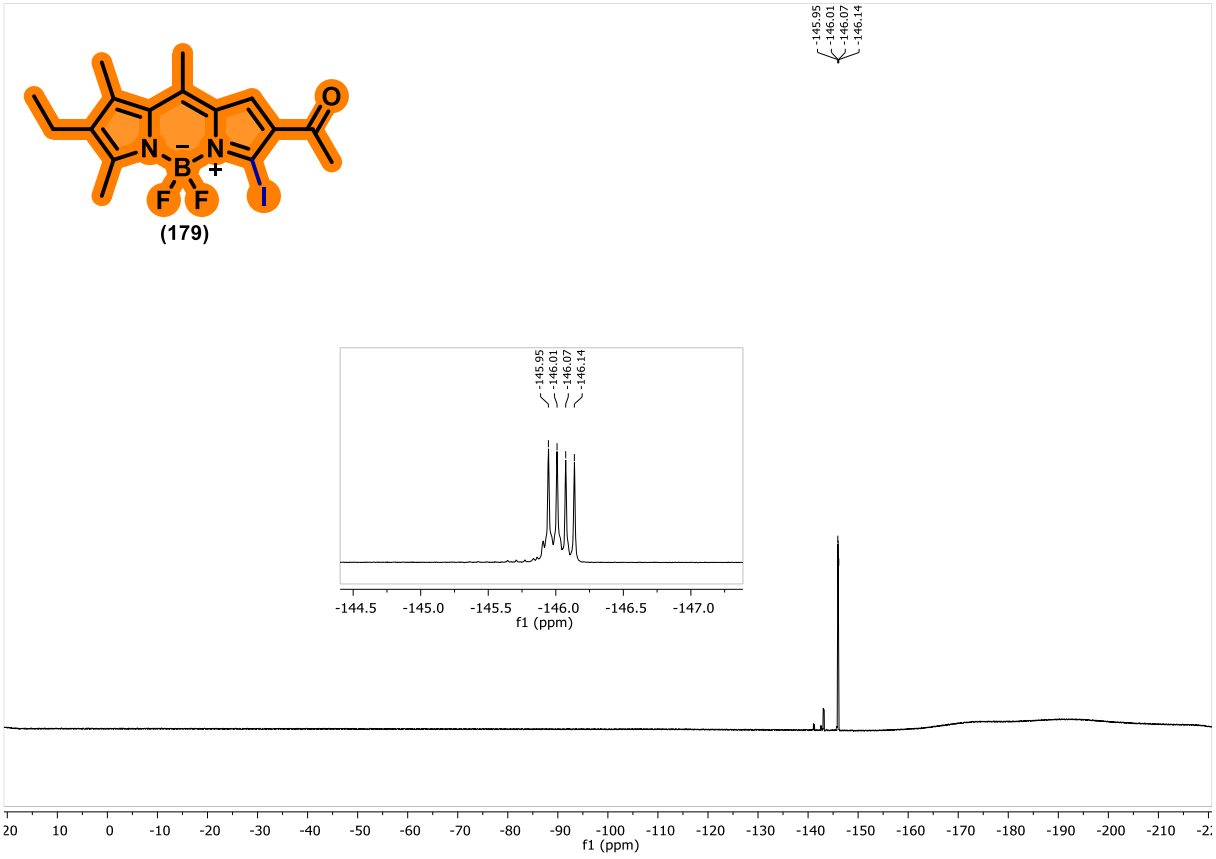

Figure C17. FTIR Spectrum of compound **179**.

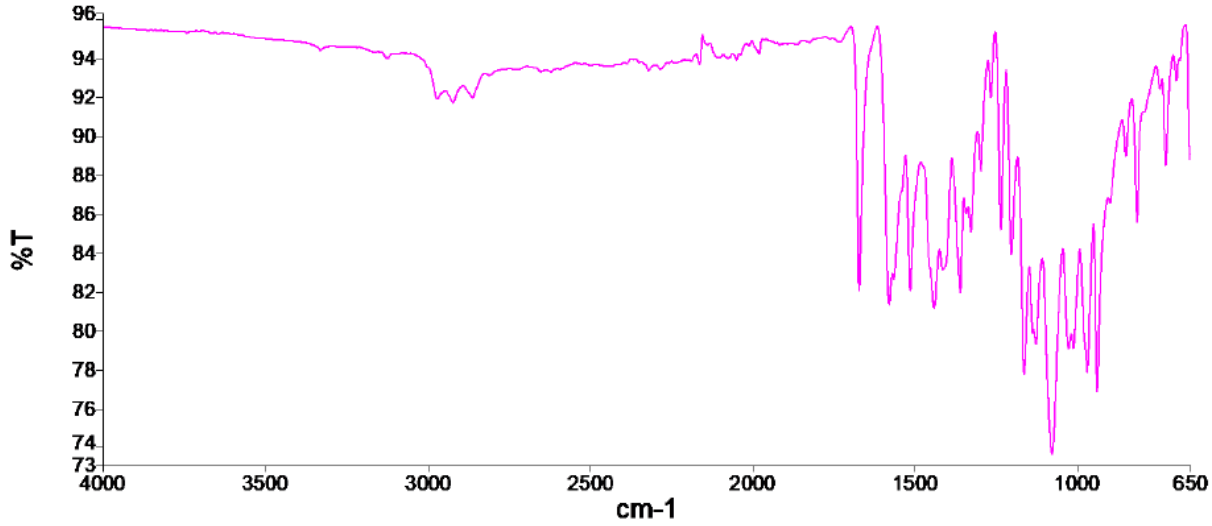

Figure C18. HRMS (ESI +) of compound **179**.

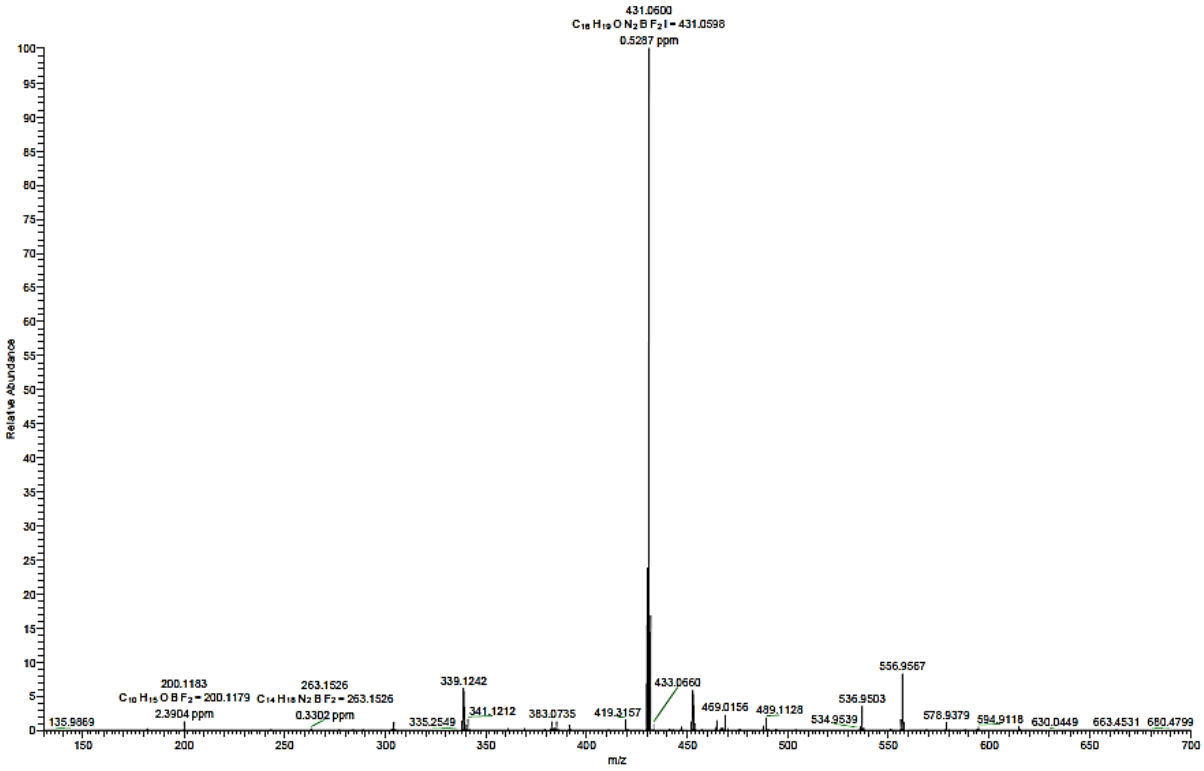

Figure C19. ^{1}H NMR spectrum of compound **180** (400 MHz, $CDCl_3$).

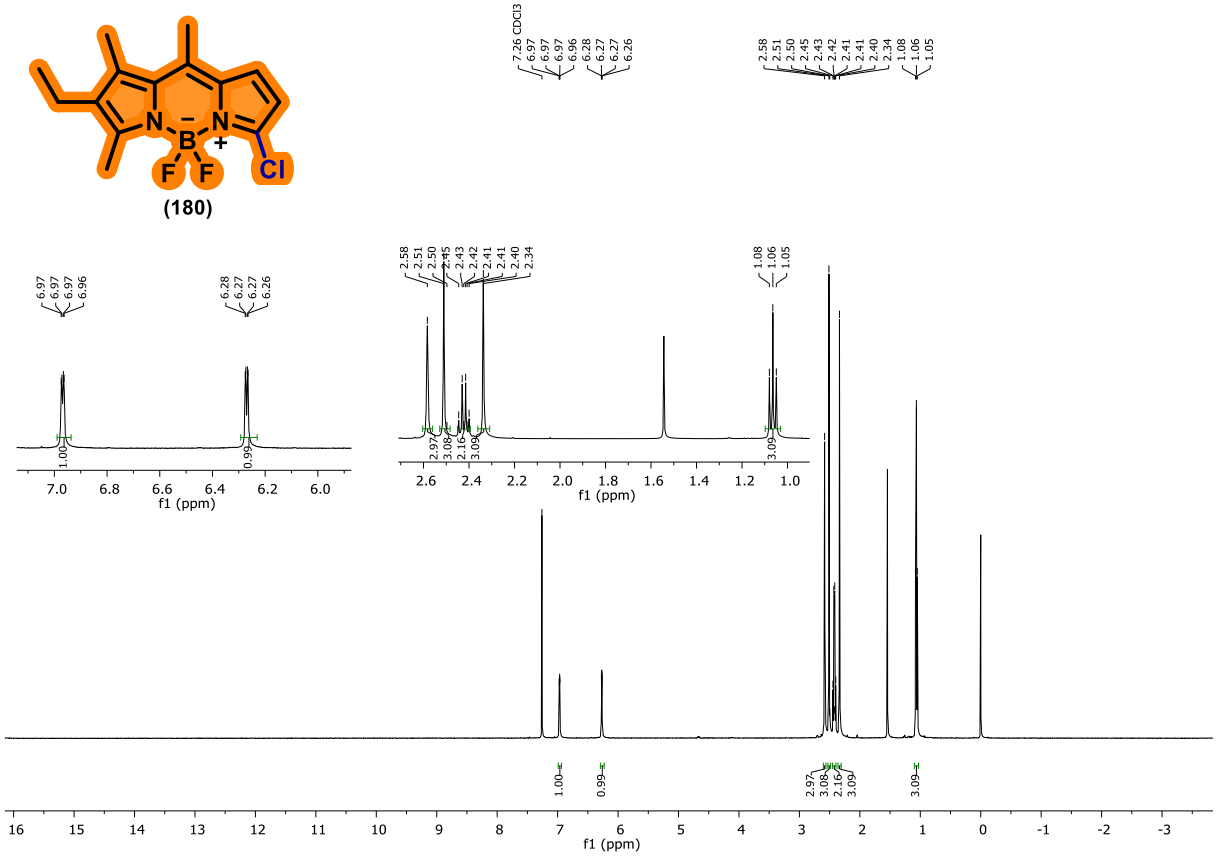

Figure C20. ^{13}C NMR spectrum of compound **180** (100 MHz, $CDCl_3$).

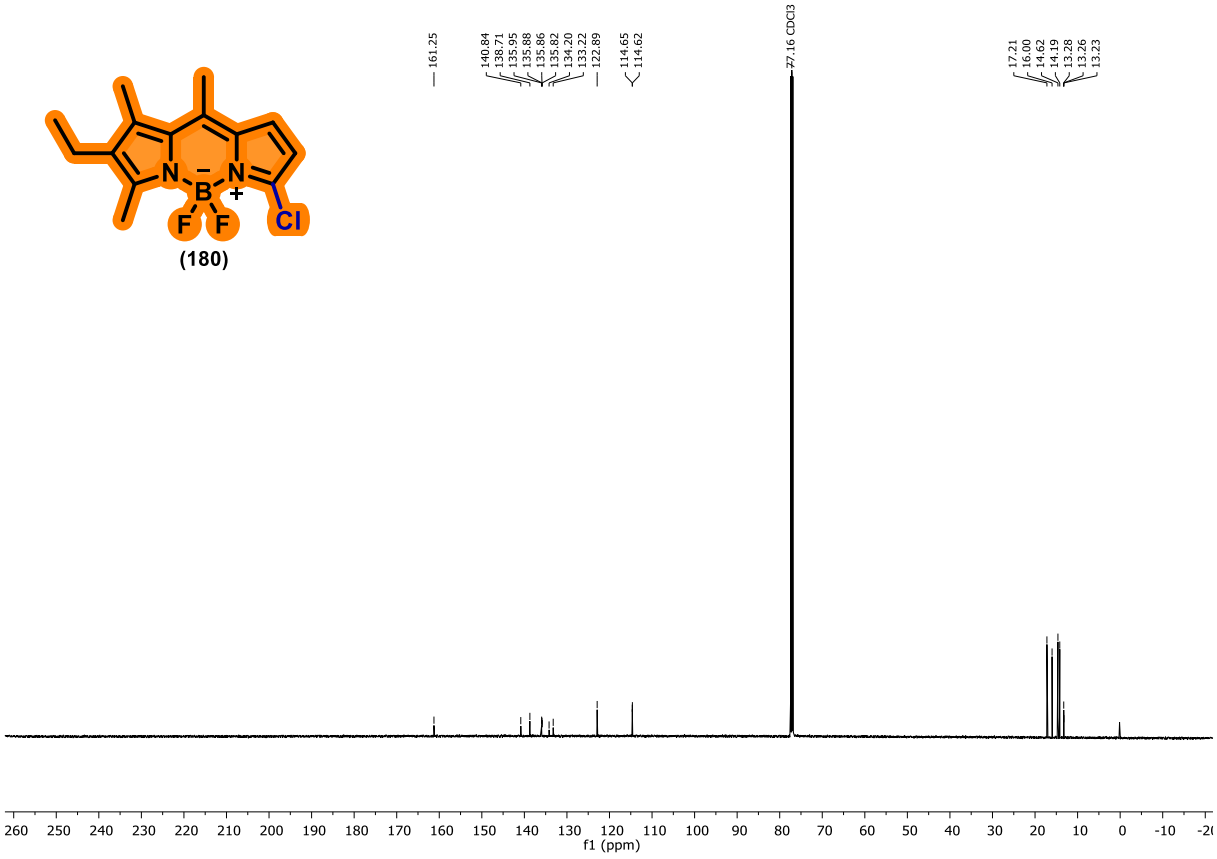

Figure C21. ^{11}B NMR spectrum of compound **180** (564.7MHz, $CDCl_3$).

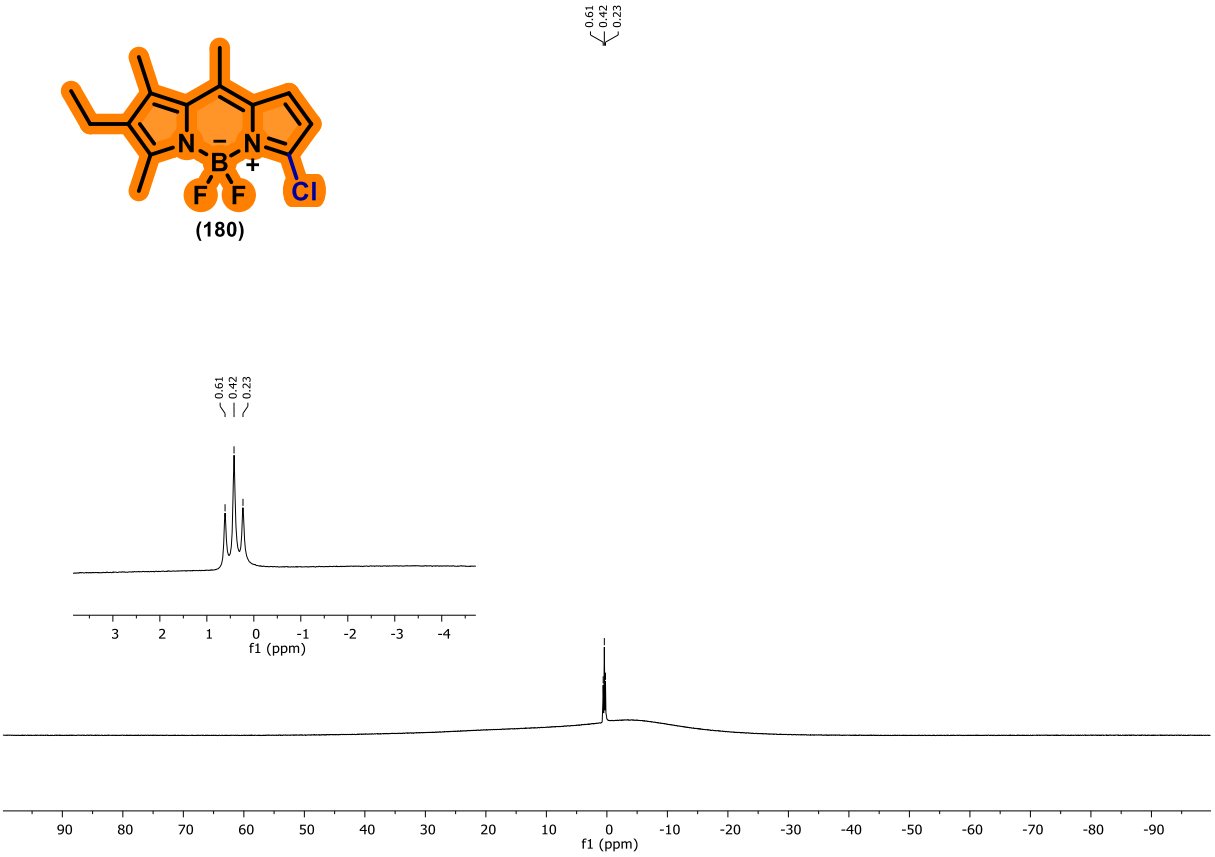

Figure C22. ^{19}F NMR spectrum of compound **180** (564.7MHz, $CDCl_3$).

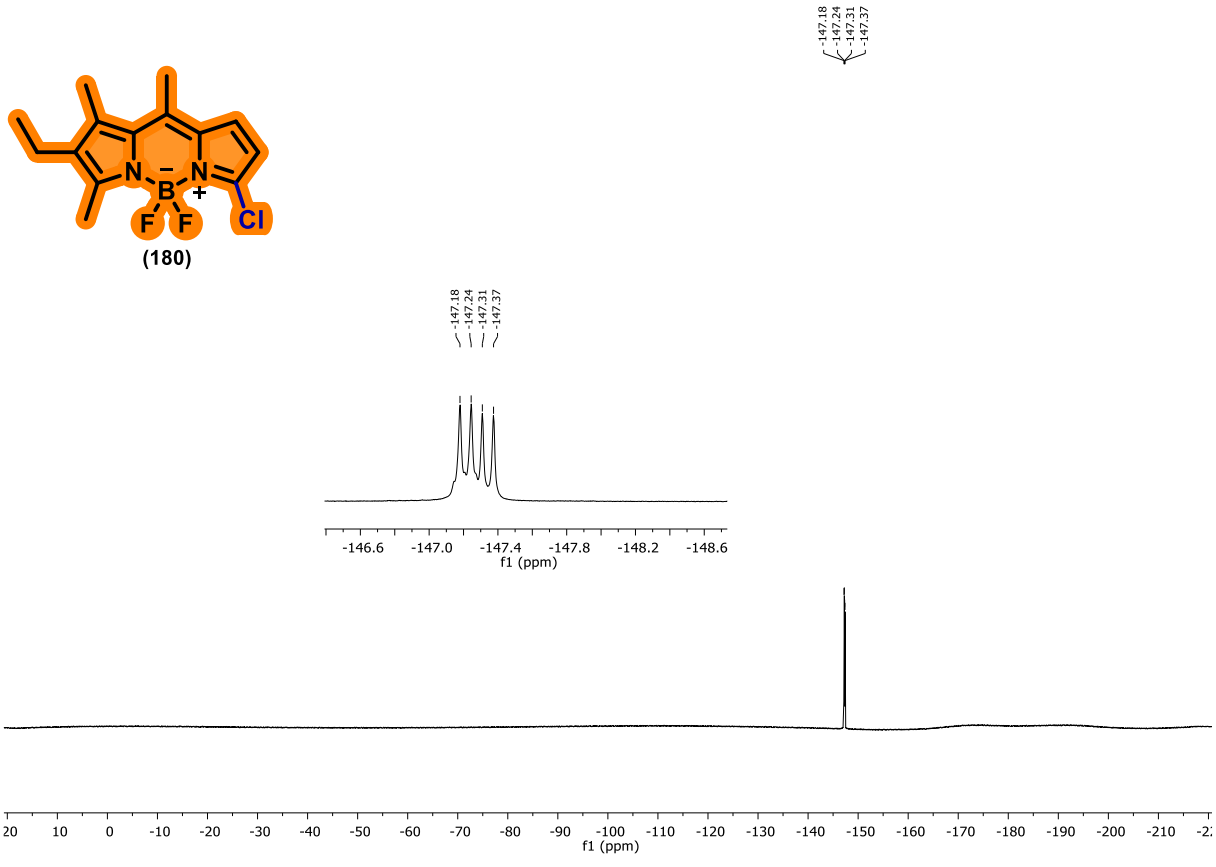

Figure C23. FTIR Spectrum of compound **180**.

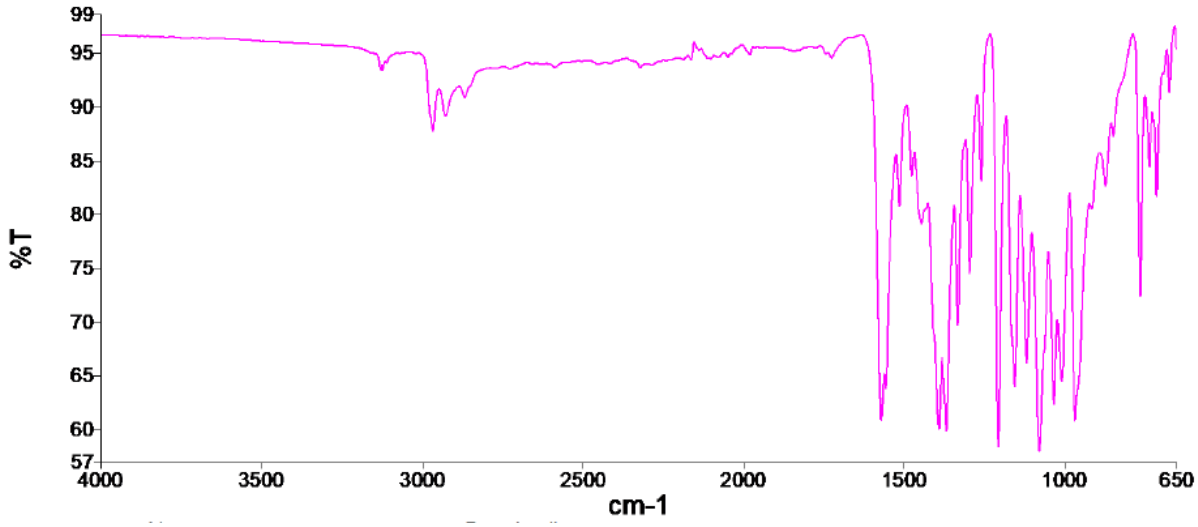

Figure C24. HRMS (ESI +) of compound **180**.

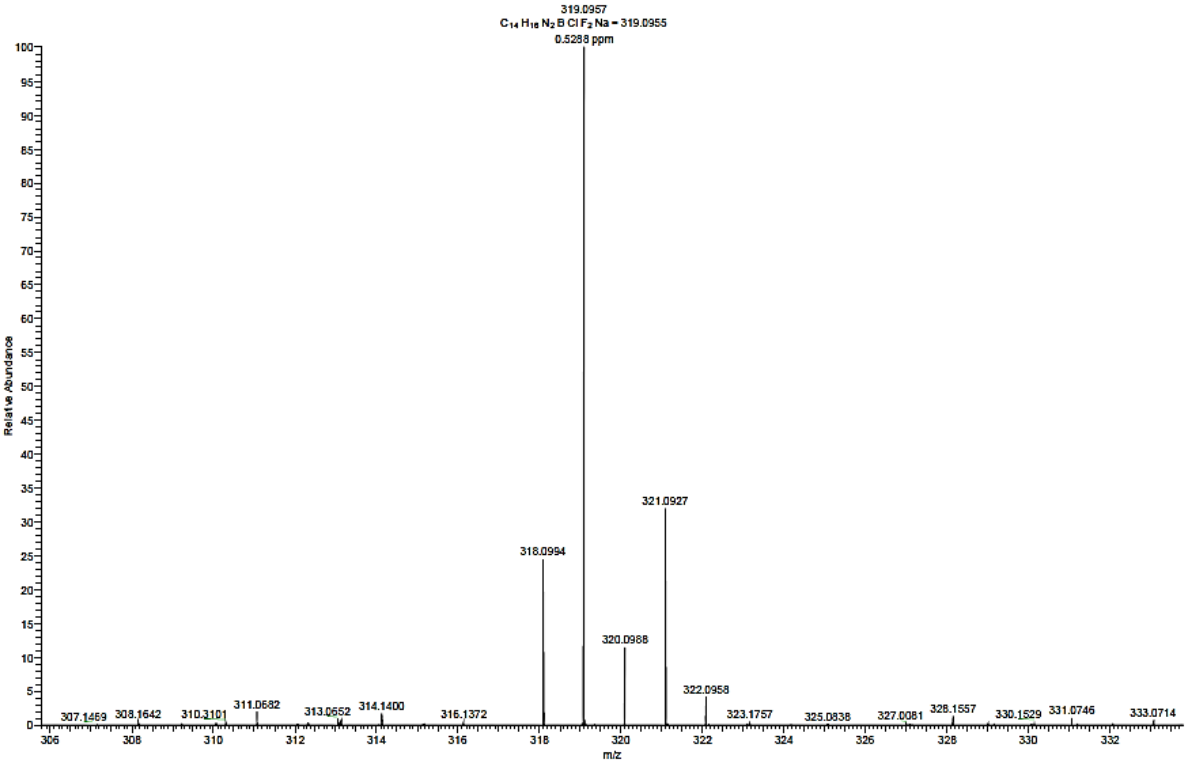

Figure C25. ^{1}H NMR spectrum of compound **181** (400 MHz, $CDCl_3$).

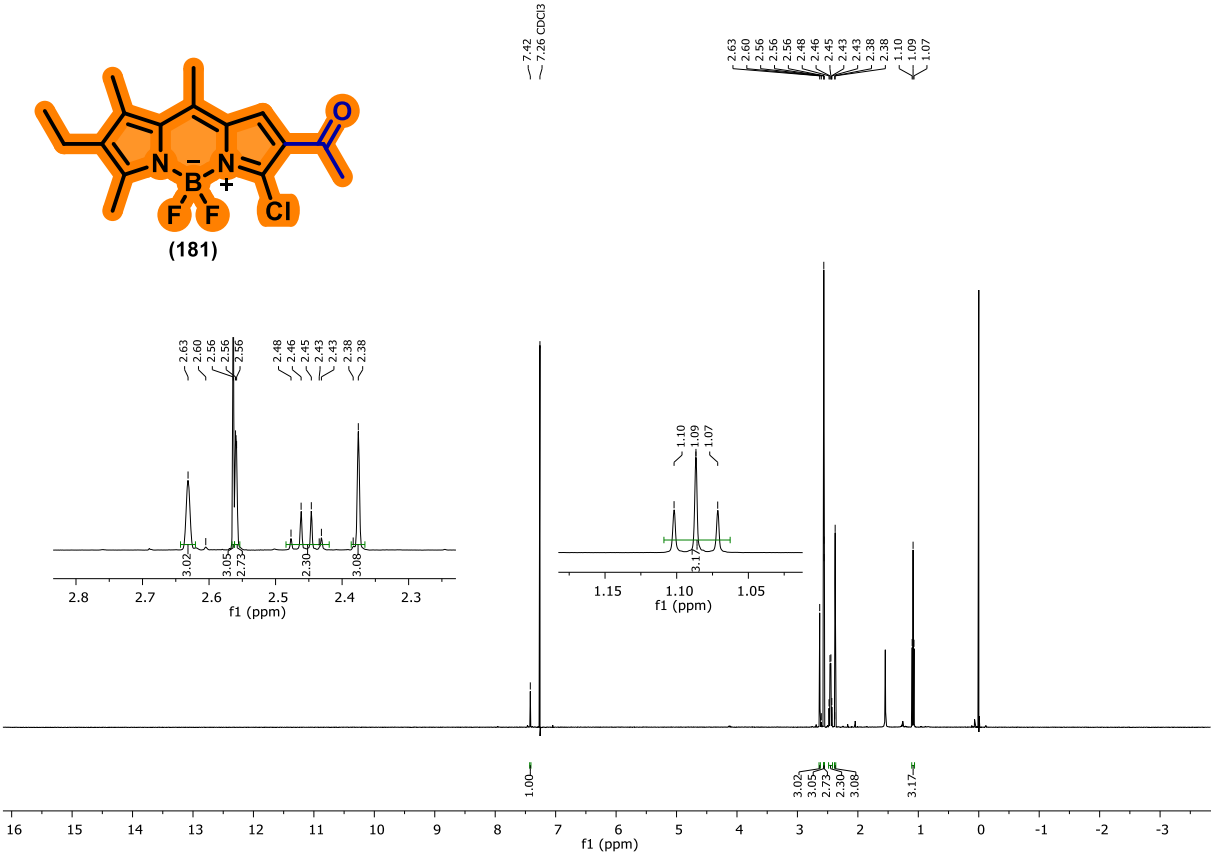

Figure C26. ^{13}C NMR spectrum of compound **181** (100 MHz, $CDCl_3$).

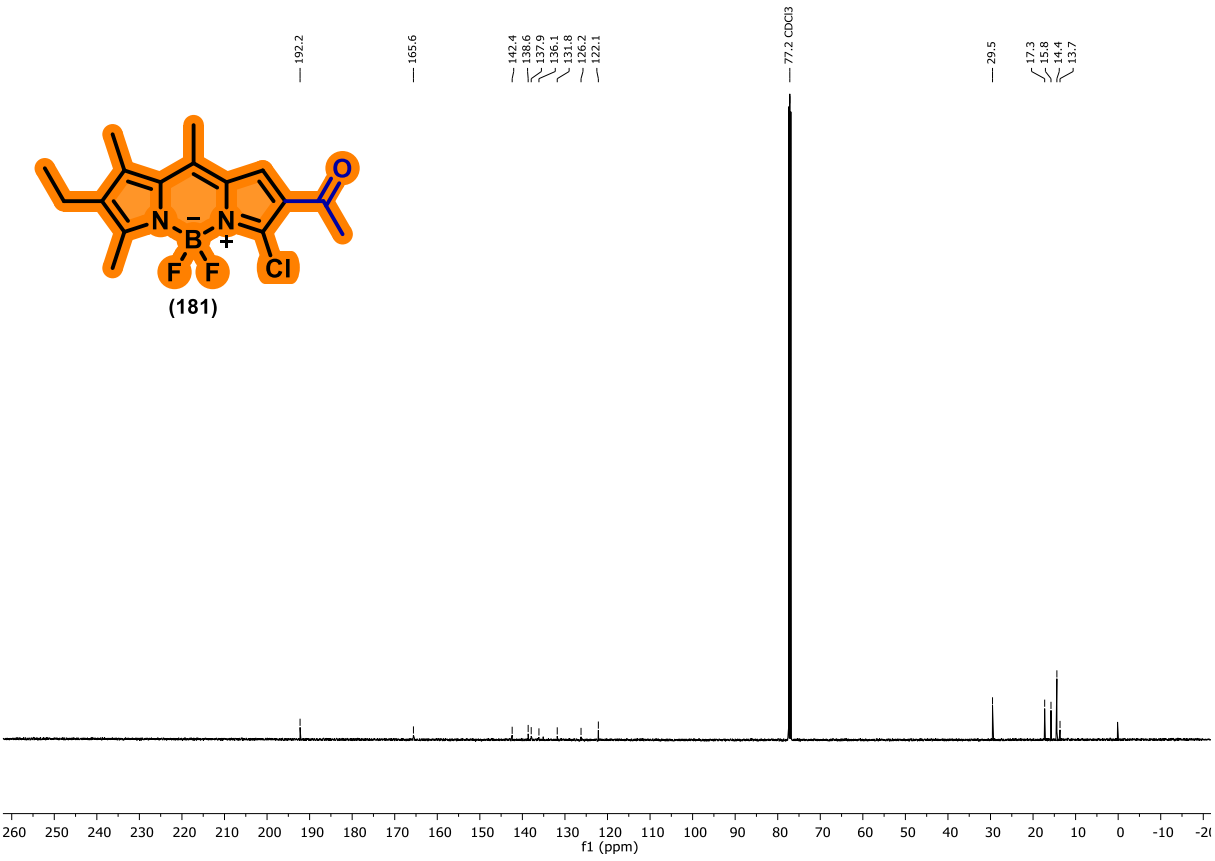

Figure C27. ^{11}B NMR spectrum of compound **181** (564.7MHz, $CDCl_3$).

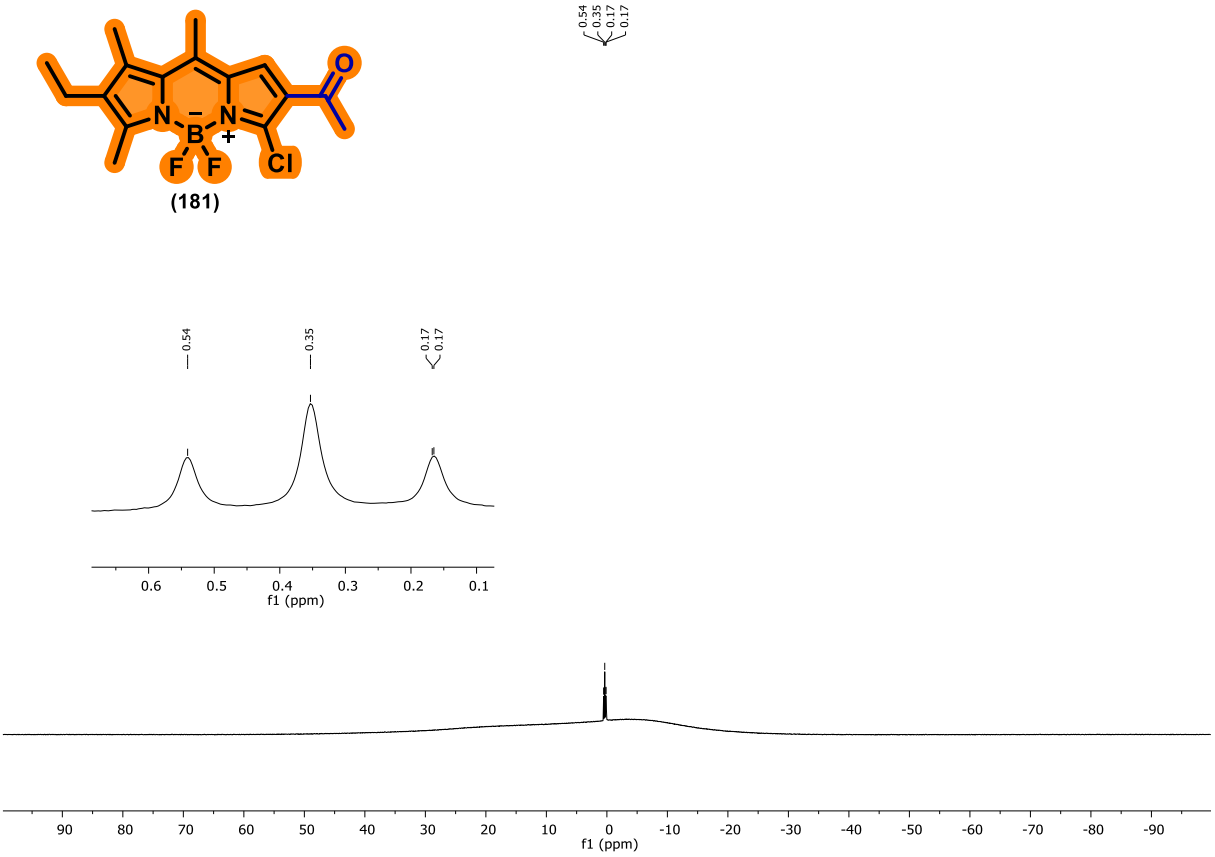

Figure C28. ^{19}F NMR spectrum of compound **181** (564.7MHz, $CDCl_3$).

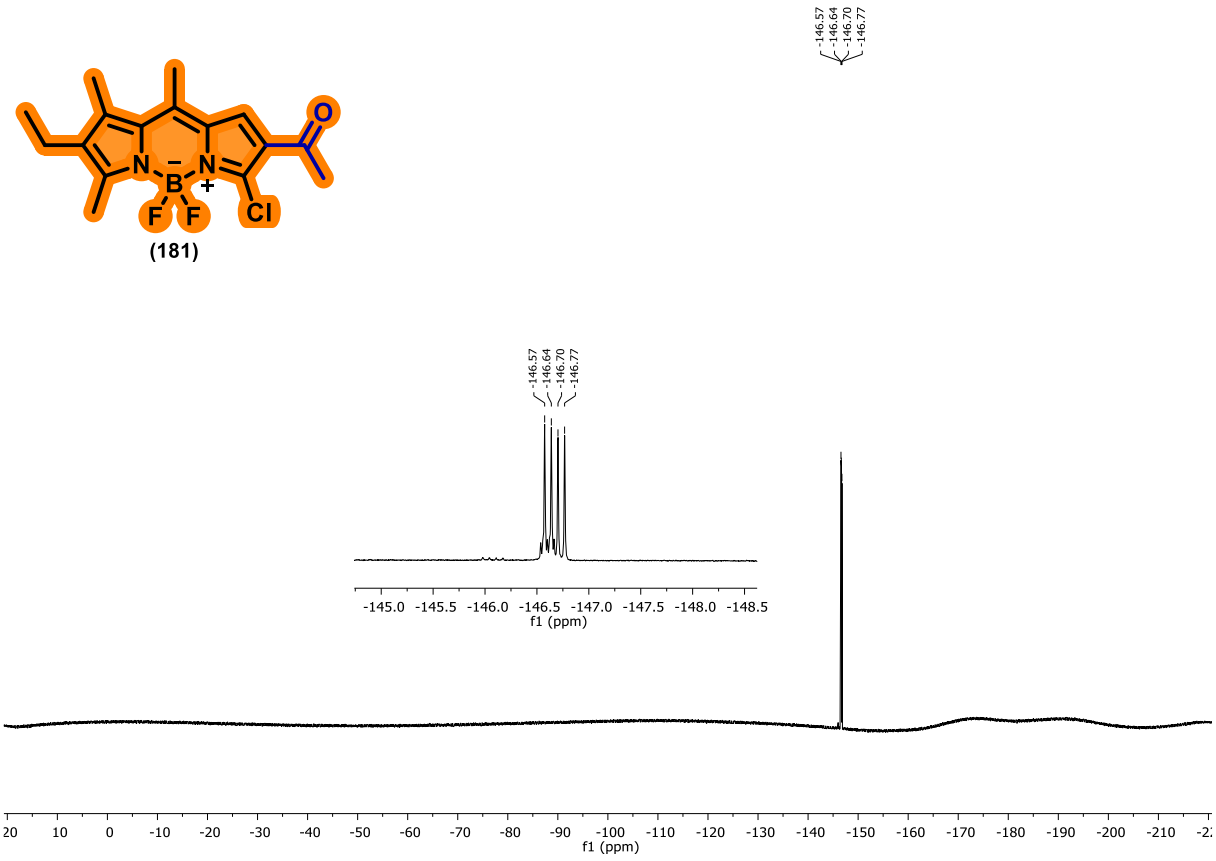

Figure C29. FTIR Spectrum of compound **181**.

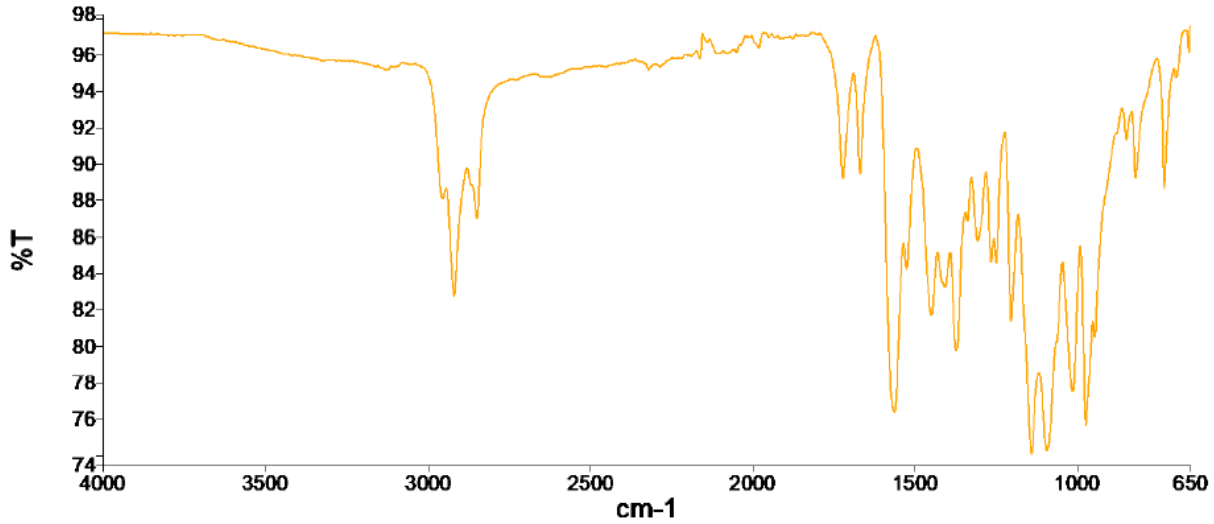

Figure C30. HRMS (ESI +) of compound **181**.

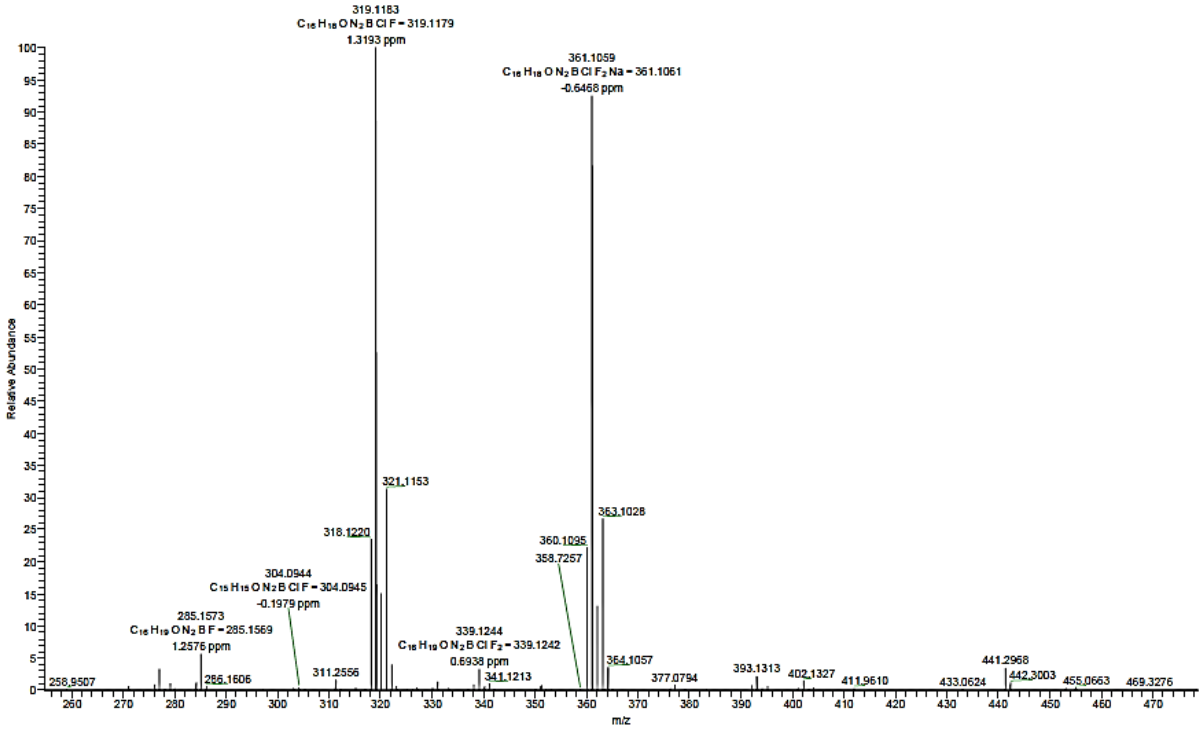

Figure C31. ^{1}H NMR spectrum of compound **181** (400 MHz, $CDCl_3$).

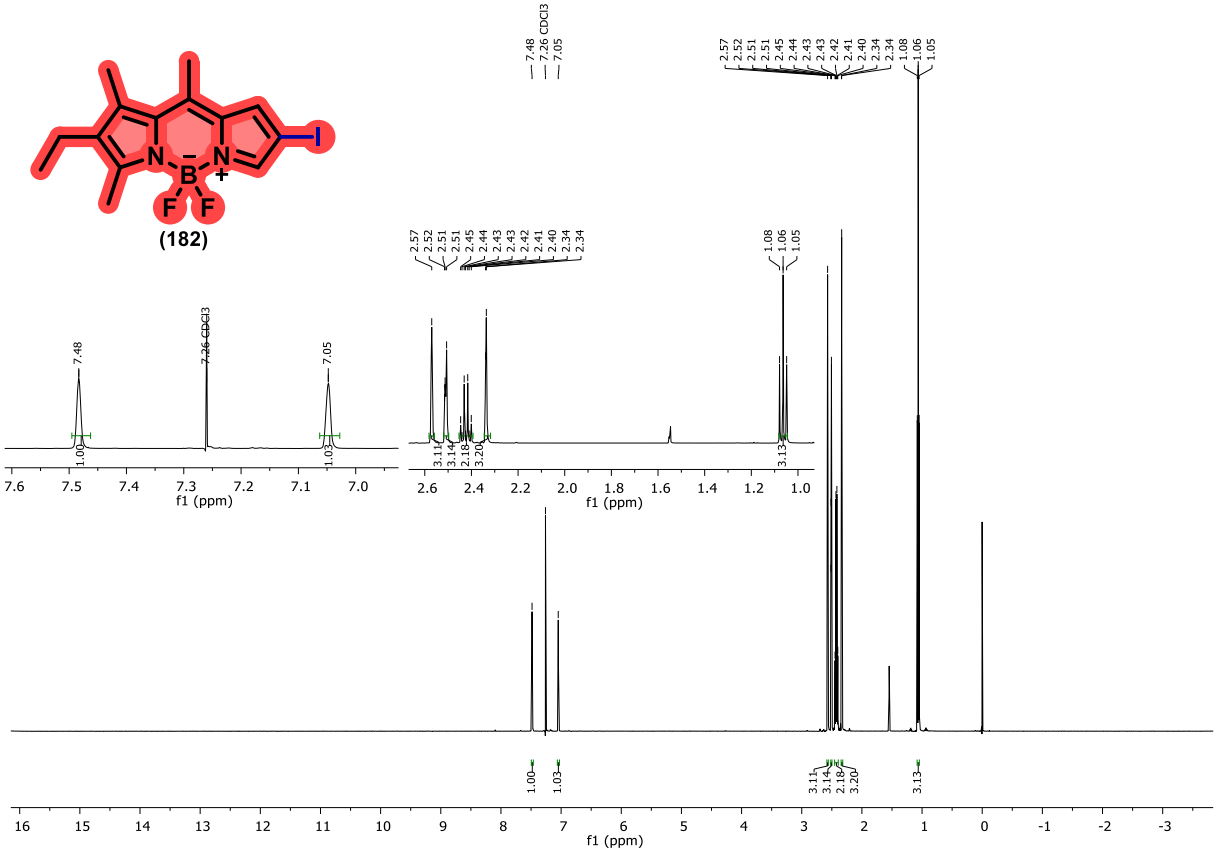

Figure C32. ^{13}C NMR spectrum of compound **182** (100 MHz, $CDCl_3$).

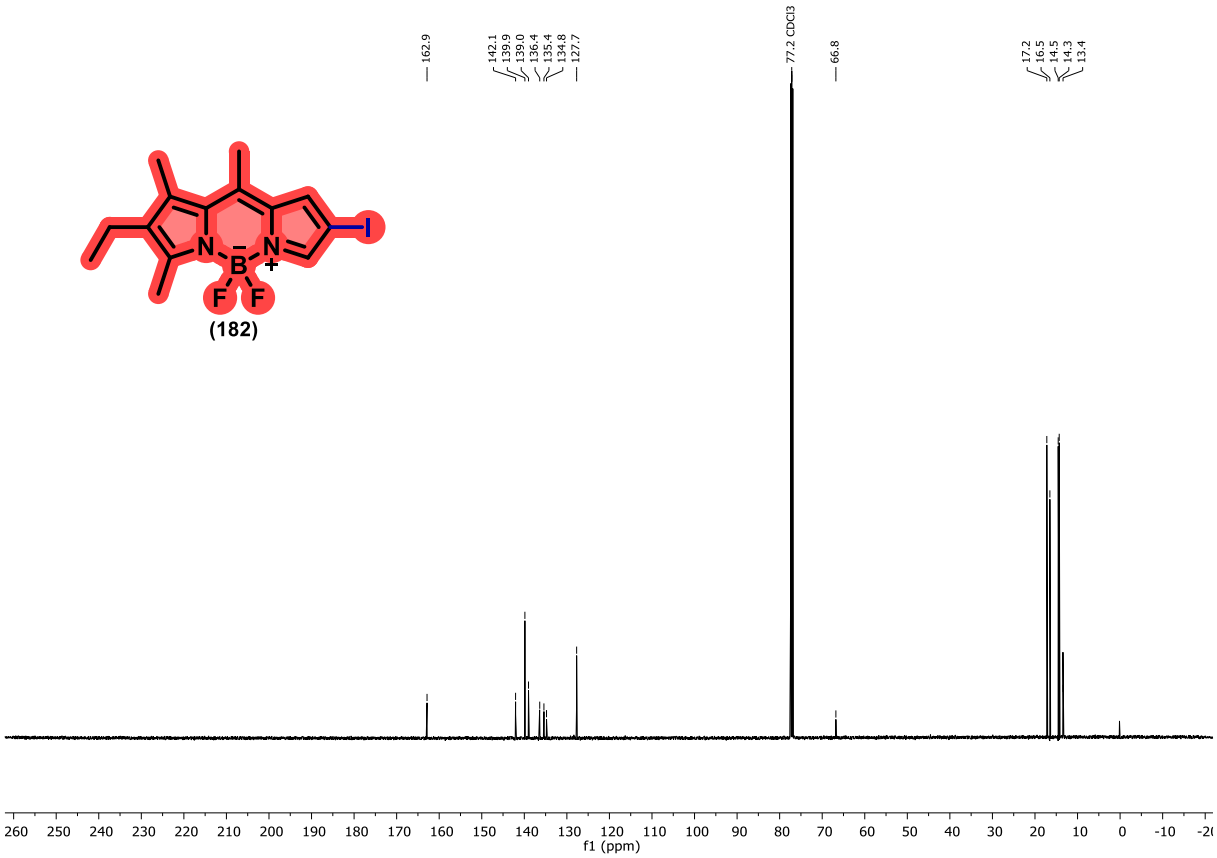

Figure C 33. ^{11}B NMR spectrum of compound **182** (564.7MHz, $CDCl_3$).

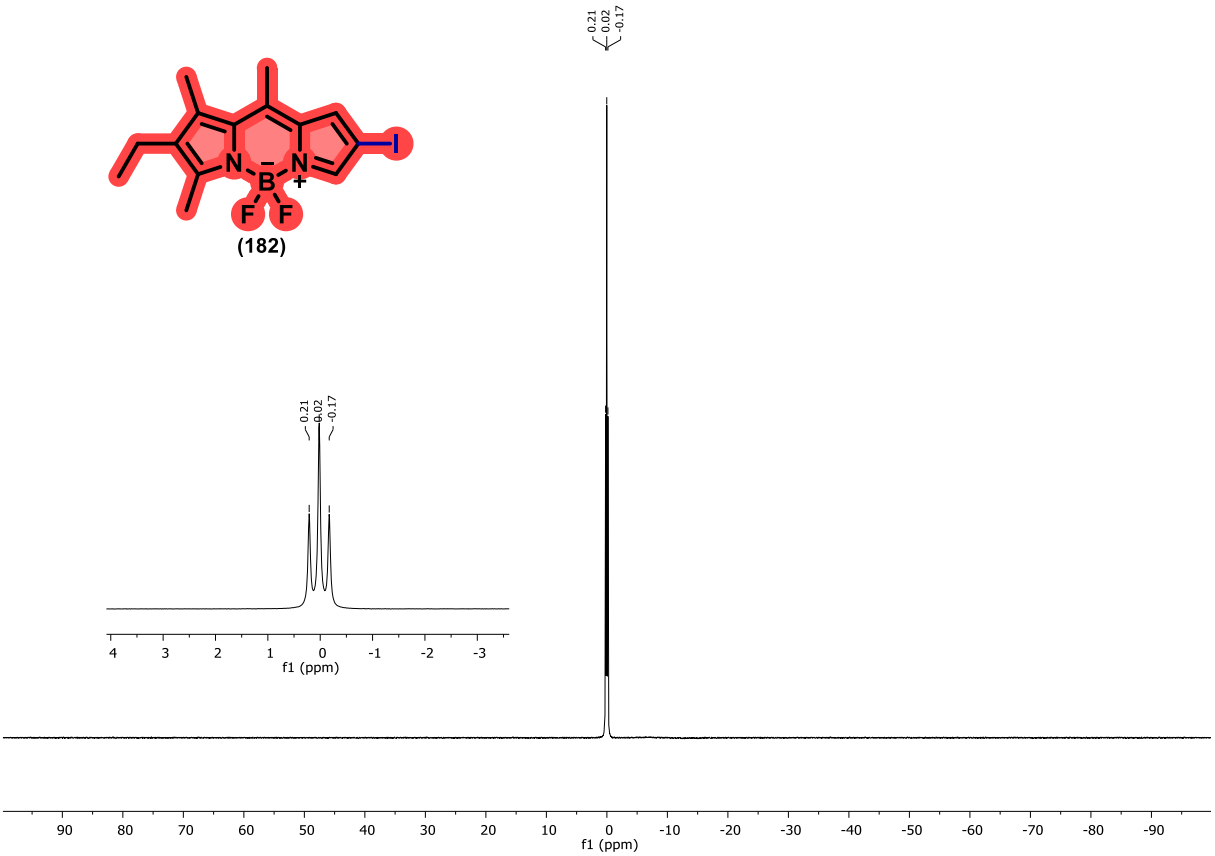

Figure C34. ^{19}F NMR spectrum of compound **182** (564.7MHz, $CDCl_3$).

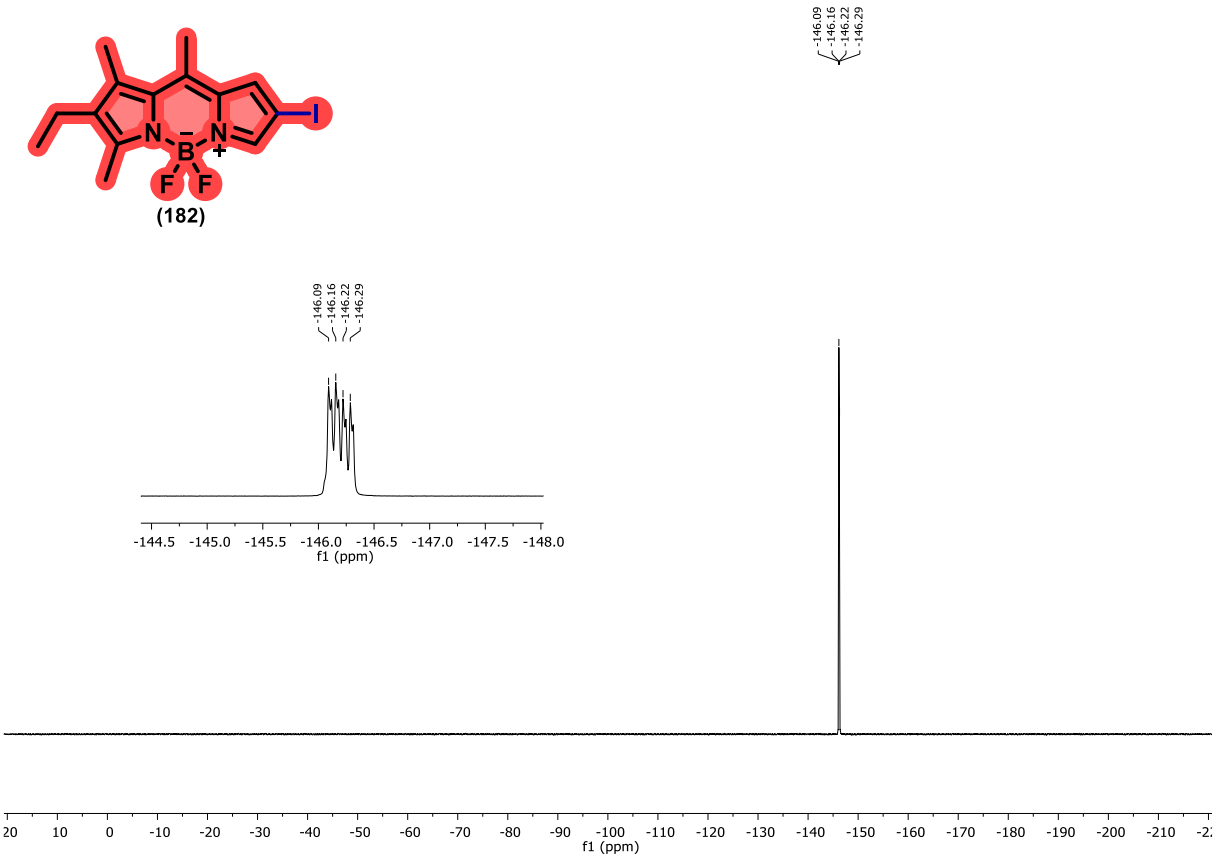

Figure C35. FTIR Spectrum of compound **182**.

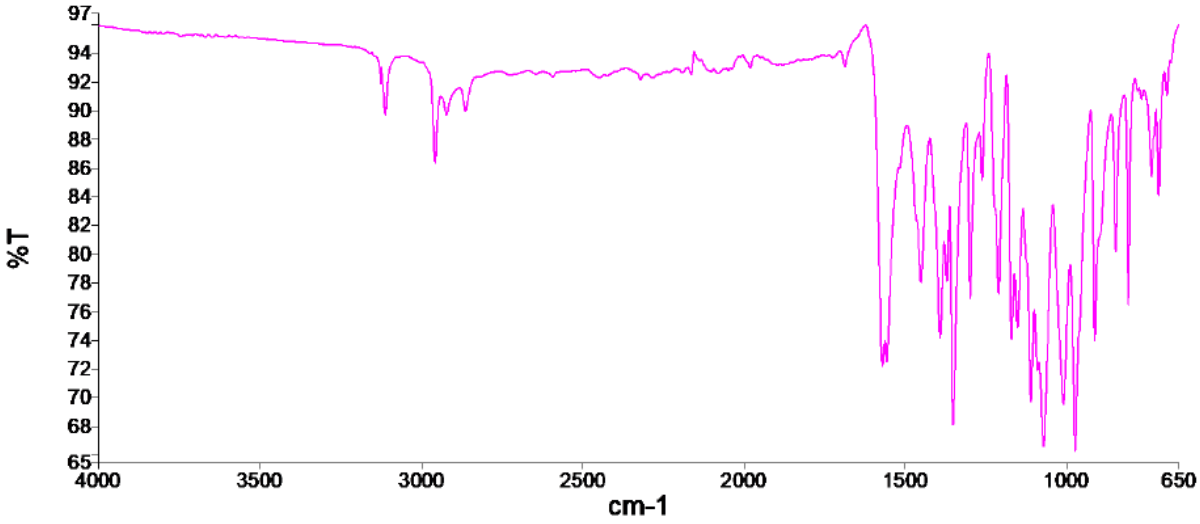

Figure C36. HRMS (ESI +) of compound **182**.

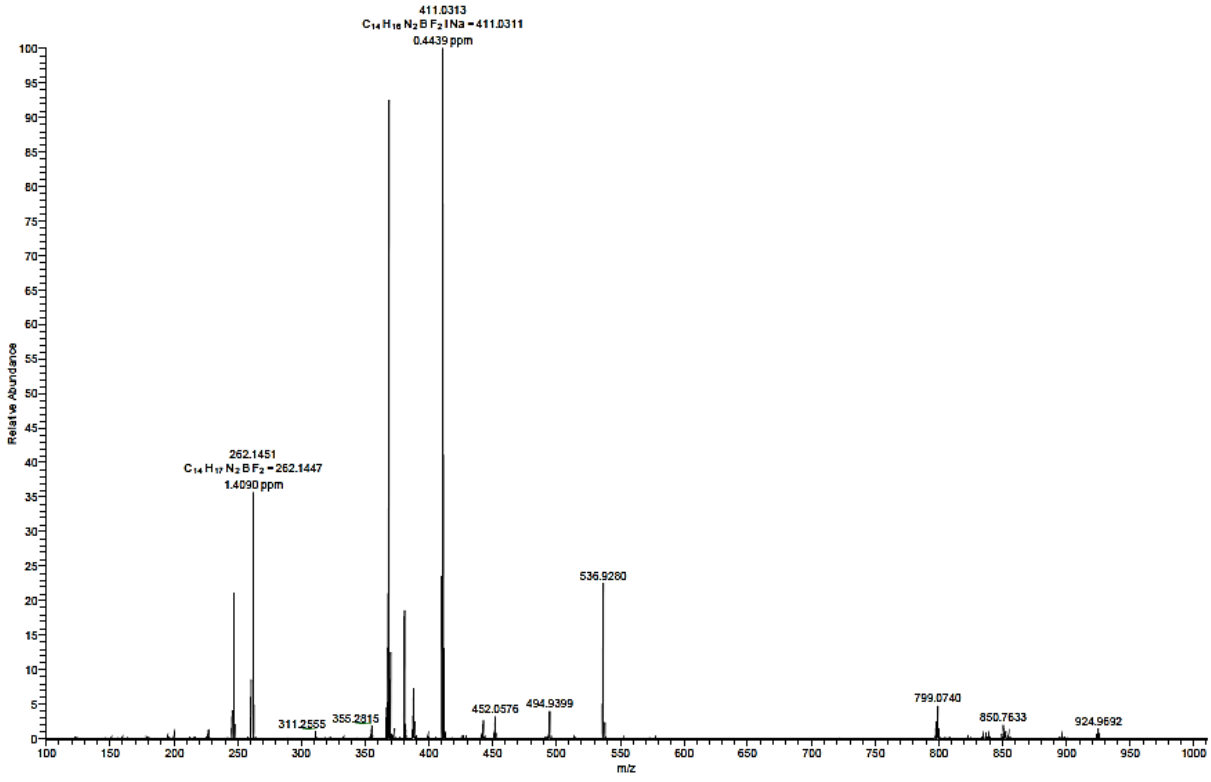

Figure C37. ^{1}H NMR spectrum of compound **183** (400 MHz, $CDCl_3$).

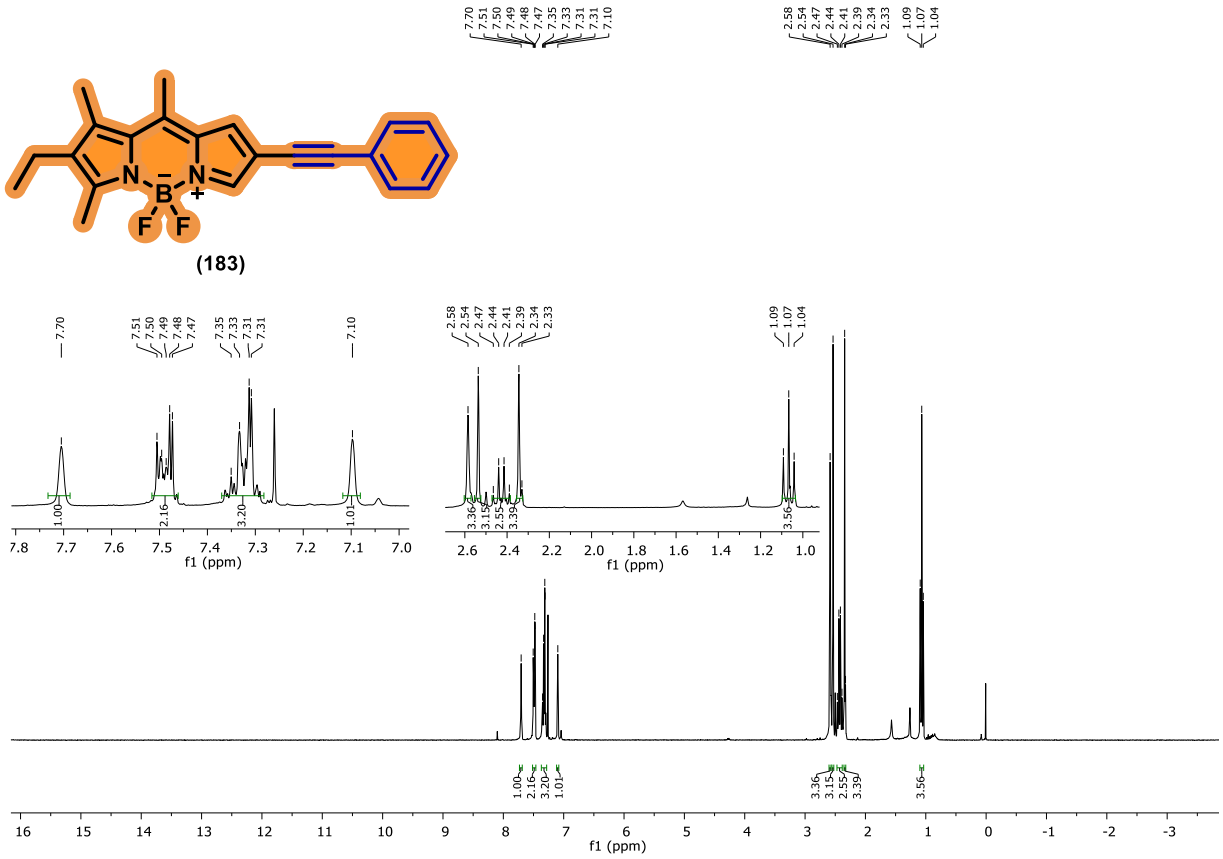

Figure C38. FTIR Spectrum of compound **183**.

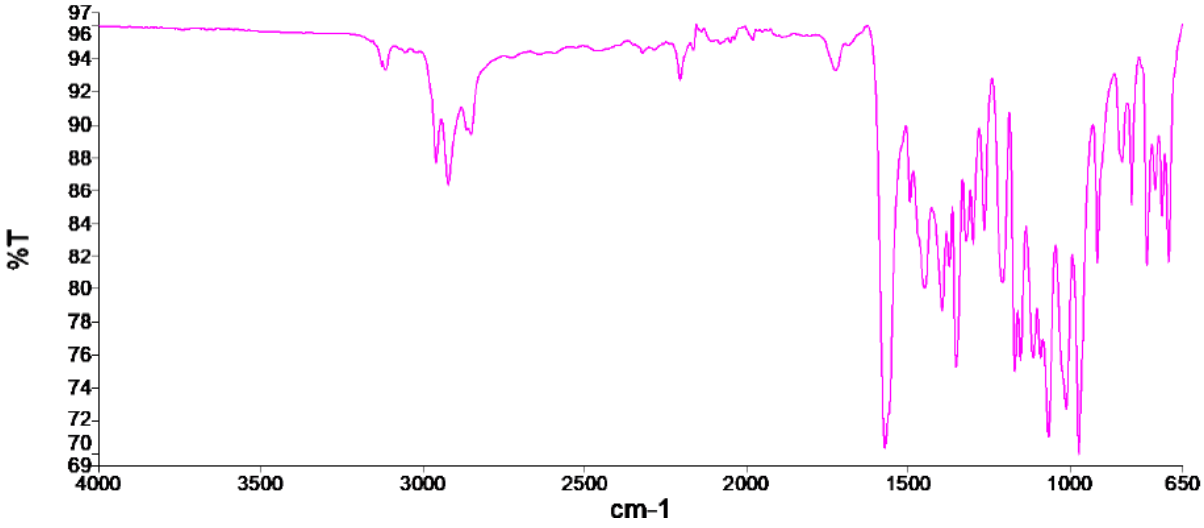

Figure C39. HRMS (ESI +) of compound **183**.

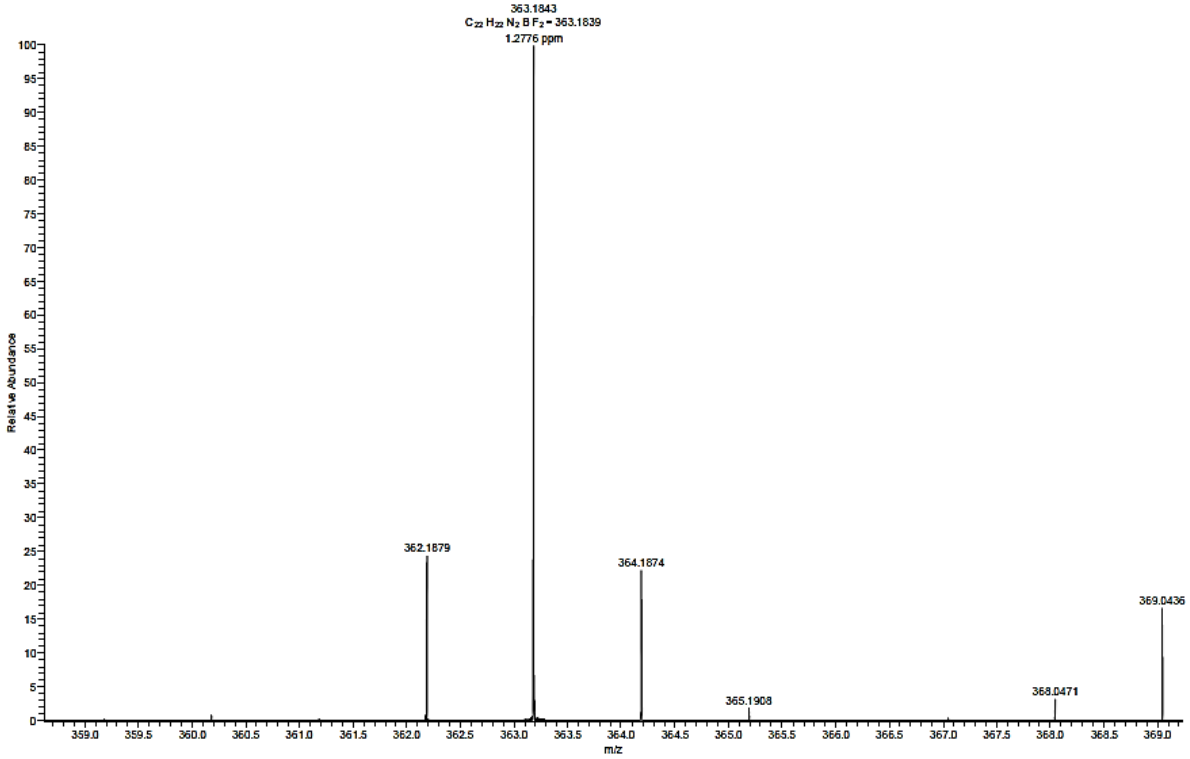

Figure C40. ^{1}H NMR spectrum of compound **184** (400 MHz, $CDCl_3$).

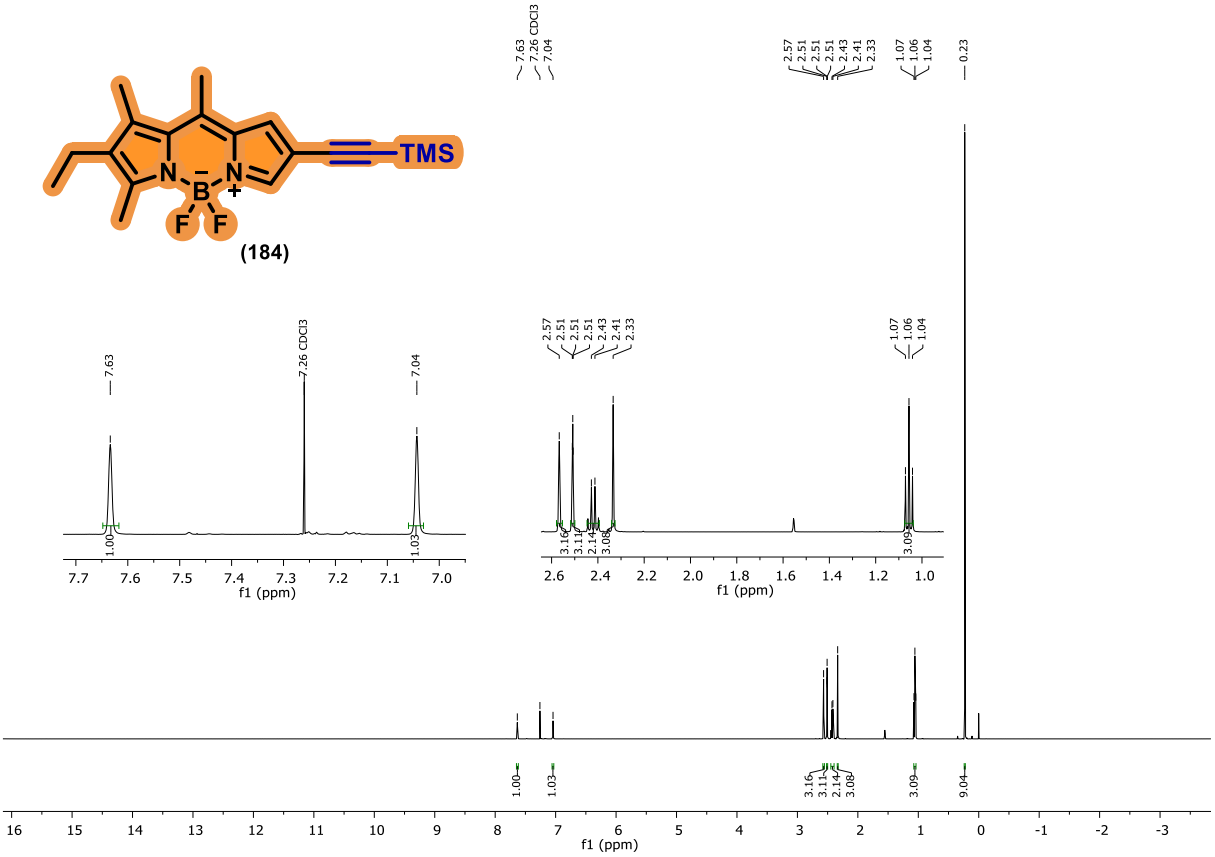

Figure C41. ^{13}C NMR spectrum of compound **184** (100 MHz, $CDCl_3$).

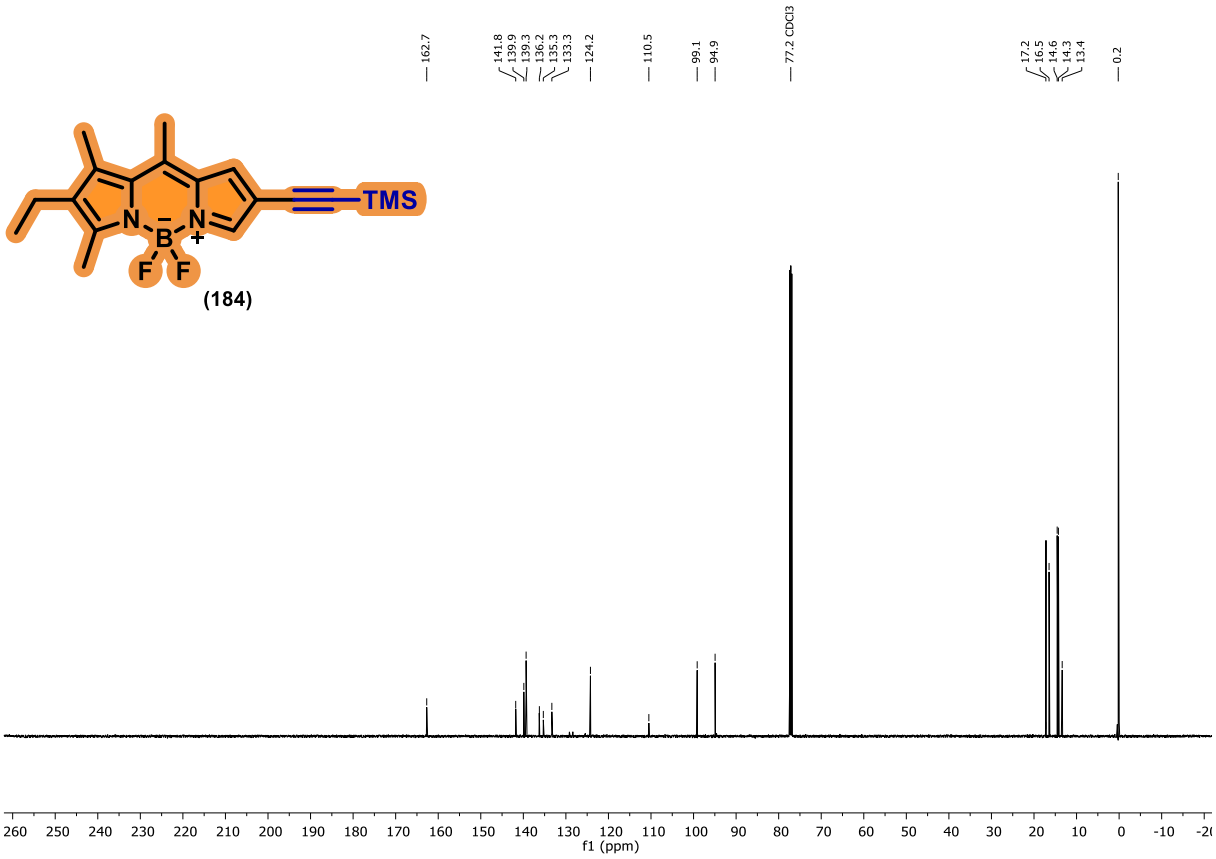

Figure C42. ^{11}B NMR spectrum of compound **184** (564.7MHz, $CDCl_3$).

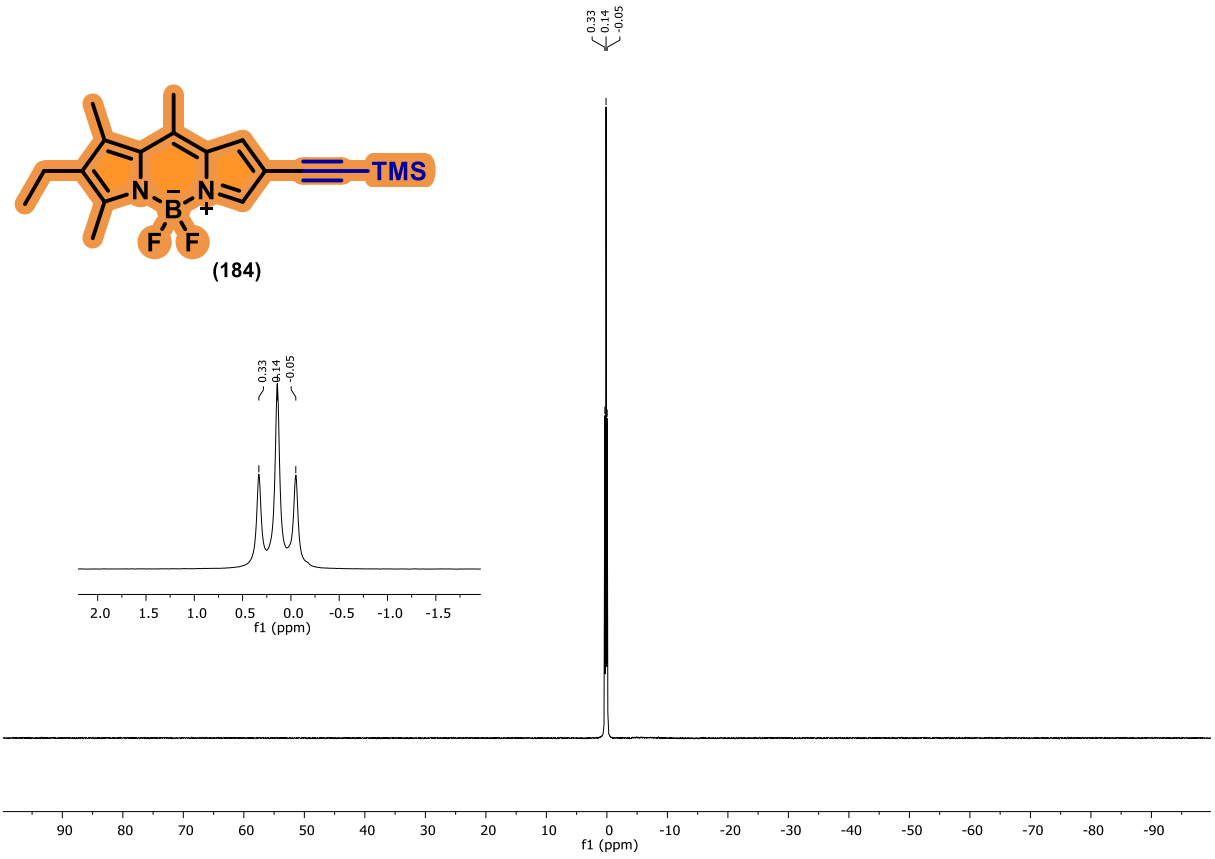

Figure C43. ^{19}F NMR spectrum of compound **184** (564.7MHz, $CDCl_3$).

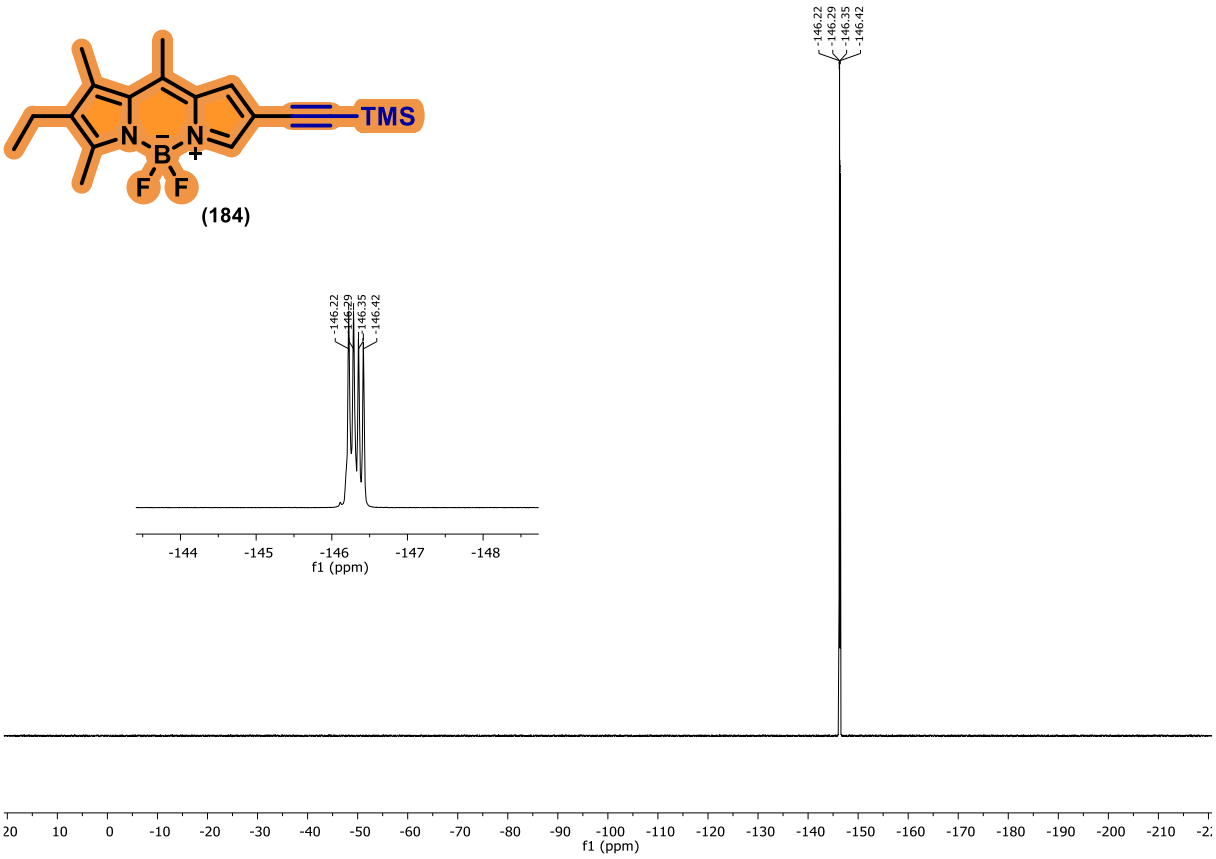

Figure C44. FTIR Spectrum of compound **184**.

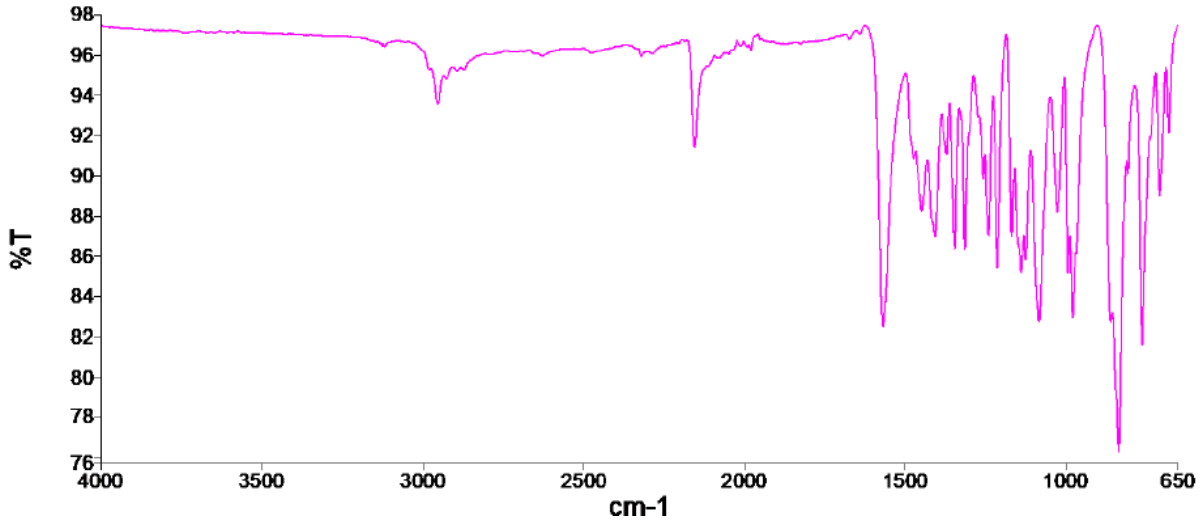

Figure C45. HRMS (ESI +) of compound **184**.

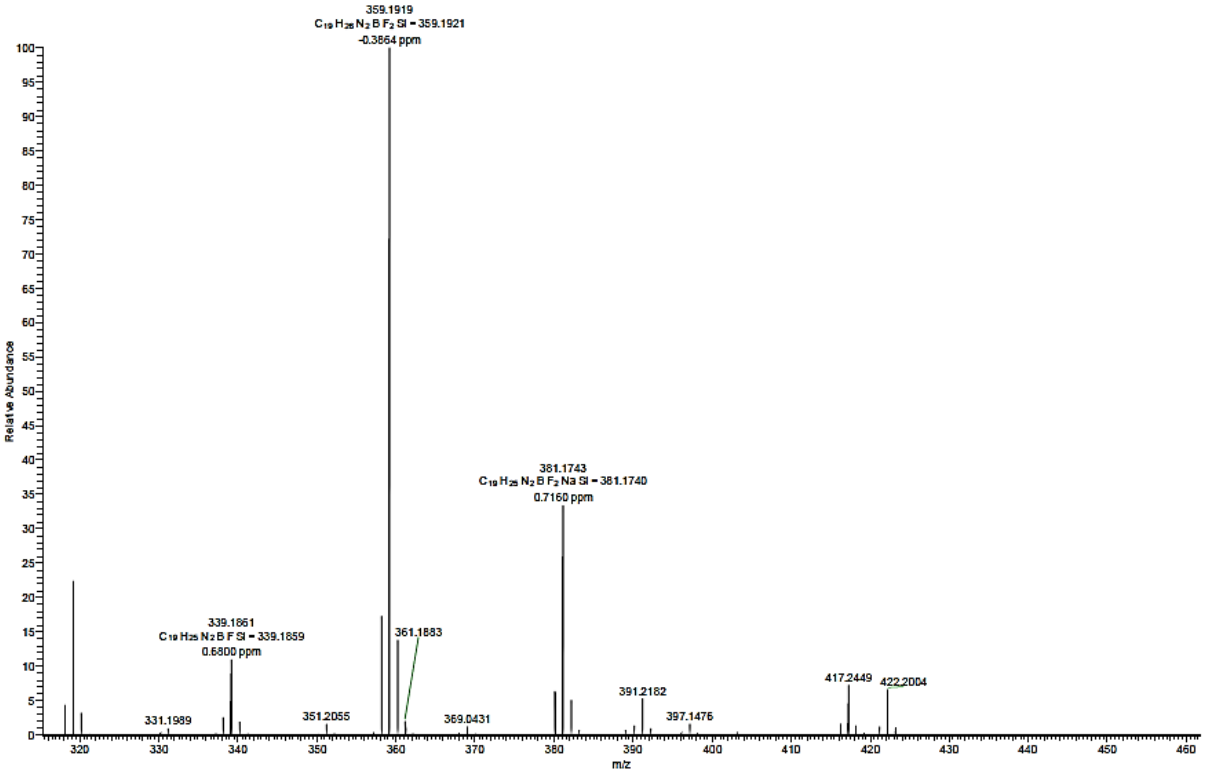

Figure C46. ^{1}H NMR spectrum of compound **185** (400 MHz, $CDCl_3$).

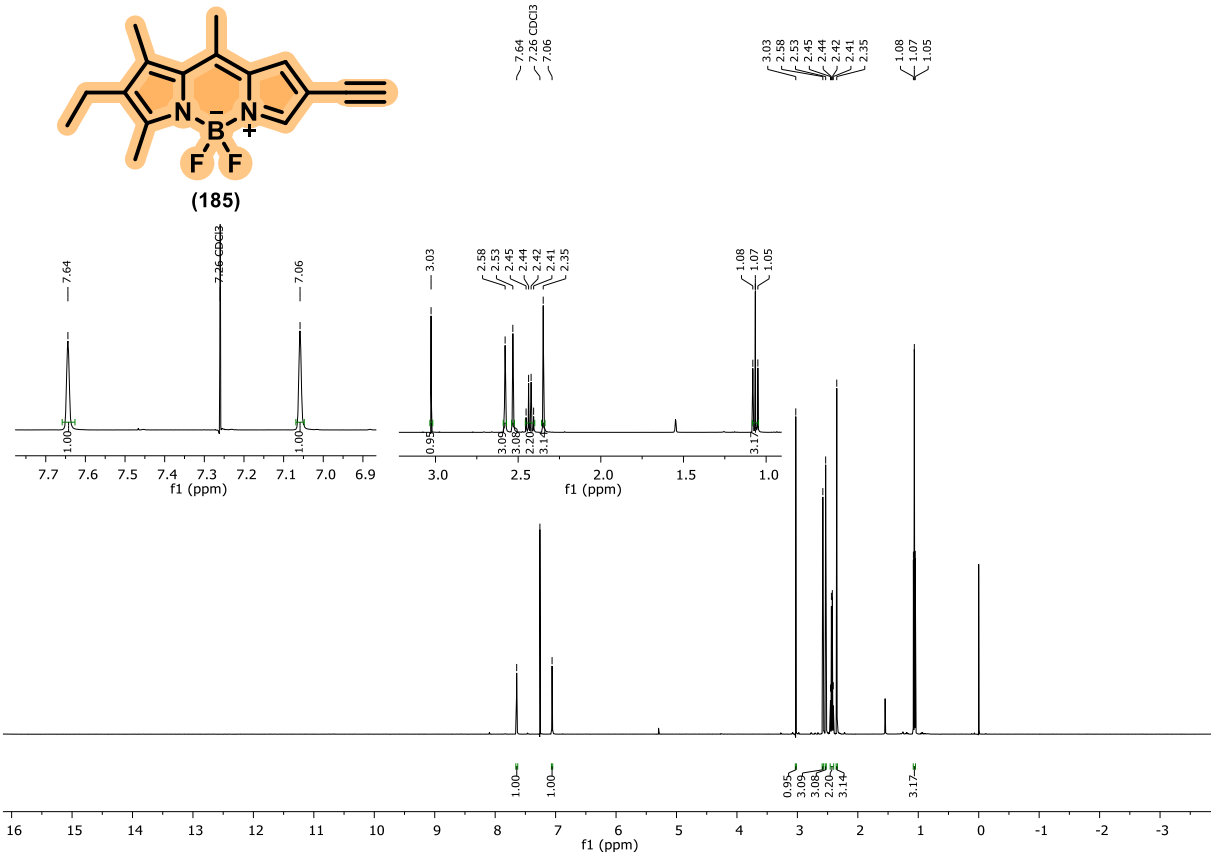

Figure C47. ^{13}C NMR spectrum of compound **185** (100 MHz, $CDCl_3$).

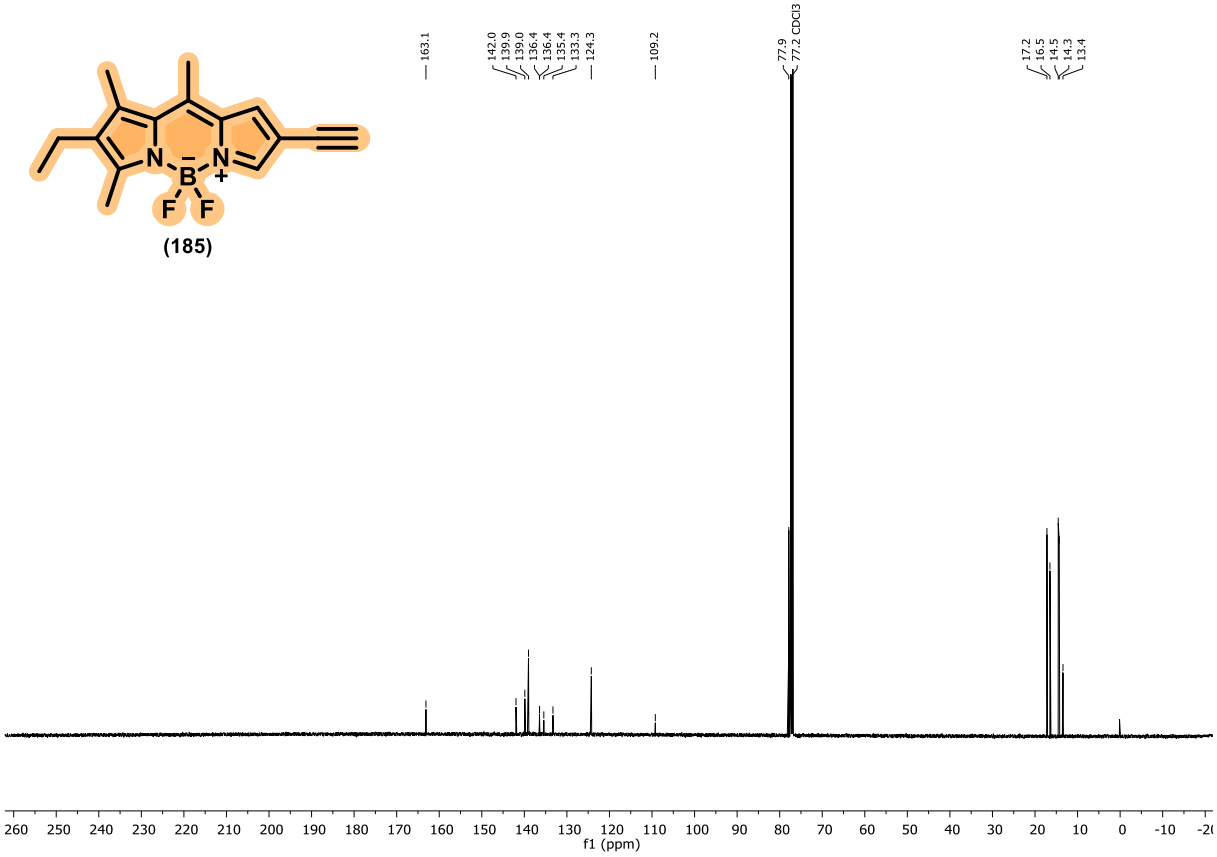

Figure C48. ^{11}B NMR spectrum of compound **185** (564.7MHz, $CDCl_3$).

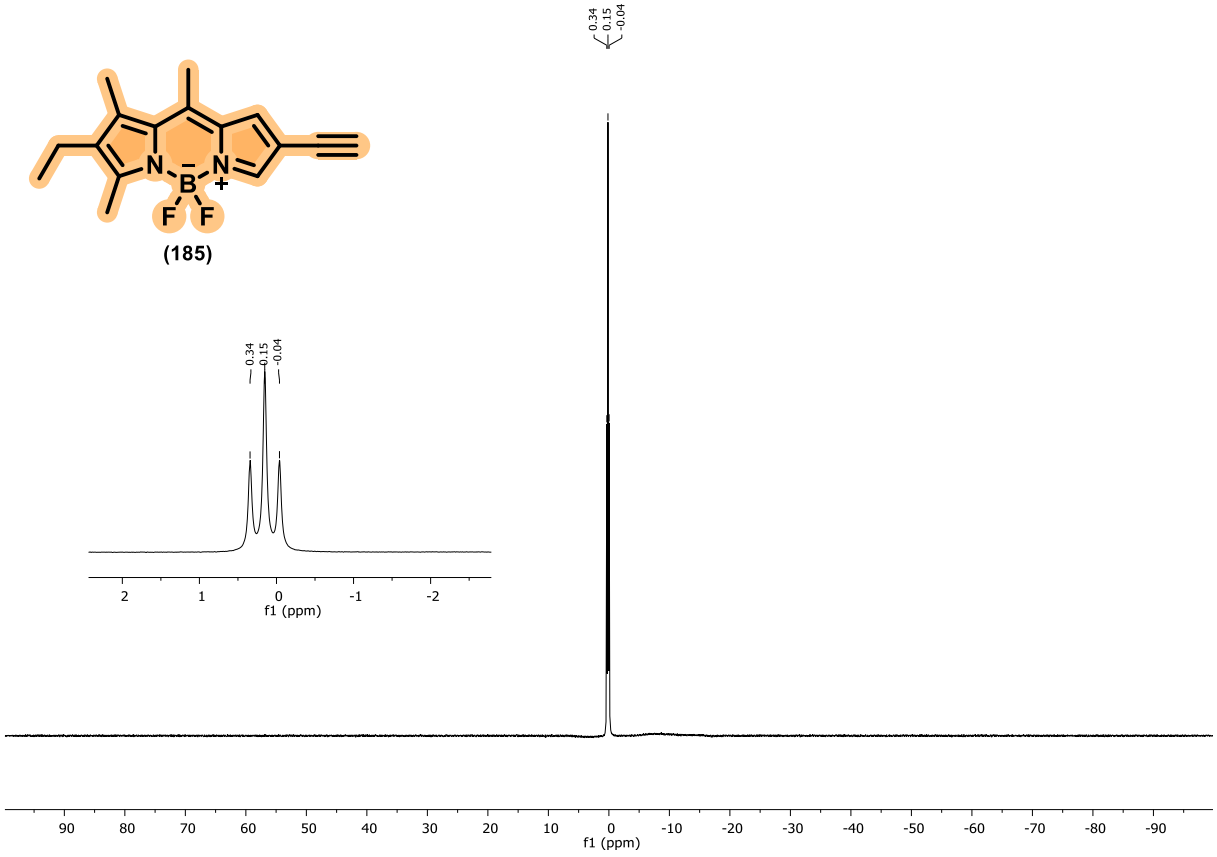

Figure C49. ^{19}F NMR spectrum of compound **185** (564.7MHz, $CDCl_3$).

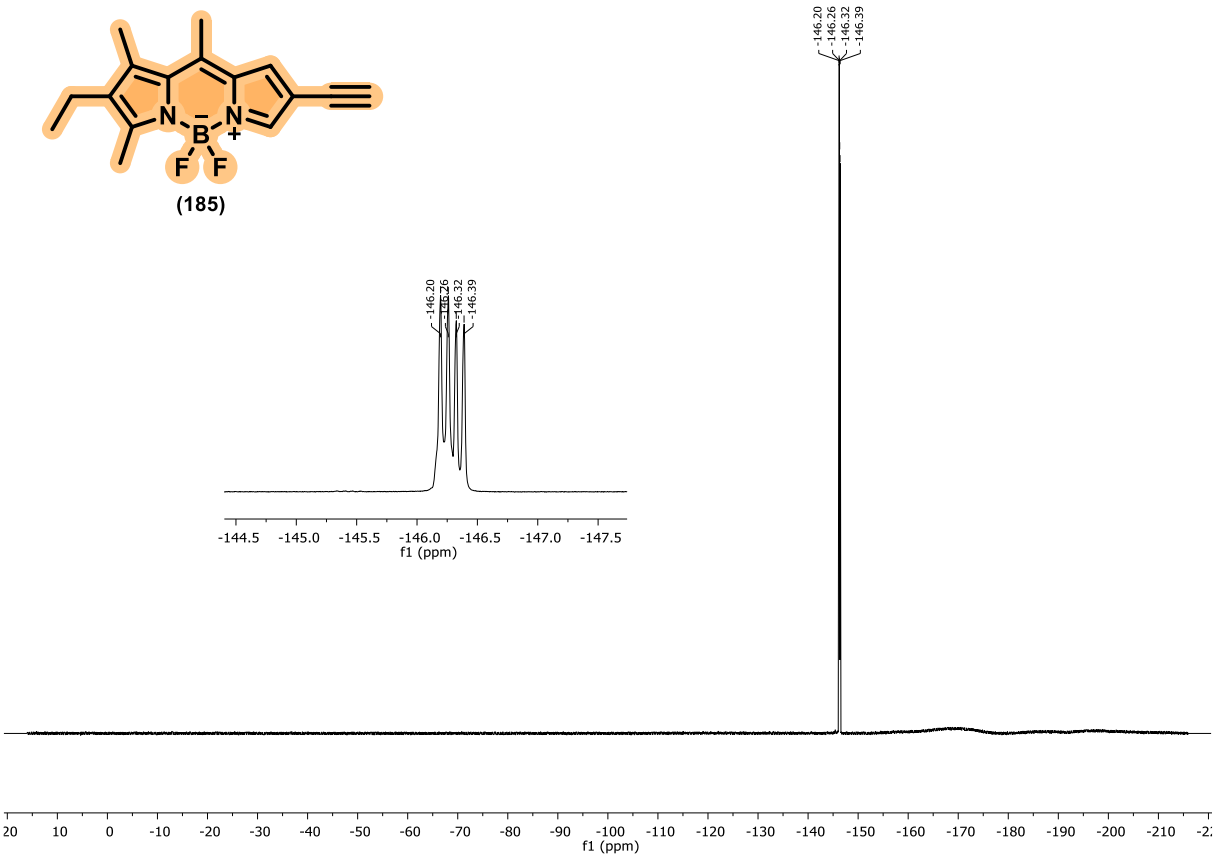

Figure C50. FTIR Spectrum of compound **185**.

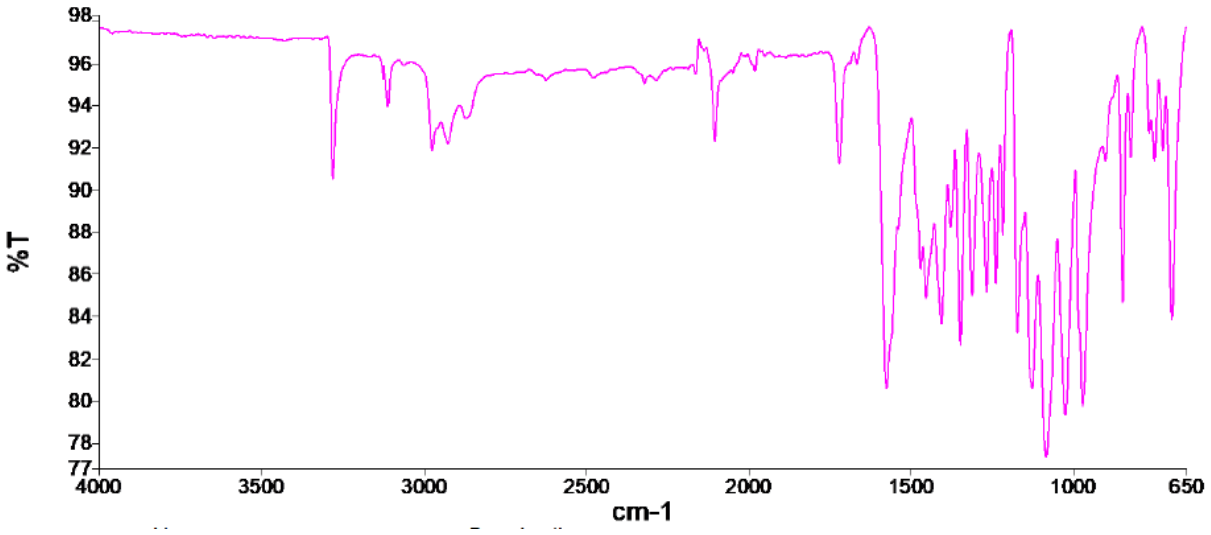

Figure C51. HRMS (ESI +) of compound **185.**

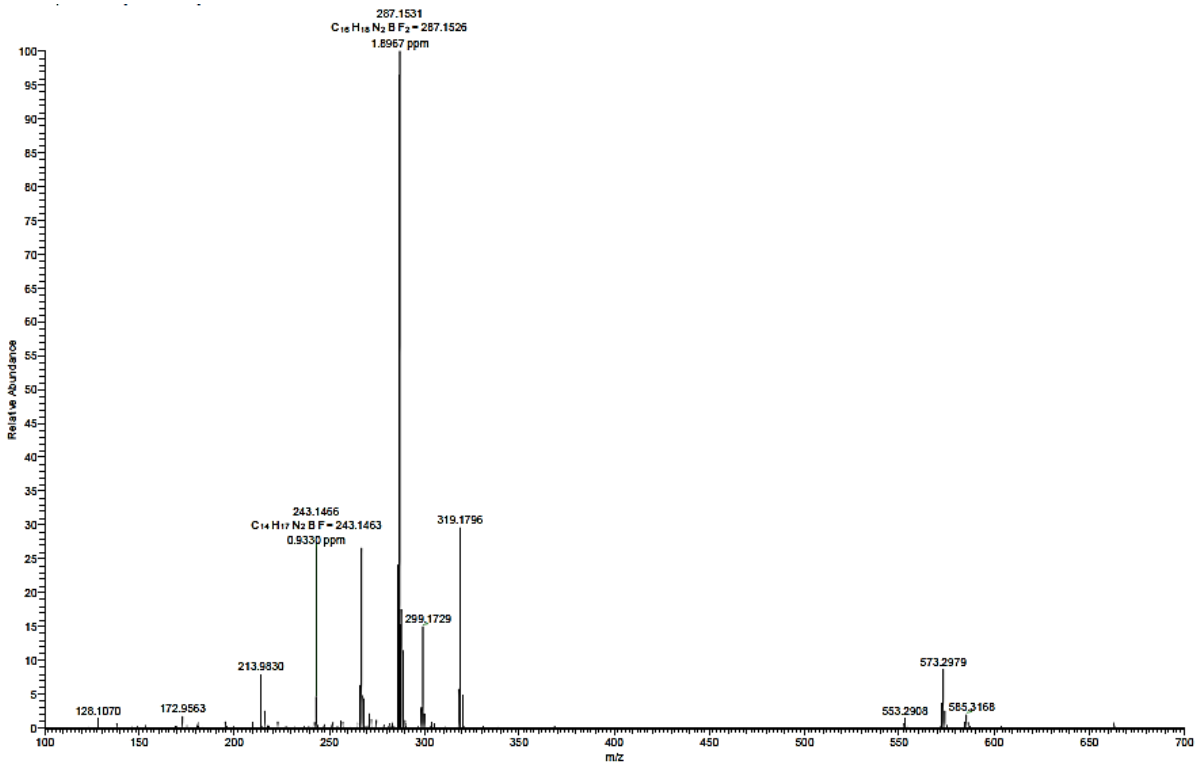

Figure C52. ^{1}H NMR spectrum of compound **186** (400 MHz, $CDCl_3$).

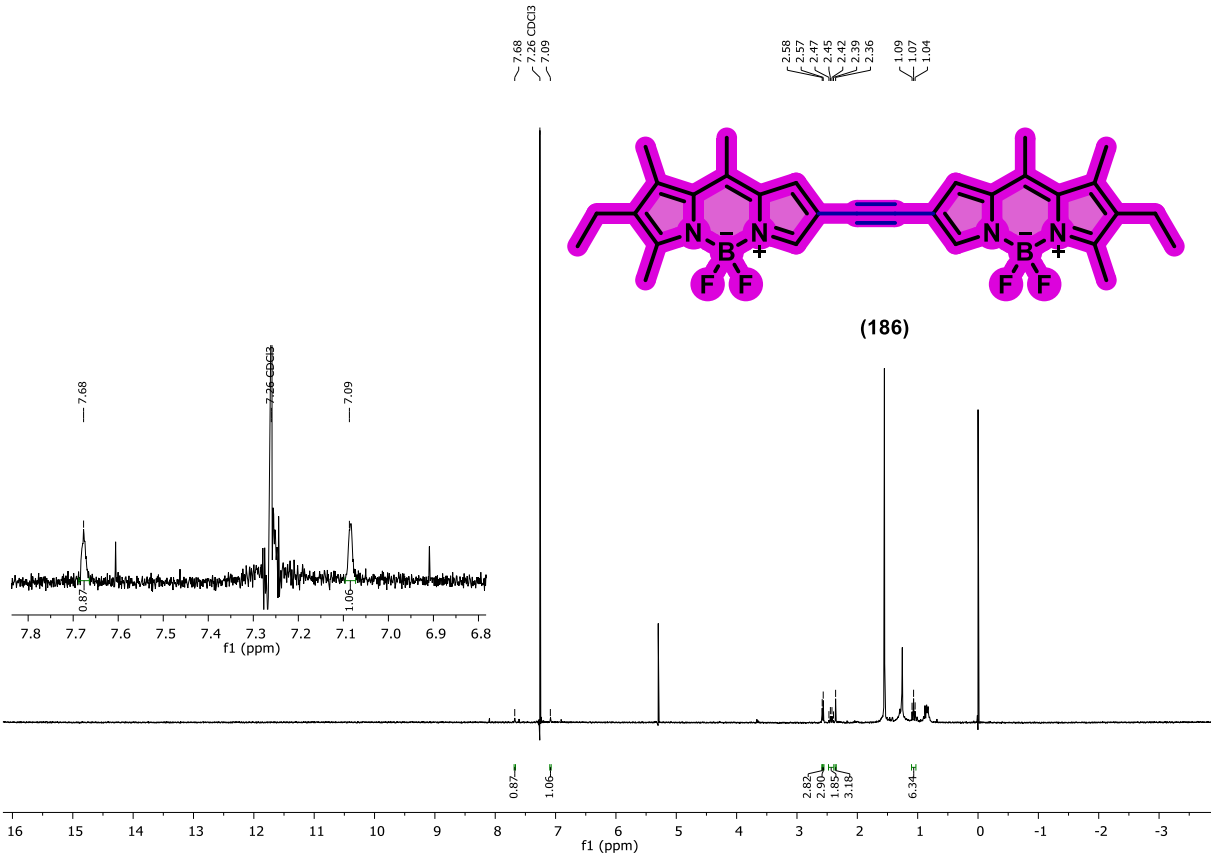

Figure C53. FTIR Spectrum of compound **186**.

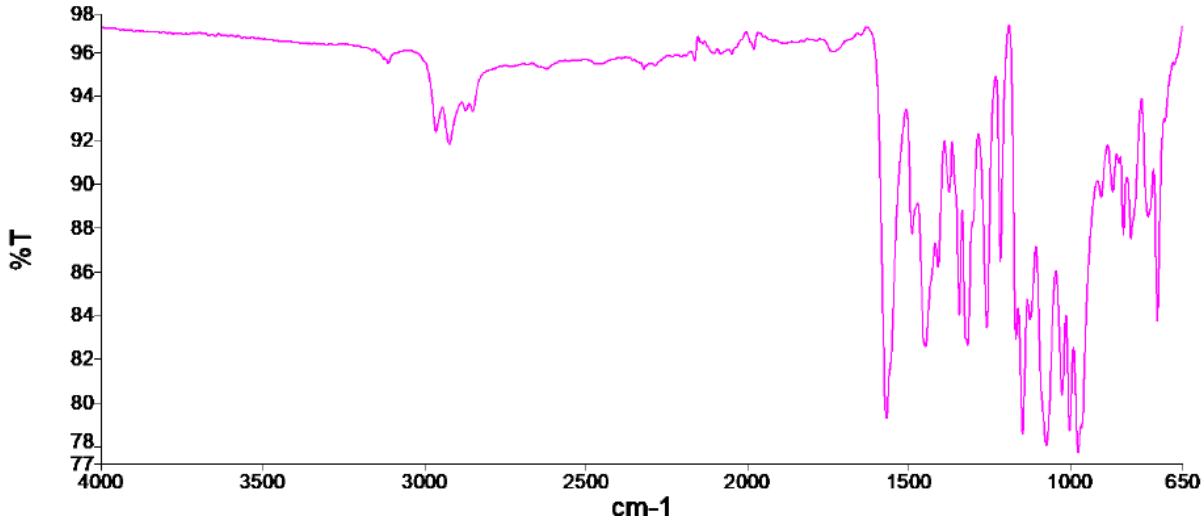

Figure C54. HRMS (ESI +) of compound **186**.

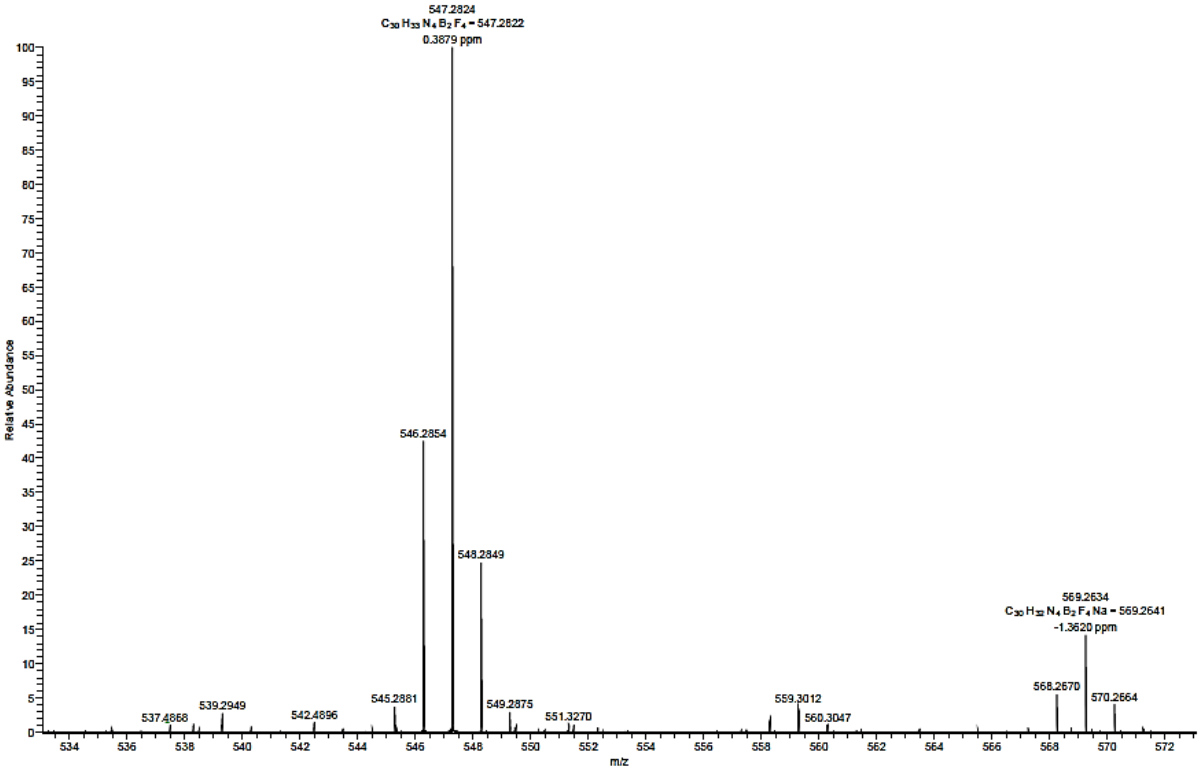

Figure C55. ^{1}H NMR spectrum of compound **187** (400 MHz, $CDCl_3$).

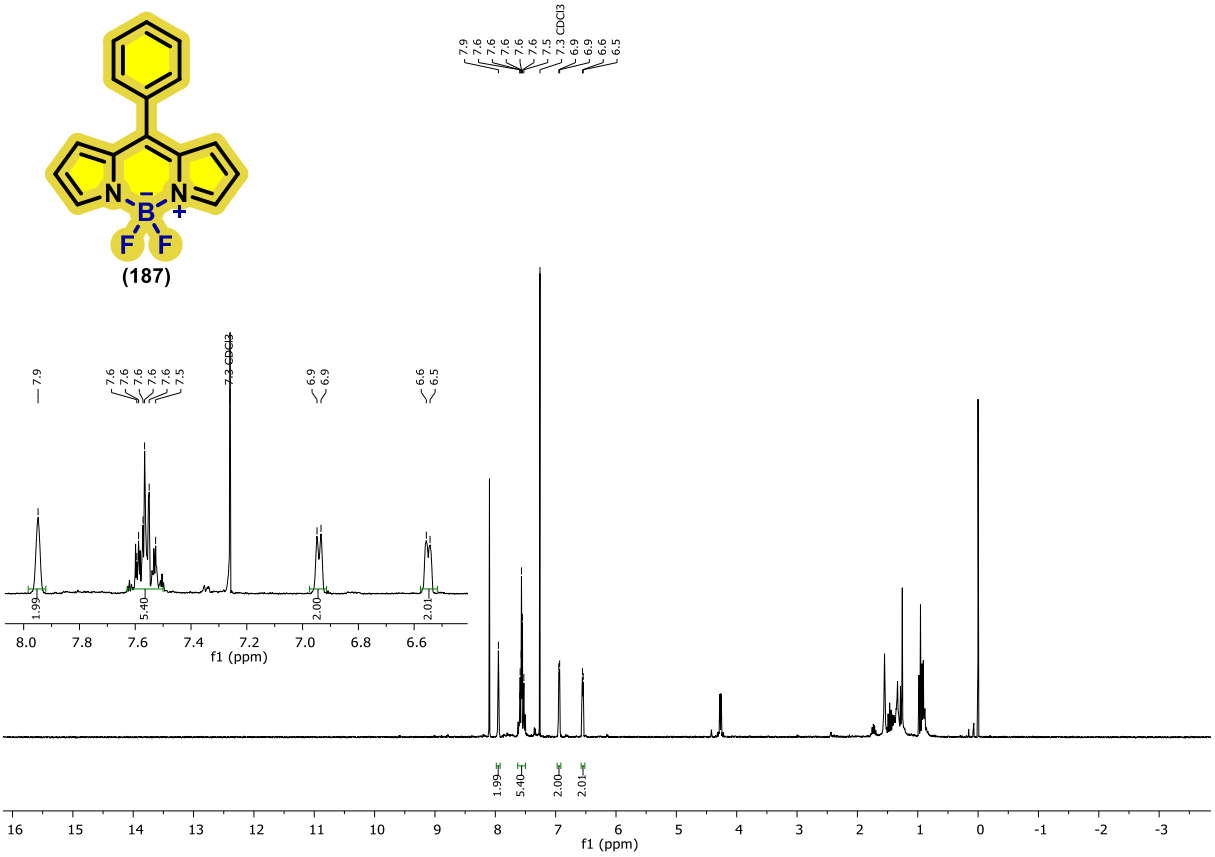

Figure C56. FTIR Spectrum of compound **187**.

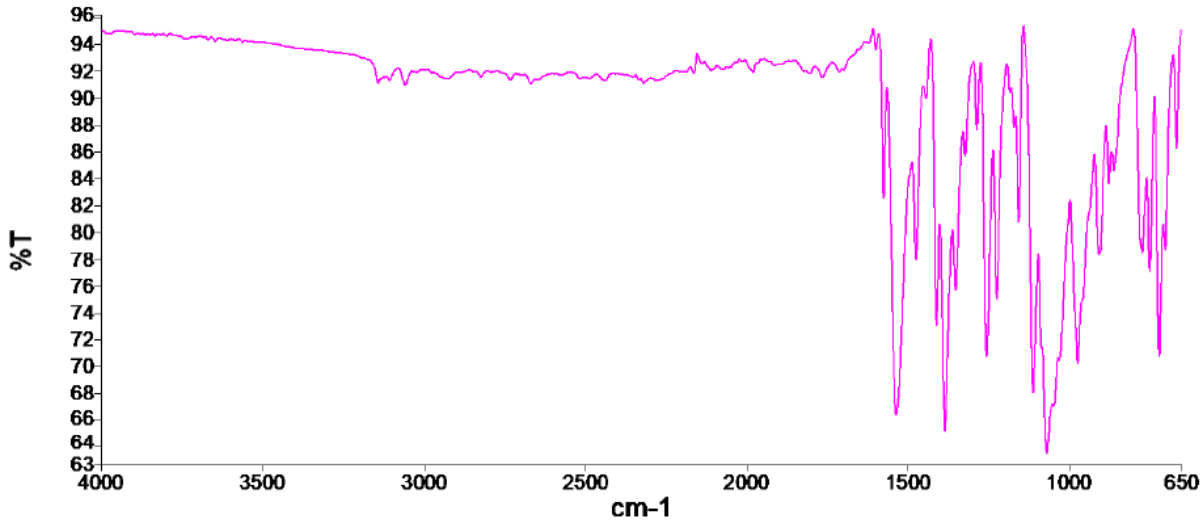

Figure C57. HRMS (ESI +) of compound **187**.

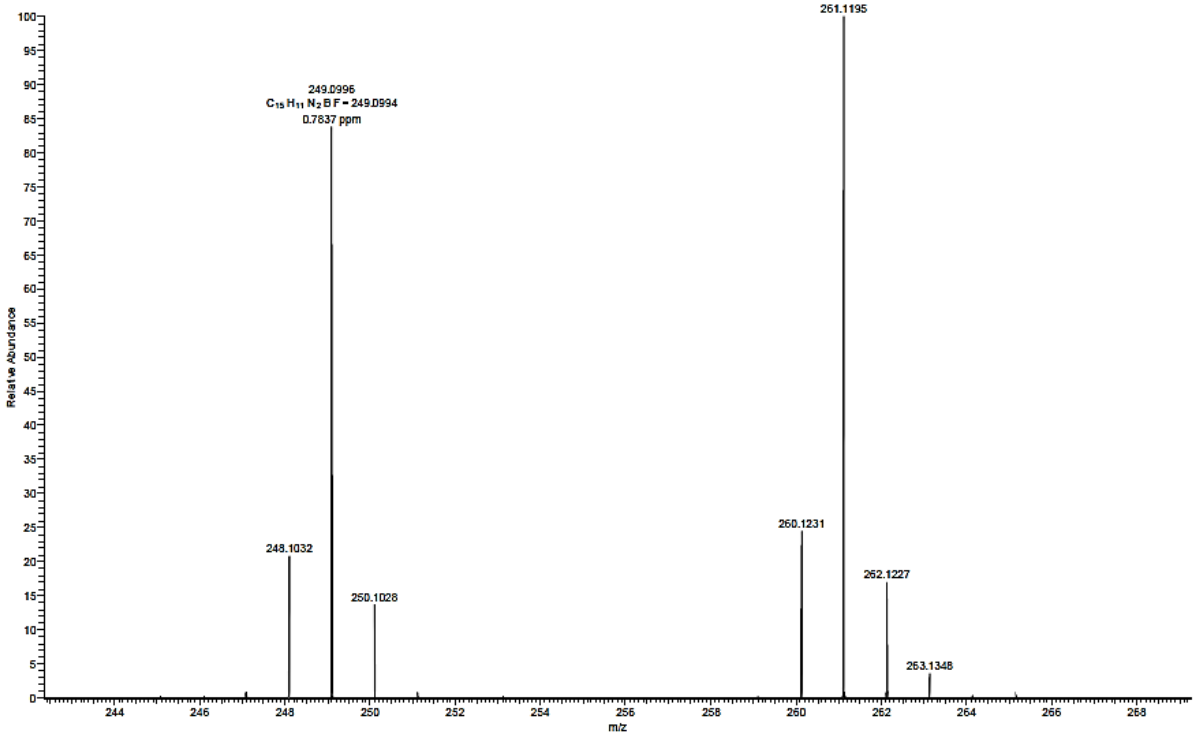

Figure C58. ^{1}H NMR spectrum of compound **188** (400 MHz, $CDCl_3$).

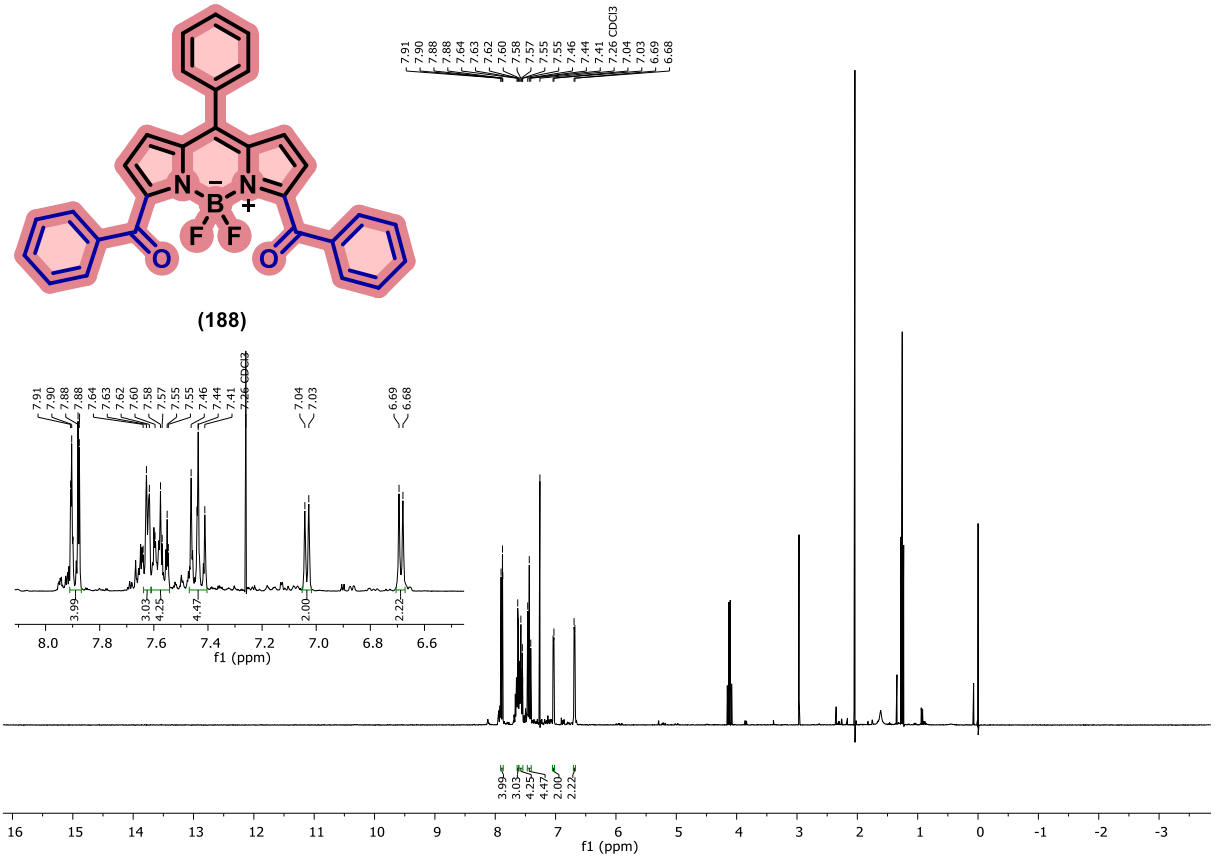

Figure C59. HRMS (ESI +) of compound **188**.

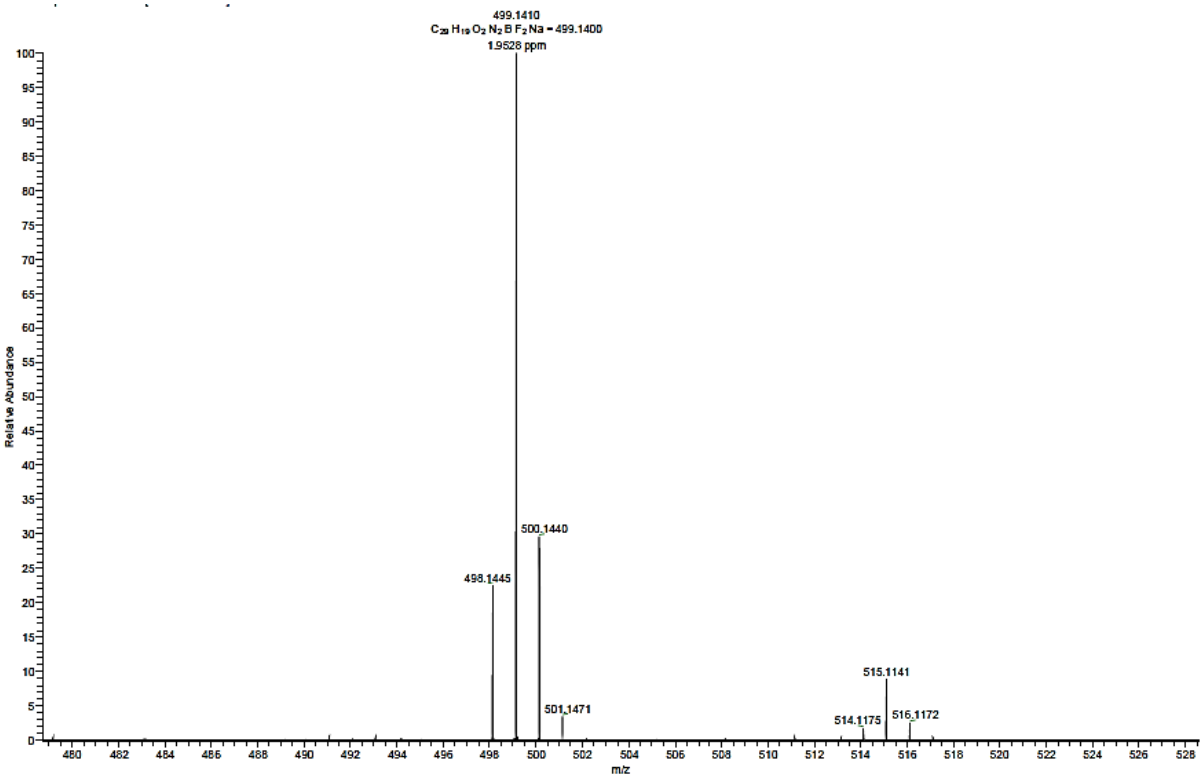

Figure C60. ^{1}H NMR spectrum of compound **189** (400 MHz, $CDCl_3$).

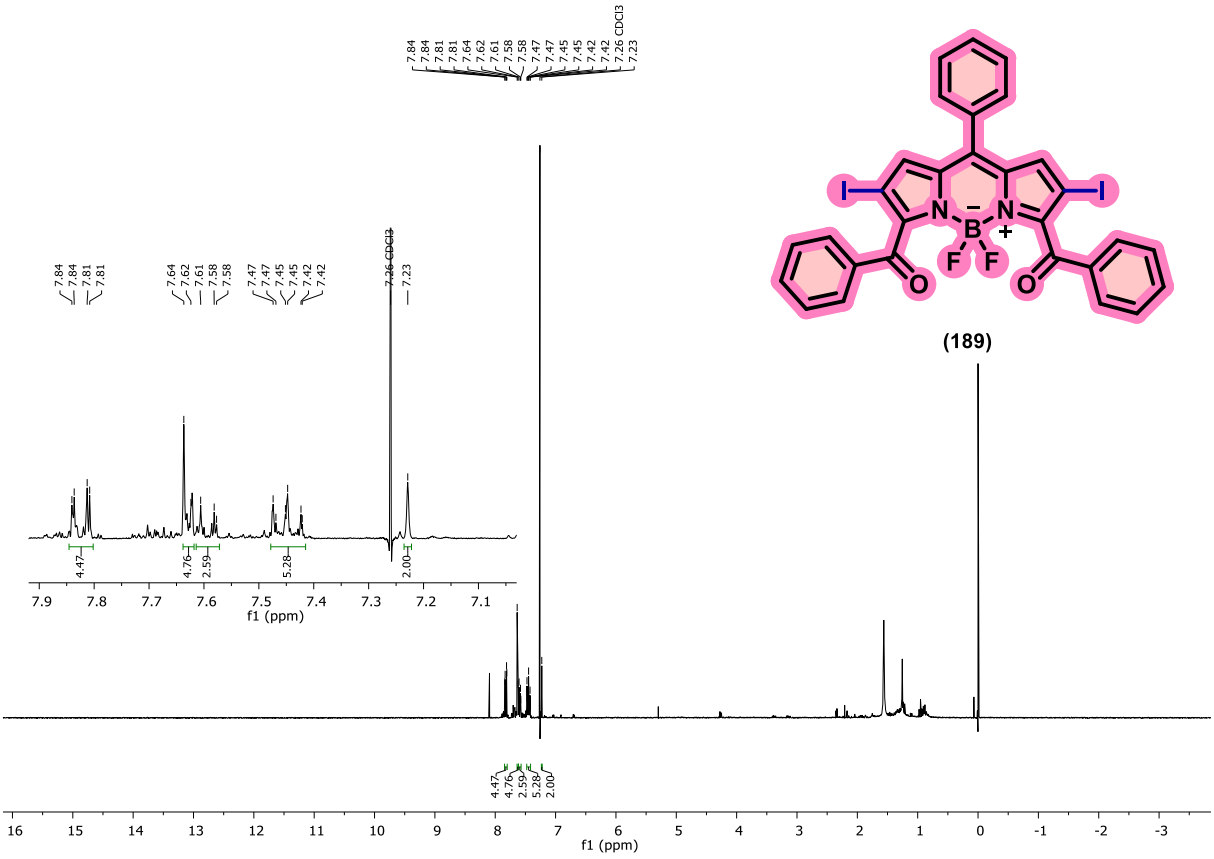

Figure C61. FTIR Spectrum of compound **189**.

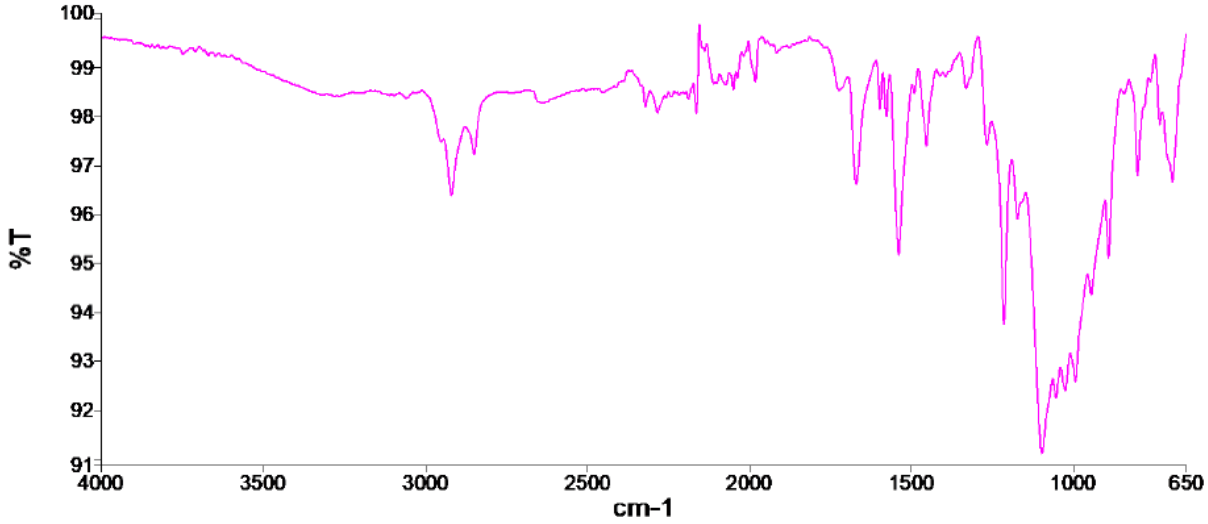

Figure C62. HRMS (ESI +) of compound **189**.